Plio-Quaternary Sediments and Neotectonics of the Isparta Angle, S.W. Turkey.

Clare Paula Glover

Thesis submitted for the degree of Doctor of Philosophy
The University of Edinburgh
1995

I hereby declare that this thesis was written by me and that its content is the result of my own work, except where otherwise stated

For Paula and Chris

Abstract

An integrated approach, combining sedimentology, structural geology and geomorphology, has been used to reconstruct the Pliocene and Quaternary evolution of the Aksu basin, located on the Mediterranean coast of Turkey. The present basin opened in the Lower Miocene (Flecker, PhD, 1995). The shallow marine, bioclastic Gebiz Limestone, originally thought to be Messinian in age is believed to date from the late Tortonian. Selenitic gypsum in the Aksu basin is related to the Messinian dessication of the Mediterranean Sea, which produced widespread evaporite deposits. Right-lateral shear is recognised during the late Miocene-early Pliocene. Pre-existing structural lineaments, that were orientated sub-parallel to the shear direction, were reactivated as right-lateral shear zones. Between these defined lineaments broader zones of distributed shear are thought to have deformed by clockwise rotation of small blocks bounded by sinistral fault planes. Flooding of the Mediterranean at the beginning of the Pliocene resulted in deposition of the Yenimahalle Formation. The onshore sediments of the Yenimahalle Formation are dated as *Globorotalia puncticulata-Globorotalia margaritae* zone, using planktic foraminifera. Benthic foraminifera assemblages show that maximum water depth at this time was of the order of 150m. Seismic profiles in Antalya Bay indicate that the Pliocene sediment package is approximately 500m thick and that it was deposited onto a block-faulted topography. Three transgressive phases are recognised, that can be related to sea-level changes during the Lower Pliocene highstand. The Yenimahalle Formation shallows and coarsens upwards in the upper 25m of section. The sediments change from blue-grey silts to yellow sands containing gravel lenses, shallow-water burrows and large macrofossils. The benthic foraminifera assemblage of the upper part of the section indicates a water depth of 50m or less. The Yenimahalle Formation grades into the Çalkaya Formation. This consists of non-marine fanglomerates in the far north; braided stream deposits in the northern Aksu basin; and deltaic marine and transitional marine deposits (marine sands and conglomerates, muds, soils and coals) in the south. A tuff deposit in the Çalkaya Formation is interpreted as the basal surge deposit of a small phreatomagmatic eruption. K-Ar dates from biotites extracted from pumice clasts in the tuff were inconclusive, due to excess atmospheric argon. Along the steep basin margin in the west, fanglomerates were deposited during the development of smooth mature slope surfaces, which are thought to have begun to evolve in the early Pliocene and to have continued to develop until the early Quaternary. A period of normal faulting occurred in the ?Late Pliocene/Early

Quaternary, mostly affecting the western basin margin, although it is also recognised in the east. As a result the Pliocene sediments were tilted towards the west. This normal faulting event is thought to be associated with a change of regional stress field, which facilitated gravitational collapse of the Aksu basin, and which has been recognised elsewhere in Turkey. Uplift of the Bey Dağlari, possibly related to underthrusting of the Anaximander mountains, is also thought to be a factor in the development of the Kemer normal faults. During the Early-mid Quaternary deposition of the Antalya tufa infilled the fault block topography. U-Th dating shows the majority of the tufa to be >400,000 years old. A complex depositional environment of tufa depositing lakes, swamps and streams existed. With time the flow of water supplied to the basin reduced and depocentres became less defined. The tufa became less lacustrine and more paludal. During the Quaternary, and probably also during the Pliocene, regional uplift affected the area. Thus relative sea-level fell, although relative subsidence of the basin with respect to the Taurus Mountains occurred. The interaction of this uplift with glacial climate fluctuations has produced the terracing of the tufa and the conglomerate terraces of the Aksu river. Karstification and stream erosion have subsequently modified the tufa terraces. Terra rossa soils are the most recent sediments documented in the basin.

Acknowledgements

Firstly, thank-you to Alastair Robertson who so cheerfully supervised this project and must be the fastest chapter reader in the department. I was generously funded by Shell International Petroleum Limited (UK) as part of their postgraduate sponsorship - Rick Preston, Sharon Munroe and Griff Cordey are thanked for their help during this time.

My time in the field has been the most memorable part of this PhD and thanks are due to a number of people in Antalya. I never failed to feel at home in that city. In particular, Ayhan, Feyzi, Hasan and the various waiters at Ünal Kebab Salonu; all the staff at Zamora Börek Salonu; the various owners of the Garden Pansion; Mustafa and Semre Gerger; Selçuk and Ifakat Erden; the builders at Aksu; Nafis Öz and his family in Tönguslu; and all the Foresters at Çandir were always ready to feed me, house me, help me or simply amuse me. Ismail Faraçlar at Grand Rent-a-Car continued to let me rent his cars, even after we had crashed them and rattled them to pieces. Most of all I have to thank my field assistants: Seb Hodgkin, Ned Pegler, Alan Dunmur, Norman Dalgleish and Harriet Randle who were all unfailingly cheerful in adversity and who cannot be thanked enough. All the people at the Institüt für Geologie und Paleontologie, Stuttgart are thanked for providing a welcoming refuge and haven, in particular Hannelore Krawinkel who organised use of the SEM and accommodation.

I was lucky enough to receive excellent technical assistance from all quarters and thank Tony Fallick and Jim Emlach from SURRC at East Kilbride for help with K-Ar dating; Ben Harte for introducing me to the joys of mineral separating; Graham Shimmield and Colin Chilcott for help with U-Th dating. Dodie James and Geoff Angel operated and helped with XRD and XRF analyses and Mike Hall prepared the thin sections. Finally, but most importantly, Diane Baty and Yvonne Cooper are thanked for their help with photography and drafting, however difficult the request!

This thesis has benefited from discussions with: André Poisson, Günter Schweigert, Bill Austin, Dirk Kroon, Erhan Altunel, Martyn Pedley, Sandy Tudhope, Rachel Flecker, Dieter Schmid, Patience Cowie, Elizabeth Pickett, Sandra Gadd, James Jackson, Serdar Özüs, Clive Pinder and Mustafa Karabiyikoğlu.

Finally, a word for the KB dinner team Graham and Steve and to those who have been such support and help during the last few weeks (months!!), whose patience, proof-reading, sticking, copying and tea-making skills have been equally excellent: Ralf, Fiona, Elizabeth, Rachel, Sandra, Clare, Ian, Tim and Al - Thanks.

Selten wird dem Reisenden, selbst wenn er grosse Theile des Orients durchwandert, ein anziehenderes Bild geboten, als dasjenige, welches sich ihm an einem hellen Frülingstag auf der Rhede von Adalia darstellt. Links im Westen die wildgezackten, dicht an's Meer herantretenden Berge der lykischen Halbinsel, rechts im Osten, die ruhigeren Kämme des pisidischen Taurus, alle diese Berge in ihren höhren Theilen mit leuchtenden Schneefeldern bedeckt, und endlich zwischen diesen verscheidenartig gestalteten Seitencoulissen des Hintergrundes vorne die Steil gegen das Meer abfallenden Ufer der pamphylischen Ebene durch zahlreiche, jäh in das Meer stürzende Wasserfälle unterbrochen und überragt von den malerischen Mauern und Zinnen einer Festung mittelalterlichen Styls, von schlanken türkischen Minarets und den Häusergruppen einer ansehnlichen, inmitten der üppigsten Gertenvegetation gelegenen Stadt: das ist der Anblick von Adalia.

Emil Tietze (1885).

Contents

Chapter 1: Introduction

This project focuses on the Pliocene and Quaternary sediments and neotectonic development of the Isparta angle in southern Turkey. It forms part of a broad area of research interest within the department of Geology and Geophysics at the University of Edinburgh, which goes back some years. The development of the Tethyan oceans from the Permo-Triassic Palaeotethys to the Quaternary Mediterranean has been studied extensively in Turkey, Greece and Cyprus. The location of the present study area and previous Edinburgh studies in the Eastern Mediteranean region are shown in Fig. 1.1. The Tethyan realm has been closing since the Permian (Fig. 1.2) and provides a unique opportunity to study the closure of major ocean basins. The Mediterranean Sea represents the final stage of closure of this long-lived system. Related, contemporaneous projects concern the development of the Late Miocene to Recent Polis graben system in SW Cyprus (Payne, 1995) and the Miocene basins of the Isparta Angle (Flecker, 1995). The study of Flecker (1995) is particularly pertinent to this work as it is concerned with the evolution of the Isparta angle during the Miocene, which directly influences the Plio-quaternary basins. Her results are summarised below.

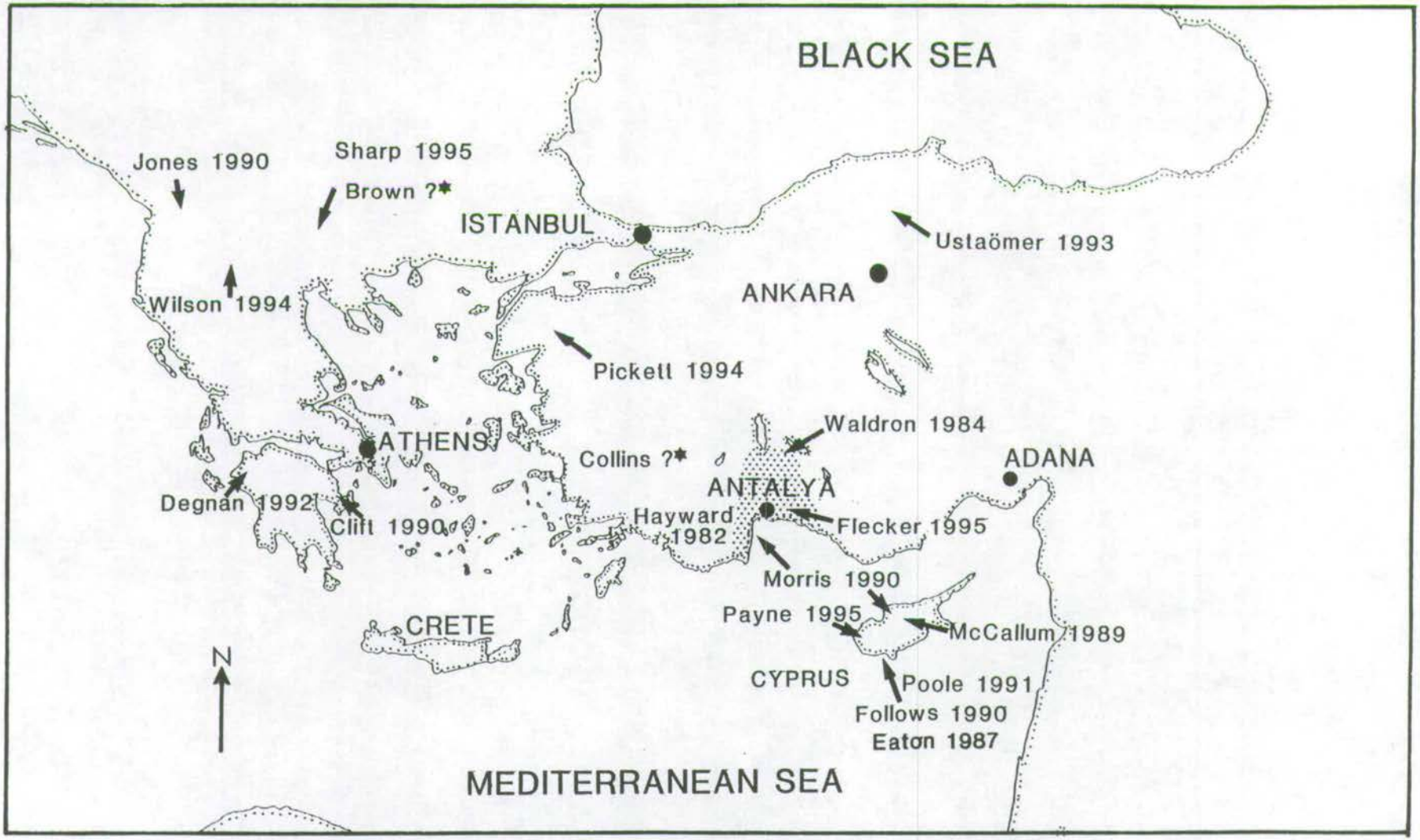

Fig. 1.1: Map of the eastern Mediterranean indicating the area of study (shaded) and the field areas of recent Edinburgh research students with interest in the development of Palaeotethys, Neotethys and Neogene basins of the region. Most of these will be referred to in the course of this chapter. All dates refer to unpublished theses of the university of Edinburgh. The symbol ?* refers to theses in progress at the time of writing.

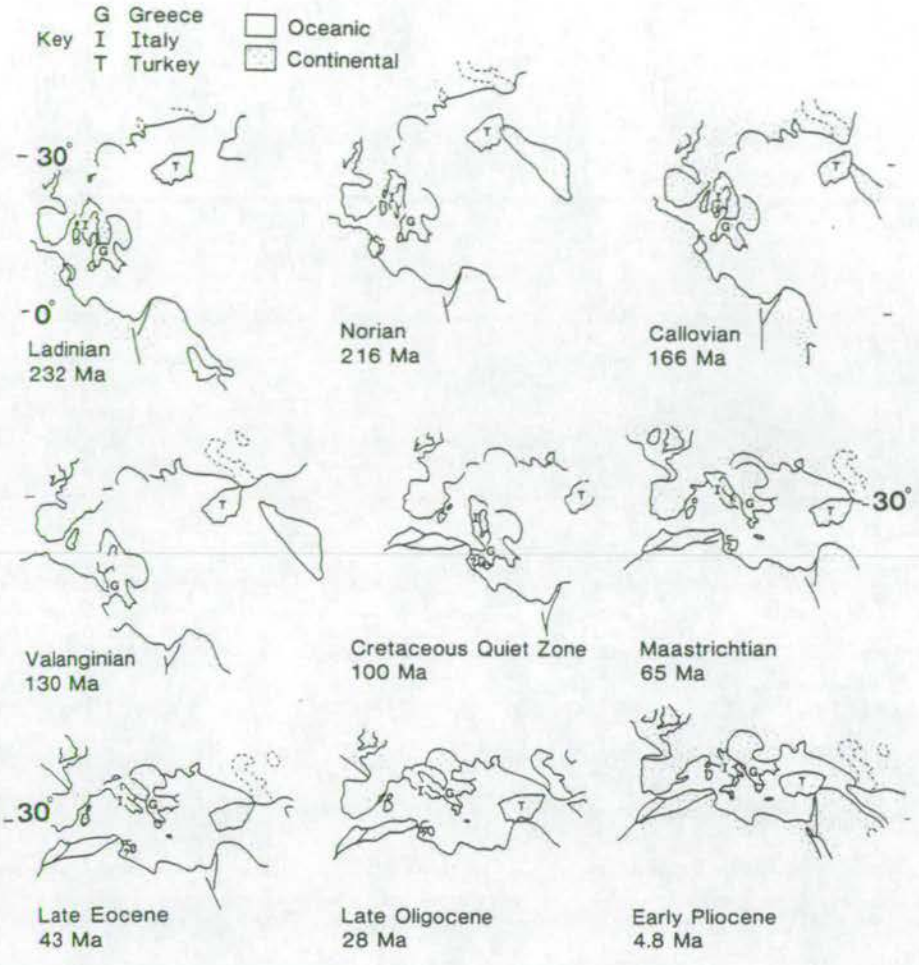

Fig. 1.2: Palaeogeographic reconstructions of the Tethys from the Jurassic to the Early Pliocene from Robertson, Clift, Degnan and Jones (1991)* . Details of the reconstruction and some of the problems associated with it are given in the original caption. It shows clearly the progressive closure of a large wedge shaped ocean and the complex movement of landmasses that produced the present-day Mediterranean.

The Isparta angle is situated on the Mediterranean coast of Turkey. It is a triangular region bounded to the east and west by arcuate thrusts related to emplacement of the Tertiary Lycian nappes in the west and the Beysehir-Hoyran-Hadim nappes in the east. The oldest units of the Isparta angle are the Tauride carbonate platform units (Bey Dağ lari, Anamas Dağ and Davras Dağ) and the deep

---

* The first citation of a given paper quotes all authors, thereafter the normal convention of using *et al* for papers with more than two authors is adopted. This practice has been chosen, due to the frequent occurrence of some workers as later authors on many papers, in an attempt to give the reader an impression of the grouping and variance of opinion.

water units of the Antalya Complex (Fig. 1.3). In the centre of the region lie the Neogene basins, the Miocene Köprü, Aksu and Manavgat basins, and the Pliocene/Quaternary Aksu basin (Fig. 1.4). Major roads and cities in the area are also shown on this map. The term "Antalya basins" has been adopted in this thesis to mean all three of these basins from their initiation to the present day.

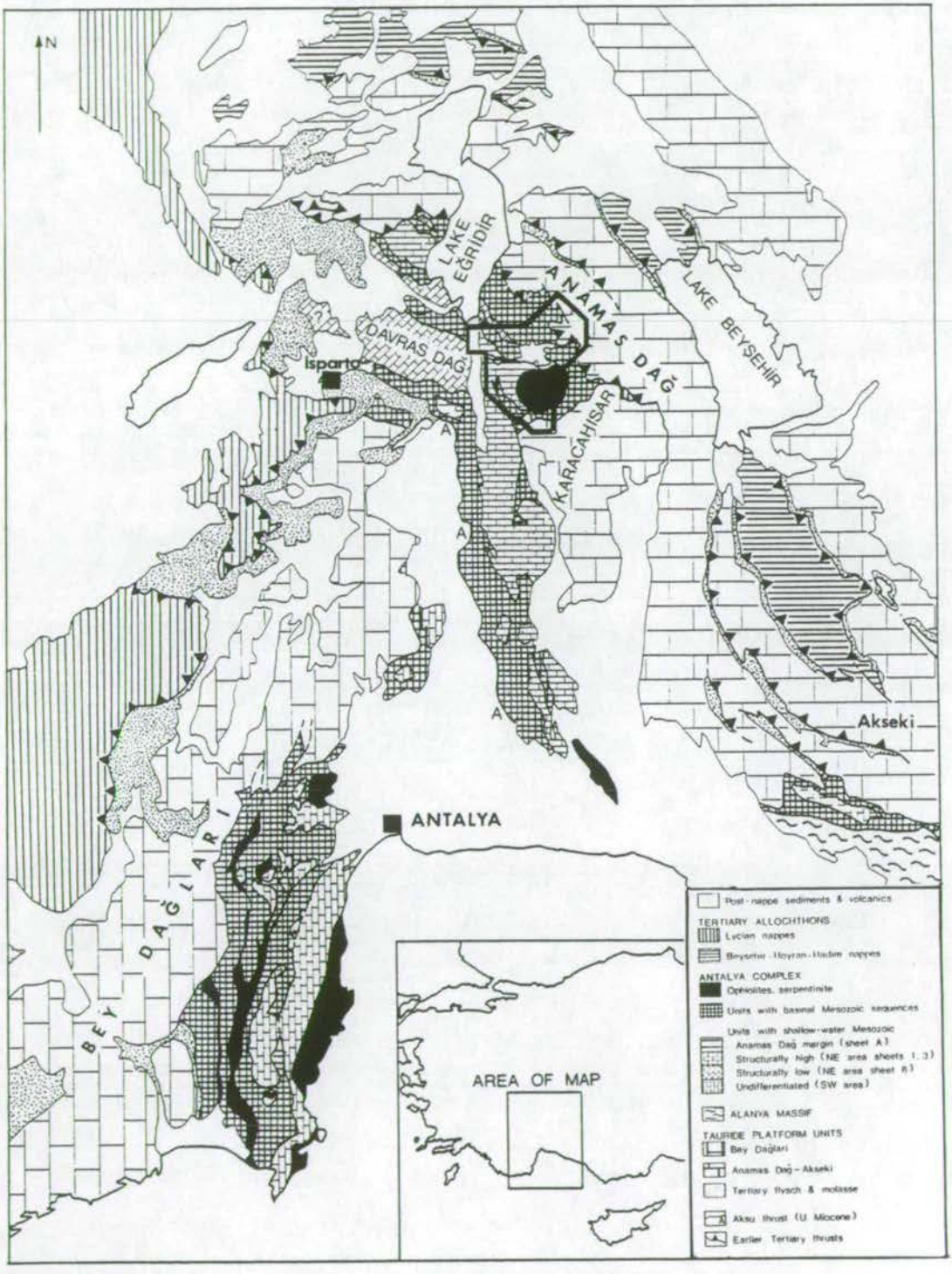

Fig 1.3: Mesozoic geology of the Isparta angle from Waldron (1984).

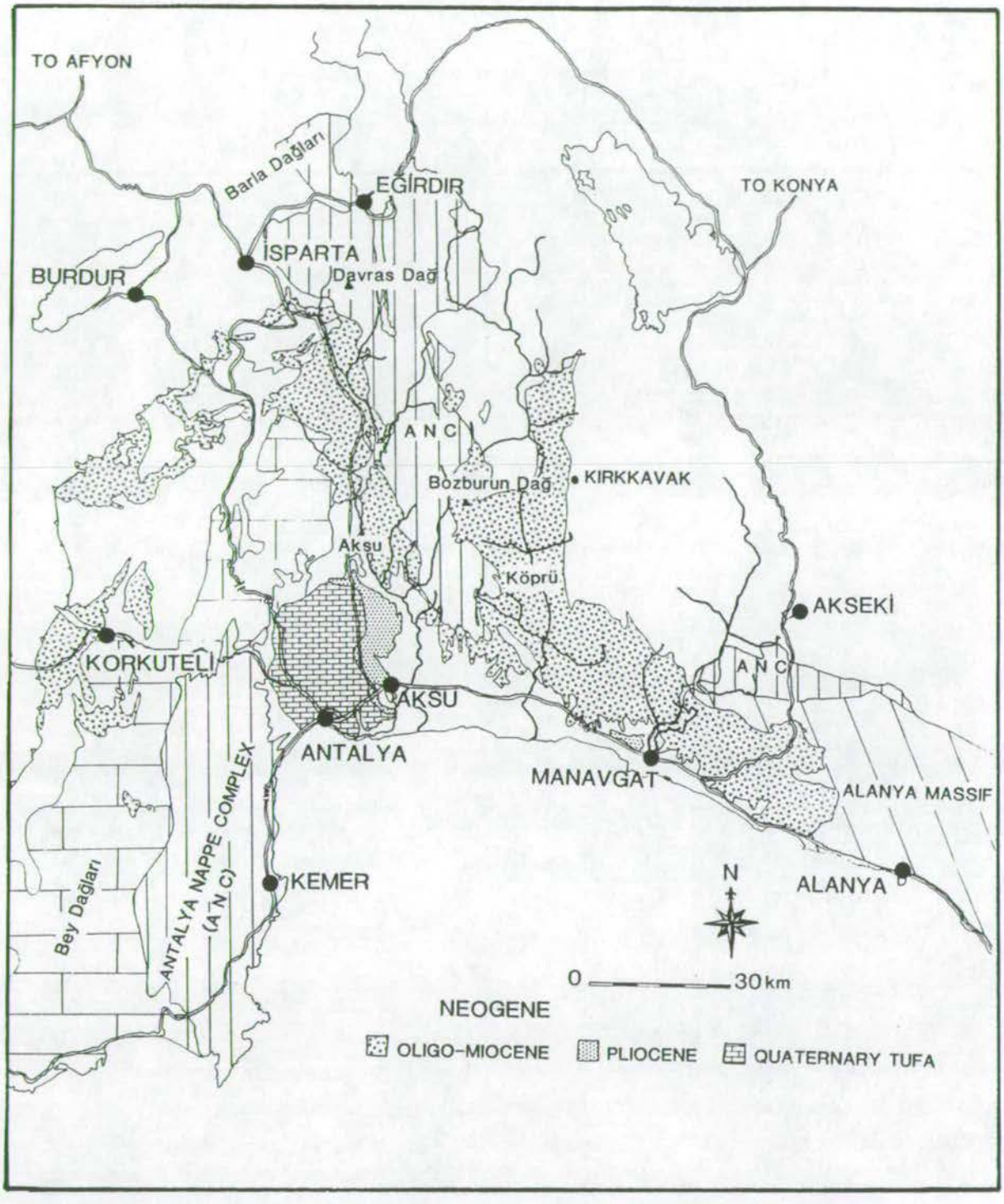

Fig 1.4: Map of the Neogene geology of the Isparta angle. The Miocene sediments are undivided. For more detail on the Miocene see Flecker (1995). Major cities and the villages of Akseki and Aksu basins are marked, as are the major roads in the area. The road from Aksu to Isparta was under construction during the field research for this project and provided particularly good exposure in new road cuttings.

The review in this chapter aims to set the general scene for the project. The history of Tethys and the Mesozoic and Miocene history of the Isparta angle give rise to the geological framework of the region. The general climatic conditions and sea-level fluctuations that affected the Mediterranean, and, thus, the Aksu basin, during the Pliocene and Quaternary are also reviewed. Chapters 4 and 6, respectively include extensive reviews of tufa sedimentology and of the Neotectonics of the eastern Mediterranean, which relate specifically to the content of those chapters.

1.1: Palaeotethys and Neotethys

The existence in the Permo-Triassic of a large, westward-narrowing ocean (Tethys) separating Eurasia and Africa was first proposed by Wegener (1924). This was later recognised to have been an essentially Palaeozoic ocean (Palaeotethys) and a number of younger, smaller oceans dating from the Mesozoic and Tertiary (Neotethys), which formed as a result of rifting along the northern Gondwanan margin (Laubscher and Bernouilli, 1977; Sengör, 1979) (Fig. 1.5). The Tethyan suture zone runs along the Alpine/Himalyan orogenic belt (Fig. 1.6).

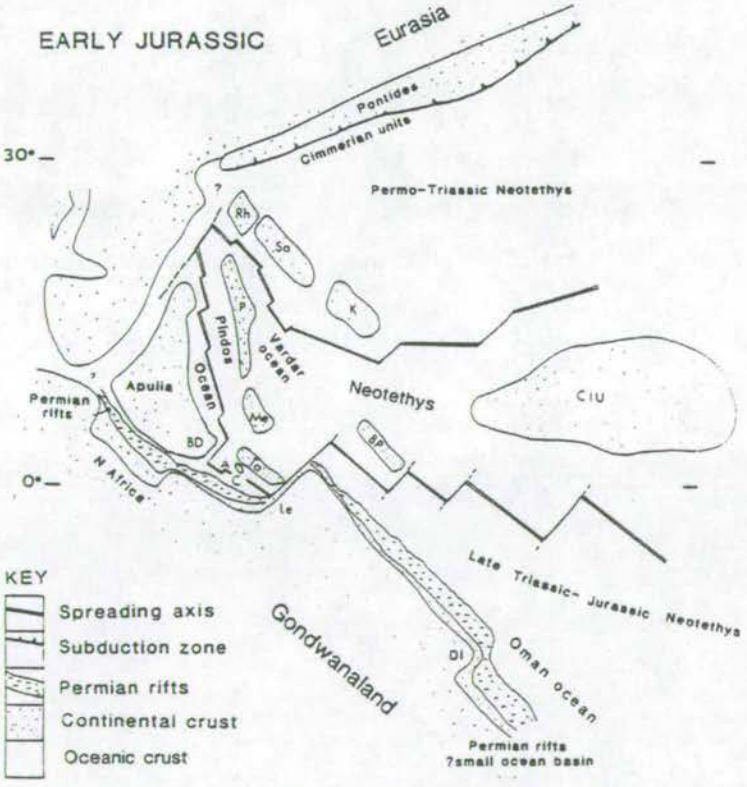

Fig. 1.5: Plate tectonic sketch map of the Eastern Mediterranean in the Early Jurassic from Robertson, Clift, Degnan and Jones (1991). Neotethys is seen as a flexible collage of small ocean basins and microcontinents. The sketch map indicates the permissible positioning of units in the light of field and palaeomagnetic data.

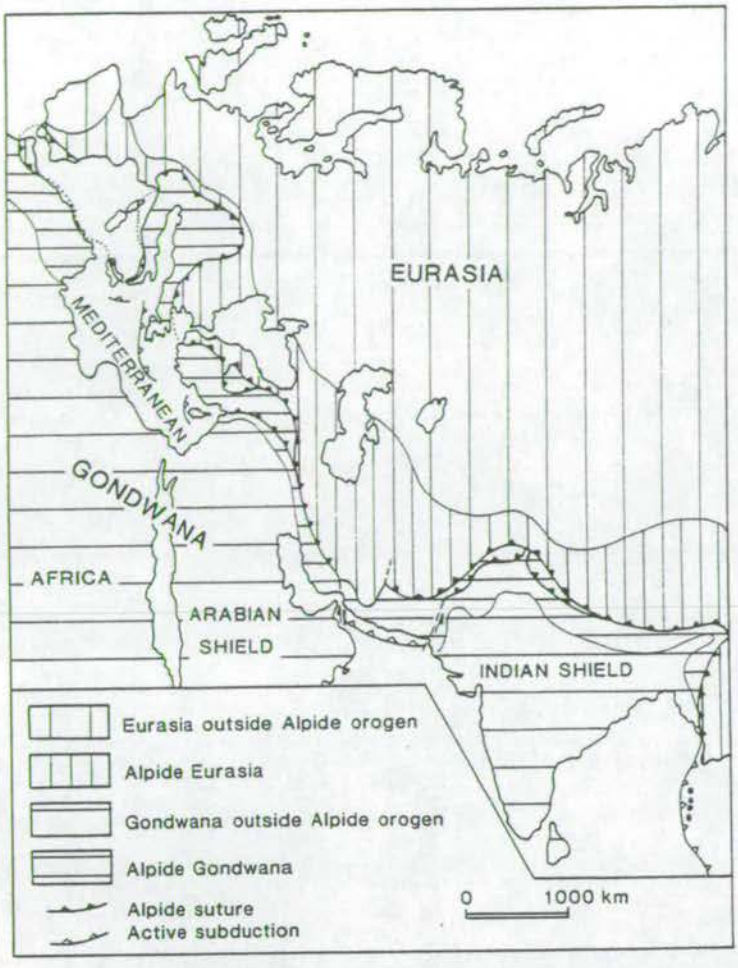

Fig 1.6: Tectonic map of the Alpine-Himalyan orogenic belt, showing the major Alpide sutures from Pickett (1994) (after Okay, 1989)

Palaeotethys is assumed to have closed by subduction during post Triassic times. Continuing debate exists as to whether subduction was southward (Sengör, 1979; Sengör, Yilmaz and Ketin, 1980; Sengör, Yilmaz and Sungurlu, 1984), or northward (Adamia, Chkhotua, Kekelia, Lordkipanidze, Shavishili and Zakariadze 1981; Robertson and Dixon, 1984), or possibly both. A review of the arguments in 1984 can be found in Robertson and Dixon (1984) and Sengör *et al* (1984). More recent support of southward subduction can be found in Okay, Siyako and Burkan (1991) and Tüysüz (1990). Northward subduction in the central Pontide region is supported by Ustaömer and Robertson (1993, 1994) and in the Caucasus by Adamia and Belov (1989). Pickett (1994) concluded that southward subduction of the Karakaya Complex in NW Turkey occured within a dominantly northwards subducting Paleotethys, perhaps as the result of "jamming" of subduction in the extreme western end of the Palaeotethys ocean by a large oceanic plateau or many small platforms.

A greater concensus exists concerning the behaviour of Neotethys. (Robertson and Dixon, 1984; Sengör *et al*, 1984). Early Mesozoic breakup of

Gondwana occured behind the closing Palaeotethys. Fragments of the Gondwanan margin drifted northwards and accreted to the Eurasian margin, as separate strands of Neotethys rifted from the Gondwanan margin. The eastern Mediterranean Neotethys can be envisaged as a series of small ocean basins, which underwent a predictable set of stages: rifting, spreading, subduction / accretion, displacement / emplacement and collison (Robertson, Clift, Degnan and Jones, 1991). Diachronous collisions ensued from the Late Jurassic onwards; these were particularly dominant in the Mediterranean during the Late Eocene and Miocene. Intra-oceanic carbonate platforms and volcanic seamounts are also a common feature of these Neotethyan basins.

A second theory of Neotethyan evolution was put forward by Ricou, Marcoux and Whitechurch (1984) (see also: Ricou, Argyriadis and Lefevre, 1974; Ricou, Agyriadis and Marcoux, 1975). These authors believe that the Neotethys formed a single, large ocean basin situated to the north of the Antalya Complex. A phase of ophiolite obduction and nappe transport emplaced all the ophiolites along the Tauride belt including the Syrian Hatay/Baer Bassit and Troodos ophiolites (Fig. 1.7). The calcareous platforms of the Bey Dağ lari, and other areas, represent a "calcareous axis" now preserved as a window, over which all these ophiolitic units were thrust.

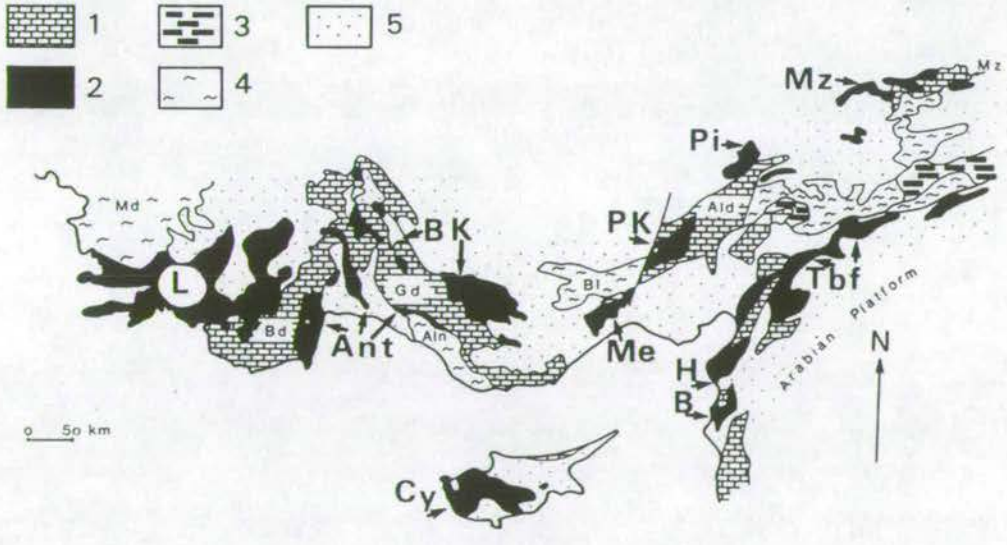

(1) Platform units: Bd, Bey Dağları; Gd, Geyik Dağ; Ald, Aladağ; and Md, Munzur Dağ constitute the Calcareous Axis of the Taurus.
(2) Ophiolites and slope-basin units: L, Lycian Nappes; Ant, Antalya; B, Beyşehir; K, Karaman; Cy, Cyprus; Me, Mersin; H, Hatay; B, Bäer Bassit; PK, Posantı, Karsantı; Pi, Pinarbaşı; Mz, Munzur; and Tbf, Turkish border folds.
(3) Malatya-Eliazığ ophiolites and associated rocks.
(4) Metamorphic massifs: Md, Menderes; Aln, Alanya; and Bl, Bolkar Dağ
(5) Post tectonic formations.

Fig. 1.7: Geological sketch map of the Taurides from Ricou, Marcoux, Whitechurch (1984). The ophiolite units which they considered to be sourced from the same northern ocean are shown in black.

The arguments of Ricou *et al* (1974, 1975, 1984) rely heavily on the similarity of facies between the basin and horst deposits in the different areas, a supposed common spreading axis trend between many of the ophiolite units and a similarity in timing of obduction and tectonic style of obduction. None of theses arguments really seem sufficient to distinguish between a single or multiple basin hypothesis. These authors argued that the similarity in timing of sedimentation styles and obduction preclude the existence of a number of small ocean basins. It can be argued that the broad controlling tectonics of continental collision would actually lead us to expect that closure of many of these basins was approximately synchronous. Robertson *et al* (1991) showed that the whilst timing of rifting and collision was similar in the Neotethyan realm they were indeed diachronous, at least in the Pindos, Antalya and Cyprean regions. Thus, the arguments for a single, northerly Neotethyan ocean no longer stand up.

These two Neotethyan scenarios (Fig. 1.8) are the basis for the opposing views of the Mesozoic history of the Isparta angle as presented in the next section.

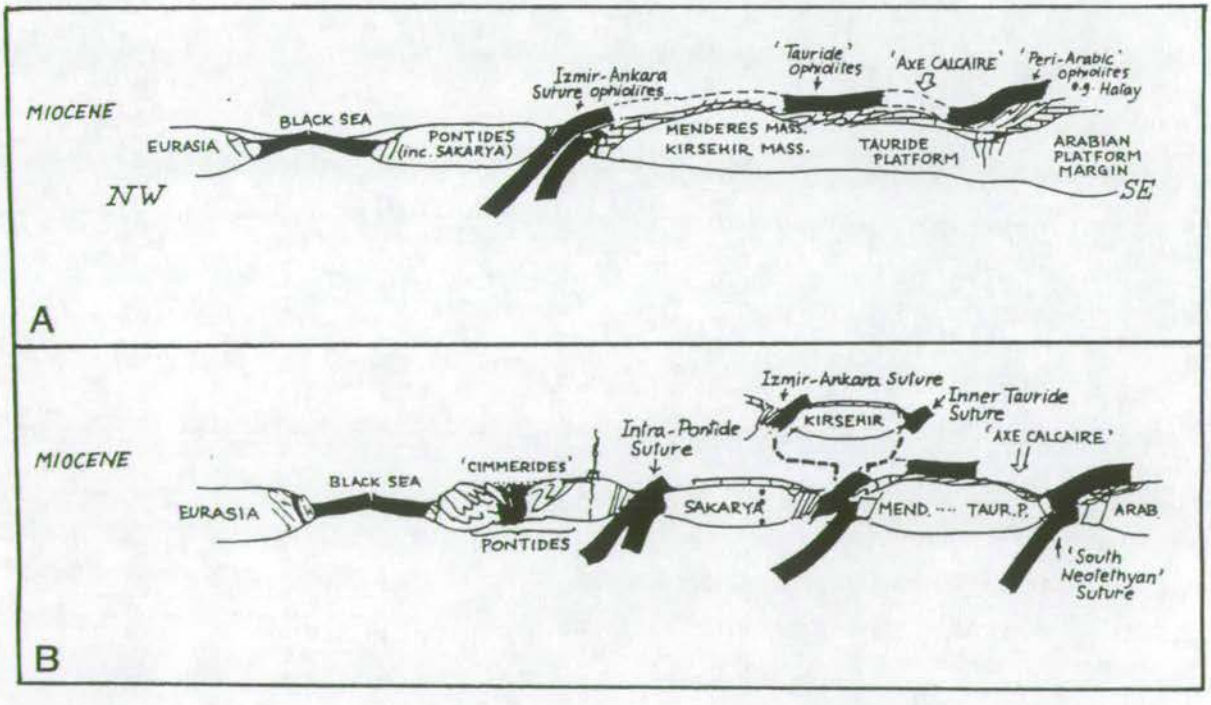

Fig. 1.8: Alternative hypotheses for emplacement of the Eastern Mediterranean ophiolites from Robertson and Dixon (1984). **A** shows a single ophiolite sheet sourced from the north and thrust over the carbonate platform units. **B** shows the multiple-root-zone model with ophiolites from a number of small ocean basins obducting diachronously as closure occurs between Africa and Eurasia.

1.2: Pre-Pliocene development of the Isparta angle

The pre-Neogene development of the Isparta angle has long been controversial. The French protagonists (Lefèvre; 1967, Brunn, 1974; Brunn, Dumont, Graciansky, De Gutnic, Juteau, Marcoux, Monod and Poisson, 1971) argued that the authochthonous and allochthonous units of the Isparta angle were emplaced as "lower" "middle" and "upper" Nappes thrust from a Neotethyan ocean far to the north (Ricou *et al*, 1974, 1975; Ricou, Marcoux and Poisson, 1979; Ricou *et al*, 1984) (or south; Dumont, Marcoux, Monod and Poisson, 1972; Monod, 1977). It has already been shown in the previous section that there are problems with this model. Robertson and Woodcock (1984) and Poisson (1984) subsequently argued that the units are much more locally derived, thrust only short distances onto the margins of a small Neotethyan ocean basin. The Bey Dağ lari and Anamas Dağ are considered to be relatively authochthonous platforms on which passive margin sedimentation occured (Monod, 1977; Gutnic, Monod, Poisson. and Dumont 1979; Waldron, 1984, Poisson and Robertson 1990). Robertson and Woodcock (1984) discuss the nature of the Antalya Complex as a braided rift in the Neotethyan realm. The Antalya Complex represents the passive continental margin of a small ocean basin and consists of carbonates, tuffs, radiolarites, ammonitico rosso, mafic extrusives, turbiditic quartzite clastics and conglomerates (Robertson and Woodcock, 1982). Emplacement of the Antalya Complex occured during the latest Cretaceous to Miocene. Anastomosing serpentinite screens are thought to be intrusions of hydrated mafic substratum through the active braided strike-slip fault system along which emplacement occured. Hayward (1982) showed that the eastern margin of the Kasaba basin in the west was overthrust only a short distance by the Antalya complex, consistent with a dominantly strike-slip emplacement. This argument and observations on the western margin of the basin (discussed further below) lead Hayward (1982) to the conclusion that the Lycian nappes and Antalya Complex approached from opposite directions bringing their respective ophiolitic units from separate oceanic basins, which were separated by the carbonate platform (Bey Dağ lari-Susuz Dağ) that now floors the Kasaba basin. The Antalya Complex is also present as a belt in the centre of the Isparta angle. Waldron (1984) documented the north-eastern part of this belt, south east of lake Eğ ridir. Late Cretaceous thrusting of deep-water sediments over shelf-edge units was followed by further folding and thrusting (NW vergent) during the Late Eocene to produce chaotic mélange-like terranes. The Antalya Complex in this area is reconstructed as a wide (i.e. >300km) ocean basin with carbonate platforms to the east and west and at least one smaller platform between. At the southern end of this central belt thrusting was complete by

the Late Oligocene and the allochthonous and authochthonous sequences in the area were then overlain by sedimentary sequences dated as Late Oligocene/Early Miocene (Poisson, Akay, Cravatte, Müller and Uysal, 1993).

Further evidence was subsequently presented by the French to argue that the "Antalya Nappes" were indeed thrust from the north (Marcoux, Brunn, Burg and Ricou, 1987; Marcoux, Ricou Burg and Brunn, 1989). These latter studies were primarily based on shear sense criteria from the basal units of the thrust sheets and showed each of the nappe units to have been thrust in slightly different directions at different times. However, they did not recognise the possibility that some of these structures may be associated with the emplacement of the Lycian Nappes. These were transported from the northwest during the late Oligocene-Miocene, from another Neotethyan ocean basin, and would certainly have produced S to SE shear criteria in ductile beds. Also, some structures relate to thrusts from the NE in the Late Eocene and/or to neotectonic deformation. Robertson (1993) presents a very detailed sedimentological and structural description of units around the Isparta angle to show that many of the carbonate platforms in the area are associated with slope and basinal

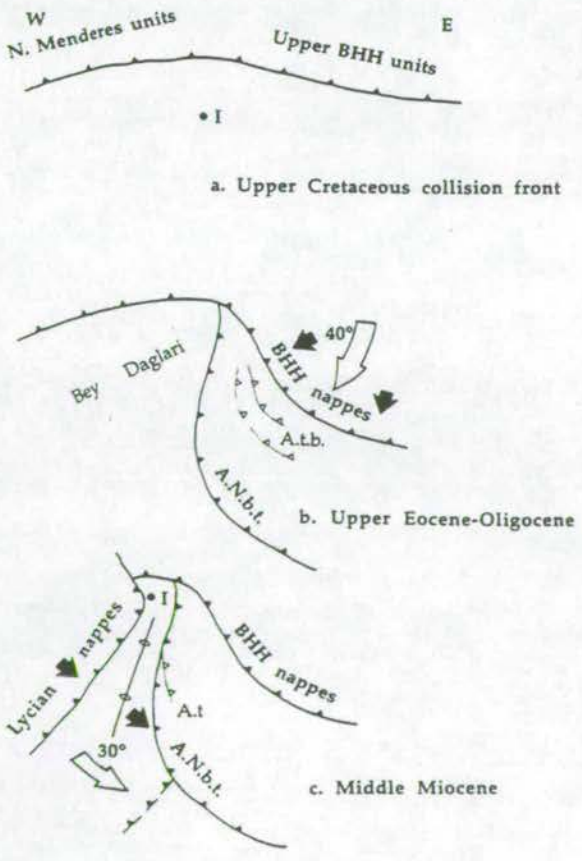

Schematic model of the development of the Isparta angle from Kissel, Averbach, Monod and Allerton (1993). Note the development of a basal thrust to accommodate rotation of the Bey Dağlari.

A.N.b.t. = Antalya Nappe basal thrust
A.t.b. = Akseki thrust belt
A.t. = Aksu thrust
I = Isparta

facies and MORB-type basalts that prove they must have been carbonate platforms sitting on strands of a Neotethyan ocean basin that were subsequently thrust onto the autochthonous margins towards the east and west.

Two other theories concerning the origins of the Isparta angle also appeared in 1993. Dilek and Rowland (1993) support the model of local derivation of the units of the Antalya Complex and go on to suggest that the ocean behaved as a passive conjugate pair dating from the Mid-Cretaceous. However, this theory is flawed as there is no evidence of a major rift event in the Upper Cretaceous. The passive margin phase begins in the Triassic and continues through to the upper Cretaceous/Paleocene. They also do not account for the ophiolite on the eastern side of the Isparta angle.

Kissel, Averbach, Frizon de Lamotte, Monod and Allerton (1993) presented new data to show that the eastern margin of the Isparta angle has rotated 40° clockwise. They presented a model of an approximately straight Upper Cretaceous collision front which was subsequently rotated clockwise 40° in the east and then 30° counterclockwise (Kissel and Poisson, 1986a) in the west as the Lycian Nappes are emplaced from the NW (Fig. 1.9). They assumed the development of a basal thrust (A.N.b.t in Fig. 1.9) which is not fully explained. This will be discussed further in chapter 6. The 30° counterclockwise rotation of the Bey Dağ lari is accounted for in the reconstruction of the Isparta angle (Fig. 1.10) (Robertson 1993).

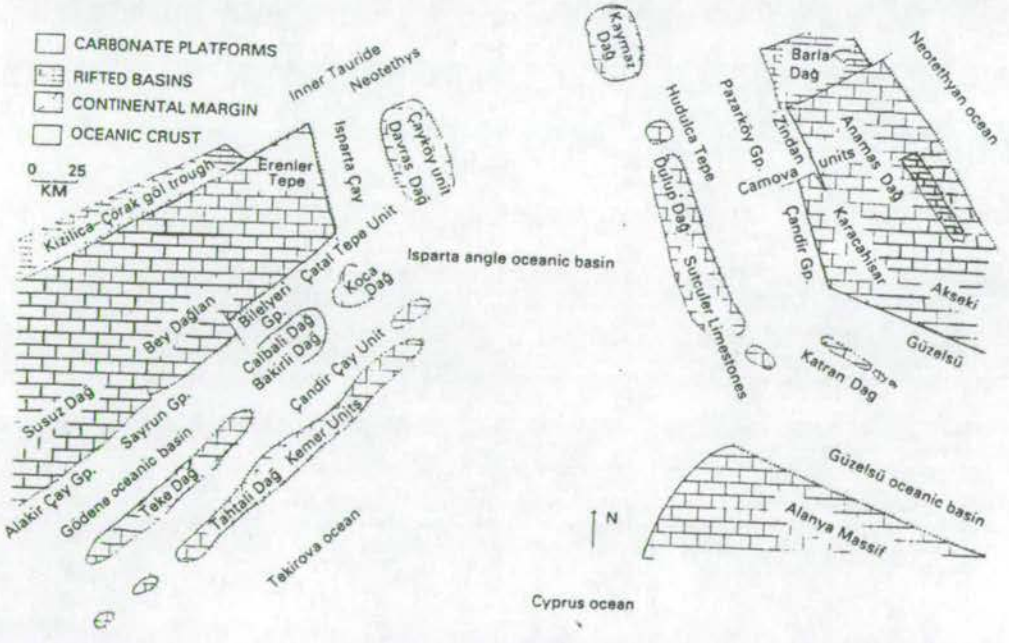

Fig. 1.10: Palaeogeographic sketch of the Isparta angle during the Upper Jurassic-Early Cretaceous from Robertson (1993). 30° counterclockwise rotation of the Bey Dağ lari is taken into account, but the 40° rotation of the eastern margin was unknown at this time. Its effect is to broaden the angle between the eastern and western margins.

It was recognised at this stage that the degree of rotation of the eastern margin of the basin was unknown. The new data (Kissel *et al,* 1993) showing a 40° rotation produces a broadening of the angle of the original Neotethyan ocean basin depicted by Robertson (1993) and does not affect the model proposed therein.

During the Early Tertiary, first, the Hoyran-Hadim nappes (Late Eocene) and then the Lycian Nappes (Late Miocene) were emplaced (Kissel *et al,* 1993; Robertson, 1993). Narrow exposures of Eocene flysch indicate flexural loading during emplacement of the Hoyran-Hadim nappes (Flecker, 1995). The emplacement of the Lycian nappes in the Late-Oligocene-Early Miocene also caused the development of a flexural foreland basin (Kasaba basin) along the thrust front (Hayward 1984). Thrusting is recurrent throughout the Miocene (Gutnic *et al*, 1979). Hayward (1982) showed that this continued emplacement throughout the Miocene resulted in progressive overthrusting of the western margin of the Kasaba basin. Final emplacement in the late Miocene is probably responsible for the Aksu phase of deformation (Poisson, 1977; Flecker, 1995).

In summary, the Isparta angle can be considered as a region formed as a result of the northwards movement of Africa towards Eurasia, closing Palaeotethys and opening a number of small ocean basins, similar to the present-day Red Sea, which closed by the Early Tertiary. The Isparta angle oceanic basin contained a number of allochthonous carbonate platforms separated in places by oceanic rifts. These were accreted by the Early Eocene (Fig. 1.11).

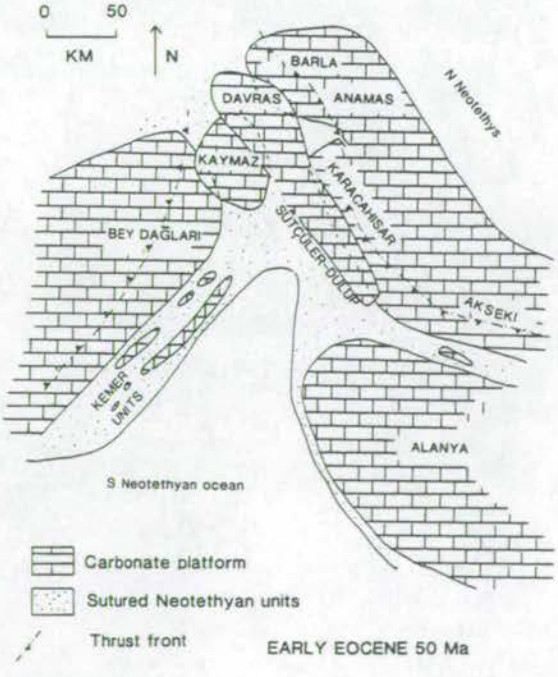

Fig. 1.11: Palaeotectonic setting of the Isparta angle after suturing of the carbonate platforms, but before Late Eocene and Late Miocene deformation from Robertson (1993).

The result of this Mesozoic activity was to leave a strong structural fabric on the region. Flecker (1995) considers this to be the dominant control on the Miocene tectonic development of the area. Its influence on the Plio-Quaternary tectonics is discussed in chapter 6.

The Miocene sediments of the Kasaba foreland basin, which is situated between the thrust front of the Lycian Nappes and the Antalya Complex were discussed in detail in Hayward (1982). The basin contains a series of alluvial and marine fans, originating from both the western and eastern margins of the basin. The western margin alluvial fans of the Kemer Formation prograde into a shallow-marine sea where small patch reefs developed. The Salir Formation in the east was deposited by sediment gravity flows in small submarine fans. Irregular subsidence with local uplift and subaerial exposure of older carbonate platform rocks which form the basement of the basin are documented by these sediments.

Flecker (1995) and Flecker, Robertson, Poisson and Müller (1993) show that the Miocene basins of the Isparta angle were bounded by palaeotopographic features localised along older sutures related to closure of Tethyan ocean basins. Initial sediments are continental fanglomerates derived from an uplifted hinterland, tentatively linked to south-southeastward movement of the Lycian Nappes, causing pull-apart basin formation within a north-south strike-slip zone. Burdigalian to Langhian sea-level rise produced diachronous transgression from south to north in the Manavgat basin. Simultaneously, the continental fan-deltas in the Aksu and Köprü basins became coastal fan-delta successions with local patch-reef development. Extensional faulting, lasting on the order of 1 Ma, occurred during the Late Langhian-Serravalian. This resulted in rapid deepening of the basins. During a subsequent period of tectonic quiescence, turbidites filled the Aksu and Köprü basins from the north and several hundred metres of planktic foraminiferal marls accumulated in the Manavgat basin. The Tortonian is marked by shallowing, to continental and coastal conglomarate deposition, again with reef colonisation within the conglomerates. Dramatic uplift occurred in the Manavgat basin at this time. Block faulting in the underlying basement is thought to have controlled this contrasting behaviour of the northern and southern basins.

The Aksu phase of compression which had been recognised by Poisson (1977) as producing west-vergent structures, was also shown to have produced east-vergent structures. Previous interpretations (Poisson 1984; Sengör *et al*, 1986) attributed the Aksu phase to westward movement of the Anatolian block.

Late Miocene	"Aksu phase" compression caused by final emplacement of the Lycian Nappes from the NW
Late Miocene (Tortonian)	Differential block faulting causes dramatic uplift of the Manavgat basin and shallowing of the Aksu and Köprü basins
mid Miocene onwards	Onset of 30° counterclockwise rotation of the Bey Dağ lari and Antalya Complex
Mid-Miocene (Langhian-Serravalian)	Rapid subsidence of the Antalya basins caused by loading and basement reactivation.
Late Oligocene-Late Miocene	SE thrusting of the Lycian Nappes. Opening of the Antalya basins, possibly as strike-slip pull-apart basins
Late Eocene to Oligocene	40° clockwise rotation of the Beysehir-Hoyram-Hadim nappes
Late Eocene	Emplacement of Beysehir-Hoyran-Hadim nappes
Late Palaeocene -Early Eocene	Collision and imbrication of carbonate platforms completed
Latest Cretaceous (Maastrichtian)	Subduction-accretion begins
Late Cretaceous	Further sea-floor spreading, possibly of supra-subduction zone type.
Late Triassic	Continental break up and sea-floor spreading forms continental slivers, volcanic seamounts and carbonate platforms within the Neotethyan, Isparta angle ocean
Early Triassic	Rifting
Late Permian	Stable shelf deposition along northern margin of Gondwana

Table 1.1: Summary of the tectonic evolution of the Isparta angle prior to the period of study.

Flecker (1995) suggested that movement of the Lycian Nappes in a southeasterly direction and thus obliquely to the main N-S trending lineaments may have dominated the area close to the thrust front and be responsible for many of the east-west compressional structures.

1.3: Previous work on the Pliocene and Quaternary deposits and Neotectonics of the Isparta angle

Very little work has concentrated on the Pliocene and Quaternary deposits of the Aksu basin. The first observations on the area were those of Tietze (1885), Penck (1918) and of Phillipson (1918). These were all very descriptive observational studies, primarily geomorphological, encompassing vast areas of Turkey. Planhol's (1956) study concentrated on the Antalya region and, whilst again primarily geomorphological, included observations on the sedimentology and tectonics including basic maps and sections. Poisson (1977) looked at the planktic foraminifera biostratigraphy as part of a study of all the Neogene deposits of the area and Akay and Uysal (1985) mapped all the Neogene basins. Both studies were more concerned with the Miocene deposits and the Pliocene is really only superficially documented. Du Poux (1984) conducted a Neotectonic study of the area, again as part of a wider study, but did not produce any significant results. The Quaternary tufa has been somewhat more extensively studied. Değirminci and Günay (1984) looked at hydrological aspects of the deposit, and Burger (1990, 1992) studied the karstification of the tufa and associated soil development. His study also incorporated geomorphology and a discussion of the origins of the tufa. All these studies will be discussed in more detail in the relevant chapters.

1.4: Chronological framework

The standard chronological framework (Harland, Cox, Llewellyn, Pickton, Smith, Walter and Fancett, 1982) is used throughout the thesis and is presented in Fig 1.12. Calcareous nannofossil and planktic foraminifera biostratigraphic zones and the most recent eustatic sea-level curve (Wornardt and Vail, 1991) are incorporated.

1.5: Global climate during the Pliocene and Quaternary

Ruddiman and Raymo (1982) present a climatic curve for the North Atlantic covering the last 2.5 Ma, the final half of the period considered in this study. This period represents the glacial period (Fig. 1.13). The essential details of the curve are:

1) While the warm periods remain at approximately the same temperature the cold periods become progressively colder.

2) From 2.5-0.8 Ma climatic fluctuations have a periodicity of 100 Ma.

3) From 0.8 Ma to the present fluctuations are occurring with a periodicity of 40 Ma. These relate to the Milankovitch cycles of precession and obliquity.

The best climatic indicators available are the oxygen and carbon isotope data from the Tyrrhenian basin in the western Mediterranean.

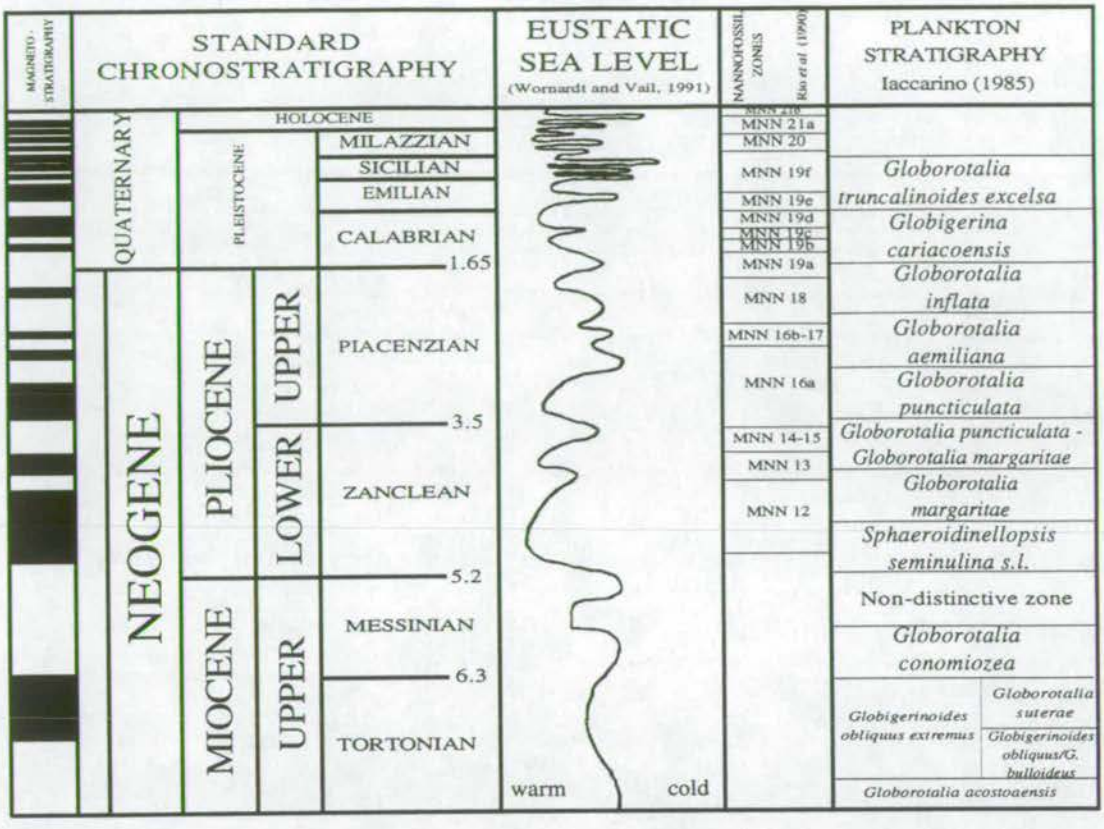

Fig: 1.12: Compiled chronology for the Plio-Pleistocene Mediterranean basin. The standard chronostratigraphy is used for the period. Against this are plotted the magnetostratigraphy; the most recent sea-level curve (Wornadt and Vail, 1990); Mediterranean nannofossil zones (Rio *et al*, 1990); and Mediterranean plankton stratigraphy (Iaccarino *et al*, 1985). This diagram forms the basic stratigraphic framework for this thesis.

The Deep Sea Drilling Program (DSDP), Leg 107, drilled cores 650-656 from the deep centre of the Tyrrehnian basin. Two isotope studies of these cores give very similar results. Many of the climatic effects observed are thought to be a result of dryness. This has also been indicated by pollen studies (Pons, Suc, Reille and Combourrieu-Nebout, 1991)

The $\delta^{18}O$ studies of Vergnaud Grazzini, Saliège, Urrutiager and Iannece (1990) allowed them to split the Plio-Quaternary into a number of different stages. They are summarised below:

4.6-3.1 Ma: The onset of elevated $\delta^{18}O$ fluctuations during the early Pliocene is attributed to an increased dryness over the area coupled with an increasing seasonal contrast. The dryness did not become drastic until seasonal contrast was well developed.

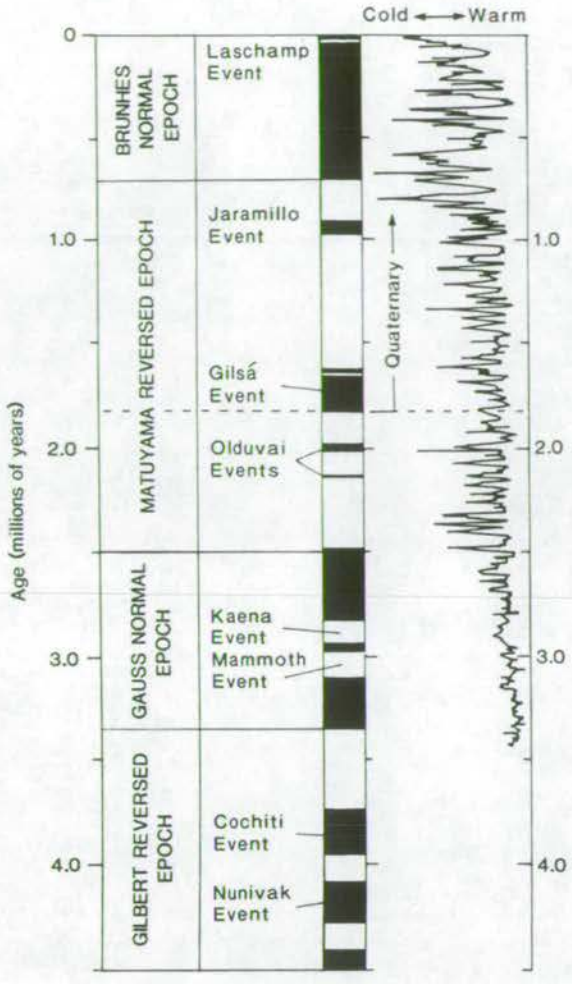

Fig. 1.13: Climatic curve for the glacial period from Ruddiman and Raymo (1982).

3.1-1.55 Ma: During this period, gradual increase in the average $\delta^{18}O$ fluctuations occured. In the Tyrrhenian basin the period 3.1-1.5 Ma was characterised by a temperate foraminifera assemblage which gradually replaced the warm associations, which had become extinct near 3.1 Ma.

3.1 Ma: A climatic step to a cooler climate is widely recognised at this point in time (Zacharisse and Spaak, 1983; Sprovieri, 1978; Van der Swann, 1983; Rio, Raffi and Villa, 1990; Suc 1984)

2.7-2.2 Ma: A period of climatic instability resulted from the transition between pre-glacial and glacial Pliocene. As a result, increased seasonal contrast and summer dryness affected the whole Mediterranean. The reintroduction of the *G. inflata* group of planktic foraminifera at 2.1 Ma corresponded to a short warming trend in the $\delta^{18}O$ curve.

1.55-1.35 Ma: The Pliocene-Pleistocene boundary (1.55 Ma) corresponded to initiation of a long term increase in $\delta^{18}O$ values, which finally culminated at 1.35 Ma. An important local evolution of Mediterranean climate was a sharp fall in winter

temperatures and a drop in rainfall. During this period surficial waters became cooler and summer dryness obliterated the $\delta^{18}O$ increases expected by global warming and identifiable in global climate cycles from elsewhere.

1.35-0.95 Ma: This period was one of relative stability during which glacial $\delta^{18}O$ values remained steady.

0.95-0.34 Ma: A sharp decrease in the abundance of warm-temperate forminiferal species corresponded to higher glacial $\delta^{18}O$ values during this period. At 0.94 Ma a climate jump, giving rise to increased $\delta^{18}O$ variability and average $\delta^{18}O$ values, occurred. More severe climate fluctuations at this time were probably due to larger polar front migrations in the north Atlantic.

0.34 Ma-present This period is marked by a further increase in $\delta^{18}O$ variability, corresponding to increased glacial $\delta^{18}O$ values and decreased interglacial $\delta^{18}O$ values. The increase in fluctuations may be due to increased continental seasonality. The global control by ice volume changes was superimposed by a dryness effect and cooling of surface (and deep) waters. Pons *et al* (1991) showed a change to arid and cold conditions, which produced a steppic and herbaceous vegetation.

In general, the $\delta^{18}O$ fluctuations in the Quaternary have an amplitude twice that of the Pliocene. Significant steps in climate occured at 0.95 Ma and 0.34 Ma. A general cooling trend throughout the period is also recognised. The base of the Quaternary (1.55-1.3 Ma) represents a step increase in dryness in the region. The Mediterranean has acted as an amplifier of the global climate signal due to dryness in the area and the evolution of the basin towards an isolated, concentration basin.

The work of Thunnell, Williams, Tappa, Rio, and Raffi (1990) at site 653 also recognises these climatic events. They identify a general cooling trend with specific cooling steps ($\delta^{18}O$ enrichment) at 3.1, 2.7, 2.1, 1.6, and 0.4 Ma related to either decrease in surface water temperature or changes in global ice volume. They also recognise unstable climatic conditions in the early Pliocene and cooling across the Plio-Quaternary boundary.

Evidence for the climatic dryness which is thought to have such an influence on the Mediterranean during the Pliocene and Quaternary comes form the cores of DSDP Leg 108 on the Atlantic shelf, off North Africa. Dust fluxes measured in these cores (Ruddiman, Sarnthein, Backman, Baldauf, Curry, Dupont, Janacek, Pokras, Raymo, Stabell, Stein and Tiedemann, 1989) suggested major aridification of north Africa, possibly with amplification of the aridity/humidity cycles during the Plio-Quaternary. These changes were not related to glaciation or to local factors, such as the tectonic development of the Mediterranean.

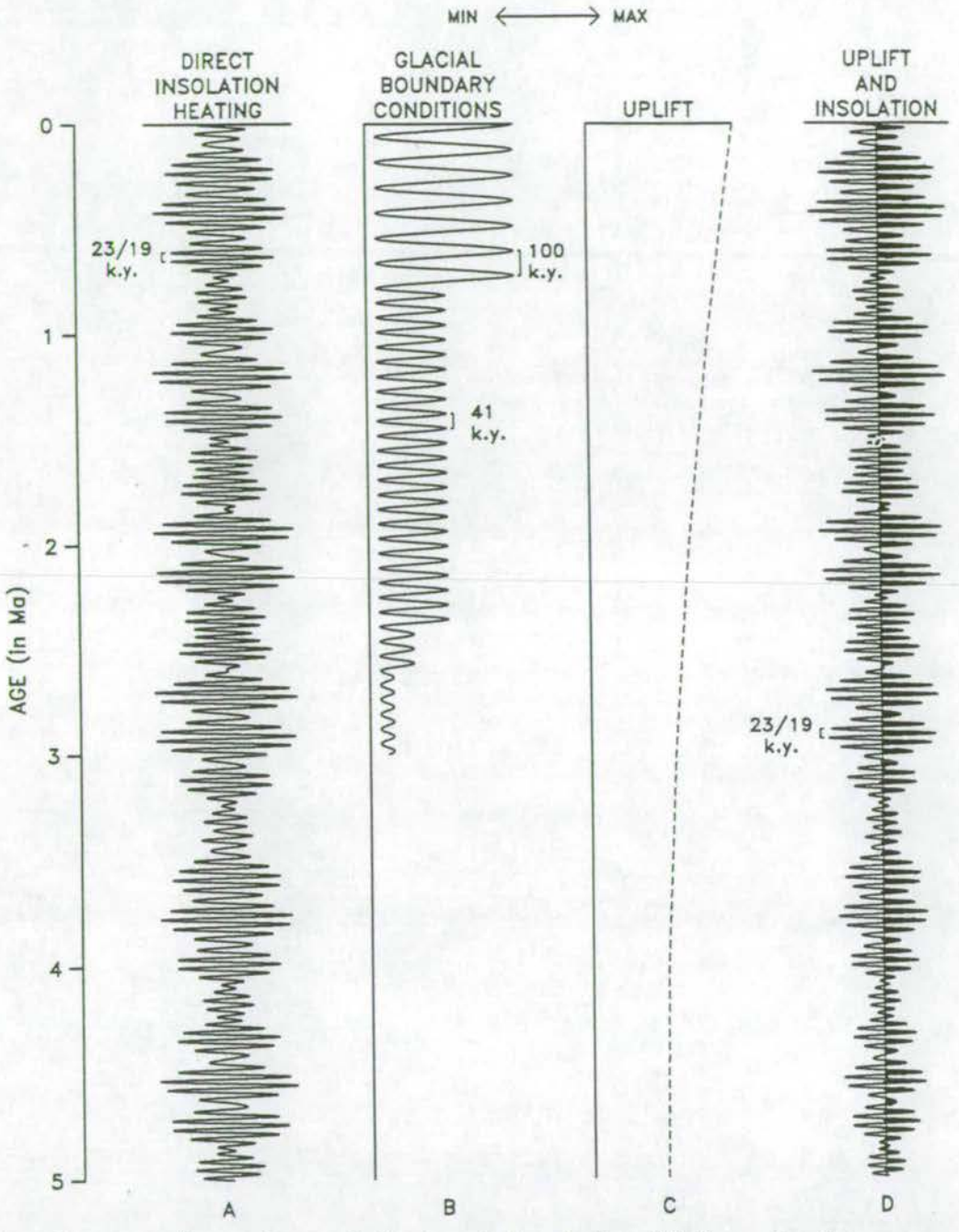

Schematic cartoon of several types of climate controls and of possible linear climatic responses over North Africa and the Atlantic during the last 5 My. Maximum amplitudes of controls and responses are arbitrarily normalised. Dominant periodicities are shown by brackets. Lengths of periods are schematic and do not exactly match the time scale. A = direct insolation heating at precessional period. B = size of northern hemisphere ice sheets (and high latitude North Atlantic cooling). C = gradual uplift of the Tibetan Plateau. D = combined effects of uplift and precessional insolation. For D two responses are suggested. 1) "two-sided" (full curve D) in which the amplitude of variation increases in both directions. "one-sided" (shaded part of curve D) in which the amplitude only increases in one direction.

Fig 1.14: Theoretical climate controls for North Africa and the Atlantic from Ruddiman *et al* (1989). The original caption is given.

It is thought that uplift of the Himalayas and rearrangement of global atmospheric circulation was the dominant factor controlling this change (Ruddiman *et al*, 1990). Theoretical curves combining Milankovitch effects, glacial cyclicity and the Himalayan uplift are presented (Fig. 1.14). This theoretical curve is not dissimilar to that presented by Ruddiman and Raymo (1982).

1.6: Mediterranean sea-level during the Pliocene and Quaternary

Since the Pliocene, the Mediterranean has been a relatively closed basin with only limited inflow of fresh Atlantic water over the Gibralter Ridge. This fact means that, when considering sea-level, only data from the Mediterranean region should be considered. The extreme tectonic activity of the entire Mediterranean region means that extreme caution must be taken to separate tectonic and base level effects when applying sea-level results from one area to another. The term eustatic cannot be strictly be applied to the Mediterranean, as it is a silled basin, only connected to the open ocean by the Gibralter ridge. Local climatic or tectonic effects, can cut the basin off entirely. In the case of the Messinian salinity crisis increasing evaporation caused the water level to drop below the sill with the result that the Mediterranean evaporated almost to dry. Thus, although the eustatic sea-level curve (Wornardt and Vail, 1991), which was constructed from records in the Gulf of Mexico, can be broadly used to look at the fluctuations of the Mediterranean, more regional factors must not be forgotten. The term eustatic in the remainder of this thesis refers to a Mediterranean wide sea-level, which is often related to the eustatic curve, but not identical to it. The Wornardt and Vail (1991) curve is used as a general representation of this.

The best indicator of sea-level since onset of the glaciation between 3.1 and 2.2 Ma is the climate curve. Sea-level can be considered as high during interglacials and low during glacials. As the glacials become colder during the Quaternary the lows will become lower. The specific cooling events identified by Vergnaud Grazzini *et al* (1990) can be interpreted as points of eustatic sea-level fall, related to the onset of glaciation. Prior to this we know that during the Messinian a widespread dessication of the basin occured (Hsü, Montadert, Bernoulli, Cita, Erickson, Garrison, Kidd, Mélières, Müller and Wright, 1978). The Mediterranean basin, already isolated from the Tethys to the east during the Middle Miocene, was cut off from the Atlantic to the west as the Betic and Rif straits closed. The now isolated Mediterranean basin suffered evaporitic drawdown, as evaporitive loss considerably exceeded precipitation and influx from rivers. Two salt units, interrupted by a flooding event, which may have refilled the Mediterranean basin to the brim, were

deposited over the entire Mediterranean basin. The upper unit shows a characteristic bull's eye saline zonation pattern. Episodic flooding events occurred and produced shallow-water diatom and stromatolite beds, which occur cyclically within the unit. Towards the end of the Messinian the Mediterranean was a series of desert and salt lakes. An inundation of brackish water is recognised in the eastern Mediterranean at this time. In shallower basins, perhaps only tens of meters below eustatic sea-level evaporite deposits formed in semi-isolated, silled basins e.g. Cyprus (Robertson, Eaton, Follows and Payne, 1995); Crete (Meulenkamp and Zacharisse, 1975); and the Italian Appenines (Ricci-Lucci, 1973). Gypsum formed subaqueously and selenitic gypsum was transported, via sediment gravity flows, to deeper parts of these basins. Presumably, these shallow basins were periodically flooded just as the deeper water basins were. The final flooding of Atlantic waters into the Mediterranean basin and the rapid restablishment of normal open marine conditions is also well established. McKenzie, Palmer and Müller (1990) documented oceanographic conditions in the Tyrrhenian sea, from the Messinian to the present day, using Sr isotope stratigraphy from the DSDP cores. The Earliest Pliocene is represented by a period of instability, probably related to unstable palaeo-oceanographic conditions as the Mediterranenan was flooded. Between 4.5 and 2.4 Ma the $^{87}Sr/^{86}Sr$ ratio remains constant, possibly representing a period of relative stability. The period from 2.4 Ma to present (i.e. the glacial period) shows an increase in the $^{87}Sr/^{86}Sr$ ratios and fluctuations with both positive and negative slopes. This may be related to the climatic instability of the period.

Thunnell *et al* (1990) recognised from the $\delta^{18}O$ signal, and from sedimentological and micropalaeontoloical observations, that during the Earliest Pliocene, as open marine conditions were re-established, productivity was very low. The latest sea-level curve of Warnadt and Vail (1991) shows a sea-level high during the Zanclean. This is a well documented trend. The sea-level curve throughout the Pliocene and Quaternary can be considered reliable (Fig. 1.12)

Despite the strong tectonic influence on local conditions eustatic events have been identified in Pliocene and Quaternary sediments during periods of tectonic quiesence. In Cyprus, McCallum (1989) was able to recognise the effects of eustatic sea-level in the Pliocene of the Mesaoria basin, during periods of relative tectonic quiesence. The Messinian salinity crisis is marked by thick evaporite deposits and the development of an unconformity surface. The flooding back of the sea and the establishment of open-marine conditions are marked by deposition of the Nicosia Formation. During the mid-Pliocene it is thought that glacioeustatic effects may have begun to affect the basin, prompting incision during periods of lowered sea-level. A

marked transgression which deposited the upper Athalassa formation is definitely attributed to eustatic sea-level rise during the ?Upper Pliocene to Pleistocene. At this time, as seen in Section 1.5, an intensification of climate conditions occurred and sea-level fluctuations changed from the order of 40m to the order of 100m. Subsequent eustatic sea-level fall may have been a contributory factor to the deposition of coarse conglomerates above the Athalassa formation. However, rapid tectonic uplift at this time is a more probable cause. Poole and Robertson (1991) showed that, during the Quaternary, glacioeustatic effects modified the coastal deposits of Cyprus, overprinting and adding to the signature of tectonic uplift. During the latest Pleistocene glacioeustatic effects dominated the relative sea-level signature. This may be due to the step up in intensity of these cycles from 0.35 Ma on.

1.7: Overview of the study

This study aims to integrate new sedimentological, stratigraphic, structural and geomorphological data to synthesise the Plio-Quaternary evolution of the Isparta angle and to place it in the context of the eastern Mediterranean. This is hoped to shed new light on the tectonic behaviour of the eastern Mediterranean during the past 6 Ma. In addition, the Pliocene and Quaternary sediments are documented in detail and palaeoenvironments are reconstructed.

A total of 8 months fieldwork was carried out over four seasons in autumn 1991, spring and autumn 1992 and autumn 1993. Standard sedimentological and structural field techniques were used. The first season was a short reconnaissance of the entire area. In 1992, detailed sedimentological studies of the tufa and the Pliocene deposits were made and the macro-tectonic structures and geomorphology were studied. U-Th dating was done during the summer of 1992. During the final season the majority of the meso-fracture data was collected and the Çalkaya area was mapped in detail. K-Ar dating and biostratigraphy were primarily undertaken during 1994.

The stratigraphic framework of the Pliocene and Quaternary sediments is set out in chapter 2. Dating of the Pliocene and Quaternary sediments was attempted by Poisson (1978) as part of a wider study of the Neogene sediments of the basin. He assigned the sediments of the Manavgat region to the Lower Pliocene. However, the upper part of the Pliocene marine section and the Quaternary continental sediments have not been previously dated. A number of techniques were used to try and tie down the stratigraphy more accurately. Detailed sampling of Pliocene sections in the western half of the basin was used for calcareous nannoplankton and planktic foraminifera stratigraphy. K-Ar isotope analysis of biotites from the Çalkaya tuff was

carried out to date the uppermost units of the Pliocene succession, and U-Th isotope analysis was used to try and date the Quaternary tufa more accurately. Although all these techniques have met with limited success they do allow the Plio-Quaternary sediments of the basin to be dated more precisely than previously. A more detailed lithostratigraphic framework for the Plio-Quaternary is presented as a result of these studies (chapter2).

The sediments will be discussed in chronological order in chapters 3 and 4. The "clastic" sediments are described in detail in chapter 3. "Clastic" includes bioclastic and siliciclastic sediments. These deposits have not been previously described and all aspects of their sedimentology are considered. The continental (Quaternary) sediments are studied in chapter 4. They consist of an unusually large deposit of tufa. The deposit has been described in detail and sedimentary facies analysis has led to a depositional model that has not been observed by previous tufa studies.

Geomorphological observations in the area are discussed in chapter 5. They provide an important link between the sedimentology and the neotectonic studies and allow better resolution of the timing of tectonic events and sediment deposition.

Finally, in chapter 6, the results of meso-fracture analysis throughout the Isparta angle are presented and a neotectonic evolution in the context of eastern Mediterranean plate tectonics is suggested.

This integrated study allows a complete understanding of basin development in this complex region. The evolution of the basin combining the data from all previous chapters will be presented in chapter 7.

1.8: The use of Turkish words

The Turkish words Çay (river) and Dağ/Dağlari (mountain/s) are used in the thesis as they form an intrinsic part of the geographical names. In addition, it is helpful to know that, in place names, köy means village, mahalle (Mah.) indicates a small hamlet that is part of a village, but geographically removed, yukari- and asağ i- mean upper- and lower- respectively, tepe means hill, and selalesi means waterfall. The Turkish alphabet does not contain the letter j. There are eight vowels in the Turkish language. The four back vowels o, u, a and ı (uh) and the four front vowels e, i, ö (oe), ü (ue) spoken at the back of the mouth and the front of the mouth, respectively. Words usually only contain vowels from one group or the other (vowel harmony). ğ (yumusak g) is silent and lengthens the preceding vowel, ç and s are pronounced ch and sh respectively and c is pronounced as j. G is always short and hard as in get.

Examples from place names in the field area are:

Çalkaya	Chalkaya
Bucak	Boojak

1.9: Key to sedimentary logs

A standard key for sedimentary logs is given in Figure 1.15 and is used throughout the thesis. Tufa logs (chapter 4) are slightly differently presented due to their non-standard features.

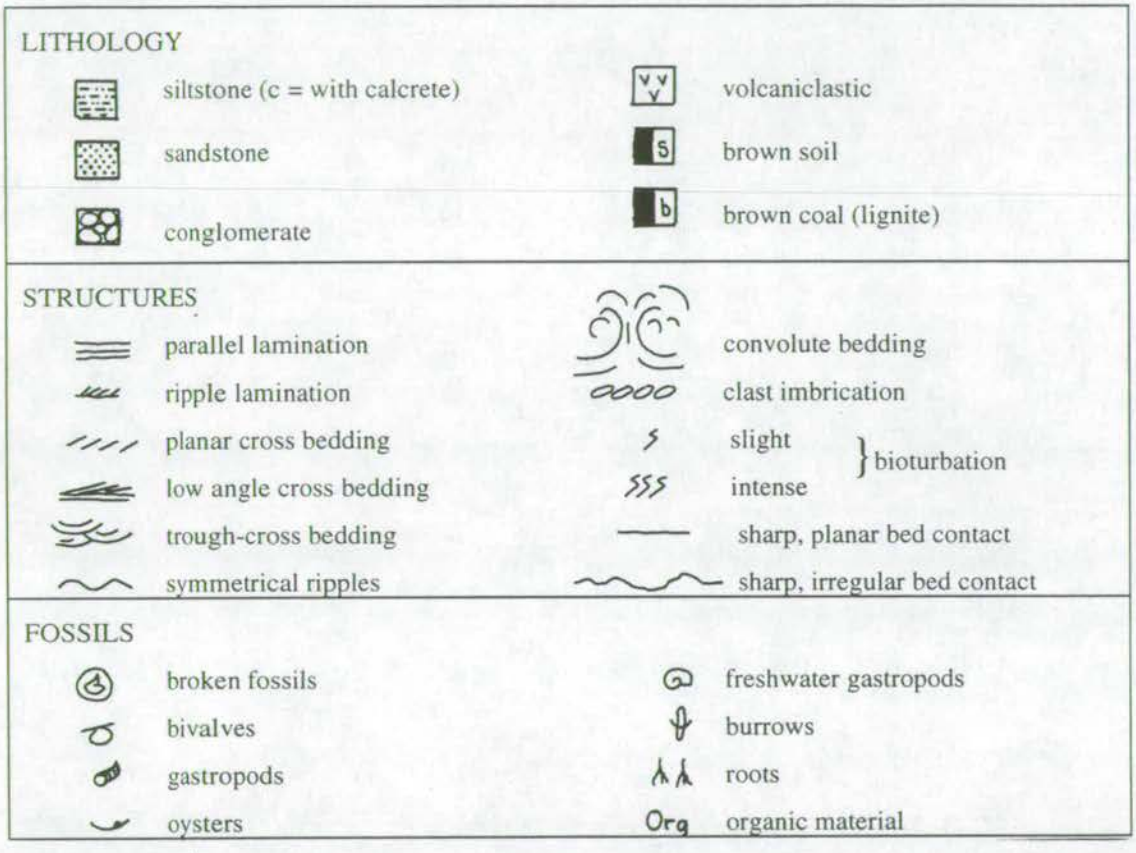

Fig. 1.15: Key to sedimentary logs (modified after Tucker, 1982)

Chapter 2:
Chronological framework

This chapter sets up the chronological framework utilised during this study. The framework is based on previous and new biostratigraphic information and isotope studies (K/Ar, U/Th).

2.1: Existing stratigraphy

Poisson (1977) dated a section south of the Antalya-Manavgat road, as lower Pliocene, spanning the *Globorotalia margaritae* and *Globorotalia puncticulata* zones Fig. 2.1. Varol (1982) studied the calcareous nannoplankton of the same succession and found it within zone NN15. Poisson's section is representative of the lower part of the marine succession exposed in the basin. The upper part of the section has not been dated and one of the aims of this study was to constrain the age of the upper part of the Pliocene section.

The principal biostratigraphic study of the Neogene Antalya basins is that of Akay (1984). This work involved the mapping and dating of the Neogene sediments in the Isparta angle and forms the background to much of this study. The Miocene sediments were studied in detail by Flecker (1995), who modifed Akay's original stratigraphy.

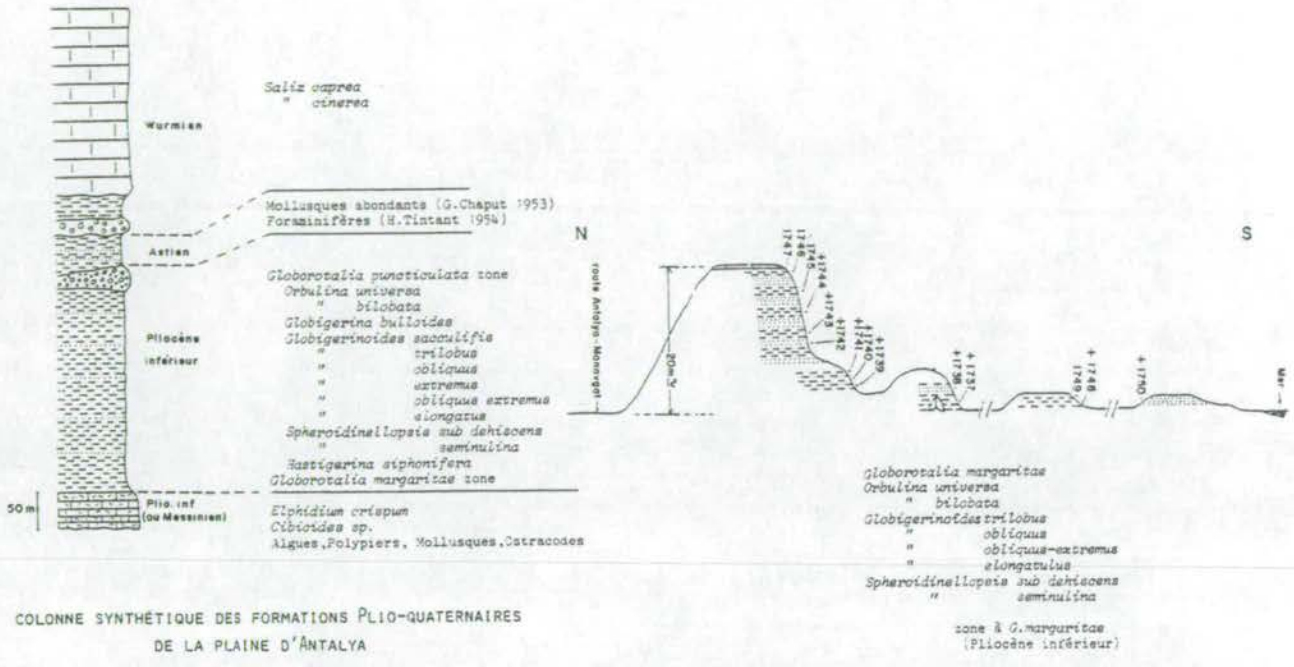

Fig: 2.1: Poisson's (1977) sketch column and biostratigraphy of the Plio-Quaternary section near the Aksu Manavgat road.

Akay and Uysal (1985) subdivided the Pliocene and Quaternary into seven formations, as summarised in Table 2.1. The Gebiz Limestone is reported to show lateral gradation into the Eskiköy Formation (Akay, Uysal, Poisson, Cravatte and Müller, 1985).

The distribution of these sediments, as mapped by Akay and Uysal (1985), is shown in Figs. 2.2 and 2.3. The maps show that the main belt of Pliocene sediment is situated to the west of the basin, dipping below the Quaternary tufa deposits. The Eskiköy Formation crops out north and north west of Gebiz (Fig 2.2). Pliocene sediments also crop out in the Manavgat area (Fig. 2.3).

A number of changes are made to Akay and Uysal's scheme, although it remains the essential framework for the Pliocene of the area. The abundant *Porites* corals (very abundant in the Tortonian; D. Kroon, pers comm., 1995) within the Gebiz Limestone and the conformable contact of the limestone with underlying blue-marls (Karpuzçay formation) of Mid-Miocene age (A. Poisson, pers. comm. 1995) suggest that the Gebiz Limestone may have an earlier age than Messinian, probably upper Tortonian to Early Messinian. The presence of the echinoid *Clypeasterina,* which were widespread in the lower Tertiary (E. Clarkson, pers comm, 1995) also suggests an earlier age then Messinian for the Gebiz Limestone.

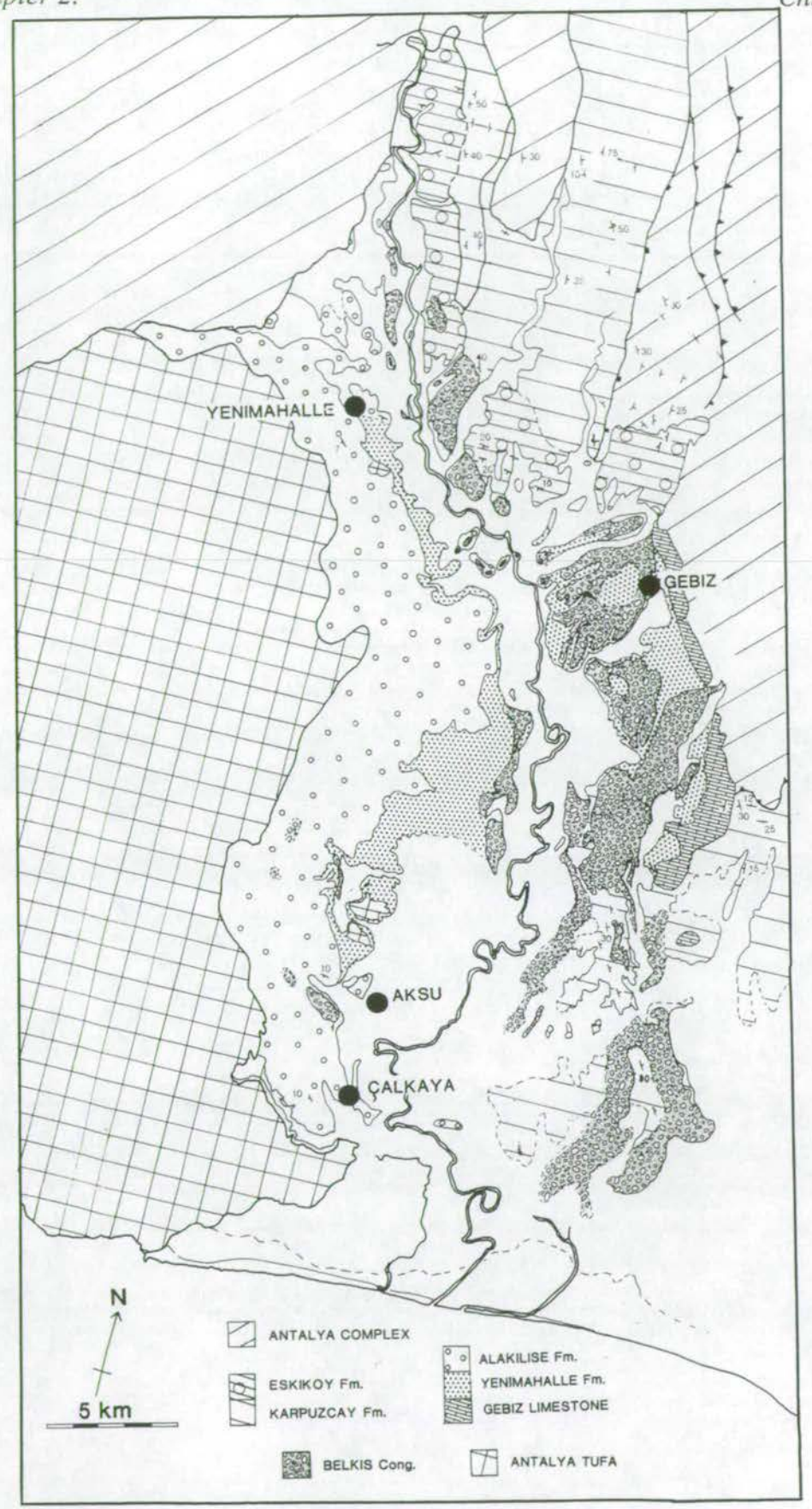

Fig. 2.2: Geological map of the Neogene sediments of the Aksu basin after Akay and Uysal (1985)

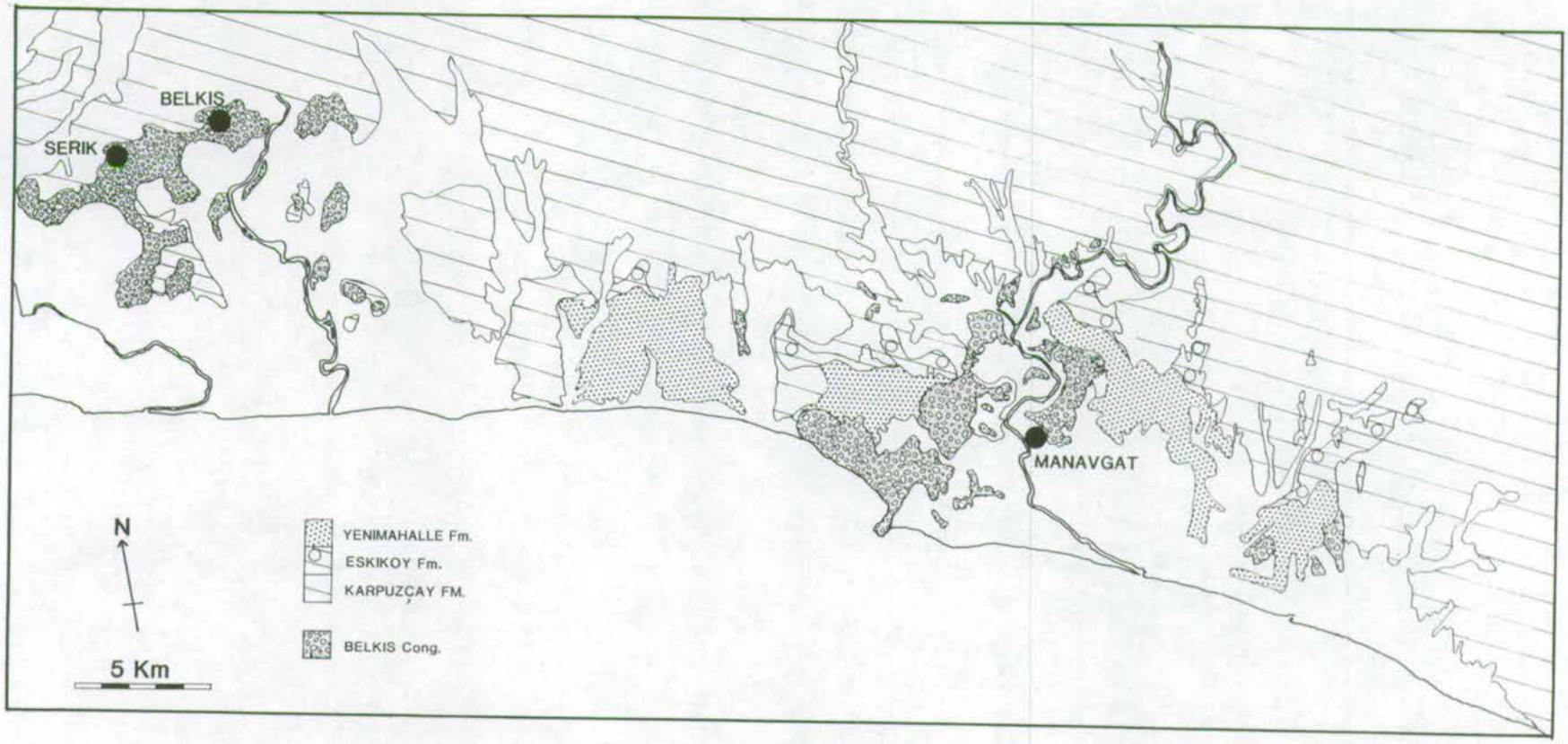

Fig: 2.3: Geological map of the coastal section between Serik & Manavgat after Akay and Uysal 1985

FORMATION	AGE	DESCRIPTION
Antalya Travertine	Upper Pliocene-Pleistocene (?)	plants, oolite-pisolith travertine
Belkis Conglomerate	Upper Pliocene-Pleistocene (?)	Rounded pebbles, Fluvial terraces.
Düzağaç Conglomerate	Upper Pliocene-Pleistocene (?)	Conglomerate, non-rounded pebbles and debris flows.
Alakilise Formation	NN15, Upper Pliocene	Lower part: macrofossils, cross-bedded sandstones (tuff in paces), Upper part: conglomerate-mudstone, regressive character.
Yenimahalle Formation	NN15-16, Lower and Upper Pliocene	Lower part: fine sand, mudstone, Uppper part: laminae-thin, bedded with sandstones and local interbedded tuff.
Eskiköy Formation	Upper Messinian - Lower Pliocene	continental conglomerate-mudstone, transitional belt conglomerate-sandstone (cross-bedded).
Gebiz Limestone	Upper-Messinian-Lower Pliocene.	White, beige compact, thick bedded-massive with benthic foraminifera, poorly reefal.

Table 2.1: Summary of Akay's (1984) division of the Pliocene and Quaternary.

Furthermore, the presence of evaporites within the basin, related to the Messinian salinity crisis, preclude an age later than Mid-Messinian. Samples were taken from marls interbedded within the limestone, but yielded no stratigraphic age, as the foraminifera were almost entirely benthic.

The main Pliocene section, comprising the western part of the margin is a continuous section representing deposition in a deltaic environment (chapter 3). Road-cuttings for the new main road, show that in the northern Aksu basin, non-marine conglomerates lie unconformably on eroded marine Pliocene marls (chapter 3). Basal conglomerates are not found in the area and the Eskiköy Formation is considered equivalent to the upper part of the marine sequence i.e. the Alakilise Formation of Akay and Uysal (1985). It is therefore proposed that Akay and Uysal's Formation names (Yenimahalle, Alakilise and Eskiköy) be grouped into two Formations. The Alakilise Formation and Eskiköy Formation are renamed the Çalkaya Formation, as it is studied in detail in the Çalkaya area (chapter 3), and the Yenimahalle Formation remains. For reasons given in Chapter 4 the Antalya Travertine is renamed the Antalya Tufa.

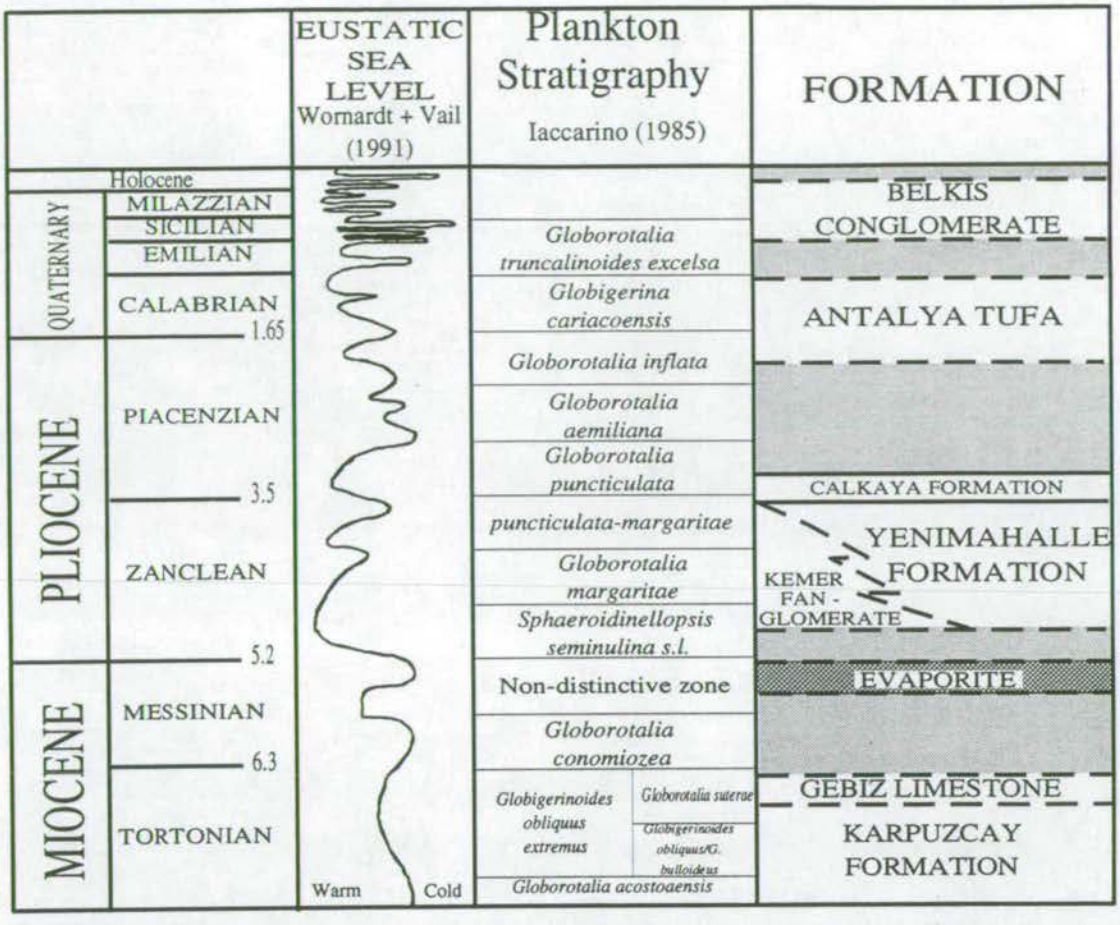

Fig 2.4: Revised stratigraphy of the Plio-Quaternary stratigraphy Aksu basin. Dotted lines indicate uncertain stratigraphic boundaries, solid lines are more certain. The positions of the units have been determined using a combination of planktic foraminifera and calcareous nannofossil dates, sedimentological field observations, K-Ar and U-Th isotopic dates.

The Quaternary conglomerates are not divided as the sedimentary features described by Akay and Uysal (1985) as differentiating the Düzağaç Conglomerate are not recognised (in particular, debris flow deposits). All Quaternary conglomerates are called the Belkis Conglomerate. An entirely new formation is also included. Along the coast from Antalya to Finike a series of conglomerates occur in fan deposits. These are thought to be of Pliocene age, as their upper surfaces form part of the mature ?Pliocene surfaces in the Tauride mountains, and as they are cut by faults which are thought to be Late Pliocene-Early Quaternary in age. These conglomerates have been termed the Kemer Fanglomerates.

A revised stratigraphic framework is set out in Fig. 2.4. The sedimentology of these Formations is discussed in chapter 3 (except the Belkis Conglomerate which is discussed in chapter 5).

Aksu sections	Ak11/92b and Ak12/92b	Lower Pliocene s.l.
	Ak16/92b	NN15/NN16
Yurtpinar section	Yu22/92b and Yu23/92b	Lower Pliocene s.l.
	Yu30/92b	probably NN15
Yenimahalle section	bottom of section	could be Messinian

Table 2.2: Tentative nannoplankton dates obtained by C. Müller, 1993.

2.2: New biostratigraphic data

Pliocene sections were carefully sampled in order to refine the dating, particulary of the upper part of the section. The finest-grained sediments to be sampled were silts and all the samples were of unconsolidated sediment.

Nannoplankton dating was undertaken by C. Müller (A. Poisson, pers comm., 1993) but did not yield good results, due to significant reworking. Nannoplankton from the Cretaceous, Eocene and Miocene (Lower and Middle) are all present in the samples. Tentative dates for a few samples are given in Table 2.2. Exact sample locations are marked on the sedimentary logs in chapter 3.

Samples from the Manavgat section and Yurtpinar section were sieved at 63µm to recover foraminifera. The foraminifera recovered were well preserved, but rather sparse due to the large volume of >63µm sediment in the samples. A composite section of the Pliocene sequence, showing the approximate stratigraphic position of the sampled sections, is given in Fig. 2.5. Accurate sample locations are marked on the sedimentary logs in chapter 3. Planktic foraminifera were identified using the classification of Kennet and Srinivasan (1983) (Plates 2.1 and 2.2). Details of species present within each sample are given in Appendix 1. The presence of *Globorotalia margaritae* (in a well-evolved form), *Globorotalia puncticulata*, *Sphaeroidinellopsis kochi*, and *Globigerina nephenthes* throughout the sequence allow it to be firmly tied down to the *Globorotalia puncticulata* - *Globorotalia margaritae* zone (upper Zanclean) (Fig. 2.6). This zone ranges from the first appearance of *Globorotalia puncticulata* to the last appearance of *Globorotalia margaritae* (Cita, 1975). The *Globorotalia puncticulata* - *Globorotalia margaritae* zone corresponds to NN13-NN15. The absence of Miocene species, the excellent preservation and the good zonation of the foraminifera collected provides good evidence that reworking is not a problem. Reworked sediment must be limited to the clay fraction.

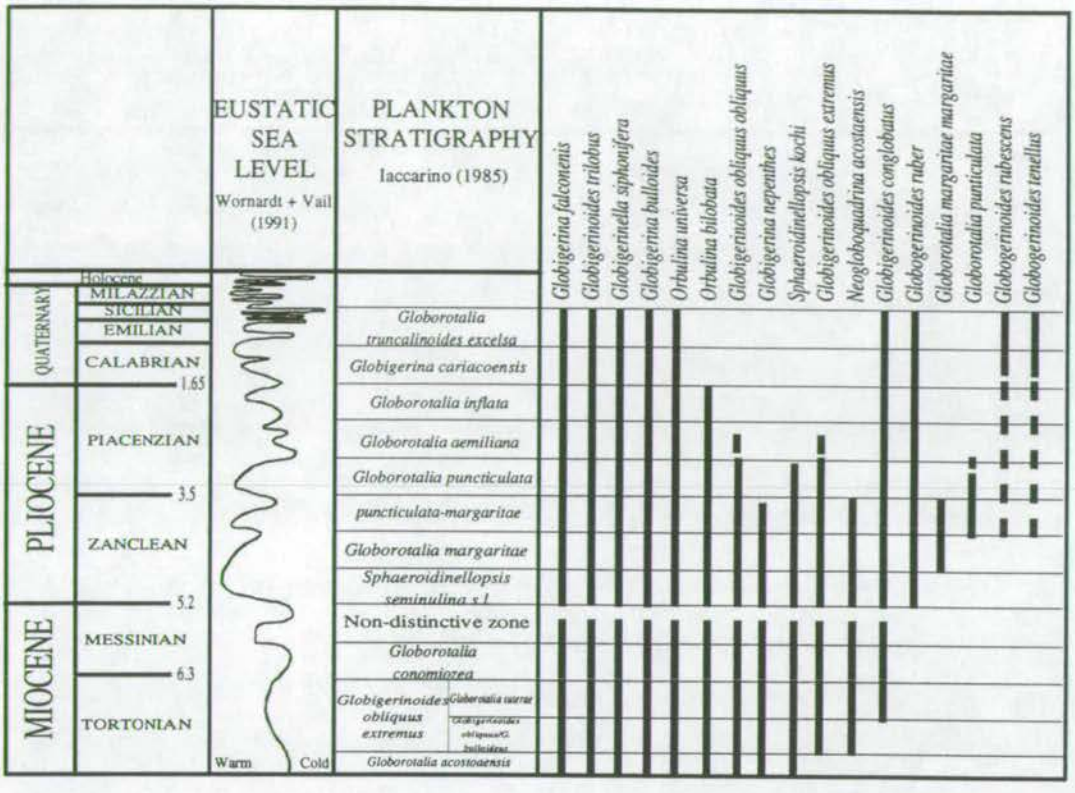

Fig 2.6: Stratigraphic table for the Yenimahalle Formation. The ranges of all the planktic foraminifera found in samples from the Yurtpinar, and Manavgat sections are included. The assemblage is such that assignation to the *Globorotalia puncticulata-Globorotalia margaritae* zone is unequivocal.

The planktic foraminifera dates and the nannofossil dates link together remarkably well. The nannofossil ages, which actually define a zone, are from the very upper parts of the Yenimahalle section, directly above the marine sediments (Yu30/92b) and within the Çalkaya Formation (Ak16/92b). Thus, the Çalkaya Formation is within the very early *Globorotalia puncticulata* zone (NN16). Seismic data (chapter 3) shows that the Yenimahalle Formation is of the order of 500m thick. In the Antalya basins we are sampling only the very upper part of the sequence. It is projected that the entire period of deposition spans the *Globorotalia margaritae* to early *Globorotalia puncticulata* planktic foraminifera zones.

The eustatic sea-level curve, which is well understood for this period (Wornardt and Vail, 1991), shows a sea-level highstand in the mid Early Pliocene, during which time sea-level was at its highest during the Neogene.

Plate 2.1:

1-3) *Globigerina bulloides*
1) sample Ma9/92b (M9/11b) x160
2) sample Ma9/92b (M9/12) x230
3) sample Ma5/92b (2/15) x230

4) *Globigerina falconenesis*
sample Yu22/92b (22/10) x330

5) *Globigerina nepenthes*
sample Ma2/92b (M2/1) x160

6) *Globigerina rubescens*
sample Ma9/92b (M9/16) x250

7) *Globigerinoides obliquus*
sample Yu26/92b (26/36) x270

8-9) *Globigerinoides obliquus extremus*
8) sample Ma5/92b (3/20) x160
9) sample Ma3/92b (M3/4) x140

10) *Globigerinoides triloba*
sample Yu8/92b (8/5) x330

11-12) *Globigerinoides ruber*
11) sample Ma5/92b (1/26) x210
12) sample Ma13/92b (M13/2b) x150

Plate 2.2:

1) *Globigerina sacculifera*
sample Ma5/92b (M5/28) x230

2) *Globigerinoides tenellus*
sample Ma9/92b (M9/28) x240

3) *Neogloboquadrina acostoensis*
sample Yu25/92b (25/8) x360

4) *Orbulina universa*
sample Ma9/92b (M9/7) x190

5) *Orbulina bilobata*
sample Yu25/92b (25/4) x140

6) *Globigerinella siphonifera*
sample Ma6/92b (M6/3) x120

7) *Sphaeroidinellopsis kochi*
sample Ma5/92b (3/18) x100

8) *Globorotalia puncticulata*
sample Ma2/92b (M2/7) x150

9-12) *Globorotalia margaritae*
9) sample Yu38/92b (38/3) x270
10) sample Yu23/92b (23/17) x*s*200
11) sample Ma6/92b (M6/1)x180
12) sample Ma5/92b (3/26) x150

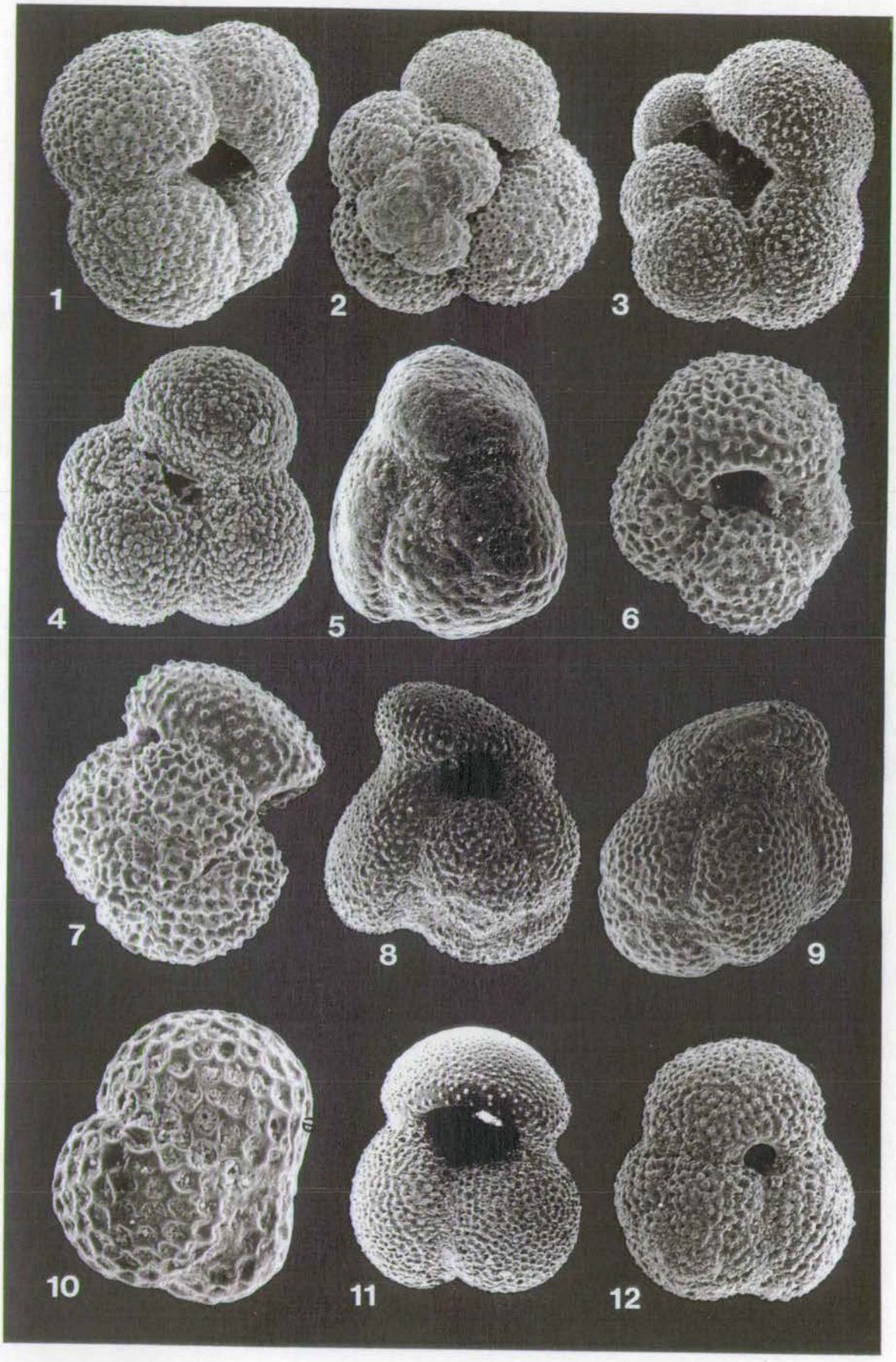

Plate 2·1

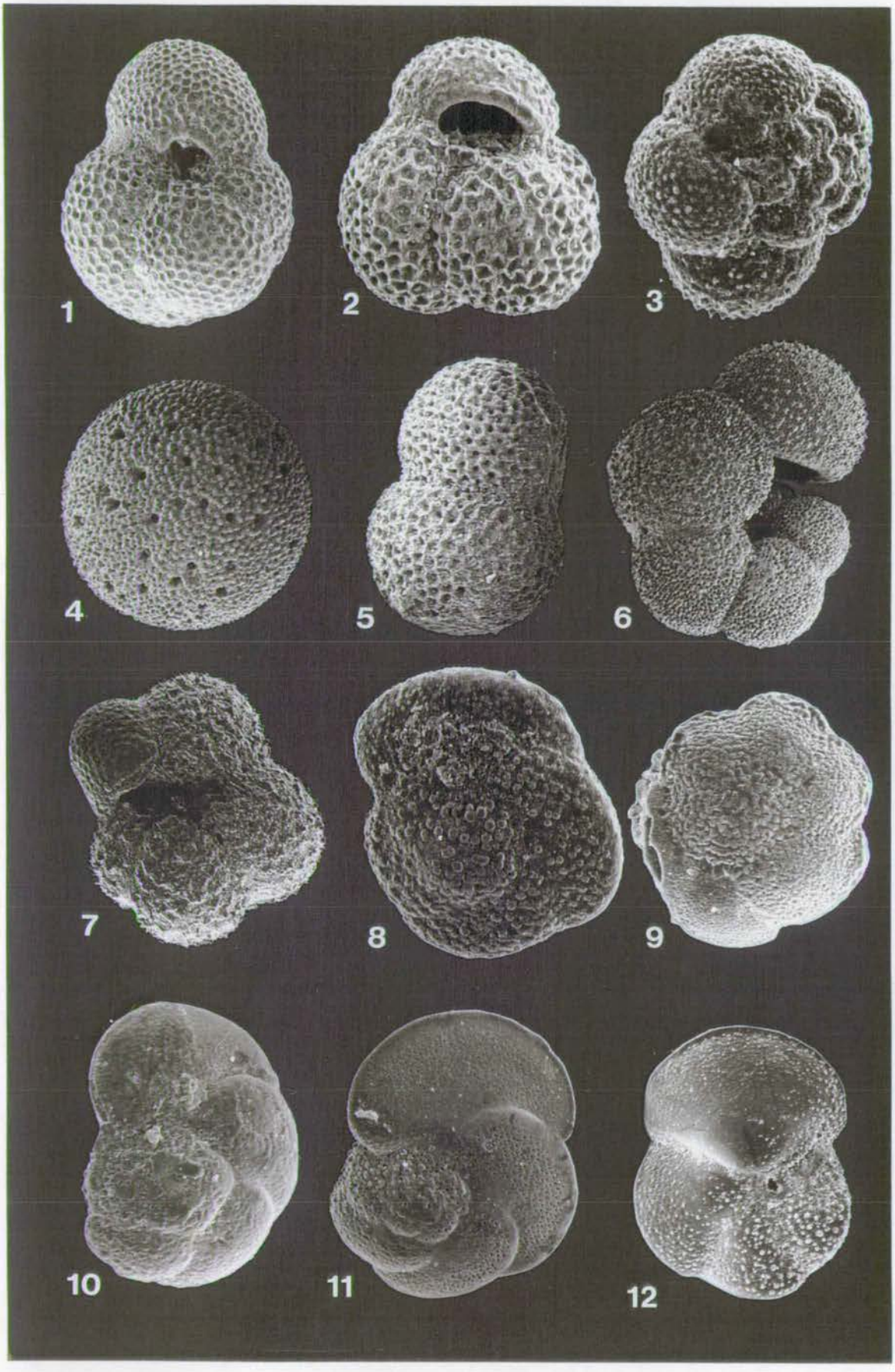

Plate 2·2

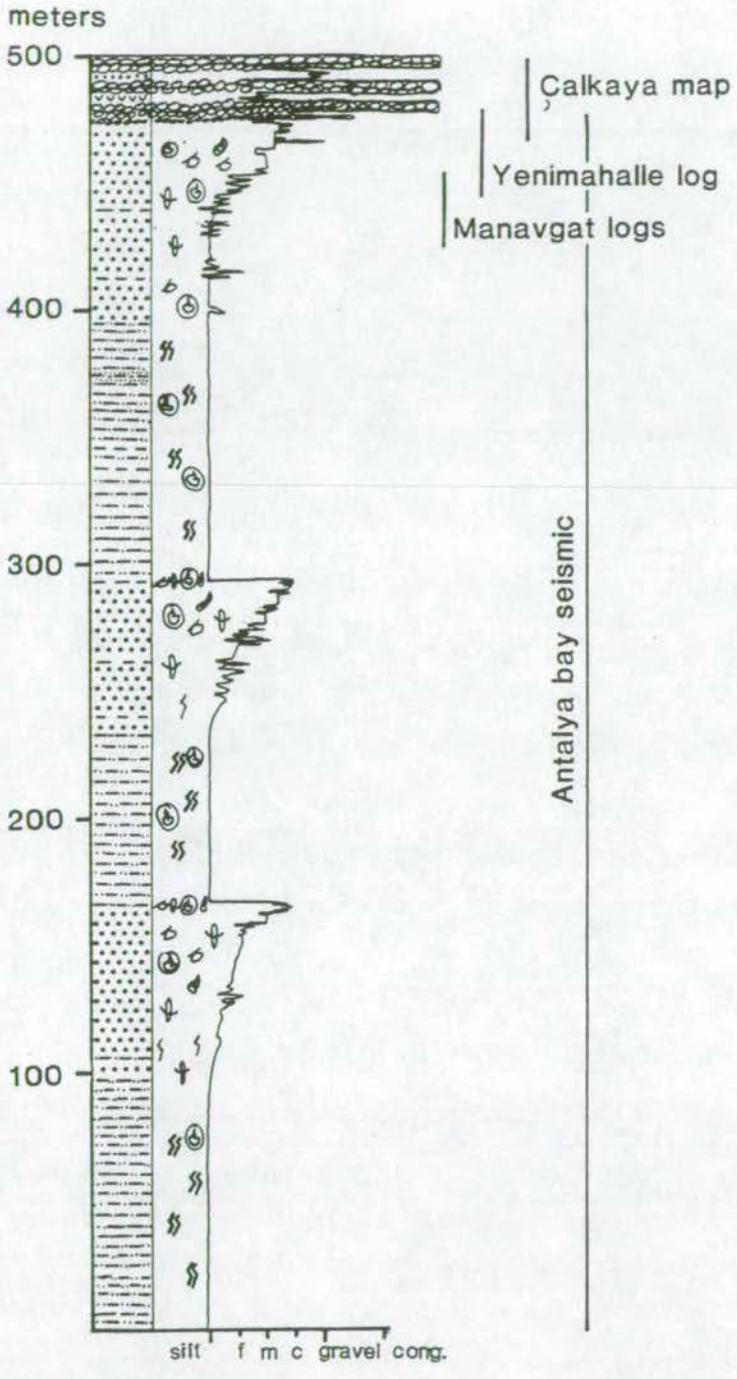

Fig. 2.5: Schematic log of the Pliocene sediments to indicate the information available over the entire sequence. Fossil symbols and lithologies are inferred in the majority of the section which is only known through seismic data.

It is probable that the majority of deposition occurred during this highstand and that the upper marine-continental transition facies (Çalkaya Formation) correspond to the relative drop in sea-level that resulted from the onset of cooling at about 3 Ma.

2.3: K-Ar dating of biotites

The K-Ar method relies on the fact that Ar is not retained in a melt and that volcanic minerals that contain significant quantities of potassium are present within certain minerals. Decay of ^{40}K to ^{40}Ar proceeds and the system remains closed unless affected by metamorphism, weathering or alteration. Measurement of the K/Ar ratio gives the age of the sample from the equation:

$$t = \frac{1}{\lambda_e + \lambda_\beta} \log_e \left[\frac{Ar^{40}_{rad}}{K^{40}} \left(\frac{\lambda_e + \lambda_\beta}{\lambda_e} \right) + 1 \right] \quad (1)$$

where λ_e is the decay constant for ^{40}K to ^{40}Ar and λ_β is the decay contant for ^{40}K to ^{40}Ca. By substituting in the values of these decay constants the equation is simplified. Errors are larger at younger ages and the method is limited for young samples by contaminating atmospheric ^{40}Ar. Since $Ar^{40}_{rad} = Ar^{40}_{tot} + Ar^{40}_{atm}$ if atmospheric argon makes up a large proportion of the sample than the error introduced into quantifying radiogenic argon is large. Biotite is a paticularly good mineral for the technique, but is also particularly susceptible to contamination by atmospheric argon and is generally not useful below ages of 1-2 Ma.

Detailed discussion of the method and techniques can be found in Dalrymple and Lanphere (1969).

2.3.1: Sample preparation and analysis

Biotites were separated from the samples Tuff1/93, Tuff2/93, Tuff3/93 and Tu1/92b from tuffs of the Çalkaya Formation (chapter3). The samples were initially centrifuged in pure tetrabromoethane. This separated quartz, feldspar, biotite, volcanic glass and zircon into the light fraction (float) and amphibole, magnetite, and some biotite into the heavy fraction (sink). The <63μm and the >180μm fractions were sieved out and discarded. From the float quartz, feldspar, zircon and some of the volcanic glass were removed with a Frantz magnetic separator. The samples were treated with 10% HCl to remove any carbonate present and then placed on a tilted vibrating board. Much of the remaining glass rolled off the board leaving a concentrate of biotite adhered to the board. More volcanic glass was removed from

the biotite-rich fraction using the Frantz magnetic separator. The final fraction of volcanic glass was separated out by centrifuging with tetrabromoethene diluted with acetone sufficient to cause the biotite to sink. This left the biotite samples 99% pure with very minor quantities of volcanic glass adhering to biotite flakes.

Amphibole separation was also attemped, but it proved that the fraction of amphibole was too small to make this worthwhile.

The biotite samples were analysed at the Scottish Universities Research and Reactor Centre (SURRC) at East Kilbride. Potassium content was measured directly in a flame photometer. After acid digestion (hydrogen flouride and sulphuric acids), analyses were carried out, in duplicate, on a Corning 410 instrument. Argon was extracted and purified on a high vacuum extraction line. The quantity of ^{40}Ar was determined by the isotope dilution method, using ^{38}Ar (Berne) tracer. Samples, each weighing <0.1g, were fused at a temperature of 1200°C. Purification of the extracted gas was achieved by passing it through a zeolite and then over titanium, heated to 800°C. The analyses were performed on an MS-10 mass spectrometer, operated in static mode.

Errors on the analyses were calculated using a combination of K and Ar normal measurement standard deviation, derived from measurements of standards (BS133 and others) with ^{38}Ar, which is pre-calibrated against air shots of known volumes of air. In-run standard deviation statistics, of the multiple integrated voltage measurements of each mass (36,38,40) and background counts are calculated. The percentage radiogenic ^{40}Ar and percentage sample admitted to the mass spectrometer are also taken into account. All statistical calculations were performed by the computer controlling the analysis.

2.3.2: Data analysis

Results are summarised in Table 2.3. It can be seen that the dates obtained from the four samples vary by over 5 Ma and that the errors are very large. This is the result of excessive contamination by atmospheric ^{40}Ar. The cause was discussed briefly above. Partial resetting of the " radioactive clock", due to metamorphism, can be ruled out in this case as the sediment is unconsolidated. Contamination by atmospheric argon may result from the presence of atmospheric argon in fluid inclusions, this may be a problem if the melt was not fully degassing. The trachytic composition of the tuff (chapter 3) indicates that the melt was highly viscous and full degassing may not have occured. However, there is no evidence for large numbers of fluid inclusions within the biotites and initial atmospheric argon is thus an unlikely source of excess atmospheric argon.

Sample	Sample weight (g)	Radiogenic ^{40}Ar (10^{-10} mol/g)	% radiogenic ^{40}Ar	K (Wt%)	Age ± 1σ (Ma)
Tu1/92b	0.10108	0.776	10.33	6.43	6.95 ± 0.84
Tuff1/93	0.10131	0.141	2.10	6.35	1.28 ± 1.31
Tuff2/93	0.09990	0.193	2.22	5.74	1.93 ± 1.77
Tuff3/93	0.09725	0.337	4.24	5.76	3.37 ± 1.16

Table 2.3: Results of K/Ar isotope analyses of samples from the Çalkaya tuff (28/10/94).

Loss of radiogenic argon may also occur due to weathering and alteration. This is ruled out as the biotites in both the unconsolidated sediment, from which the samples were taken, and the pumice clasts are pristine and show no sign of alteration. The most probable source of error is atmospheric argon adsorbed onto the surface of biotite flakes. This can be very unpredictable but is a particular problem with young biotites (Dalrymple and Lanphere, 1969). The effect of atmospheric argon is to give anomalously old ages.

In an attempt to free the samples of atmospheric argon they were rerun after being ashed in a plasma furnace. This should liberate and burn off the surface ^{40}Ar. In addition the samples were left on the sample "tree", from which the samples are loaded, and the line left to evacuate for several days to rid the system of as much atmospheric contamination as possible. Problems occurred due to exploding samples and several runs had to be undertaken. Only one repeat run was successfully acheived: Sample Tu1/92b repeated within error.

The 6.95 Ma age of Tu1/92b is thought to be older than the true age due to the presence of atmospheric argon. The other samples are swamped by atmospheric argon and have associated errors which indicate that no reliance can be placed on the ages determined.

From the results, an age of 3 Ma is suggested for the true age of the tuff. This is within the limits of the data and not unreasonable. It is chosen as it is consistent with the biostratigraphic results, which are significantly more reliable.

2.4: Uranium series disequilibrium method

Uranium series disequlibrium was used in an attempt to date the Antalya tufa. The most common and most widely applicable dating method of the series uses the ratios $^{230}Th/^{234}U$ and $^{234}U/^{238}U$. The method most commonly has been applied to corals (Bloom, Broecker, Chappell, Matthews and Mesolella, 1974; Chappell, 1983; Poole, Shimmield and Robertson, 1990), but has also been successfully applied to

speleothems and travertines (Liritzis and Galloway, 1982; Schwarcz, 1980) and tufas (Magnin, Guendon, Quinf, Roiron and Thinon, 1990). It uses the decay of ^{238}U to ^{234}U and ^{230}Th. The method is limited by mean lifetime of ^{230}Th and is effective between 5000 and 400,000 years. The method relies on the fact that when $CaCO_3$ is precipitated from natural waters uranium becomes trapped within the carbonate crystal lattice. Thorium is virtually absent, comprising ≤ 0.01ppm, as it tends to be quickly trapped in clay minerals and in hydroxides in soils. This includes not only the ^{234}U decay product, ^{230}Th, but also detrital ^{232}Th. With time, ^{234}U decays to ^{230}Th and the age is proportional to the $^{230}Th/^{234}U$ ratio, if the host carbonate is a closed system and no initial ^{230}Th is present. This can be described by the following relationship:

$$\left(\frac{^{230}Th}{^{234}U}\right)_t = \left(\frac{^{238}U}{^{234}U}\right)_t \left(1-\exp(-\lambda_{230}t)\right) + \frac{\lambda_{230}}{\lambda_{230} + \lambda_{230}} \cdot \left(1-\left(\frac{^{238}U}{^{234}U}\right)_t\right) \cdot \left(1-\exp\left((\lambda_{234}-\lambda_{230})t\right)\right) \quad (2)$$

where λ_{230}, λ_{234} are the decay constants for ^{230}Th, ^{234}U respectively.

The activity ratio $^{234}U/^{238}U$ varies with time as follows:

$$\left(\frac{^{234}U}{^{238}U}\right)_t - 1 = \left(\left(\frac{^{234}U}{^{238}U}\right)_0 - 1\right)\exp\left(-l_{234}t\right) \quad (3)$$

The equations can be represented graphically so that time (t) can be solved simply if $^{234}U/^{238}U$ and $^{230}Th/^{234}U$ are known (Fig. 2.7) (Schwarcz, 1979, 1980). The steeply inclined isochrons are derived from equation (2) and the horizontal curves are growth curves of $^{234}U/^{238}U$ derived from equation (3).

These calculations apply to pure calcium carbonate which has been a closed system since precipitation. Whereas this may apply in some instances, it is unlikely to be the case for freshwater carbonate samples. The two principal problems are: a) that the system is not closed and the sample suffers leaching of ^{234}U or incorporation of ^{238}U and ^{234}U during diagenesis; and b) that the initial precipitate is impure and detrital ^{230}Th and ^{232}Th are initially present within the sample.

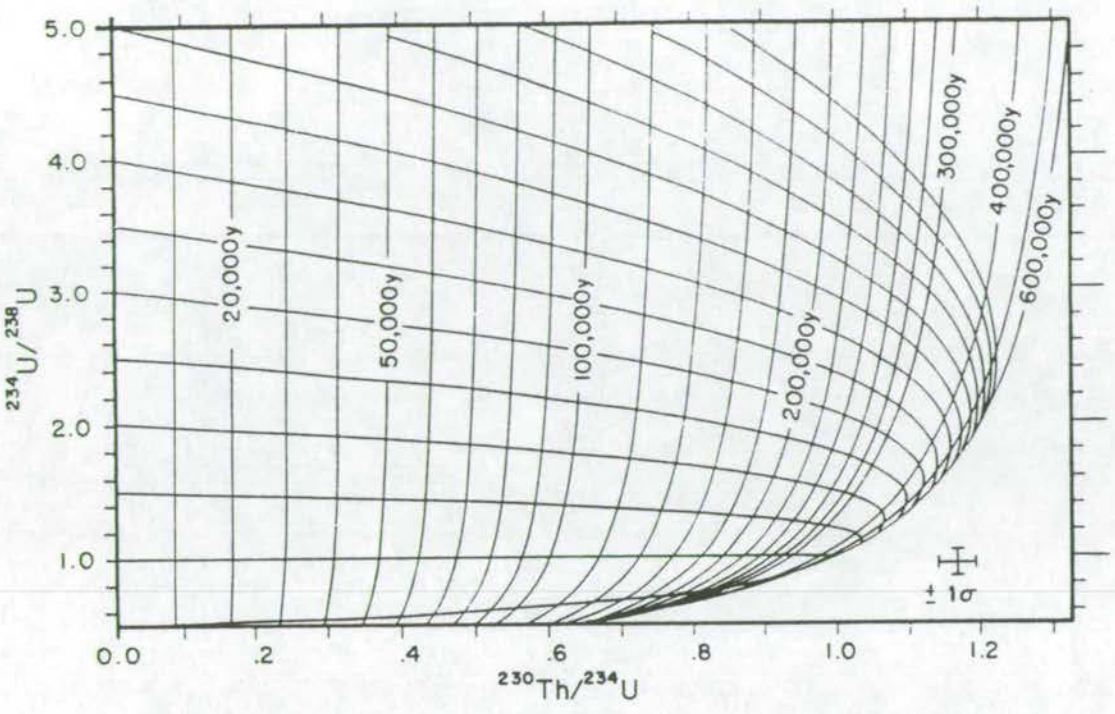

Fig. 2.7: Graphical solution of equations (2) and (3) (section 2.4) which allows calculation of U-Th ages from the ratios $^{234}U/^{238}U$ and $^{230}Th/^{234}U$ (Schwarcz, 1979, 1980).

Although an empirical method has been postulated for calculating U/Th ages for open systems (Rosholt, 1980) the technique is not applicable in this case. The empirical model relates primarily to alluvial, colluvial and glacial sediments and to altered ash deposits, all of which are almost certainly much more open than the Antalya tufa system. Also, the method cannot be used without independently dated horizons to calibrate the analysed section. It must be assumed that the Antalya tufa system was essentially closed, although minor leaching may have occurred. Tests can be applied to ascertain the degree of leaching which has affected samples. Firstly, samples are chosen that visually and petrographically have unfilled pore space and no obvious recrystallisation or dissolution textures. Secondly, the effects of leaching can be recognised isotopically by (i) anomalously high $^{230}Th/^{234}U$ ratios; (ii) anomalously low $^{234}U/^{238}U$ ratios; (iii) anomously low uranium concentrations (Schwarcz, 1980). If leaching or new crystal growth has affected the samples an age younger than the true date of deposition will be calculated.

A number of procedures have been used to correct for detrital thorium. In freshwater carbonate samples the presence of ^{232}Th can be related entirely to the presence of detrital material. Associated ^{230}Th will also be present. If it is assumed that the ratio $^{230}Th/^{232}Th$ is the same in the detrital component of a selection of

samples, each with a different absolute detrital content, then at time t = 0 the simple relation

$$\left(\frac{^{230}Th}{^{232}Th}\right)_t = \left(\frac{^{230}Th}{^{234}U}\right)_a \cdot \left(\frac{^{234}U}{^{232}Th}\right) + B_t \qquad (4)$$

holds where $(^{230}Th/^{234}U)_a$ is the authigenic ratio of $^{230}Th/^{234}U$ and B_t is the detrital ratio of $^{230}Th/^{232}Th$ at time t. This is a simple first order polynomial equation which can be solved graphically; the gradient of the regression line giving $(^{230}Th/^{234}U)_a$. This value coupled with the value of $^{234}U/^{238}U$ allows the age of the sample to be calculated. This method was evaluated by Kaufman (1993). The system was shown to be robust for a series of impure carbonates in the Dead Sea basin, where independent dating could be completed. The technique was compared to three other methods, SL (single leachate), I and II (involving analysis of an insoluble residue), and found to be the most accurate. Kaufman (1993) called the scheme L/L (multiple leachate). It was first proposed by Osmond, May and Tanner (1970) and justified mathematically by Ku and Liang (1984), Schwarcz and Latham (1989) and Kaufman (1993).

2.4.1: Sample collection

The results presented here are a preliminary study carried out primarily on one terrace edge thought to be coeval. Samples were collected from a number of sites along the lower terrace edge near Çalkaya. (Fig. 2.8) At two sites multiple samples were taken. Specimens that appeared unaltered and with good crystal structure were chosen preferentially, although this was not always possible. Five other samples, from relatively nearby were also analysed. Petrographically, all those samples that were solidified enough for thin-sections to be made are free of secondary crystalline calcite and show no sign of dissolution. Exceptions are Ku1/92b and Ku2/92b which show minor infilling of porosity by secondary crystalline calcite. It is assumed that those samples too unconsolidated to be sectioned have not undergone recrystallisation. X-Ray Diffraction analysis of all samples showed them to be pure Mg-Calcite, except A1.1/91 which contains minor low quartz (<1%) and Ca3/92b with approximately 1/3 low quartz and some minor clays.

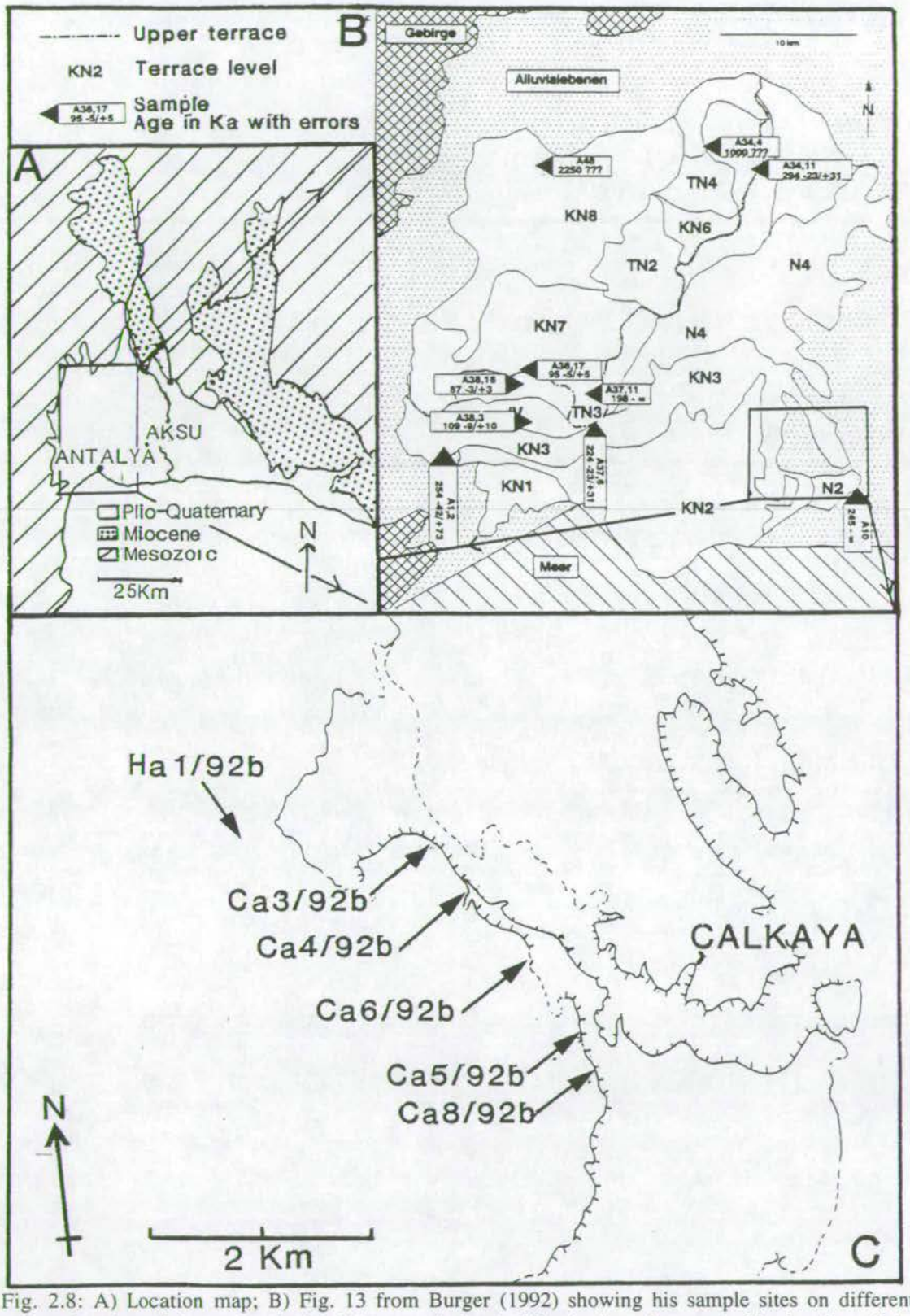

Fig. 2.8: A) Location map; B) Fig. 13 from Burger (1992) showing his sample sites on different terrace levels and the ages calculated from each site (within the boxed arrows). The locality of the present study is boxed; C) Location of sample sites for preliminary U/Th study on the Antalya tufa. Samples were collected along the edge of the tufa terrace near Çalkaya. Several samples were collected at each site.

2.4.2: Analytical Procedure

Powdered samples weighing approximately 2g were digested in a mix of 20ml concentrated HCl and 5ml concentrated HNO_3. A 0.02 ml mixed spike of ^{232}U and ^{228}Th was used. After digestion, iron was extracted with di-isopropyl ether. The solutions were put through a standard set of ion exchange resins (Biorad AG1-X8) to separate U and Th. These were electroplated onto steel discs and the isotopic activity was measured using α-spectrometry. The procedures are described in Ivanovich and Harmon (1982) and are detailed in Appendix 2.1.

The counts were entered into a spreadsheet devised by C. Chilcott (after Ivanovich and Harmon, 1982) to give corrected values (with errors) of the activities of ^{238}U,^{234}U,^{232}Th,^{230}Th; the chemical yields and concentration of U and Th; and calculated $^{234}U/^{238}U$ and $^{230}Th/^{234}U$ ratios (Appendix 2.2.). $^{230}Th/^{232}Th$ and $^{234}U/^{232}Th$ were calculated by hand. All errors are propagated using the standard technique for combined errors based on 1σ counting statistics. Samples Ca3/92b and Ca4b/92biii failed due to blockage in the ion exchange column. A summary of the data is given in Table 2.4.

2.4.3: Data Analysis

Petrographic studies showed that leaching should not be a problem and the plot of $^{234}U/^{238}U$, $^{230}Th/^{234}U$ and uranium concentration show this to be the case (Fig. 2.9). Only sample Ko/92b shows significant evidence of leaching, with low uranium, relatively low $^{234}U/^{238}U$ and associated high $^{230}Th/^{234}U$ ratios. Ca8/92bi and Ku1/92b may also have minor leach signatures.

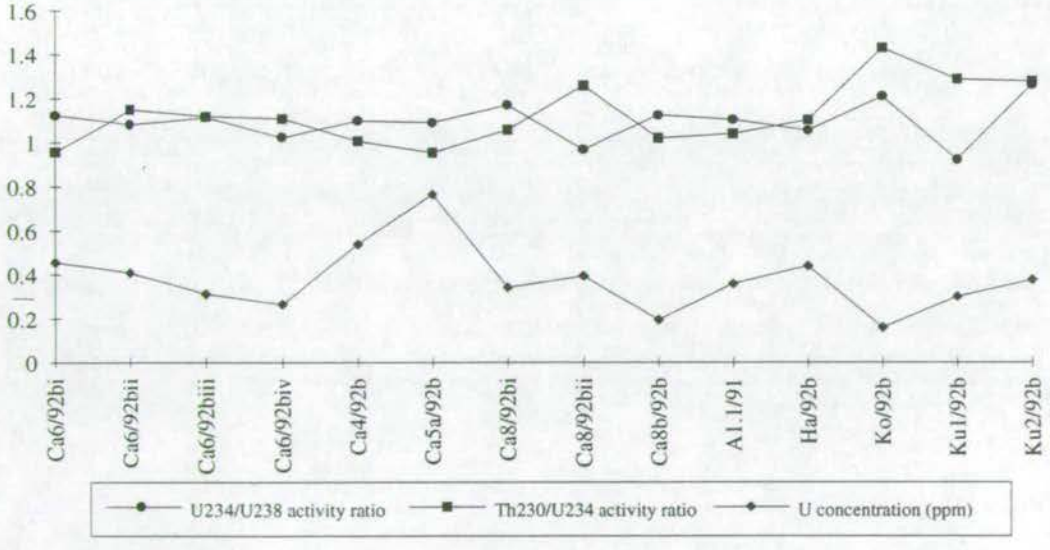

Fig. 2.9 Plot of indicators of leaching within the samples processed for U/Th dating.None of the samples show a strong leach signature and it is concluded that this is not a serious problem.

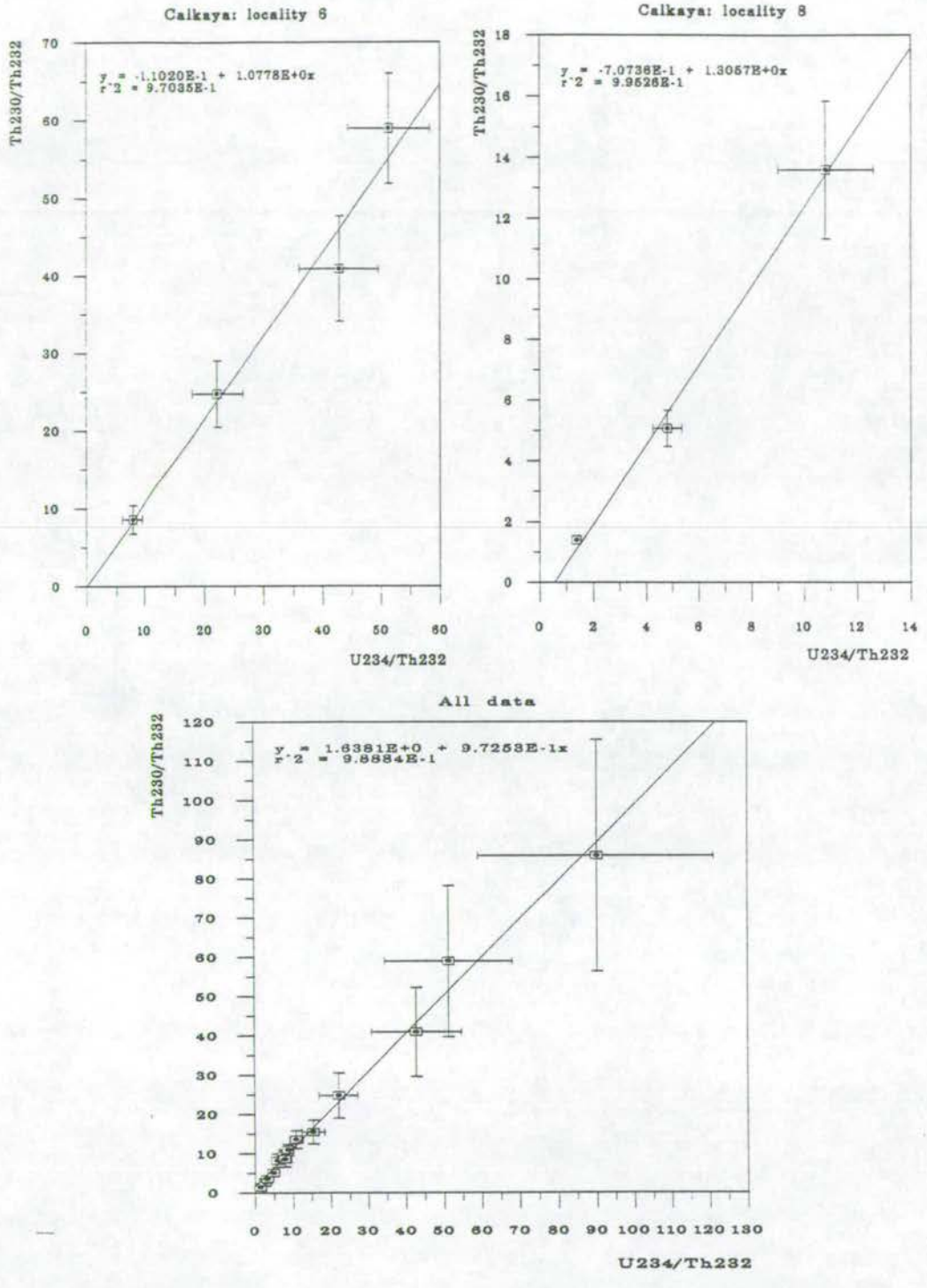

Fig. 2.10: Regression graphs for suites of samples from the Çalkaya terrace. The uppermost graphs are plots of individual samples from individual sample sites, which would therefore be expected to be of the same age. The lower graph is a plot of all samples from the Çalkaya terrace. In all three cases the regression is a good fit. However the slope of the line is also in all cases very close to 1 indicating that the samples have gone to equilibrium and that a U/Th date cannot be obtained.

High levels of ^{232}Th showed that detrital contamination was a significant problem. Consequently, the L/L correction method was used. Good regression lines were produced. The correlation statistics and values of $(^{230}Th/^{234}U)_a$ and $^{234}U/^{238}U$ are given in Table 2.4. Graphs are presented for the local groups Ca6/92bi-iv (Çalkaya: locality 6); Ca8/92bi,ii, Ca8b/92b (Çalkaya: locality 8) and for all the lower terrace data (All data) (Fig. 2.10). The results are also plotted on the isochron graph (Fig. 2.11) The data are considered to be of good quality and clearly show that the lower terrace is older than 400,000 years. If leaching had been a problem it would have had the effect of lowering the computed age of the samples and it can be seen that even at a potentially younger age, the sample is beyond the resolution of the technique.

Burger (1990, 1992) presented U-Th ages for the Antalya deposit. Eight samples were analysed and 6 samples produced results. Two of these had maximum ages of infinity. Notably, this included the sample from the region where this study was conducted. Minimum and maximum ages are given for the other samples. Burger's sample localities and average ages are shown in part B of Fig. 2.8. From these data Burger recognised three stages of terrace building.

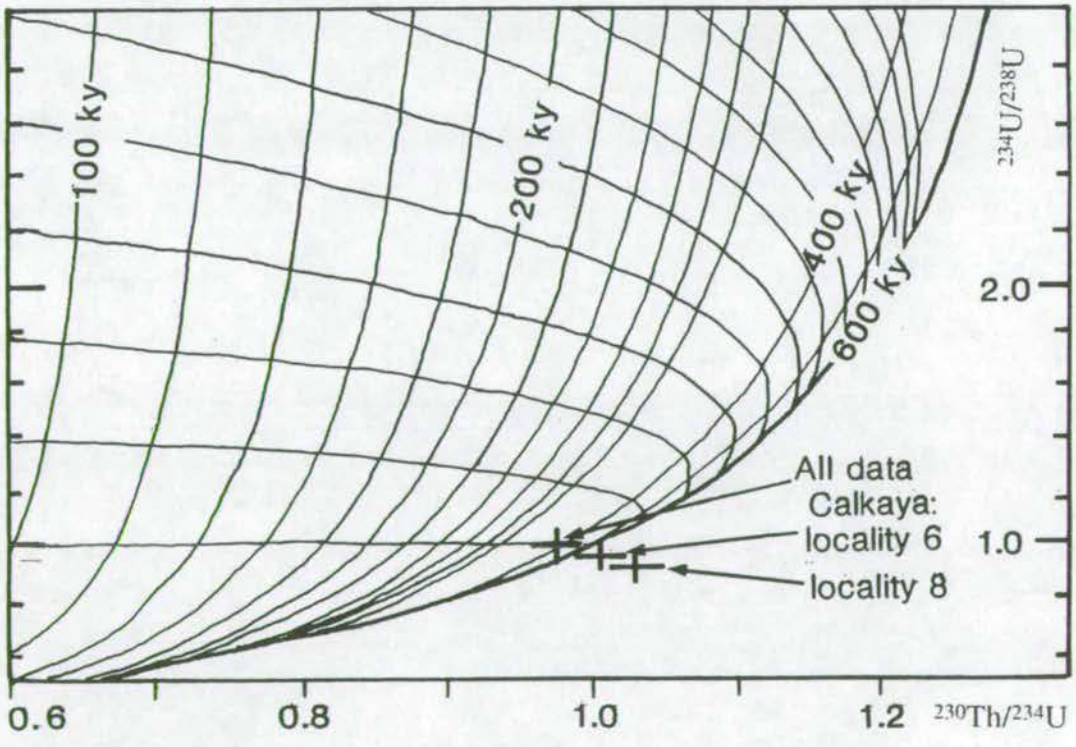

Fig. 2.11: Isochron plot of the data from the three suites of data presented in Fig. 1.10. As predicted the plots are beyond the resolution of the technique or in the case of the All data plot too close to the limit of the technique to be reliable.

For a number of reasons it is felt that Burger's (1992) results do not accurately reflect the age of the terraces and certainly the data are not sufficient to allow separate terrace "events" to be distinguished. Firstly, details of the analytical technique were not discussed. No information regarding the treatment and analysis of the samples was given and most importantly it is not known whether the presence of detrital thorium was recognised, or accounted for. Of twenty six samples eight, which were expected to give ages under 400,000 years were analysed. It appears that single samples were used as individual data points, in which case detrital thorium almostly certainly renders many of the results inaccurate. Secondly, although details of sample sites are not clear, at least one was sampled from a cave on a lower terrace. Localities such as this are prime sites for recent tufas, which are seen at present-day springs, waterfalls and in some streams. These surficial deposits are almost certainly not representative of the terrace as a whole. Indeed, what Burger's data does show is that tufa deposition has continued throughout the Quaternary, as suggested by the observation of present-day deposition (e.g. at Kursunlu Selalesi).

It is suggested in chapter 4 that deposition of the majority of the tufa occurred between 2.1 and 1.5 Ma during a general period of climatic instability, when a warming event is detected in both $\delta^{18}O$ and on the eustatic sea-level curve. This period is thought to be climatically most favourable for deposition of the tufa. In order to be really sure about the age of the deposit a much larger study would need to be carried out. However, the preliminary study of one small area suggests that the deposit is of an age beyond the resolution of U/Th dating and that the time and effort of a full study is almost certainly not justified.

2.5: Conclusions

1) A revised stratigraphical framework is proposed, based on that of Akay and Uysal (1985). The Gebiz Limestone is though to be older than previously suggested (late Tortonian?) but no definitive stratigraphic evidence could be obtained. The Pliocene, deltaic deposit is divided into the Yenimahalle Formation (marine silts and sands) and the Çalkaya Formation (marine, transitional and continental conglomerates). The Antalya Travertine is renamed the Antalya Tufa. All Quaternary conglomerates are named the Belkis Conglomerate.

2) The Yenimahalle Formation is biostratigraphically assigned to the *Globorotalia puncticulata - Globorotalia margaritae* zone (upper Zanclean). The

uppermost part of the formation, the Çalkaya Formation is placed within nannofossil zone NN15/16. Deposition of the entire Pliocene sediments probably occurred during the lower Pliocene (Zanclean) sea-level highstand, ceasing at the onset of inferred cooling at about 3 Ma.

3) K-Ar dating gives uncertain results, probably due to surface adsorbtion of atmospheric ^{40}Ar, but is not incompatible with deposition of the Çalkaya tuff around 3 Ma.

4) U-Th dating of the Antalya tufa shows it to be older than 400,000 yrs. It is suggested that deposition of the Antalya tufa occurred between 2.1 and 1.5 Ma, based on correlation with climatically favourable periods for tufa deposition. This will be discussed further in chapter 4.

Chapter 3:
Clastic sedimentation

This chapter describes the marine sediments of the Gebiz Limestone, the Early Pliocene Yenimahalle and Çalkaya Formations and Kemer Fanglomerates. The depositional environment and palaeogeography of the Aksu basin during these times will be deduced from basic sedimentological observations and sediment distribution. The sediments are described in stratigraphic sequence (see chapter 2). The relationship between each sediment type is discussed at the beginning of each subsection.

3.1: Previous work

Although some work was carried out concerning the stratigraphy and distribution of Pliocene sediments (Poisson, 1977; Akay and Uysal, 1985), as set out in chapter 2, no detailed work on their sedimentology was undertaken prior to the present study. Penck (1918) listed marine fossils from the grey marls and sands opposite Perge. Planhol (1956) briefly described the clastic sediments of the area. At this point, no stratigraphic details had been researched. The base of the series was described as conglomeratic. The marine Pliocene was recognised as an argillaceous marly sediment which passed up into grey sands, in which Chaput (1953) identified

marine fossils. A M. Tintant (in Planhol, 1956) examined the benthic foraminifera from the sequence. These suggested to him a large epicontinental sea with maximum water depth between 30 and 50m. A transitional phase to the Quaternary tufa was described as continental or very reduced lagoonal sediments with variable facies.

In 1985 mapping of the Neogene of the area was completed (Akay and Uysal, 1985). This map forms the basis of this study. No more detailed mapping has yet been undertaken, except in the Aksu and Çalkaya area. A modified version of the map (Akay and Uysal, 1985) with the revised stratigraphy, new dip and strike data and palaeocurrent data from the present study are presented in Fig. 3.1. Place names mentioned in the text, the locations of logged sections and the area of the Çalkaya map are also indicated.

The Pliocene "Isparta ignimbrite" exposed around Gölçük lake has already been thoroughly studied (Lefèvre, Bellon and Poisson, 1983; Özgür, Pekdeger, Schneider and Bilgin, 1990) and further work is beyond the scope of this project. Lefèvre *et al* (1983) dated the ignimbrite, using whole rock K-Ar methodology, as Lower Pliocene (4 - 4.7 Ma). They recognised a maar-type deposit, in the form of a trachytic ignimbrite cone around the central Gölçük lake. Özgür *et al* (1990) defined three stages of an alkalic sequence: I) tephriphonalite; II) pyroclastic series (friable tuff, ignimbrite and pumice tuff); III) trachyandesite with trachyte. The rocks consist of sanidine, oligoclase, biotite, pyroxene, hornblende, sphene, fluorite and fluorapatite in a glassy groundmass. The three stages are thought to be differentiation products of a single magma chamber. The evolution of the Isparta ignimbrite, according to Özgür *et al* (1990), is presented in Fig. 3.2.

3.2: Gebiz Limestone

The Gebiz Limestone demarcates the eastern edge of the Aksu basin and forms the main divide in the southern area between the Aksu basin and the Köprü basin. It crops out along a north-south trending lineament. The strike of the limestone is north-south and it dips approximately 25° to the west, as shown in Fig. 3.1. As discussed in chapter 2, the limestone is thought to be Late Tortonian in age, although this still remains to be proven.

3.2.1: Field observations

The Gebiz Limestone is a typical bioclastic limestone (Plate 3.1A). Clastic fragments identifiable in the field are echinoid spines and tests, bivalves (including pectens and oysters), gastropods, bryozoa, benthic foraminifera, encrusting algae and rhodoliths (Plate 3.1B,C).

Plate 3.1: Gebiz Limestone:
A) Surface of Gebiz Limestone with echinoid spines. **B)** Surface of Gebiz Limestone with gastropo
and bivalves. **C)** Algal rhodoliths. **D)** *Porites* coral colony. **E)** Small *Porites* coral colony
particularly fossiliferous limestone. **F)** *Clypeastrina* echinoid.

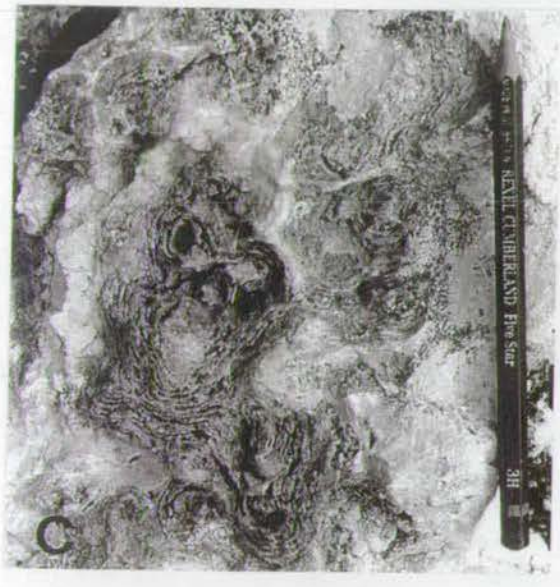

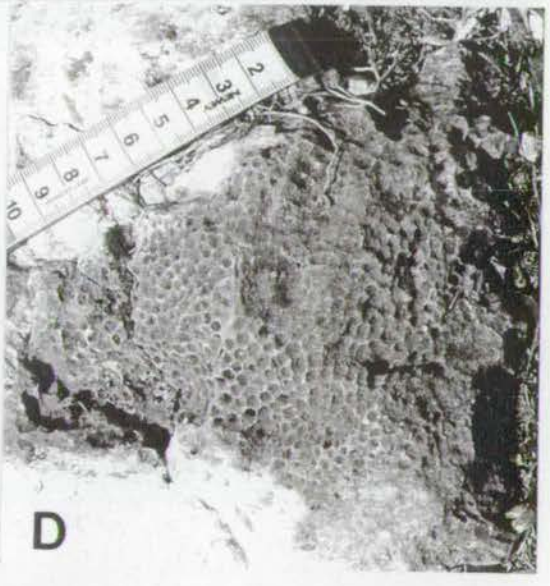

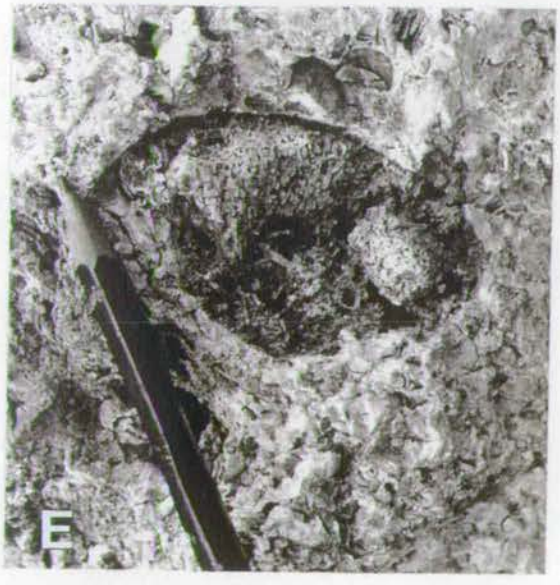

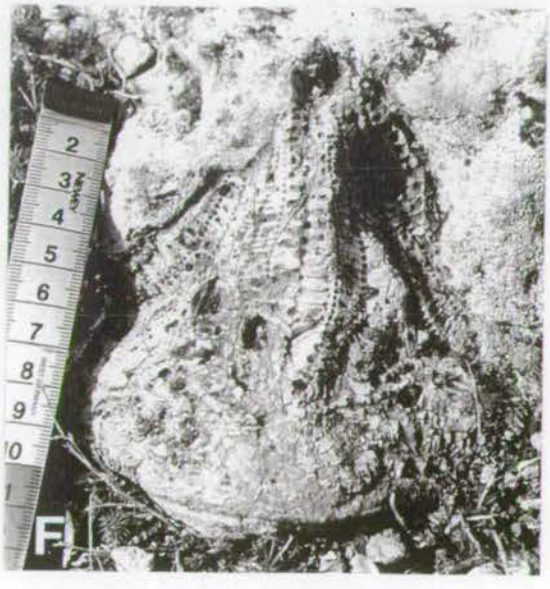

Plate 3·1

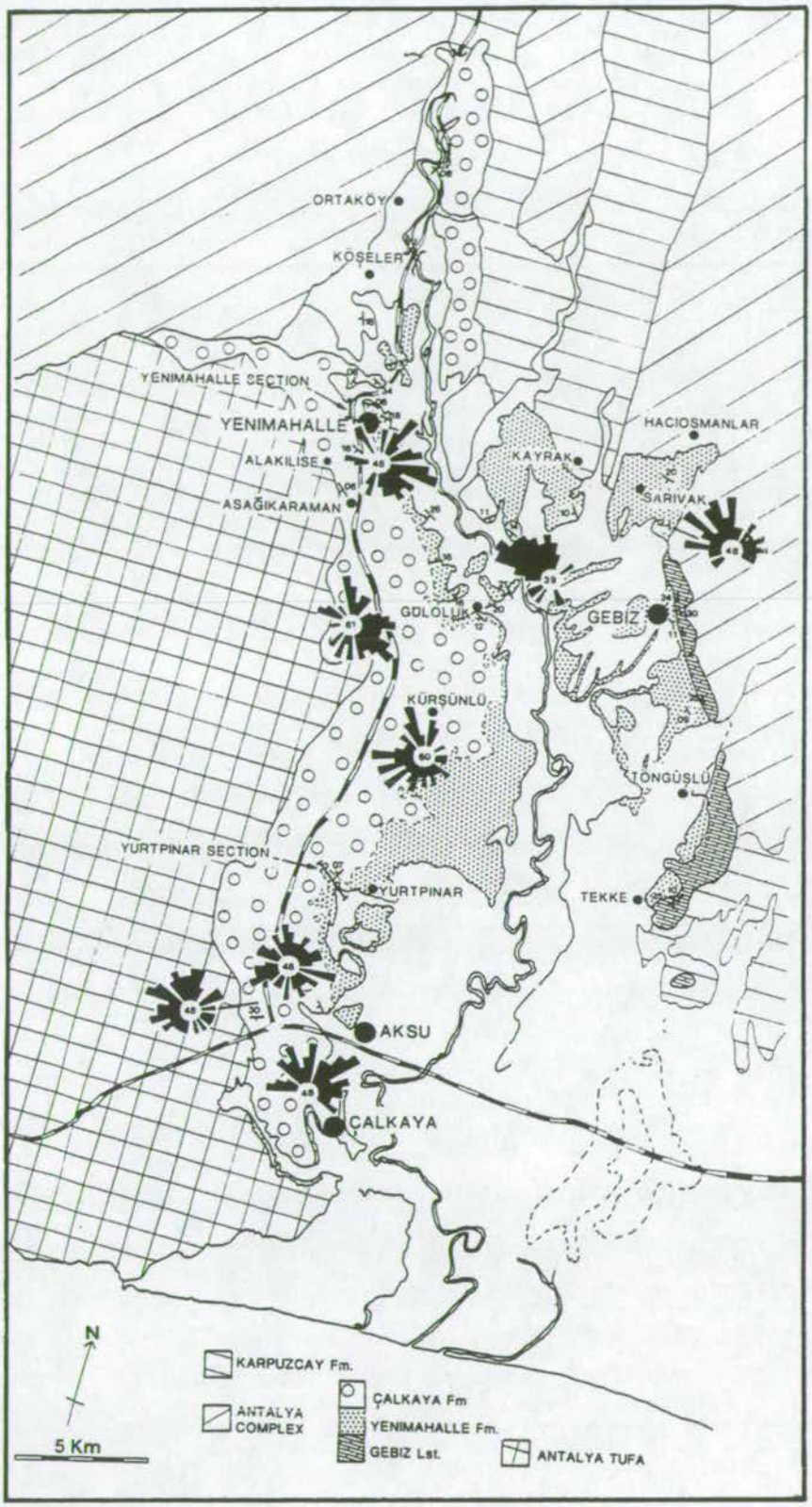

Fig. 3.1: Modified map of the Aksu basin after Akay and Uysal (1985) showing the new stratigraphy, bedding data and palaeocurrent data. Palaeocurrent data are from clast imbrication measurements. The count number is given in the centre of each plot. The two logged sections (Yurtpinar and Yenimahalle) are indicated on the map. All place names mentioned in the text are included.

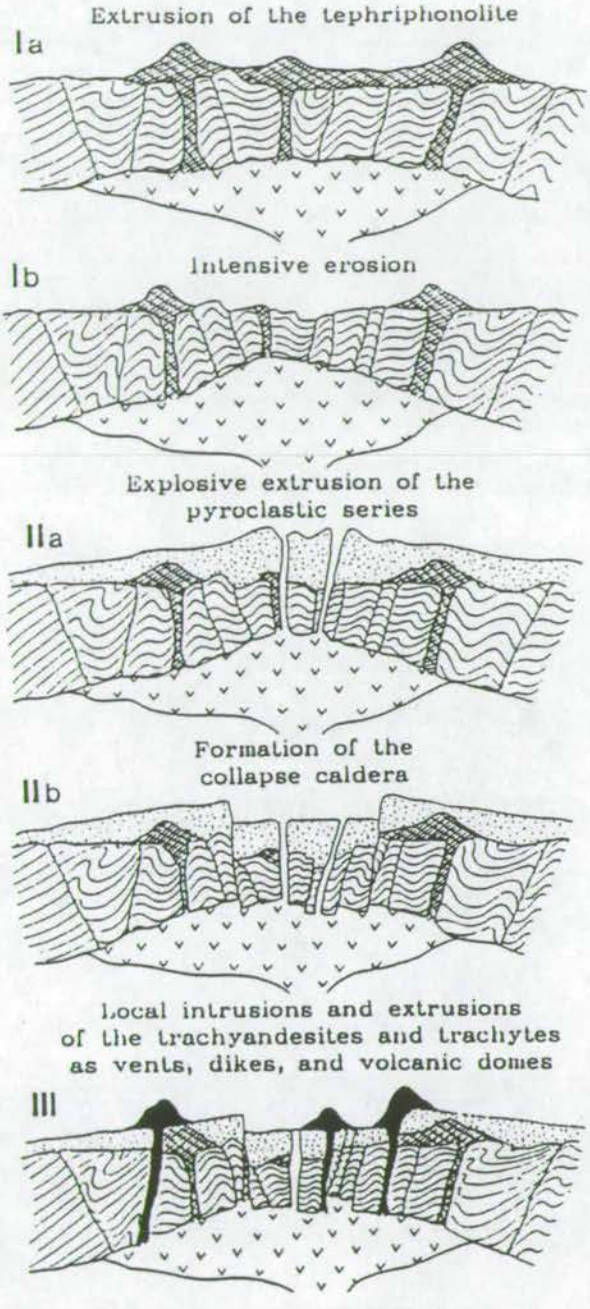

Fig. 3.2: Model of evolution of the Isparta ignimbrite from Özgür *et al* (1990).

Small colonies of *Porites* sp. (50cm in diameter) are also found (Plate 3.1D,E). These are confined to the southern part of the outcrop, around Tekke. Individual colonies are of the order of 20-30 cm in diameter. Several specimens of an echinoid belonging to the suborder *Clypeasterina* exist near the Roman quarry at Tekke (Plate 3.1F). Occasional well-rounded pebbles of ophiolitic material are present.

Other beds are found within the limestone sequence: channels of coarse sand with erosional bases, containing ophiolitic material and small shells; a bed of gritty limestone (1.5m thick); layers of lime mud; calcarenite and marine marl. Dewatering structures were observed within one of the lime mud layers. Two hardgrounds were also noted. The hardground layers are iron-rich and sandy with dense reworked fossils and prolific burrowing. Two marls, sampled near Tekke, proved to contain only benthic foraminifera. No stratigraphic indicators were found. Species identified are *Cibicides lobatalus*, *Bolivina* spp., *Melonis* sp., *Pyrgo* sp., *Trifarina* sp., *Planulina* sp., *Textularia* spp., *Elphidium* sp., *Patellina* spp., *Bulimina spinensis*, *Spirillina* sp., *Stilosigmoilinella* sp., *Neoconorbina terquem*, *Haynesia depressula*, *Quinqueloculina* sp. and *Fursenkonia* sp.

3.2.2: Petrography

Sixteen thin sections from twelve localities were studied. In general, very similar characteristics were observed in all sections and the description here is a summary of all the data. The majority of the limestone can be classified as a packed red algal biomicrite after Folk (1959, 1962), or as a packstone after Dunham (1962) (Plate 3.2A,B). One section is red algal bindstone and one is a foraminiferal grainstone (Plate 3.2C). Porosity is generally around 10-20% with only one section displaying significant sparry calcite cement infilling.

Corallinacean red algae, some encrusting and some free-standing, dominate the sections, with one section containing up to 80% red algae. Encrusting foraminifera are also common (Plate 3.2D) and were identified, primarily by their wall structure and chamber form, as similar to *Rupertina* sp., although the growth form is frequently not upright, but often appears to be rather flat. *Rupertina* sp. is often closely associated with growth of red algae, encrusting the red algae and vice versa. The encrusting foraminifera *Gypsina* sp. (Acervulinidae) was also identified in many sections. A third encruster with chambers very similar to those of *Rupertina* sp., was also observed; the chambers were typically twice the size of those of *Rupertina* sp. and form a more radiating pattern. This species was not identified.

Foraminifera are common in all sections, with *Elphidium* spp. being the most common. Various Miliolid forms (including *Quinqueloculina* sp. and possibly

Plate 3.2: Thin sections of the Gebiz Limestone.
A) Red algae in bioclastic matrix. Field of view 2.8mm x 3mm. **B)** Red algae and foraminifera in bioclastic matrix. Field of view 4.8mm x 5mm. **C)** Foraminiferal grainstone. Field of view 3.8mm 4mm. **D)** Red Algae and encrusting foraminifera cf. *Rupertina*. Field of view 4.6mm x 5mm **E)** Bioclastic fragments within a fine carbonate/clay matrix. Field of view 3.2mm x 3.3mm **F)** Brecciated red algae. Field of view 5.4mm x 5.8mm.

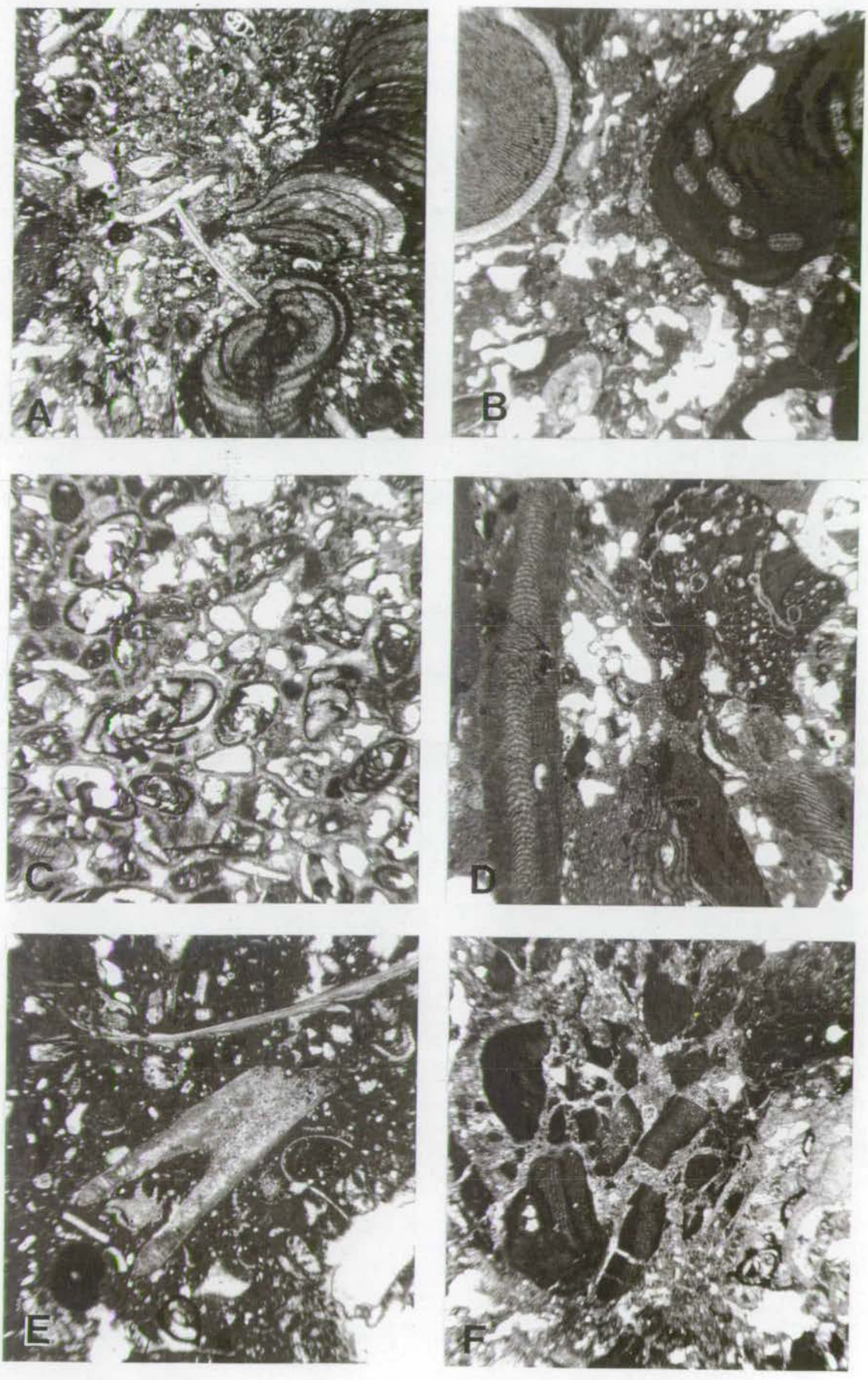

Plate 3·2

Triloculina sp.) are also frequent and occur in many sections. Other foraminifera identified were *Textularia* sp., small rotaliid benthics, *Cympaloporidae* spp., an aveolinid foraminifera with globular form., ?*Pateoris sp.*, ?*Pyrgo sp.*, and, in one section, Globigerinids. An unidentified fossil, which is tentatively included here as a large, probably encrusting foraminifera was also seen in many sections. The calcite of the chambers was always a pale brown colour, the chamber walls varied from thick to thin and chambers were chaotic, sometimes very elongate. All these species are inner shelf species, preferring a temperate to warm climate.

Other common bioclastic components are echinoid spines and plates, serpulids, bivalve fragments, *Ostrea* fragments, occasional siliciclastic grains, and rare broken corals (Plate 3.2E). One section had a significant number of Dasycladacean algae and scattered peloids within the micritic matrix. A further section, which contained many large serpulids, contained a peloidal layer approximately 1cm thick. Most sections are grain supported with about 15% micrite matrix. The maximum percentage matrix is in sections collected from the Sillyon plateau (the southernmost locality of Gebiz limestone) and contained 60% matrix. One section is distinctly brecciated, with many fragments of red algae (Plate 3.2F), the others remain intact.

3.2.3: Environment of deposition

It is probable that the Gebiz Limestone formed in a very shallow water environment with open circulation, close to wave base, within which patches of colonial corals grew. This environment typically gives rise to bioclastic wackestone or bioclastic micrite containing fragments of diverse organisms (Wilson, 1975; Flügel 1972, 1982). The brecciation of one section, which included a large number of red algae fragments, strongly suggests that storm reworking affected the sediment. The presence of calcarenite, ophiolitic pebbles, grit and sand within the sequence show that it was not far from a shoreline. It is possible that the foraminiferal grainstone originated as a tidal bar or lagoonal channel within this shallow water environment (Wilson, 1975; Flügel 1972, 1982). The presence of peloids, serpulids and occasional Dasycladacian algae suggests that, at times, water circulation may have been restricted and that a more lagoonal environment existed (Wilson, 1975; Flügel 1972, 1982).

3.3: Messinian gypsum

No *in situ* gypsum was found in the Aksu basin; however, its presence beneath the Pliocene sediments is inferred from two boulders of selenitic gypsum at

the edge of the Gebiz limestone south of Gebiz. Swallowtail selenite crystals are up to 30cm in length (Plate 3.3A) and the boulder itself has dimensions of approximately $2m^3$. The growth of large crystals of swallowtail selenite indicates a shallow water environment, as has been shown in Messinian deposits around the Mediterranean (Hardie and Eugster, 1971, Robertson, Eaton, Follows and Payne, 1995) and in recent salt lakes (Warren, 1982). Locals report that the gypsum block was removed from a water conduit, located beneath the ground, along the edge of the limestone. Further evidence for the presence of gypsum beneath the sediments was found in the Çalkaya area. In one outcrop, numerous rosettes of gypsum were found on the surface and gypsum was precipitated along cracks in the sediment. It is surmised that groundwater flowing through the sediment dissolved gypsum from lower layers and redeposited it at the present day sediment/air interface.

3.4: Contact relations between the Gebiz Limestone and the Yenimahalle Formation

The relationship between the Gebiz Limestone and the Yenimahalle Formation is most clearly seen opposite the cemetery south of Gebiz and at the location of Poisson's (1977) cross-section just north of Töngüslü. It is clear at the first locality that the gypsum onlaps the Gebiz Limestone approximately 5m below the surface. The marine Pliocene sediments then onlap the entire sequence. The onlap of the marine Pliocene onto the Gebiz Limestone is seen particularly well just north of Töngüslü where Poisson's (1977) cross-section is located.

At the first locality, the front edge of the Gebiz Limestone is characterised by an almost vertical succession of rocks (Plate 3.3B). A small gully separates this sequence from the more gently dipping Gebiz Limestone. The gully is filled with fossiliferous marls and a purer lime mud. Notably, the dip of the limestone is steeper here than in any other part of the succession (42° as opposed to 25°). The vertical succession consists of layers of breccia, containing clasts of the Gebiz Limestone, but also with common clasts of chert and mudstones. In between the breccia, layers of laminated limestone undulate over the lower breccia layer (Plate 3.3C).

The sequence is interpreted as evidence of a palaeo-fault scarp down which breccia tumbled. The fault must have acted as a water pathway carrying carbonate-supersaturated waters to the top of the fault from where it flowed down the slope surface cementing steeply dipping talus into place. Fresh talus buried the cement from time to time and then the process repeated. The ophiolitic clasts within the breccia show that the Mesozoic rocks which crop out to the east of the Gebiz

Plate 3.3:
A) Swallowtail selenite gypsum from a boulder near Gebiz. **B)** Almost vertical beds adjacent to th Gebiz limestone, interpreted as a palaeo-fault scarp. **C)** Close up of arrowed part of B). Breccia i intercalated with carbonate cement. **D)** New road cut, site of the Yenimahalle logged section. The clif comprises blue-grey silts at the base and yellow sands and the top. Under the lone tree to the right o centre a white bed can be made out that is lacustrine carbonate. This sits directly on top o conglomerate. **E)** Channels in the lower silts along the canal section near Güloluk.

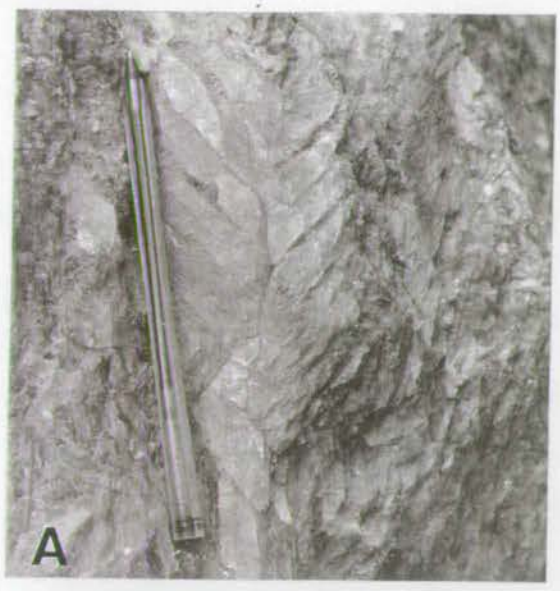

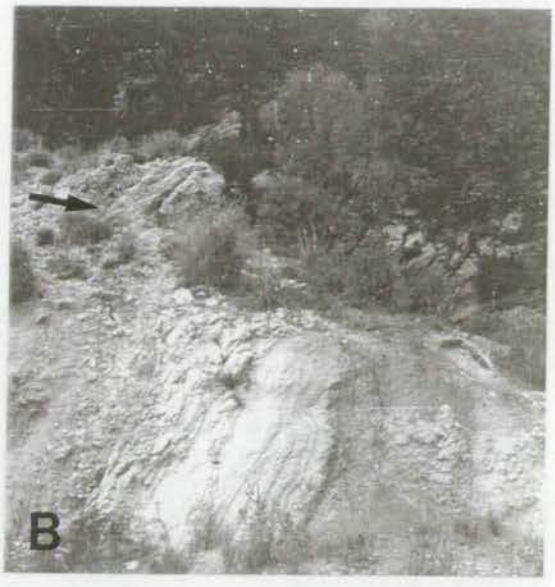

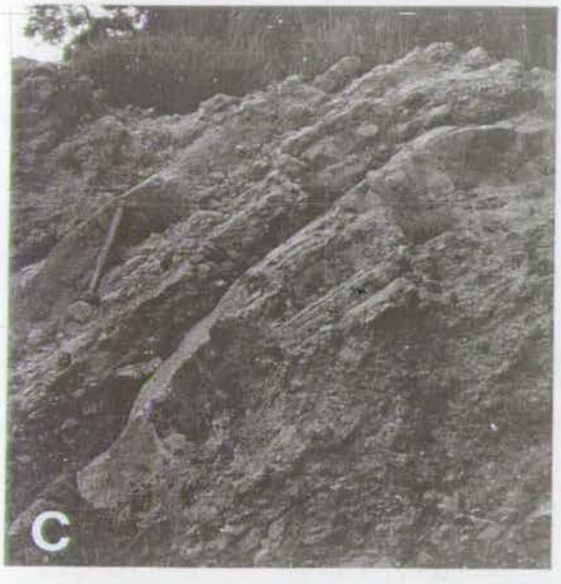

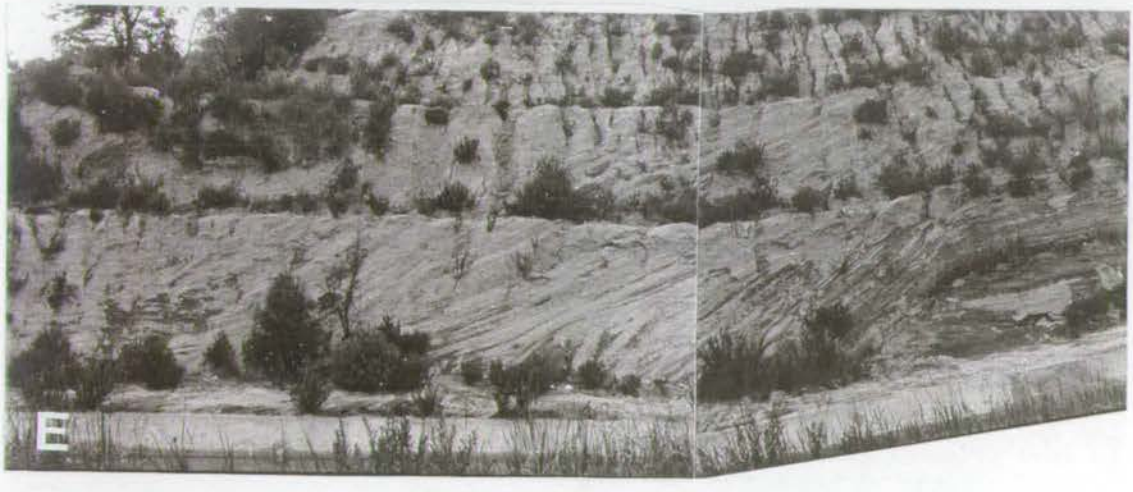

Plate 3-3

Limestone in this locality were also involved in the footwall uplift. The gypsum is not involved in this process in any way and must post-date active faulting.

3.5: Yenimahalle Formation

The Yenimahalle Formation crops out in the Aksu basin and the Manavgat area. In the Manavgat area the marine Pliocene onlaps on to marine Miocene which is very similar in appearance. The Yenimahalle Member constitutes all but the last 20m of marine Pliocene sediments, which is the Çalkaya Formation. Sections from the western side of the Aksu Çay, at Yurtpinar and Yenimahalle, are compared with the Manavgat sediments and with sediments from the Gebiz area. In general the sediments are unconsolidated. However, calcite cemented concretion horizons occur within all sections and were sampled for thin-sectioning.

The lowest part of the Yenimahalle Formation exposed onshore is exposed in the western half of the basin around Manavgat (Fig. 3.4). Two representative sections (A (Fig. 3.3) and B (Fig 3.5)) are shown from just south and just north of the main road and both were sampled for foraminifera.

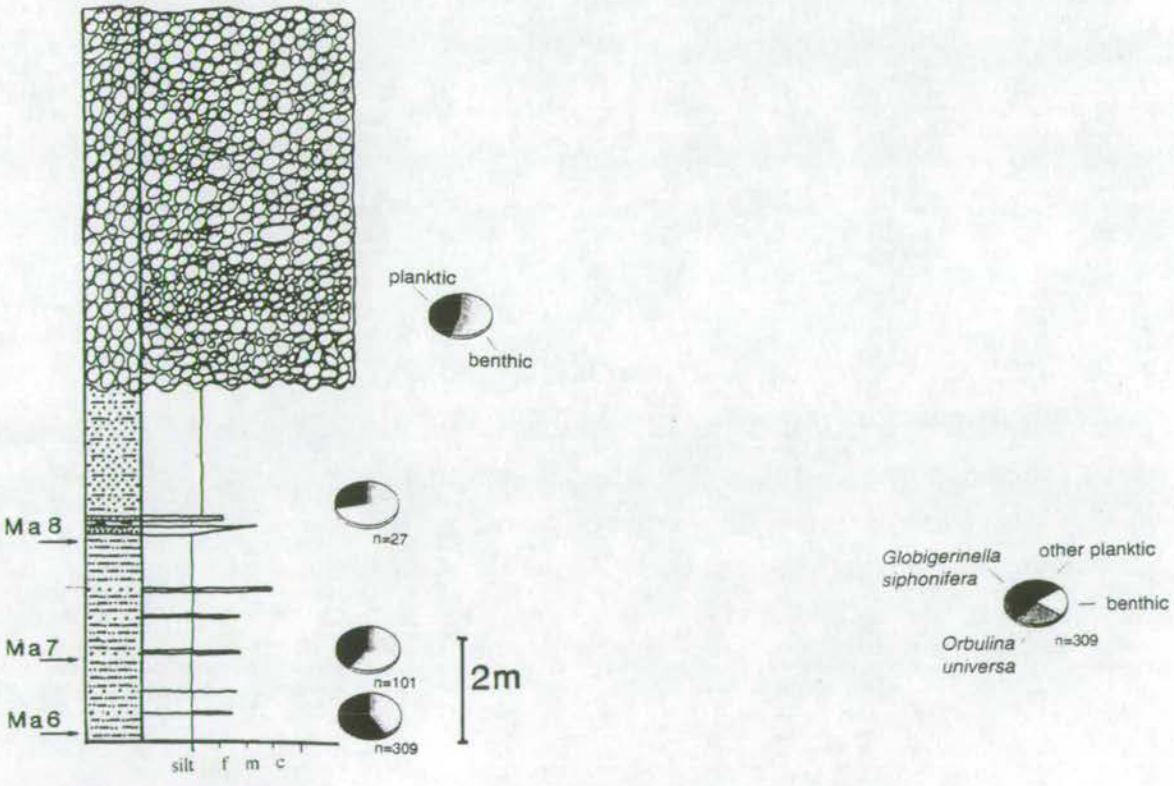

Fig: 3.3: Sedimentary log of Manavagat section A, located just south of the main road. Samples are marked on the left-hand side of the log. Pie charts represent Planktic/Benthic ratios. Ma6 is broken down further to demonstrate the dominance of *Orbulina universa* and *Globigerinella siphonifera*.

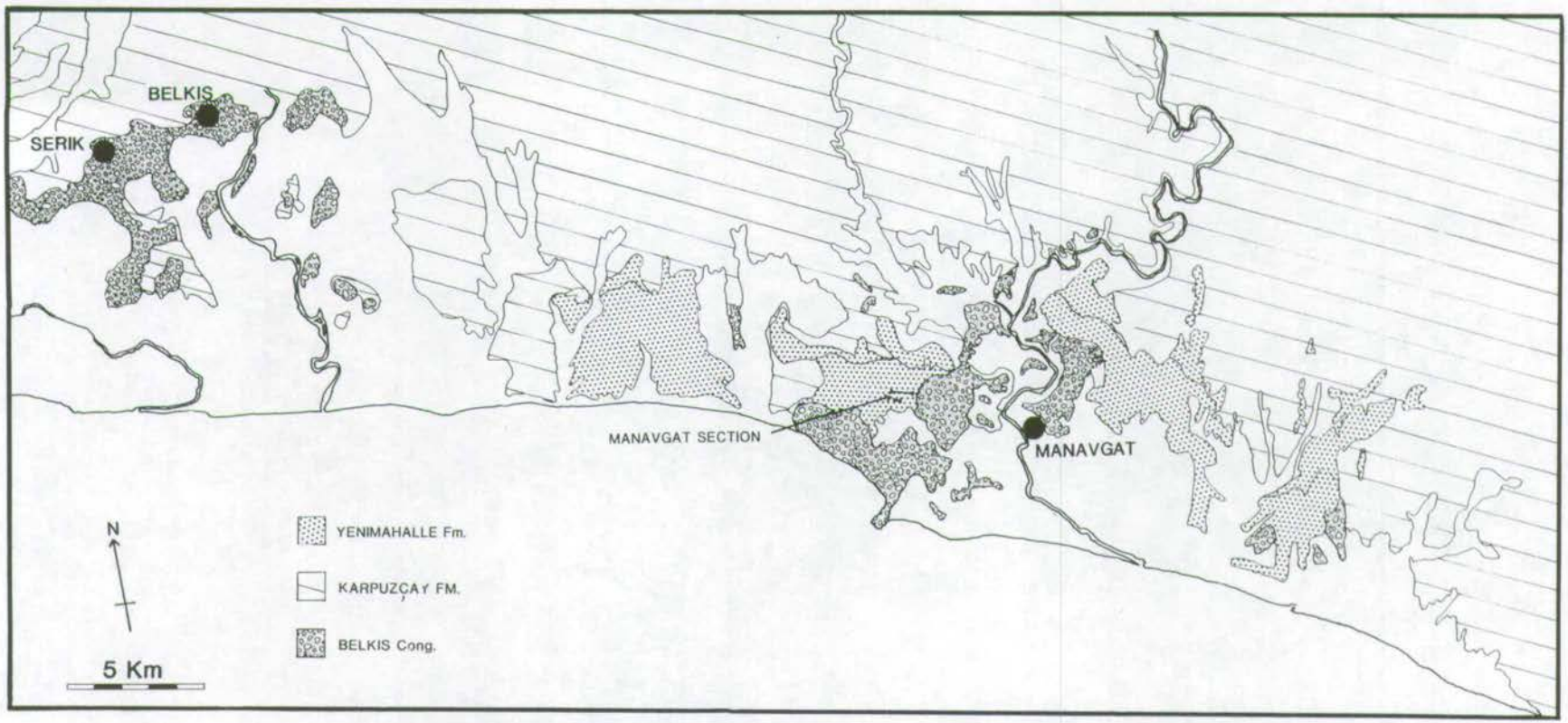

Fig. 3.4: Map of the Manavgat area after Akay and Uysal (1985). Location of the Manavgat sections just to the west of Manavgat is shown.

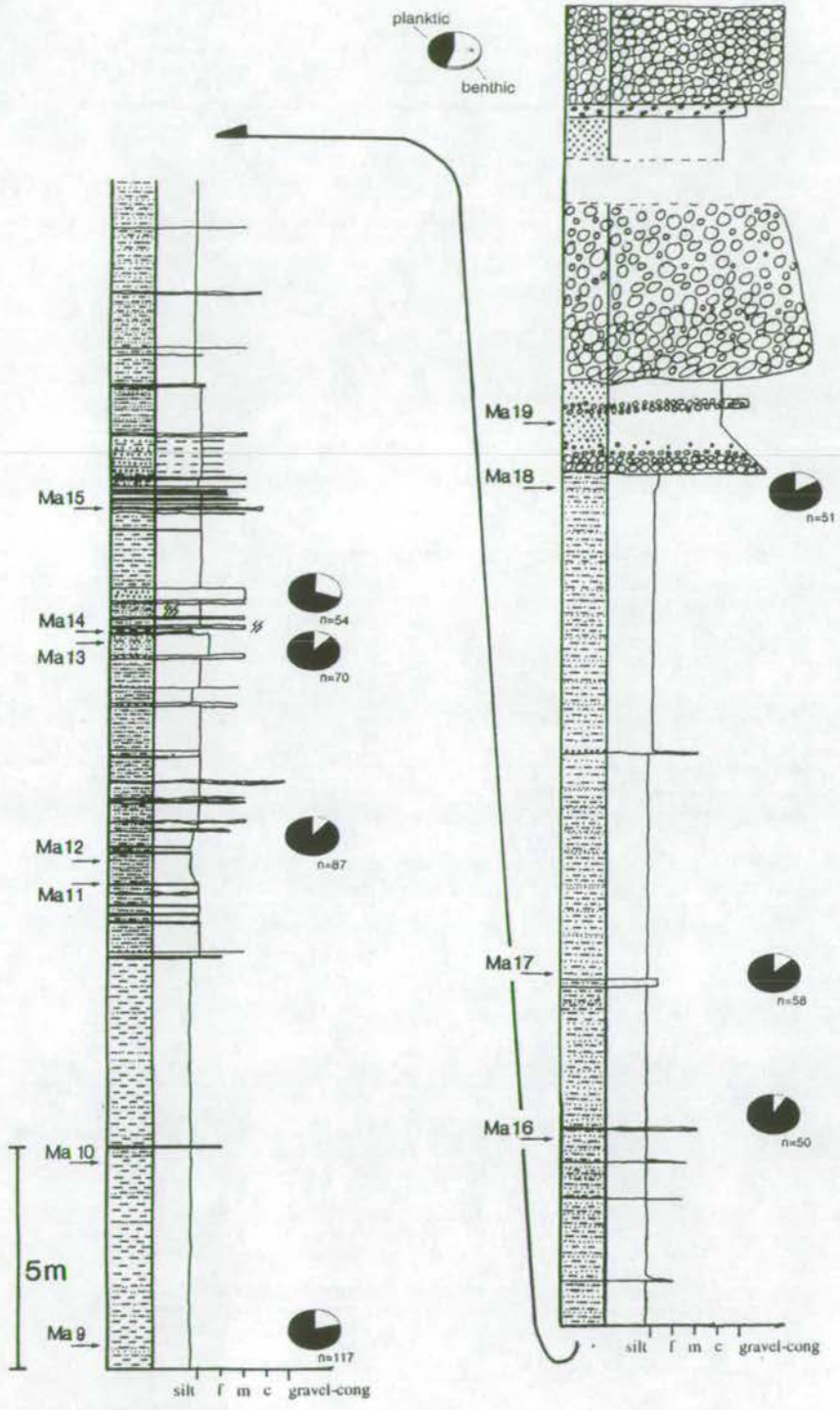

Fig. 3.5: Sedimentary log of the main Manavagat section B, located on the Manavagat road. Sample localities are indicated on the left-hand side of the log. Pie-charts are representative of Planktic/Benthic ratios.

The two samples Ma5/92b and Ma6/92b are approximately laterally equivalent and samples Ma6/92b-Ma8/92b are from the logged section south of the road (A). The remainder of samples (Ma9/92b-Ma18/92b) from this area are from section B. Samples were also collected from small outcrops close to the coast (Ma1-4/92b). Both sections are dated to the *Globorotalia puncticulata - Globorotalia margaritae* zone (see also chapter 2). The sedimentary logs (Fig. 3.4 and 3.5) show this section to be primarily blue-grey silts with thin interbeds of medium and fine sands. Macrofossils are sparse to absent. At the top of section B, coarser, graded, gravel beds and a 3m-thick conglomerate body show that coarser material was input into this environment. A thick conglomerate body on top of log A may be part of the sequence, or a later fluvial deposit.

Benthic foraminifera were identified using Loeblich and Tappan (1988) Wright (1978); Haynes (1981); van Marle (1989, 1991); Hasagawa, Sprovieri and Poluzzi, (1990) and Sprovieri and Hasegawa, (1990) (Appendix 1; Plates 3.4-3.11). The Manavgat sections are dominated by species such as *Uvigerina* spp., *Lenticulina* spp., *Pullenia* sp., *Karreriella* sp., *Globocassidulina* sp., *Planulina sp.*, *Bulimina sp.*, *Bolivina* sp., and *Cibicides* sp. Planktic/Benthic ratios range from 0.42 and 11.50 and are typically between 1.5 and 7.0. They are represented by pie charts alongside the sedimentary logs. Ma5/92b and Ma6/92b are particularly interesting samples from a micropalaeontological viewpoint. They come from silts which look identical to the rest of the section, but the foraminiferal content is much denser; the sizes of the foraminifera are larger, and the diversity greater. The samples are dominated by *Globigerinella siphonifera* and *Orbulina universa* and *bilobata* which make up 39% and 26%, respectively. Benthic foraminifera constitute only 14% of the sample (n=309).

In the Aksu basin two logged sections represent the Yenimahalle Formation. The Yurtpinar section follows a small road and is exposed in the road-side stream. The Yenimahalle section follows the new trunk road from Aksu to Isparta and documents a road-cut 50m in height, as it passes from the valley up to the upper terrace. The section was particularly fresh at the time of the study. The two sedimentary logs and other sediments studied along the terrace front are representative of the same stratigraphic level. Only the Yurtpinar section was studied micropalaeontologically. It was also dated to the *Globorotalia puncticulata - Globorotalia margaritae* zone (see chapter 2). The lowermost sample of the Yenimahalle section (Ye1/92b) was examined for foraminiferal content and contained the same faunal assemblage as the Yurtpinar log.

Plate 3.4:

1) *Textularia agglutinans*
sample Yu25/92b (25/45) x130

2) *Karreriella bradyi*
sample Ma4/92b (M4/6) x120

3-6) *Quinqueloculina* sp.
3) sample Yu6/92b (6/8) x130
4) sample Yu27/92b (27/12) x220
5) sample Yu23 (23/7) x120
6) sample Yu27 (27/1) x240

7) *Pyrgo* sp.
sample Yu26/92b (26L/6) x80

8) *Amphicoryna* sp.
sample Ma5/92b (2/5) x240

9) *Lagena* sp.
sample Ma5/92b (3/25) x200

10) *Lenticulina rotulata*
sample Ma5/92b (1/10) x160

11) *Neolentilculina* sp.
sample x170

12) *Dentalina filiformis*
sample Ma5/92b (2/14) x110

13) *Dentalina* sp.
sample Ma5/92b (2/11) x110

Plate 3.5:

1) *Sigmoilinitae tenuis*
sample Ma5/92b (2/1) x200

2) *Bulimina alazanensis*
sample Ma5/92b (1/17) x140

3) *Bulimina spinensis*
sample Yu29/92b (29/28) x140

4) *Bulimina gibba*
sample Yu29 (29/14) x300

5) *Praeglobobulimina pupoides*
sample Ma9/92b (M9/4) x140

6-8) *Reussella simplex*
6) sample Yu18/92b (18/7) x230
7) sample Yu33/92b (33/12) x210
8) sample Yu13/92b (13/12) x190

9) *Trifarina bradyi*
sample Yu10/92b (10/5) x210

10-11) *Trifarina* sp.
10) sample Ma4/92b (M4/7) x130
11) sampleYu6/92b (6/4) x220

Plate 3.6:

1) *Uvigerina peregrina*
sample Yu14/92b (14/7) x290

2) *Uvigerina pigmea*
sample Yu8/92b (8/1) x250

3-4) *Uvigerina* sp.
3) sample Ma7/92b (7/3) x 110
4) sample Yu2/92b (2/2) x 330

5-6) *Pleurostomella alternans*
5) Ma5/92b (2/13) x100
6) Ma7/92b (M7/4) x 80

7) *Globocassidulina subglobosa*
sample Ma4/92b (M4/3) x170

8) *Spheroidina bulloides*
sample Yu14/92b (14/9) x30

9) *Siphonia reticulata*
sample Ma5/92b (1/29) x160

10) *Valvulineria* sp.
Sample Yu22 (22/2) x180

11-13) *Hanzawaia rhodiensis*
11) sample Ma5/92b (3/16) x100
12) sample Ma5/92b (2/7) x170
13) sample Yu19/92b (19/10) x390

Plate 3.7:

1-3) *Cancris oblongus*
1) sample Yu25/92b (25/49) x130
2) sample Yu25/92b (25/48) x150
2) sample Yu25/92b (25/50) x110

4-5) *Neoconorbina terquem*
4) sample Yu4/92b (4/10) x230
5) sample Yu36/92b (36/4) x300

6-7) *Patellina* sp.
6) sample Yu37/92b (37/5) x390
7) sample Yu22/92b (22/15) x430

8) *Bolivina robusta*
sample Yu29/92b (26/39) x180

9) *Bolivina plicatella*
sample Yu27/92b (27/8) x300

10) *Bolivina* sp.
sample Ma9/92b (M9/2) x290

11) *Brizalina subreticulata*
sample Yu2/92b (2/6) x300

Plate 3.8:

1) *Brizalina alata*
sample Ma8/92b (8/1) x170

2) *Brizalina hastula*
sample Yu25/92b (25/43) x190

3) *Brizalina macella*
sample Yu19/92b (19/17) x170

4-5) *Stilostomella antillea*
4) sample Ma5/92b (1/1) x290
5) sample Yu29/92b (29/24) x170

6) *Fursenkonia* sp.
sample Yu25/92b (25/26) x190

7) *Nonion fabum*
sample Yu6/92b (6/15) x270

8) *Florilus bouneaum*
sample Yu25/92b (25/32) x130

9) *Haynesia depressula*
sample Yu14/92b (14/4) x230

10) *Melonis affinis*
sample Ma9/92b (M9/6a) x250

11) *Pullenia osloensis*
sample Ma5/92b (1/9) x220

—

Plate 3.9:

1-2) *Cibicides kullenbergi*
1) sample Ma5/92b (1/20) x170
2) sample Yu17/92b (17L/3b) x90

3-9) *Cibicides lobatulus*
3) sample Ma5/92b (3/5) x190
4) sample Yu13/92b (13/3) x220
5) sample Yu26/92b (26/40) x160
6) sample Yu38/92b (38/1) x220
7) sample Yu26/92b (26L/3) x80
8) sample Yu26/92b (26L/4) x80
9) sample Ma6/92b (M6/5) x140

10-11) *Cibicides refulgens*
10) sample Yu2/92b (2/13) x290
11) sample Yu30/92b (30/8) x250

12) *Dyocibicides biserialis*
sample Yu26/92b (26L/5) x190

Plate 3.10:

1-2) *Planulina arimensis*
1) sample Ma5/92b (1/2) x130
2) sample Ma5/92b (3/6) x90

3-4) *Planorbulina mediterrenensis*
3) sample Yu26/92b (26L/8) x90
4) sample Yu19/92b (19/9) x170

5-6) *Ammonia beccarii*
5) sample Yu25 (25/31) x130
6) sample Yu26 (26/5) x140

7-8) *Aubiguyna perculida*
7) sample Yu30/92b (30/12) x330
8) sample Yu26/92b (26/15) x330

Plate 3.11:

1) *Elphidium advenum*
sample Yu26/92b (26/35) x330

2-3) *Elphidium crispum*
2) sample Yu17/92b (17L/1) x40
3) sample Yu26/92b (26L/7) x80

4-5) *Elphidium macellum*
4) sample Yu25/92b (25/30) x120
5) sample Yu 26/92b (26L/2) x60

6) *Elphidium* cf *macellum*
sample Yu26/92b (26/9) x330

7) *Elphidium excavatum*
sample Yu28/92b (28/7) x21

8) *Elphidium* sp. A
sample Yu26/92b (26/13) x30

9-11) *Elphidium* sp.
9) sample Yu30/92b (30/13) x250
10) sample Yu13/92b (13/1) x390
11) sample Yu13/92b (13/8) x390

12) *Gyroidinoides laevigata*
sample Ma5/92b (3/13) x130

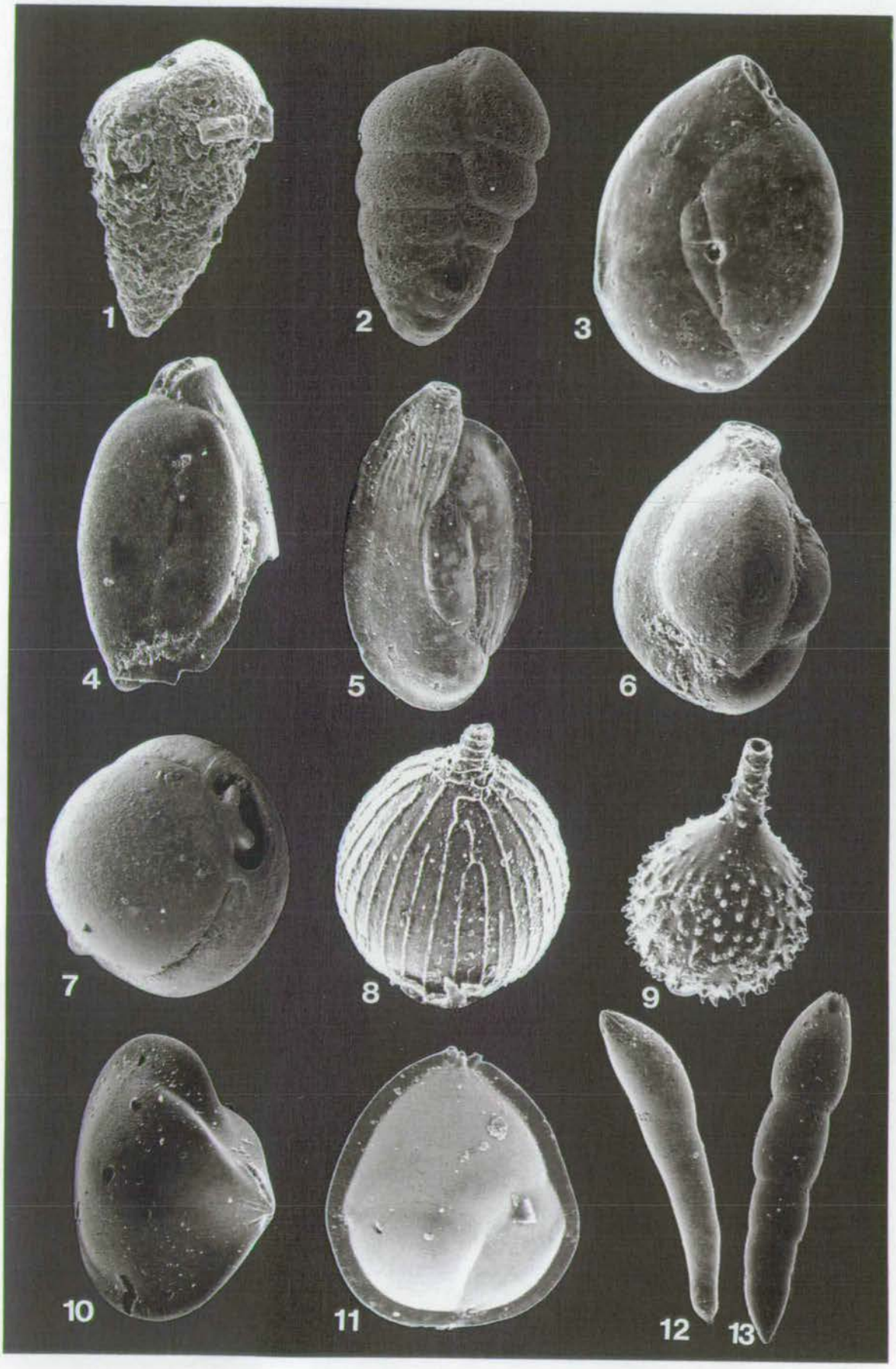

Plate 3·4

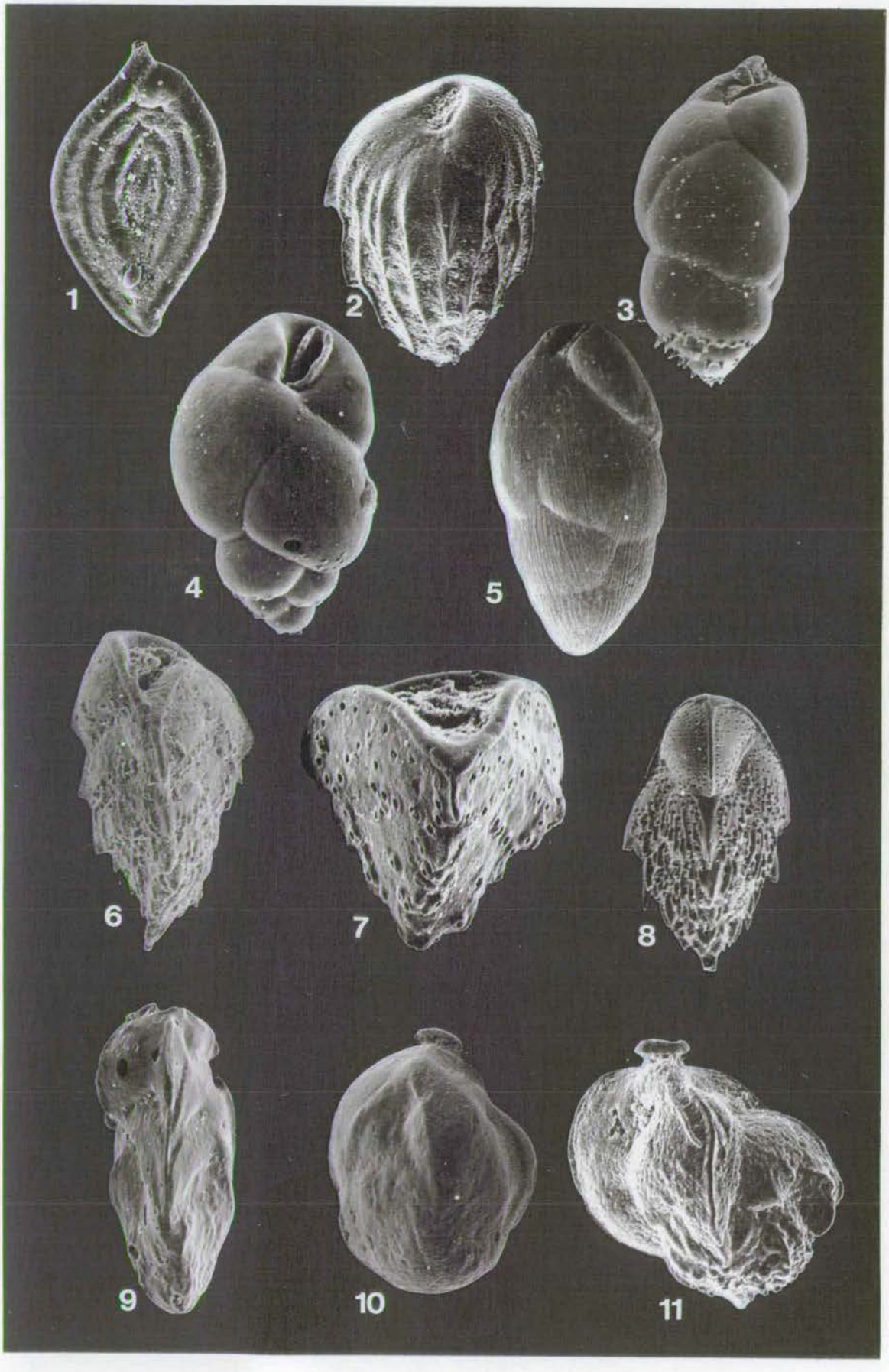

Plate 3·5

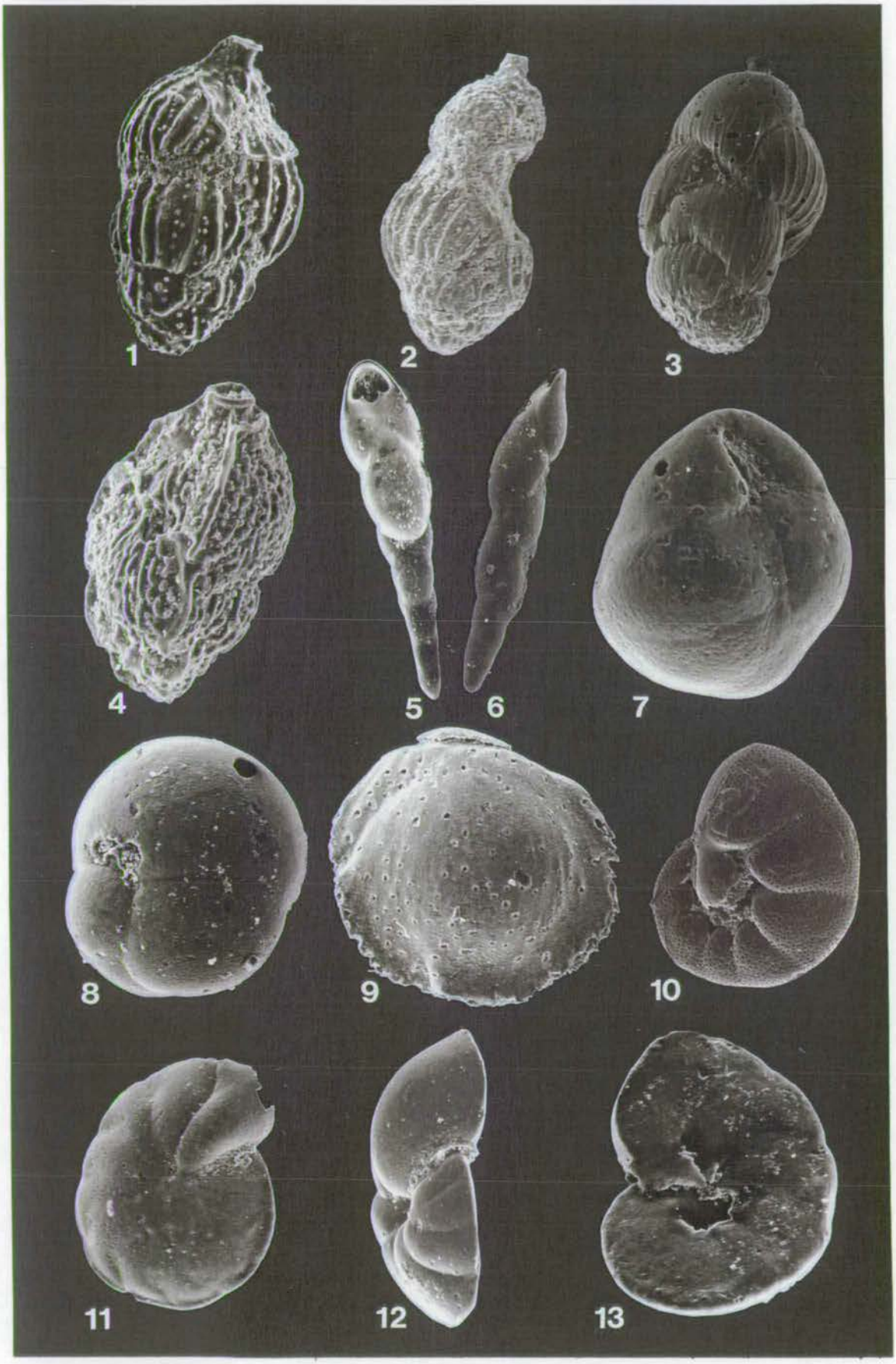

Plate 3·6

Plate 3·7

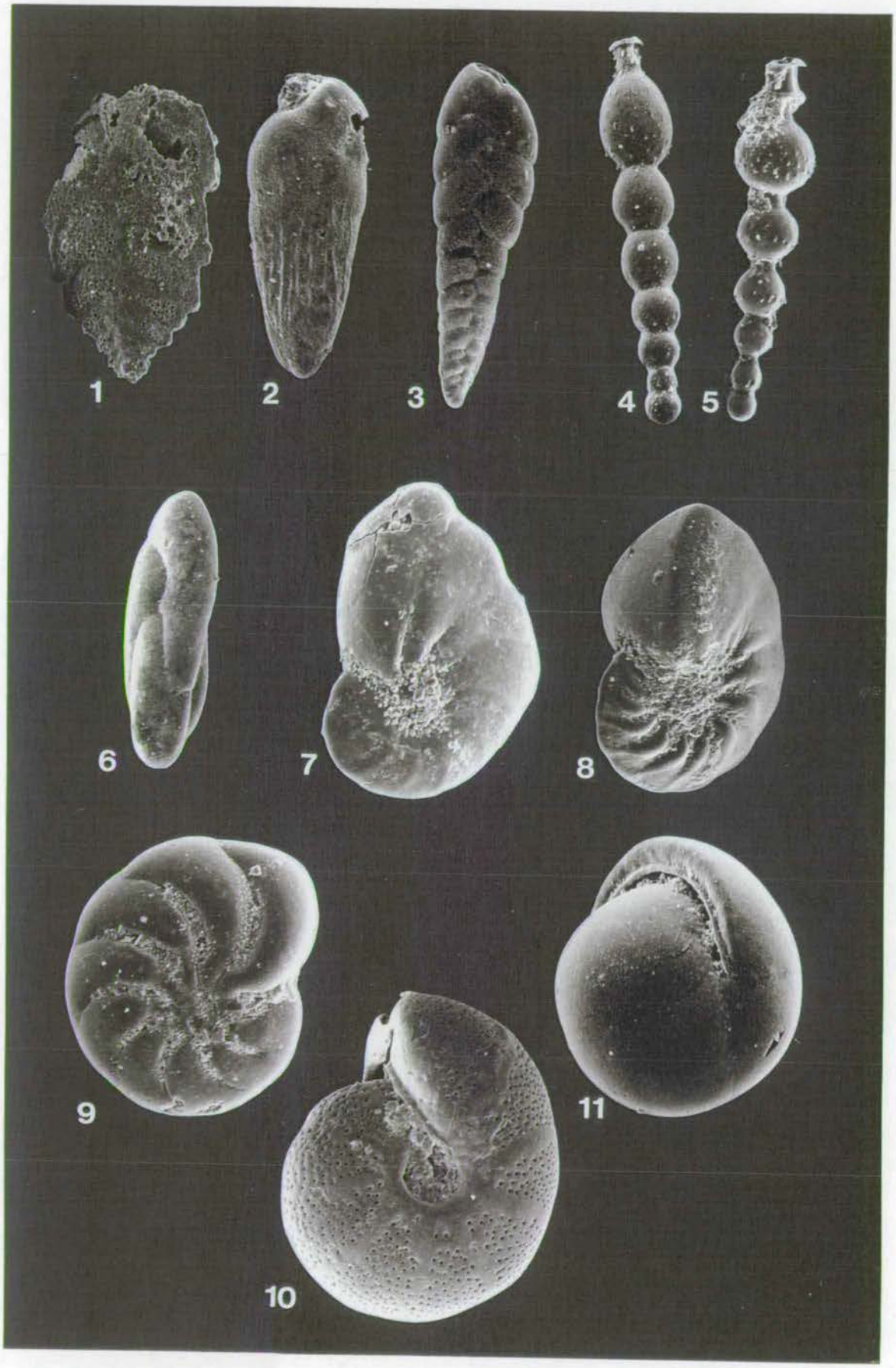

Plate 3·8

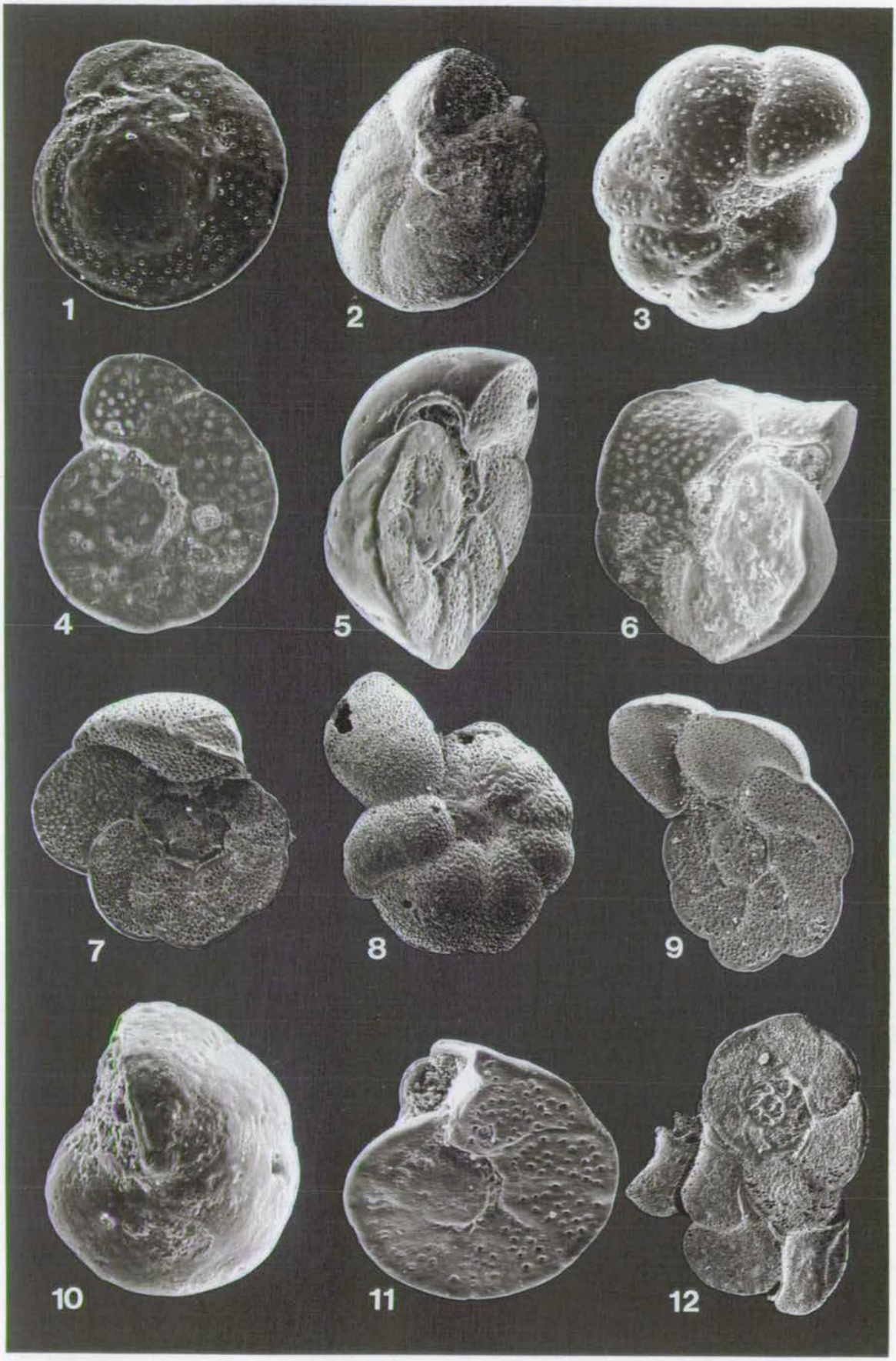

Plate 3·9

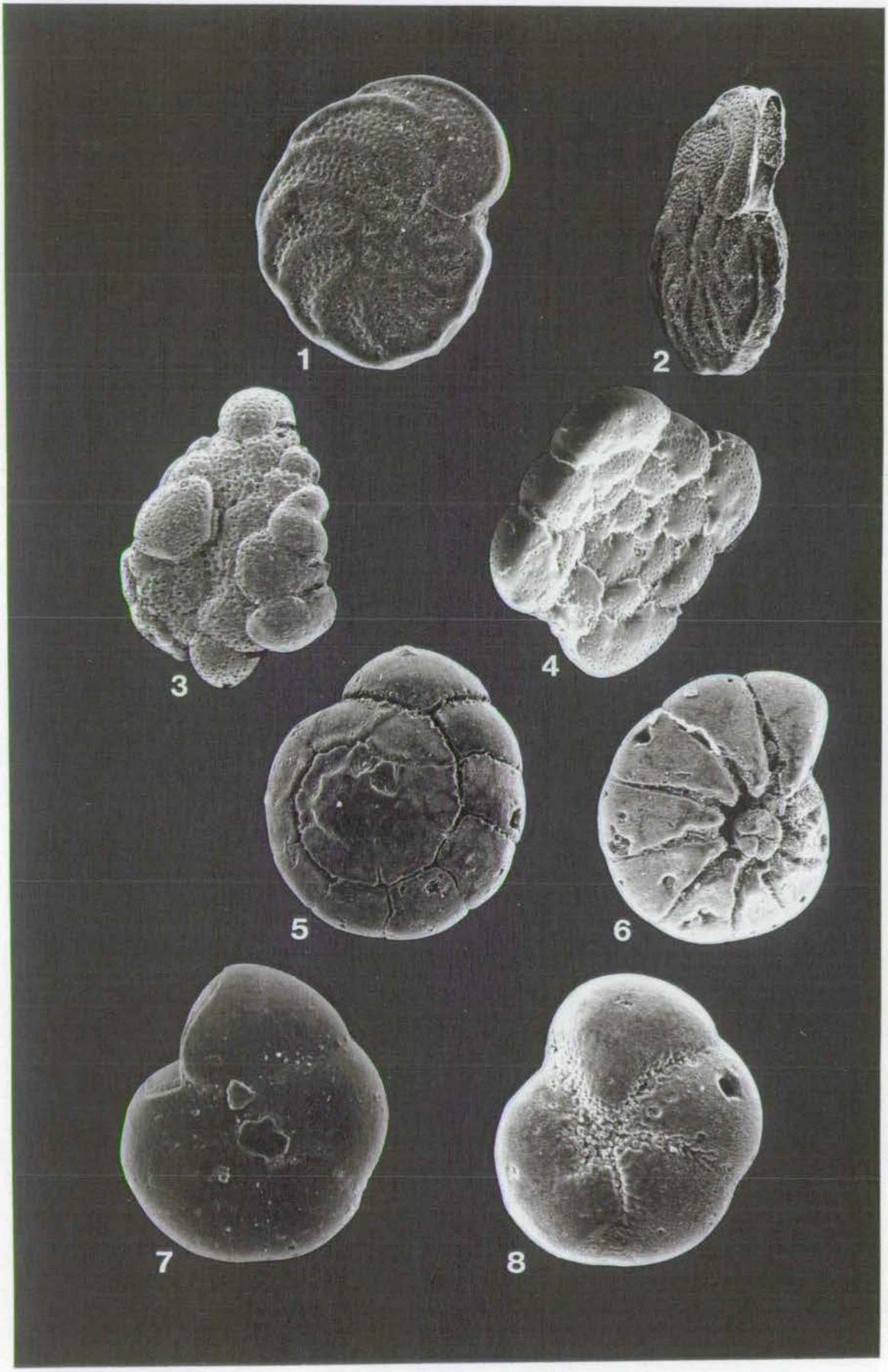

Plate 3·10

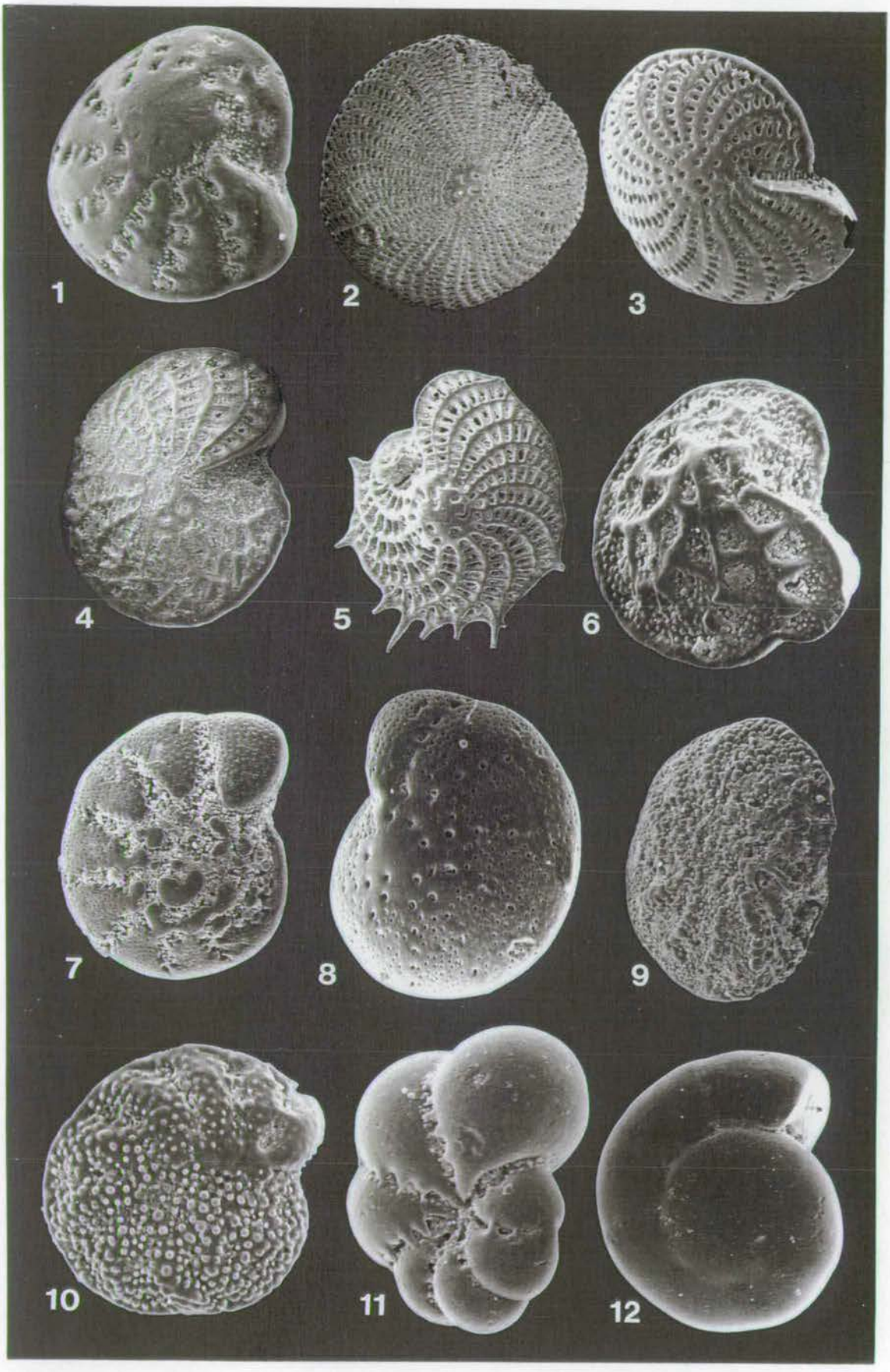

Plate 3·11

In the Aksu basin the lowest exposure of the marine section is beside the canal along the lower part of the Pliocene terrace from Aksu to Yenimahalle via Yurtpinar and Guloluk. The sediment, just as at Manavgat, is a blue-grey silt with sparse macrofossils. Channels approximately 5m in width are exposed along the canal section (Plate 3.3E), in the main cliff section at Yenimahalle and also near Sarivak to the north of Gebiz. Similar to the Manavgat region, these lower blue marls contain only sparse and broken macrofossils. The logged sections pass from the canal section to the terrace plateau (Figs. 3.6 and 3.7). The sections grade from silt-dominated sediment to fine to medium sands. Towards the top of the section these are a rich golden brown colour. The Yurtpinar and Yenimahalle sections are representative of the sequence along the entire terrace front from Aksu to Yenimahalle. The sediments of the terrace scarp are exposed all along the canal section. Channelisation, lenticular sands, shell concentrations and soft-sediment deformation have all been observed in the blue-grey silts of the section. Where roads pass from the lower level up to the Pliocene terrace level, sedimentary features in the upper sands can also be observed. The changing sedimentary characteristics of the logs are shown by the Yurtpinar and Yenimahalle sections. The most visual feature is the increase in shell size and concentration up section, in conjunction with a change from blue-grey silts to orange-brown sands. Petrographically, all sections are immature. The lowermost sections (Yu5/92b, Yu9/92b, YU11/92b, YU20/92b, Yu24/92b, Ye3/92b, Ye14/92b) are classified as a lithic greywacke (Folk, 1974; Pettijohn, 1975) or a clayey siltstone (Picard, 1971) (Plate 3.13A) and contain angular grains, 0.1-0.25 mm in size, of quartz, plagioclase, calcite, chert, biotite, muscovite, opaques, chlorite, mudstone and organic material plus pelagic and benthic forams, and occasional thin shell fragments. The clay matrix makes up between 50% and 70% of these samples. In addition, Yu24/92b which came from a bed with a particularly rich blue colour and contains biotite flakes, muscovite and green pyroxene. The sandier sections (Yu31/92b, Yu34/92b, Ye16/92b, Ye18/92b, Ma10/92b Ma12/92b and Ma14/92b) are classified as litharenite (Folk, 1974; Pettijohn, 1975) or as sandstone (Picard 1971) (Plate 3.13B). They contain moderately sorted, subangular and subrounded grains, 0.5mm in size, of chert, quartz, calcite, plagioclase, and mudstone. Biogenic components include benthic forams, shell fragments and echinoid spines. Original porosity was of the order of 30% and is now infilled by a coarsely crystalline calcite cement. This only applies to the samples collected for thin-sectioning, as the majority of sediment is unconsolidated. Sample Ye20/92b is a claystone, with a high percentage of organic material, and sample Ma11/92b is a calcite cemented claystone.

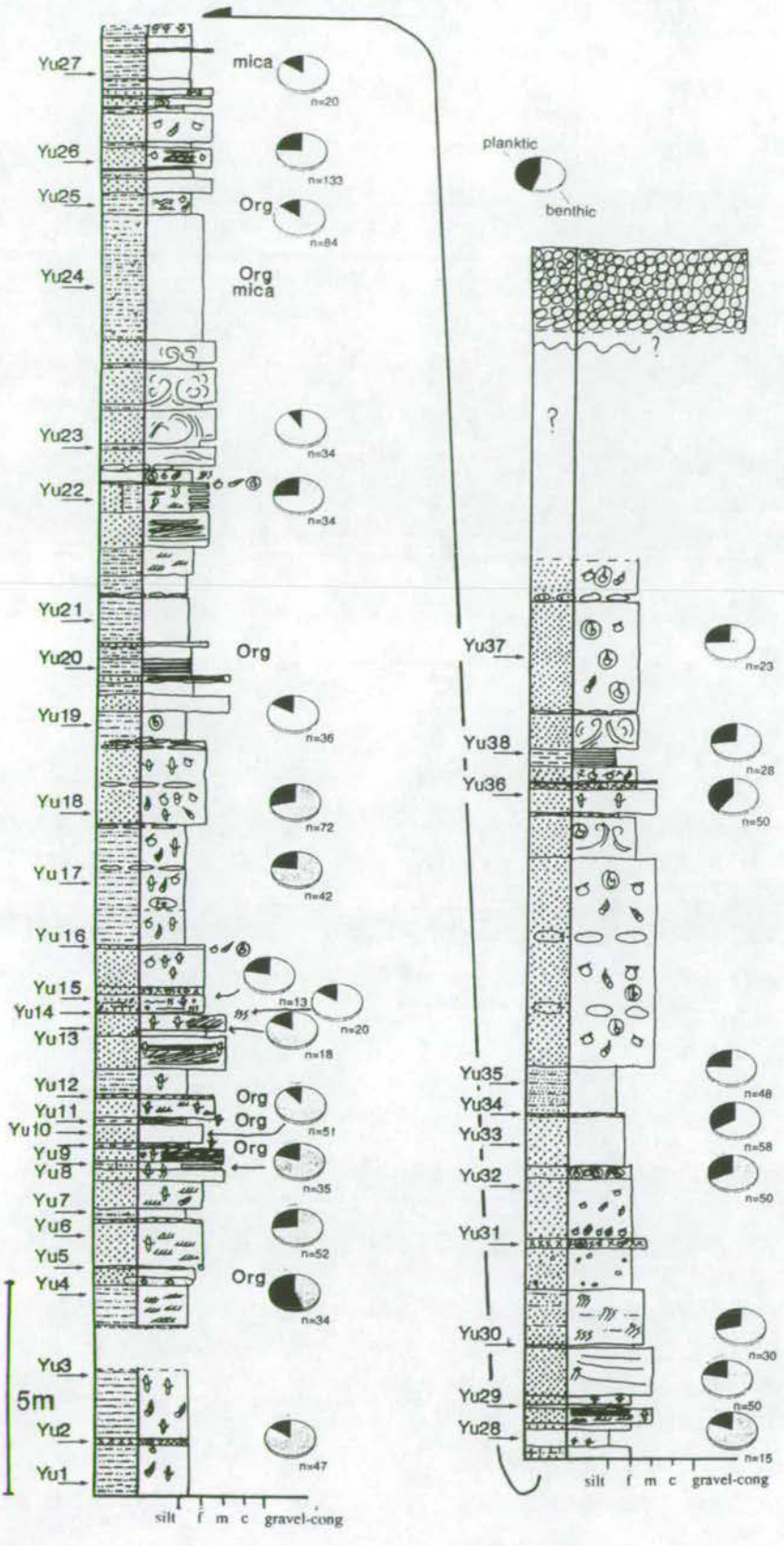

Fig. 3.6: Sedimentary log of the Yurtpinar section. Sample localities are indicated on the left-hand side of the log. Pie-charts are representative of Planktic/Benthic ratios.

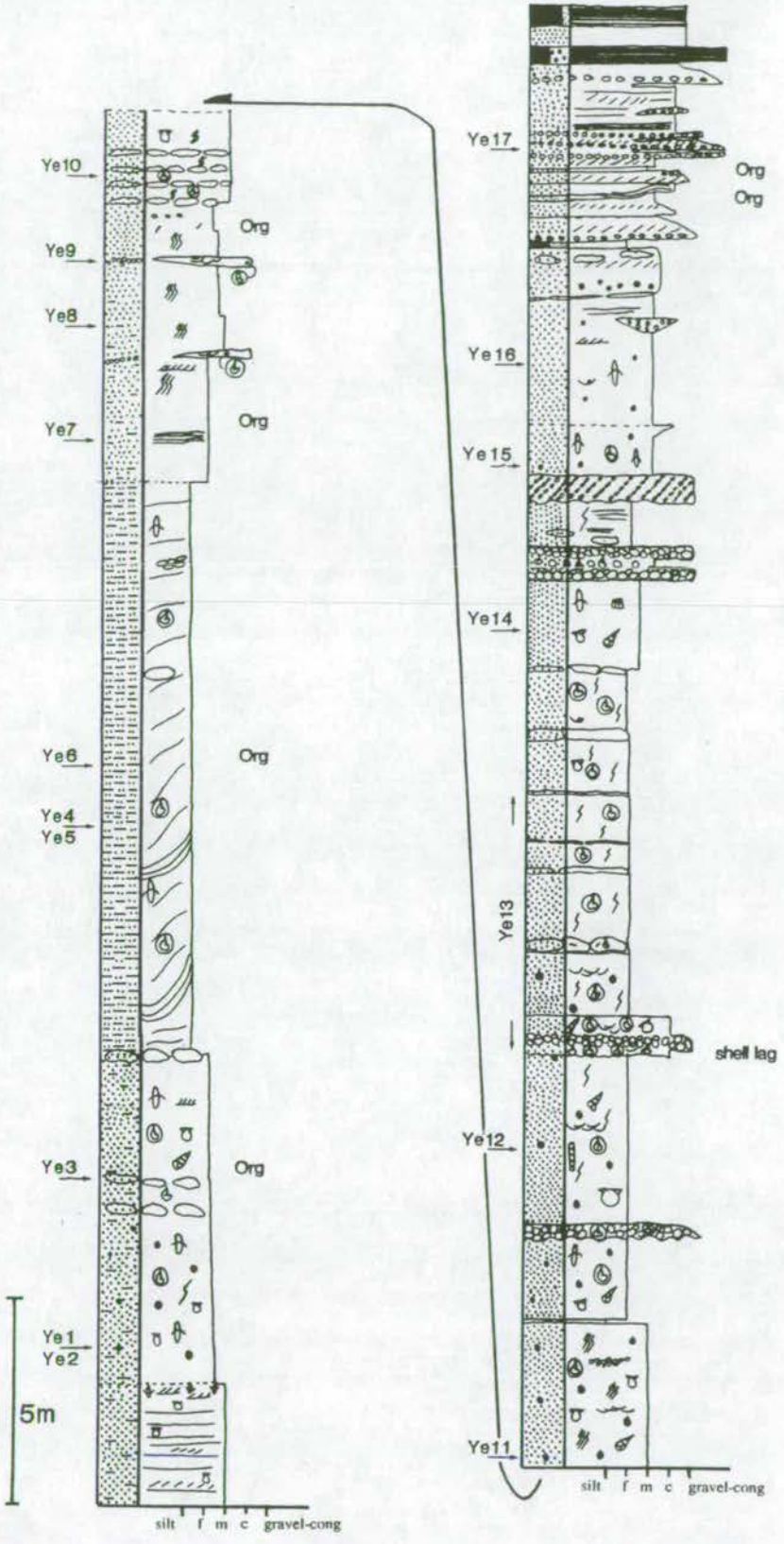

Fig 3.7. Sedimenatry log of the Yenimahalle section, located along the road from Aksu to Isparta. Samples are marked on the left-hand side of the log.

Macrofossils were identified using Davies (1935), Murray (1985), and Boardman, Cheetham and Rowell (1987). Macrofossils present within the sections and the sands in general include:

Bivalves: *Acanthocardia echinata*, *Acanthocardia edule*, *Anadara* sp., *Cerastoderma edule*, *Circumphalus foliaceolomellosa*, *Crassostrea* sp., *Glycymenis* sp., *Ostrea* sp., *Paphia* sp. *(large)*, *Pecten* spp., *Psammobia* sp. and *Solen* sp.
Scaphopods: *Dentalis* cf. *elephantium* and *Antalis* sp.
Gastropods: *Apporhais pesceliani*, *Appollon* (*Aspa*) cf. *marginatus*, *Buccinum* spp., *Cerithium* sp., *Conus mediterrinensis*, *Drupa* cf. *arachnoides*, *Fusinus* spp., *Galeodea* (*Cassidaria*) spp., *Gibbula* sp., *Littorina* sp., *Mitra* sp., *Murex* spp., *Natica* sp., *Turitella communis*, *Turitella* spp., *Turricula* sp., and *Turris* sp.
Miscellaneous: *Balanus crenatus*, Serpulids, *Cladicora* sp. (reworked, one sample only). Bryozoa, annelids, sponge spicules (tetracts with rays not at 90°, probably demospongea), and echinoid test fragments are also present.

Burrows also increase up-section, although in many cases weathering does not enable identification. Typical burrows are those of *Skolithos*, *Chondrites*, *Thalassanoides*, *Rind burrows*, *Scoyenia* and *Planolites* (Plate 3.12). General bioturbation and destruction of sedimentary features is also common, particularly in the lower parts of the section. Where bedding features are preserved low-angle cross-bedding, trough cross-bedding, and parallel lamination are present. In the Yenimahalle and Aksu marine sections (Fig. 3.8) the uppermost part of the section shows ripple lamination in places. Sediment dewatering on the scale of 0.5m- to 1m-thick disrupted beds is also a common feature of the upper parts of these sections. Gravel lenses are common in the upper part of the Yenimahalle section (Plate 3.13E) and towards the very top, poor soil horizons are developed. The uppermost part of the Yenimahalle section must thus be considered as the Çalkaya Formation (Plate 3.13F). Occasional blackened wood fragments are also found within the sequences.

The microfossil content of the entire Yurtpinar section is very different to the Manavgat section. Planktic/Benthic ratios (displayed as pie charts in Fig. 3.6) are generally between 0.15 and 0.5 (with one exception) and are dominated by the benthic species: *Ammonia* spp., *Bolivina* spp., *Cancris oblongus*, *Cibicides* spp., *Elphidium* spp., *Haynesia depressula*, *Neoconorbina terquem*, *Nonion* sp. and *Planorbulina mediterrenensis* (Appendix 1).

Plate 3.12: Burrows in the upper sands.
A) Skolithos. **B)** Rind burrows. **C)** Chondrites. **D)** Planolites. **E)** Thalassoinides. **F)** Shrimp burrow?.

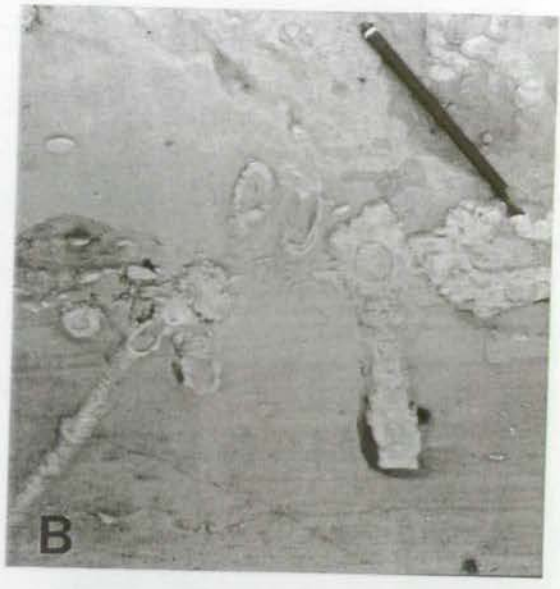

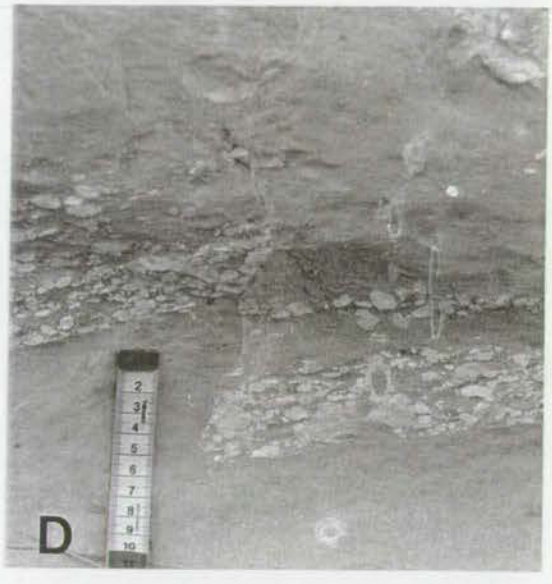

Plate 3·12

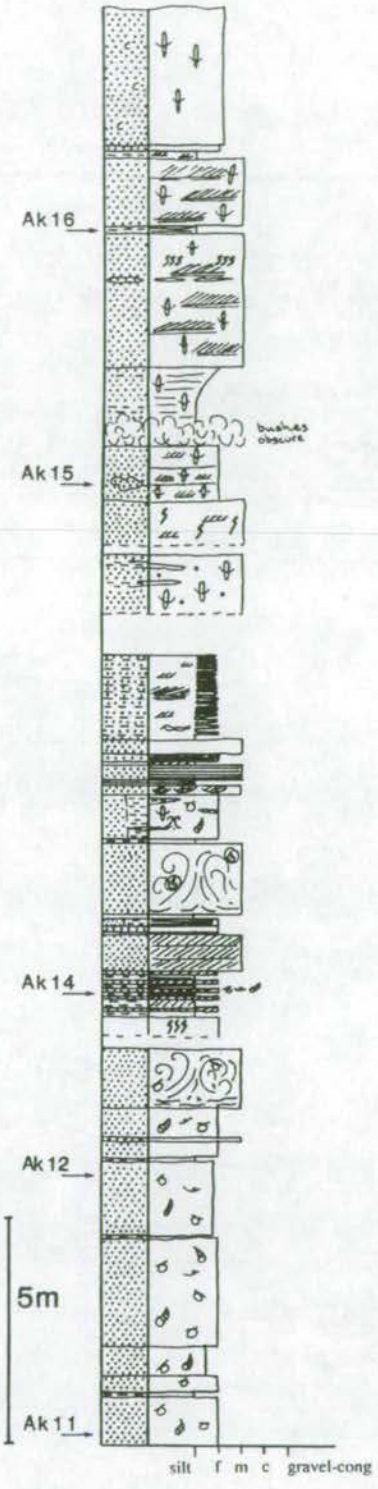

Fig: 3.8: Sedimentary log of the marine Pliocene section near Aksu. Samples are marked on the left-hand side of the log.

3.5.1: Pliocene around Sarivak and Kayrak

In the Gebiz region and to the north-west of Gebiz around Sarivak and Kayrak, the sediments are assigned to the Yenimahalle Formation. The sedimentary log (Fig. 3.9) from a quarry just south of Gebiz shows this well: marine silts with a normal Pliocene macrofauna grade up to sands displaying trough cross-bedding, burrows, ripples and conglomerate channels. Along the road to Haciosmanlar, Pliocene sediments are observed. Interbedded sandstones and marls contain reworked *Cladicora* corals, gastropods, bivalves, oysters, scaphopods and wood fragments. Scattered pebbles and pebble lenses are more common in this northern area. The sands themselves are cross-bedded or parallel laminated. Fining-upwards sand channels and channelised conglomerates are present, as well as thicker conglomerate successions. Conglomerate clasts can reach up to 30cm in diameter. Just before Haciosmanlar itself, these Pliocene sediments pass down into Mesozoic sediments. The contact is not observed.

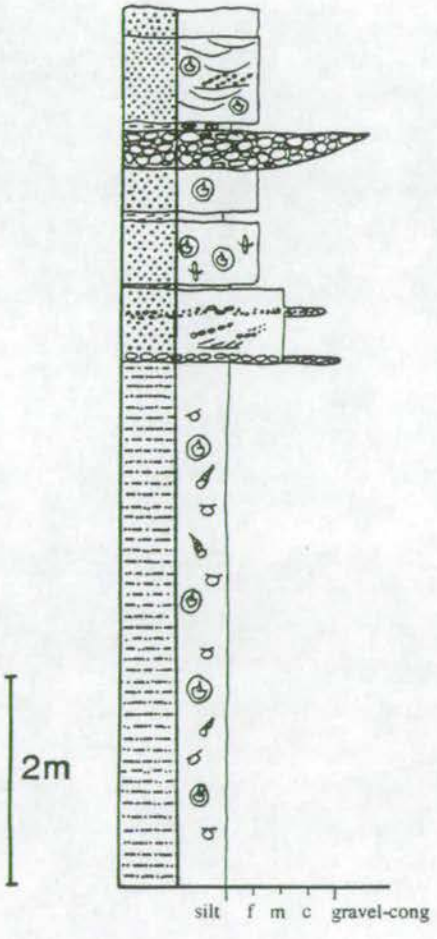

Fig. 3.9: Log of the marine Pliocene near Gebiz.

In the Kayrak area, Pliocene sediments are observed along the water course. These sediments dip to about 20° and contain a typical marine Pliocene macrofauna, soft-sediment deformation structures, and pebbles. Just beyond Kayrak village itself Miocene turbidites are deformed to vertical. The Pliocene, thus, onlaps the Miocene approximately at Kayrak village.

As discussed in chapter 2, no evidence of the basal conglomerates described as the Eskiköy Formation (Akay and Uysal, 1985) is recognised in this area.

3.6: Çalkaya Formation

The Çalkaya Formation is the uppermost 20m of the marine Pliocene. It crops out over much of the upper part of the Pliocene terrace and is gradational with the underlying marine silts and sands of the Yenimahalle Formation. Marine and marginal marine and subaerial deposits are interbedded in the southern part of the basin. Marine sands are interbedded with marine conglomerates, tuffs, brackish water facies, soils and coals which often occur as lenticular bodies. Each of these facies will be discussed in turn. In the northern part of the basin the Çalkaya Formation consists of fluvial conglomerates.

The marine Pliocene has been mapped in the Aksu and Çalkaya area (Fig. 3.10). The Yenimahalle Formation forms the lower part of the sequence, exposed in the valleys and along the terrace edge, while the Çalkaya Formation is exposed on the terrace plateau. A number of sedimentary logs from the Aksu section and the Çalkaya area demonstrate the relationships between the various facies types (Figs. 3.11 and 3.12). Most contacts appear to be stratigraphic. It is unfortunate that the lower contact of the Çalkaya tuff is not exposed.

3.6.1: Sands

Much of the Çalkaya Formation consists of sands indistinguishable from the upper sands of the Yenimahalle Formation and containing the same fossil assemblage. In one of these sands a *Murex* sp. gastropod was found 7cm in height. In general, the marine gastropods and bivalves in the Çalkaya Formation are larger than their counterparts in the upper part of the Yenimahalle formation. Many are found in life position. Sedimentary structures include symmetrical ripples, low-angle cross-bedding (Plate 3.13C), trough cross-bedding (Plate3.13D), mud drapes, ripple lamination and shell lags. In the Çalkaya area, hummocky-cross stratification is seen. Plant fragments are relatively common. Burrows include *Skolithos* and *Thalassanoides*. The sands are interpreted as shallow marine sands, sometimes subject to storm activity.

Plate 3.13:
A) Photomicrograph of blue-grey silts. Field of view 7mm x 7.5mm. **B)** Photomicrograph of sands Field of view 7mm x 7.5mm. **C)** Cross-bedding within upper Yenimahalle Formation sands. **D** Trough cross-bedding in the Çalkaya Formation. **E)** Lenticular conglomerate body in sands in th Çalkaya Formation. **F)** Lenticular conglomerates and sands in the Çalkaya Formation.

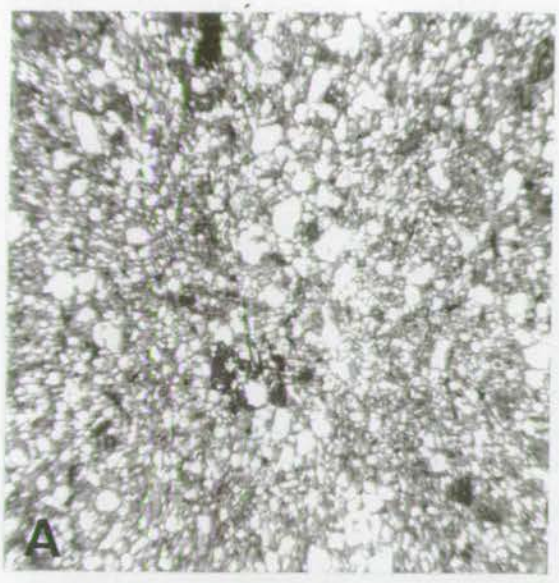

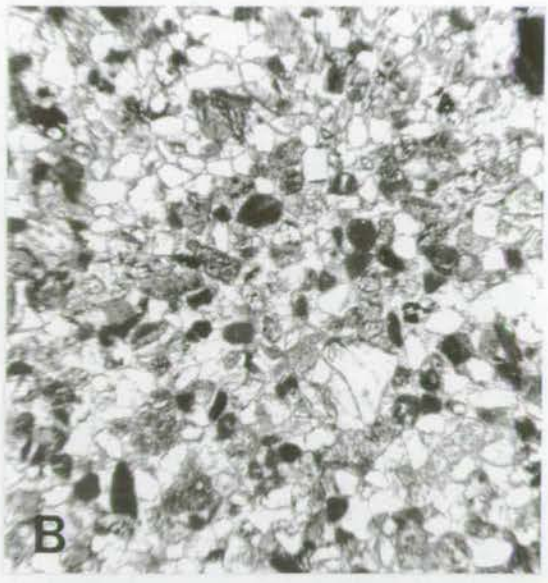

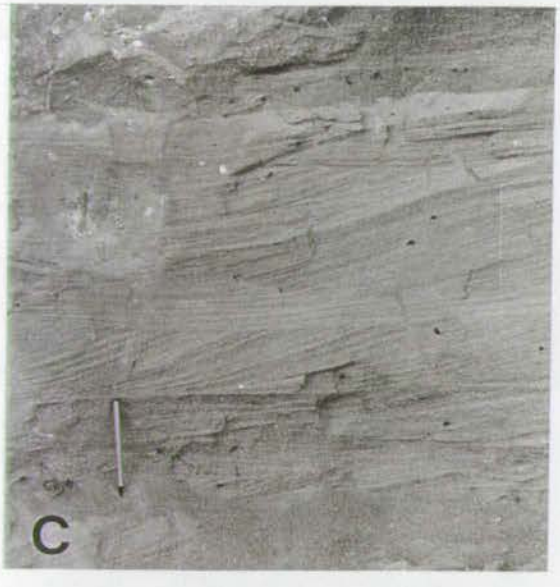

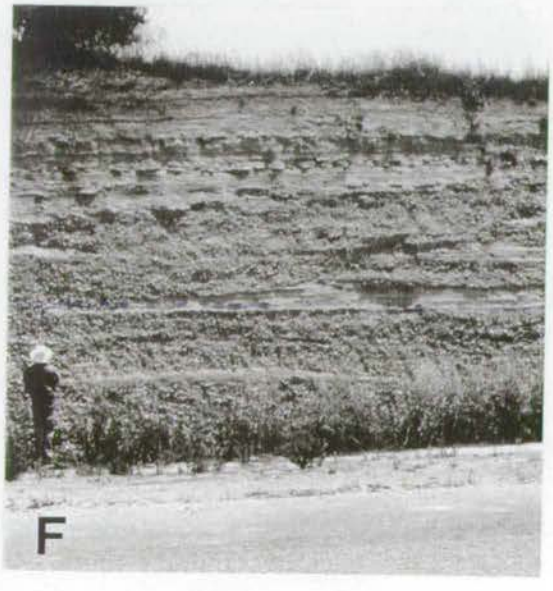

Plate 3·13

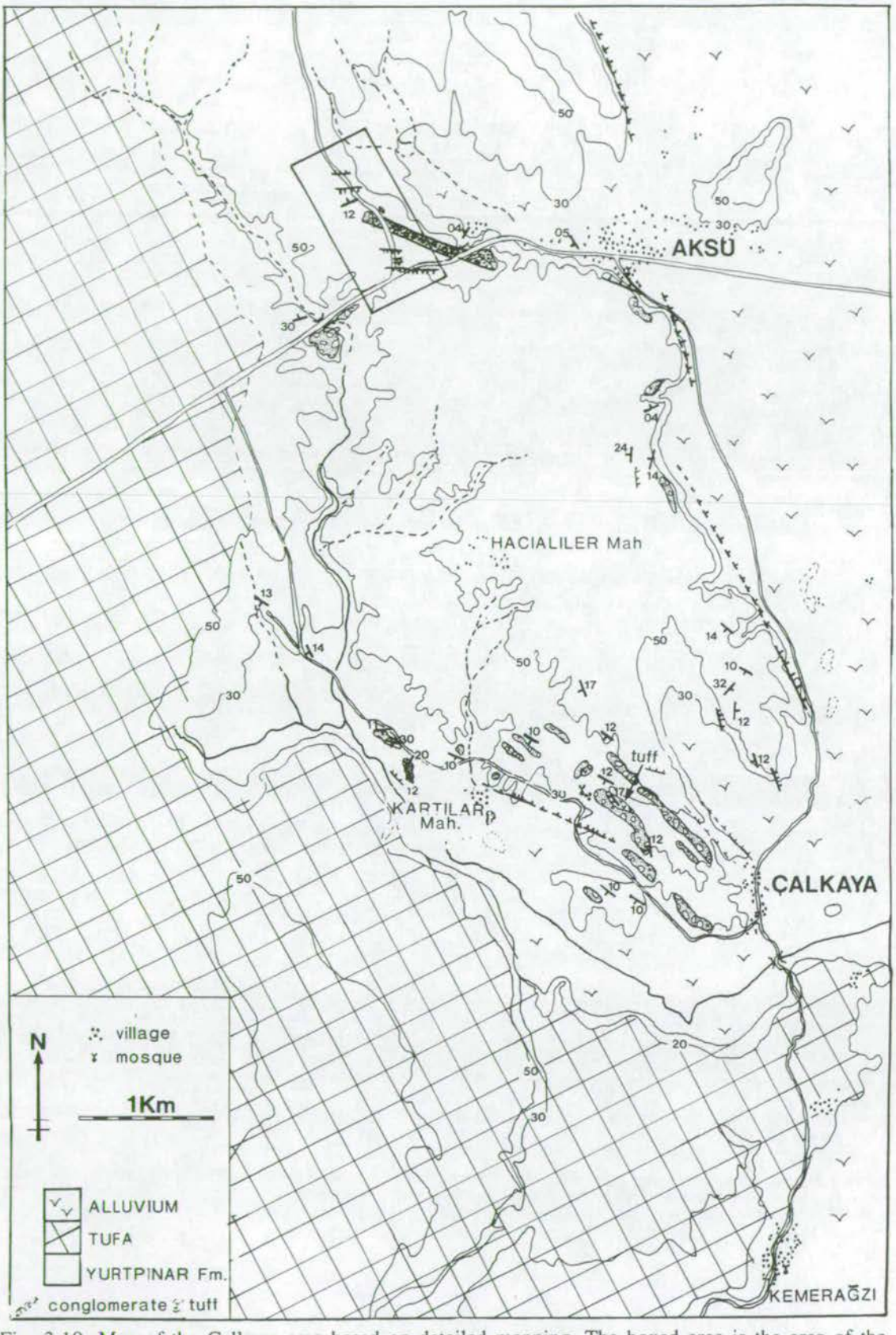

Fig. 3.10: Map of the Çalkaya area based on detailed mapping. The boxed area is the area of the detailed map in Fig. 3.18.

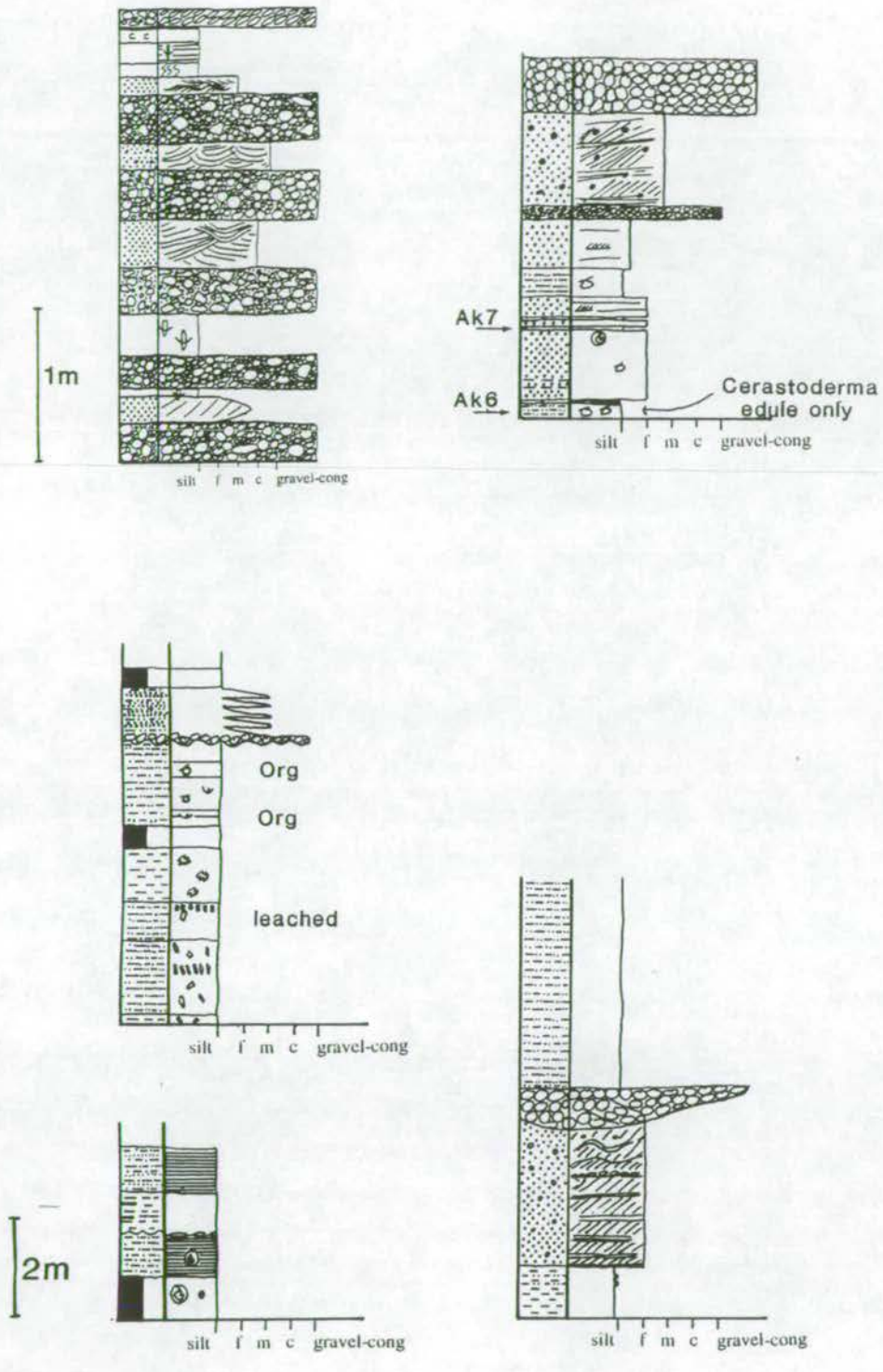

Fig. 3.11: Logs from the Aksu area. These logs were measured on the new road cuttings during construction of the bridge just to the west of Aksu.

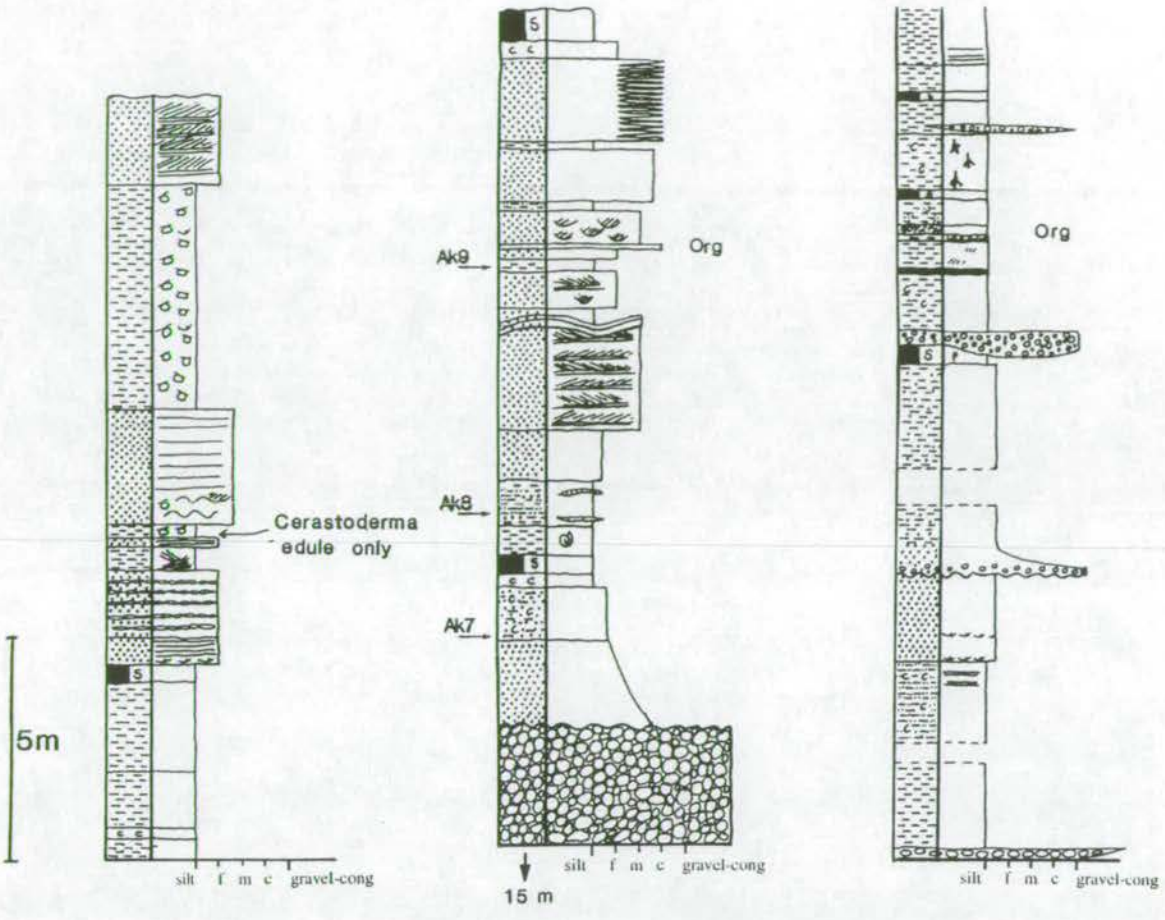

Fig. 3.12: Logs from the Aksu area. These logs were measured on the new road cuttings during construction of the bridge just to the west of Aksu.

3.6.2: Conglomerates

Conglomerates crop out as topographic ridges and map out as elongate bodies, parallel to bedding. The beds are several metres thick and often cross bedded (Plate 3.14 A,B). Clast-imbrication data and provenance were collected from these thick conglomerate bodies. Similar, locally thick conglomerate deposits are formed in areas such as Kursunlu and Yesilkaraman and crop out along the main road to Yenimahalle. In appearance, these conglomerates are very difficult to distinguish from the Quaternary conglomerates of the Aksu valley. Provenance data (Fig. 3.13) do not allow a distinction to be made between the conglomerates of the Çalkaya Formation and Quaternary fluvial conglomerates (chapter 5). The size distribution shows a median in all conglomerates of between 1-5cm with clasts reaching a maximum size of 12cm.

Plate 3.14:

A) Channelised cross-bedded conglomerates in the Çalkaya Formation. **B)** Cross-bedde conglomerates in the Çalkaya Formation. **C)** Typical Çalkaya Formation marine conglomerate i sandy matrix. Note the bed of smaller clasts at the top of the picture. **D)** Sponge bored pebble in th Çalkaya Formation conglomerates. A cerastoderma shell appears in the matrix just above and right o the tape measure. **E)** Sponge bored pebbles and pebble encrusted with barnacles in the Çalkay Formation. **F)** Oysters (cf *Pododesmus* sp.) encrusting a pebble in the Çalkaya Formation.

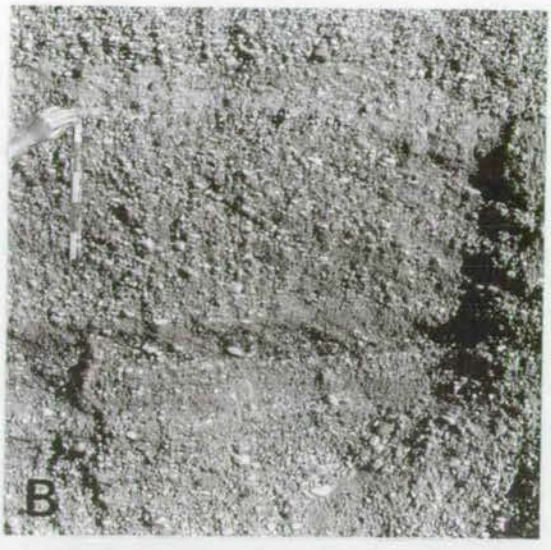

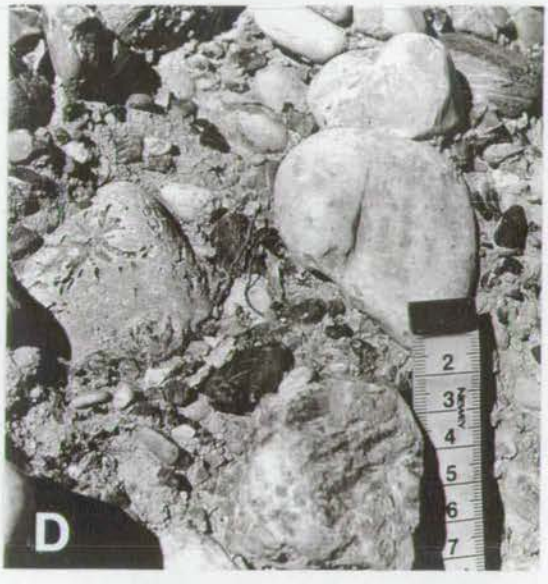

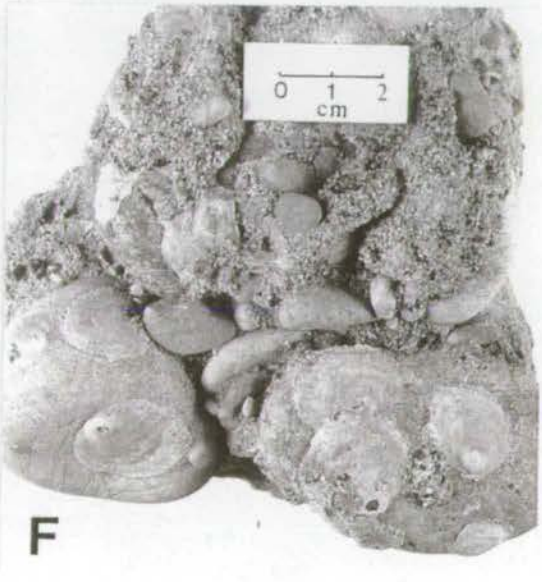

Plate 3·14

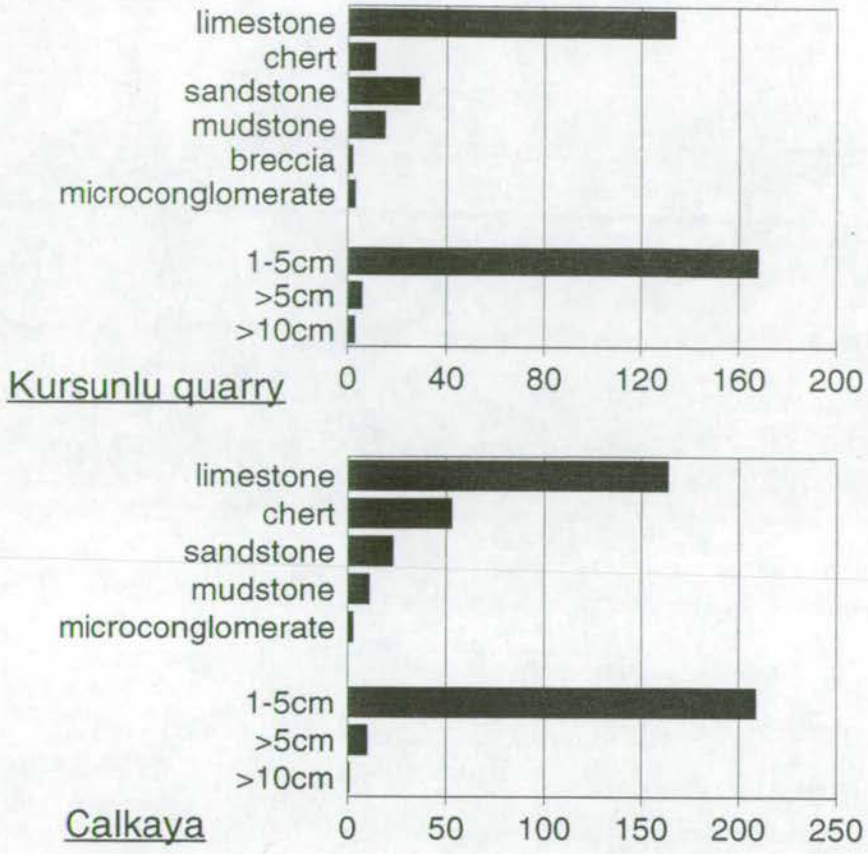

Fig. 3.13: Two examples of provenance data from Çalkaya Formation conglomerates.

The conglomerates are dominated by limestone, the other principal components being chert, sandstone and mudstone (Plate 3.14C). Pumice clasts were found at only one conglomerate locality, in the Çalkaya area. A number of rare features do allow the Çalkaya Formation conglomerates to be differentiated from the Quaternary conglomerates. It is possible to find in many of the outcrops bored pebbles, primarily sponge borings (Plate 3.14D), but occasionally bivalve borings. *Balanus* sp. have been found attached to one pebble (Plate 3.14E). In some of the conglomerates attached bivalves (cf *Pododesmus* sp.) occur in life position attached to limestone pebbles within the conglomerate (Plate 3.14F). Very rare marine shells can also be found within the matrix of the conglomerate. The conglomerates are usually bimodal, with matrix varying between 10% and 50% and may be silt-coarse sand. In some of the conglomerates, partial cementation has occurred with slight dissolution of limestone clasts and small quantities of calcite cement forming around pebble edges. This is, however, not a widespread or significant phenomena. The conglomerates often contain thin lenticular sand bodies, particularly in the more

northern area (a typical example is 1m x 13m). Thin, tabular beds and small lenticular deposits of conglomerate and gravel are frequently interbedded with the sands.

The presence of bored pebbles, encrusted oysters, *Balanus* sp. and shells in the sandy matrix of these conglomerates confirm that deposition occurred in a marine environment. While faunal evidence is the best evidence for the marine deposition of conglomerates, other distinguishing characteristics have been discussed in the literature. The sorting of pebbles into oblate, disc and rounded pebbles (Bluck, 1967) can be used to distinguish zones in the nearshore and shoreface environment However, as Bluck (1967) recognised, the pebble shapes are only sorted in the beach environment and are not produced there. In the Antalya region the pebbles are all naturally rounded in shape and, therefore, this theory cannot be applied. This natural rounding of pebbles creates difficulty with palaeocurrent measurements from clast imbrication. Measurements were not able to be taken from single bed sets, but were taken from imbricated clasts over a large outcrop. This does have the advantage of providing longer-term, more general data than that provided by a bed representing a single event. Palaeocurrent data are included on the map in Fig. 3.1, but are often ambiguous. In general, the conglomerates show a mixture of onshore, offshore and longshore current activity, assuming that the coastline was approximately parallel to the present-day coastline. Clifton (1973) showed that a combination of good pebble segregation and low lenticularity are qualitative indicators of wave-worked conglomerates. The Çalkaya Formation conglomerates conform to this observation, with pebbles occuring as tabular bodies within sands. Small lenticular bodies of pebbles may also be found within well-sorted sands. These are interpreted as lag concentrations within the lower shoreface zone, possibly a result of accumulation in hollows or as storm deposits (Bougeois and Leithold, 1984; Kumar and Sanders, 1976). Well preserved symmetrical ripples of gravel covered by fine matrix suggest an upper shoreface environment (Bougeois and Leithold, 1984) (Plate 3.15A). The large mapped outcrops of cross-stratified conglomerates are interpreted as migrating bars. Channelised conglomerates are also recognised. These may contain sand bars. (Plate 3.15B).

3.6.3: Brackish-water facies

In some of the sections of the Aksu area it can be seen that some beds contain a restricted fauna of either thin-shelled oysters or *Cerastoderma edule*. These are interpreted as brackish-water deposits.

Plate 3.15:

A) Large-scale symmetrical ripples in gravel in the Çalkaya Formation. **B)** Sand bar in thick conglomerate body in the Çalkaya Formation. **C)** Small symmetrical sand ripples draped by white clay in the Çalkaya Formation. **D)** Palaesol in the Çalkaya Formation. **E)** Çalkaya Formation coals near Kursunlu selalesi. **F)** two thin coal layers in the Çalkaya Formation near Çalkaya above the coals are fossiliferous marine sands.

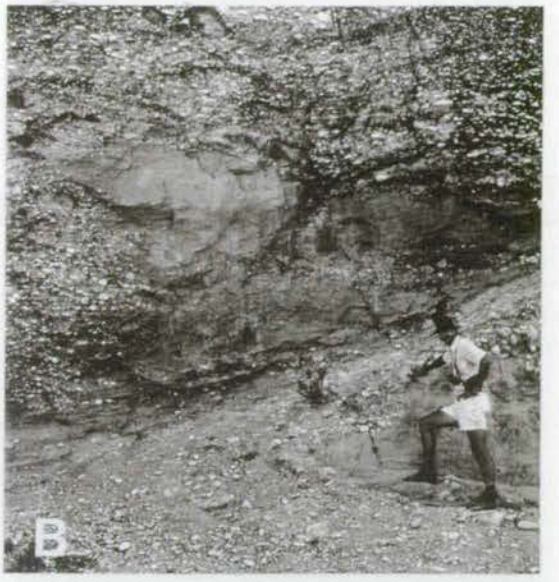

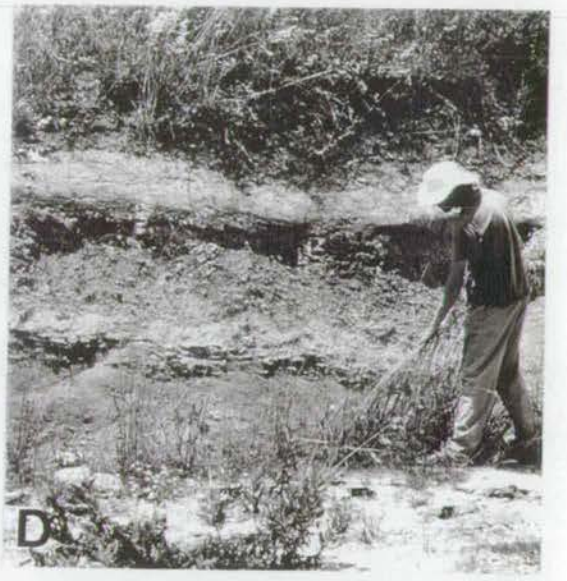

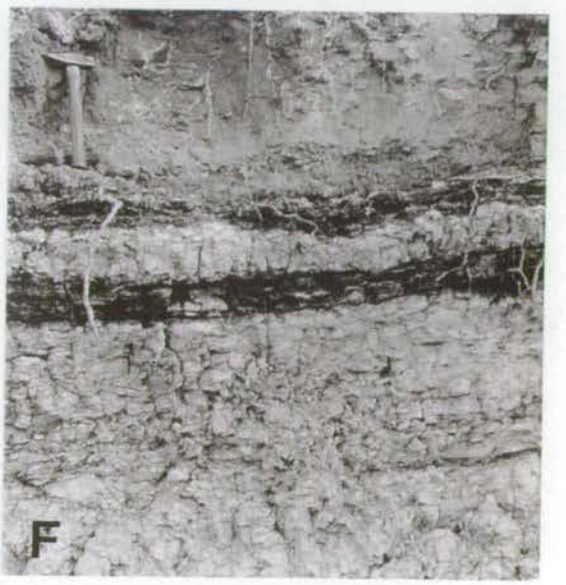

Plate 3·15

3.6.4: White clays

Thin bands of carbonate-rich claystone are observed throughout the Çalkaya Formation. For example, they are found as matrix within conglomerates, as thin beds within sands, draping symmetrical ripples and as thin bands within the Çalkaya tuff section (Plate 3.15C). The thickest clay bed observed was 1m thick and occurred directly above a dark soil with caliche development. In some cases thick sequences of more clayey marls are developed. A good example of this is a new cutting on the main Aksu road in which particularly chalky marls are interbedded with sandy and soil horizons.

Beyond the car park to Kursunlu selalesi a sequence of sands and gravels is locally topped by a carbonate layer containing small flat and pulmonate gastropods.

Carbonate-rich clays in the Dead Sea basin (Frostick and Reid, 1989) are deposited from hypersaline waters in undisturbed pools. It is probable that similar depositional processes occurred in isolated, evaporative seawater lagoons and pools.

It is unclear whether some of the oncolitic limestones on the main Yenimahalle road belong to the lower beds of the tufa deposit or to the Çalkaya Formation. The lack of other deposits of this sort in the Çalkaya Formation has led them to be attributed to the tufa. However, it is possible that the lacustrine carbonates are a part of the Çalkaya Formation.

3.6.5: Soils and coals

Soils and coals are found relatively frequently within the Çalkaya Formation. Typical soils are pale, Brown Mediterranean soils with an upper humic layer about 50cm thick, a visible leached zone and a lower zone of reprecipitation containing caliche nodules. The entire soil profile is generally 1-2m thick (Plate 3.15D).

Coals are well developed at two localities. The thickest coal is found at the conglomerate quarry opposite Kursunlu selalesi (Plate 3.15E). Above 10m of conglomerate is a thick (75cm) layer of flaky brown coal. A 1m-thick bed of silt separates this from a second coal layer, 50cm thick. The coals are not continuous, but form lenticular bodies within the conglomerate. The 20-30cm of conglomerate immediately below the coal is firmly cemented and displays a reddish weathering colour. In the Çalkaya region two 15cm-thick coal bands are separated by 15cm of sands (Plate 3.15F). Below these coal layers are silts containing thin-walled gastropods. Above the coals are some 12m of sand containing a fauna of *Turritella* sp., *Cerastoderma edule*, bivalves, oysters, pecten, *Cladicora*-type coral, serpulids, and bored pebbles. Small quantities of coal were also seen in other localities, for example in a pit dug as part of the new bridge in the mapped Aksu area.

The soils and coals were not studied beyond their recognition in the field.

3.6.6: Tuffs

Two significant occurrences of tuff within the Çalkaya Formation are documented.

A pure tuff deposit occurs in the Çalkaya region (Fig. 3.10). Almost 10m of pure tuff grade into a tuffaceous sandstone and finally conglomerate (Fig. 3.14). Bedding is planar, low-angle cross-bedded, wavy or trough cross-bedded and can be defined by sorting into mafic and felsic minerals. Thin, white clay beds occur higher up the sequence. Planar bedding, symmetrical ripples, trough cross-beds, low-angle cross-bedding and convolute bedding/flame structures form the principal sedimentary structures (Plate 3.16A,C-E). Pumice clasts are ubiquitous and locally form channel-fill deposits. Towards the top of the section a soil horizon and a shell bed are present.

The tuff was studied petrographically using a grain mount (Plate 3.16B) from the unconsolidated sediment and a section of pumice clast. Both contain the same mineral assemblage: biotite, green pyroxene, alkali feldspar, plagioclase feldspar, amphibole, sphene, zircon, quartz and opaques. The grainmount also contains lithic fragments, mainly mudstone and carbonate grains. The minerals are unaltered. The groundmass of the pumice clast shows a trachytic texture consisting of small laths of plagioclase with domains of preferred orientation in a dark glassy matrix. The predominant phenocrysts are alkali feldspar, which has both concentric and random zonation, and biotite. X-Ray Diffraction analysis of powdered pumice clasts give the following mineral content: quartz, sanidine, anorthite (minor), augite (aegerine), diopside (hedenbergite), sphene, zircon and apatite. (hydroflouroxyapatite and carbonate-hydroxyapatite). X-Ray Fluoresence analysis of pumice clasts gives very consistent results in both trace and major element analysis. Details of XRD and XRF analysis and full results are given in Appendix 3. A total alkalis versus silica plot (Le Maitre *et al,* 1989) is used to classify the pumice as trachyte (Fig. 3.15).

The trace-element patterns (Fig. 3.16) from the contaminated tuffs at Yenimahalle, the pure tuffs at Çalkaya, and samples collected from Gölçük lake show almost identical patterns.

In the Yesilkaraman region, a channel filled with tuffaceous clastic material and pumice pebbles cuts down into a sandy soil layer (Plate 3.16E). A gravelly point bar can clearly be distinguished at the edge of the channel. A tuffaceous bed is also observed nearby. Petrographically, the pumice pebbles are correlatable with those from the Çalkaya region, containing zoned feldspars and biotite phenocrysts in a trachytic textured groundmass.

Plate 3.16: Çalkaya Tuffs

A) Typical Çalkaya tuff with fine banding and ubiquitous pumice pebbles. **B)** Photomicrograph of pumice pebble. Feldspar, biotite and pyroxene appear in a trachytic matrix. Field of view 4.6mm 5mm. **C)** Symmetrical ripples in the tuff. **D, E)** Water escape structures in the tuff. **F)** Channel nea Yesilkaraman, containing pumice pebbles and volcanic minerals. The channel cuts into soils.

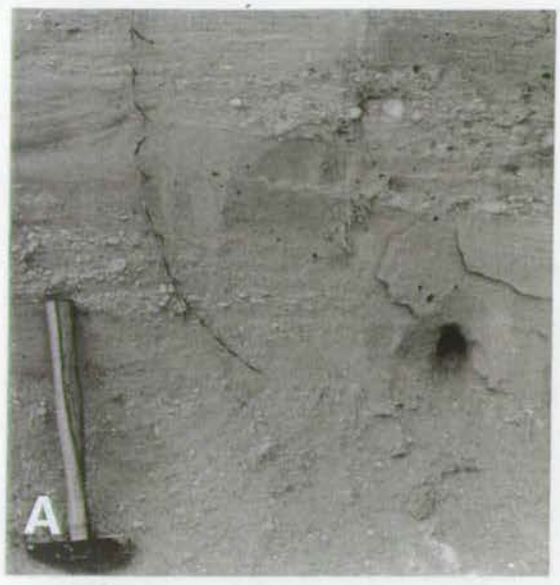

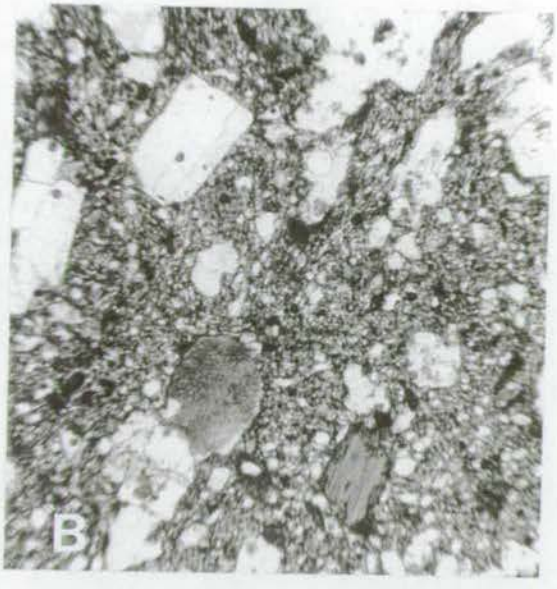

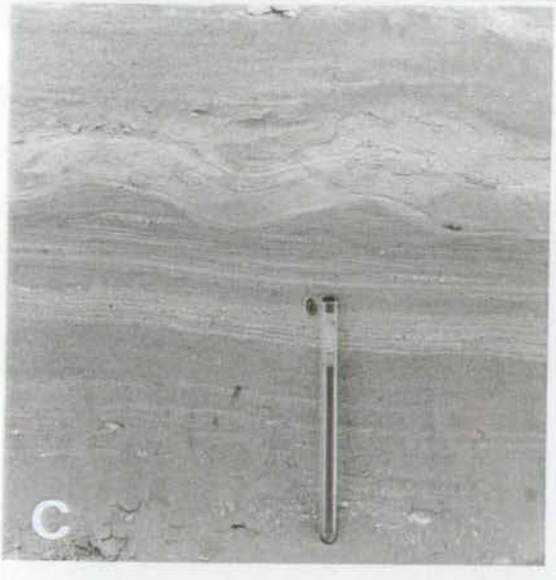

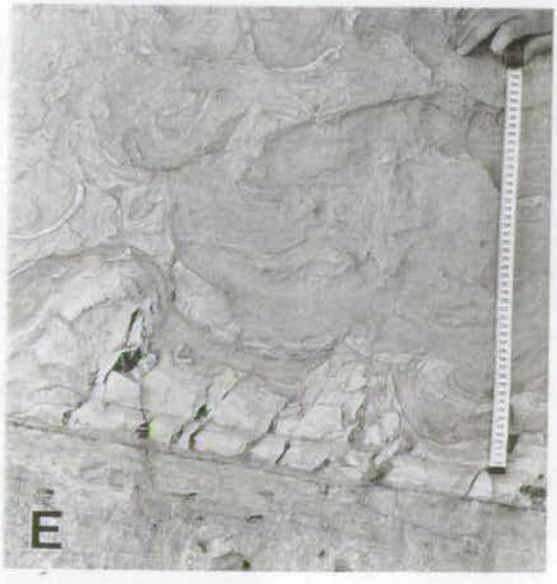

Plate 3·16

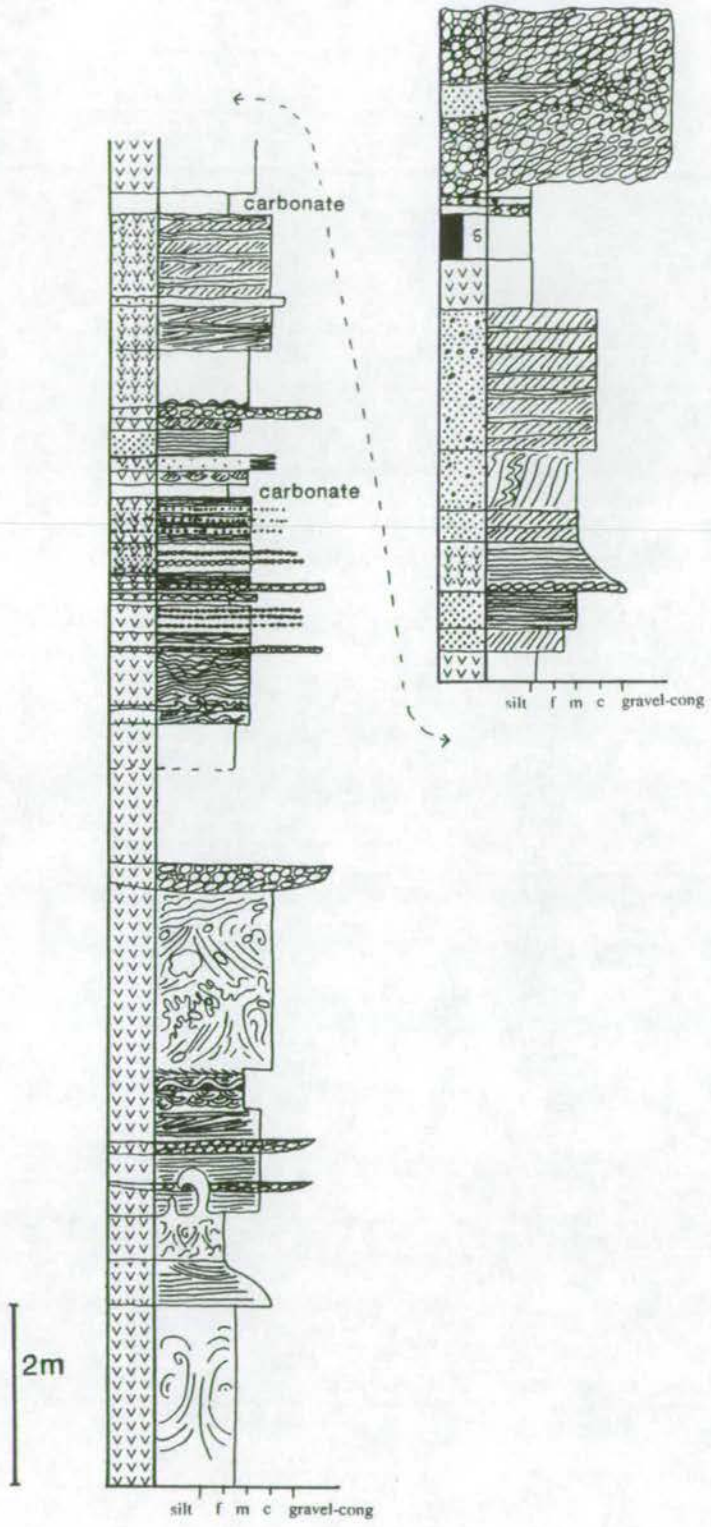

Fig: 3.14: Log of the tuff section near Çalkaya. The exact locality of this section is marked on Fig. 3.9.

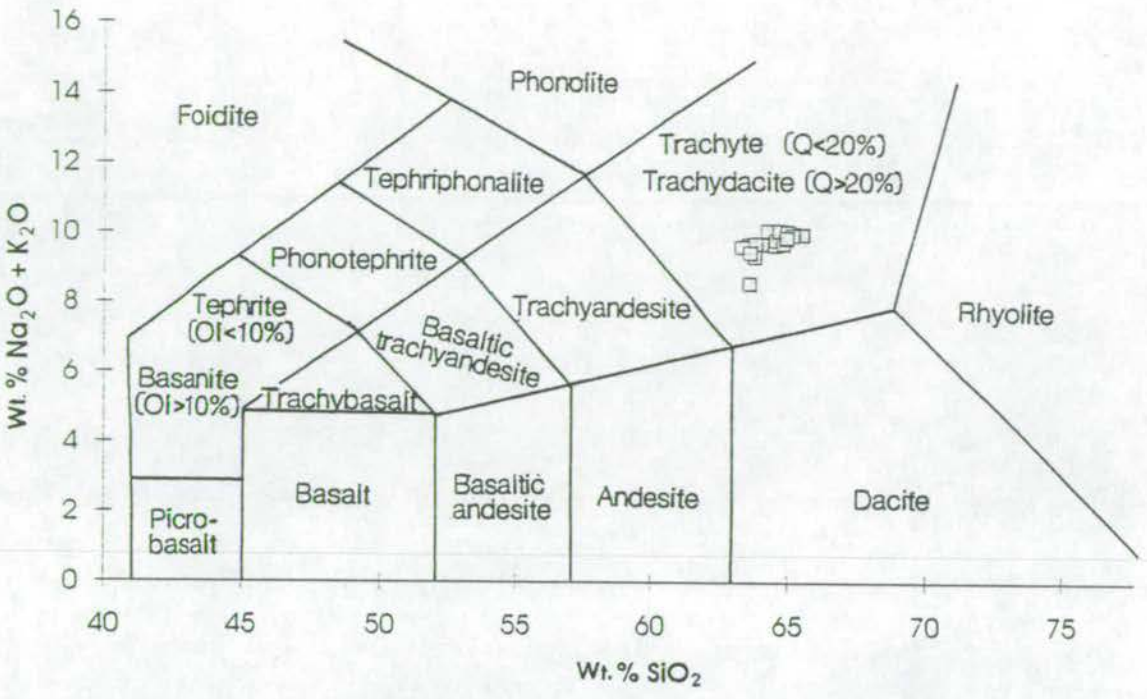

Fig. 3.15: Total alkali versus silica plot for pumice pebbles in the Çalkaya tuff. The pumice pebbles clearly plot in the trachyte field.

Thin sections of the clastic material contain a large number of grains of the trachytic groundmass, in addition to clastic and volcanic mineral grains of quartz, feldspar, biotite, sandstones and muds.

The trachyte composition of the Çalkaya tuff shows that it is the product of a highly differentiated, probably shallow, alkalic magma chamber. These types of magma chamber commonly develop appropriate conditions for explosive pyroclastic eruptions (Fisher and Schminke, 1984). This was also the case for the Isparta ignimbrite (Özgür *et al*, 1990) where trachytes were found to be the final composition in the suite of alkalic eruption deposits. The similarity between the composition of all three deposits suggest a genetic relationship between them. The timing of eruption, however, spans approximately 2Ma (Lefèvre *et al*, 1983; chapter 2). Thus, persistent but localised volcanism due to crystal fractionation appears to have occurred throughout the Early Pliocene.

The Çalkaya tuff deposit is interpreted as the basal surge deposit of a small, shallow, phreatomagmatic eruption (tuff-ring). The term phreatomagmatic is defined, after Fisher and Schminke (1984), as an eruption during which the ascending magma interacts with water. It is known that the Çalkaya tuff deposit was deposited in a marine environment, but this interpretation is made primarily because of the highly localised nature and the sedimentary structures of the deposit.

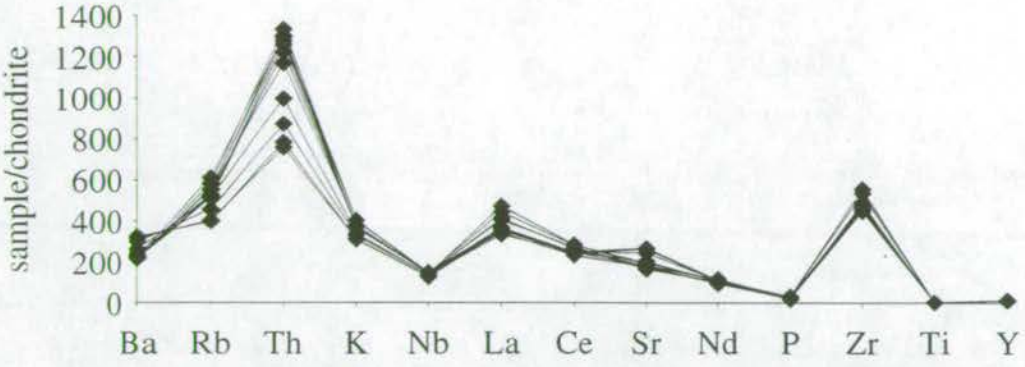

Fig: 3.16: Trace element plot for samples from Gölçük lake, the Çalkaya tuff and the Yesilkaraman channel. Similarity between all samples indicates a similar origin.

In particular, the varied bedforms (planar and sandwave lamination) represent deposition under different flow regimes. The purity of the lower 10m argues against subsequent reworking of the deposit and confirms that the bedforms are primary depositional features. The sedimentary features described are indicative of a phreatomagmatic surge deposit (Fisher and Schminke, 1984). Convolute lamination is probably a result of shear deformation from the overiding surge flow (Fisher and Waters, 1970). Gravity sliding is not seen in this deposit, probably because of its small size. Similar eruptions are probably responsible for the beds containing low concentrations of pyroclastic grains lower in the sequence (Yu24/92b for example). It is probable that this small fragment of the resultant tuff-ring was preserved because of migration of a conglomerate bar over the deposit, protecting it from dispersal. The soil and shell horizon indicate that the upper part of the tuff-ring became subaerially exposed and was subsequently resubmerged. The impure Yesilkaraman tuff is thought to be the result of dispersal of a similar tuff-ring into a clastic channel which retained a significant proportion of tuff in its sediment. This interpretation is consistent with the interpretation of the Isparta ignimbrite as a maar deposit (Lefèvre *et al*, 1983). A maar deposit is defined by Fisher and Schmincke (1984) as a volcanic crater cut into country rock below general ground level and possessing a low rim of coarse- to fine-grained tephra.

3.6.7: Fluvial conglomerates

Beyond the Yenimahalle terrace the sediment sequence is somewhat different. The main road passes through the central Aksu valley crossing the river at Köseler. Before the bridge, the road only cuts through small outcrops of typical marine Pliocene sediment. Either side of the road, tilted fault blocks of Pliocene sediment crop out (Plate 3.17D), capped with conglomerates, containing sand lenses. These

Plate 3.17: Northern Çalkaya Formation:
A) Fluvial conglomerates on the northern section of the Çalkaya Formation. The conglomerates ar
interpreted as Scott-type braided stream facies (see main text). They are unconformable on blue-gre
silts of the Yenimahalle Formation. **B)** Channel within the conglomerates. **C)** Rip-up raft of Pliocen
Yenimahalle Formation in the Çalkaya Formation conglomerates. **D)** Bedded conglomerates on top o
a tilted fault block near Yenimahalle. **E)** Conglomerates dipping away from Mesozoic limestone (wit
trees) in the northern part of the Aksu basin. The Aksu Çay emerges onto the plain just to the left o
this picture.

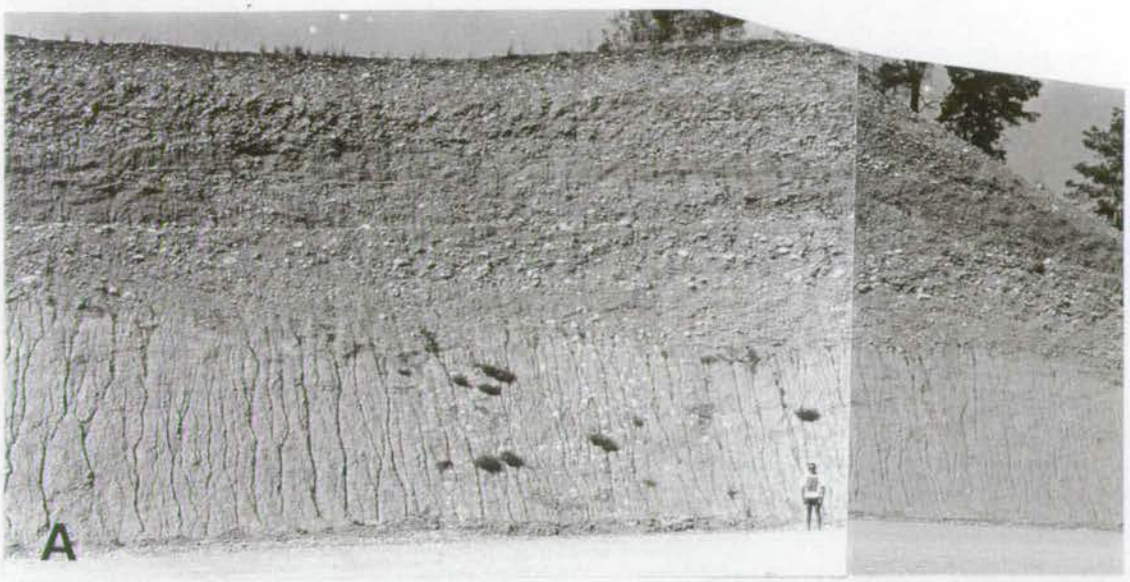

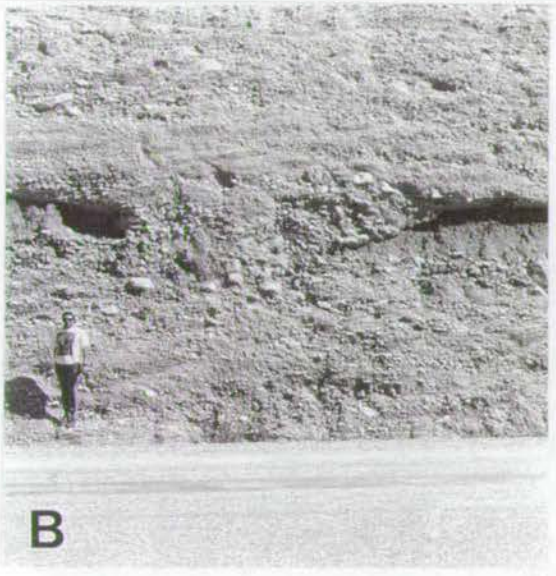

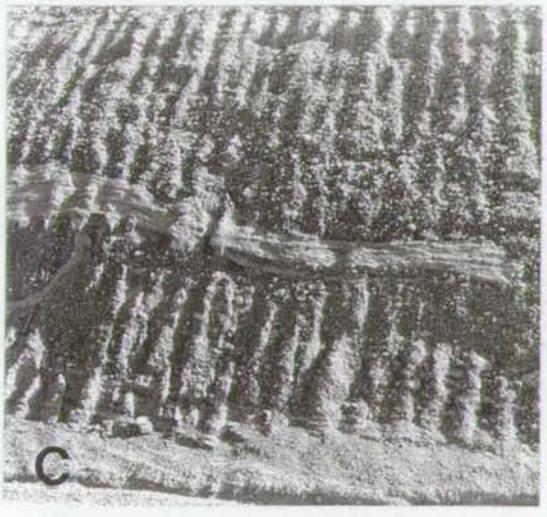

Plate 3·17

tilted fault blocks may, in fact, be seen along the edge of the central terrace to south of Güloluk (chapter 5).

Beyond the bridge, where the Aksu basin narrows significantly, the sequences once again become thicker and the road cuts reveal that blue-grey Pliocene silts (the lower part of the Yenimahalle Formation) are unconformably overlain by a thick sequence of channelised conglomerates (Plate 3.17A). Akay and Uysal (1985) mapped this section as basal conglomerates of the Eskiköy Formation. However, the unconformable contact between the conglomerates and the underlying Pliocene of the Yenimahalle formation is clearly exposed by the new road cutting and this fact allows correlation of these conglomerates with the Çalkaya Formation. The total thickness of conglomerate is about 20m, unlike that in the Çalkaya area which is of very limited extent. They are highly erosional at their base and contain intra-conglomerate erosional channels (Plate 3.17B). The conglomerates are generally massive or horizontally stratified, may show cross-stratification, and contain thin sand lenses. In one outcrop along the road to Yenimahalle large rip-up "rafts" of Pliocene marl are caught up in the conglomerate (Plate3.17C).

The northern Çalkaya Formation conglomerates are interpreted as gravel-dominated braided-stream deposits (Rust, 1978) analagous to the Scott-type (Miall 1978). The Scott-type braided stream model was erected for proximal braided stream deposits, including those on alluvial fans, where gravel is the dominant facies and interbedded sandy units occur. The horizontally-bedded, massive gravels may show some imbrication and are interpreted as the deposits of longitudinal bars, lag deposits and sieve deposits. Cross-stratified deposits are interpreted as channel fills and possible linguoid bars. Thin sand lenses are deposited in small zones of lower flow regime.

Beyond Ortaköy, in the vicinity of the second baraj and the new tunnel, the conglomerates reach 50m in thickness, have a related steep original dip (25°W) and are thus classified as fanglomerates. The deposit is limited in extent and shows no evidence of significant mass-flow type deposits; the main sediment transport process was probably creep (Nemec, 1990b). In this area, the Aksu river emerges from the Taurus Mountains through a steep-sided gorge in the limestone. It cuts deep down into the dipping conglomerates (Plate 3.17E). The conglomerates themselves are steeply unconformable on Miocene sediment, of which only a thin sliver remains before it itself is unconformable on the Mesozoic limestone through which the Aksu river emerges. In places the fanglomerate rests directly on Mesozoic basement.

3.6.8: Syn-sedimentary faulting

In the Aksu region, sediments of the Çalkaya Formation are faulted. A stereoplot of the measured fault directions in this small area show that they are very consistently east-west orientated (Fig 3.17) (as will be seen in chapter 6 this is not compatible with other fault trends measured in the Isparta angle). This region was mapped in detail (Fig. 3.18). Faults were correlated using strike measurements and correlation of sedimentary facies between individual faults. Anastomosing fault patterns are clearly brought out by this map. The faults are clearly syn-sedimentary in origin. Broad-scale folding and is associated with the faults in some sections. (Fig. 3.19).

Two of the best examples of syn-sedimentary deformation are sketched in Fig. 3.17. They relate to faults A and B on the map (Fig 3.18).

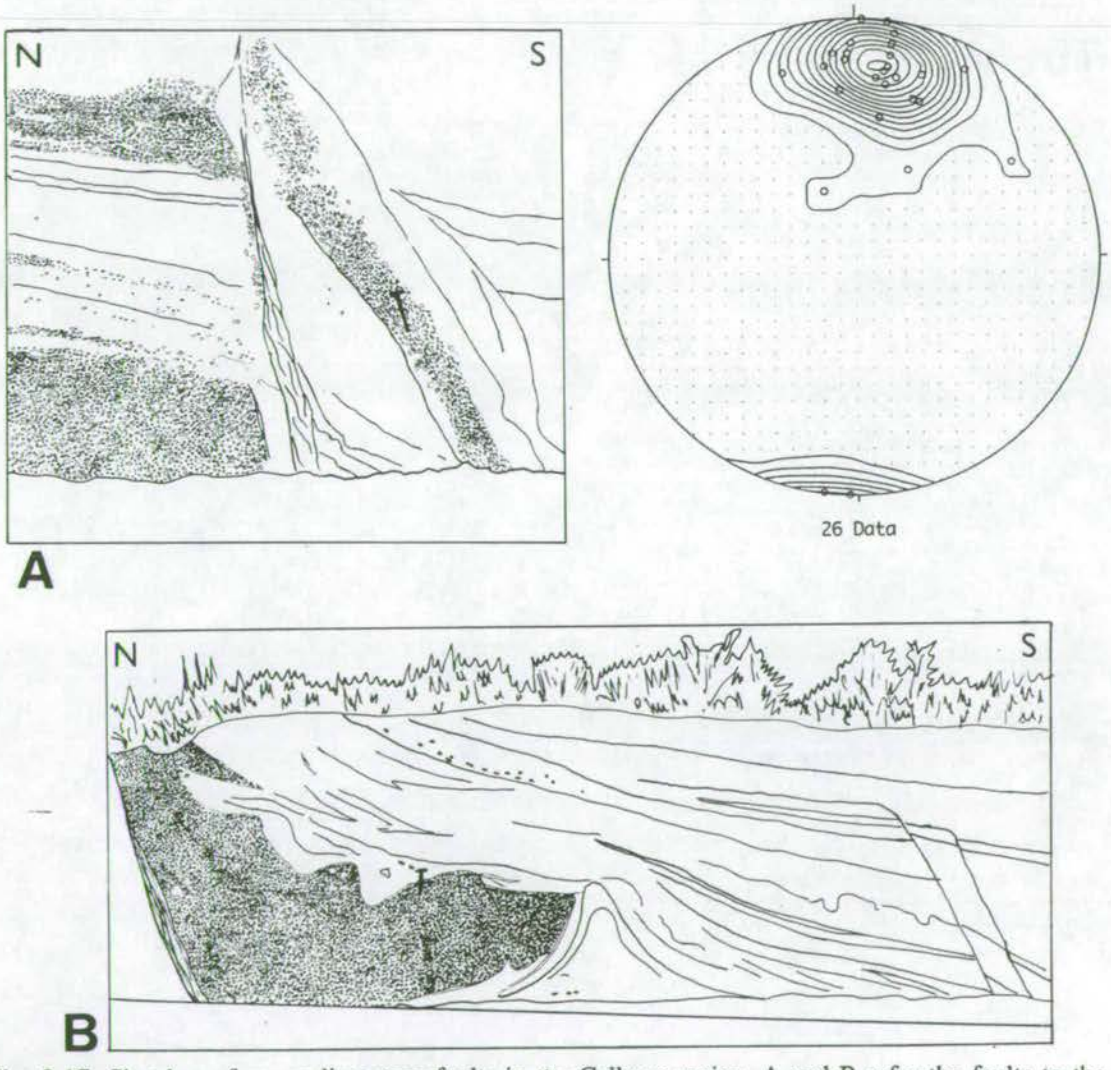

Fig. 3.17: Sketches of syn-sedimentary faults in the Çalkaya region. A and B refer the faults to the map of the area (Fig. 3.18). The faults are fully described in the text (page 82).

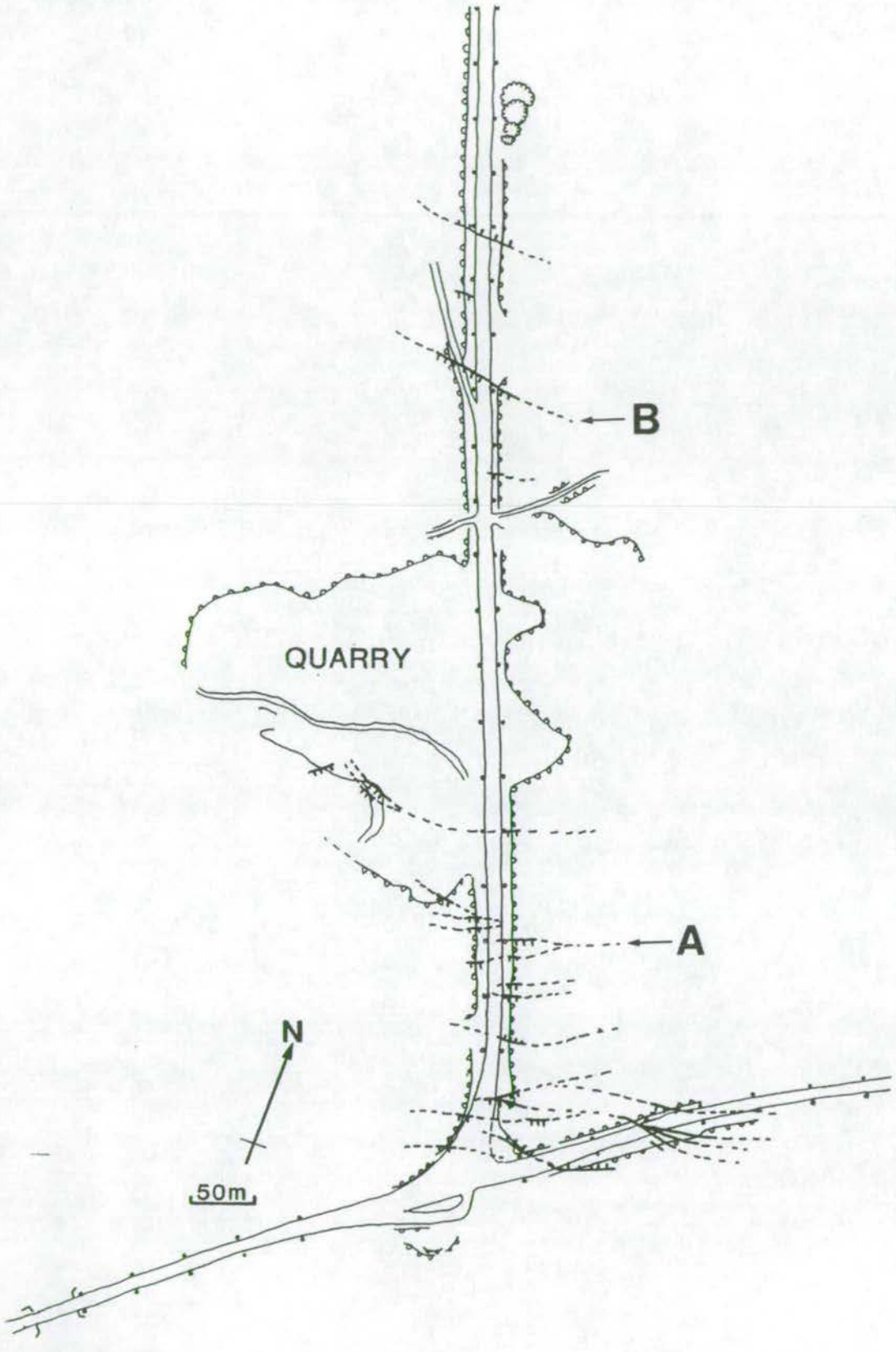

Fig. 3.18: Detailed map of the faults in the Aksu area. The exact location of this map is marked on Fig. 3.10.

Fault A shows a fault scarp down which conglomerate was deposited as talus, presumably from uplifted sands and conglomerates of the hanging wall. This talus section was refaulted to form a narrow strip of almost vertical conglomerate, as pictured, and has been subsequently onlapped by sands. Conglomerate talus was also shed from Fault B, as a small wedge-shaped deposit. Again, the clasts are of conglomerate pebbles, locally reworked. Sediment has then pushed up to the south of the conglomerate, probably due to the weight of the talus on the underlying soft sediment. This "diapir" of fluidised sediment has caused both the conglomerate body and the sands, which had already deposited on top, to deform. The entire deformed sequence has been faulted again, to the south of the original fault, and the whole faulted section is onlapped by sands in the top right of the sketch.

Syn-sedimentary faulting is best developed in this localised area and is not seen particularly in the Çalkaya or Yenimahalle region. Some of the roadside conglomerates on the approach to Yesilkaraman show evidence of disturbed bedding, chaotic structures and possible faulting which may be syn-sedimentary, but the general lack of bedding makes this difficult to determine precisely.

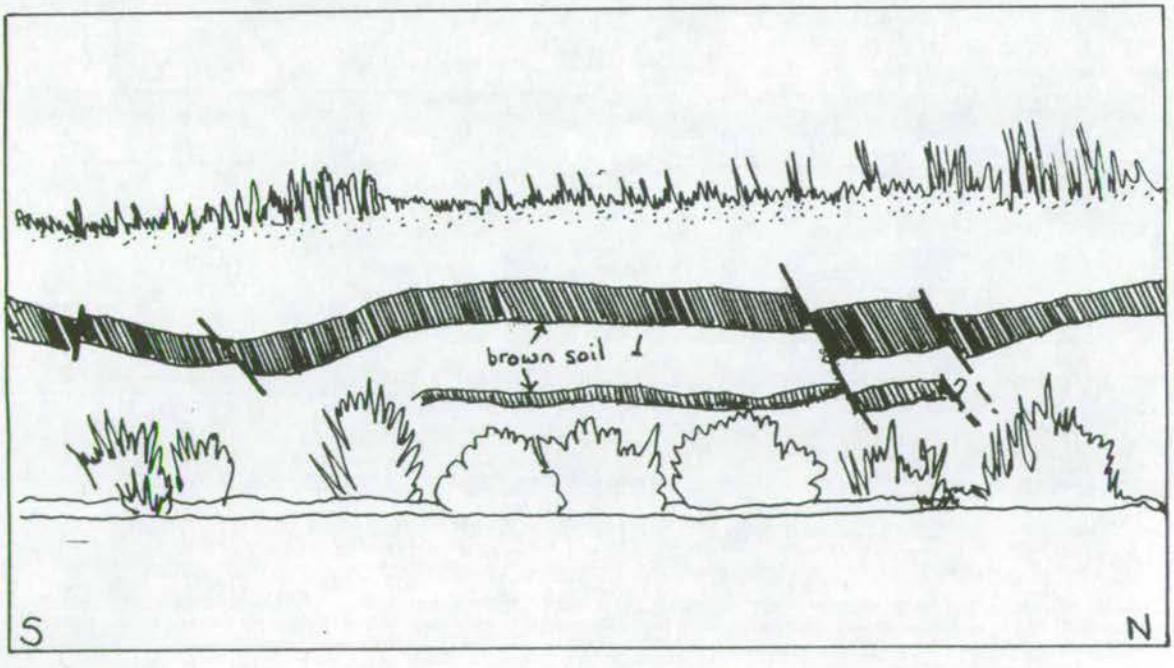

Fig. 3.19: Field sketch of warped soil beds in the Çalkaya Formation. Minor fault offsets also occur. The section was located between two of the faults mapped in Fig. 3.18.

3.7: Environments of deposition

3.7.1: Yenimahalle Formation

The Yenimahalle Formation is interpreted as the deposits of a shallow-marine shelf sea. Coarse clastic input is thought to be minimal at this time. There is no evidence of early fluvial, fan or beach deposits near the present day Aksu emergence point. It is probable that a freshwater plume transported silt and clay particles far into the sea, reworking calcareous nannoplankton from the Miocene sediments to the north.

Benthic foraminifera from the Manavgat section and the Yurtpinar section can be used to determine palaeowater depths. The species diversity and distribution are indicative of a normal marine environment, although the small size of both the planktic and benthic foraminifera indicate that the sea was extremely shallow. Douglas (1979) discusses the applicability of modern foraminiferal distribution to fossil assemblages. It is known that foraminifera may adapt to different ecological niches if conditions require, thus, modern day distributions may not be representative of past habitats. From plate tectonic reconstructions (Smith, Hurley and Briden, 1981; Scotese, Gahagan and Larson, 1988; Rowley and Lottes, 1988) it is known that the present-day oceanographic situation began to develop 14 Ma ago and by the late Miocene was well established. Thus, modern distributions are generally accepted to be applicable back until about the Mid Miocene (Douglas, 1979). Care must be taken with silled basins such as the Mediterranean, which have a restricted circulation, as taxa which under normal conditions would be found at 1000m, for example, may be found at much greater depths. Restricted oxygen conditions at depth could also alter the assemblage in these basins (Douglas, 1979). However, at the depths of the Pliocene Antalya basin (<150m) these factors are not a problem and comparison with modern distributions can be considered a reliable indicator of past conditions in this case. Fig. 3.20 is a genus list with ecological information for all the benthic foraminifera species found in the samples which are indicative of water depth and environment, compiled from Murray (1991). They are arranged in approximate depth order, with those species that live in the shallowest water depths at the top of the list. The order is not definitive as figures are only available for half of the species. Of particular importance are *Ammonia* sp., *Planorbulina* sp. and the keeled *Elphidium* sp., which indicate water depths of 50m or less, and *Planulina* sp. *Uvigerina* sp., *Lenticulina* sp., and *Pullenia* sp., which indicate depths of 100m and greater. *Nonion* sp. which lives between depths of 0 and 180m is the shallowest species found on the Manavgat samples.

SPECIES	DEPTH	ENVIRONMENT	% / C	HABITAT	SEDIMENT
Ammonia	0-50m	marine, inner shelf	0-30 C	infaunal	muddy sand
Planorbulina	0-50m	marine, inner shelf		epifaunal	hard substrate
Elphidium (keeled)	0-50m	marine, inner shelf	35-70 %	epifaunal	sand
Patellina	0-100m	marine, inner shelf		epifaunal	hard substrate
Nonion	0-180m	marine, shelf	30-35 %	infaunal	mud, silt
Nummulites	0-130m	marine, inner shelf		epifaunal	muddy carbonate
Cancris	50-150m	marine, shelf		epifaunal	sediment
Elphidium (non keeled)		lagoons + marshes; marine, inner shelf	0-70 %	infaunal	mud, sand
Quinqueloculina		marine, shelf, rarely bathyal	32-65 %	epifaunal	sediment
Neoconorbina		marine, inner shelf		epifaunal	hard substrate
Hanzawaia		marine, inner shelf		epifaunal	hard substrate
Pyrgo		marine, inner shelf		epifaunal	
Eggerella		lagoons; marine, inner shelf - bathyal	20-37 %	infaunal	silt-fine sand
Haynesia		lagoons + marshes; marine, inner shelf	0-30 %	infaunal	mud-silt
Cibicides	0-1000m	lagoons; marine, shelf - bathyal		in-epifaunal	hard substrate
Fursenkonia	0-1200m	lagoons; shelf - upper bathyal	30-35 %	epifaunal	mud
Brizalina		marginal marine - bathyal		infaunal	muddy sediment
Bulimina		marine, inner shelf - bathyal		infaunal	mud-fine sand
Bolivina		marine, inner shelf - bathyal		infaunal	muddy sediment
Trifarina	0-400m	marine, shelf + upper bathyal		infaunal	mud, sand
Textularia	0-500m	marine, shelf - bathyal		epifaunal	sand, hard substrate
Melonis		marine, shelf - bathyal	<10 C	infaunal	mud, silt
Planulina		marine, shelf - bathyal		infaunable	hard substrate
Globocassidulina		marine, shelf - bathyal		infaunal	mud
Uvigerina	100-4000m	marine, shelf - bathyal		infaunal	muddy sediment
Lenticulina		marine, outer shelf-bathyal		epifaunal	mud
Pullenia		marine, outer shelf - bathyal		infaunal	mud
Karriella		marine, outer shelf - bathyal	<10 C	epifaunal	mud and silt

Fig. 3.20: Genus list and ecological information for benthic formainiferal species found in the Yurtpinar and Manavgat sections. Data, compiled from Murray, (1991), are based on known modern distributions of benthic foraminifera.

Infaunal, epifaunal and encrusting foraminifera are all present and nothing can be deduced from the distribution of infaunal and epifaunal foraminifera in this data set. The order of species compiled in Fig. 3.20 was used to plot a matrix of the genus content of all the picked samples in the Manavgat and Yurtpinar sections (Fig. 3.21). Species ranging from shallow to deep are plotted down the side of the table and samples from the Manavgat section and then the Yurtpinar section plotted from bottom to top across the table. Crosses indicate the species present in each sample. A clear difference in benthic assemblage exists between the two. Whereas the Manavgat section contains the deeper-water species, *Planulina* sp., *Uvigerina* sp., *Lenticulina* sp., and *Pullenia* sp., the Yurtpinar samples all contain one or more of *Ammonia* sp., *Planorbulina* sp. and the keeled *Elphidium* sp. indicating a water depth of 50m or less.

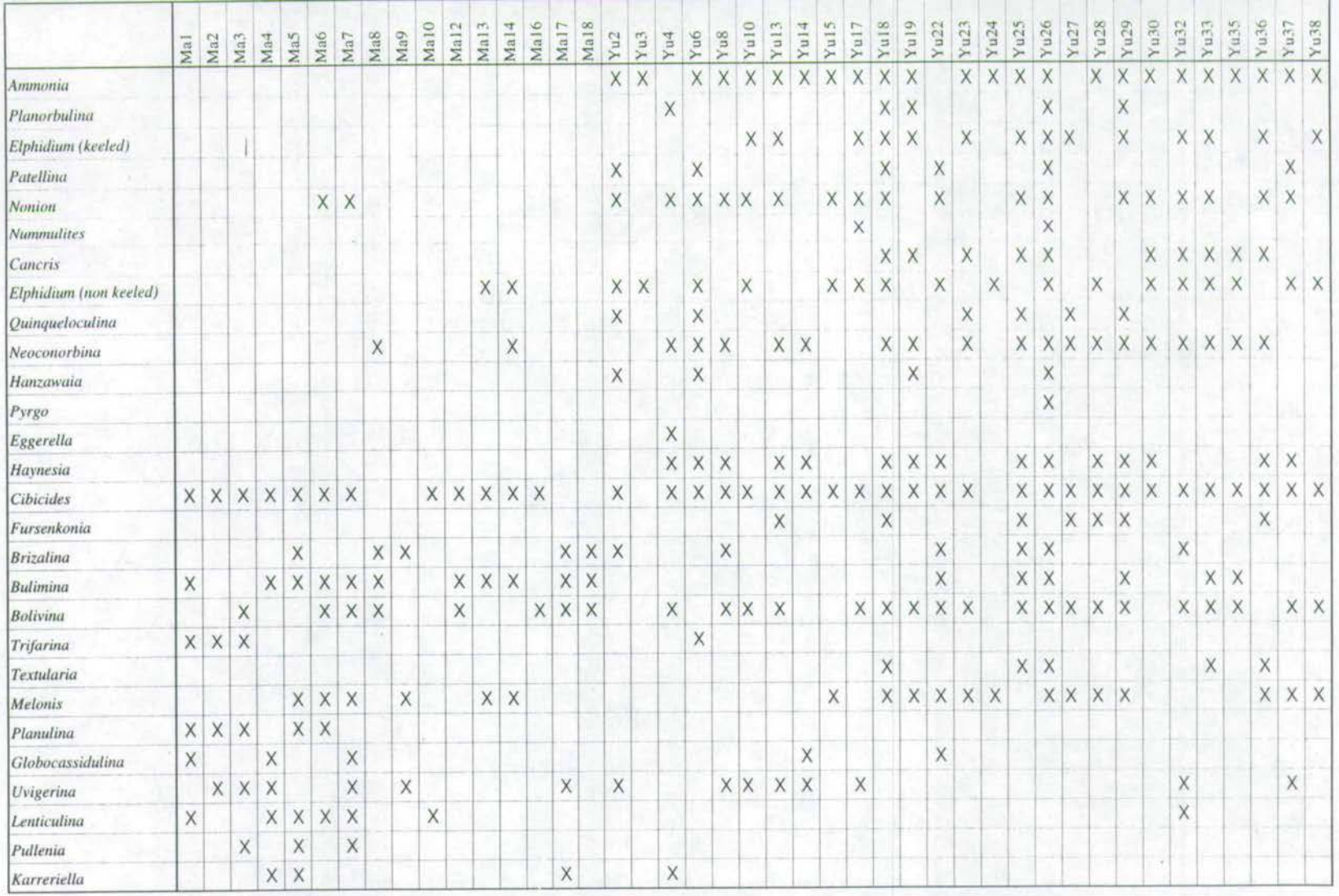

Fig. 2.21: Matrix of benthic foraminifera found in the Manavgat and Yurtpinar sections. The samples are listed from bottom to top, Manvagat section and then Yurtpinar section. Benthic foraminifera are arranged in approximate order of the water depth in which thay live (after Fig. 3.20). The presence of a particular genus in a sample is marked by a cross. The figure clearly shows that the Manvagat section contains a deeper water assemblage than the Yurtpinar section.

The presence of *Nonion* sp. in two of the Manavgat section samples suggests that water depth was approximately 150m. Comparison of the assemblages with ecological data from modern environments (Murray, 1991: Table 18.1) also shows the Yurtpinar assemblage to resemble an inner shelf assemblage, of water depth 0-100m. The lack of large numbers of planktic *Globorotalia* species, and the small size of most of the planktic specimens are still further evidence that this was a very shallow sea, probably <100m in depth. This was previously indicated by Planhol (1956). The abundance of *Globigerinella siphonifera* and *Orbulina universa*, and the increased numbers and increased size of foraminifera in samples Ma5/92b and Ma6/92b, indicate that a flooding event occurred during the deposition of this horizon. During a flooding event the input of water and nutrients from the open ocean reduce the stress of an extremely shallow-water environment; numbers of planktic foraminifera increase and they are able to grow to a normal size. This event was probably short lived and cannot be identified sedimentologically. The ease of identification of this flooding event, using foraminifera, suggests that detailed work on cores through the entire, offshore, sequence could be a valuable tool for documenting small-scale eustatic sea-level changes in the Mediterranean Pliocene.

The upper sandy sections at Yenimahalle and Yurtpinar are characterised by burrows (skolithos), macrofossils (barnacles, oysters, large spiney gastropods), and sedimentary structures (ripples, low-angle cross-bedding, gravel and shell lags) that indicate a nearshore setting (Crimes, 1975; Johnson and Baldwin, 1978 and references therein.).

Water-escape structures occur as the result of sudden loss of the support between grains reducing the shear strength to nothing and causing disruption of the sediment. The structures observed in the Yenimahalle Formation are volcano structures, resulting from the vertical movement of fluid from one layer (silt) upwards through the overlying layer (sand), resulting in the lower silt layer becoming mixed into the overlying sand layer. This may be caused by a number of mechanisms. The concept of a reversed density gradient, arising from the deposition of denser beds over less dense beds, is probably the most popular explanation for water escape structure formation (Anketell, Cegla and Dzulynski, 1970; Lowe 1975). Earthquakes may also act as a triggering mechanism for fluid escape, as the sediment destabilises due to vibration (Lowe, 1975). Experiments conducted by Nichols, Sparks and Wilson (1994) showed that water flowing through layers of fine and coarser grained sediment will collect in voids at the base of the coarser layer, until a critical point is reached and the water ruptures through the upper layer fluidising the sediment. The volcano-type structures produced by these experiments bear a closer

resemblance to the structures documented in the Yenimahalle Formation than the structures pictured by Lowe. However, Nichols *et al* (1994) suggest that the pillar structures described by Lowe (1975) may also result from water flowing through the sediment and this process is thought to be the most probable causal mechanism.

3.7.2: Çalkaya Formation

Interpretation of individual facies of the Çalkaya Formation has already been made (section 3.6). The Çalkaya Formation consists of marine, marginal marine and continental facies. It is interpreted as a regressive deltaic system which was deposited during eustatic sea-level drop resulting from onset of Arctic glaciation. No large scale Gilbert-type foresets exist and this is a shallow water delta. The complexity and diversity of delta environments have resulted in the proposal of a number of classification schemes. These are reviewed in detail in Nemec (1990a). In brief, the three most satisfactory classification schemes are those of Galloway (1975), McPherson, Shanmugam and Moiola (1987) and Postma (1990). The Ternary diagram of Galloway (1975) distinguishes between fluvial, wave and tide dominated deltas. Its extension by Orton (1988) to include dominant grain size makes this more generally applicable, as the degree of reworking is directly related to the grain size. McPherson *et al* (1987) classify deltas by the nature of their feeder systems into fan deltas, braid deltas and "common" deltas (referring to finer grained deltas with meandering or straight rivers of mixed or suspended load). Postma (1990) produces a complex classification scheme (Fig. 3.22) that relies on identification of sedimentary facies types and depositional architecture and regards the nature of the feeder system and the degree of reworking as secondary features. Since these are the features which are studied as a matter of course by field sedimentologists this is an ideal scheme for application to "ancient" delta systems. It is, however, valuable to assess the fluvial supply system and the degree of fluvial as opposed to wave or tidal influence, where exposure allows. Thus, using a combination of these schemes the southern Çalkaya Formation deposit may be classified as a wave influenced, shoal-water, Type C delta (Postma, 1990). Shoal water refers to the shallow nature of the gradient of the delta, which displays no Gilbert-type foresets. Type C refers to a feeder system of a moderate gradient, with a gravelly and sandy alluvial system, of closely spaced, but relatively stable channels emanating from well defined points of sediment supply. Stabilisation of outlets is enhanced by vegetation on point bars. These may be subsequently flooded and the transition from soils or coals to marine sands and silts is not uncommon.

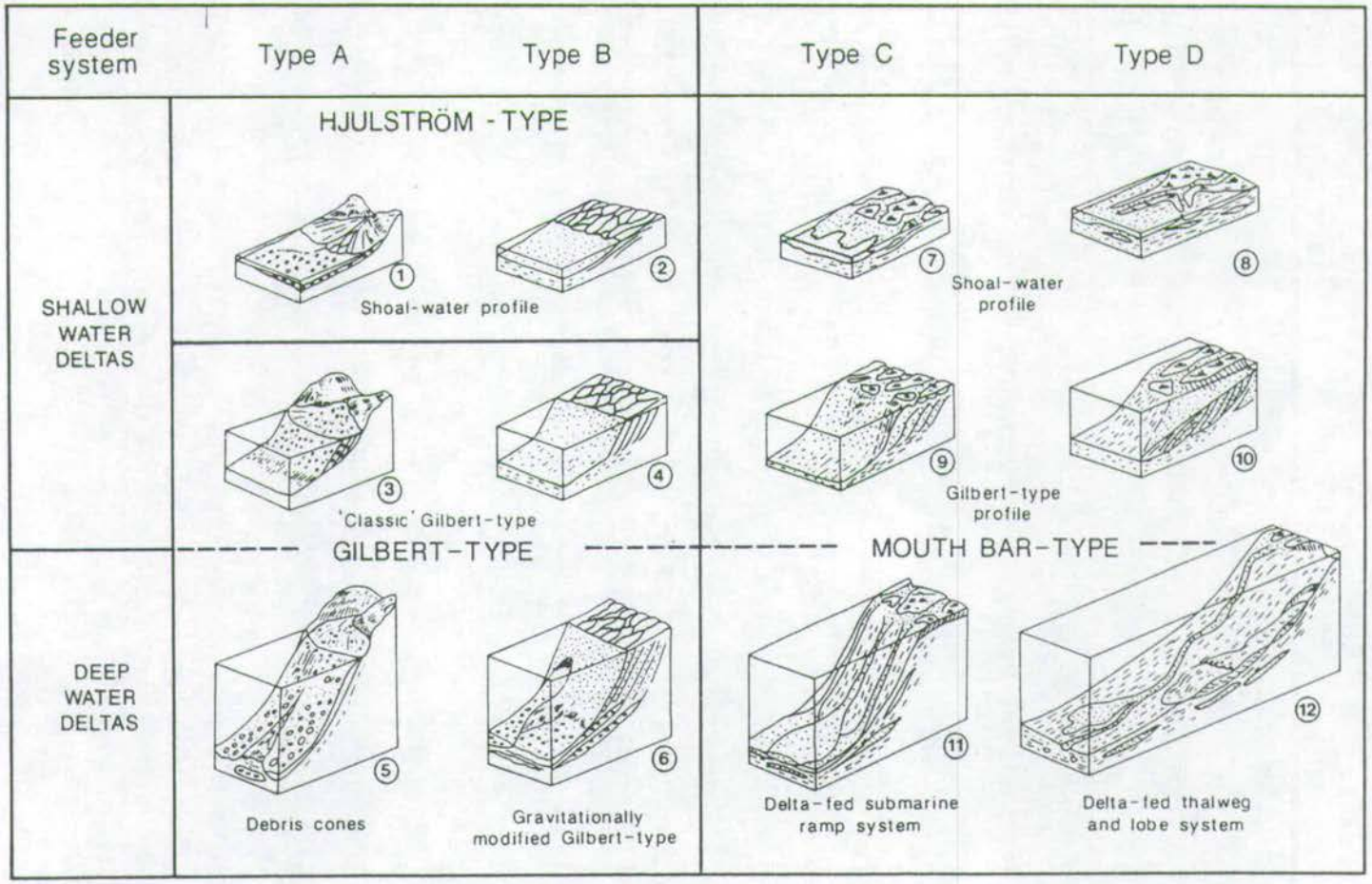

Fig. 3.22: Classification of deltas (Postma, 1990) Twelve major prototypes are presented, all dominated by fluvial processes. Wave-dominated and tide-dominated deltas may also exist for each prototype. The prototypes are distinguished on the basis of four different types of distributary system and two ranges of depth ratios, and take into account the variation due to inertia, friction and buoyancy dominated effluent.

The presence of coals and soils within the predominantly marine deposits of the southern Çalkaya Formation is interpreted as the product of significant periods of subaerial exposure on stable bars. The thick conglomerate deposit near Kursunlu is an excellent example of this. This is one of the thickest conglomerate deposits in the southern Çalkaya Formation area and is likely to have formed a stable, subaerial bar for a significant period of time. The hardening and reddening of the upper surface testifies to subaerial exposure, as does the metre thick coal deposit on top. However, the coal contains a 0.5m thick deposit of marls, probably representing a flooding event prior to a second shorter period of coal development. Finally the whole stable bar is flooded. Marine sands extend far into the delta mouth and symmetrical wave ripples are seen and are indicative of the wave influence on the delta front. The larger conglomerate bodies have been interpreted as gravel bars. Assuming a coastline approximately parallel to that today, these are interpreted as longitudinal bars, possibly mouth bars in a wave-influenced fluvial delta distributary front. Isolated patches of marine, brackish or freshwater may remain stable for periods of time in this environment, leading to the deposition of draping clays, carbonates and restricted fossil assemblages. The nature of the feeder system is thought to be represented by the thick sequence of conglomerates north of Ortaköy which have been interpreted as braided stream deposits. The feeder system is thus a braid plain. This gives the deposit some characteristics of a B-type delta, however, this only applies to the northernmost, truly fluvial part of the Çalkaya Formation and the delta mouth itself is not braided. The fan delta system (Type A) at the emergence point of the Aksu must also be included into the general model. Syn-sedimentary faulting is rare within shoal-water deltas, but may occur, possibly as a result of seismic shock. The very localised faulting described in the Aksu region is interpreted as seismic-shock related syn-sedimentary faulting, perhaps directionally influenced by the delta morphology.

3.8: The Kemer Fanglomerates

Along the coast from Antalya to Kemer and Olympos the coastal road cuts through a number of fanglomerates. These are lobe shaped and occur at regular intervals along the coast. Individual lobes are separate and no interfingering of deposition from adjacent lobes occurs. Most of the fan deposits are inaccessible and only exposures on the main road could be observed. Two conglomerate facies are present in the fans. The most common (A) is clast-supported and contains angular - subangular clasts, ranging from a few centimetres to tens of centimetres. Bedding occurs on a metre scale; the less coarse beds may display a low-angle cross bedding. This is particularly well seen in the large fan section just before Phaselis. The lowest

part of this section was logged (Fig. 3.23). The majority of the deposit consists of bedded conglomerate, as represented in the upper part of the log. Beds varied by sorting and clast size, but were not chaotic. The second conglomerate facies (B) is extremely poorly sorted, matrix supported and contains angular clasts up to 3m in size. Plate 3.18 shows both these in one fan deposit. Facies A is exposed to the left of the conifer, and facies B is exposed above the bushes. There is a sheared texture to the muds separating the two types. Facies A is interpreted as the deposit of a steep alluvial fan, whilst facies B is interpreted as a debris flow deposit.

3.8.1: Environment of deposition

The Kemer Fanglomerates are interpreted as a series of small coarse-grained fan deltas depositing from the steep scarps of the western Taurides. The principal depositional processes within these fan deltas were alluvial processes and gravity driven debris flows. The Kemer Fanglomerates can be compared with similar deposits in the Miocene Kasaba basin (Hayward, 1982) and in the Gulf of Elat (Gvirtzman and Buchbinder, 1978). Both these examples are much better exposed than the Kemer Fanglomerates. Lateral transition from alluvial to marine sediments and detailed observations on sedimentation style are documented.

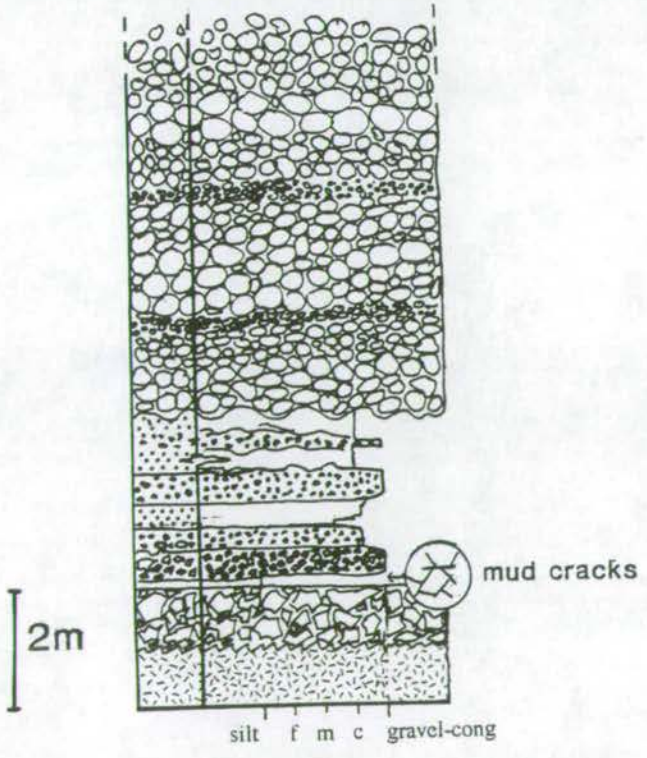

Fig. 3.23: Log of the lower part of the Phaselis fan section. The conglomerates at the top of the log continue for approximately another 25m.

Plate 3.18: Kemer Fanglomerate.
Facies A is a well bedded conglomerate resulting from normal alluvial fan conditions. The chaotic
facies B is interpreted as a debris flow deposit. The pale band between the two facies types is thought
to be a sheared layer resulting from the force of the debris flow that deposited facies B.

Plate 3·18

3.9: Seismic reflection profiles in Antalya Bay

Seismic reflection profiles, provided by Prof. Dr. M. Ergün and shot by M.T.A. Sismiki, have been interpreted with emphasis on the sediment distribution. No cores are available and so the age of the sediment is unknown. However, a strong reflector, which can be equated to the -M- reflector (Woodside, 1977) of the Messinian unconformity surface and evaporites, at the base of the sediment package and the lack of seismic penetration below this reflector suggest that the sediment packages imaged are of Plio-Quaternary age. The significance of the faulting inferred on the profiles will be discussed further in chapter 6. Copies of the original profiles are included in Appendix 4. It must be stressed that the quality of the seismic data is very poor, but that a number of interesting features can still be identified which tie in well with the field observations. The principal feature of sediment distribution in Antalya Bay to come out of the profiles is that the sediment was deposited on a fault-block topography. This is shown and discussed further in chapter 6. Minor syn-rift packages (Fig. 3.24) are developed on the Messinian fault-block topography which have been covered by the majority of the deposit. A further phase of extension has reactivated some, but not all, of these faults, cutting through the Pliocene sediment package. The clearest and most informative profile is that of A1 (Fig. 3.25). Three transgressive phases are identified. Two of these phases are also identified on the northern part of line A4 (Fig. 3.26). The main sediment package does not cover the entire Antalya Bay area, but appears to be restricted to a lobe approximately around the mouth of the present-day Aksu river. The total thickness of the sediment package imaged in line A1 is one second of two way travel time. By comparison with onshore deposits, the sediment is likely to be unconsolidated silt. Assuming a travel time through unconsolidated silt of 1000m/s (J. Underhill, pers comm, 1995) puts the total thickness of sediment at 500m. Thus, onshore we are able to study only one fifth of the total sediment thickness.

In the western side of the bay the sediment has been channelised by a fault controlled gully which is narrow at its northern end but widens out rapidly to the south. Sediment flows down this gully and is deposited as a stacked channel deposit. This is shown particularly well in line A2 (Fig. 3.27). It is also important to note that a significant quantity of material has also been deposited from the Kemer coastline, as fan delta deposits, which presumably correlate with the Kemer fanglomerates. This is imaged in line A2 where a sediment package, of limited extent is identified at the western end of the profile (Fig. 3.27).

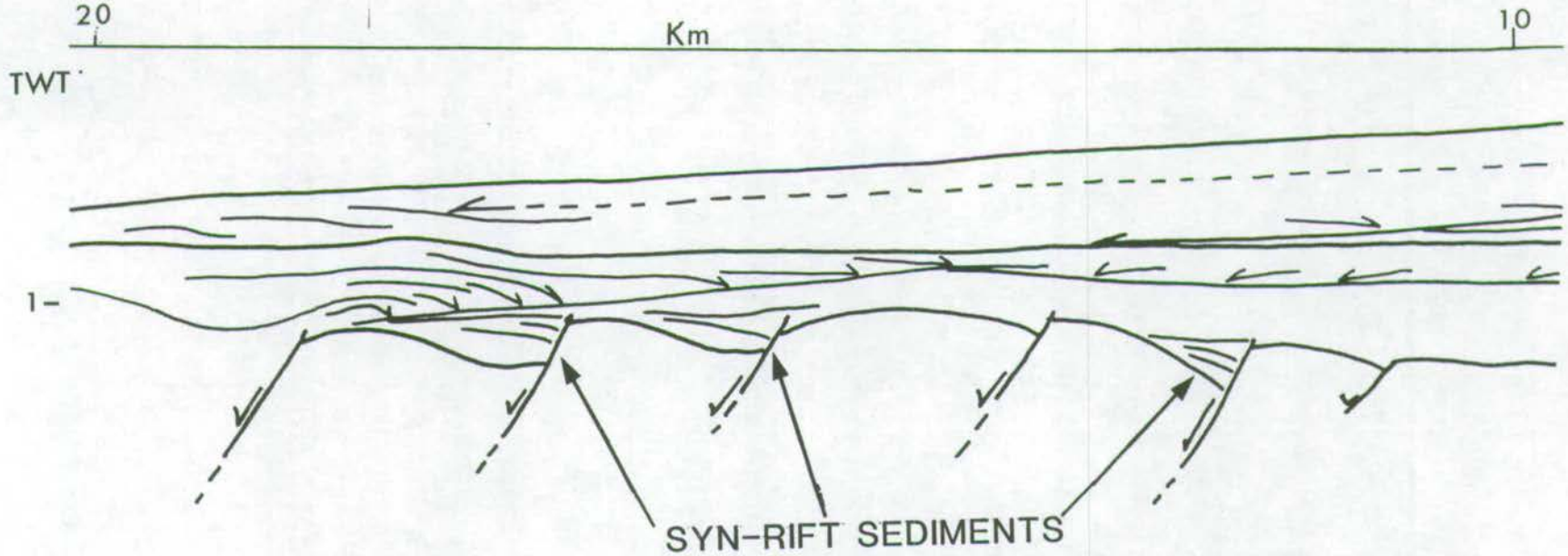

Fig. 3.24: Synrift sediment packages interpreted in seismic profile A1.

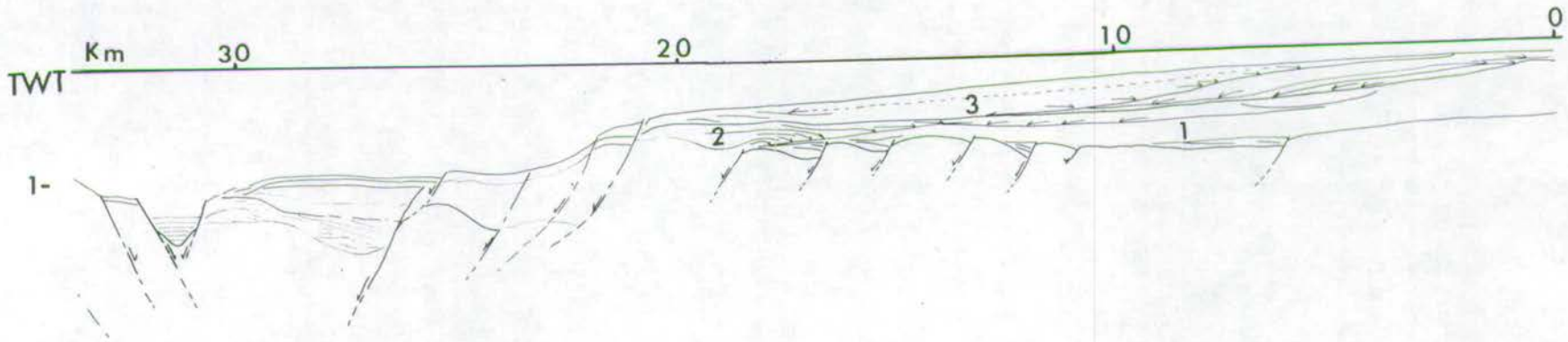

Fig. 3.25: Interpretation of seismic profile A1. Three transgressive phases are marked: 1, 2 and 3. The very western part of the profile is not shown.

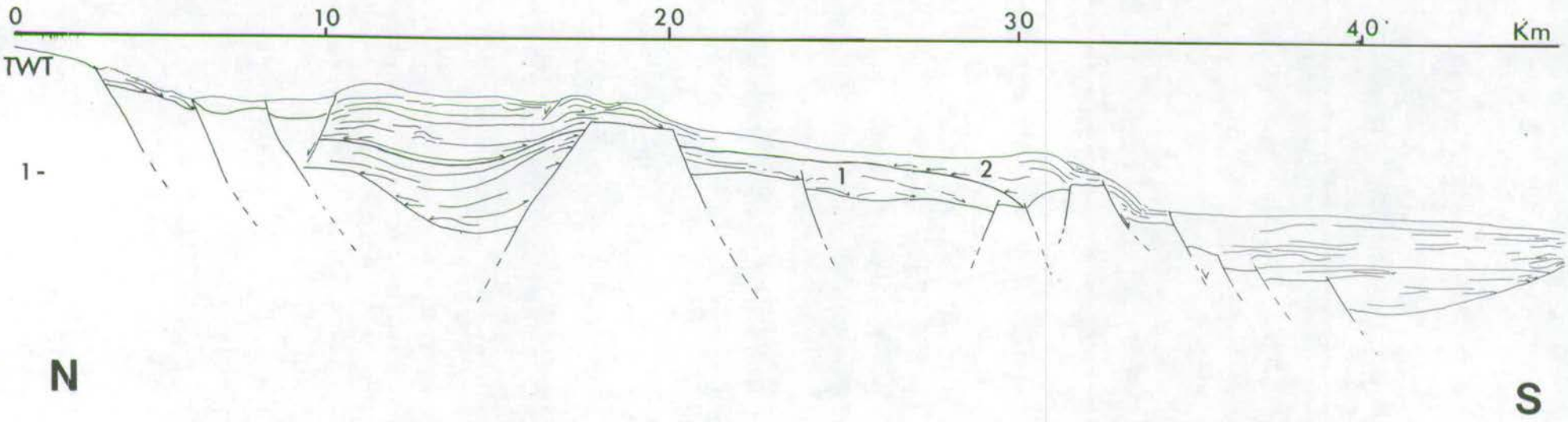

Fig. 3.26: Interpretation of northern section of seismic profile A4. Two transgressive phases are identified, marked 1 and 2.

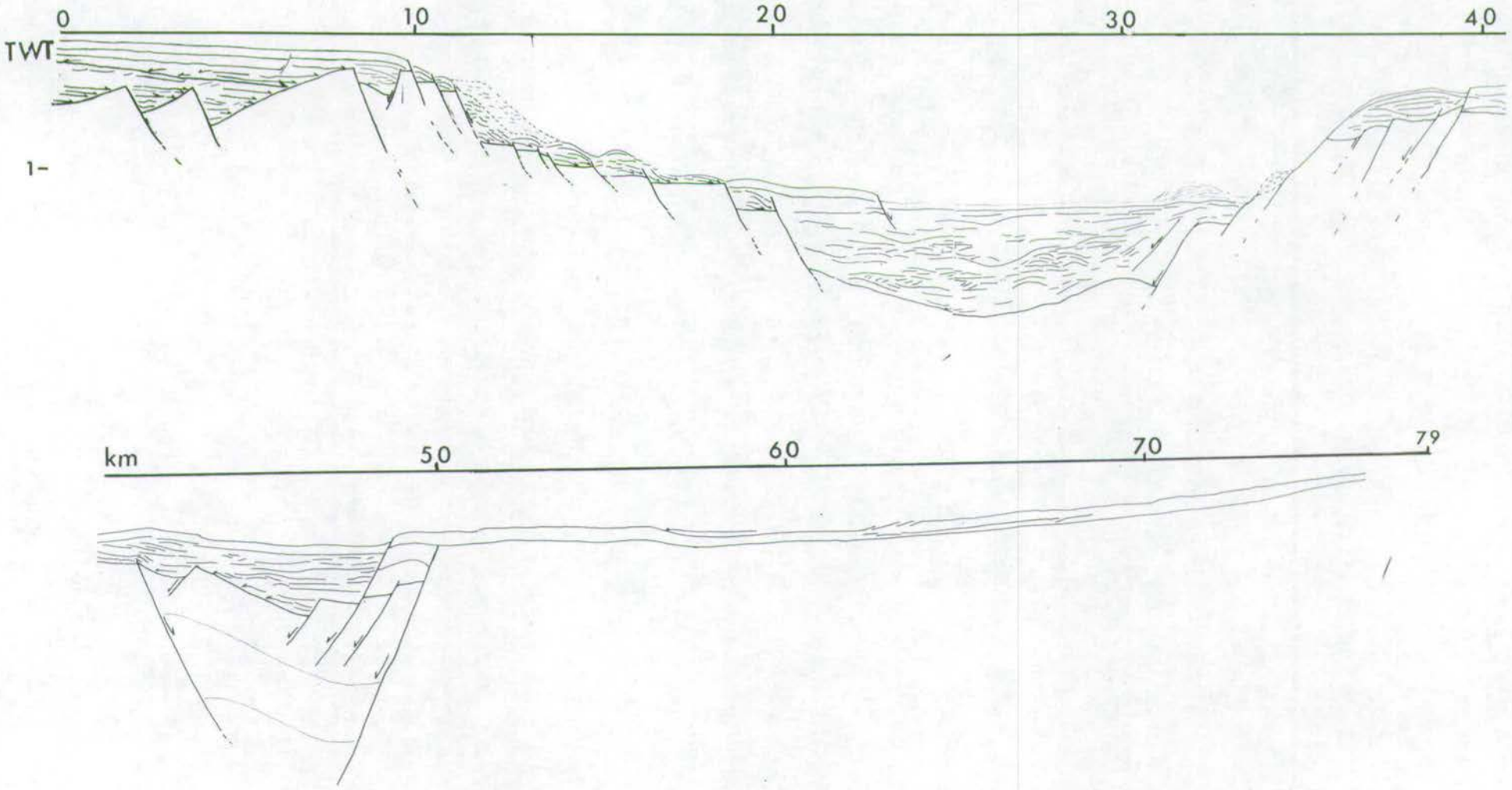

Fig. 3.27: Interpretation of seismic profile A2. In the west the sediment package is interpreted as part of the Kemer Fanglomerates. Note the channel forms in the central graben.

A similar comparison between offshore seismic and onshore geology was made on the south coast of Cyprus (McCallum, Scrutton, Robertson and Ferrari, 1993). Again the Messinian reflector was recognised as a strong reflector below which the basement was characterised by poor seismic penetration. Core was able to confirm this interpretation. Above the Messinian reflector, seismic units were identified which could be correlated with known onshore geology. The Plio-Quaternary sediment package was thinner than that in Antalya, but as in Antalya no active faults were seen during the Plio-Quaternary.

3.10: Evolution of Pliocene sedimentation

The majority of Pliocene sedimentation occurred in a shallow-marine sea. Clay and silt size sediment was transported into Antalya bay probably via the channels documented in the lower Yenimahalle Formation. This was almost certainly a low-gradient system characterised by a low bedload/total load ratio. It is probable that little coarse grained material was supplied to the basin at this time, since reworking of nannoplankton, but not of foraminifera is seen. In addition, if a significant quantity of coarse-grained material had been supplied, an alluvial fan/fandelta sequence of significant proportions would be expected in the north of the basin. However, blue-grey silts and sands crop out at the very northern end of the basin. Benthic foraminiferal species, the absence of rotaliid planktic foraminifera and the small size of all foraminifera indicate that the basin was never more than 150m deep. The sequence shallows-up gradually and the foraminifera, macrofauna and trace fossils of the Yurtpinar and Yenimahalle sections show that for a significant period the basin was less than 50m deep. Phreatomagmatic eruptions may have occurred in the vicinity, depositing volcanic minerals in certain horizons (sample Yu24 of the Yurtpinar section, for example). Evidence from seismic profiles shows that the sequence is of the order of 500m thick. Three transgressive phases can be identified. These can be directly related to the eustatic sea-level curve which shows that during the Lower Pliocene highstand, there were two periods of lowered sea-level. At the end of the Pliocene highstand rapid climatic cooling and onset of Arctic glaciation resulted in a large sea-level drop. This marks the end of marine deposition in the Aksu basin. The rapid regressive phase resulted in the deposition of the Çalkaya Formation shoal-water deltaic system, which laterally develops from Type A through to Type B then to Type C (Postma, 1990). Coarse clastic input marks this phase and a small, coarse alluvial fan was deposited at the emergence point of the Aksu river (Type A). It cuts into the earlier fanglomerate of the Miocene Aksu Formation indicating that the emergence point of the Aksu has remained fixed at

least since the Mid Miocene. The fan rapidly shallows onto a coarse proximal braid plain (Type B), the sediments of which erode strongly into the underlying marine sediments of the Yenimahalle Formation. This braid plain was fluvial at its northern proximal end, but rapidly deposited the majority of its coarse load and a sandy, wave-influenced, shoal water delta-top (Type C) covered most of the basin area. The fluvial system did not prograde southwards and it is probable that the final regression was so rapid that the river system did not manage to keep up with the retreating shoreline. The further development of the Aksu river course will be discussed in chapter 5. The localised syn-sedimentary faults could either be growth faults or tectonic faults. The well confined E-W direction of the faults suggests that they are not purely tectonic, as tectonic faults in the area are orientated around a N-S direction (chapter 6). However, in such a shallow delta, growth faults would not be expected. It is possible that growth faults were triggered by earthquakes. The laterally continuous beds of soft-sediment dewatering structures could also result from seismic activity, athough it is felt that water flow through the sediment is a more probable cause. Tectonic aspects will be discussed further in chapter 6.

Phreatomagmatic activity during deposition of the Çalkaya Formation is responsible for the tuff ring deposit at Çalkaya, channelised volcaniclastic sediments near Yesilkaraman and volcanic grains in the Yenimahalle Formation.

3.11 Comparison and discussion

In the eastern Mediterranean Neogene sediments are exposed onshore in the Antalya and Adana basins in Turkey, the Mesaoria basin in Cyprus, and in Crete. Comparisons are made between the Antalya basins and the other areas, primarily the Cyprus Mesaoria basin and the Adana basin.

3.11.1 The Mesaoria basin

The Aksu basin sequence bears a remarkable similarity to the Pliocene Nicosia and Kakkaristra Formations of the Mesaoria basin in Cyprus (McCallum, 1989, McCallum and Robertson 1995a,b). The majority of Pliocene sediment in the Mesoaria basin (900m of 1000m) is shallow marine background sedimentation of the Nicosia Formation, remarkably similar in aspect to the Yenimahalle Formation. Coarse mass-flow dominated lobes are present in the Nicosia Formation which are not seen in the Yenimahalle Formation, suggesting that the margin of the Mesaoria basin (the fault controlled margin of the uplifting Troodos ophiolite) was steeper at this time than the margin of the Aksu basin. Shallowing of both the Nicosia Formation and the Yenimahalle Formation resulted in a gradual change to deposition

of shallow marine sands. In both cases these sands comprise the upper 20-30m of section. The total thickness and facies associations of the Kakkaristra Formation and its interpretation as a Type C Gilbert-type profile in a shallow water delta system bear very close comparison to the Çalkaya Formation. Again the fundamental difference is the absence of gravity flows in the Çalkaya Formation. This difference indicates that tectonic activity influenced the Mesaoria basin deposits.

The entire marine Pliocene of the Mesaoria basin, Cyprus and the Aksu basin is very similar, with the exception that the Mesaoria basin deposits were flanked by a steeper, tectonically active continental margin adjacent to the uplifting Troodos ophiolite to the south. Consequently, mass flow deposits are present within the Nicosia and Kakkaristra Formation deposits. The Mesaoria basin was very active by the Late Pliocene.

3.11.2 The Adana basin

The Pliocene sediments, of the Adana basin, located on the easternmost section of Turkish Mediterranean coast, are poorly described. The Pliocene of the Adana basin is named the Handere Formation. It is described as consisting of detrital sediment; conglomerate and coarse-medium sandstone in the west and fine sandstone and siltstone in the east. In general, the sediments are greyish-yellow siltstones and shales with cross-bedded sandstone and conglomerate interbeds and lenses, occasionally containing abundant oysters. In the western area, gypsum lenses are present in the Formation and 400-450m of bioclastic and oolitic limestone and sandstone/shale alternation form the basal part of the section (Yetis, 1988; Yalçin and Görür 1984). The thickest section reported is 120m, although the total thickness of the sequence is greater than this. *Globorotalia margaritae* is reported from the Handere Formation, dating it to the Lower Pliocene (Yetis, 1988). The Handere Formation is interpreted as deltaic, shallow marine, fluvial and lagoonal sediments. (Ünlügenç and Gürbüz, 1992). During the Pliocene, the Adana basin underwent local compressive or transgressive deformation and clockwise rotation (Ünlügenç and Gürbüz, 1992). Again, the shallow water deltaic sedimentation of the Pliocene Adana basin is similar to that of the Aksu basin.

3.11.3 Crete

The situtation in Crete is somewhat different (Peters, Troelstra and van Harten, 1985). A number of wave-cut platforms are recognised which are locally covered by Pliocene marls spanning the Pliocene from the *Spheroidinellopsis* ACME zone of the Lower Pliocene to the *Globorotalia crassaformis* zone of the Middle

Pliocene and probably beyond. Foraminifera and ostracods indicate water depths of >500m for the marls that comprise the majority of the deposit. Palaeo-bathymetric lows are filled with mass-flow deposits. The platform sediment association is interpreted as evidence of rapid step-wise subsidence of the south Aegean during the Lower Pliocene. Stabilisation in the Mid Pliocene and subsequent inversion and uplift has brought the island back to sea-level, but uplift has not yet exceeded Pliocene subsidence (Peters *et al*, 1985). The strong tectonic control over Pliocene sedimentation in Crete resulted in a sequence very different to that in the other eastern Mediterranean basins. Although it cannot be used as a comparison to the Aksu basin sediments it serves to emphasise the relatively low tectonic control affecting the Antalya, Adana and Mesaoria basins during much of the Pliocene.

3.12: Tectonic versus eustatic controls

With the advent of sequence and seismic stratigraphy and the recognition of eustatic sea-level change (Vail, Mitchum and Thompson, 1977a,b) and the subsequent realisation of the modification effect of regional and local tectonics (Bally, 1982; Cloetingh, 1986) the interpretation of deltaic facies in terms of these parameters has become increasingly important. Fan deltas in particular are usually deposited in active tectonic environments, from extensional and transtensional basins to foreland basins. Tectonic control is frequently cited to account for changes in fan morphology and facies changes (McCallum, 1989; Gawthorpe and Colella, 1990; Colella, 1988; Alexander, Nichols and Leigh, 1990). Frostick and Reid (1989) show that, in the active tectonic environment of the Dead Sea pull-apart basin, details of fan geometry are controlled by fluctuations in lake level. The facies types and associations described by Frostick and Reid (1989), particularly the rapid transitions from muds to conglomerates are reminiscent of many aspects of the Çalkaya Formation. These features in the Dead Sea fans are attributed to fluctuating lake levels and to the rapid input of large volumes of coarse material by flash floods. Many similar facies features in the marine Pliocene can be attributed to small changes in sea-level and to shifting bars, lagoons and islands in the shoal face delta. The flooding event identified in Ma5/92b and Ma6/92b testify that this extremely shallow sea was highly sensitive to small sea-level fluctuations. Storm activity is recognised, which produces similar superposition of coarse deposits in relatively low-energy environments as the flash floods in the Dead Sea basin.

Excellent stratigraphy dates the onshore marine sediments to the *Globorotalia puncticulata-Globrotalia margaritae* zone and parts of the Çalkaya Formation sediments to the NN15/16 (chapter 2). The seismic evidence that the Yurtpinar

Formation is 500m thick and the recognition of three transgressive events within the formation also link deposition to sea-level. During the Mid Pliocene sea-level high, two regressive phases occur. Thus, three transgressions are expected, just as were inferred from the seismic data.

It is thus suggested that the sedimentary facies changes of the marine Pliocene are the result of eustatic sea-level fluctuations and not of tectonic events.

McCallum (1989) attributes the change from Nicosia Formation sedimentation to Kakkaristra Formation sedimentation to a pulse of tectonic uplift of the Troodos uplift. The transition between the Yenimahalle and the Çalkaya Formations is a gradational one, whereas the contact between the Nicosia Formation and the Kakkaristra Formation is sharp. In addition, the contrast between the shoal water profile of the Antalya delta and the Gilbert profile of the Cyprus deltas shows that Cyprus was tectonically more active, creating steeper basin margins.

The localised uplift of the Troodos ophiolite which directly affected the Cyprus Nicosia and Kakkaristra Formations is probably superimposed on a regional uplift, which may also have affected Antalya. Evidence for this regional uplift is also seen in Cyprus, Israel, and eastern Turkey/Syria (Piorazzoli, Laborel, Saliège, Erol, Kayan, Person, 1991), although drowned shorelines are characteristic of western Turkey (Flemming, 1971) and were observed in Adrasan Bay at the very southern limit of the field area. The general shallowing of the Yenimahalle Formation and the increase in sand size sediment may be the result of this gradual tectonic uplift, coupled with sediment infilling of the basin, but finally controlled by eustatic sea-level. The possible causes of this uplift and its continuation to the present day will be discussed in chapters 5 and 6. The question still remains as to the source of the coarse material of the Çalkaya Formation. However, the rapid climatic cooling that accompanied the onset of Arctic glaciation is likely to have been responsible for accelerated weathering rates and greater erosive ability of the Aksu river resulting in increased pebble supply to the Aksu basin.

The similarity between the sediments of the Adana, Aksu and Mesaoria basins adds further evidence to support an overriding eustatic signal in the eastern Mediterranean at this time. All three basins were flooded at the start of the Miocene and shallow water, deltaic sedimentation ensued. Tectonic modification of the style of sedimentation differs in each basin. Whereas, very little tectonic activity is recognised in the Antalya basins during the Pliocene, the northern margin of the Mesaoria basin uplifted with the Troodos ophiolite and the Adana basin underwent local compressive or transgressive deformation and clockwise rotation (Ünlügenç and Gürbüz, 1992).

3.13: Analogues

A close analogue to the Aksu basin delta deposition is the Lake Hazar pull-apart basin in south-eastern Turkey (Dunne and Hempton, 1984). Although the tectonic setting is not analogous and the basin is non marine, comparison is made to the sedimentation style in the basin. Two delta types are recognised: fandeltas, sourced from the steep basin margins, and a shallow water mouth-bar delta, arising from the progradation of the central drainage system into Lake Hazar. The latter facies types can be compared to the Yenimahalle and Çalkaya Formations, particuarly the Çalkaya Formation. The former equates to the coarse Kemer Fanglomerates. The controlling factor over sedimentation style in both Lake Hazar and the Pliocene Aksu basin is topography. In both cases a steep basin margin was responsible for the deposition of numerous, small coarse-grained Gilbert-type deltas, whilst a shoal-water delta developed from a shallow-gradient, central drainage system.

3.14: Conclusions

1) Deposition of the Gebiz Limestone occurred in a shallow shelf sea which may at times have seen restricted circulation or lagoonal conditions. Its age is probably Late Tortonian.

2) Messinian and Pliocene deposits onlap onto the tilted Gebiz Limestone.

3) Evaporite deposition, possibly in a sub-basin similar to those in Cyprus, occurred in the Aksu basin. The presence of swallowtail selenite gypsum indicates shallow-water growth in hypersaline silled basins or lagoons.

4) The Yenimahalle Formation was deposited in a shallow sea, 50-150m in depth. No coarse clastic input into the basin occurred, but silt sized particles and clays, reworked from the Miocene deposits were transported into the basin. The deposit shallows and coarsens up, possibly due to gradual tectonic uplift and basin infilling.

5) Seismic data indicates that the marine Pliocene is approximately 500m thick and contains three transgressive events that can be related to eustatic sea-level change. This helps relate deposition of the entire sequence to the duration of the Lower Pliocene highstand.

6) The Çalkaya Formation was deposited as a shoal water Type C delta (Postma, 1990) and represents regression due to rapid sea-level drop at the onset of Arctic glaciation.

7) Phreatomagmatic eruptions occurred during deposition of the Lower Pliocene sediments. The Isparta ignimbrite is the largest of these, but a small tuff-ring within the Pliocene sediment represents the same magmatic processes.

8) Coarse fan delta deposits originating from the steep-sided basin margin along the present-day western coast of Antalya Bay were probably deposited synchronously with the marine Pliocene.

Chapter 4:
The Antalya Tufa

This chapter includes an extended literature review covering all aspects of tufa sedimentology. Rapid developments in the sedimentological study of tufa and the paucity of in-depth reviews on the subject merit this as an introduction to the current study. The study is not only an integral part of the entire project, but a piece of sedimentological research of its own. A description of the facies types observed and the distribution of these facies both locally and regionally are presented. These data are then incorporated to develop a model of deposition. The uniqueness of this deposit in both size and depositional environment is striking and this study should significantly improve our understanding of tufa, and indeed terrestrial carbonate, as an important part of the sedimentological realm.

4.1: Travertine versus tufa - a question of semantics

Throughout the discussion the Antalya freshwater carbonate deposit is referred to as a tufa. This is in line with the conclusions drawn below.

There are currently no clear and generally accepted definitions of travertine and tufa and many consider them as synonymous (Ford, 1989). In the Mediterranean region all terrestrial carbonates deposited from carbonate supersaturated spring

waters have traditionally been named "travertine" e.g. Golubic (1961); Folk and Chafetz (1983); Weijemars, Mulder-Blanken and Wiegers, (1986); Emeis, Richnow and Kempe, (1987); Heimann and Sass (1989); Violante, Ferreri, D'Argenio and Golubic (1994). The Antalya deposit is no exception (Penck, 1918; Planhol, 1956; Aydar and Dumont, 1979; Burger, 1990; Özüs, 1992). Notably, Tietze (1885) and Phillipson (1918) referred to the deposit as "Kalktuff", the German equivalent of "tufa". In northern Europe cool water, terrestrial carbonates are generally called tufas e.g. Couteaux (1969), Marker (1971), Pedley (1993), and deposits from thermal waters are known as travertines e.g. Pentecost (1990), Koban and Schweigert (1993). Previous attempts to distinguish between the two have been made using porosity and lithification (Challinores dictionary of Geology, Wyatt, 1986; Burger, 1990, after Flügel, 1978; Guendon and Vaudour, 1971); and temperature of the spring water (Penguin Dictionary of Geology , Whitton and Brooks, 1988) All definitions agree that both travertine and tufa refer to $CaCO_3$ deposited from solutions of calcium bicarbonate.

The Antalya Tufa deposit reveals that lacustrine limestone and tufa are intimately associated within the deposit and cannot be differentiated as separate rock formations.

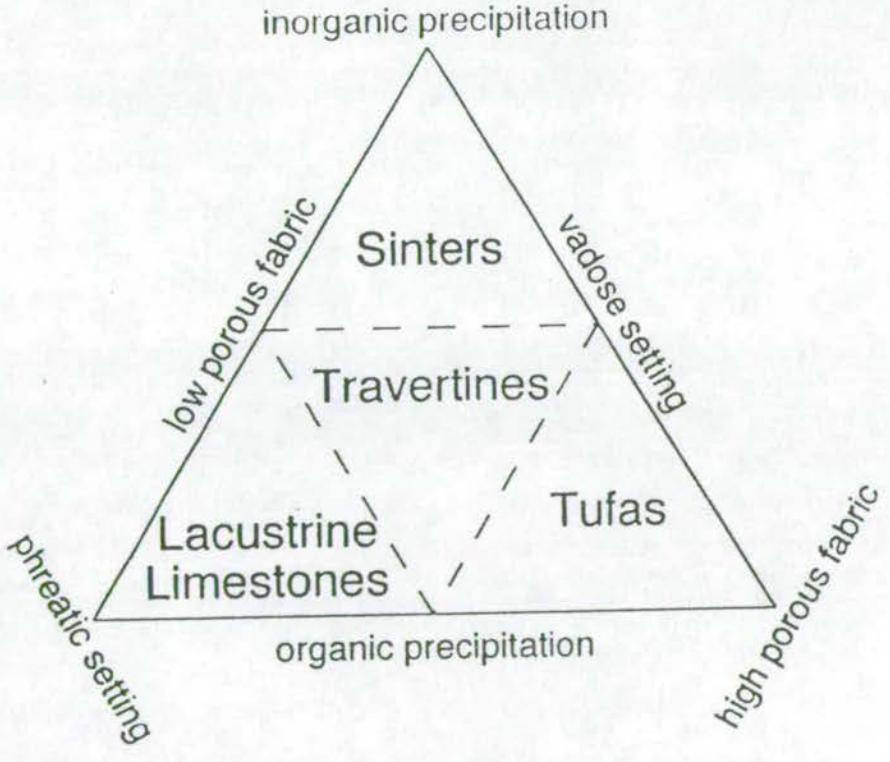

Fig. 4.1: Diagram showing the genetic relationship between different non-marine carbonate facies devised by Koban and Schweigert (1993).

The close relationship between all terrestrial carbonates: lacustrine limestone, travertine, tufa and sinter has been recognised in the classification scheme of Koban and Schweigert (1993). As the term sinter is more usually used for siliceous deposits, the term calc-sinter would be more appropriate in this case. It is interesting to note that Challinor (1978) suggests the word travertine to be equivalent to calc-sinter. Calc-sinter is here taken to be a hard calcareous encrustation formed by inorganic chemical precipitation from mineral enriched waters. Its predominant environment of deposition is in caverns (speleothem) and as fissure fill. Whilst it is predominantly a vadose precipitate, some sinter may form in the phreatic environment. The classification scheme of Koban and Schweigert (1993) utilises three variables: porosity, biological/chemical control, and vadose/phreatic waters (Fig. 4.1). It does not take into account temperature, which is one of the most important controls leading to distinctive fabrics in travertine and tufa (see discussion in sections 4.3 and 4.4). A modified diagram is proposed which addresses more effectively the problem of classification of freshwater carbonates (Fig. 4.2). Processes, environments and deposits are all represented on the diagram. These three elements are all discussed and reviewed further in the following sections. Processes are represented by the arrows along the sides of the triangle. 100% biogenic precipitation and 100% physico-chemical precipitation define the left and right edges respectively. The importance of these processes decreases perpendicular to the centre of the edge as shown by the dotted lines. The top of the triangle is cropped as it is impossible to have abiogenic and biogenic precipitation at a single point. Biogenic precipitation is algal at the base and changes gradationally to bacterial at the top. The base of the triangle represents 0°C and relates to the process of hydrothermal heating which increases perpendicular to the base. The gradient of hydrothermal heating from 0°C to 90°C is shown beside the main triangle. The environments where the the rock types are most commonly deposited are shown at the corners of the triangle and are from bottom left clockwise cold spring, hot spring and vadose. The environments grade towards each other along the edges of the triangle. The deposits expected in the different environments, due to the indicated processes, are shown in the fields within the triangle. The boundaries between these fields should not be taken as fixed. The importance of this diagram is that all terrestrial carbonates are inherently related and no definite distinctions can be made between tufa, travertine, lacustrine limestone and calc-sinter. It is significant that lacustrine limestone is the central field as it represents a deeper water facies which may be related to any of the others.

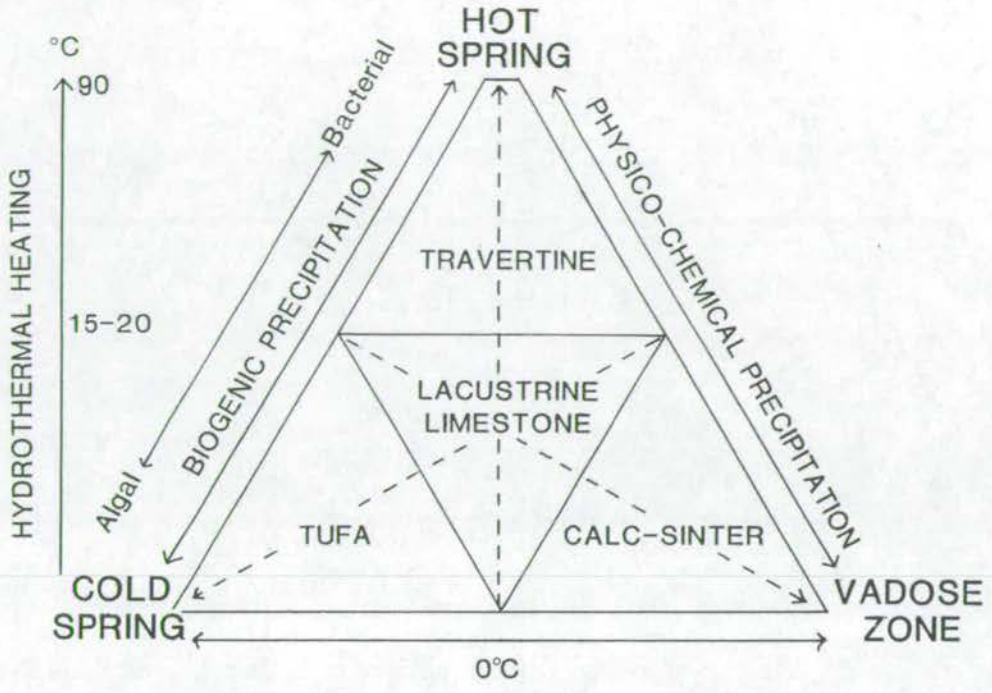

Fig. 4.2: New classification of terrestrial carbonates. The corners of the triangle represent environments of deposition. Terrestrial carbonate types are shown by the four fields within the triangle and processes controlling precipitation are represented by the edges of the triangle and the dotted lines perpendicular to them. A quantative representation of the hydrothermal heating line is given on the left.

4.2: Modes of deposition - Chemical and Biological factors

Calculating the solubility of calcium carbonate in natural waters is a complex problem. A full discussion and calculation is presented in Faure (1991). It is valid to consider the solubility as a function of the partial pressure of CO_2, temperature and pH.

Processes which decrease the quantity of dissolved CO_2 cause precipitation of calcite due to the reaction:

$$Ca^{2+} + 2HCO_3^- \rightarrow CaCO_3 \downarrow + H_2O + CO_2 \uparrow.$$

In general, it has been found that, due to loss of CO_2 , water downstream becomes increasingly supersaturated with respect to calcite (Barnes, 1965) and supersaturation as high as 63 times saturation with respect to calcite has been reported (Chafetz, Rush and Utech, 1991). CO_2 is probably the most influential of the three factors with respect to tufa deposition. Meteoric waters percolating through soil and karst systems and underground hydrothermal waters will equilibrate with CO_2 at a higher partial

pressure than the atmospheric pressure and become an effective calcite solvent. On exposure to atmospheric air, either in caves or at springs, CO_2 will re-equilibrate and $CaCO_3$ will be forced out of solution. CO_2 degassing is enhanced in areas of high turbulence such as the edges of channels, at rapids and at waterfalls; hence these are preferential sites for deposition. As discussed below, algal and bacterial activity also causes $CaCO_3$ precipitation by removal of CO_2 from water.

Temperature is an important factor in travertine deposition, directly influencing loss of CO_2. CO_2 solubility decreases with increasing temperature. This means that at thermal springs the emerging water is less capable of retaining $CaCO_3$ in solution, when CO_2 degasses as a result of exposure to the atmosphere. Warming of cool, shallow water by the sun may cause micrite precipitation to occur.

CO_2 solubility increases dramatically with acidity but this is unlikely to be of real significance within a natural tufa/travertine depositing environment. Acidic, industrial pollutants finding their way into freshwater, carbonate-rich streams may have an effect on the natural behaviour of the river and Pedley (1993) suggests this may be one of the factors inhibiting present day precipitation of the Derbyshire barrage tufas. It will be seen later in this section that the mucilaginous sheath associated with cyanobacteria is important for $CaCO_3$ precipitation and it is also suggested that inhibition of the growth of this sheath by nitrate may be an important factor inhibiting tufa precipitation in the area.

All the analysed tufa and travertine deposits which have been reported in the published literature are monomineralic low Mg-calcite. Some studies of recent, rapidly depositing, thermal travertines have found small quantities of aragonite to be present (Kitano, 1963; Pentecost, 1990; Chafetz *et al*, 1991). Aragonite is also present in the rather unique tufa towers at Mono Lake where spring waters emerge into a highly alkaline lake (Scholl and Taft, 1964).

In thermal waters (above 30°C) sedimentation is generally observed to be the result of physicochemical processes (Herman and Lorah, 1987, 38°C; Pentecost, 1990, 30-65°C; Chafetz *et al*, 1991, 33°C; Amundson and Kelly, 1987, 30°C). Rapid deposition occurred on a copper substrate placed in the thermal springs at Yellowstone (Chafetz *et al*, 1991). Since copper poisons bacteria and algae (Huntsman and Sunda, 1980) it can be concluded that deposition was entirely due to physicochemical processes.

At lower temperatures (studies of thermal waters between 19°C and 22°C) bacteria become increasingly important, although there has been some debate as to the exact rôle played by these organisms. Chafetz and Folk (1984) became convinced of the importance of bacteria as calcifiers after finding numerous bacterial forms in

the Tivoli region. Most distinctive are the bushy "shrubs" which contained bacterial structures. Koban and Schweigert (1993) found identical bacterial forms in the Stuttgart and Riedöschinger travertine deposits. However, Pentecost and Terry (1989) conducted experiments using forty-four strains of bacteria isolated from travertines and found that calcite was not nucleated. It is possible that bacteria merely thrive in moderate temperature waters and are readily preserved. The rapidly precipitating travertine may use the bacteria as a template or primary and secondary nucleation may occur on trapped seed crystals associated with the bacteria (see discussion in section 4.13).

There is little doubt that at lower temperatures (cold spring water) algae, in particular the blue-green algae (cyanobacteria), play an extremely important rôle to play. In the Plitvice deposits Emeis *et al* (1987) found that $CaCO_3$ did not precipitate on a copper substrate and thus it may be concluded that physicochemical deposition is not important in the cold-water, tufa depositing environment. Pentecost and Bauld (1988) conducted experiments which succeeeded in nucleating calcite on a limited number of cyanobacteria isolates, including the freshwater *Scytonema,* and demonstrated that different species differed in their ability to nucleate calcite. In the siliciclastic Walker Lake of Nevada blue-green algal stromatolites, which occur around the lake margin, contained three types of algae that directly precipitated carbonate and many other genera with the ability to trap clastic particles (Osbourne, Licari and Link, 1982). However, Pentecost (1978) showed that direct $CaCO_3$ precipitation from cyanobacteria isolates from British tufas, in particular, *Schizothrix*, only accounts for, at most, 5% of the total carbonate present in the tufa deposits.

The role of cyanobacteria as calcifiers has been studied in both marine and non-marine modern stromatolite environments (Monty, 1976; Riding, 1991b; Golubic, Violante, Ferreri, and D'Argenio, 1993). The main calcifying cyanobacteria are *Scytonema, Schizothrix, Phormidium, Oocardium* and *Rivularia*. These occur as epiphytes on aquatic mosses, fallen leaves or simply as stromatolitic mats. Monty and Hardie (1976) undertook a detailed study of the freshwater algal mats of the Florida-Bahaman region. Owing to the harshness of the $CaCO_3$ supersaturated waters, higher plants were absent and the fauna was restricted to rare gastropods and ostracods. The harsh environment, coupled with periodic wetting and drying of the area, allowed the blue-green algae to flourish. Logan, Rezak and Ginsburg (1964) also found periodic wetting was an important factor influencing the growth and morphology of stromatolite mats. Monty and Hardie (1976) made the important observation that, during times of exposure, desiccation and disintegration of the mat were common, causing large amounts of calcitic mud to be produced. This may result

in the complete loss of the original algal structure and preservation of the mat as a fine structureless limestone.

Whereas in the marine to brackish environment algal mats are often of the trapping and binding form, in the freshwater environment stromatolites are calcified as a result of impregnation in, or encrustation of, $CaCO_3$ crystals on the mucilaginous sheath coating the algal cells. This mucilaginous sheath is a sticky film of mucopolysaccharide secreted by many bacterial filaments and freshwater diatoms. Small calcite crystals were observed adhered to the mucilaginous sheaths of the cyanobacteria isolated in experiments (Pentecost, 1978). In particular, Merz and Zankl (1991) investigated the importance of the sheath in relation to carbonate precipitation by cyanobacteria. Emeis *et al* (1987) and Pedley (1992) noted that the higher plants often have an encrusting "fur" of cyanobacteria and pennate diatoms which appeared to have a direct influence on calcite precipitation. Pedley (1992) also observed an early micritic fringe cement on which a later sparry calcite cement developed. Emeis *et al* (1987) attributed this early micrite to entrapment of resuspended grains in the mucilaginous sheath associated with the "fur" of diatoms and cyanobacteria; these trapped grains then acted as a "seed" for further carbonate precipitation. In addition, Pedley (1992) noted that micrite development requires the presence of the biofilm and thus is limited to sluggish or paludal environments and that later, sparry cement probably develops in slightly faster flowing waters. It is important to note that cyanobacteria only stimulate $CaCO_3$ precipitation; it does not appear to be a necessary part of their life cycle. In fact, not all cyanobacteria are calcifiers (Défarge, Trichet and Couté, 1994) and yet in the presence of a highly $CaCO_3$ supersaturated environment many cyanobacterial species are found coated in $CaCO_3$ simply because they act as nuclei for precipitation. Thus, the formation of tufa requires the presence of specific cyanobacteria and carbonate supersaturation of the water. Since the presence of diatoms and cyanobacteria is seasonal, a layering of algal micritic tufa and cementing, sparry calcite develops. Cyanobacterial deposits may occur as a coating around plants and other submerged matter, stromatolitic mats or stomatolitic bioherms, as in the cases discussed above or as detached oncoliths. These can occur in high or low energy environments (Riding, 1991a; Nickel, 1983; Folk and Chafetz, 1983). Non-algal pisoliths may also occur in both travertine and tufa environments (Folk and Chafetz, 1983).

Labyrinthine brain-like furrows are often observed as layers within algal mats and micrite deposits. These are chironomid traces, the living and feeding burrows of insect larvae, probably *Lithotanytarsus emarginatus* GOEGTH (C. Pinder, pers comm., 1995) They are highly seasonal, indicative of springtime deposition. The

ecology of chironomids can be found in Theinemann (1957). Carbonate is deposited along the sticky threads with which the larvae line their tubes, thereby strengthening them (Irion and Müller, 1968).

Green algae and mosses also act as a substrate for tufa deposition. Parihar and Pant (1975) described a number of bryophytes, algae and some angiosperm which appeared to be contributory to tufa building. They saw the primary role of these organisms as that of an absorbent substrate on which thin films of water were retained and exposed, allowing loss of CO_2 and associated deposition of $CaCO_3$. In Checa, central Spain, Weijemars *et al* (1986) observed that tufa appeared to be associated with the photosynthesis of the lower plants and algae (i.e. the uptake of CO_2 or H_2O through the cell membrane to produce glucose - $C_6H_{12}O_6$). Encrustation occurred around the base of the mosses and algae causing them to grow upwards. The carbonate assumed the form of the moss substrate around which it precipitated. Different species were characterised by different growth rates; growth tended to be faster in the summer months giving rise to seasonally laminated deposits of spongy and dense layers. In fossil tufas the presence of the original moss or plant is usually only evident from moulds.

Fragments of stems and leaves, within a tufa depositing stream or pond, also act as substrates onto which $CaCO_3$ will precipitate. Although changes in the macrochemistry of waters are undetectable, the microchemistry in the immediate vicinity of the algal/plant material will cause $CaCO_3$ to precipitate (Chafetz *et al*, 1991). It is likely that these higher plants act as substrates because they are home to epiphytal cyanobacteria.

Travertine and tufa deposition is a self-building, self-regulating system which, once established, becomes self-perpetuating, as is evident in the models of depositional environment described in section 4.7.

4.3: Travertine

As defined in section 4.1 the word travertine is considered only to apply to terrestrial carbonate deposits precipitated from thermal waters (generally 20°C and above). The word travertine derives from the Latin *Lapis Tiburtinus* or stone of Tibur (now Tivoli), situated 25km east of Rome. This is a true thermal travertine which was, and still is, quarried as an ornamental building stone.

Travertine is uncommon, though spectacular, and most studies have been undertaken on a limited number of well known areas. Currently active travertine depositing hot springs are those at Mammoth Springs in Yellowstone National Park, Wyoming, U.S.A. (Barger, 1978; Chafetz and Folk, 1984; Pentecost, 1990);

Pammukale in western Turkey (Altunel and Hancock, 1993), Japan (Kitano, 1963) and Karlovy Vary in Czechoslovakia. Inactive deposits have been studied in Tivoli and nearby localities (Cortesi and Leoni, 1955; Folk and Chafetz, 1983; Chafetz and Folk, 1984), East Africa (Casanova, 1986) and in southern Germany (Koban and Schweigert, 1993). Thermal spring waters emerge at the surface containing a high concentration of dissolved ions which are then free to precipitate.

Travertine classification has been primarily based upon environmental setting and morphology, largely because the setting often has a strong influence on the morphology. Thus, the travertine facies from different settings are frequently distinctive. However, it is also because these studies have been based on currently active or very recent examples, where original depositional morphology is still preserved. Thus, 1) waterfall/cascade, 2) lake fill, 3) sloping mound, 4) terraced mound, 5) fissure ridge, 6) range front, 7) eroded sheet and 8) self-built channel forms have all been recognised and described (Chafetz and Folk, 1984; Altunel and Hancock, 1993). Relatively few petrographic and facies studies have been undertaken, although this is potentially a more useful interpretational tool for the study of ancient deposits.

Good descriptions of travertine facies can be found in Chafetz and Folk (1984) and Koban and Schweigert (1993). Many of the minor facies they describe from the travertines are comparable with those seen in tufa e.g. pisoids, intraclast layers, teepee structures and stromatolite-like mats. However, two facies are particularly important for identifying thermally deposited travertine. Bushy or shrub layers with a moderate-high macroporosity are most dominant. These are laminated with denser micrite layers and the resulting cyclicity is thought to be annual. Carbonate encrusted gas bubbles, "foam rock", are frequently, and exclusively, seen in thermal carbonate depositing environments. Microterracing is common on the surface of mounds and terraces and although this feature is not restricted to travertine deposits it is more prevalent in these environments.

4.4:– Tufa

The word tufa derives from *Tophus,* originally used by Pliny to describe porous rock. A number of tufa sites exist in Britain, for example: Matlock Bath, Alport by Youlgreave and Lathkill Dale in Derbyshire; Malham in north Yorkshire; and Caerwys in north Wales (Ford, 1989; Pedley, 1993). A map of all the British tufa locations can be found in Pentecost (1978). Further deposits have been described from the Hindu Kush (Jux and Kempf, 1971); the Transvaal (Marker, 1971); India, China and the U.S.A. However, it is the Quaternary of the Mediterranean region and

central Europe that has been the focus of most recent studies (Golubic, 1969; Kempe and Emeis, 1985; Brancaccio, D'Argenio, Ferreri, Damiano, Bruno and Maria, 1986; Brancaccio, D'Argenio, Ferreri, Stanzione, Taddeuci and Voltaggio, 1988; Weijemars *et al*, 1986; Emeis *et al*, 1987; Ordóñez and García del Cura, 1983; Szulc and Cwizewicz, 1988; Magnin, Guendon, Vaudor and Martin, 1991; Violante *et al*, 1994). It is only in these recent publications that the question of facies associations and depositional environments of tufa formation begins to be properly addressed.

It is noteworthy that such a large number of significant tufa sites exist around the Mediterranean. Widescale carbonate deposition around the Mediterranean during the Triassic-Cretaceous followed by compression and uplift have created depositional basins surrounded primarily by carbonate. Climatic conditions during the Quaternary have, at times, led to extensive karstification of these carbonate deposits and associated deposition of tufa at sites within the basins. Therefore the entire Mediterranean basin satisfies the unique criteria of significant quantities of carbonate basement coupled with climatic condtions favourable for tufa deposition.

4.5: Favourable Climates for Tufa deposition

Pedley (1990) states that a warm, humid, temperate climate is most favourable for tufa deposition. Under semi-arid conditions insufficient water exists to produce extensive karstification and under cold conditions tufa growth appears to be retarded. Marker (1971) also pointed out that above a critical value of rainfall, fluvial erosion dominates. She suggested that tufa deposition in the Transvaal was at a maximum during the transitional period from a glacial to an interglacial. Many authors attributed periods of maximum deposition to the postglacial and interglacials. Jux and Kempf (1971) believed the Afghanistan tufas to have been predominantly formed in a cool, humid, continental climate with a warm summer. Emeis *et al* (1987), after Horvatincic (1985), through radiometric dating of tufas, showed that carbonate in the Plitvice system precipitated mainly during warm, humid, Pleistocene interglacials and Pedley (1993) dated the Lathkill and Wye valley tufas as the same age. Analysis of oxygen isotopes gives a good indication of the climatic conditions under which a tufa was deposited: using this method Buccino, D'Argenio, Ferreri, Brancaccio, Ferreri, Panichi and Stanzione (1978) were able to identify the Tanagro deposits as temperate interglacial deposits. Interestingly, two authors, Szulc and Cwizewicz (1988) and Casanova and Nury (1989), as a result of oxygen isotope studies, suggested a tropical climate for deposition of tufas. Both noted that seasonality was important. This observation is supported by the preference of algal mats for a periodic wet/dry environment and by Marker (1971) and Weijermars *et al*

(1986). In the Holocene of central Europe both Coûteaux (1969) and Magnin *et al* (1991) found that tufa deposition was related to a cooling of climate and reflected an associated forestation. In Gaume, Coûteaux (1969) related tufa deposition to the cool, humid, Preboreal and Atlantic periods whilst in the intervening warm, dry Boreal, peats developed. In conclusion, the most favourable climate for tufa deposition is a temperate, humid one with marked seasonality.

4.6: Tufa facies

Tufa has been classified variously in terms of the fossil plants preserved within it (Irion and Müller, 1968; Schneider Schroder and Le Campion-Alsumard,.1983; Pentecost and Lord, 1988); its depositional environment (Chafetz and Folk, 1984; Marker, 1971); and the type of deposit (allocthonous/autochtonous) (Julia, 1983). Often it is not clearly distinguished from travertine deposits (Chafetz and Folk, 1984).

In order to properly utilise the concept of facies, their distribution and their environments of deposition, a facies scheme based on structures and textures is more useful. Algae and plants are not a useful guide to environment, although it is important to understand which organisms are involved in tufa formation. Classification in terms of depositional environment is, in fact, a classification of facies associations and does not subdivide the facies sufficiently to allow other environments to be identified, through the study of facies associations. In addition it relies heavily on recognition of original gross morphologies which are unlikely to be clearly recognisable in the fossil record.

Buccino *et al* (1978) first classified tufas on the basis of their structures and textures following the ideas of other sediment classification schemes. They recognised the following facies types (Note that they use the word travertine - this should properly be replaced by the word tufa):

1) Stromatolitic travertine (travertine bindstone) - *in situ* algal laminites
2) Phytohermal travertine (travertine framestone) - *in situ* encrustation of plants
3) Phytoclastic travertine - lensoid accumulations of phytoclasts
4) Phytoclastic calcarenite-calcirudite - smaller phytoclasts than phytoclastic travertine.
5) Foliar travertine- phytoclastic travertine in which the phytoclasts are predominantly leaves.
6) Phytoclastic sands - chalky deposits of coarse arenitic size.
7) Charophyta sands - as chalky sands with an important constituent of Chara fragments.

Ordóñez and García del Cura (1983) used a different scheme for their fluvial tufas. Many of the terms, however, are rather imprecise and the terminology is not consistently related to fabric alone. In particular moss tufa derives from the scheme of Irion and Müller (1968).

1) Vertical tube facies - applied to *in situ* encrustation of higher plants.

2) Crossed tube facies - also encrusted plants but with a high porosity and an orientation defined as relating to palaeocurrents.

3) Detrital tufa facies - relates to broken and redeposited fragments of tufa and has associated sedimentary structures e.g. cross-bedding, fining-up sequences.

4) Moss tufa -contains calcified bryophytes.

5) Stromatolites - subdivided into planar and mamillary after Logan *et al* (1964)

6) Oncolites - algal coated grains.

More recently Pedley (1990) combined, redefined and expanded the work of the above authors in an attempt to provide a more coherent scheme. His definitions follow:

1) *Autochthonous tufa deposits*

1.1) Phytoherm framestone - living anchored framework of encrusted floral and faunal organisms.

1.2) Phytoherm boundstone - stromatolite heads and algal mats (the latter was not specifically included in his original definition, but should have been).

2) *Clastic tufa deposits*

2.1) Phytoclast tufa - allochthonous, cement encrusted plant fragments.

2.2) Cyanolith "oncoidal" tufa - oblate to sub-spherical, detached stromatolites.

2.3) Intraclast tufa - silt and sand grade detrital tufa fragments reworked from the above deposits.

2.4) Microdetrital tufa - Very fine chalky sediment either structureless or clotted or peloidal in texture.

2.5) Paleosols - paleosols are included because they are commonly associated with tufas, particularly in a paludal environment.

At this stage in the development of sedimentological studies concerning tufa it is important that authors accept and use a common framework and terminology. Pedley (1990) clearly sets out a workable facies model and using this, the Antalya facies have been described. Two additional facies types, important in the Antalya area, are also described and these should be incorporated into the general model:

1) Pisolith tufa - inorganic pisoliths and oolites;

2) Tufa breccia - reworked tufa clasts up to tens of centimeters in size.

Tufa facies types

Autochthonous deposits	
Phytoherm framestone	*In situ,* cemented plant material.
Phytoherm boundstone	*In situ* stromatolite build-ups.
Clastic deposits	
Phytoclast tufa	Allochthonous fragments of plant material cemented before and/or after transport.
Cyanolith "oncoidal" tufa	Subspherical laminated stromatolites.
Pisolith tufa	Finely-laminated, inorganic, spherical balls. "Oolites" up to 2mm in size, pisoliths often approximately 0.5 cm in size.
Microdetrital tufa	Micrite, usually massive. Peloidal and aggregated textures also occur.
Tufa breccia	Intraformational breccia of all above facies type.
Intraclast tufa	Silt and sand grade detrital material, usually rich in plants.
(Paleosols)	Usually moderately developed, carbonate rich and in close association with microcrystalline material.

Fig. 4.3: Facies types observed in the Antalya Tufa taken from the classifiaction scheme of Pedley (1990). Two new facies types have been added a) Pisolith tufa (equivalent to the inorganic pisoliths described by Folk and Chafetz (1983) from hot spring deposits) and b) Tufa breccia. (not previously described). The right-hand column is from the field observations in the Antalya area.

The former (pisoliths) have been recognised from both tufa and travertine (Folk and Chafetz, 1983) but are not included in Pedley's scheme. They are highlighted specifically because the environment in which they form is likely to be much higher energy than an oncolite environment and thus they are important indicators of local regime.

The latter (breccia) has previously not been formally recognised and it is therefore proposed here as a new facies type. One previous mention of tufa breccia has been made; that of Planhol (1956a) who described an intraformational breccia facies within the Antalya deposit (note that he attributed this to tectonic movement but it is interpreted here as a sedimentary deposit). Both are described in more detail in the facies description of the Antalya deposits.

Since a paleosol is not a carbonate facies, but a relict soil it should not strictly be included within the facies scheme for tufa. However, paleosols are important within the freshwater environment and consideration of their presence is necessary to correctly intepret depositional environments.

An expanded facies scheme containing this new information, but essentially that of Pedley (1990) is presented in Fig 4.3 and it is this that is used to interpret the Antalya deposit.

4.7: Depositional environments and facies associations

The following review of depositional environments reaches much the same conclusions as Pedley (1990). It is somewhat expanded and incorporates more recent publications which make a significant contribution to our understanding of the systems involved. Facies description and sedimentological modelling of tufa systems are still in their early stages and future, more detailed work on tufa deposits will certainly refine, improve and add to existing models. My own study of the Antalya Tufa, conducted entirely from basic sedimentological principles, as will be seen, has elucidated the complexity of what must have been a very varied environment incorporating many aspects of the following models.

4.7.1: The barrage/lake system

The best understood and most commonly recognised environment of tufa deposition is the barrage/lake system, exemplified by the spectacular Plitvice lakes of Yugoslavia (Golubic, 1969; Kempe and Emeis, 1985; Emeis *et al,* 1987). This depositional environment has also been recognised at Bande Amir, Afghanistan (Jux and Kempf, 1971); the Transvaal, (Marker, 1971); Malta (Pedley, 1980); southern France (Magnin *et al,* 1991) and Derbyshire (Pedley, 1993).

The barrage/lake system develops when carbonate supersaturated waters flow down a confined river. Magnin *et al* (1991) refer to this system as "un véritable système morpho-bio-sédimentaire, regi par le developpement de la construction travertineuse". At rapids, breaks of slope and areas of pronounced river bed widening, colonisation by cyanobacteria and bryophytes plus increased water turbulence cause carbonate to preferentially precipitate. Tufa phytoherm framestone begins to grow and the area becomes elevated, thus enhancing its position as a preferential site for deposition. The phytoherms begin to act as barriers and upstream accumulation of water occurs. Pedley (1993) observed that the barriers often show an overall downstream-facing morphology and that smaller phytoherms cluster upstream from the principal barrage. Golubic (1969) first noted that the largest barriers tend to be found downstream and that the lakes accumulated behind these may flood over smaller barriers (Fig. 4.4A).

In general, it seems that two distinct facies associations can be recognised from this system: one from the barrage environment and the other from the lacustrine

environment. The barrage facies is a porous, bryophyte dominated, phytoherm framestone. The encrusted bryophytes may have a parabolic form inherited from the cascade flow of water over the barrage (see discussion of waterfall tufas in section 4.7.2). Magnin *et al* (1991) also noted the presence of laminated, algal and stromatolitic fabrics in the barrage deposits. Inorganic sinters may form in the splash zones of cascades and waterfalls and often a secondary sparry cement infills cavities. Golubic (1969) stressed the cyclicity of barrier growth with clearly definable phases of growth and cementation superimposing themselves as the barrier grows upwards and outwards. This cyclicity is also recognised in the Bande Amir system (Jux and Kempf, 1971). The lake deposits develop concurrently with the barrage deposits but produce a very different and distinct facies association. Typically, the sediment is dominated by micrite which may or may not be biogenically controlled. In the lake waters diatoms are common and seasonal diatom blooms may cause varves to develop. The lakes may also contain insect larvae, gastropods, ostracods and crustaceans and some fish. Around the lake margins oncolites and stromatolites develop and encrustation occurs around semi-aquatic plants. Jux and Kempf (1971) described in detail the plant and animal associations found in the Bande-Amir lakes.

4.7.2: The waterfall system

Waterfall and cascade deposits are very distinctive and spectacular, but tend to be very localised and thus have a poor preservation potential. They are essentially the product of fossilisation of a waterfall or cascade and occur protruding from cliffs or as plugs in incised valleys. (Marker, 1971).(Fig. 4.4B) The deposits are extremely porous and consist largely of cemented bryophytes; detrital material, twigs and leaves may also get caught up in the deposit. Marker (1971) described a horizontal upper surface that grades back upstream into the valley floor. Downstream the sheer face of the deposit is characterised by carbonate sheets, often bryophyte dominated, whose laminae follow the curve of the water face - the cones and chutes of Pedley (1990) or the hanging curtains of Chafetz and Folk (1984). These are the result of encrustation around mosses and plants which have been caught up in the parabolic path of the flowing water and are subsequently encrusted in place resulting from the action of the bryophytes and associated cyanobacteria and the high turbulence of the water. The cemented vegetation then acts as a course for the water and the structure becomes accentuated. This form is also seen developed in barrage deposits, as discussed in section 4.7.1, and care must be taken not to confuse the two as Chafetz and Folk (1984) did. Waterfall deposits are not associated with bryophyte framestones from the stream bed, nor do they have an upstream lacustrine association

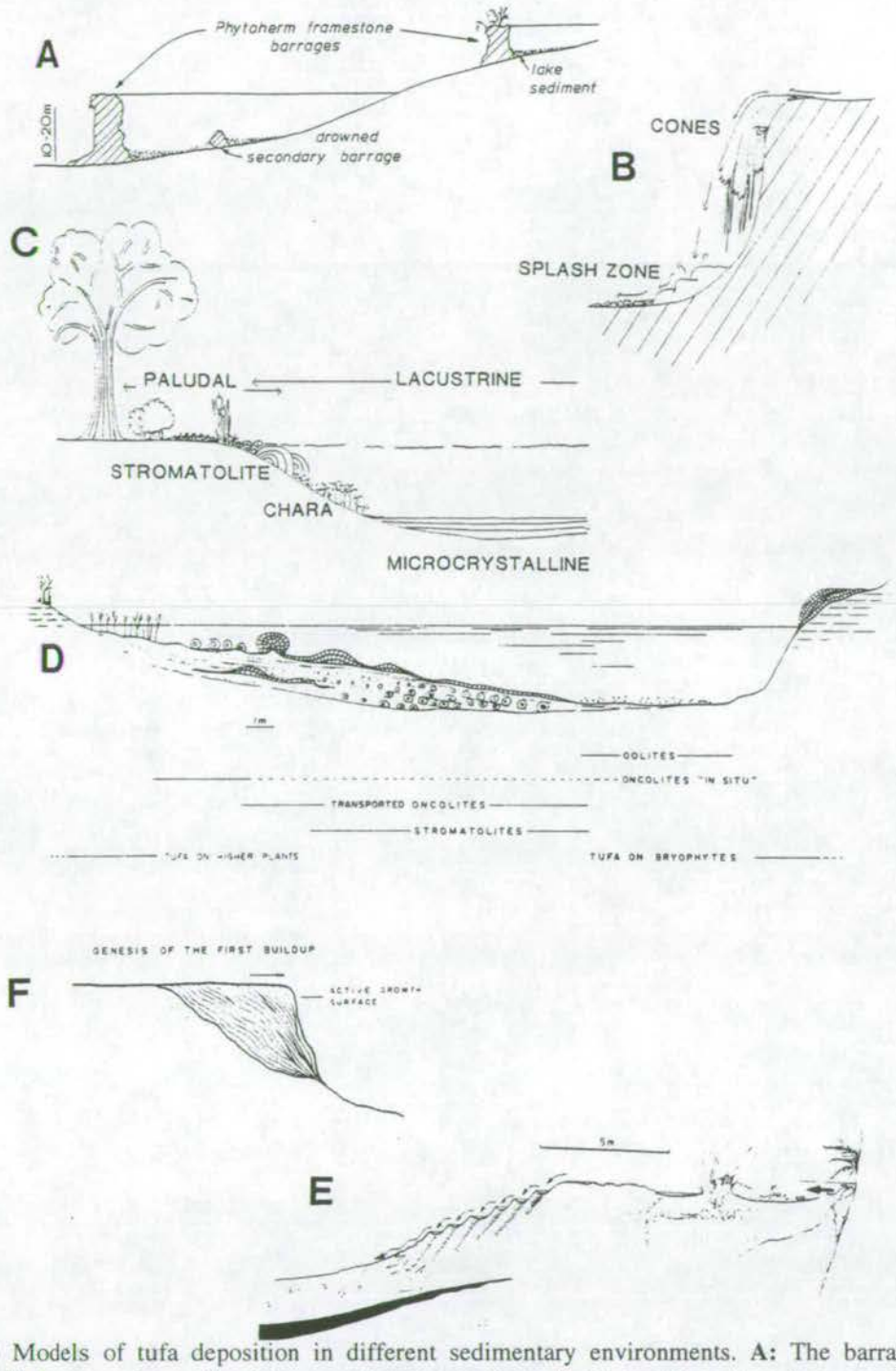

Fig. 4.4: Models of tufa deposition in different sedimentary environments. **A:** The barrage/lake system which occurs in confined rivers and streams, where phytoherm framestone barrages dam the river and cause lakes to form upstream (from Pedley, 1993); **B:** The waterfall system, where carbonate encrusts vegetation in the waterfall path and creates "cushions" at the base of the falls; **C:** The lacustrine and paludal systems, showing the associated flora and fauna of the complex paludal system and its association with the deeper lacustrine microcrystalline carbonates; **D:** The fluvial system, showing distribution of oncolites, stromatolites and sediments in the bar system of the channel (from Ordóñez and García del Cura (1983); **E:** The slope system or perched springline model of spring waters running down a shallow slope to create step-like terraces (from Pedley, 1990) **F:** The prograding model of waterfall carbonates proposed by Ordóñez and García del Cura, (1983) which can be compared to the progradation of the slope carbonates at Rochetta a Volturna (from Ordóñez and García del Cura, 1983).

At the base of the falls plants are strung out and cemented parallel to the direction of flow. In addition large, flat topped, moss cushions develop where the water pounds onto the ground. This is particularly well illustrated at Sitting Bull Falls in New Mexico, U.S.A. The tops of these cushions are dominated by thick, coarse, spar layers while the flanks are moss dominated (Pedley, 1990). Again the large hollows in the deposit may be filled by a later calcite cement or calc-sinter.

Weijermars *et al* (1986) describe a particularly well developed waterfall system at Checa in central Spain. They suggested that the 8m high, flat topped terrace formed as a result of lateral migration of a spring sourced waterfall. The tufa has a bryophyte dominated, spongeous texture. However, the facies description given is not sufficiently detailed to verify that this is indeed the case.

4.7.3: The lacustrine and paludal systems

Lacustrine sediments occur in deeper water areas and, just as in the barrage/lake system, consist of seasonally varved micrite, possibly with some organic content, rare gastropods, ostracods and molluscs. In the paludal environment rapid encrustation of the dense aquatic vegetation produces highly porous, phytohermal and phytoclastic deposits and may be associated with stromatolites, chironomids and a marsh fauna of gastropods and molluscs. Typically the two facies types are intimately associated. Paludal deposits occur around the shallow margins of lakes and pools and in a strongly seasonal climate may transgress out over lacustrine deposits as water levels drop during the summer months. In a dominantly paludal environment hollows of deeper water will develop a micritic lacustrine facies (Fig. 4.4C).

A mixed lacustrine and paludal system has been recognised from the Slawkow Graben, Poland (Szulc and Cwizewicz, 1988) and at Tanagro, Campania (Buccino *et al*, 1978).

The tufas of the Slawkow graben were deposited in a series of local hollows located down-slope from a set of springs. They include stromatolite mats and domes, algal varved micrite and a palustrine assemblage of calcified plants, algal and moss vegetation and some detrital input from the surrounding sediment regime (conglomerates and basalts).

Oxygen isotope studies suggest that the waters which deposited the Tanagro carbonates were in fact thermal (20°-30°C). However, the facies descriptions have all the characteristics of tufas (algal phytoherms and phytoclasts, preserved vegetation, micrite) and none of those of travertines (bushy, bacterial fabrics, regular lamination). The Tanagro tufas are thought to have been deposited in a trough shaped

depression (D'argenio, Ferreri, Stanzione, Brancaccio and Ferreri, 1983; and Fig. 18 of Buccino *et al*, 1978) although the English abstract of Buccino *et al* (1978) gives a slightly different interpretation " .... the travertines (sic) were deposited ..... on very low angle slopes in systems of shallow pools". This possibly equates directly to the Polish example where the pools are located downslope from the springs.

4.7.4: The fluvial system

This system, developed on non-confined fluvial plains, is well described by Ordóñez and García del Cura (1983) based on their studies in central Spain (Fig. 4.4D). Channels, containing oncoids and detrital tufa, are frequently cross-bedded and show fining-up sequences. Oolites may occur in the deeper parts of channels. Rapid cementation and algal binding create stabilised substrates, which cause frequent evolution of the flow regime in the system. Thus, lateral and vertical facies changes occur very rapidly. In the lower flow regimes of the channel margins, bryophytes, stromatolite mats and bioherms flourish. Encrusted plants and green algae, particularly Charaphytes, are common at gently sloping channel edges and on the flood plain. Current alignment of stromatolites, phytoclasts and encrusted plants is common. As the channels migrate with time, cross cutting and erosional features develop just as in siliciclastic river systems. It should be possible to distinguish between braided and meandering systems by straightforward sedimentological techniques (e.g. sediment size and distribution; bar distribution and form; cross-bedding directions).

4.7.5: The slope system

Springs often emerge along a line, some distance up sloping hillsides. If these springs are carbonate rich, tufa deposition will occur downslope relative to the springline. This system is similar to the "perched springline model" of Pedley (1990). New interpretation of the Rochetta a Volturno deposits (Violante, Ferreri, D'argenio and Golubic, 1994), previously ascribed to the barrage lake system (Brancaccio *et al*, 1986), has added to our understanding of this particular environment. The deposits are highly porous and dominated by phytoclast tufa and stromatolites. Some ponding may occur within the system giving rise to lenses of micritic or paludal tufa.

The overall morphology of the deposits is fan-shaped in plan view and wedge-shaped in profile. This wedge may either be thickest proximal to source as at Cozzo Marotto in southern Sicily (Pedley, 1990) and Pontecagnano (D'Argenio *et al*, 1983), or thickest distal from source as at Rochetta a Volturno (Brancaccio *et al*, 1988; Violante *et al*, 1994). The difference in profile is related to the way in which

the deposit builds out from the surrounding slope. In the first case water drains away from the spring forming a series of small step-like terraces, maintaining the profile of the slope and diminishing into a thin deposit of fine intraclast tufa at the base of the slope (Fig. 4.4E). At Rochetta a Volturna it is suggested that, in a similar manner to a prograding delta, the deposit modifies the slope shape, shallowing the upper surface and steepening the scarp surface until a flat topped terrace is produced. Paludal or shallow lacustrine deposits may develop on the flat upper surface in the late stages of development of the system. This model is very similar to the sedimentological model of waterfall carbonates proposed by Ordóñez and García del Cura (1983) (Fig. 4.4F). In the Hula Valley of Israel the large deposits of tufa are thought to have formed by a widespread, slow moving sheet of water flowing down a gentle slope (Heimann and Sass, 1989). Unfortunately, no cross-sectional profile of the deposit is provided. It may be that the deposit formed as the result of the coalescence of a line of springs along the hillside effectively forming a sheet-like slope deposit (see also Pedley, 1990).

4.8: Previous work on the Antalya Tufa

Early descriptions of the Antalya Tufa were made by the "travellers" of the early part of the century whose geological and geographical wanderings took them over vast areas of western Turkey. One of their main interests was the origin of the spectacular terraces which dominate the landscape around Antalya and their ideas will be presented and discussed in chapter 5. There exist only two recent studies directly concerning the Antalya Tufa deposits: Burger (1990, 1992) and Özüs (1992). Neither are primarily concerned with formation of the deposit. The former Burger paper considers the geomorphology, construction and karstification of the tufa and the thesis (1992) also includes a lengthy study of soil formation as an example of Pleistocene subtropical weathering. The latter study, an unpublished thesis from Çukarova University (Özüs, 1992), is concerned primarily with the geochemistry of the karst waters of the region, dealing only briefly with the formation of the deposit. Thus, although both authors have considered the formation of the tufa, it was not their primary objective.

Firstly, those aspects of previous work which are not directly relevant to the current study but nevertheless provide useful information to aid our understanding of the deposit are considered.

Burger (1990, 1992) sets out the post-depositional history of the deposit, which can be either diagenetic alteration of the surface or corrosion and weathering of the surface.

Two types of surface crust (essentially a cementation of the suface limestone) are described:

a) Case hardened, formed directly on the surface.

b) Bodensinter, formed under soil cover.

The latter gives a very clear ringing sound when knocked with a hammer.

Three corrosive forms are recognised from the Antalya Tufa:

a) Polje (or sink holes); created by collapse of a cave roof leaving a surface depression, usually circular. A number of these are described from the 40m level and one from the 280m level.

b) Karst marginal plains; caused by lateral erosion in small embayments, slightly higher than sea-level, which contain springs. Burger recognised these embayments, around the source of the Düden Çay, and related them to a former higher sea-level at the 40-50m level.

c) Karren, (the solution of the limestone surface into innumerable pinnacles or steep-sided ridges; these can be produced by subaerial (rain water) corrosion giving pits on a centimetre scale (rillenkarren) or subsoil (groundwater) corrosion giving pits on a metre scale (rundkarren). Their extensive development underlines the significance of corrosion on the travertine plains, particularly the lower one. At the 50m level subsequent soil erosion leaves large standing blocks exposed at the surface and small rillenkarren are developed on the tops of these blocks.

These observations are particularly useful in the field as they aid in the recognition of alteration and loss from the original surface deposits.

Burger (1990) recognises eleven levels of plain, eight of which are tufa plains. He divides these into a lower group and an upper group. The lower plains are typified as laterally corrosive and related to changing sea-level and groundwater resurgence. The upper plains are modified by constructional "travertine basin" tufa with corrosion marked by fields of rundkarren on the upper surfaces. "Travertine basin" construction is discussed in more detail below. Burger (1990) considers that the upper surface of the plains at 200, 240 and 270m are primary plains developed by the construction of the tufa. Burger (1990) also showed that springs occur at three main topographic levels around the complex: 300m (including the Kirkgöz spring group); 100m; and sea-level. These are essentially the two main terrace levels. The precise location of these springs is shown on the map (Fig. 4.5).

The geochemical results of Özüs (1992) which relate to the present day system are very probably indicative of the regime in the past and essentially show that the system was an open one from which carbonate was free to precipitate.

1) The Kirkgöz springs have a discharge of 15.62 m^3/sec. Hydrological, hydrogeological and hydrochemical analyses show that the spring waters discharge from a karstic aquifer with a very large groundwater reservoir which is not significantly affected by local rainfall. The calculated average decreasing coefficient value (α) which is a function of permeability, porosity and geometry of the Mesozoic limestones is of the order of 10^{-3} suggesting that the karst systems have a well-balanced flow, continuous feeding and storage. The pH values are in the range of 6 -7 and Ca^{2+}, Mg^{2+}, HCO_3^- and SO_4^{2-} values are high.

2) Geochemistry shows that for every 1 litre of springwater 40mg of carbonate are lost through sedimentation.

3) The upper travertine plateau is not an aquifer but does have an important rôle feeding the lower plateau. Conversely the lower plateau is an unconfined aquifer with widespread underground water.

4) Despite the lack of treatment of Antalya sewage, the bacterial contamination of the water is low indicating natural filtration, bacterial trapping and bacterial diminution within the porous tufa deposit.

It is interesting to note that the aquifer properties of the upper and lower plateaux may be directly responsible for the different karst characteristics of the two levels. It is only where groundwater is pervasive that large fields of karren are able to develop. The fact that this is not the case on the upper terrace implies that these karst pillars will not be strongly developed. Burger's (1990) argument that the upper plains are constructional, because the rundkarren are not so well developed, is thus not so convincing. It is not clear from the work of either Burger or Özüs why this fundamental difference exists. The origins of the terraces are discussed further in chapter 5.

Previous work on the sedimentology and formation of the Antalya Tufa deposit has been rather more sketchy and is of limited use to the following study. However, it forms a broad basis for the current study and the observations are in agreement with the current findings.

_ Tietze (1885) described the deposit as a freshwater calcareous tufa, containing plant stems while Philippson (1918) considered that the tufas were carbonate river deposits.

Planhol's contribution to the sedimentological study of the tufa deposits was somewhat more substantial: a discussion of the facies (1956a) and the stratigraphy (1956b) which, although simplistic, are the only real attempt to describe the Antalya deposit in this way prior to the current study.

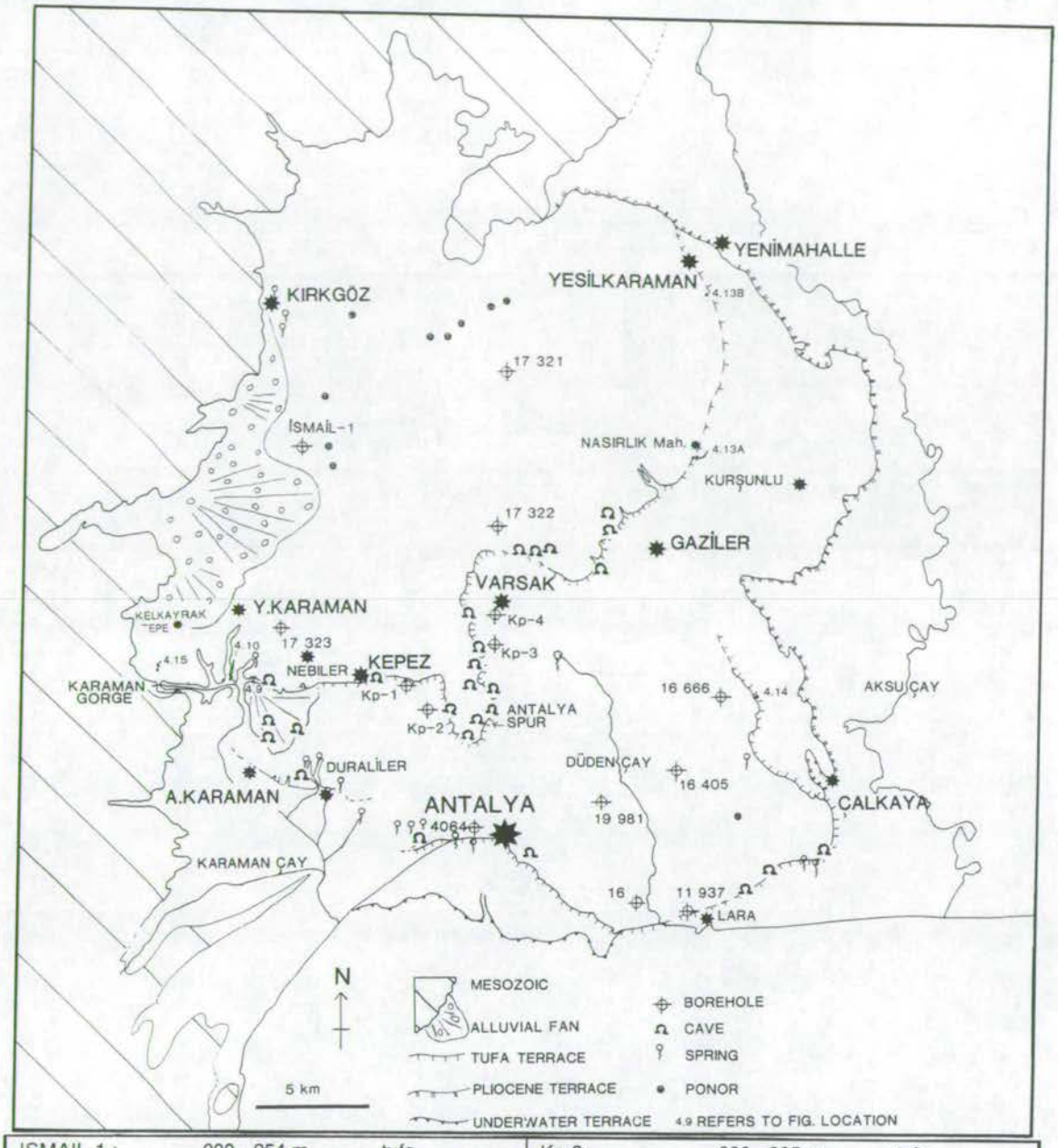

ISMAIL 1 :	000 - 254 m	tufa	Kp-3 :	000 - 085 m	tufa
	254 - 340 m	radiolarite		085 -150 m	radiolarite
	340 - 795 m	peridotite	Kp-4 :	000 - 065 m	tufa
17 321 :	000 - 099m	tufa		065 - 150 m	radiolarite
	099 - 274 m	conglomerate	16 666 :	000 - 055 m	tufa
17 322 :	000 - 200 m	tufa	16 405 :	000 - 058 m	tufa
17 323 :	000 - 251 m	tufa	19 981 :	000 - 060 m	tufa
Kp-1 :	000 - 078 m	tufa	11 937 :	000 - 030 m	tufa
	078 - 120 m	radiolarite	16 :	000 - 151 m	tufa
Kp-2 :	000 - 082 m	tufa	4064 :	000 - 011 m	tufa
	082 - 135 m	radiolarite			

Fig. 4.5: Map of the western Antalya basin showing the series of major terraces which dominate the present-day landscape. The location of springs on three major levels and the intense cave systems, particulary around the spur north of Antalya are indicated. Borehole data from Özüs (1992) are presented in the table. All place names mentioned in the text and the locations of logs and sketches figured in this chapter are also marked.

Planhol (1956a) recognised three main facies. A classification relating to the present facies scheme is given in parenthesis.

1) a friable, argillaceous facies, always relatively soft and whitish in colour, which he attributed to strongly terrigenous sedimentation in disturbed waters (microcrystalline tufa?)

2) a regular, crystalline facies, always very hard, and attributed to a calm lacustric phase which is further subdivided into 2a) a "tranquil" facies, essentially that described above (phytoherm boundstone; laminated algal mat) and 2b) a "jumbled" facies consisting of crystalline carbonate tubules (with a diameter of 5cm on average and up to 10 or 20 cm at most) representing cementation around undetermined plants and reeds. He observed that the "jumbled facies" occur around resurgences and discharge channels (phytoclast tufa).

3) an intraformational breccia facies seen only in an area to the west of Antalya which he attributes to localised tectonic movements (tufa breccia).

He considered the transition from facies 1 to 2 to be the result of gradual change over time from a disturbed environment to a calm one. In contrast he considered the relationship between 2a and 2b to be distributional with 2a found in the heart of the basin and 2b found around the basin margins.

Burger (1990) described a number of facies types: a) a porous tufa which can either be *in situ* or alluvial; b) a consolidated "travertine" with secondary crystalline cement; and c) a silty powdery "chalk". These can presumably be described under the present classification scheme as: a) phytoherm framestone and intraclast tufa b) surface crust or possibly phytohermal tufa and c) microcrystalline tufa.

Thus between the two, most of the facies types present have been described, albeit rather sketchily. The notable exceptions are oncoidal and pisolith tufa and phytoherm boundstone of the large stromatolite dome form.

Planhol's stratigraphic study (1956b) used the evidence of Depape and Arènes (1952), who found *Salix caprea* and *Salix cineria* leaves from the 40m terrace level near Antalya, and comparison with flora from tufas near Burdur lake (*Quercus* cf. *Q. pendulata*; *Glyceria* cf. *G.*; and *Salix babylonia*) to infer a cold humid climate with conditions favourable to carbonate dissolution, for example at the start of a post-glacial warming. The period of deposition is, thus, attributed by Planhol to the end of the Würmien. This is a rather arbitrary classification and the term Würmien itself is largely meaningless. The term comes from the Quaternary classification scheme of Penck and Bruckner (1909). Only four glacials were recognised during a period in which it is now known there were ten. Originally, Würmien represented the last period of glaciation, but, in fact, it represents more than one glacial advance and the

intervening glacials (Bowen, 1978). Consequently, no importance is attached to Planhol's hypothesis.

Only Burger (1990) seriously tackled the problem of deposition of this large quantity of tufa. He proposed two constructional processes which he believed produced the Antalya Tufa deposit

The most important of these was the construction of what are called, by Burger, travertine basins (Fig. 4.6). The limiting walls of these basins were constructed as one layer of travertine precipitated over another from water flowing down from the Kirkgöz source group. Primary caves were produced by overhangs in the outer parts of the walls. Stratified fillings of chalk and "alluvial tufa" were deposited in the pools. These are typified by the depressions on the spur north of, and currently being engulfed by, Antalya city (Fig 4.6A, B). Burger considered that a whole series of these spurs transgressed into the sea and created the majority of the Antalya Complex.

There are a number of objections that, together, refute this model. Firstly, it is hard to envisage how the barrier system of Plitvice, with which he compared the construction, can operate, without a narrow, confining, channel, to form a series of transgressing circular pools. In addition, no pre-existing roughness of topography is called for to initiate barrage (or pool wall) formation and in his Fig. 7 (Fig. 4.6C) the barriers are shown occurring directly over "alluvial" tufa deposits and not over a protruding cemented barrier from the previous system, where it would be expected that preferential tufa deposition would occur. Secondly, he stated that alluvial tufa is developed towards the upper parts of the pool fill and yet these do not appear to erode either the chalky sediment or the barriers themselves. Thirdly, there are many facies types that are not recognised or incorporated into the model (e.g. stromatolites). Finally, Burger claimed that similar structures can be seen in the cliffs of the Karaman river, however the current study cannot confirm this. Observations from the present study suggest the the features observed on the spur north of Antalya are karst features. This is discussed further in chapter 5.

– The second constructional process was the formation of bands and cones of alluvial tufa: these are recognised as especially typical for the upper part of the sequence. He described them as well stratified and containing fragments of fragile hollow stem tufa thought to have formed upstream, where the river gradient is lower and the water flow slower. Cones are seen constructed at the foot of escarpments. These may be equivalent to the cascade deposits of other authors, as discussed in section 4.7.2. Burger did not explain how these deposits relate to the previous deposits or what the changes in environment were which increased their dominance

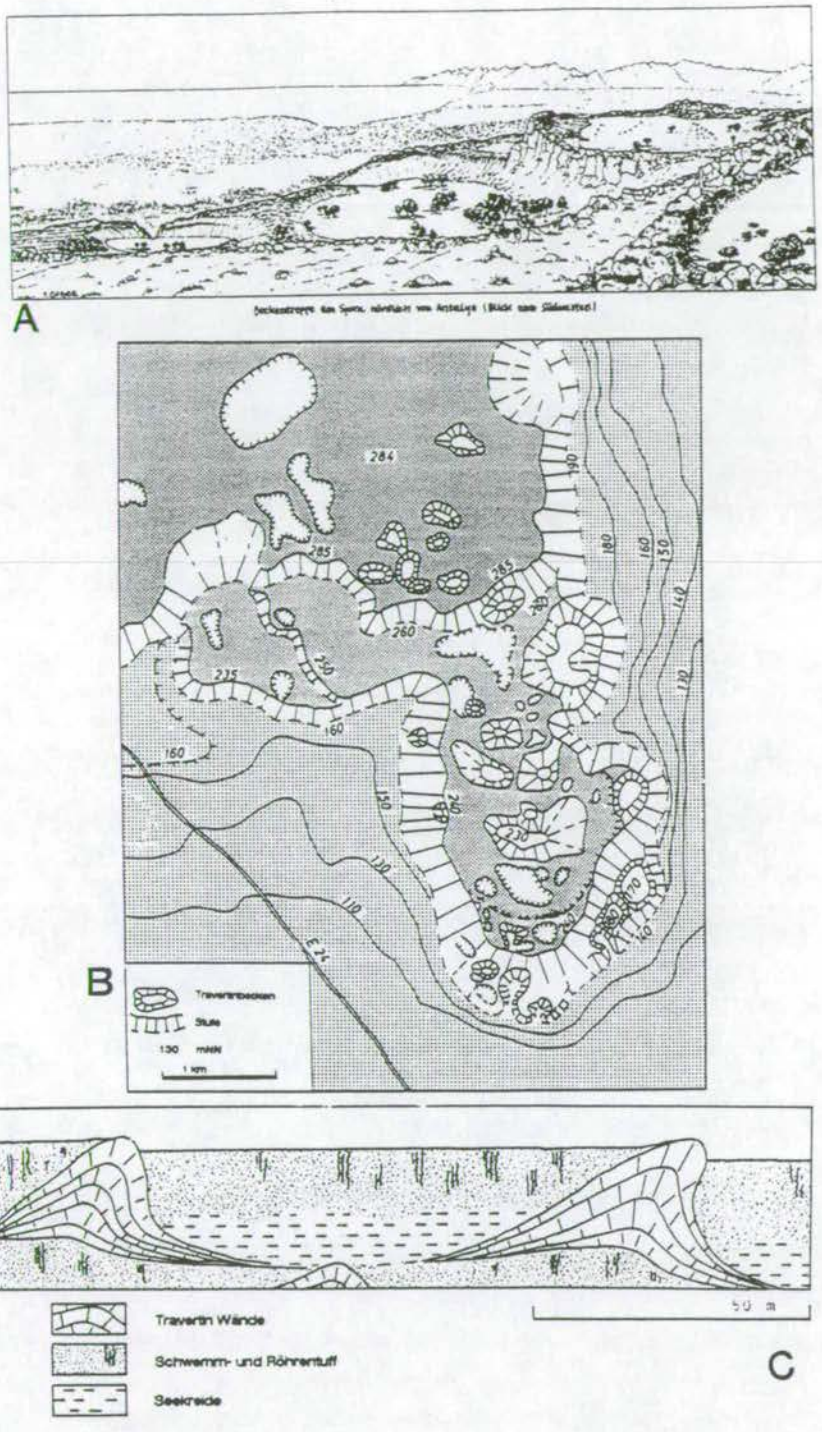

Fig. 4.6: Models of tufa formation in the Antalya area from Burger (1992) **A:** sketch of the depressions on the Antalya spur. **B:** map of the Antalya spur showing the large number of depressions. **C:** model of basin construction: walls of hard tufa create basins into which chalky sediment deposits. With time the system progrades out and new deposits cover old ones.

towards the upper part of the sequence. He believed that the lower terrace was built by the Düden river which meandered over the 40m level, constructing the platform. It is now fixed in its course. This is in direct contrast to the opinion of Planhol (1956) who viewed the lower terrace as an erosional product of the meandering Düden river. This will also be further discussed in chapter 5.

Both Burger (1990/1992) and Özüs (1992) described a third major plateau which exists below sea-level, extends some 2.5 - 3.0 km south of the present day shoreline and drops 150m at its edge. Unfortunately, I have not had access to the data which could confirm this.

4.9: The present day system

It is probable that the hydrologic regime which existed in the past is little changed from that which exists today. A number of studies have focused in particular on the hydrology of the system because of its importance to the drinking water supply and the sewage disposal of the Antalya district. However, the volume of water that flows through the system must be significantly less than in the past, as demonstrated by the limited deposition in the present day and the calculations of past rates of deposition and water flux set out in 4.9.3.

4.9.1: Location and source waters of the Antalya Tufa

The tufa deposits of Antalya occupy approximately 600 square kilometres of the northwestern corner of the Aksu basin. They outcrop as a series of major terraces which dominate the present day landscape of the area. (Fig. 4.5) Borehole data presented in Özüs (1992) shows that tufa on the upper terrace varies between 99m and 254m thick and on the lower terrace between 65 and 85m thick. However, in the Yesilkaraman area where tufa sits directly on Pliocene terrace the thickness of the formation is only 20-30m.

The water sources for the spring systems in the Aksu and Köprü basins are thought to be the lakes of Eğirdir, Burdur and Beysehir, situated some 100km to the north, and the polje system (now dry) at Kestel, Planhol (1952), Burger (1990), Özüs (1992). Değirminci and Günay (1992) establish good evidence for hydrological connection between Beysehir lake and the Olukköprü springs in the adjacent Köprü basin, mainly following the line of the Kirkkavak fault. They see a strong relationship between structural trends in the area and karstification and identify limestones as the dominant aquifers. They do not discuss the recharge system of the Aksu basin, but do identify a groundwater divide between the Köprü and Aksu basins effected by the impermeable ophiolitic spur running N-S between the two (Fig. 4.7).

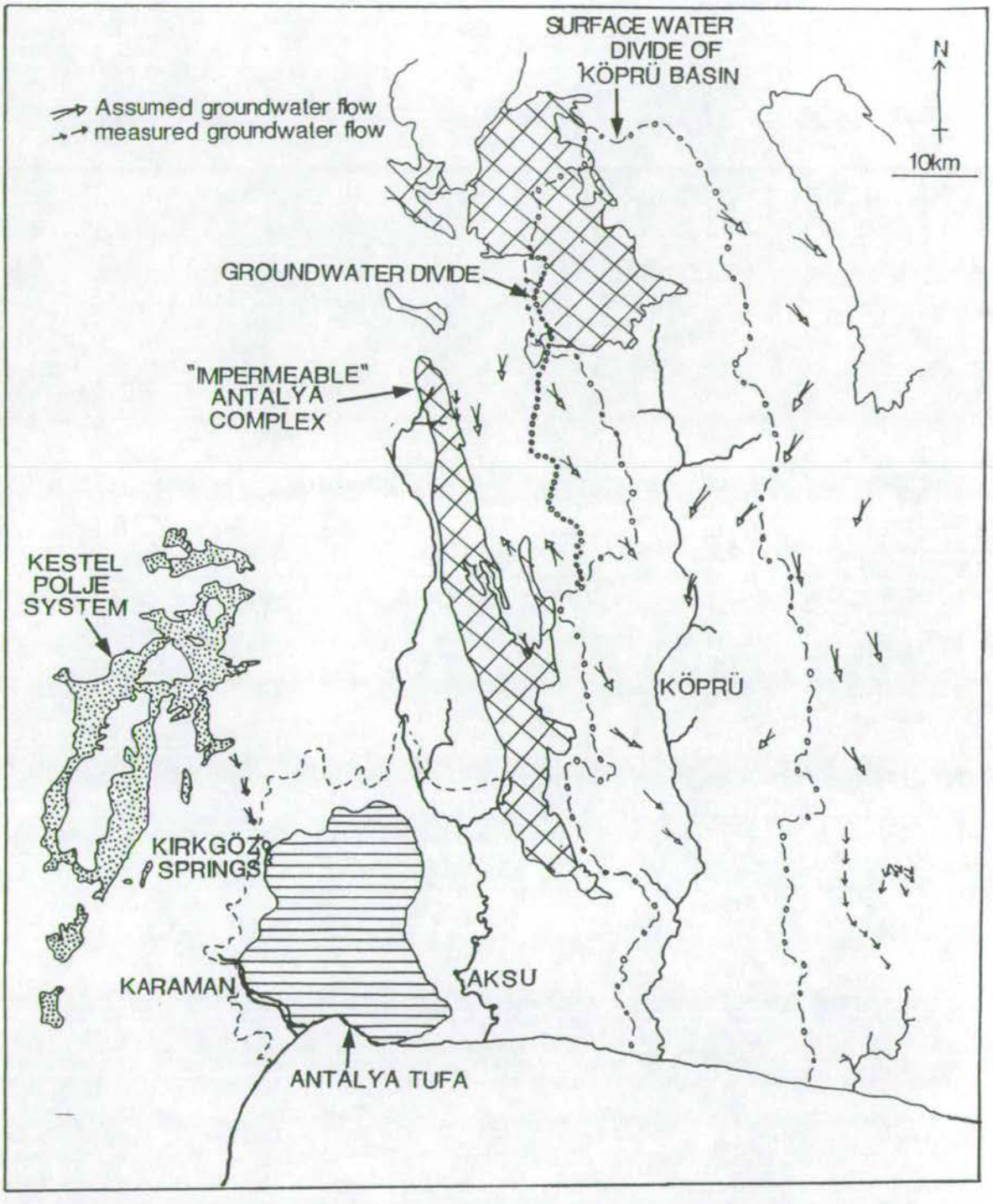

Fig. 4.7: Groundwater flow in the Köprü Basin from Değirmenci and Günay (1992) demonstrating the assumed water flow from the Eğirdir/Beysehir region to the Köprü Basin. Groundwater to the Aksu basin almost certainly travels similar distances. The groundwater divide created by the impermeable Antalya Complex is also clearly shown, as are the Kestel Polje, thought to have been a important source area for the Antalya Tufa.

Extensive karst systems through the Mesozoic carbonates of the Taurus Mountains bring large volumes of carbonate supersaturated waters from these source areas to the Antalya plain. The area of Kirkgöz (forty springs) situated in the northwest corner of the upper plateau is currently the major spring area, although numerous other springs exist in the region (Fig. 4.5).

4.9.2: Present day deposition in the region

At the present time deposition of tufa on the Antalya plain is very limited. Dramatic deposition occurs at the waterfall sites of Düden, inland and at the coast, and at Kursunlu (Plate 4.1A). In addition, very small quantities of carbonate encrust water plants in the springs at Kirkgöz and microcrystalline tufa is seen to be present in the pools and streams developed in the area. Locally, some small streams deposit carbonate. At Duraliler, fine examples of intraclastic tufa bars, encrusted leaves and twigs were found (Plate 4.1B,C). Two successive visits to the mouth of the major gorge system at Asağ ikaraman revealed that the drying up of shallow water left a film of carbonate associated with the algae which had flourished on the surface of the shallow water (Plate 4.1D). Even in the Manavgat river carbonate is seen to precipitate on water plants (Plate 4.1E,F) although there is no evidence that the Köprü basin was ever a site of major tufa deposition. Although many of these phenomena would have been found in the past, the present day system is a mere relict of what existed and in many ways bears no comparison to the system described below.

4.9.3: Duration of precipitation

In order to assess the time scale involved in deposition of the tufa and to gain a better appreciation of the scale of the deposit, a number of calculations were made. Firstly, an estimate of the volume of tufa was calculated as follows. The surface area of the upper terrace was evaluated from the topographic map by a simple square counting exercise. The result was 485 km^2. Borehole data (Fig. 4.5) suggests that, for the upper terrace, the tufa is of the order of 250m thick in the west (Ismail-1, 17 323) 200m in the south (17 322) and 100m in the centre (17 321). On the eastern terrace edge the tufa is about 30m thick and sits on Pliocene sediments. On the basis of this limited data it seems reasonable to approximate the form of the upper terrace to a wedge with the major axis running SW-NE and the thickest part of the wedge in the SW. In reality it is certain that the underlying topography is irregular, however it is not possible to more accurately characterise the shape of the formation in more detail

from the data available. From this assumption the volume of the upper terrace is calculated to be 6.412×10^{10} m^3 .

Two authors have investigated rates of precipitation of tufa: Emeis *et al* (1987) and Heimann and Sass (1989). Based on measurement of the loss in total dissolved ions and conductivity in the system at Plitvice National Park Emeis *et al* (1987) estimated deposition over an area of 2 km^2 as 10×10^6 kg a^{-1}. Heimann and Sass (1989) based their calculations on radiocarbon ages of two samples separated by a known vertical interval (2.5m) They then calculated from the area of the Hula valley deposit (18 km^2) and assuming a bulk density (1.5g cm^{-3}) a rate of accumulation of 8.6×10^6 kg a^{-1}.

The time required for deposition for the Antalya Tufa can be calculated from these data. The similarity between the description of the Hula valley tufa and the Antalya Tufa justify assuming the same bulk density. This gives a mass of 9.618×10^{13} kg for the upper terrace of the Antalya Tufa. Assuming 8.6×10^6 kg a^{-1} per 18 km^2 gives a period of deposition of 440,000 years. Applying the Plitvice rate of 10×10^6 kg a^{-1} per 2 km^2 gives a period of deposition of only 42,000 years.

The difference between 440,000 years and 42,000 years is significant! The meaning of this must be considered. The prime depositional setting in each case is the important factor. At Plitvice the water is fast flowing and turbulent over the barriers and it is reasonable that precipitation rates seem to be much higher here than at Hula where the waters are thought to have been sluggish and widespread over an area of lush vegetation. The situation at Hula is much closer to the situation proposed for the Antalya Tufa and it is to be expected that the rates applied there are more realistic than those at Plitvice.

The calculations only apply to the upper terrace of the tufa as it is relatively simple to calculate its volume. From the results it is reasonable to suggest that the entire tufa mass was deposited in the order of half a million years.

4.10: Facies descriptions

The facies types observed in the Antalya Tufas have been classified according to the scheme of Pedley (1990) and are systematically described in the following section (4.10). The new facies types: pisolith tufa and tufa breccia, are described.

4.10.1: Phytoherm Framestone

The definition of a phytoherm framestone given by Pedley (1990) suggests a large "reefal" type structure consisting of *in situ* plant material, either recumbent or vertical, and an associated fauna of ostracods, larvae and molluscs.

In the Antalya area the phytoherm tufa is more commonly of a patchy nature and is not of a significant "reef" building nature, except when developed under cascade or waterfall conditions. In general, layers of cemented, vertical plant stems alternate with more crumbly microdetrital layers (Plate 4.2A). In these layers the stems tend to be uniformly cemented to approximately 0.5 or 1 cm in diameter but can reach up to 15cm in diameter.

Where waterfalls and cascades occur, large volumes of plant material, mostly reeds and mosses, become cemented in the stream of flowing water. Individual strands can reach meters in length. The result is a highly porous "stringy" fabric which is occasionally infilled by a secondary cement but more often remains as it was originally deposited (Plate 4.2B). On shallow slopes, encrusted vegetation follows the line of slope in a recumbent manner. In the most extreme cases, where water flow is fast, large conical structures form. The cones themselves are well cemented but large cavities exist below the cones. These can be seen developed at both falls of the Düden river - inland (where it is possible to walk around in the cave system behind the falls) and on the present day coastline (Plate 4.1A). These deposits are directly analogous to the waterfall and cascade deposits documented by Marker (1971) and others (as discussed in 4.7.2).

In both hand specimen and thin section it can be seen that calcite precipitates radially around the stems. Thin section evidence suggests that algae play an important rôle. In thin section it is also clear that around the stem itself a micritic layer, rich in organic material forms and that it is on this that the calcite crystals begin to grow (Plate 4.1C). Later, void filling, cements are coarse crystalline carbonates. In many cases the stems have an outer layer of very bobbly, iron-rich carbonate. In thin section these can be seen to be microstromatolites. This, and the algal structures observed within the crystalline material will be discussed further in section 4.14.

4.10.2: Phytoherm Boundstone

Phytoherm boundstone occurs most frequently in the area as stromatolitic tufa. Frequently, it is associated with the brainlike, lenticular, texture of chironomid; the highly seasonal indications of the presence of large numbers of insect larvae (Plate 4.2D).

The algal deposits are clearly laminated. Chironomid textures indicate that this is a seasonal banding. In thin section, the chironomid houses are surrounded by a thin coating of micrite with coarse crystalline calcite between the lenticular voids. Where chironomids are not so important the laminae occur as layers of radiating

Plate 4.1: Present day deposition of tufa in the Antalya area:
A) Dramatic deposition occurs at the inland waterfall of the Düden Cay. B) Examples of intraclastic tufa bars, encrusted leaves and twigs found in a small stream near Duraliler C) Recent encrusted leaves and twigs picked out of the Duraliler stream. The surface texture of the leaves is well preserved. D) Carbonate encrusted algal film, broken and left lying on the ground surface after ephemeral waters dried up. E) Part of the Manavgat river south of the main road. The white colouration is carbonate encrustation on patches of grass within the river. F) Close up of the white areas showing carbonate encrustation around individual stems of grass.

Plate 4.2: Facies types of the Antalya tufa I:
A) Phytoherm framestone: layers of cemented, vertical plant stems alternate with more crumbly microdetrital layers. The absence of root structures within the microdetrital layers suggests that a thin paleosol may have existed, but has now weathered away. B) Phytoherm framestone: cascade deposit where long strands of reeds and mosses are cemented in the flowing water. C) Photomicrograph of crystalline calcite which grow radially around a plant stem. The innermost layer is an organic rich micrite, black in colour, and represents the surface on which the carbonate started to precipitate. Field of view 3.5mm x 3.8mm. D) Phytoherm boundstone: Chironomid traces within a stromatolite mat. The upper half is a plan view and demonstrates the complex furows caused by the feeding insect larvae. The lower half shows the lenticular shape of the traces in cross-section. E) Scanning electron micrograph of the calcite fringes within laminated algal mat showing the highly fibrous nature of the crystals which is attributed to precipitation around cyanobacteria. F) Scanning electron micrograph of the same fibres at over 10x greater magnifcation. The fibres have complex form and may bifurcate The ends of some bunches of crystals have flat faces.

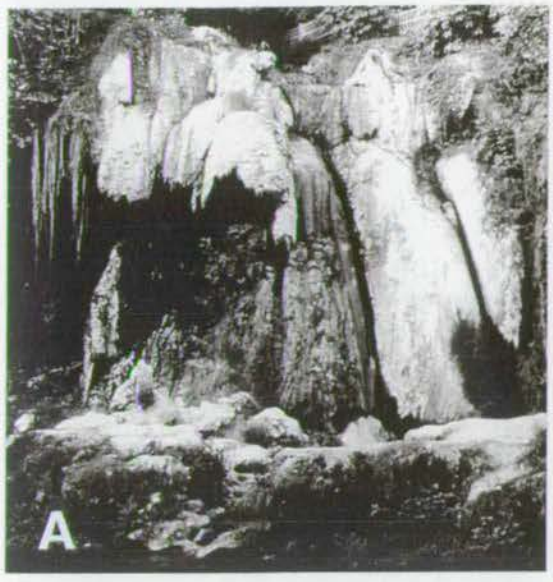

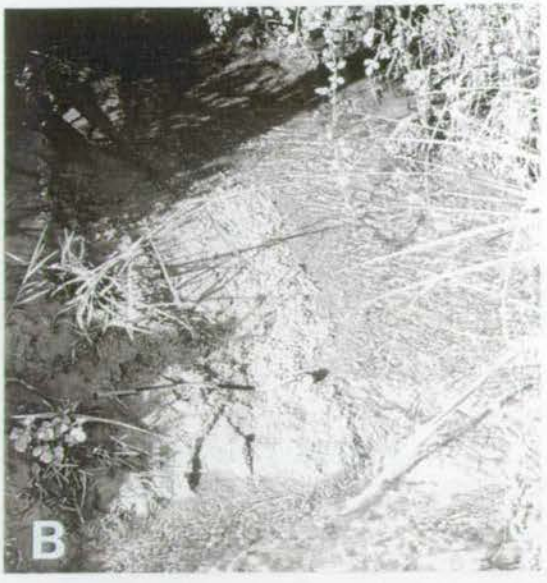

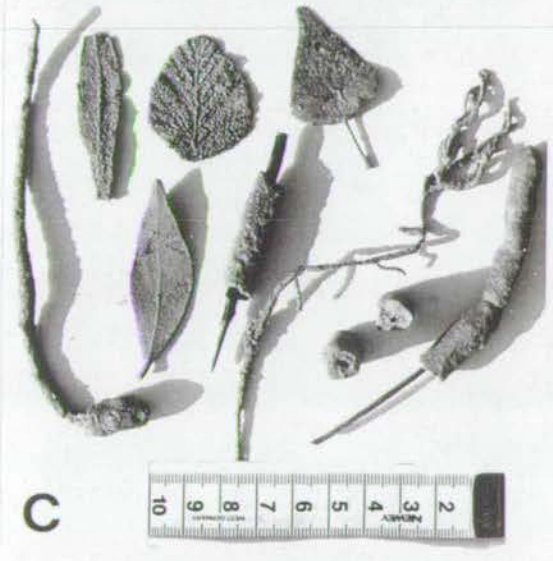

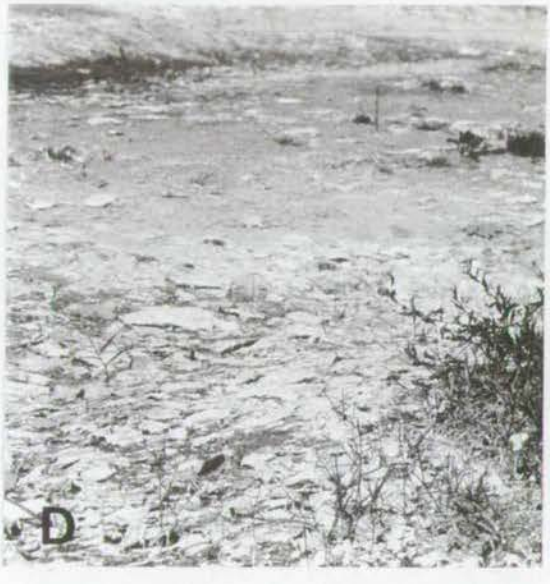

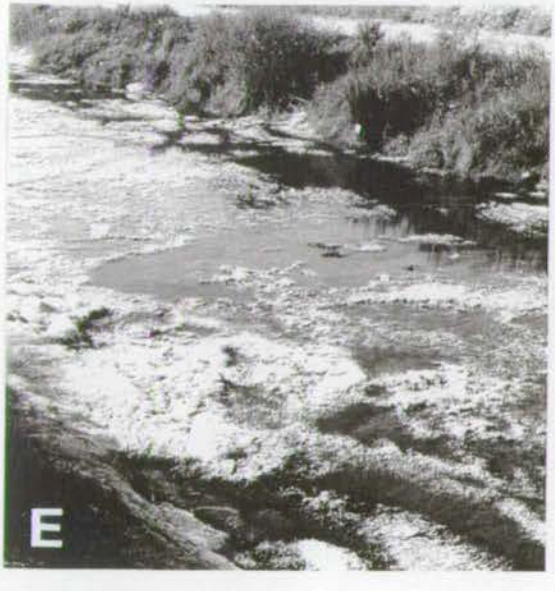

Plate 4·1

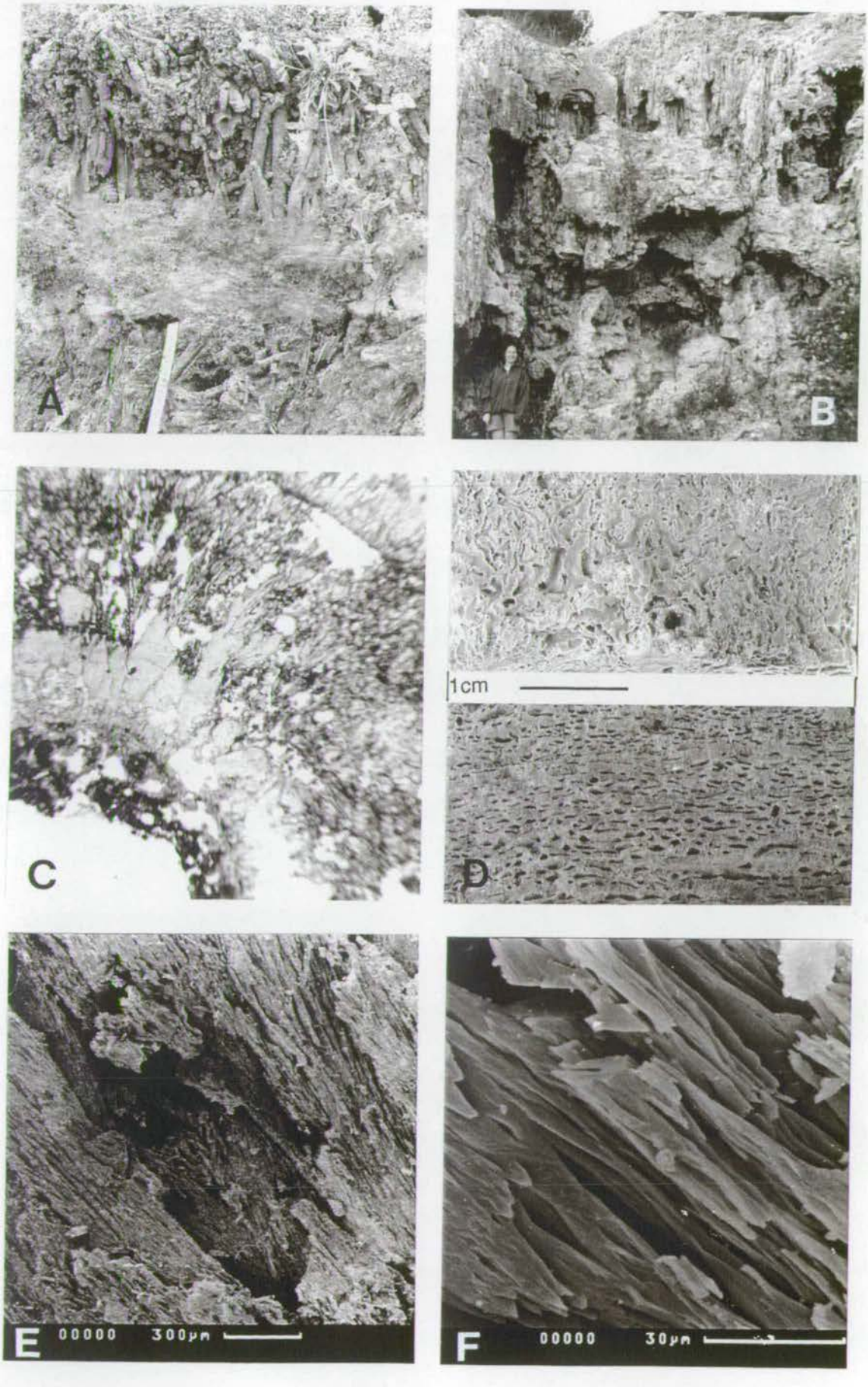

Plate 4·2

calcite fringes of about 1/2cm in thickness growing upward from dense microcrystalline layers. This can clearly be seen in thin sections. Scanning electron microscope images of the laminated fringes show that in some cases they consist of extremely fine crystal fibres (Plate 4.2E). In other samples, these fibres are not so well developed and the layers appear to consist more commonly of radiating calcite. However, fibrous crystals are still present and it is likely that these are at a later stage of cementation. Further magnified, these fibres can be seen to be interlinked strands of calcite (Plate 4.2F) and are almost certainly of algal or bacterial origin, probably attributable to Oscillatorian cyanobacteria. Note also the very fine strands developed between these layers. Within the more micritic layers, small rosettes of radial calcite (Plate 4.3A) have been observed, also attributable to algal origins. Similar structures have been pictured using the scanning electron microscope (section 4.13). Thick, virtually horizontal deposits of this algal mat form extensive outcrops up to 10m in height, particularly in the Gaziler and Yesilkaraman regions (Plate 4.3B).

The stromatolites often take the form of large stromatolite heads approximately 1m in diameter which may coalesce to form large domal build-ups 5 - 10m in height (Plate 4.3C,D). Individual heads as large as 3m in diameter have been observed. On shallow slopes the stromatolites form thick undulating mats with a wavelength of 2-3m and an amplitude of 0.5m. This can be clearly seen at Kepez where water flowed downslope from springs at the steep terrace edge. Even microterracing can be seen on the surface in some places.

Thin, binding, algal mats drape over sediment, smoothing and accentuating the underlying topography (Plate 4.3E). Commonly these mats are quasi-horizontal and where no existing relief exists will gently undulate. In extreme cases they have been observed as vertical drapes. Algae may also use plant stems as a substrate and have been seen, complete with associated chironomids, to encrust stems to a thickness up to 10 cm (Plate 4.3F).

4.10.3: Phytoclast tufa

Phytoclast tufa differs from phytoherm tufa in that the plant fragments are allochthonous and have been cemented during and/or after transport. Fragments of stems ranging from a few mm to a few cm in size, leaves and small detrital grains typically make up these grain-supported deposits (Plate 4.4A). Thin, binding, algal mats may also be an intimate part of the fabric.

Plate 4.3: Facies types of the Antalya tufa II: Phytoherm boundstone:
A) Photomicrograph of micritic tufa displaying a rosette of radiating crystals. This strange form i
also seen as the nucleus of some pisoliths. It is attrbuted to algal origins. Field of view 1.2mm
1.3mm. **B)** Regularly laminated deposits of algal mat. The laminations are upwards growing, fibrou
calcite crystals growing between layers of micrite. **C)** Large stromatolite heads approximately 1m i
diameter which coalesce to form a large domal build up. **D)** Stromatolite domes underneath and abov
a patch of phytoclast tufa. **E)** A 1cm thick, binding, algal mat drapes over phytoclast tufa. The ma
curves dramatically and effectively coats the uneven substrate. **F)** Algal coating of a bunch of thi
plant stems. Chironimids occur towards the bottom part of the section and the coating has include
other stems as it expands. The outer layer at the top consists of fringing calcite crystals identical t
those observed in laminated algal mats.

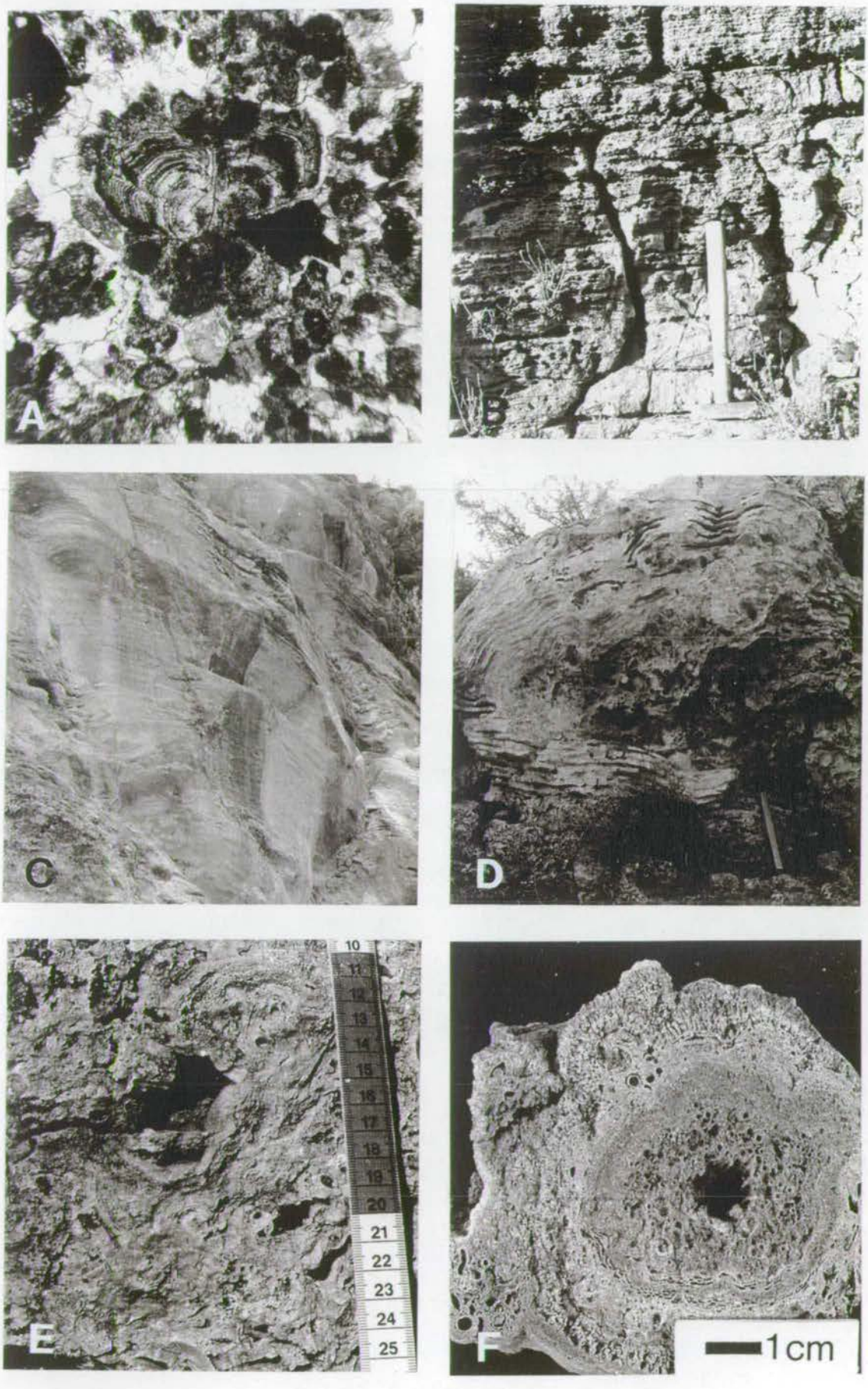

Plate 4·3

4.10.4: Oncoidal tufa

Oncolites are subspherical, laminated stromatolites generally 0.5-2cm in size. The biogenic origin of oncolites is clearly shown in the Lower Cretaceous blue-green algal deposits of eastern Spain (Monty and Mas 1979). Their shape is dependent both on the energy of the environment in which they were formed, and the nucleus (Plate 4.4B). For example, highly oblate forms may grow around elongate fragments of twig. In this situation we cannot simply assume that the higher the sphericity the higher the energy of the environment in which they were formed although the general principle still applies (Nickel, 1983; Schneider *et al*, 1983; Riding, 1983). In thin section these stromatolites are shown to be crenulated in aspect. Nuclei tend to be rather indistinct micrite (Plate 4.4C). As the oncolites develop they may coalesce and the coating envelops many nuclei. The oncolites typically occur within a matrix of micrite, often peloidal micrite, and are generally subspherical to elongate in shape. Frequently, hand specimens of consolidated oncoidal tufa have a mottled appearance.

4.10.5: Pisolith tufa

Pisoliths, usually 0.5cm in size, occur in the field as distinct clusters of hard pea-like balls, close to spherical in shape often cross bedded and deposited in small channel and lenses. Small, up to 2mm, inorganic pisoliths (oolites) have only rarely been observed but display the same characteristics as the larger pisoliths. Together these are classified here as pisolith tufa. In thin-section the cortex is seen to consist of a very fine concentric banding, often radially cracked. The shape of individual pisoliths reflects the shape of the nucleus. Individual pisoliths never coalesce and, in thin section, are rarely seen in contact, although in three dimensions point contact is made with several surrounding pisoliths. Pisolith tufa can be considered distinct from oncolitic tufa as it does not display the highly irregular, probably biogenic, structures of the oncoids. Nuclei consist of anything available and crystalline calcite, micritic peloids fragments of cortex, chara etc. have been observed (Plate 4.4D). In some cases, only a few laminae are present in the cortex; these could be defined as superficial ooids (Flügel, 1982). They are equivalent to those described as inorganic pisoliths by Folk and Chafetz (1983) and the similarity, both in the field and in thin-section, between the two is striking. The pisoliths are thought to be the only entirely inorganic sediments in the area. Oncolites and pisoliths are never found together in the same section.

Plate 4.4: Facies types of the Antalya tufa III:
A) Phytoclast tufa: Allochthonous plant fragments cemented during and/or after transpo
B) Oncoidal tufa: Oncolites in the field. Some broken oncoids have plants as nuclei. **C)** Oncoidal tuf
Photomicrograph of oncolites within micrite. The crenulated algal coatings are attributable
cyanobacterail activity. They grow evenly in all directions but tend to be elongate or subspherical
shape. In some cases several nuclei have coalesced to form one oncolite with a continuous coatin
Filed of view 7mm x 7.5mm. **D)** Photomicrograph of pisoliths showing the finely laminate
concentric banding of the cortex, often with radial cracking. Field of view 5.6mm x 6mm
E) Microdetrital tufa: Thick sequence of microdetrital tufa showing clear lamination. The dark
horizons within the deposit are thin paleosols. **F)** Microdetrital tufa: Photomicrograph of cha
fragments and ostracods in the micrite of the microdetrital tufa. Field of view 7mm x 7.5mm.

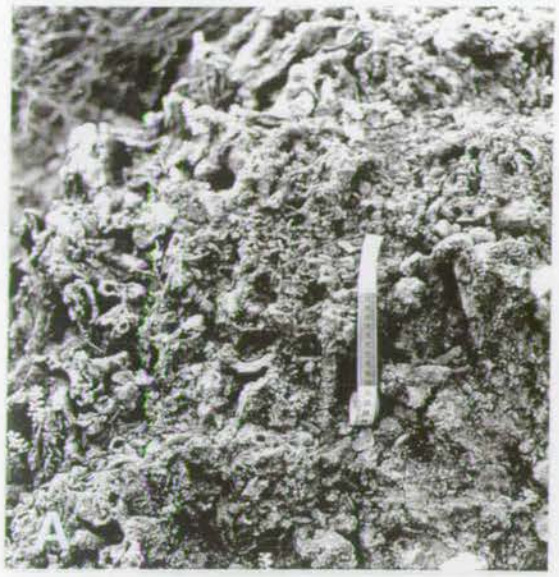

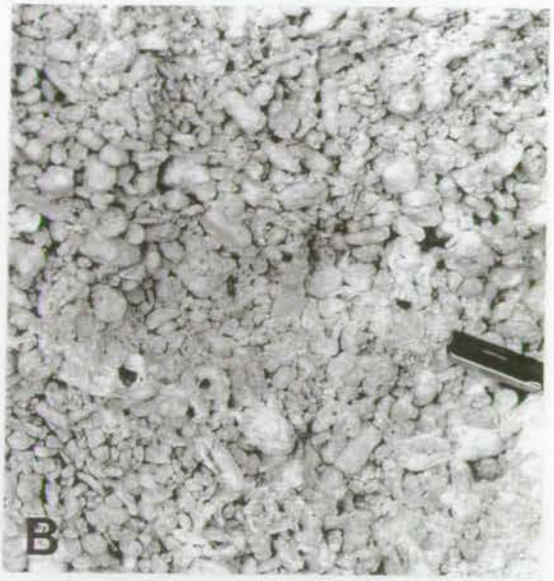

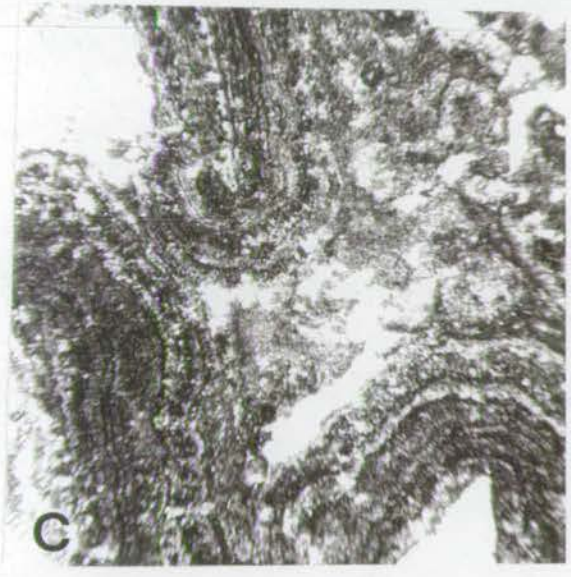

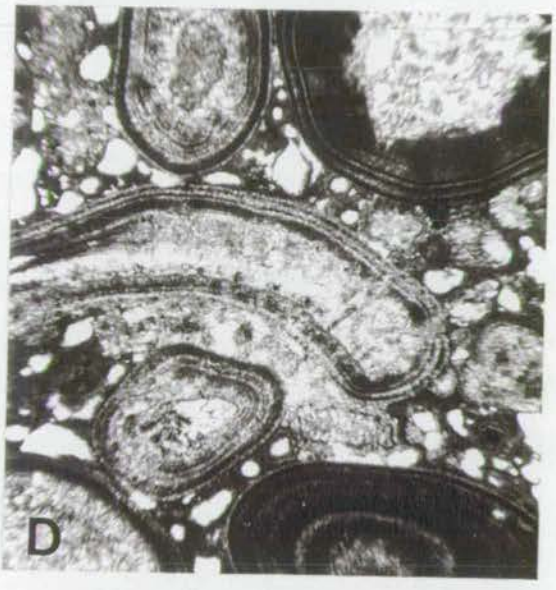

Plate 4·4

4.10.6: Microdetrital tufa

The term microdetrital tufa describes the finest sediments of the system. It is, essentially, micrite and occurs throughout the Antalya deposit (Plate 4.4E). In the field it typically occurs as a fine white, unconsolidated carbonate with little structure. Sometimes it is finely laminated, more often it is massive. Thin sections of microdetrital tufa show that it is compositionally very variable. Common constituents are microcrystalline carbonate grains with organic inclusions, peloidal micrite, dense structureless micrite and dense banded micrite. The microdetrital tufa can be filled with tiny rectangular voids which are clearly seen in thin section to be the remnants of dense chara populations. The micrite associated with these chara is always peloidal.

It is still generally unclear how much microdetrital tufa is of biogenic and how much of abiogenic origin. Thin section and scanning electron microscope evidence discussed in section 4.13 suggests that a significant quantity is biogenic. In some areas, particularly where the microdetrital tufa is thickly developed, the bedding undulates gently with a wavelength of several meters and a centimetre scale amplitude. This could be attributed to gentle compressive deformation of the tufa, but could also indicate that an undulating algal mat is the origin of much of the microdetrital material. In one section a desiccated appearance is observed; crystalline layers form small scale tepee structures (Plate 4.5A). This, coupled with the evidence of undulating layers, described above, suggests that the origin of at least some of this micrite may be desiccated algal mat which has lost its original structure, perhaps in the manner discussed by Monty and Hardie (1976).

In some cases the very fine material has a friable, porous, aggregated texture. Thin section shows this to be a peloidal micrite with no subsequent infilling of pore spaces.

Macrofossils are rare but in just a few localities freshwater gastropods can be found in moderate numbers. These will be discussed later. Thin sections reveal the presence of freshwater ostracods which are seen in many sections, but which are most common in structureless micrite (Plate 4.4F).

4.10.7: Tufa breccia

The term tufa breccia is used to describe deposits of reworked tufa, largely intraformational, which form significant deposits within the Antalya Tufa complex. The clasts are typically angular, poorly sorted fragments of phytoclast and phytoherm tufa (Plate 4.5B). Significant size variation within the deposits almost certainly reflects the different natures of the tufa facies that are reworked. Thus, clasts of

Plate 4.5: Facies types of the Antalya tufa IV:

A) Photomicrograph of layered microcrystalline tufa. cracked layers from a small-scale teepe structure giving strong evedence of periodic drying and dessication of algal mat. Filed of view 5.6m x 6mm. **B)** Tufa breccia: Tufa breccia with a strongly erosional base sits on top of microcrystallin tufa and a thin, laterally discontinuos, binding algal mat. In general the larger clasts are fragments stromatolite and the smaller fragments of phytohermal and phytoclastic tufa. Other facies can also b found within the breccia. **C)** Intraclast tufa: Cross-bedded clasts of coarse, sand-grade detrital tuf Many of the clasts are tiny hollow tubes which probably formed as coatings around grasse **D)** Paleosols within microdetrital tufa. The paleosols occur at regular intervals and are typical carbonate rich. **E)** Numerous freshwater gastropods occuring in clay-rich carbonates of the bas carbonate sequence at Yenimahalle. **F)** Scanning electron micrograph of an ostracod fro microdetrital tufa collected near Karaman.

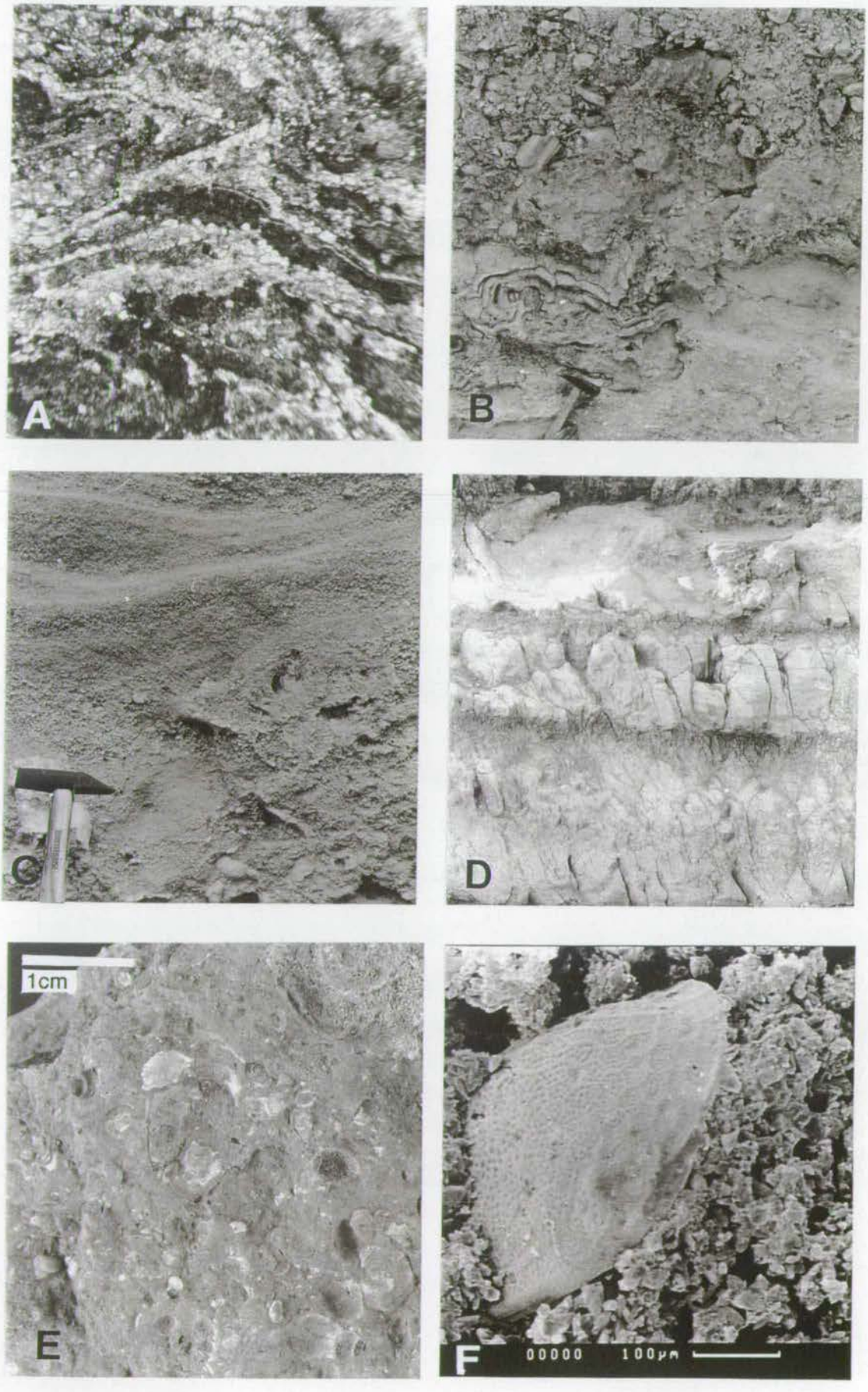

Plate 4·5

stromatolite tend to dominate and to be larger than clasts originating from phytoherm framestone or phytoclast tufa. However, the latter do not always break up completely and sizeable blocks of phytoclast or framestone tufa may be found. Occasional exotic clasts may be found, but are exceedingly rare. The breccias are clast supported but have a matrix of silt and sand grade reworked tufa.

The base of the tufa breccias is almost always erosional and no internal fabric is observed.

4.10.8: Intraclast tufa

Intraclast tufa is another form of reworked tufa consisting largely of silt- and sand-grade detrital tufa. These often contain numerous, small, elongate fragments that probably formed as coatings around grasses, as in the Manavgat Çay, together with broken pieces of larger cemented phytohermal material (Plate 4.5C). These deposits are frequently cross bedded.

4.10.9: Paleosols

As discussed in section 4.6 the presence of paleosols within the tufa environment is an important one and must be recorded. The paleosols are moderately well developed, usually carbonate rich and occur in close association with the microdetrital tufa. They can often be seen to occur at regular intervals (Plate 4.5D) and may indicate seasonal or climatic cycles.

The absence of roots beneath layers of phytoherm tufa, particularly where vertical stems alternate with micritic tufa, suggests that paleosols may once have existed within these sequences but have been lost over time. This has been observed in other tufa deposits (M. Pedley, pers. comm., 1994). A good example of this phenomenon can be seen in the logged section at Çalkaya (Plate 4.2A).

4.11: Faunal and Floral Content

4.11.1: Gastropods

In the majority of the deposit gastropods are extremely rare, even in areas where microcrystalline tufa dominates. Significant numbers of gastropods are only found in two sections, both basal, where the contact with the underlying rocks (Pliocene conglomerate at Yenimahalle; peridotite at Karaman) is exposed (Plate 4.5E). In both localities the microcrystalline carbonates are relatively impure. This probably reflects a deepening of water and a reduction of detrital input as the basement is blanketed.

4.11.2: Ostracods

Ostracods are found in most thin-sections of microcrystalline and oncolitic tufa. They are smooth, thin-walled, freshwater forms. Washing unconsolidated, microcrystalline tufa at 63μm failed to liberate any whole specimens, as the shells are very fragile. Scanning electron microscope work found ostracods in two samples; one from near Yenimahalle and the other from the Karaman area. From the latter area, one species can be seen to have a regular form with a textured surface (Plate 4.5F). The form was not readily identifiable although it is likely to be a *Cypridacea.*

4.11.3: Flora

The phytoherm framestones largely consist of the fossilised remains of algae, mosses and reeds. The latter are a common substrate for carbonate encrustation and although not formally identified it is probable that all types (*Scirpus*; *Carex*; *Schoenoplecta*; etc.) occur. The water plant *Potamugeton* is one of the most commonly preserved plants from this environment.

In the phytoclast tufas, flora ranging from reeds and algae to grasses and leaves can be found. Leaves were collected from several localities of phytoclast tufa in which they were found to be particularly abundant (Lara, Çalkaya, Nebiler). Although mostly poorly preserved, specimens of *Lonicera* sp., various (honeysuckle); *Alnus Glutinosa* (common alder); *Salix* sp., various (willow), (Depape and Arènes (1952) recognised *Salix caprea L.* and *Salix Cinerea L.*); *Betula* sp. (birch); *Parrotia persica* (Persian ironwood) and *Viburnum* sp. cf. *lantana* have been identified (Plate 4.6). A twig and thorn of *Rosa* sp. were also found (G. Schweigert, pers. comm., 1994). Of particular interest are *Alnus glutinosa* and *Parrotia persica.* Although many species of Elder still grow in Turkey *Alnus glutinosa* is now a relict species occurring only in the mountains and cooler northern regions (Meusel *et al*, 1965). It is currently far more common in Europe, where its natural habitat is alongside open water. *Parrotia persica* is also non-existent in the present day Turkish flora, although it can be found in the Caucasus, N. Iran, Hungary and Czechoslovakia. It was, however, widespread in the Mediterranean region before the onset of the glacial period (all G. Schweigert, pers comm., 1994). *Viburnum* sp. is from the sub-mediterranean climatic zone and does not tolerate a strong frost. *Lonicera* sp. require a temperate but rather wet climate.

Scanning electron microsope observations have revealed a couple of spore varieties. The former is almost certainly a fern spore. It cannot be stated with absolute certainty that these are not recent contaminations of the sample, although it is likely that they are, indeed, original components of the deposit.

Plate 4.6: Fossil Leaves collected from various localties. *Alnus glutinosa, Parrotia persica, Salix s and Lonicera sp. and Betula sp.* are pictured. Scanning electron micrographs of pollen and spo found in the tufa are pictured in the bottom left and centre of the plate.

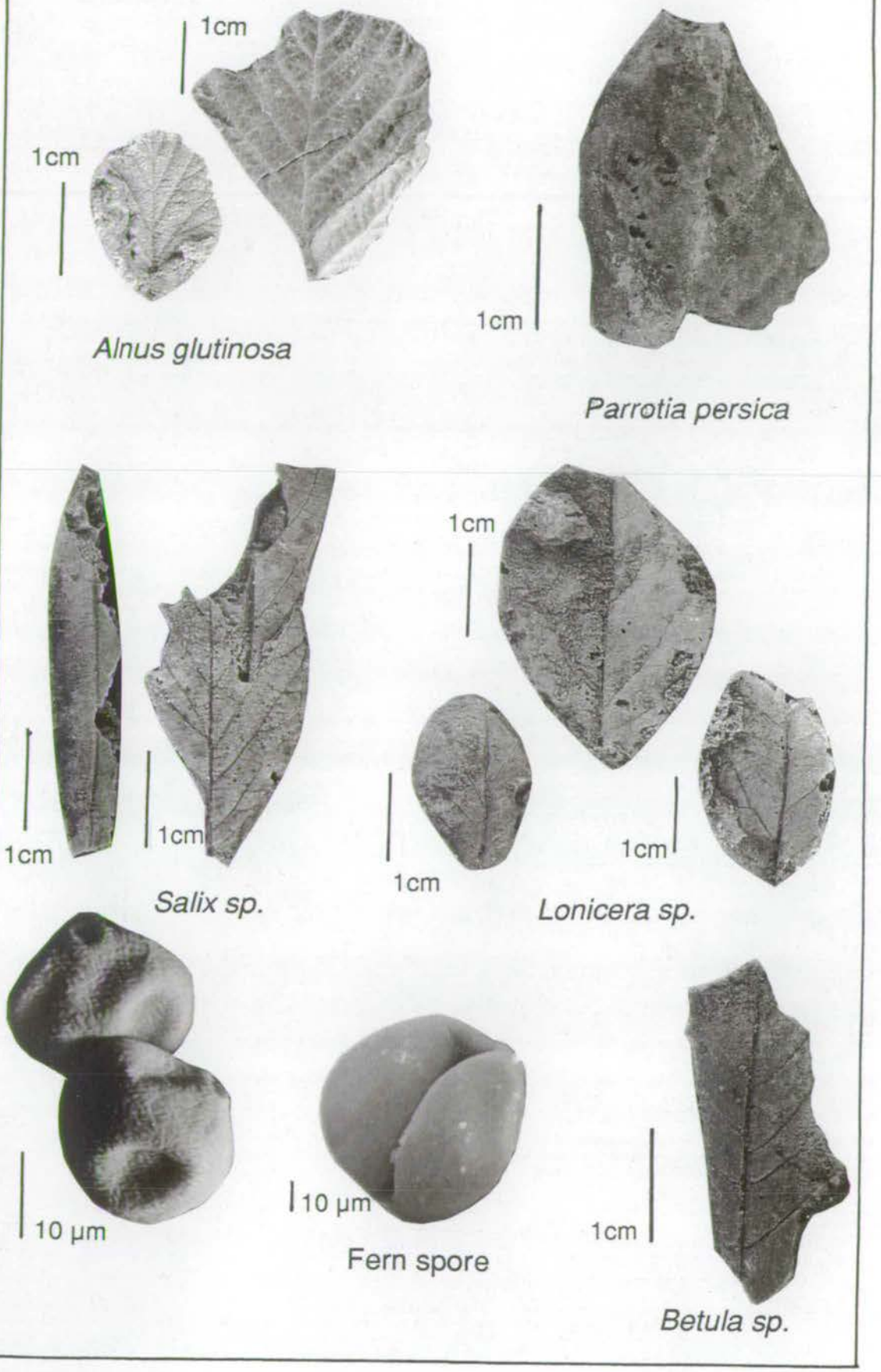
1cm
1cm
Alnus glutinosa
1cm
Parrotia persica
1cm
1cm
Salix sp.
1cm
1cm
1cm
Lonicera sp.
10 µm
10 µm
Fern spore
1cm
Betula sp.

Plate 4·6

4.11.4: Climatic implications

Although certainly not a complete list of the flora which could be found within the Antalya Tufa deposit, this assemblage gives us some idea of the climatic regime at the time of maximum deposition. We can surmise that the climate was probably cooler than at present and certainly damper. Many of the fauna present are strongly indicative of this (*Lonicera* sp., *Viburnum* sp., *Alnus glutinosa*). Dwarf birch and willow are also wetland species. They often represent the immediate post-glacial vegetation assemblage (N. Hulton, pers. comm., 1995). However, we have no indication that the *Betula* sp. and *Salix* sp. are dwarf forms. The presence of *Parrotia persica* in the assemblage suggests that the bulk of deposition occurred before the onset of the glacial period. The relict form *Alnus glutinosa* also indicates that tufa formation is not recent. All these data fit in well with the conclusions reached in section 4.5 that a temperate, humid climate displaying marked seasonal fluctuation provides the most favourable conditions for tufa development.

Chironomids are widespread throughout Europe, but according to Theinneman (1957) are absent from regions which were glaciated during the ice ages.

4.12: Chemical composition

X-ray diffraction analyses of samples of tufa from all facies types show them to be pure low Mg-Calcite (Appendix 3). This is typical of cold-water tufas and indicates a hydrologically open system.

4.13: Depositional mechanisms

The review in section 4.2 indicates that both chemical and biological mechanisms are important for the deposition of tufa. The extent to which biological control causes precipitation is not known, although increasing evidence for significant biological input is emerging. This section presents evidence for the occurrence of chemical and biological precipitates in order to assess their relative importance.

Two facies types, pisolith tufa (discussed in detail in section 4.10.5) and structureless micrite can lay claim to being purely chemical precipitates. There are, however, very few micrite sections which show no evidence of algal structures at all. Thin section studies of all other tufa facies types reveal many features which can be interpreted as of biological origin (Plate 4.7A,B).

Carbonate growths around strings of mosses are micritic and form a fuzzy, wavy structure around individual strings which closely resemble algal structures

Plate 4.7: Photomicrographs of algal structures:
A) Mat-like laminations within microdetrital tufa. Field of view 7mm x 7.5mm. **B)** Peloids and pelle within microdetrital tufa. Field of view 4.6mm x 5mm. **C)** Cross-section through "strings" encrusted mosses. The texture of the encrustation is similar to that of the peloids. Field of view 7m x 7.5mm. **D)** radiating fibres of organic material within coarse, calcite crystals. Field of view 4.6mm 5mm. **E)** Radiating calcite crystals are rounded by an organic coating. The upper part of th micrograph consists of layered algal material. Field of view 4.6mm x 5mm. **F)** Recent stromatolit coating on the outside of an encrusted plant stem. Field of view 7mm x 7.5mm.

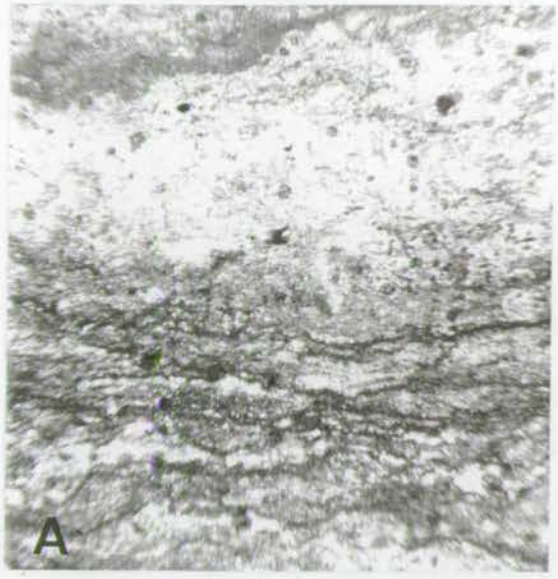

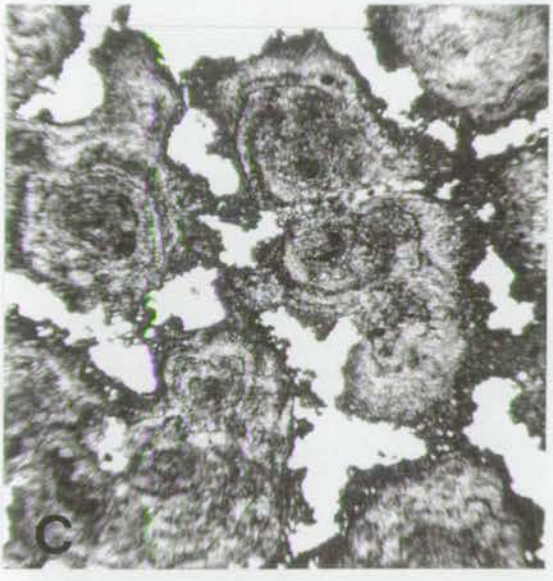

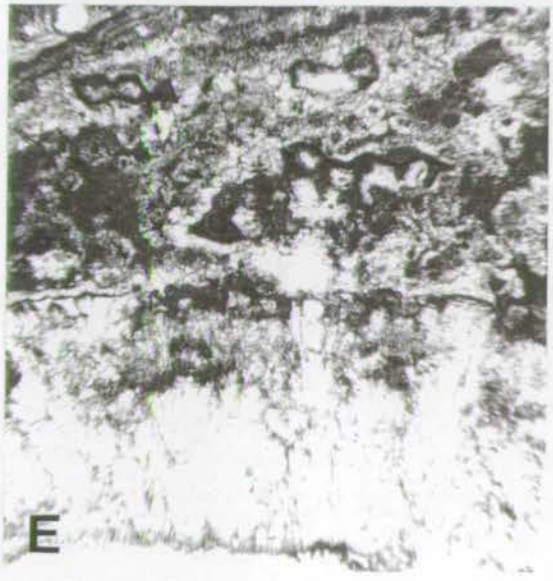

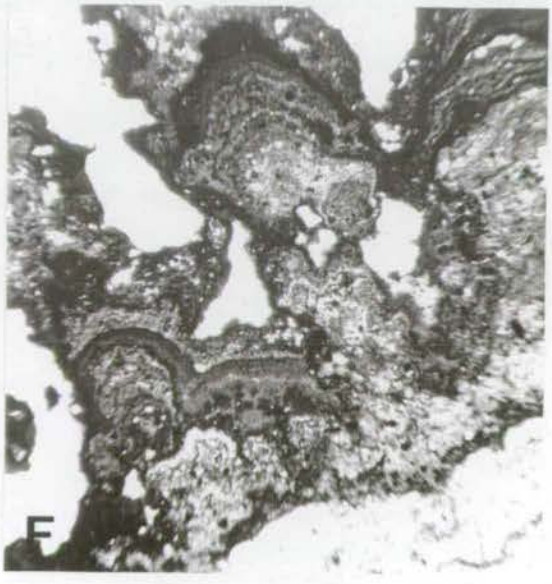

Plate 4·7

(plate 4.7C). The calcite crystals which grow around larger plant and reed stems frequently contain very thin, black lines fanned around the long axis of the crystal (Plate 4.7D). These may bifurcate and create a feathery appearance. Sometimes the radiating crystals themselves have rounded ends and upward curving black growth lines (Plate 4.7E). Occasionally, small rounded crystals containing short parallel black rods, often at the edge of a void which was once an algal stem, are observed. The edges of cemented stems often have a nodular encrustation of slightly orange carbonate. In thin section this has a fine, wavy structure resembling mini-stromatolites, which is interpreted to be algal in origin (Plate 4.7F). Abiogenic cave pearls and some speleothem deposits have a similar appearance but in thin section lack the detailed microstructure consisting of smoother more even layers.

Microdetrital carbonate has already been described in thin section as consisting either of microcrystalline calcite or micrite. Microcrystalline calcite has been observed from a section of dome stromatolite, occurring above a layer of chironimid traces. This calcite is identical to that observed in other sections. Within individual crystals spots of dark material are observed. This may be more or less dense, distributed throughout the crystal or in a central area. The structure and nature of the organic inclusions may change between different layers and patches in a single thin section. The distinctness of the different forms and their observed occurrence in stromatolite domes suggests that the crystals form around clumps of bacteria which are preserved as the dark spots. Different bacterial species probably account for the various distributions and forms which are recognised.

Within micritic material wavy laminations, often picked out by changing density of micrite, and occasional layers of feathery crystals are a common feature. The structure of these layers resembles oncolite coatings and indicates that algae were present during deposition. Sometimes these algal structures will occur in small patches, or as broken pieces within a more homogenous micrite. The layering may be cracked and broken and teepee structures have been observed showing that desiccation occurred as algal mat was subjected to periodic drying.

In some sections the whole structure is very chaotic and patchy. Peloidal micrite, calcite crystals, broken layers, mini stromatolites/algal layers occur with no preferred orientation or structure. This too may be related to drying of an algal mat and local reworking of the sediment.

The matrix observed around chara fragments is always peloidal micrite. Since we know already that chara are important carbonate generators (section 4.2) and that any micrite associated with them is bacterial in origin we can interpret these peloidal sediments as bacterial. This can be extended to peloidal sediments without chara

remains which are commonly observed constituents of microdetrital tufa. Sometimes the peloids may be strung out into long lines suggesting "chains" of algae or bacteria.

Thus, evidence from thin section suggests that bacterial and algal activity is an integral part of deposition in most environmnts.

Scanning electron microscope observations on a number of tufa samples from different facies settings reveal the intricate association between algal and bacterial activity and carbonate deposition. These observations also suggest that in all environments algal and bacterial activity was the dominant process through which carbonate was precipitated. They support the arguments and observations of Emeis *et al* (1987) and Pedley (1992) (see discussion in section 4.2).

Evidence for the influence of algal and bacterial activity on the precipitation of carbonate in the system can be seen in a variety of ways: crystallites growing around plant stems; fossilised algae; pennate diatoms and bacterial filaments; and bizarre crystallite forms indicating a relict bacterial structure.

Radiating calcite crystals form a coating up to 10cm thick around stems, preserved as hollow tubes after the original organic material has rotted away. This radiating crystal pattern can be seen in hand specimen, thin section and using the scanning electron microscope (Plate 4.8A). Typically, the innermost layer is of black highly organic material coated by micrite which rapidly gives way to larger crystals. In rare cases, one sees evidence of bacteria and/or algae which lived on the surface of the plant and may have contributed to the preferential nucleation of carbonate (Plate 4.8B,C).

The fossilised remains of chara are common in microcrystalline tufas. It can be seen clearly that carbonate crystals grow outwards from a micrite layer on the surface of the chara stem (Plate 4.8D). It can also be seen that bacterial filaments and pennate diatoms (Plate 4.8E) are closely associated with the chara and that these would have contributed towards the mucous sheath which initially attracts carbonate. The filaments and bacteria have become cemented into the crystalline mass growing around the chara. Various species of pennate diatom may also be found well preserved within more crystalline carbonate (Plate 4.9).

Bacterial filaments were observed in nearly all the studied specimens. Several different forms could be identified. They are positively identified as bacterial filaments owing to their hollow nature and general organic tube-like form. These are pictured in Plate 4.10. The micrograph 4.10A shows a typical hollow tube with small crystallites adhered to the surface. This is very similar to bacterial filaments depicted by Défarge *et al* (1994) and may be *Scytomena*. The micrograph 4.10B shows a similar hollow tube and a much smaller bacterial filament, also hollow. In the

Plate 4.8: Scanning electron micrographs of calcite growth and bacteria associated with chara stems:
A) Radiating calcite crystals which grew around a 30μm stem, probably chara, now decayed. **B)** filamentous bacteria along the interior surface of the mould, around a larger stem, probably algal. **C)** Microcystalline carbonate forming a thick coating around the hole left by a microstem. On the interior surface of the stem several bacterial filaments, with their own coatings of carbonate can be seen. **D)** The internal surface of the hollow tube has a clear texture, indicating that precipitation occured around stems of Chara. At the point where the preserved chara texture breaks off, a node occurs and a small side stem branches towards the bottom of the photomicrograph. Calcite crystals can be seen growing away from all the chara surfaces. The thin carbonate covered filament extending out of the void is probably bacterial in origin. **E)** Carbonate growth away from a chara stem. In this case both the internal and external moulds are present a thin gap between the two occurs where the original algal material was present. Incorporated into the carbonate coating are diatoms (indicated by black arrows) which would have been living within and contributing to the mucus sheath of the chara. The evidence that these are some distance from the chara wall suggests that the mucous sheath was thick and that carbonate precipitated within it.

Plate 4.9: Scanning electron micrographs of pennate diatoms from within the tufa mass. Three different species are recognised.

Plate 4.10: Scanning electron micrographs of bacterial filaments within the tufa:
A) Typical hollow tube with small crystallites adhered to the surface. **B)** A similar hollow tube and a much smaller bacterial filament, also hollow. **C)** The bacteria is clearly a chain structure and appears to be flat. Note again the crystallites adhered to the surface. **D)** Bacteria of a lumpy, irregular form with no adhered crystallites. **E)** Large group of bacterial rods. These can be seen to be rather short and to comprise the bulk of the sediment in this area. **F)** Y-shaped branch of a bacteria of the type pictured in A and B. This is a particularly unusual feature and good evidence that these filaments are bacterial in origin.

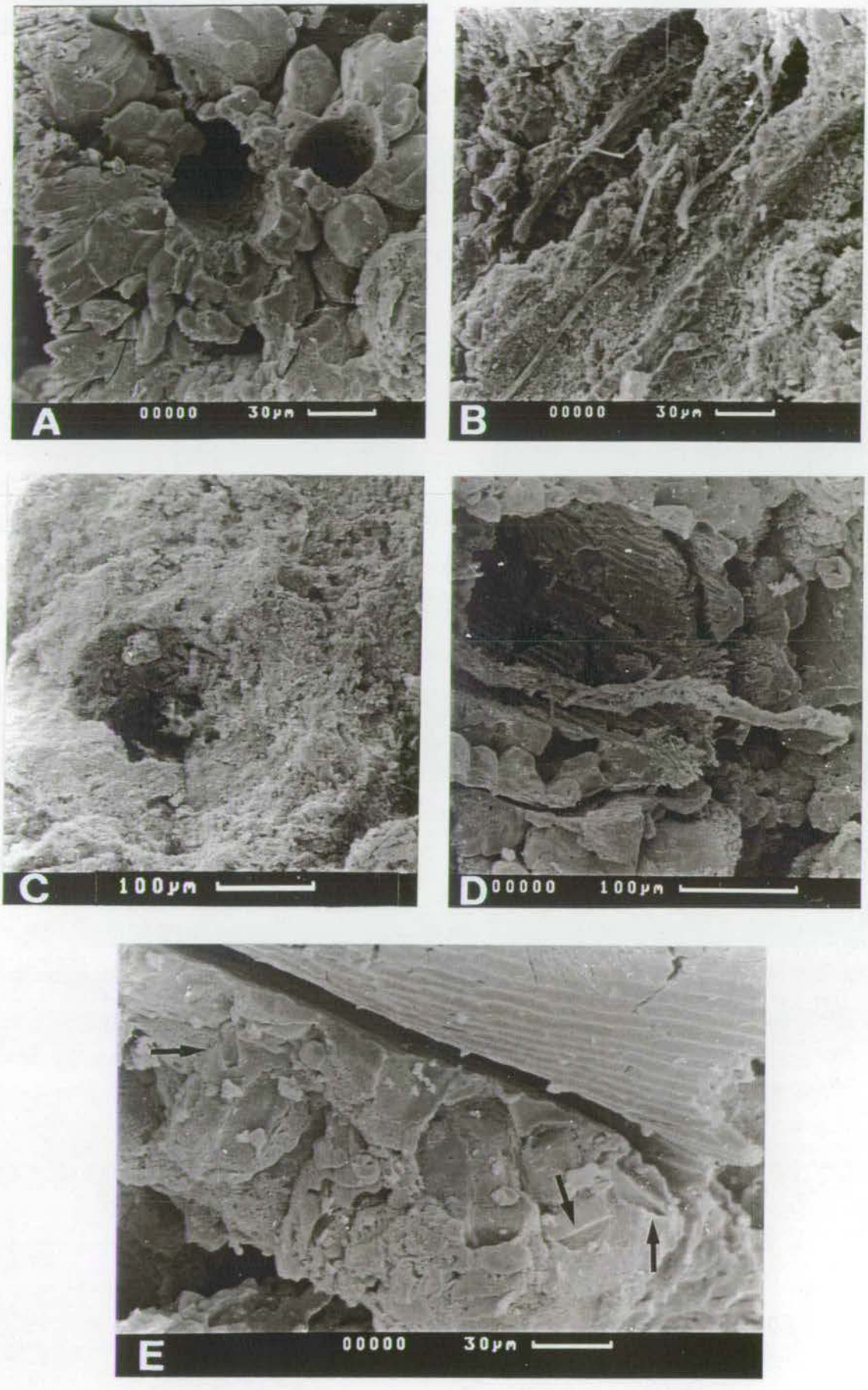

Plate 4·8

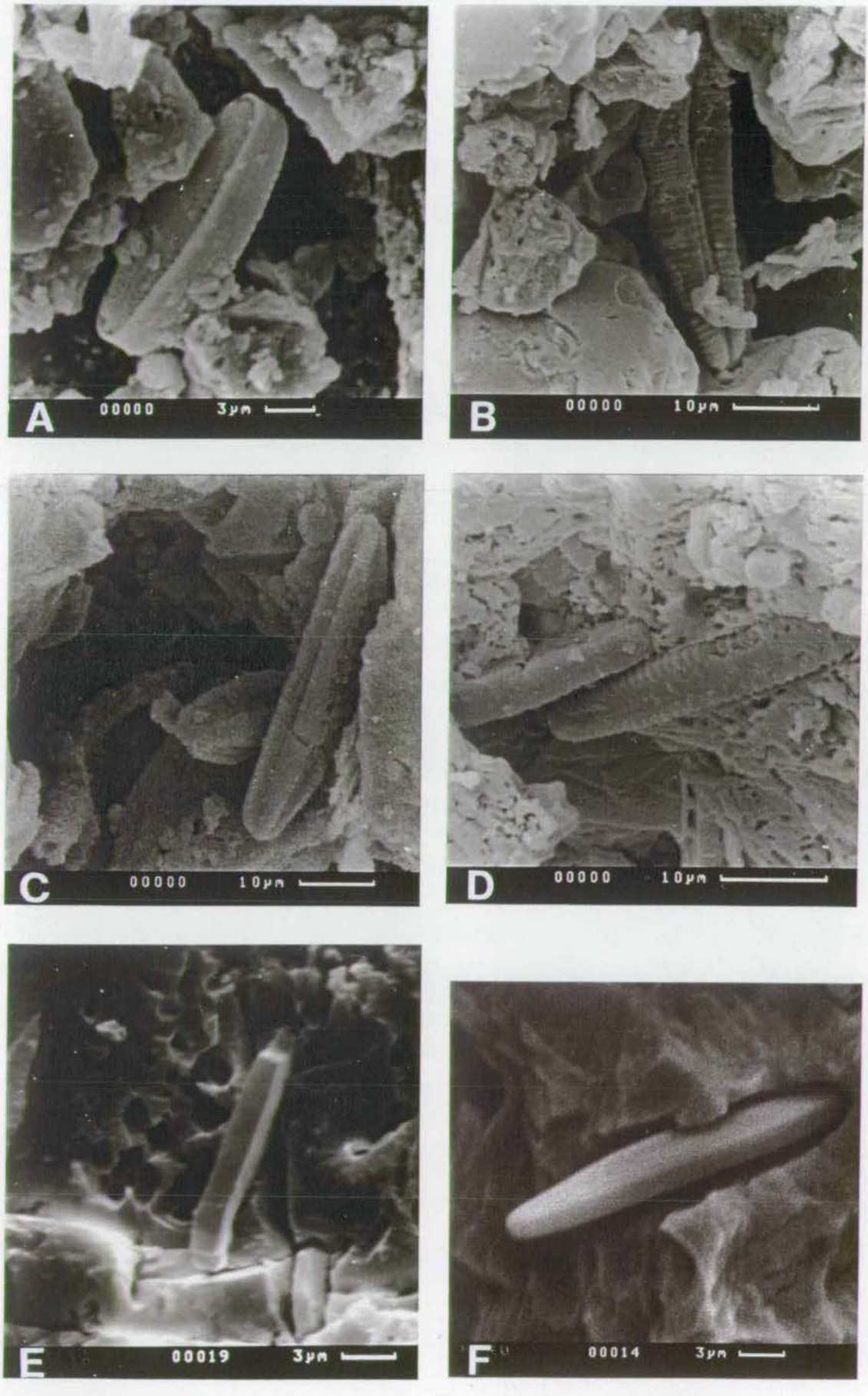
A
00000
3µm
B
00000
10µm
C
00000
10µm
D
00000
10µm
E
00019
3µm
F
00014
3µm

Plate 4·9

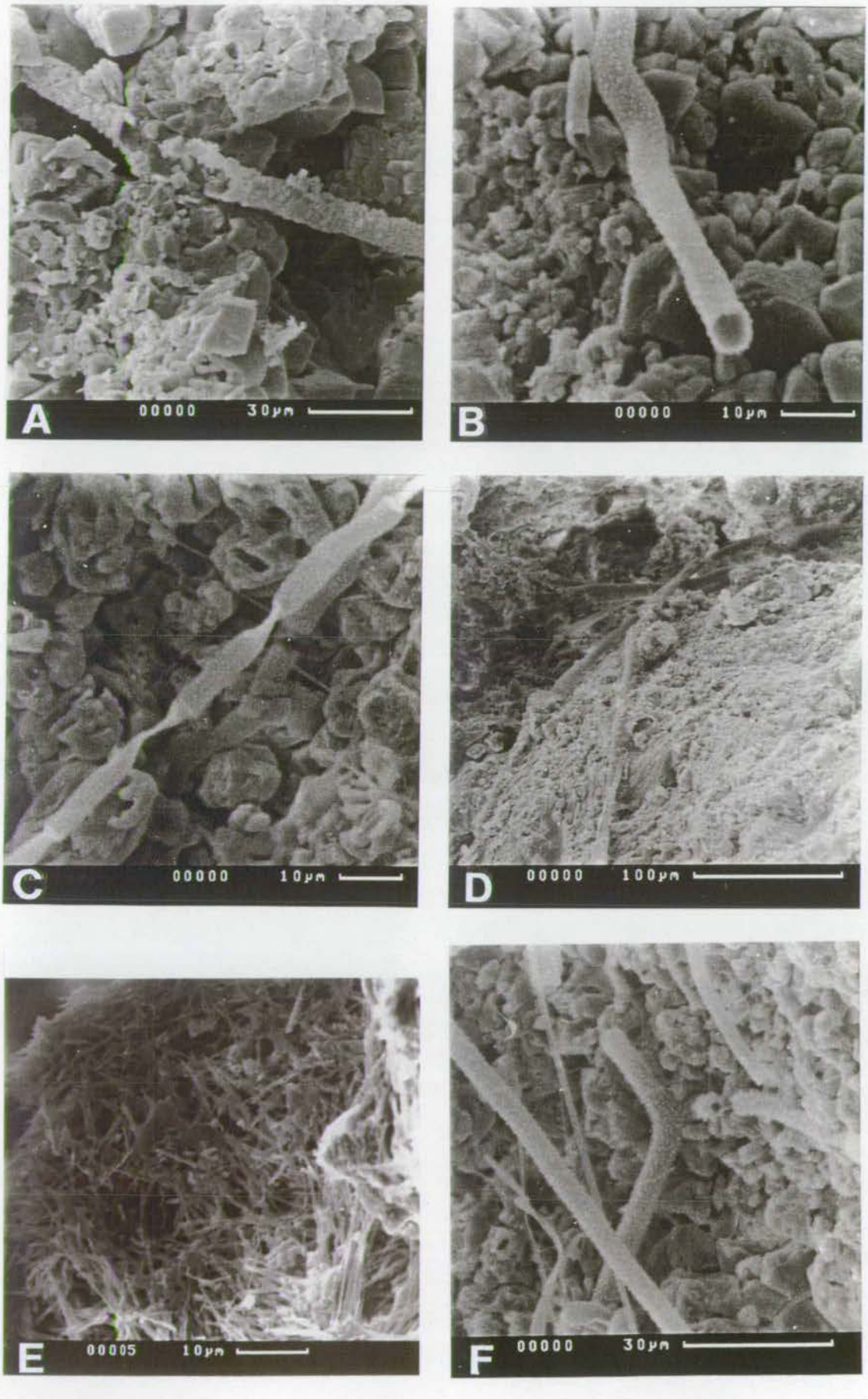
A
00000 30µm
B
00000 10µm
C
00000 10µm
D
00000 100µm
E
00005 10µm
F
00000 30µm

Plate 4·10

micrograph 4.10C the bacteria is clearly a chain structure and appears to be flat. Note again the crystallites adhered to the surface. The bacteria pictured in micrograph 4.10D are of a much less regular form and have no adhered crystallites. Note the lumpy, irregular form of the filament. Finally micrograph 4.10E shows a large group of bacterial rods. These can be seen to be rather short and to comprise the bulk of the sediment in this area. Of particular interest is the Y-shaped branch pictured in (micrograph 4.10F) which is good evidence that these filaments are bacterial in origin. It is my opinion that the small crystallites seen adhered to the surface of many of these filaments are the beginnings of crystallisation in the sticky mucous sheath. In fact, a sequence of bacterial filaments in successive stages of precipitation has been observed. These are pictured in Plate 4.11. In the micrograph 4.11A small crystallites have formed on the surface of the bacterial filament but do not cover the entire surface. These crystallites are about 1μm in size. Micrograph 4.11B shows the crystallites cover the entire surface of the filament and have grown to 1.5μm, although note the hollow centre can still be distinguished. A larger calcite crystal has also become attached to the filament. In micrographs 4.11C and 4.11D crystallisation has proceeded even further and individual crystallites start to be enveloped in the growing mass of calcite. Finally in micrograph 4.11E a thick mass of crystalline carbonate is shown, which has obviously grown around a tube structure. It is unclear whether or not this was a bacterial filament, an algae such as chara or a higher plant, perhaps a grass.

It is not only the presence of fossilised diatoms, algae and bacteria that supports the argument for a high degree of organic influence on the precipitation of carbonate. In samples where these features are rare the crystal forms themselves suggest that growth has not been by simple inorganic crystallisation. A number of typical crystal types which strongly suggest a bacterial origin are highlighted here (Plate 4.12). The micrograph 4.12A shows a euhedral crystal with a circular hole in the centre suggesting that it has grown around a single bacterial filament. Micrographs 4.12B and 4.12C show very porous crystals which may well have grown around bacterial colonies. The latter also shows a typical crystal with later, minute, spiky crystals growing on the surface. Larger crystals with a spiky form are common and are pictured in the micrograph 4.12D. Micrograph 4.12E shows spherically radiating, euhedral crystals. It is possible that this form is related to the unidentified, spherical bodies seen in thin section (Plate 4.3A). It is probable that nucleation occurred around a central point. Micrograph 4.12F shows an unidentified spherical object acting as a nucleation site. Due to their rather unusual morphologies all the crystal forms described above are attributed to growth under the influence of

Plate 4.11: Successive crystallisation of bacterial filaments:
A) Small crystallites exist on the surface of the bacterial filament but do not cover the entire surface These crystallites are about 1μm in size. **B)** The crystallites cover the entire surface of the filamen and have grown to 1.5μm. The hollow centre of the filament can still be distinguished. A larger calcit crystal has also become attached to the filament. **C)** Individual crystallites have been enveloped in th growing mass of calcite. **D)** The carbonate coating around the bacterial filaments has become eve thicker and is starting to become a part of the general mass of carbonate. **E)** A thick mass c crystalline carbonate grown around a tube structure. It is unclear whether or not this was a bacteri filament, an algae such as chara, or a higher plant, perhaps a grass.

Plate 4.12: Scanning electron micrographs of unusual crystal forms within the tufa attributed t growth under the influence of algae and bacteria:
A) A euhedral crystal with a circular hole in the centre which suggests that it has grown around single bacterial filament. **B)** Very porous crystals which probably grew around bacterial colonies **C)** Rather larger porous crystals some with later, minute, spiky crystals growing on the surface **D)** The crystals are much larger than those in C) and show a pervasive spiky texture with flat plane running parrallel to the broad side, but consisting of amalgamated spikes. **E)** Spherically radiating euhedral crystals. It is possible that this form is related to the unidentified, crystal rosettes observed i thin section (Plate 3.3A). It is probable that nucleation occurred around a central point **F)** Unidentified spherical object acting as a nucleation site.

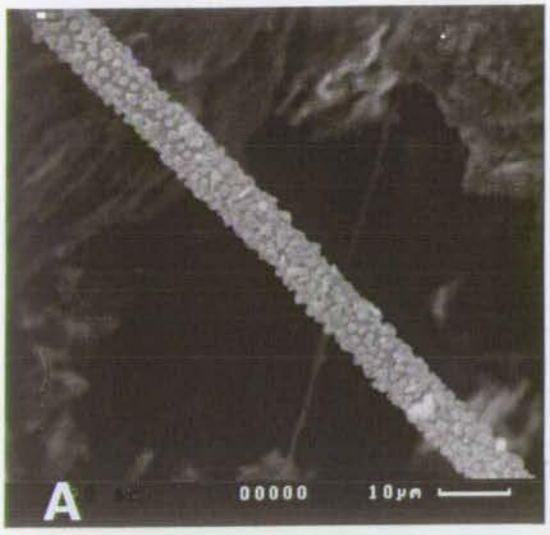

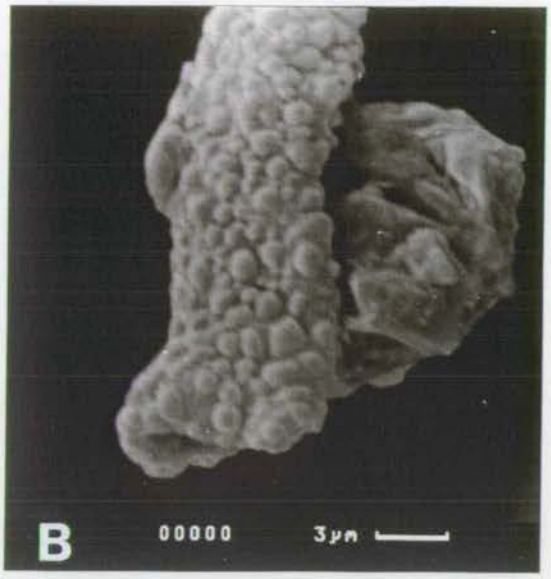

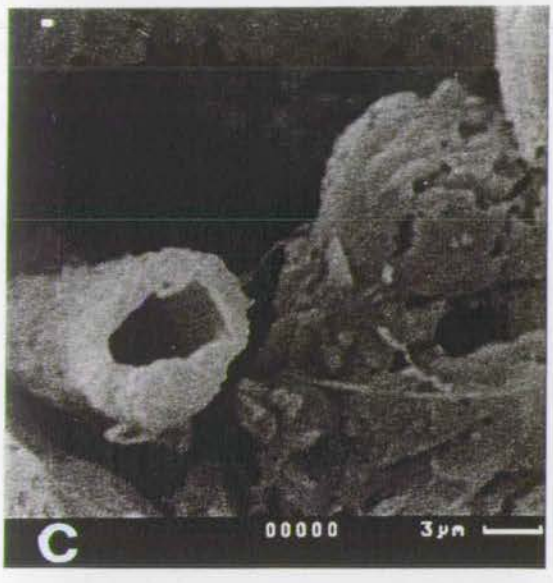

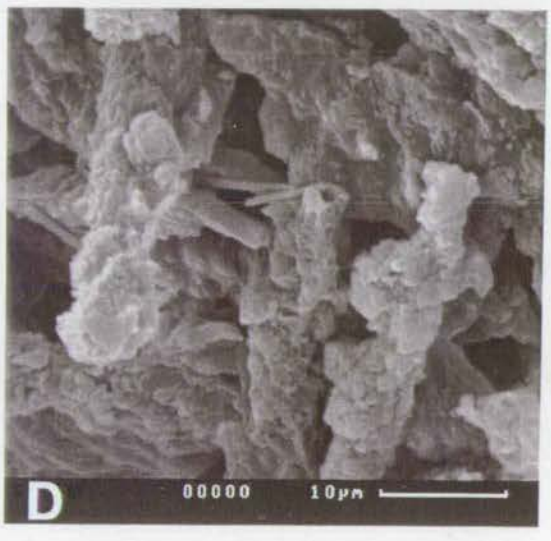

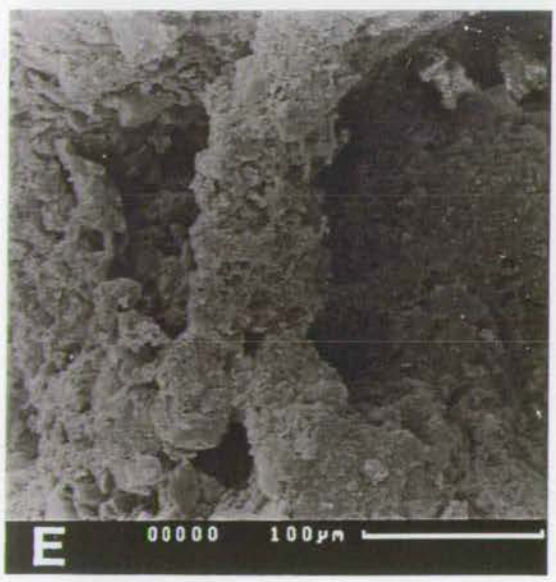

Plate 4-11

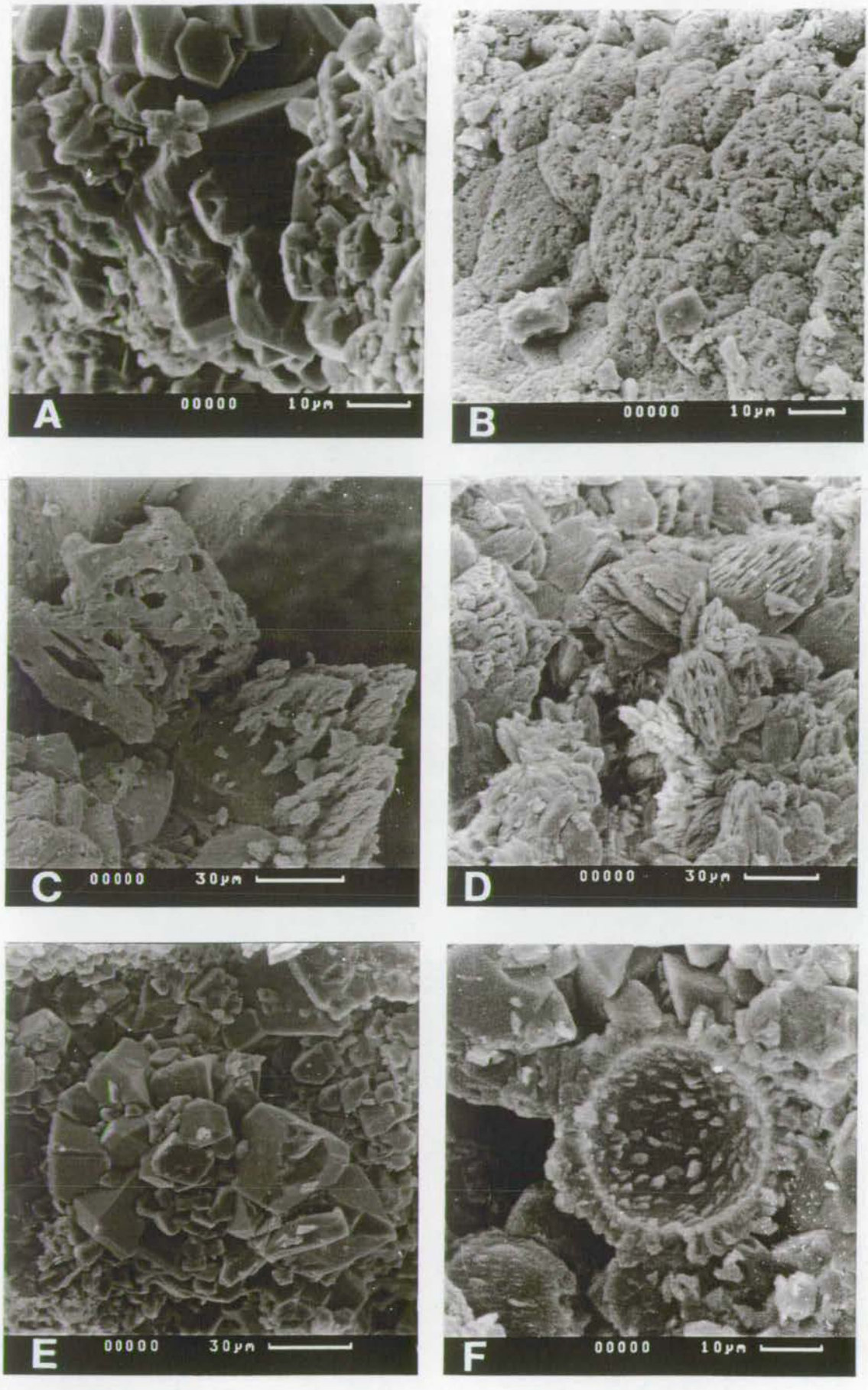
A
00000 10µm
B
00000 10µm
C
00000 30µm
D
00000 30µm
E
00000 30µm
F
00000 10µm

Plate 4·12

algae and bacteria. A number of forms have been recognised which can be more specifically related to the influence of bacteria. These can be clearly related to the experimentally induced, bacterial, crystal bundles observed by Castanier, Maurin and Perthuisot (1989) and Buczynski and Chafetz (1991) (Plate 4.13). Note that in the micrograph 4.13E the structure has almost become overgrown by the surrounding crystalline material and thus evidence for the bacterial origin of the tufa is rapidly lost. The micrograph 4.13F shows a group of these fibrous bundles constituting the total fabric of the deposit. Similar dumbell shaped crystals have also been observed in recent algal mats from French Polynesian atolls. (Défarge *et al*, 1994)

Finally, it is worth noting that interlinking fibrous strands which make up crystalline layers in the layered stromatolitic tufas, which are attributed to Oscillatorian Cyanobacteria, are also seen in other samples, for example in agglutinated, planty, microcrystalline material.

The variety of carbonate particle types associated with tufa deposition which have been observed in this study are also observed in modern microbial mats (Gerdes Dunajtschik-Piewak, Riege, Taher, Krumbein and Reineck, 1994). In the microbial mats of Lanzarote peloids, ooids and agglutinatated grains have all been described. Nuclei range from clumps and single cells of bacteria, intraclasts and bubbles. Casts and inprints of bacterial cells within precipitates are also documented. The comparison of particle forms between this Recent mat and the Quaternary Antalya example is excellent. The Antalya Tufa deposit serves to emphasise how much tufa these organisms are capable of producing.

The extent to which algae and bacteria mediate deposition of carbonate in tufa deposits is becoming increasingly clear. The wide range of facies types encountered in the Antalya deposit allow the rôle of algae and bacteria in a number of different environments to be assessed. The thin section, scanning electron microscope and field observations all point firmly towards an algal and bacterial origin for the vast majority of deposits in the Antalya Tufa. It suggests that without the presence of these organisms, deposition of carbonate from waters supersaturated with respect to calcite would be very limited.

4.14: Depositional environment

The vast majority of tufa seen in the Antalya area consists of horizontally bedded sediments comprising all the facies types described in section. 4.10 Local environments of deposition can quickly be assigned to various facies types, particularly by comparison to facies models for open carbonate lakes (Tucker and Wright, 1990) (Fig. 4.8).

Plate 4.13: Scanning electron micrographs of crystal types similar to those produced experimentall by Castanier *et al* (1989) and Buczynski and Chafetz (1991):
A) The crystal on the left side of the micrograph has spiky ends, similar to those seen in Plate 3.11D and appears to have "split". **B)** Fine crystals radiating away from a central void withi microcrystalline carbonate. **C)** Elongate bundle of fibrous calcite. The central portion looks as if it ha been "pinched in" as the edges curl towards the centre. **D)** Twinned crystals intergrowing at an angl of 30° **E)** The elongate fibrous bundle similar to those seen in B and C has almost become overgrow by the surrounding crystalline material. **F)** A group of fibrous bundles constitute the total fabric of th deposit.

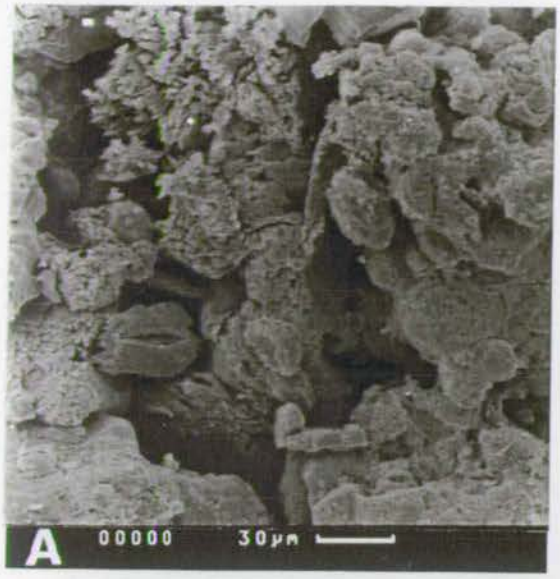
A
00000
30µm

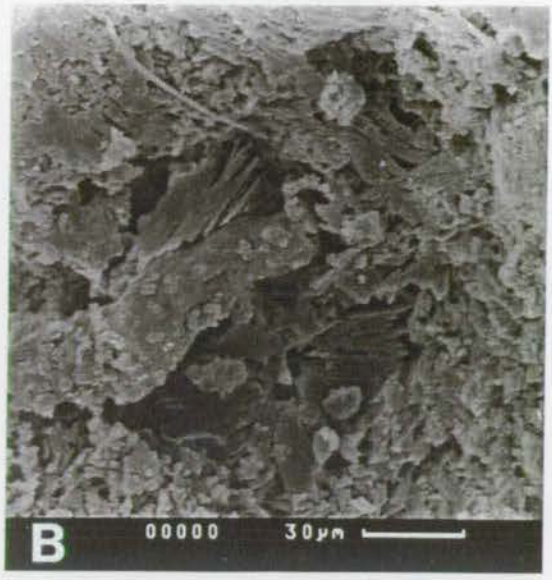
B
00000
30µm

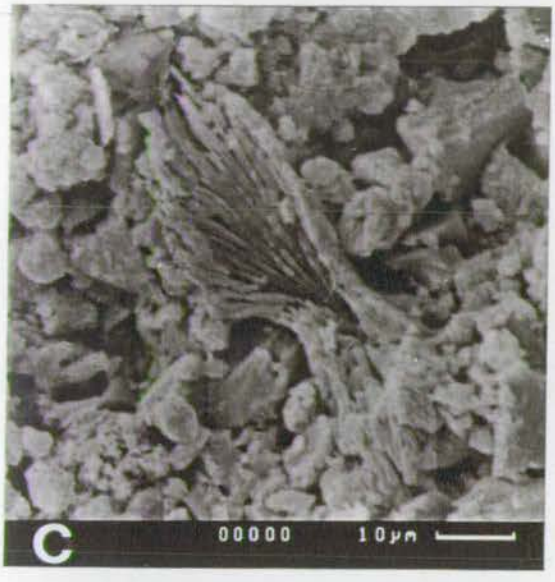
C
00000
10µm

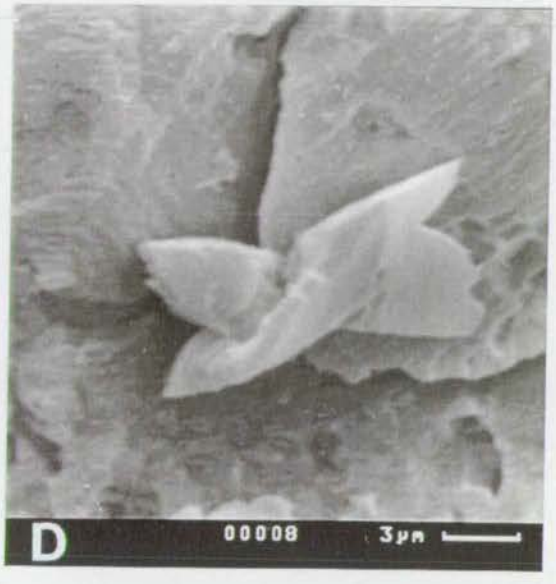
D
00008
3µm

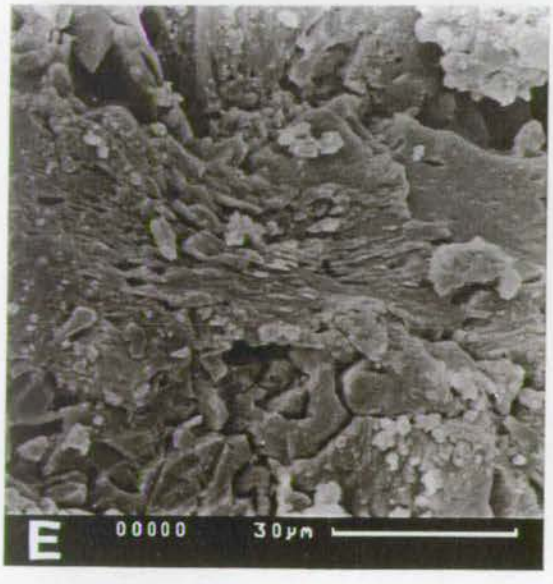
E
00000
30µm

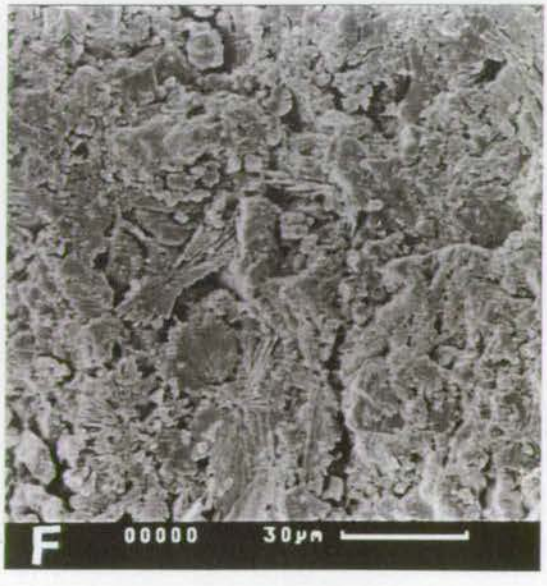
F
00000
30µm

Plate 4·13

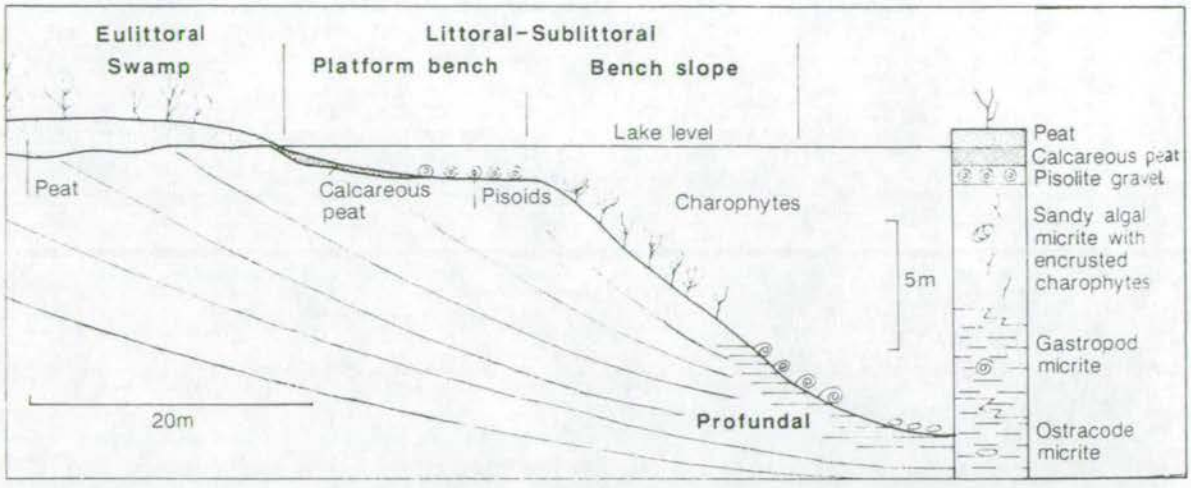

Fig. 4.8: Simple model of carbonate facies in a low energy bench margin of a hydrologically-open carbonate-rich lake. In this case the lake is permanantly stratified with anoxic conditions in the profundal one. Charophyte meadows can also occur on the bench slope. (from Tucker 1984). This model can be used to study the facies in the paludal and lacustrine environments of tufa deposits.

The most complex of these environments is the very shallow water/paludal environment where wind and wave agitation play a strong rôle. Phytoclast, oncolite, pisolith, intraclast, and possibly phytoherm tufa will all develop in this environment often closely associated with, and bound by, thin algal mats and drapes. This leads to very complex facies associations dependent upon local topography. The energy of a shallow water environment strongly controls the deposition which takes place. This can be either wind/wave energy or current energy. The value of differentiating between oncoidal tufa and pisolith tufa becomes apparant when we consider the evironments in which each grows. Oncoidal tufa is commonly believed to occur in quiet fluvial or lacustrine environmets (Nickel, 1983; Jones and Wilkinson, 1978). The examples from the Antalya Tufa support this. Commonly the oncolites sit in a fine grained substrate, the presence of occasional ostracods indicates a lacustrine setting. The coatings are wide and have grown in all directions at once, and the oncolites themselves tend to be elongate with no preferred orientation. In contrast the thin regular laminae, the spherical to subspherical shape and their occurance cross-bedded in lenses and channels (Plate 4.14A; Fig. 4.9A) strongly indicates that the pisolites formed in a highly agitated environment where carbonate precipitation was rapid. This agrees with the interpretation of Folk and Chafetz (1983) that the Tivoli pisoliths were deposited in a high energy environment. Phytoclast tufa also tends to be very localised, usually occurring as patches of reed, moss or plant stems cemented in growth position (usually vertical) and indicates a quiet, marshy environment. Algae and Cyanobacteria are opportunistic and although they do not tolerate a high

energy environment they will quickly establish themselves in an area, before plants and grazers begin to colonise. Thus, thin algal drapes and mats are particularly common and are seen covering fluvial breccia deposits and phytoclastic deposits just as often as deposits from calmer environments such as phytohermal patches. These are not usually laterally extensive but will grow on anything and in any orientation. It is probable that extensive areas of algal mat, such as in the Gaziler and Yesilkaraman areas, require calm conditions, probably in very shallow water, where periodic drying prevents higher plant and algal species (e.g. chara) becoming established. The highly cyclical laminations of the mat in these areas supports this supposition. The situation is comparable with the freshwater marsh areas of Monty and Hardie (1976) and the floodplain deposits of Casanova (1986). On the marshes documented by Monty and Hardie (1976) the mats reached no more than 6cm in thickness owing to rapid disintegration in the warm climate, but it is probable that the cooler climate during deposition around Antalya gave the mats a much higher preservation potential and indeed the deposits are observed over 10m in thickness.

It is important to remember that in shallow water fast deposition in a localised area (e.g. around thick stems or by domal stromatolites) and stabilisation of sediment by algal mats will rapidly alter the local topography, water depth and energy and hence the associated deposition. Rapid lateral and vertical facies changes are common throughout the deposit, but no more so than in the shallow-water tufa deposits. Domal stromatolite boundstone and phytoclast tufa may become the walls to small pools in which microcrystalline tufa develops (Plate 4.14B,C; Fig. 4.9B,C). These pools tend to be on a scale of a few meters, although Burger (1990) also attributes the large depressions on the Antalya peninsula to this system. It is my opinion that this is not the case (further discussion in chapter 5).

Stromatolite domes may also be indicative of water depth and energy. Generally it is shown that domal stromatolites are a nearshore facies requiring relatively calm, although possibly wave influenced, conditions. The depth of water they will grow in depends on the quantity of suspended sediment in the water which affects light levels. Anomalous examples have been found, for example stromatolites growing at 60m depth in Lake Wandergat, South Africa (Gow, 1981), but the majority of investigations show that stromatolites predominantly occur in nearshore environments and progade away from the shoreline to depths of about 10m (Eggleston and Dean, 1976; Link, Osbourne and Awramik, 1978; Golubic, 1991; Casnova, 1986)

Plate 4.14 and Fig. 3.9 (line drawings): Complex facies associations within the Antalya tufa:
A) Pisoliths, towards the top of the photograph, associated with intraclast tufa, cross bedded on 20cm scale, indicates that deposition occured in a high energy environment. **B)** Stromatolite dom form a pile on the left, behind which microcrystalline tufa deposits, presumably from water which h pooled behind the domes. **C)** Pisoliths occur as a layer within the infill between two stromatoli domes. Both form in a nearshore environment but pisoliths are higher energy deposits. The pisolit may have occurred as the result of a general change in environment or, perhaps, as a current w channel through the two, upstanding stromatolite "walls". **D)** A 0.5m thick tufa breccia deposit erosively on top of extremely pure microdetrital tufa. The breccia is generally very poorly sorted a represents sudden deposition within the environment. Above the breccia cross-bedded intraclast tu can be interpreted to represent a rather quieter period after the main flow which deposited the brec has moved away or died down. **E)** Patch of phytoherm framestone established on top of a tufa brecci **F)** Complex association of phytoclast tufa, intraclast tufa, pisolith tufa and tufa breccia which sugge that although all were deposited from a highly agitated environment, rapid stabilisation of t sediment prevents it being reworked. Thus the intraclast tufa merely fills in a rather complex g between the phytoclast tufa and the pisolith tufa.

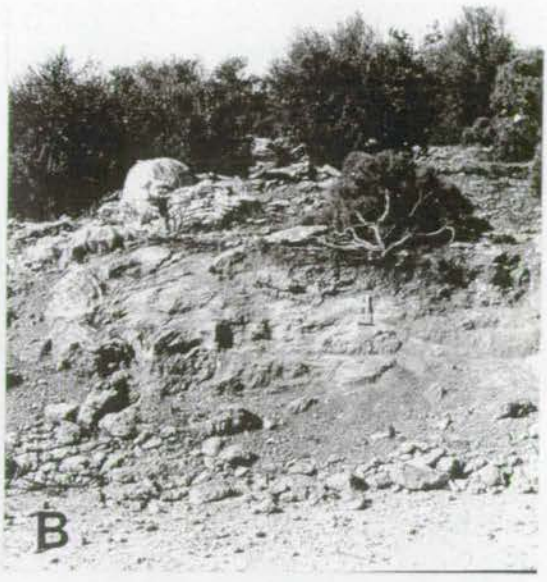

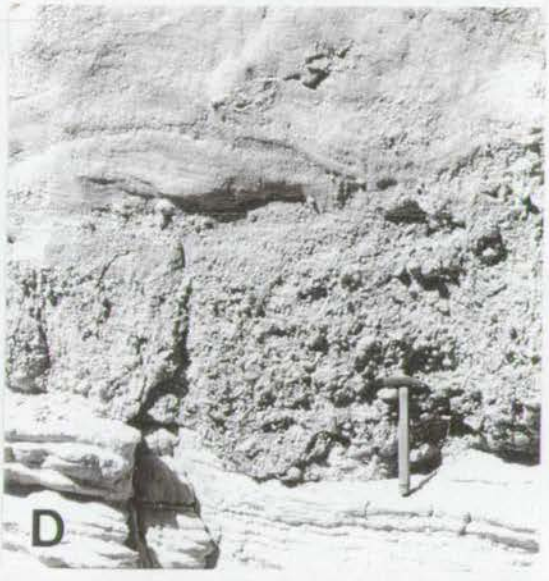

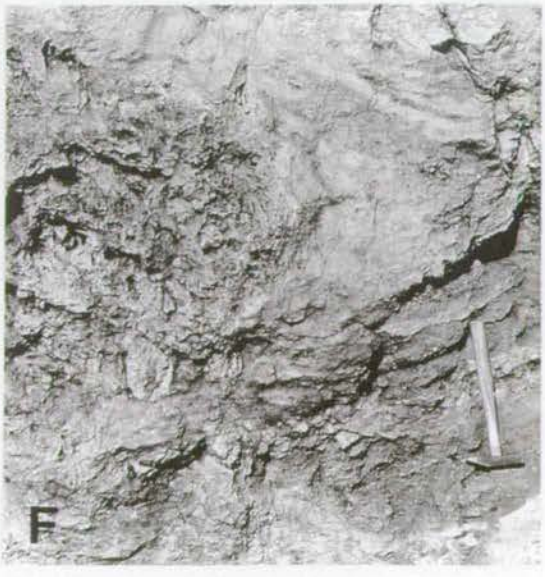

Plate 4·14

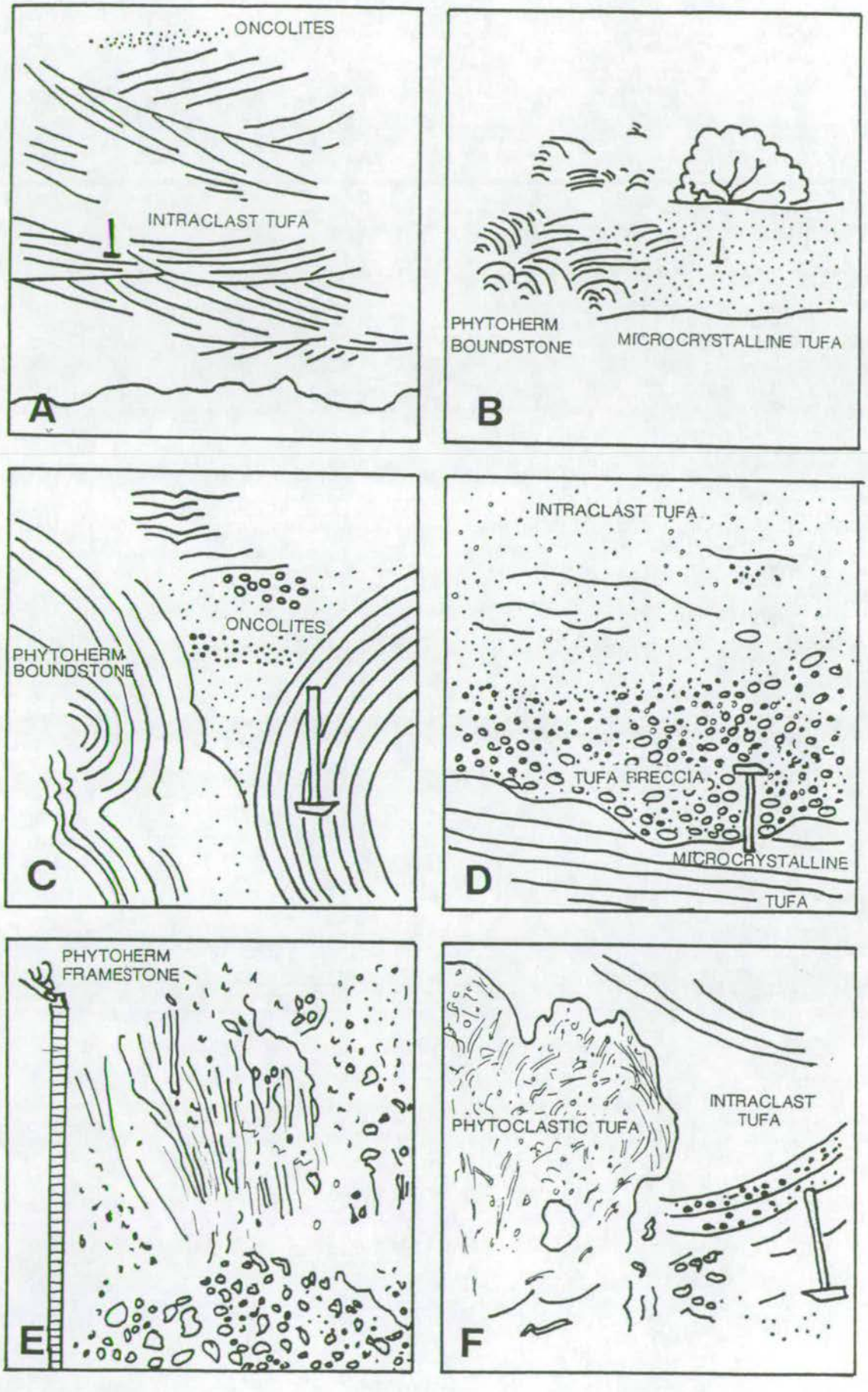
ONCOLITES
INTRACLAST TUFA
A
PHYTOHERM
BOUNDSTONE
MICROCRYSTALLINE TUFA
B
ONCOLITES
PHYTOHERM
BOUNDSTONE
C
INTRACLAST TUFA
TUFA BRECCIA
MICROCRYSTALLINE
TUFA
D
PHYTOHERM
FRAMESTONE
E
PHYTOCLASTIC TUFA
INTRACLAST
TUFA
F

Chironomids are typically found in streams but may occur in shallow, agitated (wind, areas of spring upwelling) lake margin waters. (C. Pinder, pers. comm., 1995) Thus, the presence of chironomids is a clear indication of shallow, flowing water. The fact that some algal domes are found with seasonal chironimid bands and others without means that it is possible to attribute algal domes (and mats) to shallow and deeper water environments.

In waterdepths of 4-6m, possibly even deeper, charophyte meadows may be common. These prefer a muddy substrate to a coarse one and the resulting deposit is a microcrystalline tufa rich in chara fragments, pennate diatoms and bacteria. As shown above stromatolites and oncolites may also occur in this environment and the actual deposits found are probably more dependent upon local topographic controls and not water depth.

Some stromatolite domes will grow in the littoral to sublittoral zone (depths up to 10 or 15m, possibly shallower), where low light intensity prevents higher plants gaining a foothold. Link *et al* (1978) suggest that stromatolites from these depths are relatively thin with no surface ornamentation in comparison to those growing in shallower waters which will tend to be large, flattened bioherms. The large, domal form of the stromatolites in the Antalya Tufa suggests that they grew in water depths up to 10m.

In waters deeper than 15m and below fairweather base pure microcrystalline carbonate will deposit. This tends to be pure carbonate with rare gastropods but some ostracods. Monty and Hardy (1976) showed that severe life conditions in the marsh prevented the development of a rich and diversified freshwater and fauna with rare gastropods and ostracods the sole occupiers of the environment. The rareness of gastropods and ostracods in the Antalya Tufa suggests the during deposition the waters were particularly harsh. In the stratigraphically lower, gastropod-rich sections, clay indicates some degree of external input into the system. Bands of poorly developed paleosol may also occur within these sediments.

Intraclast and tufa breccia are also important within the system, associated not with a lacustrine/paludal system but with fluvial systems. In particular, the tufa breccia can be seen to have a strongly erosional base and to occur in channels (Plate 4.14D; Fig. 4.9D; Fig. 4.10). These may be seen cutting through deposits from all environments. Intraclast tufa is likely to develop in small streams such as the present day example at Duraliler as well as in the paludal/shallow water marginal zones discussed above.

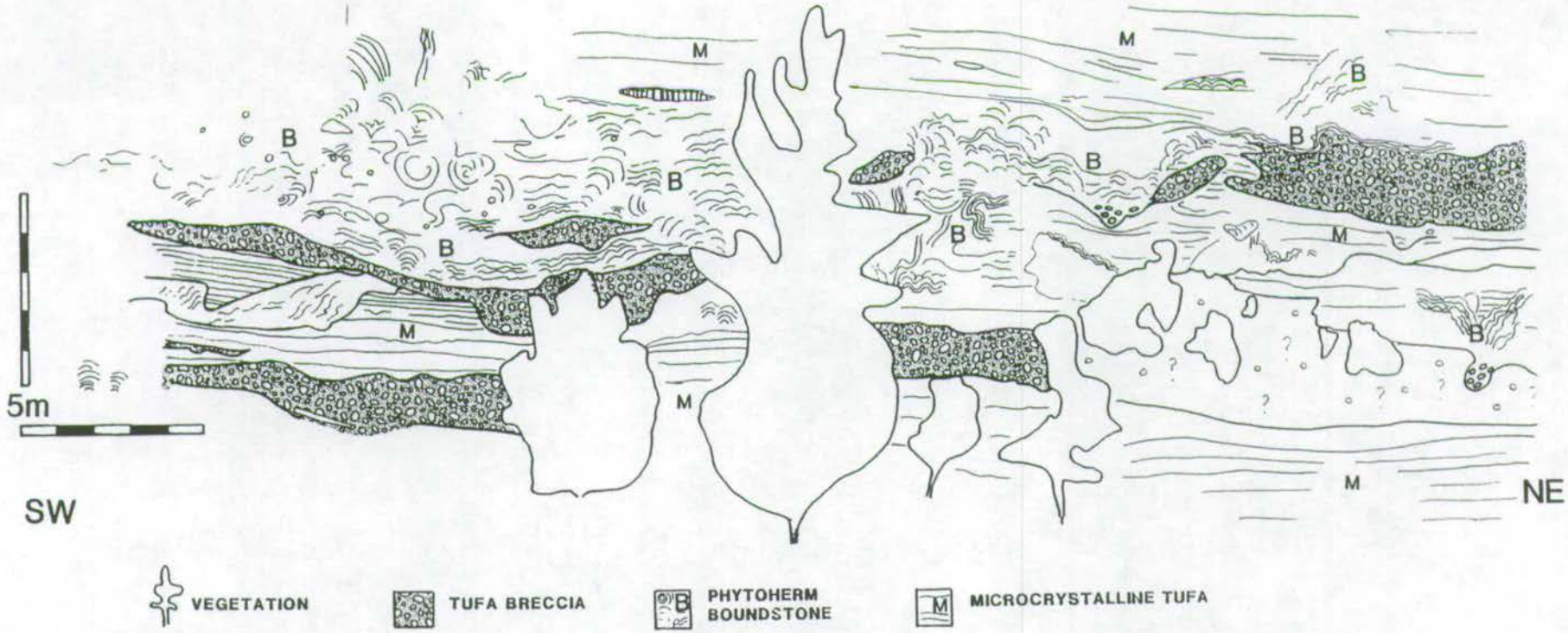

Fig. 4.10: Sketch of cliff section within the Asağ ikaraman-Yukarakaraman gorge system showing the dominance of tufa breccia in channel forms. Large quantities of phytoherm boundstone within the central part of the section suggest a general shallowing of the environment at this stage. The sketch was drawn from the opposite cliff using field glasses and a black and white photograph. It is probable that smaller scale variations, which could not be resolved, resemble those shown in the logs of Fig. 4.11.The vertical and horizontal scales are the same. The exact location of the section is shown on the inset of Fig. 4.11.

Fig. 4.10 not only shows the frequency and scale of the tufa breccia channels but also emphasises how large areas of stromatolite heads accumulate and dominate the deposit. Towards the top of the sequence microcrystalline carbonate once again dominates the cliff face. This sequence probably represents a shallowing and then a deepening of lacustrine waters. In this area it is typical to see very rapid vertical and lateral facies changes. This is illustrated by two logs drawn in the Karaman gorge section (Fig. 4.11). What, from a distance, looks like horizontally laminated microcrystalline deposits is, in fact, a complex association of microcrystalline, phytoherm, phytoclast and oncolitic tufa. In some cases unexpected associations occur: phytoclast tufa established on top of tufa breccia for example (Plate 4.14E; Fig. 4.9E). The situation is further complicated by the rapid stabilising of sediment which causes rigid topography around which new deposits form. This is well illustrated in Plate 4.14F and Fig. 4.9F.

These processes essentially describe the situation envisaged to have controlled the majority of tufa deposition (Fig. 4.12). It is proposed here that, during deposition, the plain was dominated by paludal and lacustrine environments with water depths ranging from centimetres to meters (possibly up to 20m in local depressions). Across this plain a number of small rivers (5-10m in width and probably meandering) and streams (1-2m in width) wound their way, constantly reworking the friable deposits through which they passed. The dominance of intraformational clasts and lack of detrital material within the fluvial deposits show that they were spring sourced and not runoff from surrounding mountains. This situation is a complex mix of what is seen in the Hula Valley (Heimann and Sass, 1989), the Tanagro valley (Buccino *et al*, 1978) and Slakow graben (Szulc and Cwizewicz, 1988) lacustrine and paludal environments and in the fluvial environment of central Spain (Ordóñez and García del Cura, 1983). In the Hula valley the majority of deposition is thought to have occurred on a gentle slope under a shallow sheet of water. The waters were probably more sluggish than those in Antalya. The primary difference is that there is no evidence that the Antalya deposit was formed on a slope, more lacustrine material is present in the Antalya deposit and there is significant evidence for fluvial reworking. Heimann and Sass (1989) attribute the reduction in tufa deposition and the increase in slope to tectonic activity. It is possible that the reduction in tufa deposition is climatically controlled (cf. section 4.16) and that the increase in slope represents slope steepening due to deposition, as described for the Rochetta a Volturno deposits (Violante *et al*, 1994, section 4.7.5).

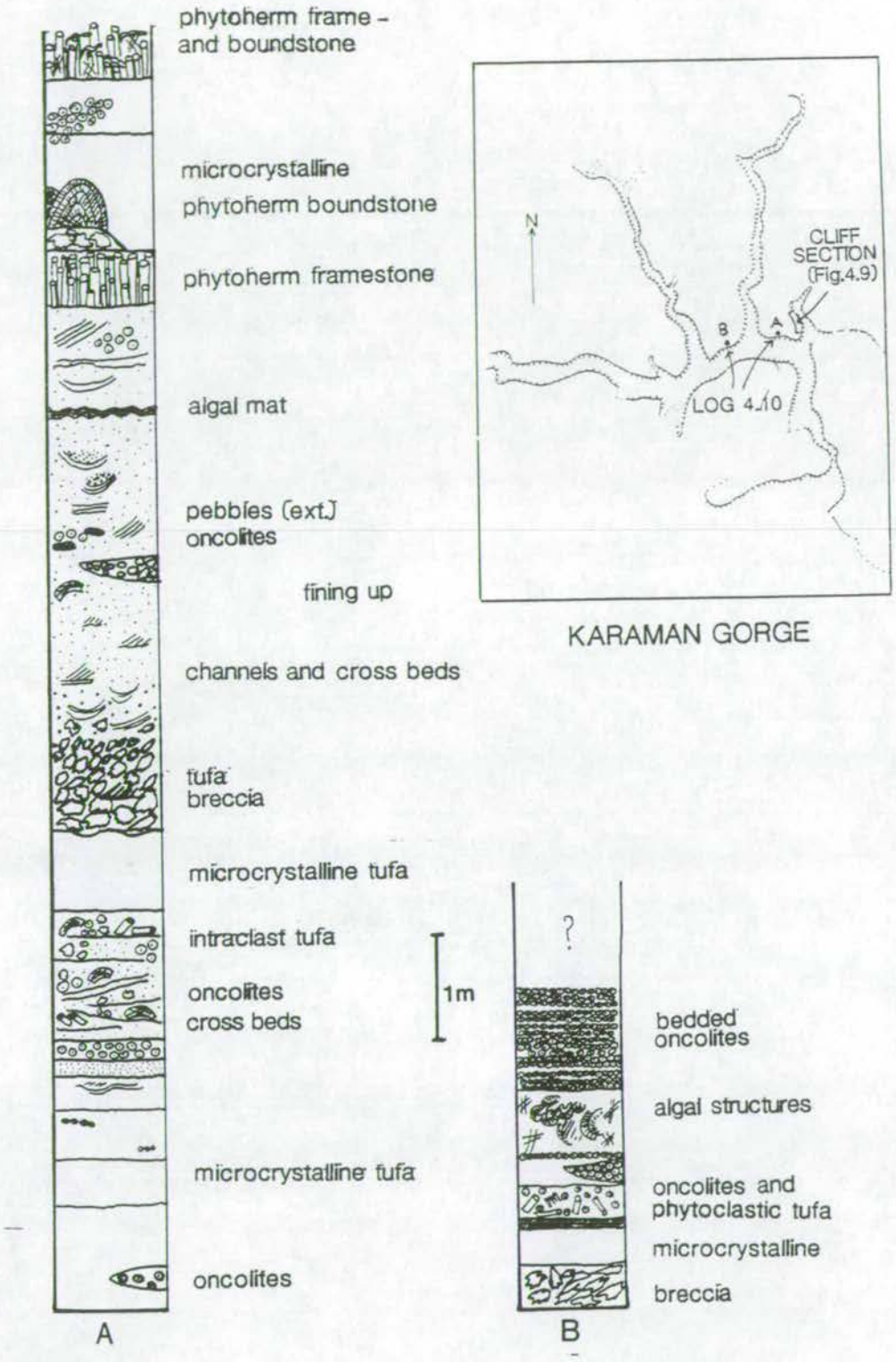

Fig 4.11: Sedimentary logs of tufa facies seen towards the base of the Karaman gorge system and their localities within the gorges (Inset). These logs emphasise the extreme complexity of the association between all facies types and the rapid vertical facies changes. This type of association is almost certainly present in the microcrystalline sections of the cliff sketched in Fig. 3.9 although this could not be verified.

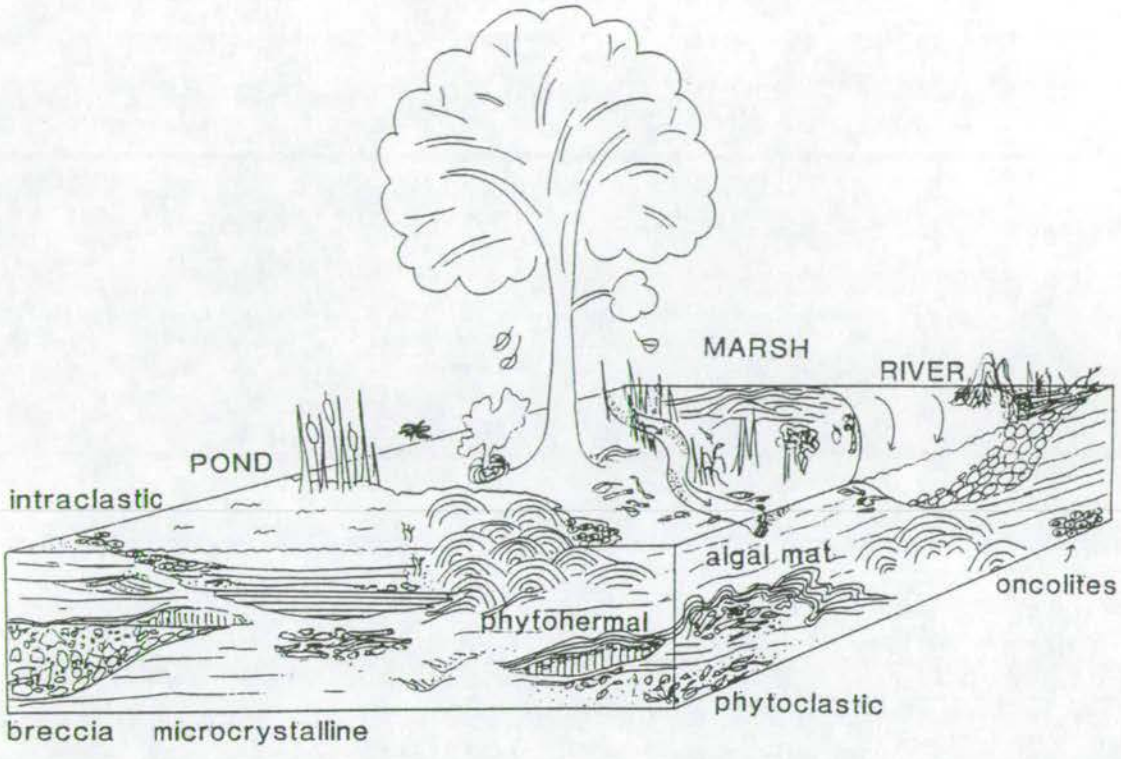

Fig. 4.12: Schematic diagram of the complex depositional environment thought to have existed during deposition of the majority of the tufa. Fluvial, paludal and lacustrine (RIVER, MARSH, POND) environments are all depicted. Facies types are indicated in lowercase letters.

If this is the case the Hula valley is not analogous to the Antalya system. In Tanagro (Buccino *et al*, 1978) and in the Slakow graben (Szulc and Cwizewicz, 1988) ponds of lacustrine carbonate and related paludal sediments are seen. Once again these seem to be in much calmer environments than the Antalya Tufa and no evidence of large-scale fluvial reworking is described. There are many similarities between the fluvial tufas of Spain (Ordóñez and García del Cura, 1983) and the higher energy deposits of the Antalya system. The Antalya Tufa thus represents deposition from a broad sheet of water, on a very gentle slope with high energy fluvial systems dissecting and reworking the quiet water paludal and lacustrine deposits.

Distinct associations occur on the terrace edges and although they are of relatively minor volumetric importance their dramatic visual impact and veneering nature means that they are one of the most noticeable features of the system. The two most common facies which occur on terrace scarps and slopes are phytoherm framestone and phytoherm boundstone. Occurrence of other facies is minor. A number of different forms can be identified: cascade, spring and slope deposits.

If the scarp is steep, water will cascade over the edge and waterfall deposits similar to those described in section 4.7.2 will develop. Long vertical stems provide the common textural fabric (Plate 4.15A). Where water flow is particularly strong, cones may develop such as those seen at the Düden falls both inland and on the coast near Lara (Plate 4.15B). Mounds of mosses and some sinter will commonly develop at the base of the waterfall, as seen at both the inland falls (Düden and Kursunlu).

At many terrace edges the water does not pour over the edge, but emerges some way down the cliff at a spring (Plate 4.15C) These springs often have many resurgence points resulting from the highly porous nature of the tufa and thus water flow tends to be somewhat slower. Typically *Potomugeton,* mosses and algae dominate the deposit, giving it a vertical porous texture (Plate 4.15D). Thin algal mats are also very commonly associated with these deposits. In some areas (Çalkaya, spur north of Antalya) relict pools can be distinguished, developed on the shallow slope below the terrace and springs (Plate 4.15E). These are directly comparable to the pool structures seen on the terrace mound deposits at the hot spring areas of Pammukale and Yellowstone. The general morphology of large algal dome structures, analogous to these terrace mounds, are also found. They are not common as the terrace edges are nearly always vertical to subvertical. However, a particularly good example is found on the slope behind Varsak where the domes are up to 20m in width and 10m in height (Plate 4.15F).

4.15: Facies Distribution

In section 4.14 a general picture of the local environments in which the tufas were deposited has been presented. These observations can be applied to all areas of the deposit and used to interpret the local depositional environment. By considering the gross lateral distribution of facies and environments together with their development through time (vertical distribution) a more general model emerges for the entire Antalya deposit.

The base of the deposit is only exposed in a few areas. In the Kursunlu region the tufa sits directly on the Pliocene conglomerates and in some places sands.

Plate 4.15: Terrace edge deposits:
A) Long vertical stems cemented during cascade of water over the edge of a terrace. **B)** Cones of tufa at the Lara falls of the Düden Çay, cemented around mosses which hang in the parabolic flow o water. **C)** Phytoherm framestone deposited around the resurgence point of a spring. The deposit i dominated by encrustations around *Potomugeon*, mosses and algae. These are often plastered fla downslope just as they trailed in the running water. Numerous exit holes can be seen within and abov the central chamber. **D)** Detail of typical spring deposits. **E)** Relict pools can be distinguished developed on the shallow slope below a terrace and springs. These are directly comparable to the poo structures seen on the terrace mound deposits at the hot spring areas of Pammukale and Yellowstone **F)** Thick deposits of large-scale, undulating algal domes, analogous to the range-front travertines o Pammukale.

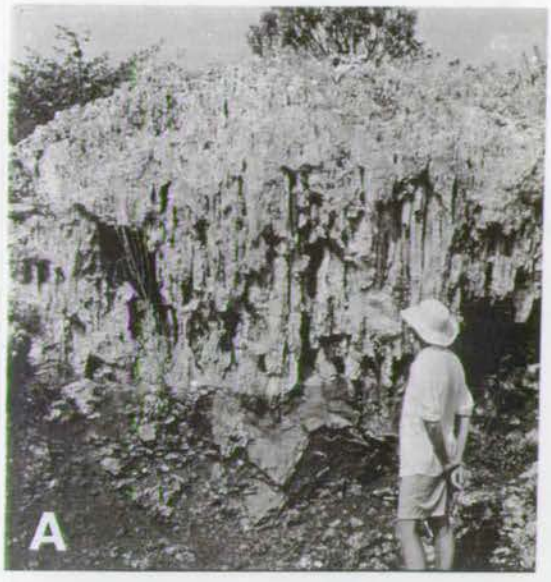

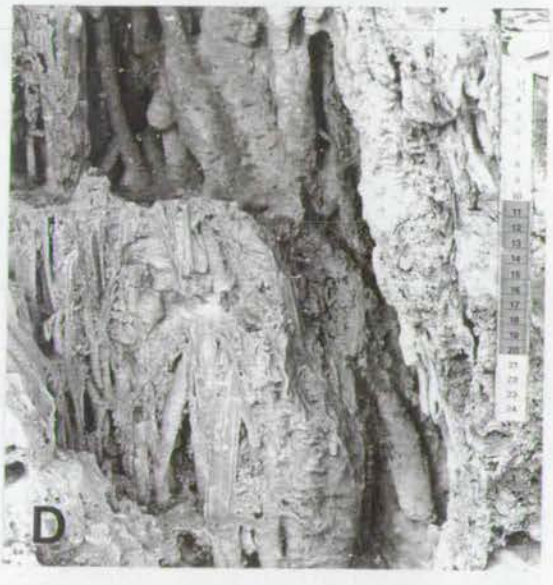

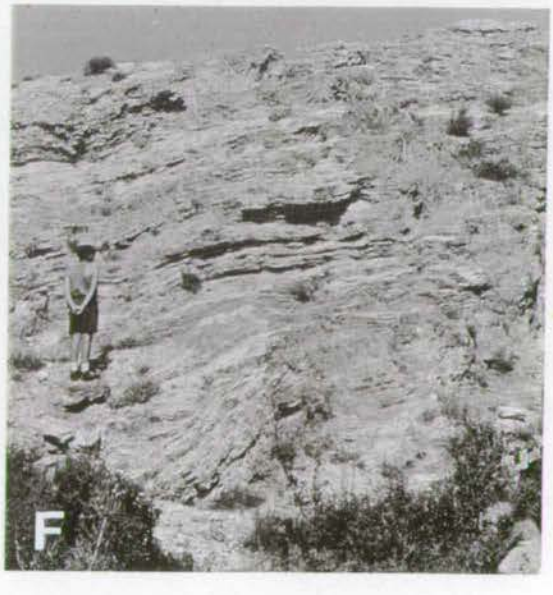

Plate 4·15

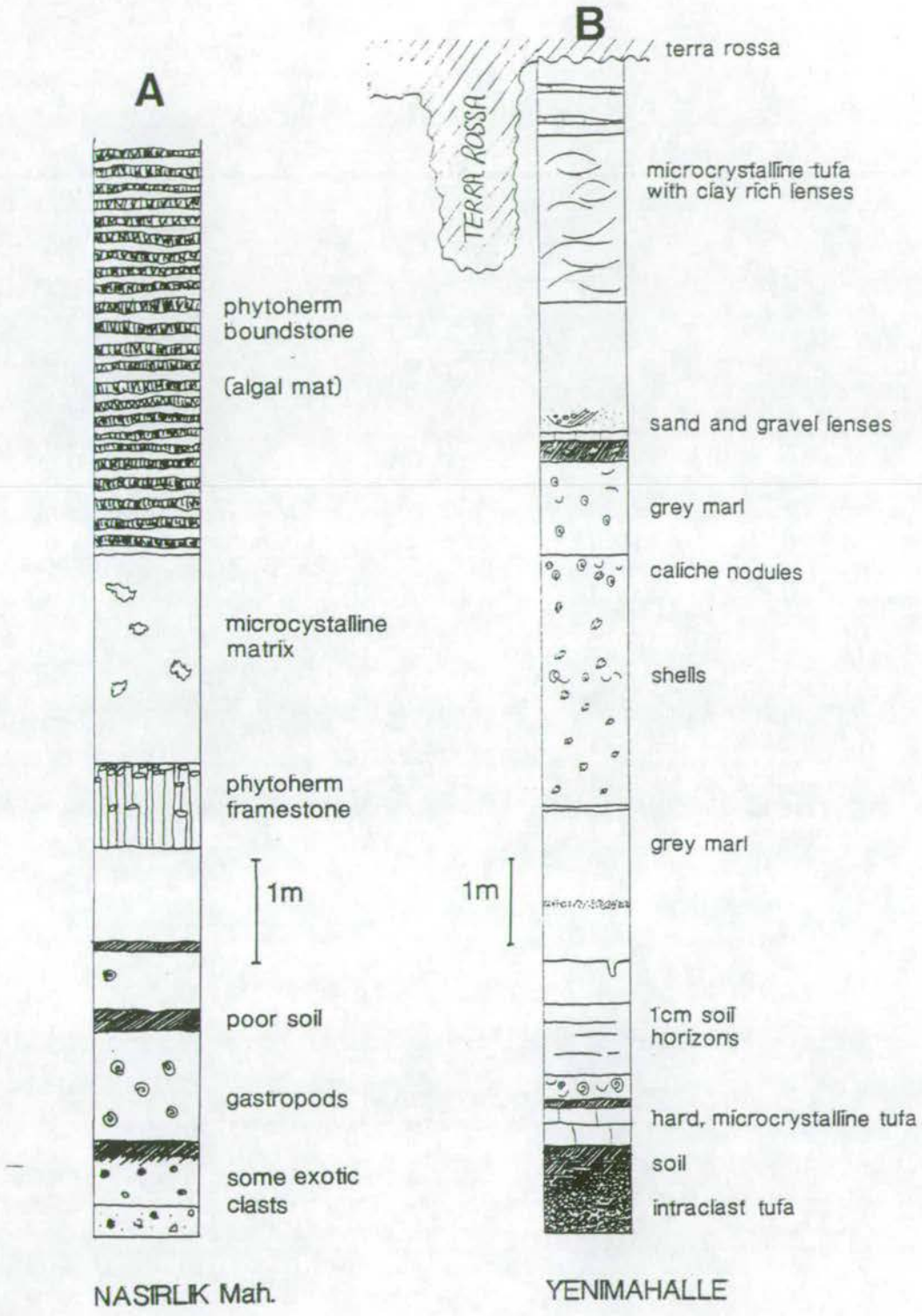

Fig. 4.13: Logs of the base of the deposit exposed on the eastern terrace edge at Yenimahalle and Nasirlik Mah.. Typically the lowermost beds are gastropod bearing, clay-rich carbonates. At Nasirlik Mah. these carbonates pass rapidly up into thick deposits of algal mat (phytoherm boundstone). This transition is not seen in the Yenimahalle section although algal mat exists further up the hillside.

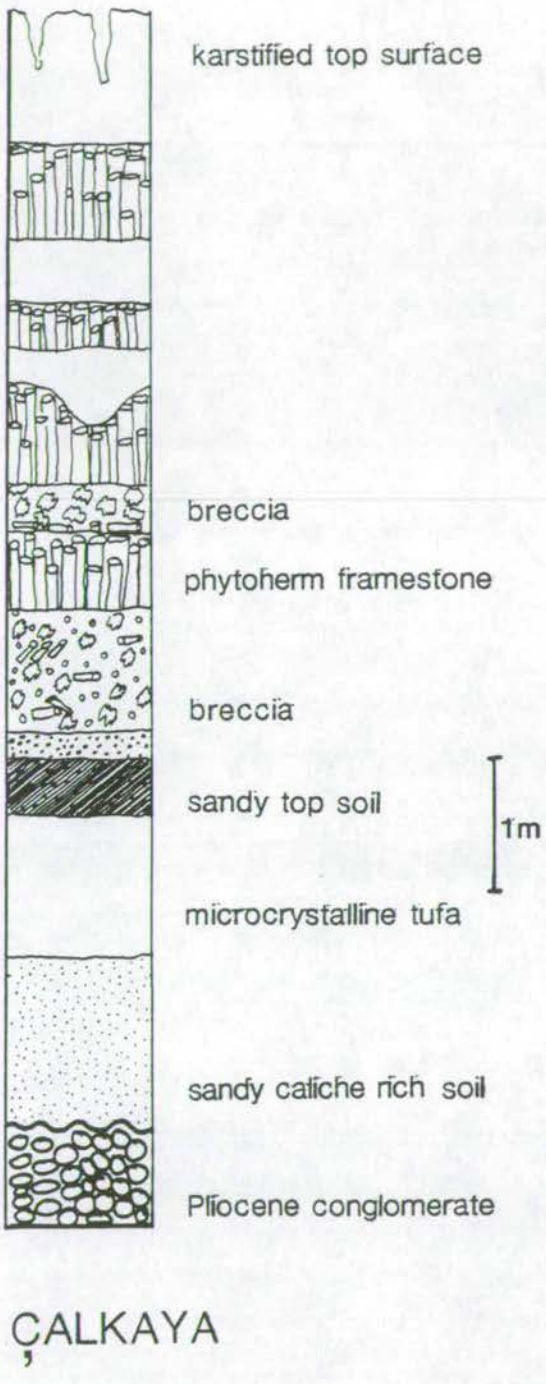

Fig 4.14: Log of the base of the tufa at Calkaya. The tufa sits directly on Pliocene conglomerate and is predominantly phytoherm framestone and micritic tufa, suggesting a marginal lacustrine area. Lack of rootlets in the microcrystalline tufa suggests that thin paleosols may have existed between them and the phytoherm framestone layers which have subsequently been eroded away.

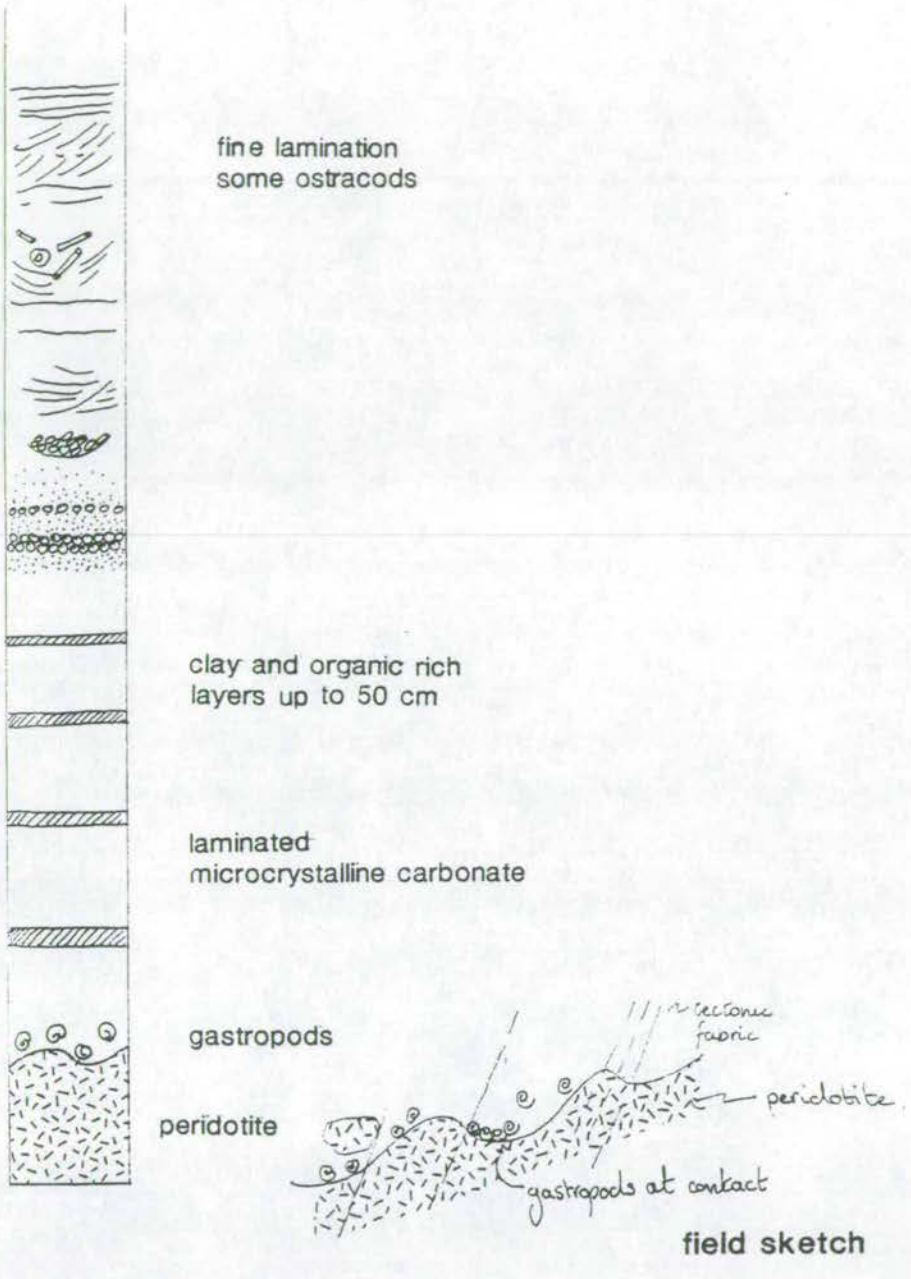

Fig 4.15: Log of the basal section in the west of the basin, near Karaman. The tufa lies unconformably on the Mesozoic peridotites and radiolarites. As in Figs. 4.13 and 4.14 the initial deposits are a clay-rich microcrystalline tufa rich in gastropods. In places, directly above the contact, clasts of peridotite can be seen within the deposit.

The contact is unconformable; the Pliocene deposits dipping westwards below the tufa. Typically the lowermost beds are gastropod-bearing, clay-rich, microcrystalline tufa, or oncolitic. The boundary between them and the underlying sediments is sharp. These lowermost beds pass rapidly upwards into thick deposits of laminated algal mat (Fig. 4.13). Further south on the same plain, around Gaziler, the deposits are more varied consisting of phytoherm, phytoclast, oncolitic and microcrystalline tufa. Further south again at Çalkaya the tufa sits directly on Pliocene conglomerate and is predominantly phytoherm framestone, paleosols and micritic tufa, suggesting a marginal lacustrine area (Fig. 4.14). Along the entire terrace edge from Yenimahalle to Lara the tufa is typically only 30m thick (Plate 4.16A). It can sometimes be seen tilting backwards into the terrace (Plate 4.16B).

In the west around the Karaman gorge area (map: Fig. 4.5) the tufa lies unconformably on the Mesozoic peridotites and radiolarites (Fig. 4.15) and is considerably over 100m thick. This can be seen in outcrop and from the borehole data presented above. Kelkayrak Tepe, on which sits a firewatch station, is composed of peridotite which is clearly a pre-tufa hill around which tufa has subsequently deposited leaving only the summit protruding (Plate 4.16C). Again the initial deposits are a clay-rich microcrystalline tufa, rich in gastropods. In places, directly above the contact, clasts of peridotite can be seen within the deposit. The sediments in this area rapidly grade up into a pure microcrystalline tufa with regular interbedded carbonate-rich paleosols. These pure microcrystalline tufas dominate the section for about 10m and then the sediments become more varied with cross bedded, oncolitic phytoclast deposits. In this area the majority of the sequence is typified by the Karaman gorge section log (Fig. 4.10) and cliff section (Fig. 4.9). It is important to remember that throughout this section microcrystalline tufa is common (Plate 4.15D,E). The top 10m of the sequence is quite different in character, consisting almost entirely of phytoclast tufa. This sequence represents a general shallowing-up of the entire deposit through time.

The occurrence of terrace edge deposits is limited to the present-day terrace scarps, where they form a thin veneer over the underlying sediment. This is the case at the present day Antalya coastline, where horizontally-bedded tufa facies are visible beneath a coating of cascade tufa only a few meters in thickness (Plate 4.16F). At the coastal falls of the Düden, it can be seen that the river has switched westwards relatively recently. This process of switching enabled the river to produce a veneer of phytoherm framestone over large proportions of the cliffline. The same process can be seen at the inland terraces, although here the veneer is not nearly so pervasive and

Plate 4.16: Distribution of Facies:

A) Above the bushes approximately 30m of laminated phytoherm boundstone crop out. Below th bushes, and next to the person, Pliocene conglomerate crops out. **B)** Laminated phytoherm boundstone tilts back away from the edge of the terrace near Çalkaya. **C)** Looking across th Karaman gorge towards Kelkayrak Tepe, on which sits a firewatch station. The hill is peridotite and i interpreted as original palaeotopography around which the tufa has deposited. **D)** Thick deposits o microdetrital tufa situated just to the north of the Karaman gorge. **E)** Horizontally bedded tufa withi the Karaman gorge at the base of the 100m high cliff. This is the section logged in Fig. 3.10 **F)** Terrace cascade deposits creating a veneer on the coastal cliffs immediately to the west of Antaly It can be seen that typical bedded tufa exists below this veneer.

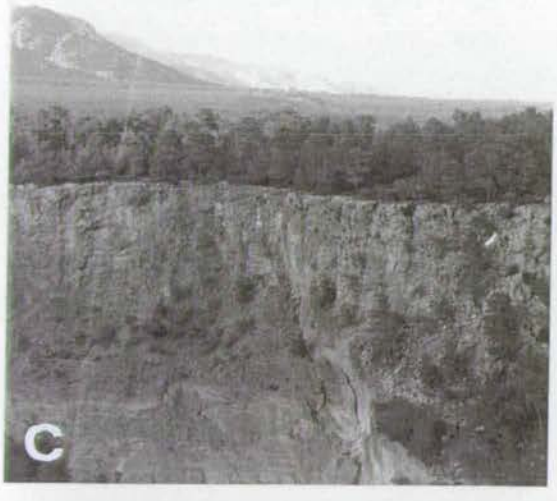

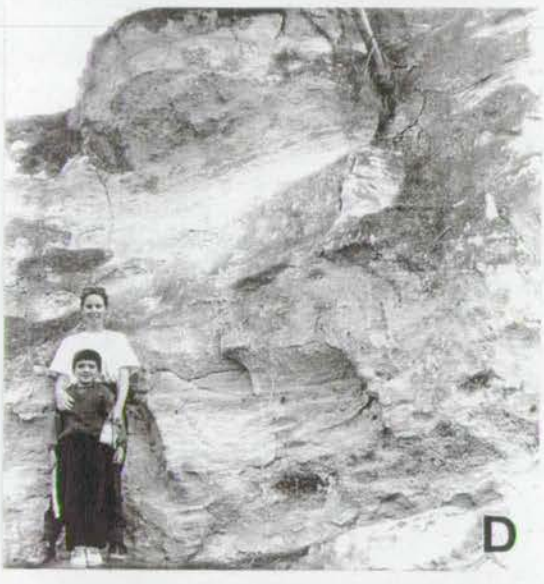

Plate 4·16

often the terrace scarps and slopes consist entirely of horizontally bedded tufa. At Kursunlu, the veneer of tufa is deposited onto conglomerate.

4.16: Deposition in space and time

It is shown in chapters 5 and 6 that the Pliocene sediments underwent normal faulting that created west-dipping fault blocks in the Aksu basin. The horizontal strata of the tufa show that it was deposited after the principal normal faulting event. The differences in basement in the east (Pliocene sands and conglomerates) and west (Peridotite) are attributable to the highly irregular, block faulted topography of the basement. The exact form of the underlying topography, for example the number of fault blocks and the relief, are unknown. Block faulting almost certainly postdated the erosion surface which is seen dipping below the tufa along the western margin. Small, localised fanglomerates along the western margin of the area interfinger into the tufa suggesting that renewed uplift caused by the normal faulting may have brought some sediment into the very west of the area in runoff streams. This effect was not great and, in general, the clastic supply to the area was not sufficient to swamp carbonate production. Clastic material from the Aksu river at this time may be the reason that the tufa is not deposited further to the east.

There is no striking evidence for cyclicity within the deposit and certainly no intraformational karstification of the deposit. At best, the Karaman cliff section (Fig. 4.9) shows a change from lacustrine to paludal and back to lacustrine. This could be related to slight changes in climate, but may equally represent a reorganisation of facies distribution. This leads to the conclusion that deposition occured during one particular climatic period (section 4.11.4). U-Th dating (chapter 2) indicates that the majority of the tufa is >400,000 years in age. Very rough calculations (section 4.9.3) suggest that deposition required approximately 500,000 years. This is a minimum period. Only the upper terrace was considered for the calculation and no account was taken of erosion. It is fully possible that the period of deposition was of the order of 1 Ma or longer. A general shallowing trend through time has also been observed (section 4.15). This also indicates that deposition occured during one climatic period. As the climate gradually became drier, tufa deposition became less until, eventually, it virtually ceased.

The climatological data from the Tyrrhenian Sea (chapter 1) show that the most favourable period for tufa deposition in the Mediterranean is during the period 2.1-1.5 Ma. The onset of cooler climate conditions is seen at 3.1 Ma and the conditions from this period to the Pliocene-Pleistocene boundary (1.55 Ma) are described as temperate. The period 2.1-1.5 Ma is marginally warmer than the

previous 5 Ma, documented by a warming trend in $\delta^{18}O$ and the reintroduction of the *G. inflata* group. Strong seasonality also increases the probablitiy of tufa deposition during this time interval. This seasonality is due to climatic instability immediately preceding to the 100,000 year glacial cyclicity of the Pleistocene and Holocene. This cyclicity corresponds to a sharp fall in winter temperatures, low rainfall and summer dryness allowing only for limited deposition. Indeed the cold, wet glacial periods are more favourable for karstification and erosion of the tufa than for deposition: evaporation rates are lower and the carbonate is more dilute due to the greater throughflow of water.

Although there is no firm evidence that 2.1-1.5 Ma was the main period of deposition a significant number of indicators all tentatively suggest the same thing. Firstly, we know that the deposition of tufa occurs most rapidly in temperate periods with strong seasonality (section 4.5). It has also been suggested that tufa deposition occurs during transitions between glacials to interglacials (Marker, 1971). The period 2.1-1.5 Ma meets all these requirements. The thickness and continuity of the Antalya Tufa suggests it must have been deposited during a significant period of favourable climatic conditons. These are not seen anywhere within the deposit. The glacial cyclicity of 100,000 years is simply too short for the Antalya Tufa to have formed during an interglacial. If deposition had occurred over several glacials during the Holocene visible indications of the glacial periods would be expected, such as erosion, soil formation, and infilled karst forms. The 0.6 Ma period at the onset of glaciation is of the right order of time thought to be required for deposition of the Antalya Tufa and also shows a gradual increase in dryness which accounts for the observed shallowing-up trend. Furthermore, the floral evidence also points towards deposition having occured prior to onset of the glacial period, in a temperate wet climate (section 4.11.4). It is possible that deposition began as far back as 2.7 Ma at the very onset of climatic instability. However, it is thought likely that this period was marginally too cool.

A series of palaeogeographic sketches of the distribution of tufa deposition and the principal facies formations through time is presented in Figs. 4.16. and 4.17. Initially the tufa is probably limited to deposition in lakes in palaeolows between tilted fault blocks. Soil layers are occasionally developed as climate fluctuates (4.16). One cluster of springs in the same geographic position as Kirkgöz seems the most probable source but a more widespread series of springs may have existed.

With time the palaeotopography is infilled and a broader zone of tufa deposition develops. The eastern margin may still be limited by a fault block high at this point. On this margin the primary deposition was due to algal mats, perhaps due

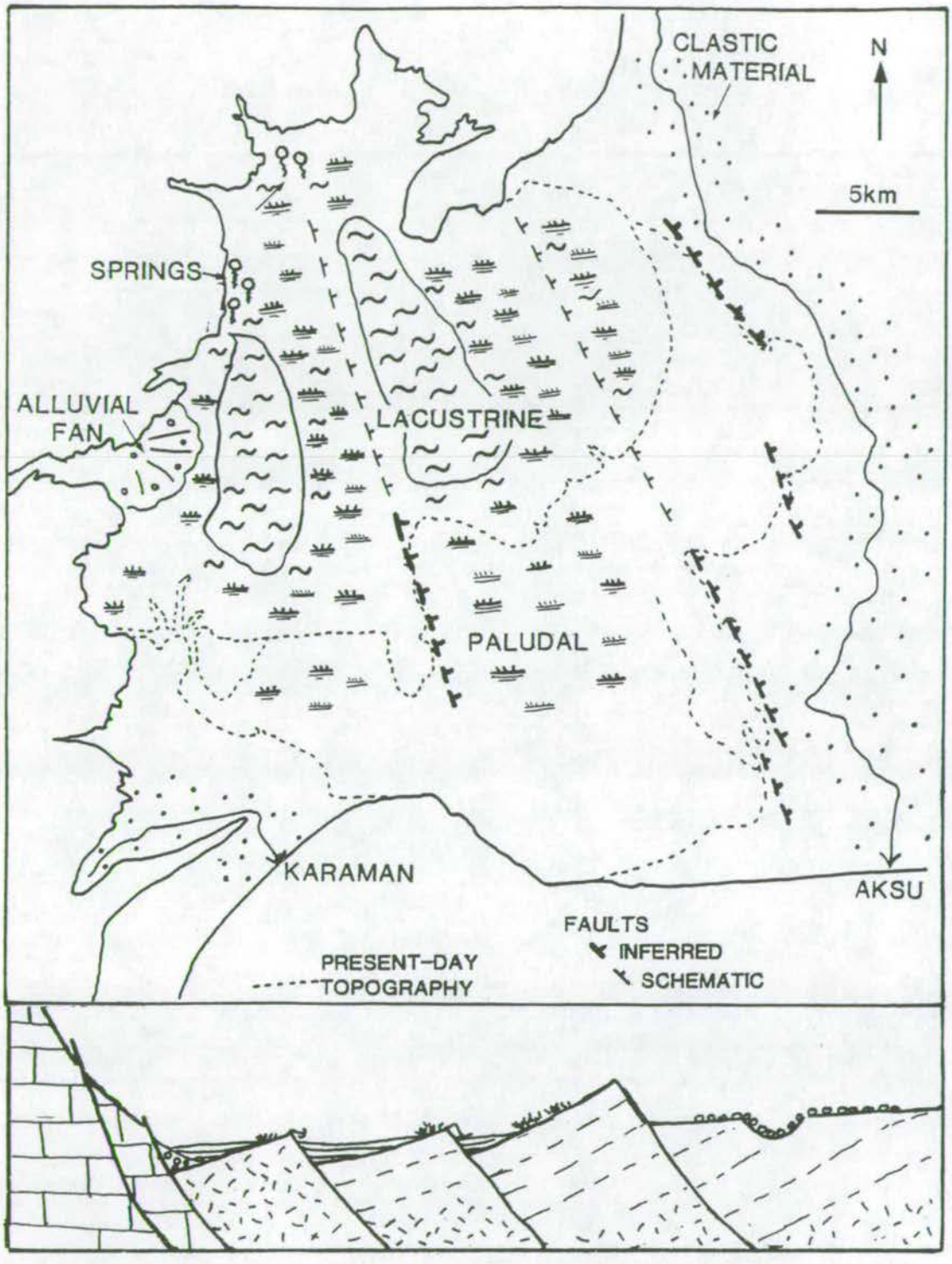

Fig. 4.16: Initial phase of deposition of the Antalya Tufa. Carbonate supersaturated waters are ponded between fault blocks in the underlying basement (Mesozoic and Pliocene). Clastic sedimentation from the Karaman Çay prevents deposition to the and southwest. In the east the fault-block topography acts as a sill, confining the tufa system to the west of the basin.

to the presence of a confined "lagoonal" area (Fig. 4.17). Deposition during this period is represented by the complex lacustrine/paludal environment described in section 4.14 and illustrated by Fig. 4.12. This represents the main phase of tufa deposition.

As the climate becomes drier, surface water is reduced and the predominatly phytoclast, phytoherm deposits of the uppermost 20m of the section are formed. During the Holocene neither the glacials or interglacials allow significant tufa formation. The glacials are too cold and wet and the interglacials too arid. Thus, only minimal tufa deposition and erosion marks the final phase of the development of the deposit.

It is to be expected that, if the terraces are original depositional features, migration would have occurred creating "fossil" terrace edges comprising large deposits of vertical phytoherm framestone onlapped by lacustrine/paludal sediments. These have not been discernible anywhere in the deposit which indicates that the present day terraces are erosional. At the onset of the Pleistocene global sea-level fluctuations become greater and it is possible that a marine incursion occurred and eroded the lower terrace. A small fan was deposited at the mouth of the Karaman Çay at this time (4.16C). No evidence of marine sediments have been found on the lower plain, but it is very heavily karstified and vegetated. Burger (1990) suggested this was a karst marginal plains on the 40-50m level and was related to a period of higher sea-level. Gorge incision and erosive retrogression of the tufa cliffs are further Quaternary features. The Aksu Çay has not cut back significantly into the tufa as the fault scarps which formed the eastern boundary of tufa deposition are topographic features and protect the tufa from erosion whilst constraining the Aksu valley. Streams on the upper terrace have produced some erosion of the eastern edge of the tufa. This final phase of erosion, karstification and terrace formation will be dicussed further in chapter 5.

Subsequent depositional modification of the terraces has occurred until present, producing slope pools, waterfall deposits and terrace mound deposits in localised areas. These are at lower levels than the main terraces because of lowered water tables. At the present day tufa deposition is very limited, despite continued high supersaturation of the emergent spring waters. It primarily occurs in the highly turbulent regimes of waterfalls and small streams. Fine particle formation occurs at source springs and in areas where water is very ephemeral and algal films occur on the water surface.

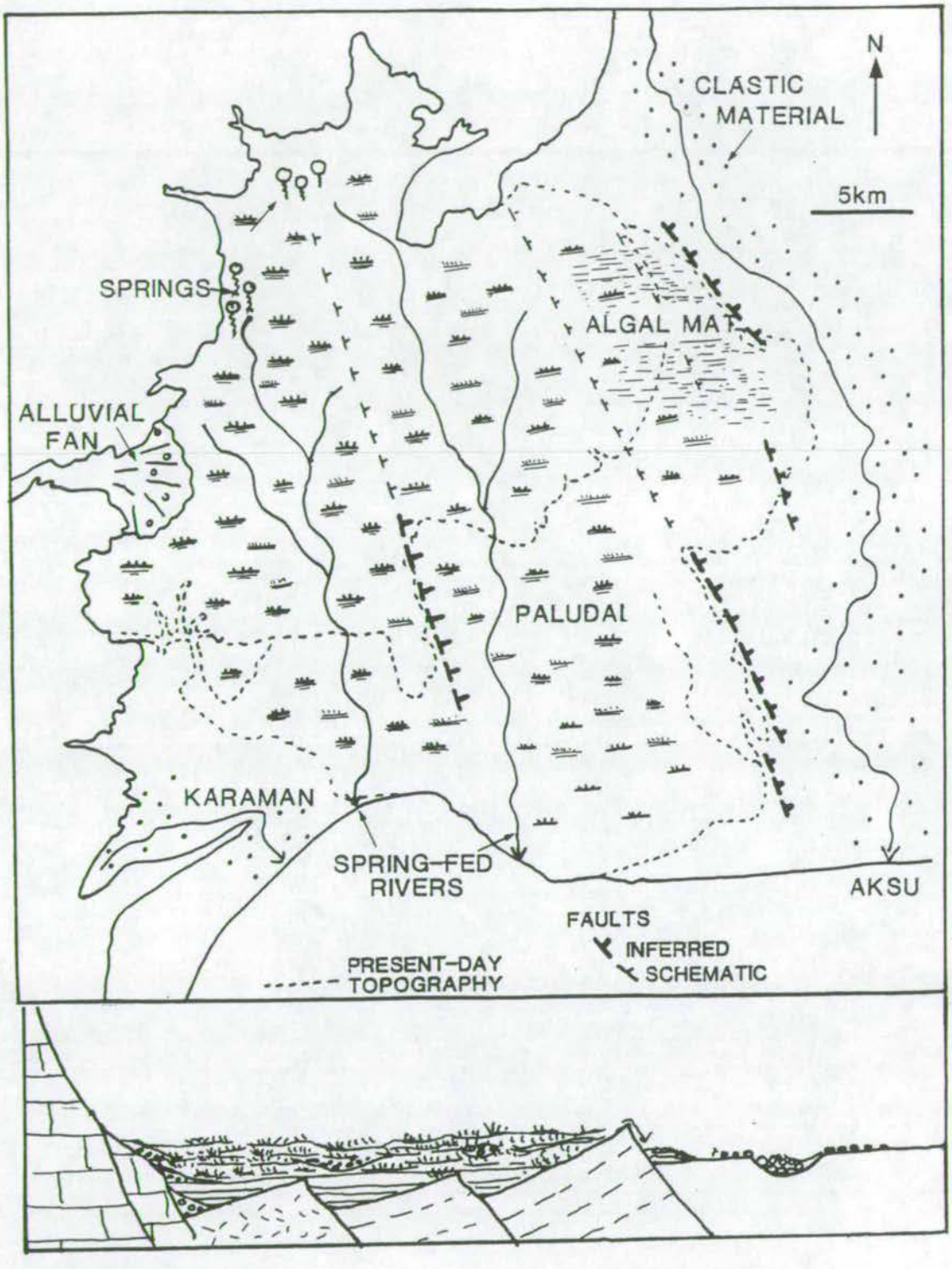

Fig. 4.17: Second phase of deposition of the Antalya Tufa: the entire system has become shallower and more paludal due to increased climatic dryness and a larger depositional area. Most of the fault block topography has been infilled. Clastic deposition continues in the Karaman and Aksu Çayi.

4.17: Conclusions

1) A modified triangular diagram for the classification of freshwater carbonates has been proposed. It is process-controlled and recognises the importance of temperature in distinguishing between travertine and tufa deposits and the importance of biogenically controlled deposition.

2) Tufa and lacustrine carbonate are intimately associated and both form an integral part of the the Antalya deposit.

3) Bacteria, Cyanobacteria and green algae are vital agents for the depositon of the tufa.

4) Two new facies types have been added to the facies scheme of Pedley (1990): tufa breccia and inorganic pisoliths. The former has not been previously recognised.

5) The initial phase of deposition was predominantly lacustrine and water was ponded between fault block highs. As the palaeotopography was infilled the region became more paludal.

6) The majority of tufa deposition occured in a complex lacustrine, paludal, fluvial environment characterised by numerous facies types and rapid lateral and vertical facies changes. The facies types are those of Pedley (1990) with the additions mentioned in 4 above.

7) The final phase of tufa deposition is represented by phytohermal and phytoclastic deposition in a very shallow water environment.

8) Deposition is thought to have occurred between 2.7 and 1.5 Ma.

9) At the present day erosion is more important than deposition.

Chapter 5: Geomorphology

This chapter describes and discusses geomorphological features of the Isparta angle. The effects of erosion, faulting and fluvial incision and aggradation will be discussed. The various geomorphological features are presented in approximate chronological order.

5.1: Previous work

The geomorphology of the region has received more attention than other aspects of the Plio-Quaternary evolution of the area. The dominant terraces of the western Aksu basin, occupied by the Antalya tufa, are probably the most striking feature of the area. Certainly, the earliest workers paid almost exclusive attention to the possible origins of these terraces.

Tietze (1885) viewed the terraces as evidence of marine erosion reflecting slow regression from the Antalya basin. He also suggested that some of the inland terraces were the result of a carbonate "overcrust" developed on older marine terraces. He pointed out the simplicity with which carbonate-rich rivers, which are free to meander over their own deposits, could change their course and produce broad flat plains of "chalk" as they deposit carbonate over the floodplain.

In contrast, Penck (1918), whilst agreeing with the last point, saw terrace creation as a response to uplift of the land. When uplift occured the relative level of the watertable sank causing springs and rivers to run dry. New springs and associated rivers then appear further towards the sea. Penck envisaged that this process occurred in repeated phases. He viewed the escarpment between the two main terraces as an old sea cliff left high and dry by uplift of the land. Both Tietze and Penck, therefore, viewed the terraces as a result of marine erosion. It was just the causal mechanism: tectonic uplift, or marine regression, which was in dispute. This is, of course, the problem of relative sea-level change which causes so much angst amongst today's sequence and seismic stratigraphers.

Philippson (1918) considered that the distinctive escarpments were fault steps.

Planhol (1956a), partially after Darkot and Erinç (1947), attributed terrace formation to subaerial erosion. This was largely from geomorphological arguments concerning the profile and trace of the terraces and the continuation of erosion surfaces from the travertine plateau into the surrounding, older rocks. In particular, he noted that there is an absence of deposits characteristic of a marine abrasion surface. He felt the agent responsible for levelling the terraces was "fluvio-karstic scouring" (i.e. river erosion) by the Aksu Çay and the spring sourced streams that flow across the plain. He believed that the upper terrace level was liable to be the original level of the tufa, relating to a lake level. He envisaged small valleys, which extended out from the interior of the mountains, being infilled by these lakes. This upper surface was then eroded by the Düden Çay. There is no evidence that the Aksu ever flowed on the upper plateau; it is a coarse sediment-bearing river whose ancient conglomerate deposits are limited to the central area of the Aksu basin. However, the Aksu Çay does have a rôle to play in the levelling of the central part of the basin and this process and the controls on it will be discussed in section 5.5.2. It is also debatable whether the Düden Çay eroded the entire lower plateau, although aerial photos suggest that some erosion between the source and the Düden waterfall at the coast has occurred. The question of terrace formation and fluvial erosion will be discussed further in section 5.4.

From his observations Planhol (1956) developed a "morpho-tectonic history" for the Quaternary of the area (Planhol, 1956 a,b). Briefly it was as follows:

Stage 1: Tufa was deposited in a period of "tectonic calm", in a cold, but humid, climate favourable to the dissolution of carbonate and extensive karstification of the Taurus Mountains. The end of this period saw the development of a huge erosion surface resulting in a shallow, seaward-sloping plain.

Stage 2: Violent tectonic movement stopped karstification and caused valleys to be incised into the tufa. In particular, the Aksu valley was created at this time. In his 1956a paper he relates the course taken by the Aksu to the development of a fault down the centre of the Pamphylian plain which had over 70m of throw down to the east. These valleys were filled by a thick mass of conglomerates towards the end of this stage.

Stage 3: Renewed "tectonic calm" and erosion resulted in the development of the lower terrace and the distinct escarpment, typical of regressive erosion, between the two terrace levels.

Stage 4: A second phase of tectonic activity deformed the lower terrace, tilted it and produced the coastal Antalya cliffs.

Stage 5: A final phase of recent rejuvenation caused much of the relief in the Taurus mountains and the incision of many of the major valleys.

Although a number of features described in this "history" have been observed (e.g. the development of erosion surfaces, tectonic rejuvenation, valley incision), the relative timing of events and the causal mechanisms of the model cannot be substantiated. It is important to remember that these ideas and those of Penck, Philippson and Tietze were developed prior to the advent of plate tectonic theory (Wilson, 1965), and that the assumption of rapid and violent phases of upheaval cannot now be considered relevant. It is, however, still valid to consider the various tectonic and erosional controls which could cause terrace formation along similar lines to those expounded above:

1) marine erosion surfaces and abandoned sea cliffs,
2) fault bounded terraces,
3) watertable fluctuation causing springs to resurge at different levels through time,
4) subaerial/fluvial erosion.

Tectonic, climatic and sea-level changes can affect all of these processes and, thus, we find we are in fact considering a very complex system.

There also exists the possibility that the terraces are primary constructional features. Penck (1918) considered this as an impossibility, but we now know that tufa does not behave in the same way as other sediments and can build its own barriers.

Özüs (1992) briefly discusses tufa terrace formation. His arguments are based on the thicknesses of tufa obtained from boreholes on the upper plateau. These showed the tufa sitting unconformably on either conglomerate or radiolarite on both the upper and lower plateaux. He considered the terraces to be developed on top of old erosional platforms. The present-day coastal cliffs are described as a product of marine erosion with some rebuilding by the coastal Düden falls, presently situated at

Lara. This idea of rebuilding of an erosional cliff line by the waterfall tufa is similar to the veneering nature of terrace front tufas described in chapter 4.

Burger (1992) considered that the terraces (of which he identifies eight levels, many more than other workers) are a combination of erosional terraces and constructional terraces. This has already been briefly discussed in chapter 4. In general, the upper terraces are described by Burger (1992) as constructional with small, more recent spurs formed as "travertine basin" superposition modified the terrace shape. The upper terrace is considered to have been built before these spurs and erosional features are observed on the upper surface. Burger considers the upper plateau to be less corroded than the lower terrace because it is primarily a constructional terrace. However, it was suggested in chapter 4 that the hydrological aspects of the tufa may mean that the restricted flow through the upper terrace in comparison to the lower terrace is the cause of the this discrepancy. The principal mechanism of constuction of the terraces was thought to be the growth of spurs, such as the one north of Antalya. It was shown in chapter 4 that this mechanism of construction is unlikely. An interpretation of the spur north of Antalya, as a collapsing zone full of sink-holes, is given in section 5.4.1. The lower erosional terraces described by Burger (1992) are also discussed in section 5.4.1. Much of Burger's (1992) study concerned the analysis of the soils that formed after tufa deposition. These soils are discussed in section 5.6.

5.2: The development of mature slope surfaces

The remnants of a mature slope surface can be identified along the entire western edge of the Aksu basin. A mature slope surface is defined as a smooth, evenly sloping surface which must have developed over a substantial period of time. Carson and Kirkby (1972) document the development of real slopes (rather than hypothetical ones) in response to physical factors such as lithology, climate, structural properties of the rock and downslope transport processes. Slope development in the Taurus Mountains is closest to their type of profile that was developed on a strong closely jointed rock in a semi-arid climate (Fig. 5.1). The term mature, as used in this discussion, refers to stages between 3b and 4 on their diagram.

The mature slope surface remnants increase in size and frequency southwards. They occur up to a level at about half the total height of the mountains. The surfaces are developed on top of the Kemer fanglomerates (chapter 3) on the lower slopes and as smooth eroded surfaces on the upper slopes. Robertson and Woodcock (1978) describe similar surfaces, associated with "capping breccias" developed in the Kumluca region to the west of the study area.

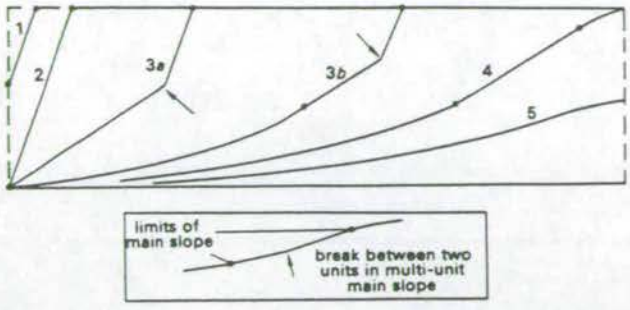

Fig 5.1: Slope profile development in a strong closely jointed rock in a semi-arid climate from Carson and Kirkby (1972). Between stages 1 and 2 erosion occurs by active stream incision. At stage 3 the rock wall is mantled by a talus slope. At stage 4 the main slope is progressively consumed through slope wash. Basal concavity extends upslope.

The topographic map and sections (Fig. 5.2) show the positions of these remnant surfaces. Contours are shown for the entire length at 100m intervals, starting at 50m. This defines the overall morphology of the mountains and valleys along this coastal region. The remnant mature slope surfaces are depicted by areas of evenly spaced contours which have been drawn in at 10m intervals. Seven surfaces are defined in this way. Five profiles are drawn A-A' to E-E', all at approximately 3.5x vertical exaggeration. Note that due to the extreme height of the mountains the profiles C-C' to E-E' are shown at half the scale of A-A' and B-B'. The vertical exaggeration remains the same allowing direct comparison between all five profiles (This also applies to the profiles of Fig. 5.8). The profiles demonstrate different aspects of the coastal geomorphology. The profile A-A' runs down the Phaselis slope surface (Plate 5.1A), which is the top surface of the Phaselis fan described in detail in section 3.6. Apart from a small notch at present-day sea-level it can be seen that this surface continues offshore. The significance of the notch will be discussed in section 5.7. Well developed soils exist on the upper surfaces of the fans. The presence of these surfaces indicates that the landscape was stable for a significant period time, probably during most of the Pliocene. That the slopes are now heavily dissected by both fault scarps and by fluvial downcutting (section 5.3.2) indicates that a period of faulting and uplift of the western Taurides created the relatively immature slopes of the present day. Plate 5.1B shows relatively intact mature slopes to the south of Kemer. Further north the slopes are much more dissected and the fragments of mature surface which remain are much smaller. (Plate 5.1C)

Plate 5.1D shows the facetted scarps of the Taurus Mountains, adjacent to the flat tufa terrace just south of Kirkgöz. This view is essentially of the upper parts of the mature surfaces adjacent to the flat plain of the tufa.

Plate 5.1:
A) The Phaselis fan surface can be traced from the mountains, as a smooth slope, down into the sea. **B)** Intact erosion surfaces south of Kemer. **C)** Dissected erosion surfaces north of Kemer. The fau scarps at the back have a stepped appearance, implying that intra-fault zone hanging wall collapse ha occurred. **D)** Erosion surfaces dipping underneath the surface of the tufa , just south of Kirkgö **E)** flat erosion surface dipping away from the Mesozoic limestone in the right of the picture. A clea break exists between to two.

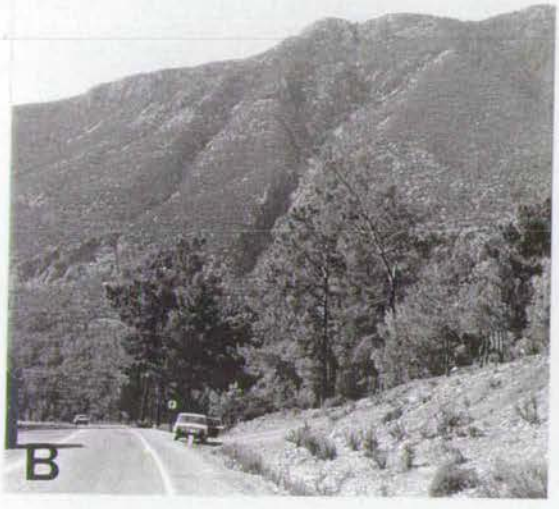

Plate 5·1

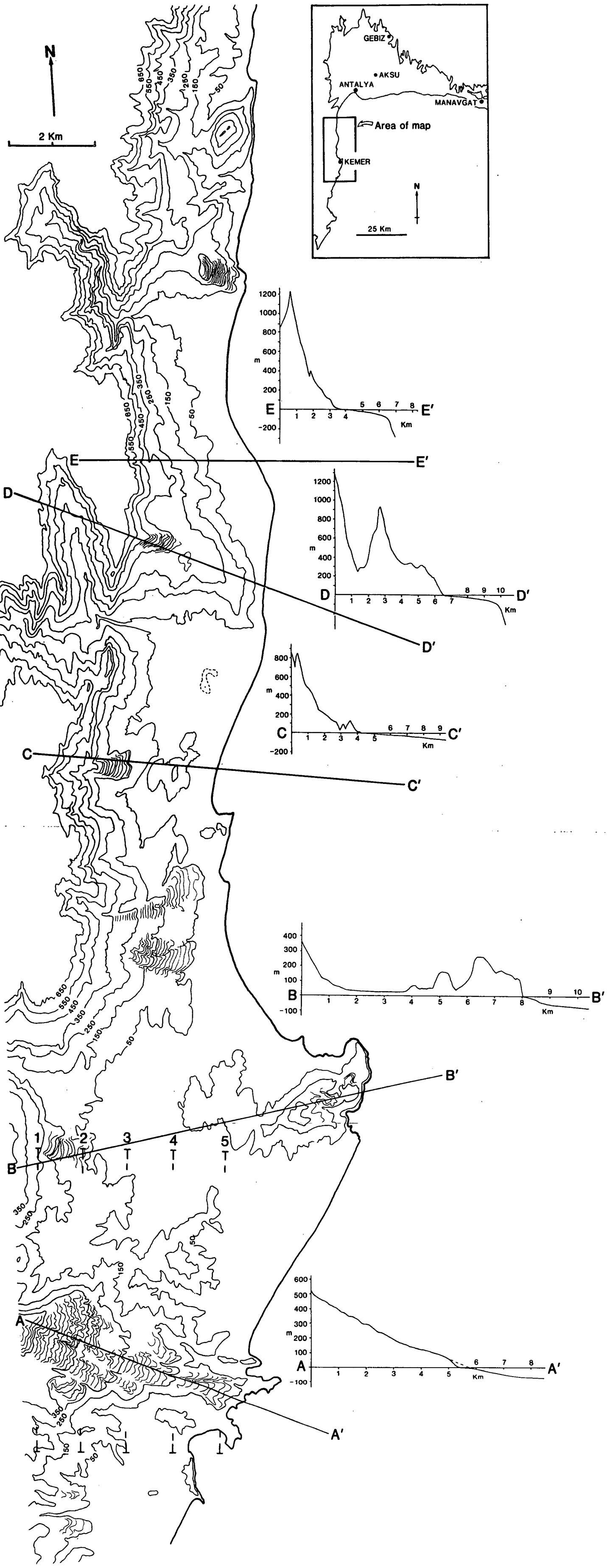

Fig. 5.2: Contour map of the west Antalya Bay coastline. Contours are plotted at 100m intervals, starting at 50m, except where mature slope surfaces are identified and a 10m interval is used. The mature slope surfaces were identified in the field and are typified on the topographic map by regular, relatively widely spaced contours. Profiles are accurate topographic cross-sections with 3.5x vertical exaggeration. Profiles C-C' to E-E' are at half the scale of A-A' and B-B'.

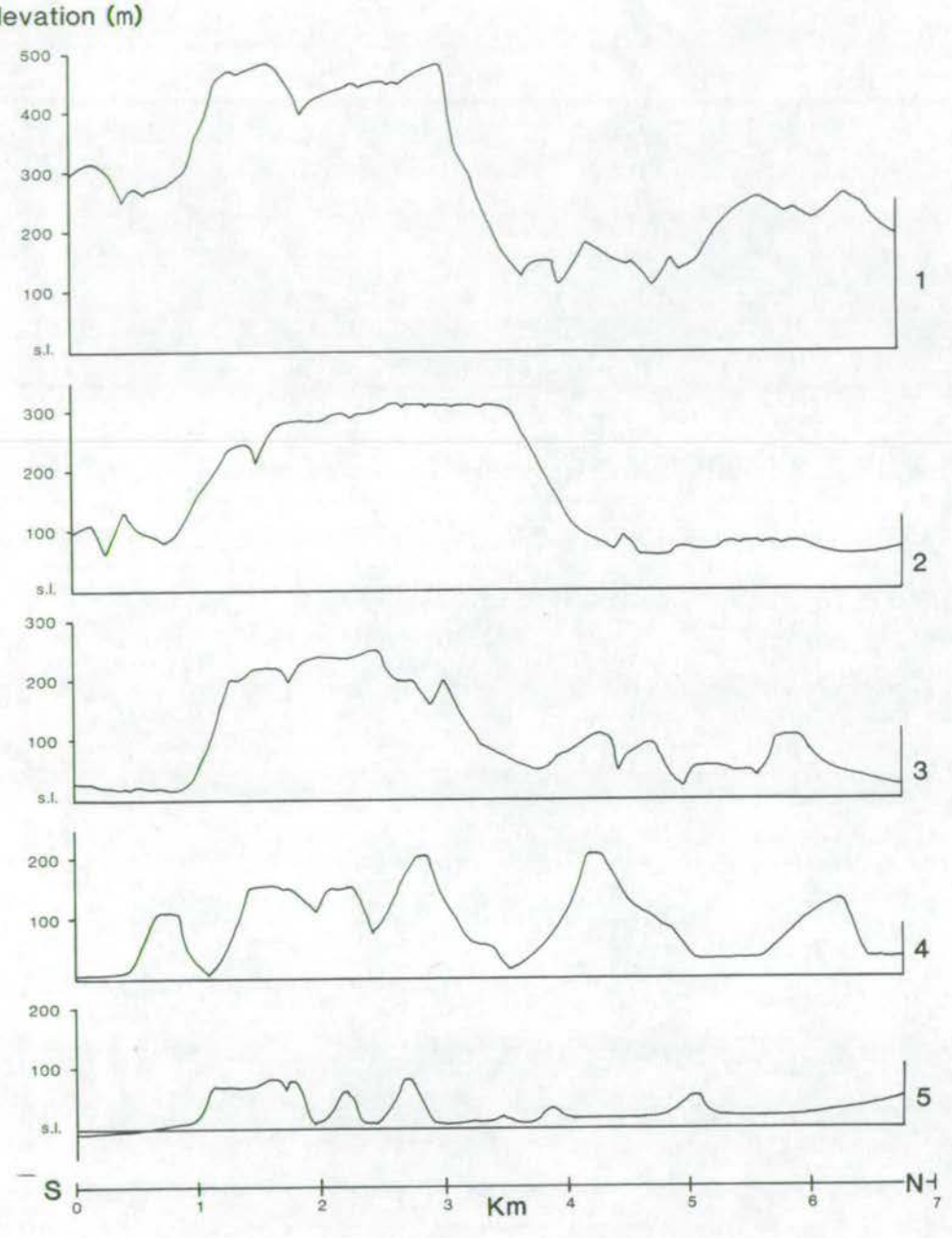

Fig. 5.3: Downslope profiles of the Phaselis fan surface demonstrating the progressive fluvial incision of the fan. Profile 1 is highest up the slope, profile 5 is at the bottom of the slope. The lines of section are marked on Fig 5.2. Towards the top of the slope the surface is relatively broad. Stream incision progressively dissects the slope into smaller segments until near the coast only small remnants remain.

The tufa appears to have infilled the basin, covering the pre-existing erosion surfaces. This indicates that the mature slope surfaces were well developed by the late Pliocene/early Quaternary.

5.2.1: Dissection of the mature slope surfaces

The two remnant surfaces in Plate 5.1C are dissected by fault scarps at their top and possibly their foot and by streams parallel to the slope. Sections B-B' to E-E' on Fig. 5.2 show the strong dissection effects of both faults and streams. The extremely steep topography represented by profile D-D' is that of a typical fault scarp. These fault scarps will be discussed further in section 5.4. Fluvial incision causes slopes equally as steep, as demonstrated by profiles C-C' and D-D'. The progressive fluvial incision of the Phaselis fan is shown by the topographic profiles 1-5 (Fig. 5.3) drawn laterally across at distances 1 km apart, beginning at Profile 1 towards the top of the surface and progressing downslope to Profile 5 close to the coast. The positions of these profiles are marked on Fig. 5.2. The original flatness of the surface can best be seen in Profile 2. A small amount of southwards dip is probably caused by the action of the stream that cut through the steep sided notch at the southern edge of the plateau. The progression through Profiles 3, 4 and 5 shows a gradual narrowing of the remnant surface as the streams affect a wider area of the slope. In addition, the number of streams cutting through the surface increases and by Profile 5 the surface occupies only 1km where it previously covered 3.5 km of the slope (Profiles 1and 2).

5.3: Neotectonic fault scarps

Normal fault scarps define strong lineaments in the Taurus Mountains, which can be mapped from the ground. These features are also highly visible in the satellite image of the area (Fig. 5.4). The strongest features are along the western edge of Antalya Bay. These faults do not continue along the entire basin margin. Rather the topography becomes less steep and many of the lineaments are orientated approximately parallel to the margins of Burdur graben. Qualitative assessment of the neotectonic fault scarps, using the observations of Stewart and Hancock (1989), shows them to be highly degraded. Stewart and Hancock (1989) define a fault zone architecture typical of the Mediterranean region, based on observations of faults in Mesozoic carbonate rocks in Greece and western Turkey. Earlier discussions of slope degradation effects were based on observations of degradation of single scarps in superficial sediments (Peterson, 1985).

Fig 5.4: Satellite image of the study area and overlay. Fault lineaments are marked by arrows.

Petreson's (1985) models are simply not applicable in the Mediterranean, where multiple scarps cut solid Mesozoic carbonate bedrocks, and where weathering rates are typically an order of magnitude less (Schumm, 1962; Lamarche, 1968).

A number of features described by Stewart and Hancock (1989) can be observed on the Kemer scarps. Firstly, they note that faults frequently act along the same plane as earlier fault events so that the contact between slope talus and the bedrock is a fault contact. In order to show that this is the case, detailed observations of the contacts are required. This was not possible in the Antalya area due to the inaccessibility of the scarps. However there is strong evidence that this is in fact the case. The majority of the talus fans (Gilbert-type fandeltas) are thought to have begun to develop in the Early Pliocene (chapter 3). Their upper surfaces define the lower portions of the mature slope surfaces already described in section 5.2. These surfaces no longer continue to the tops of the mountains, but are abruptly cut by steep scarps, interpreted as a later faulting event. In one case, visible looking north from the Göynük valley, the fan surface is clearly separated from the rising fault scarp behind it by a distance of tens of metres (Plate 5.1D). Stewart and Hancock's (1989) contact types refer to Quaternary talus and Quaternary faulting. Here the same phenomenon is described for Pliocene talus and ?late Pliocene /early Quaternary faulting. The timing of faulting is discussed further in chapters 6 and 7.

Stewart and Hancock (1989) model what they call "intrafault zone hanging wall collapse" (Fig. 5.5i). This process gives rise to a stepped sequence of faults as progressively younger faults migrate into the hanging wall. Episodic faulting on one plane may cause a similar stepped profile if significant degradation occurs between each successive fault step (Fig. 5.5ii). It is probable that the intrafault zone hanging wall collapse is responsible for the stepped nature of the faults in the Antalya region. The stepped fault scarps are well illustrated in Plate 5.5C. It can be seen that these scarps have a highly irregular morphology. Stewart and Hancock (1989) go on to model the effects of degradation in a step faulted limestone. Obviously, fresh scarps are modelled to be smooth (Fig. 5.5iii). If intrafault zone hanging wall collapse is responsible for the step faulting then fault surfaces are likely to be brecciated. In addition, the complex fault surface of a limestone is likely to be full of irregularities, pits and grooves (Hancock and Barka, 1987), vulnerable to degradation, and a cavitated appearance may be acquired (Fig. 5.5iv). Thus, the stepped and cavitated surface of the Antalya faults, by comparison with the models of Stewart and Hancock (1989) suggest a typical degraded Mediterranean neotectonic fault zone.

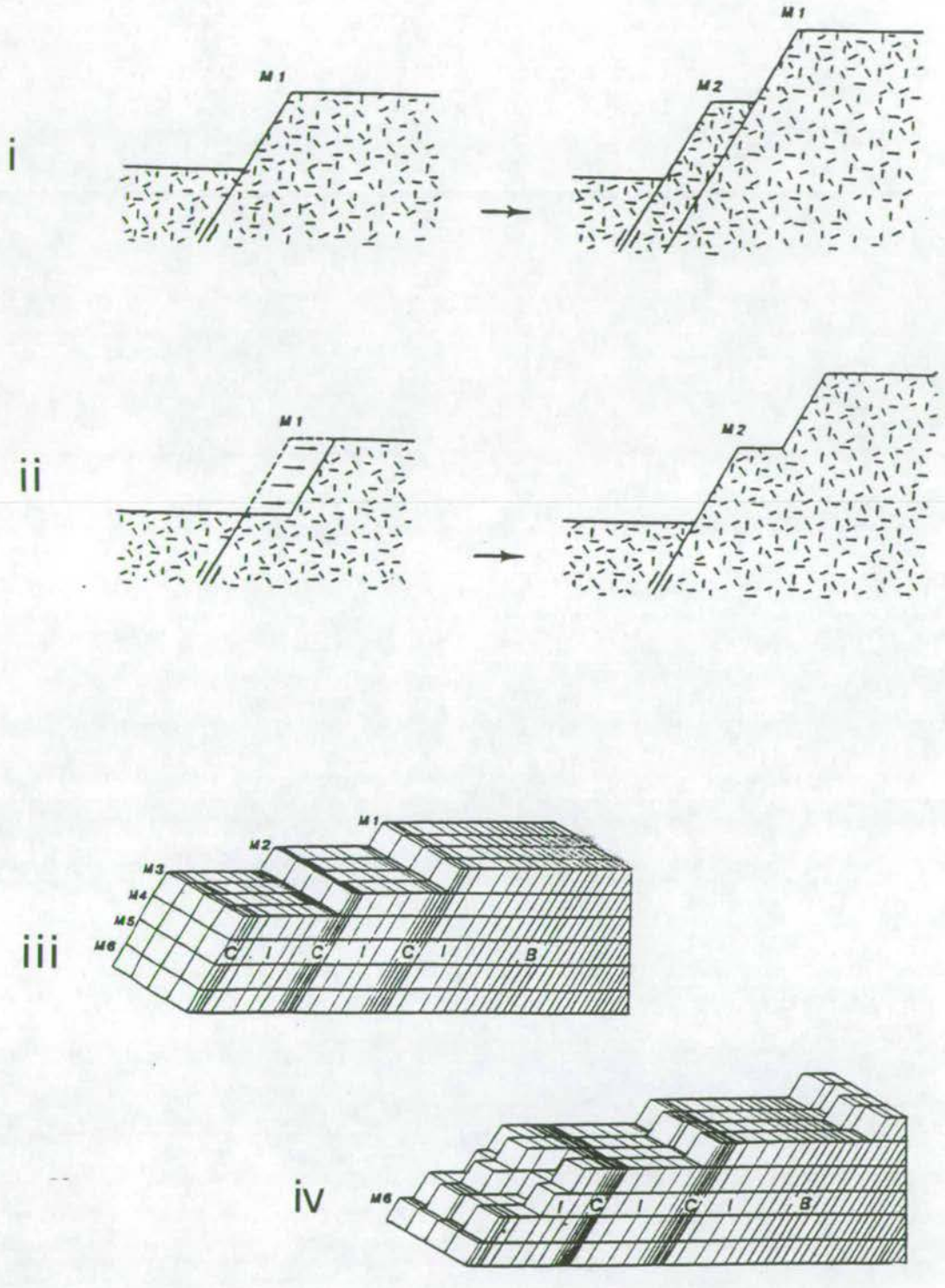

Fig. 5.5: Model of Mediterranean fault scarp degradation from Stewart and Hancock (1989):
i) Intrafault zone hanging wall collapse. A stepped fault appearance is created as progressively younger faults migrate into the hanging wall. ii) Rapid scarp degradation between successive fault movements also causes a stepped appearance. iii) Basic model of intra-fault zone hanging wall collapse with fresh scarp surfaces. iv) Model iii after degradation. Initial irregularities in the fault surface allows differential erosion and a rugged topography is created.

Stewart and Hancock (1989) note that with the large disparity between uplift and denudation rates in the Aegean, 1 Myr will make little geomorphic modification to uplifted fault scarps. Whilst uplift rates are probably significantly slower in the Antalya region, it still suggests that the fault scarps must be a few million years old to display the distinctly degraded surfaces and deep incision of the streams.

Some modern talus cones are seen along the coastal section (Plate 5.2A) and not all fault scarps are severely degraded. However, these represent only a small proportion of the scarps visible and, whilst faulting has probably not ceased in the area (earthquakes are responsible for the destruction of many of the Lycian cities), activity is almost certainly very subdued compared to the past (?early Quaternary).

5.4: Tilted fault blocks

In the northern area of the Aksu basin a number of tilted fault blocks of Pliocene sediment form many of the numerous small hills in the otherwise flat Aksu basin (Plate 5.2B). These blocks are mostly conglomerate with sand lenses. In some cases marine Pliocene silts and sands form the lower part of the block. A map of the tilted blocks, bedding readings and the possible locations of the faults which formed them is given (Fig. 5.6).

5.5: The tufa terraces

Whereas Planhol's (1956) "morpho-tectonic history" of the Quaternary of the Aksu basin clearly does not stand up to examination, his model for development of the tufa terraces is the closest to the present model. In particular, his suggestion that the upper terrace level is the result of carbonate lakes infilling a topography of palaeovalleys is not dissimilar to the current model of a lacustrine, paludal, fluvial environment infilling a basin topography controlled by fault blocks (chapter 4). The primary cause of the extensive terrace morphology remains to be discussed.

Terrace morphology was mapped by Burger (1990, 1992) (Fig. 5.7). Two accurate cross-sections, approximately 3.5x vertical exaggeration, demonstrate the extreme flatness of the tufa terraces (Fig. 5.8). It was concluded in chapter 4 that the tufa was deposited over a block-faulted half-graben topography, which limited tufa deposition to the east. The basin was infilled by the tufa which in its final stages formed in a paludal environment. The extreme flatness of the tufa terraces (Plate 5.2C) may be a result of this final stage of deposition forming a flat upper surface to the deposit. Terraces may form as a result of water table fluctuation. With changing water table levels springs may emerge at different levels on the plain. This could lead to the development of tufa terraces forming at each new spring resurgence level.

Plate 5.2:
A) Active talus fans from degraded fault scarp near Olympos implies that some faults are still active **B)** Tilted fault blocks in the Aksu valley. **C)** Behind the greenhouses the flatness of the tufa terrac can be clearly seen. **D)** Sink hole on the spur north of Antalya. half way up the collapsed wall a larg spring exists. This has been a site of focused tufa deposition. **E)** Rundkarren (karstpillars),arrowed, o the lower plain, west of Antalya. A gorge also cuts through the tufa in the foreground. **F)** Rillenkarre developed on the surface of a karst pillar.

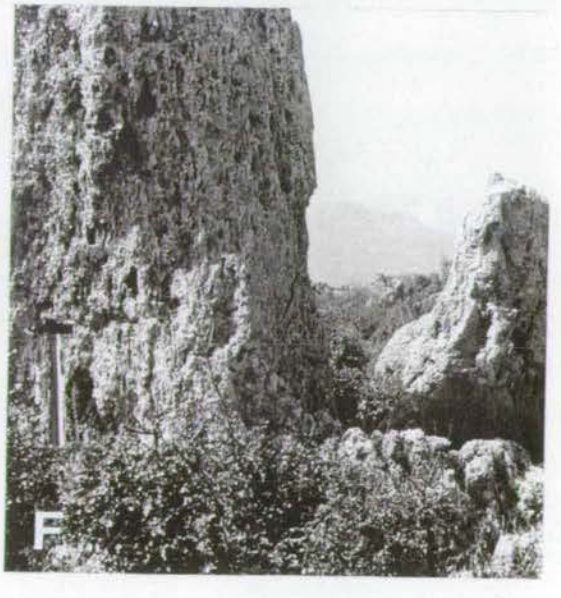

Plate 5·2

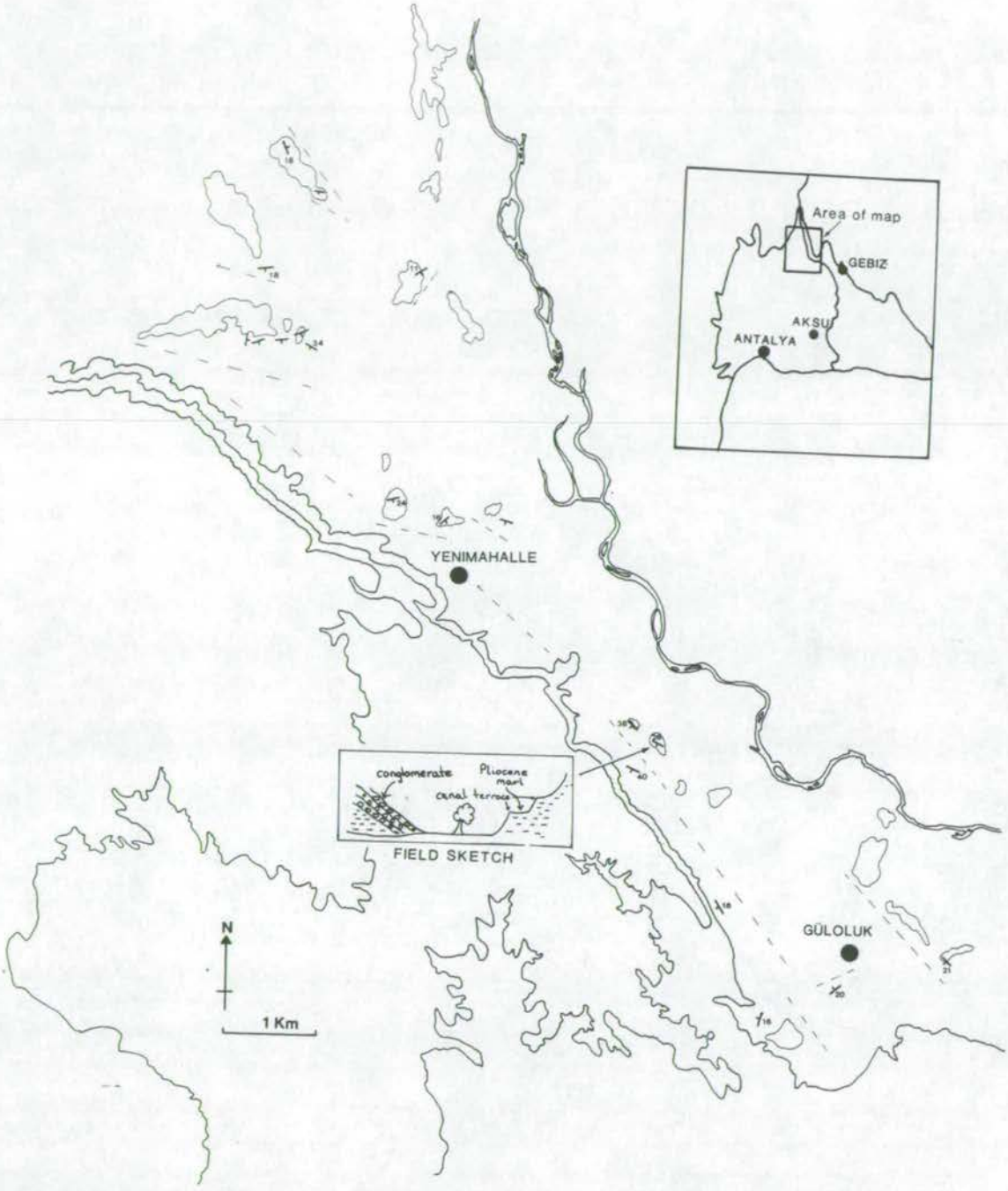

Fig 5.6: Map of tilted fault blocks in the northern area of the Aksu valley. The blocks are of Pliocene sediment, usually the sands and conglomerates from the upper part of the sequence.

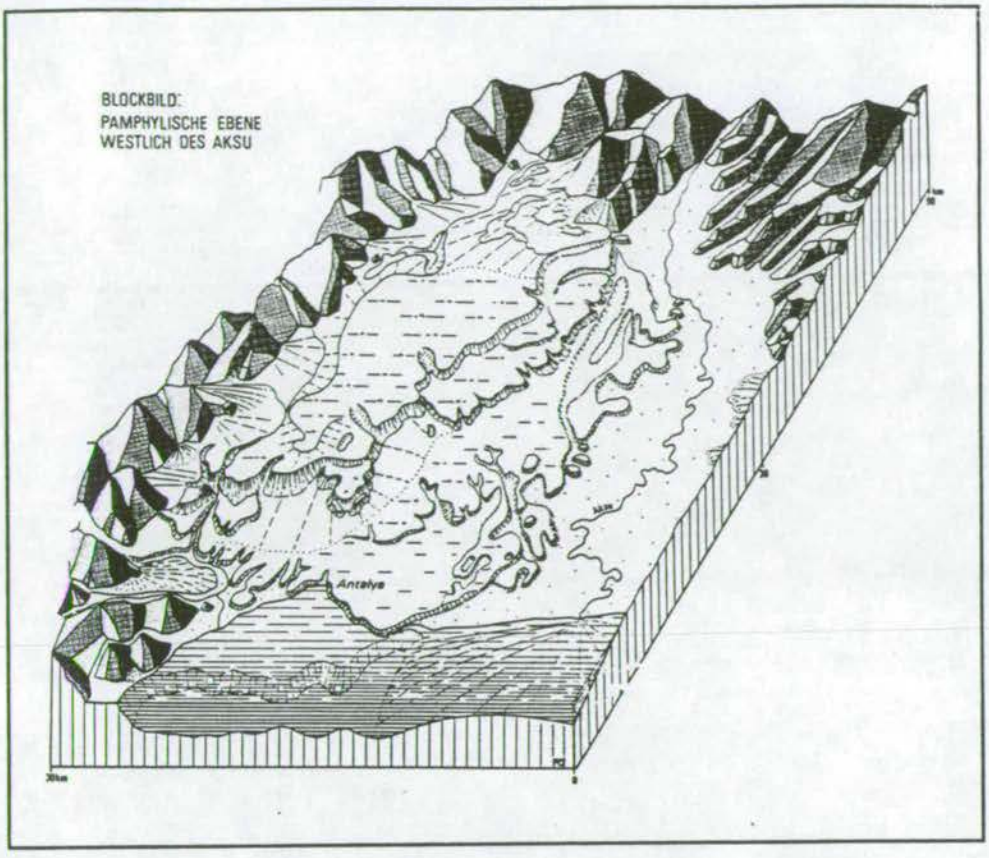

Fig 5.7: Block diagram of the tufa terraces from Burger (1990, 1992)

It is probable that this mechanism would produce a large number of small, irregular terraces, although it cannot be ruled out. Evidence against this mechanism is primarily the absence of dense spring populations along the edges of the upper terraces. Those that do exist are too high up to have sourced the lower terraces. At Varsak, where the springs are known to feed the tufa system, the spring level is exactly at the level of the tufa.

Accelerated tufa growth in areas of increased turbulence along pre-existing scarps and slope breaks may be the cause of some of the topography, for example the rise and slope on the upper terrace, labelled "A" on Fig. 5.8, which is a shallow slope. Modification of an original steep scarp slope by preferential build up of tufa, perhaps over an underlying scarp may result. A second possibility is indicated by the composition of the tufa in this region. It often comprises laminated deposits of algal mats. This may have a higher growth rate than tufa in other environments. Again, this is related to the presence of an original scarp, which caused the environment to be exposed and shallow over a long period of time. However, examination of the terrace edges themselves suggests that they are not primary depositional features.

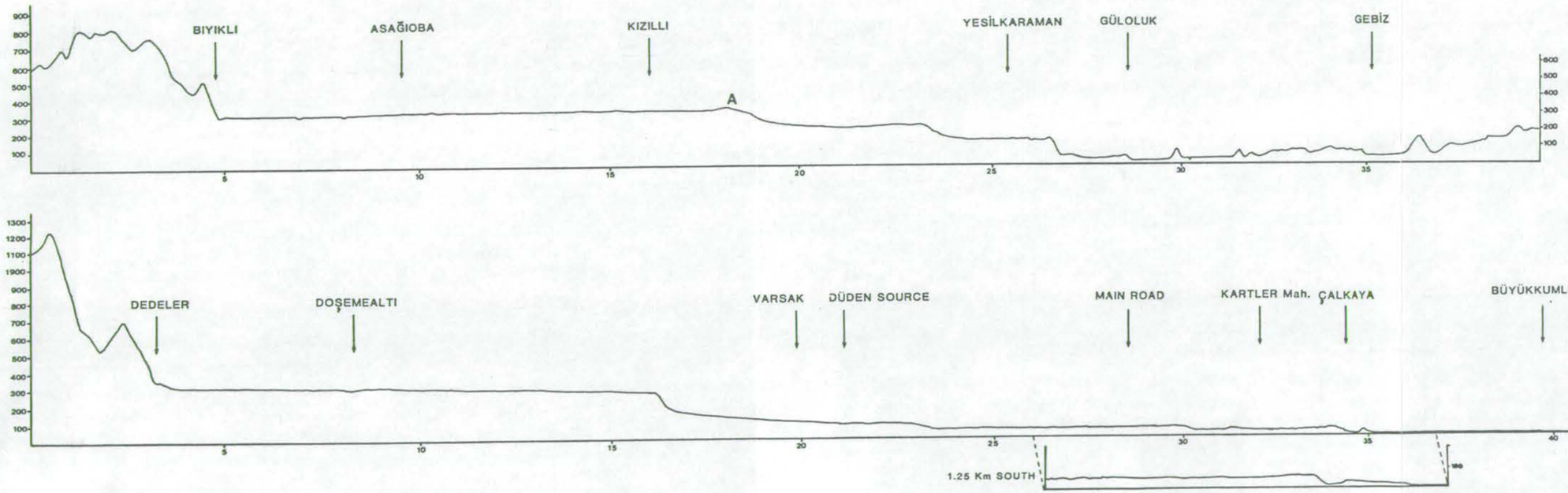

Fig 5.8: Accurate cross sections across the tufa terraces and Aksu river valley. Note the extreme flatness of the upper terrace.

Horizontal beds end abruptly and terrace edge deposits away from the coastal section are only very localised. Although it is probable that the vast upper terrace level was primarily formed as a flat depositional plain of tufa, the actual formation of the terraces must be erosional. A number of possibilities which must be considered are those that came from the previous ideas concerning the geomorphology of the area. To recapitulate, the terraces may be produced by:

1) marine incursion resulting in abandoned sea cliffs;
2) fluvial erosion;
3) subaerial erosion, related to base-level changes;
4) fault scarps.

The relative importance of tectonic, climatic and sea-level change must also be assessed. In order to evaluate these factors a review of the observations concerning karstification is necessary.

5.5.1: Tufa karstification

Tufa karstification and associated soil formation comprises much of the study of Burger (1992). Burger (1990, 1992) identifies a number of surface crusts and karst forms. Two types of surface crust are distinguished. The first formed as a result of outcrop induration on the surface and the second as a result of induration below a soil cover. They are termed, respectively, case-hardened and bodensinter (ground sinter). Both processes involve the dissolution and recementation of the tufa giving rise to a sparitic calcite texture. The thickness of the indurated layers is very variable. Bodensinter can be observed on the upper plateau, where the indurated layer is frequently broken up and piled at the edges of fields. It was observed that the layers are approximately 1m thick and that hollows within these crusts are filled with Terra rossa soil (see section 5.6). Karst processes are represented by the presence of poljes, karst marginal plains and karren (Burger 1990).

Two poljes are recognised by Burger (1990). They are collapsed solution caves within the tufa complex and the term sink hole is preferred here due to the relatively small size of these features (usually tens of metres). A number of sink holes are recognised in the present study that were not identified by Burger. They occur principally around the terrace edges, near Çalkaya and on the upper Antalya peninsula. A topographic map of the north Antalya spur (Fig 5.9) shows the intensive sink hole development that characterises the region. Burger (1990, 1992) attributes the characteristics of this region to build-out of a tufa spur by tufa basin development. This model was discussed in chapter 4.

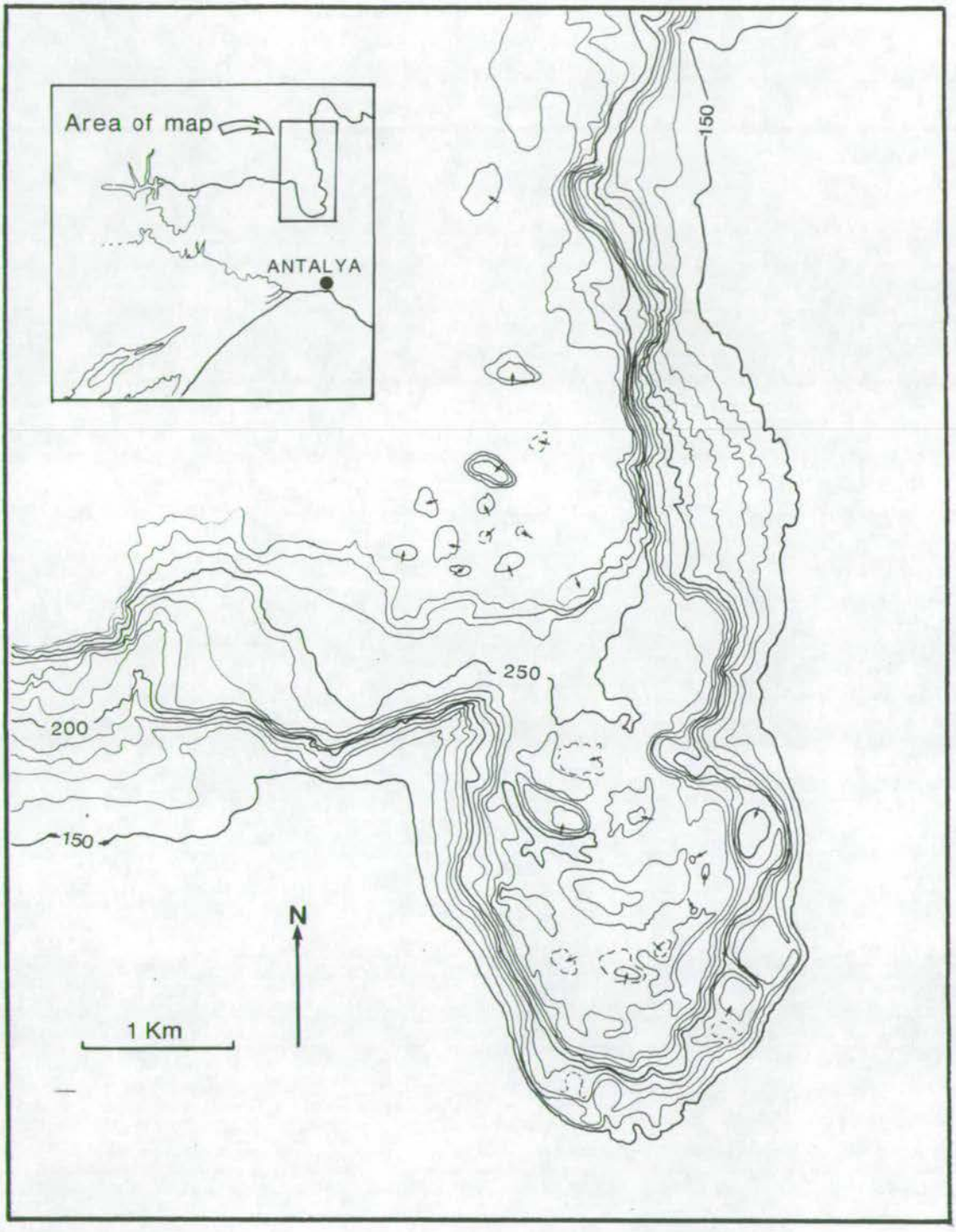

Fig 5.9: Contour map of the spur north of Antalya. Both the spur itself and the region behind it are full of sink holes indicating that a major underground stream system flowed through the spur.

The view in this thesis is that the morphology of the spur is due to intense subsurface water flow and subsequent collapse of the entire area. The field observations that support this are: 1) The presence of spring-related caves in the upper sides of the sink holes; and 2) the occasional dip of bedding in towards the holes and away from the edge of the upper cliff level. From a distance the view of the spur reveals an extremely irregular upper surface which immediately brings to mind "collapse". Apparent links between several of these depressions may represent a remnant of an original complex cave system with interlinking streams. The vicinity to the Varsak window and the source of the Düden river suggests that underground flow through the upper terrace in this region is still active.

The karst marginal plains described by Burger (1990) were defined from the Konyaalti region. They are described as small embayments, some metres higher than sea-level, where large numbers of springs emerge at sea-level. Concave erosion occurs around the spring resurgence point. The 40-50m level i.e. the level occupied by the Düden river is also interpreted as a karst marginal plane representing a former period of higher sea-level. The source of the Düden river is thought to represent an embayment similar to those seen behind Konyaalti.

The geomorphological map of the tufa complex (Burger, 1989) shows that the majority of the tufa surface is characterised by "rundkarren". These are the isolated towers of karstified tufa which form as water percolates through overlying soil and dissolves the underlying carbonate and are described as "normal corrosion plains" (Plate 5.2E). On the surface of the rundkarren, "rillenkarren" represent recent rainwater dissolution of the tufa (Plate 5.2F). Rillenkarren are millimetre- to centimetre-sized dissolution pits which affect the surface of the limestone. Rundkarren are developed most extensively on the surface of the lower plateau directly west of Antalya.

5.5.2: Erosional modification of the tufa

Burger's (1989) map shows the majority of the upper and lower terraces to be dominated by rundkarren, normal features of subaerial and subsoil erosion and karstification of carbonates. In addition, no Quaternary marine deposits are known to exist on any part of the upper and lower terraces. There is, therefore, no reason to believe that marine incursion has occurred at any time since the mid-Pliocene regression which deposited the Çalkaya Formation. Burger claims that the 40-50m level, effectively the plain occupied by the Düden Çay, is a karst marginal plain, formed by marine erosion.

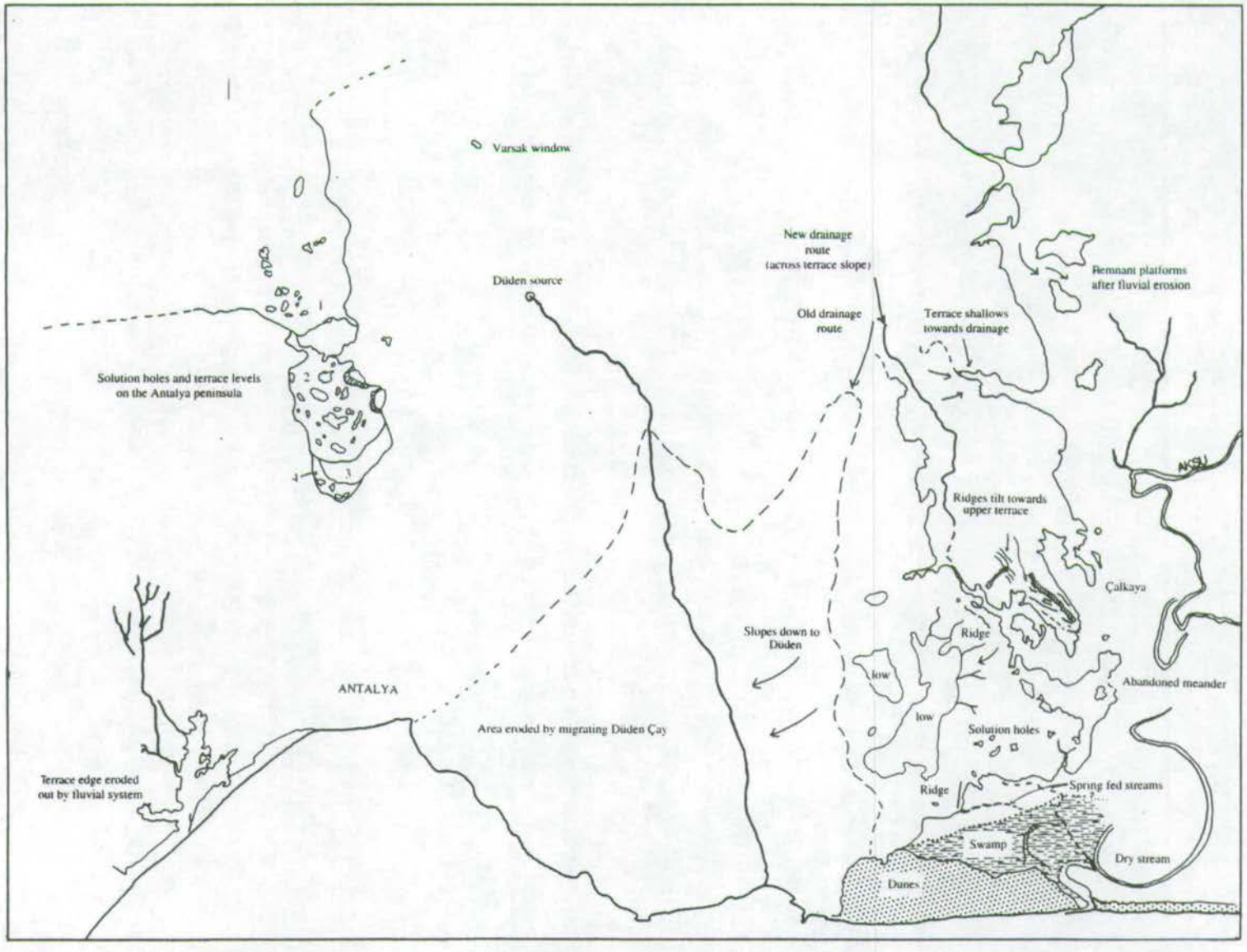

Fig 5.10: Interpretation of the geomorphology of the Antalya area from aerial photographs. Note the concentration of sink holes on the Antalya spur and in the Çalkaya area levels on the spur are marked 1-4. The erosional modification of the terraces by stream activity is clear from the patterns of headward erosion into the terrace edges.

However, it is impossible to see that this area, which currently sits above sea-cliffs 20m high, could have been flooded by the sea when the Asağikaraman region to the west of Antalya shows no evidence of marine erosion. The erosion of this area is more likely to have been the result of the migrating Düden river.

An interpretation of aerial photographs of the southern part of the Aksu basin is presented in Fig 5.10. The erosional plain of the Düden Çay can be seen, marked by the dotted line. Two erosional embayments can be seen, one occupied by the Düden Çay, the other empty. It appears that either a second river also occupied this plain at some time, or that the source of the Düden Çay has changed location. The vicinity of the second erosional embayment to the river system that now cuts through the Pliocene terrace near Çalkaya suggests that this river also once flowed over the tufa terrace. The aerial photographs show a number of other interesting features. In particular, the distribution of sink holes in the tufa is concentrated in two areas. The first on the spur north of Antalya, the second on the tufa terrace near Çalkaya. It has already been suggested that the concentration of sink holes on the Antalya spur is related to a former subsurface water pathway which created a dense cave system. Subsequent collapse of that cave system has diverted the underground river to a new course, almost certainly the underground part of the Düden Çay. The tufa terrace near Çalkaya by comparison, is also the route of a large amount of underground water. The concentration of the springs at the edge of this terrace and the swamp region on the lower plain add good evidence that this is the case. The vast amounts of water still passing through the tufa suggest that eventually the entire deposit will collapse by underground solution and subsequent sink hole formation.

The morphology of the main terraces, particularly the lower ones, has been strongly modified by feeder streams to the Aksu, which are no longer active, but presumably are significant water courses during colder, wetter, glacial periods. The cyclical Holocene glacial climate means that the Mediterranean fluctuates between its present-day semi-arid climate and a climate similar to that of northern Europe at the present-day. During the semi-arid periods, drying of the sediment produces a substrate vulnerable to the running streams of the glacial eras. This implies that during wet, glacial periods erosion was very rapid. A morphological map of the present-day topography, indicating the apparent pathways of interglacial stream systems (Fig. 5.11) shows how this erosion created the present-day landscape. These erosion events cut through the tufa, adding further weight to the supposition that the tufa was primarily deposited prior to the Holocene.

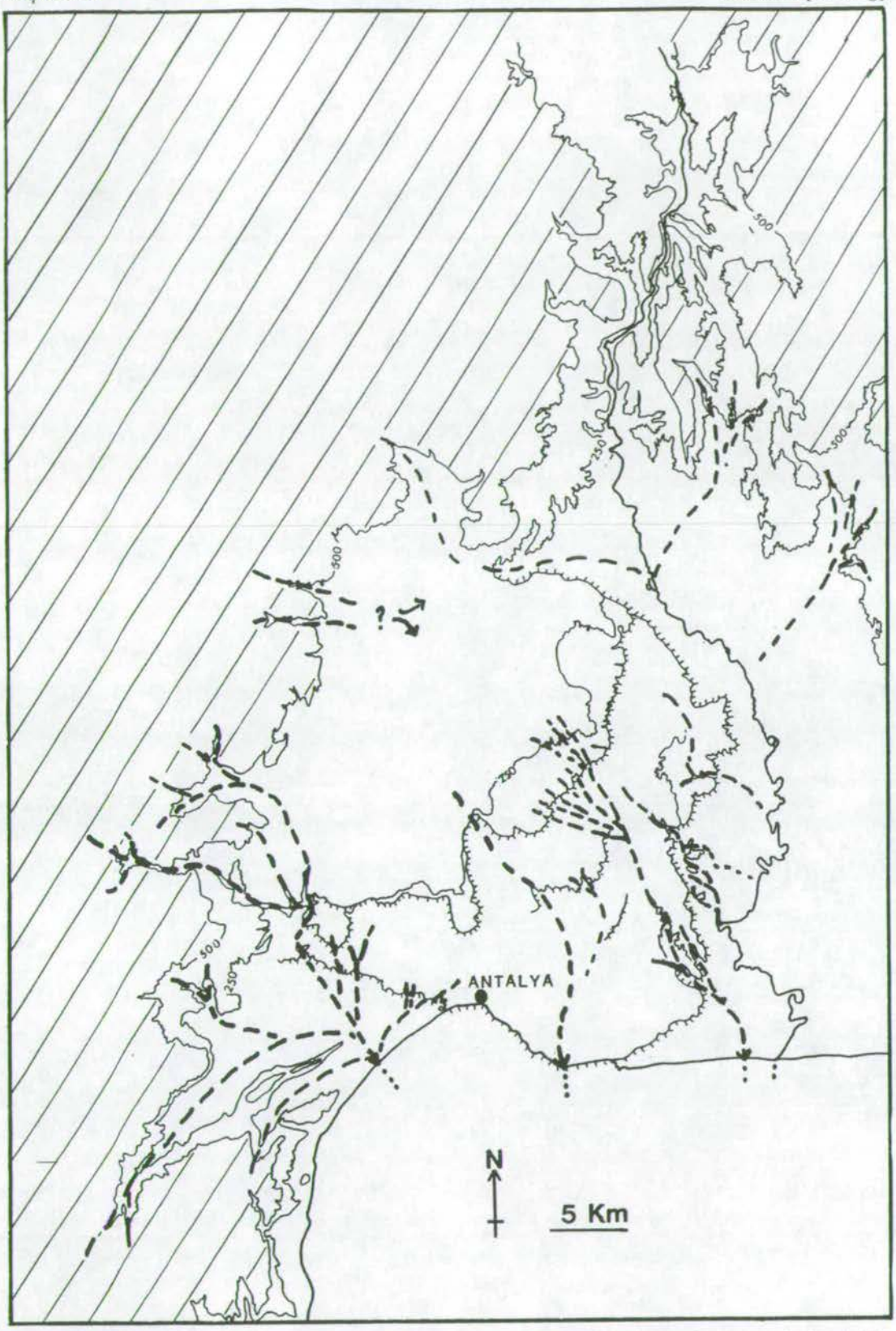

Fig 5.11: Map of the Aksu basin and terraces indicating the probable routes of streams during colder, wetter climatic periods. These routes are inferred from the erosional morphology of the terrace edges.

As there is no evidence for marine erosion of the terraces and the fluvial systems appear primarily to modify the existing terrace structure, two possibilities remain to explain terrace formation. The possibility that the tufa terrace edges are fault controlled is partially suggested by the implied subsurface fault-block topography. However, the overall shape of the terraces in plan view (highly irregular) does not support a fault origin even when the modifying effects of fluvial erosion are accounted for. Also the tufa is horizontally stratified and no evidence of faulting within the tufa was found (except local minor faulting; chapter 6). Some parts of the Pliocene terraces may be fault controlled at their edges, but this is probably a remnant of the pre-tufa faulting controlling the position of the present-day scarps. Slope evolution of the unconsolidated Pliocene sediments is likely to be a rapid process and thus the original faults are unlikely to remain.

It seems that the terracing is controlled by changes in base level associated with the fluctuating Quaternary climate/sea-level. As base level changes over time erosional levels develop. Tectonic uplift gradually elevates the terraces and subsequent changes do not erode the upper levels. This process has been documented in Cyprus, particulary in the intermontane Mesaoria basin, where marine erosion has not destroyed the terraces as it has on the southern part of the island (Poole and Robertson, 1991).

5.6: The Aksu river during the Quaternary

The Aksu river floodplain can be defined as a gravelly, meandering river plain (B3a, in the terminology of Nanson and Croke, 1992). Aggradation occurs primarily by lateral point bar, overbank vertical and abandoned channel accretion. The floodplain surface is flat to undulating with a meandering stream course. The upper reaches of the river are confined (except in the Çalkaya area where the valley opens out) and may be classed as type A1 (Nanson and Croke, 1992). The drainage is consequent (i.e. it flows downslope).

In chapter 3 it was suggested that the emergence point of the Aksu appears to have remained unchanged since the mid-Miocene. During the Pliocene the Aksu river fed the deltaic system, prograding in a braided system across the delta plain during the final mid-Pliocene regression. Subsequent tilting of the Pliocene as a series of fault blocks has already been discussed (chapters 3 and 4). This appears to have diverted the Aksu towards the east.

Leeder and Alexander (1986) demonstrated the formation of asymmetrical meander belts in tilted half grabens.

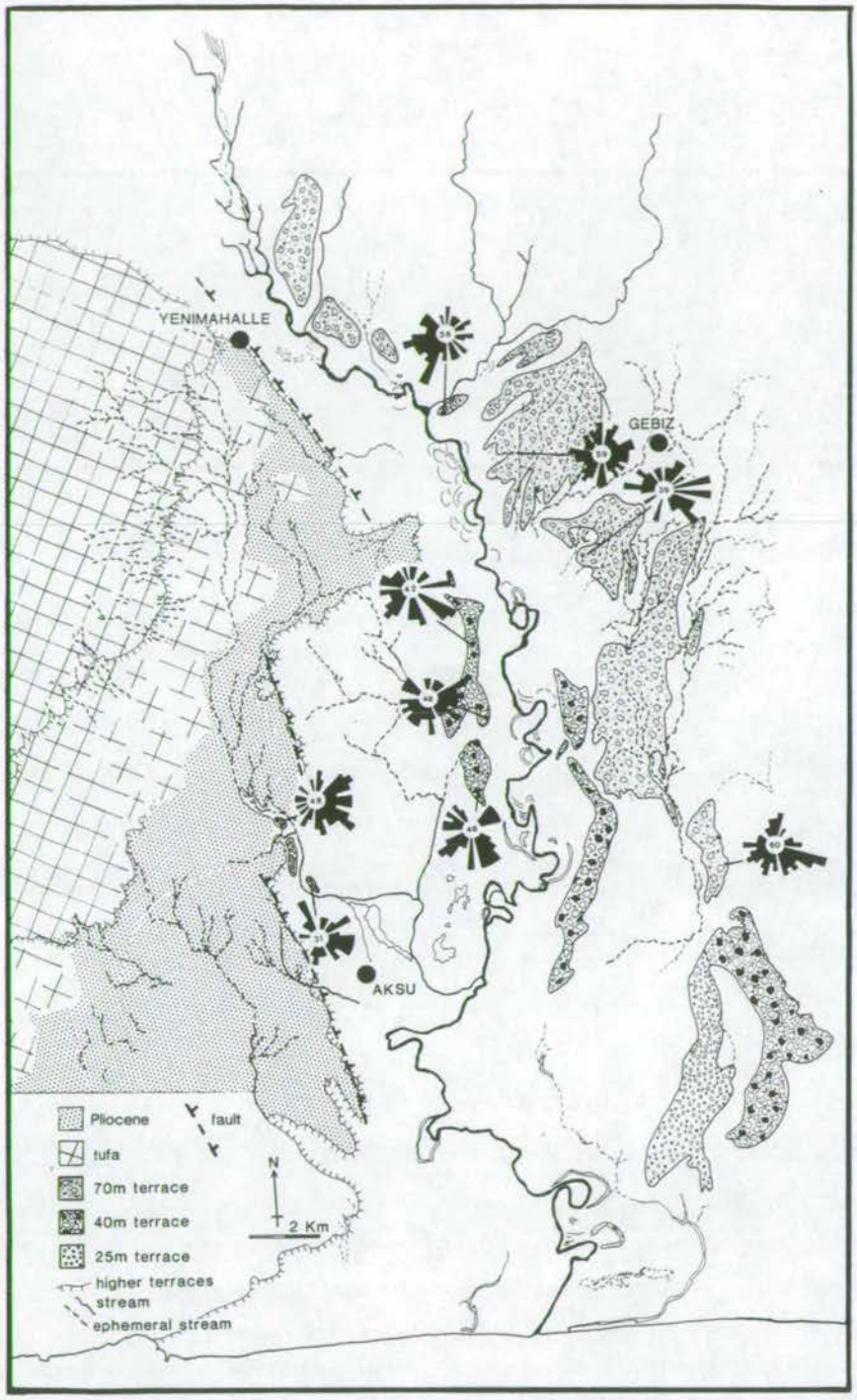

Fig 5.12: Map of Quaternary fluvial terraces in the Aksu river flood plain. Three terraces levels are recognised (70m, 40m and 25m). Palaeocurrent data are from clast imbrication measurements; the number of counts is indicated in the centre of each plot. Meander loops were identified using aerial photographs. The fault scarps and tufa terraces pre-date this phase of the rivers activity and although the tufa is not eroded by the main Aksu river, some erosion by the, now ephemeral, streams on the upper terrace has cut back the terrace edge during wetter climatic periods. Note that the faults are the same as those shown in Figs. 4.16 and 4.17.

As the active meander belt migrates towards the lowest point of the half graben it destroys the meander belts in its path leaving an asymmetrical system of belts in its wake. This phenomenon was looked for on the Aksu floodplain. Detailed topographic maps and aerial photographs were used to map the present-day Aksu, its tributaries, associated ephemeral streams and meander loops on the flood plain (Fig. 5.12). The gravelly nature of the stream bed leads to the rapid loss of detectable evidence of these loops and the data are situated rather close to the present-day channel to be conclusive. It can only be stated that it is a possibility that lateral migration of the meander belt towards the west of the basin has occurred steadily through time, leaving behind a set of asymmetrical meanders. What is clear is that the terrace/tilted fault block morphology has affected the drainage pattern and each terrace acted as its own drainage basin. Whilst the main Aksu drainage is approximately dendritic, the drainage from the Pliocene terrace has a parallel drainage pattern, as it was controlled by the structure of the fault block.

5.6.1: Fluvial terrace conglomerates (The Belkis Conglomerate)

The Aksu river deposits are represented as a number of terraces. These terraces were mapped by Burger (1992) who identified terraces at 70m, 40m and 25m. These levels are also recognised here. Terrace distribution within the Aksu basin and palaeocurrent data from clast imbrication in the conglomerates is included in Fig. 5.12. It was possible to trace the 70m and 40m terraces around the Köprü and Manavgat basins (Plate 5.3A,B,C), although a detailed correlation of the terraces was not attempted. The conglomerates of the Quaternary river terraces are extremely difficult to separate from the conglomerates of the Pliocene Çalkaya member, except by distribution. Palaeocurrent data do not show any clear flow direction, presumably due to the complex bar nature of the river that produced the deposit. The provenance of the conglomerates is identical to that of the Çalkaya member. The median clast size is again 1-5cm and the dominant clast is limestone (Plate 5.3D). The clasts are well-rounded and clast-supported within a reddish matrix. Clasts of tufa would allow Quaternary conglomerates to be recognised, but unfortunately not only is tufa extremely friable and would not survive in a bedload stream of this nature, but also the Aksu does not cut through the tufa in the first place.

5.6.2: Stream terrace genesis

The existence of unpaired Quaternary conglomerate terraces stretching from Gebiz to Abdurrahmanlar, to the east of the present-day Aksu suggest that the course of the Aksu Çay has migrated back towards the west, where it now lies close to the

Plate 5.3: Quaternary conglomerates (Belkis conglomerate)
A) Conglomerate terrace next to Manvagat Çay. **B)** Conglomerate terrace next to the Köp
C) Manavgat Falls, possibly flowing over a previous river terrace. **D)** Typical Qua
conglomerate. **E)** Steep-sided Terra-rossa channels cutting into the conglomerate near Bel
looking south towards Kemer. The shallow slopes become steep at the coast (middle and far di
indicating uplift of the mature slope surface and coastal erosion.

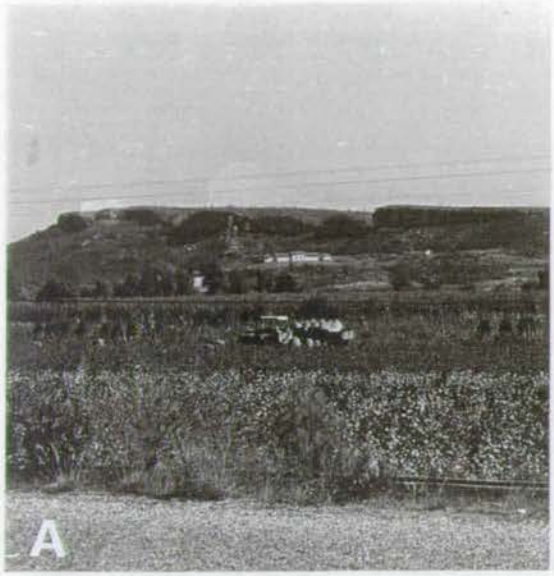

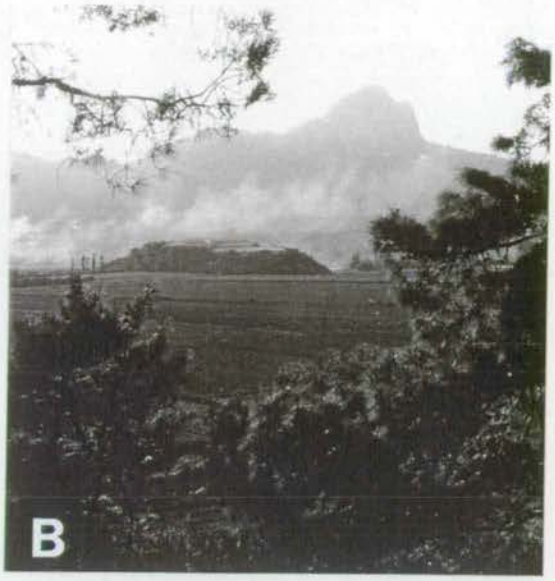

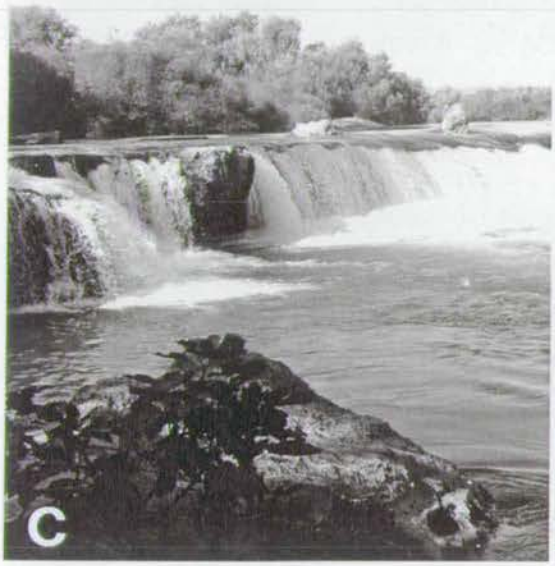

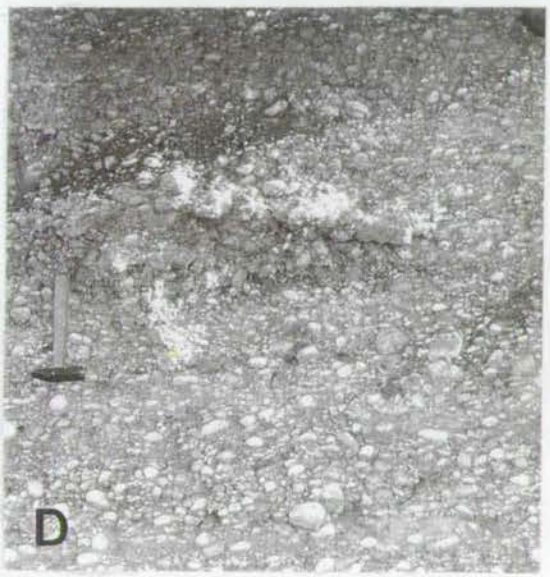

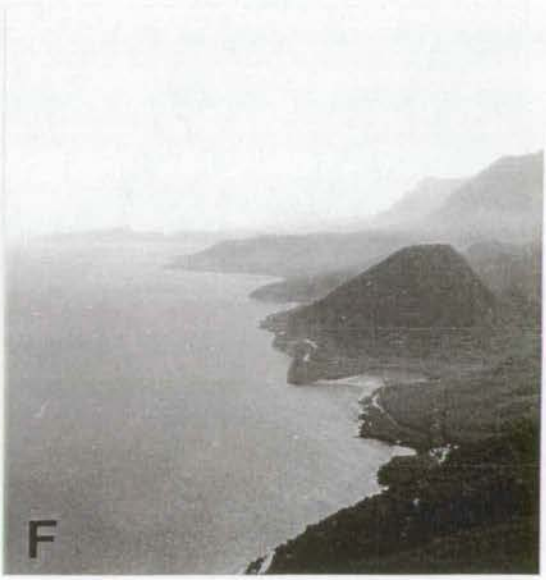

Plate 5·3

present-day Pliocene terrace. The highest of the fluvial terraces (70m) is located to the east of the present-day Aksu, between Gebiz and the central basin. A lower terrace (40m) of Quaternary fluvial deposits is more symmetrical, occurring on both sides of the Aksu. A still lower terrace (25m) occurs to the east of Aksu village.

The formation of unpaired terraces occurs when lateral shifting of the channel is relatively rapid. Often asymmetrical terraces will be cut either side of the valley floor. In the case of the Aksu only one unpaired terrace occurs (at 70m). This may indicate that only one major aggradation/incision cycle occurred, or that the present level of the valley is nearing equilibrium and that more recent aggradation/incision events have simply occured in the same temporal level, similar to the arroyos (definition 2 below) of the south-west U.S.A. (Haynes 1987).

Bull (1990) reviews in detail stream terrace formation. Stream terraces form as rivers cut down through the landscape to reach a base level of erosion. If landscape and climate are stable the result will be a single surface. However, if there are perturbations, flights of either single or paired terraces will form. Terraces can be strath terraces - cut into bedrock, or cut-fill terraces - cut into alluvium of the present system. Bull (1990) classifies terraces into three types: 1) tectonic terraces form due to fluvial downcutting in regions of tectonic uplift. 2) climatic terraces are the result of climatically controlled aggradation events followed by degradation. If no tectonic uplift occurs to isolate terraces above a base level of erosion then these aggradation/degradation cycles will tend to be buried by subsequent cycles, such as at Curry Draw in Arizona (Haynes, 1987). This may be termed an arroyo. 3) complex response terraces are the result of local adjustments (either climatic or tectonic) within individual stream systems. Complex response terraces tend to be small and localised. Larger, correlatable terraces are either a result of tectonic or climatic changes.

From the above definitions a number of criteria for recognition of climatic and tectonic terraces can be identified. If continuous tectonic uplift occurs, strath terraces will be cut into bedrock and no fill will occur. If, however, tectonic uplift is pulsed some basin fill may occur; however, the base level of erosion that is obtained by the river during uplift will not change and the fill is only likely to be thin (a few metres), unless the basin subsides. This may occur as a result of sediment loading, but is probably insignificant on Quaternary timescales. Thick deposits of conglomerate fill can, therefore, be attributed to climate/sea-level changes. During the Quaternary, climate and sea-level are intimately linked, as the controlling factor on both is the waxing and waning of the Arctic ice caps. During glacials low sea-level and a wet and corrosive climate prevail; high fluvial weathering rates produce

large quantities of clastic material. Stream gradients will be steep, facilitating transport of coarse material into the basin. During interglacials sea-level is high; the base level is consequently raised and stream gradients become less steep. Therefore, coarse material, which is not so readily transported, forms thick aggradational fill within the basin. As Bull (1990) discussed, if no tectonic uplift occurs then successive cut and fill events will be superimposed. However, if uplift occurs then thick conglomerates, deposited as a result of climatic aggradation, will form major terraces.

It may be possible to correlate climatically controlled terrace aggradation events around the Mediterranean. Vita-Finzi (1969) claimed that "Older-fill" and "Younger-fill" aggradation phases can be identified around the region. Vita-Finzi's (1969) correlations were probably premature due to the lack of dating available for conglomerates in the Meditteranean. However, more recent data also points towards the possibility of correlating climatic aggradation events around the Mediterranean. Lewin, Macklin and Woodward (1991) studied in detail the terraces of the Voidomatis basin in Greece. Whilst many of the more minor alluviation periods appeared to be controlled by local factors (complex response terraces; Bull, 1990) Lewin *et al* (1991) are able to correlate the most major alluviation period during the last ("Würmian") glacial between the Voidomatis basin, the Larissa plain (Demitrack, 1986) and the Southern Argolid (Pope and Van Andel, 1984). In contrast, in the Mula basin, SE Spain, three principal stages are recognised: 1) Late-Mid Pleistocene incision up to 60m; 2) a large-scale late Pleistocene aggradation (up to 18m); and 3) a subsequent Holocene incision up to 40m. The major alluviation event is attributed to tectonic movement, which is though to have dammed up the course of the Mula (Mather, Silva, Harvey, Zazo and Goy (1992). Care must therefore be taken before generalisations are made about the causes and controls of terrace formation in any valley.

A significant quantity of evidence points towards the Aksu terrace as a climatically-controlled aggradation terrace. The terrace consists entirely of fluvial conglomerates, cut into by later incision. As discussed above, thick terrace conglomerates are almost certainly the result of climatically controlled aggradation. The upper terrace is possibly correlatable with the last ("Würmian") glaciation. The 40m and 25m terrace levels probably represent more minor aggradation events. That the terraces can be traced in all three of the Antalya basins is further evidence that the aggradation event is a major terrace forming event and not a complex response terrace.

5.7: Terra rossa

A bright red soil cut into both the edge of the tufa terrace, and as steep sided channels in the Quaternary conglomerates occurs throughout the region (Plate 5.3E). The soil bears all the field characteristics of Terra rossa. Terra rossa is primarily developed on "pure" chalk parent rocks. It requires an extremely hot and dry summer soil climate. The soil is normally a strongly decalcified soil, its vivid red colour resulting from the presence of water deficient ferric hydroxide (Kubiëna, 1953). Terra rossa is commonly found in the karst landscapes of southern Europe. They are frequently relict soils as the present soil climate is so dry that eluviation and weathering rates are very slow (Kubiëna, 1953). Burger (1992) presents a detailed analysis of these soils. With respect to iron content, the soil has the requisite characteristics to be classed as Terra rossa. However, in Burger's (1992) opinion the carbonate content is too low and the high content of foreign materials too high for the soil to be classed as a "clean" Terra rossa after the definition of (Kubiëna, 1948). This definition (presumably the German edition of "The soils on Europe") is 5 years prior to the English version (Kubiëna, 1953) from which the definitions of terra rossa given above are derived. These state that Terra rossa is a strongly decalcified soil with a high wind blown content of foreign material. It is, therefore, felt that the soil is close enough to a Terra rossa to retain that name. Burger (1992) considers that not all the Terra rossa originates on the tufa although local pockets exist where Terra rossa formation did occur. In many cases the surface of the tufa is depleted in carbonate not enriched as would be expected if Terra rossa soil had formed above (Burger, 1992). It is probable that much of it formed on the Mesozoic limestone basement. The fact that the Terra rosa is also seen channelled into the Quaternary conglomerates around Serik and Manvagat, where no tufa is present, confirms this. Without a doubt some Terra rossa has developed on the tufa. Complex solution hollows filled with the soil which are exposed in the quarry behind Yesilkaraman demonstrate this.

The form of the channels is very striking. They usually occur as a series of closely spaced (5m separation), extremely steep-sided channels. They can be seen around the Antalya basins and whilst usually found cutting into the Quaternary fluvial conglomerates, have also been seen cutting into the Pliocene sediments, most notably at the terrace edge at the top of the Yenimahalle logged section. The very rapid downcutting that must have accompanied these channels indicates that they were deposited in catastrophic events, probably flash floods. This interpretation is compatible with the hot, dry summer climate in which they formed as it is not unlikely that this would be accompanied by periods of intense rainfall. (L. Frostick, pers. comm., 1994)

5.8: Evidence for gradual regional uplift

Bull and Kneupfer (1987) plot the percentage of fall from the headwaters of a stream against the percentage of length of the stream from its headwaters. If the resulting dimensionless plot produces a straight line then it can be said that dynamic equilibrium has been reached. This term implies that tectonically induced downcutting equals rate of uplift (Hack, 1960). The presence of strath terraces are a strong indication that this has occurred. The Bull and Kneupfer (1987) plot is applied to the Aksu river (Fig. 5.13) and clearly shows that, whereas the lower reach of the river may be close to dynamic equilibrium the upper reach is far from that state. Note the low gradient of the Aksu as it passes through the Çandir area (between 25 and 45 % stream length from headwaters). This evidence that the Aksu Çay is out of equilibrium and the gradient is still very steep in the headwater region is indicative of progressive regional uplift. In section 5.6 it was shown that climatic aggradation terraces form arroyo type deposits unless regional uplift lifts them above base level of erosion. Climatic/sea-level fluctuations alone form a series of superposed cut and fill events. Thus, the form of the Aksu Çay and its conglomerate terraces show that regional uplift has occurred throughout the Quaternary. It may be that uplift began much earlier.

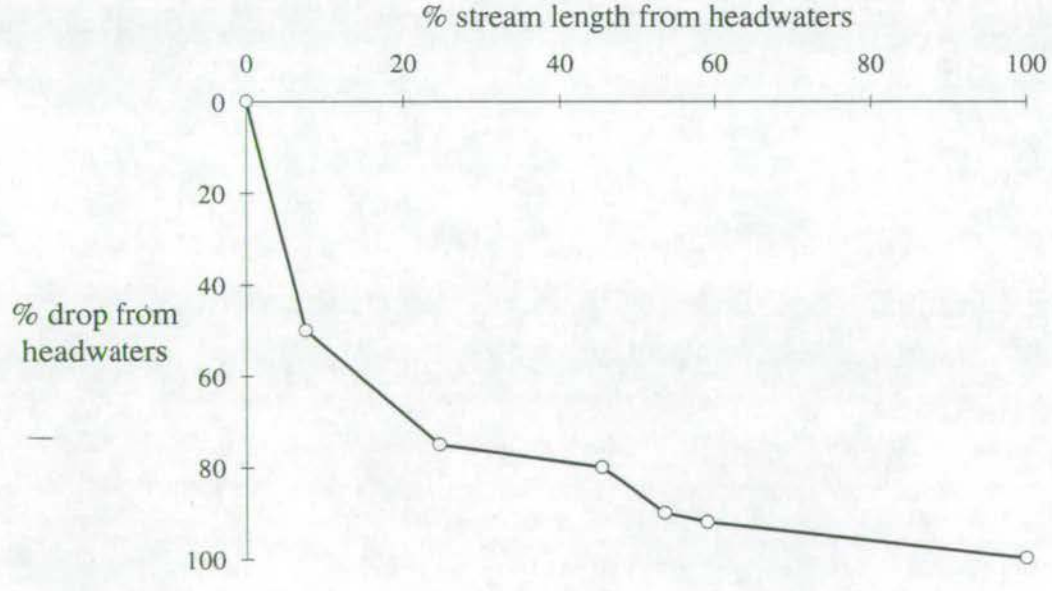

Fig 5.13 Dimensionless plot of the stream profile of the Aksu Çay. The stream is not in an equilibrium state and the profile indicates that tectonic uplift is occurring in the Taurus mountains.

It would be expected with the large fluctuations of sea-level that have occurred during the Holocene (Vail and Wornardt, 1991), that flooding of the central Aksu basin and the western coastal area to Asağikaraman would have taken place. However, it has been shown that there is no evidence for marine incursion after the Pliocene regression. This implies that the area has been uplifted out of the range of sea-level fluctuations. Other evidence also points towards this conclusion. Glacioeustatic effects have been in operation since the mid Pliocene and in the Quaternary the effect has increased and caused sea-level fluctuations on the order of 100m. If uplift had not occurred it would be expected that a number of marine incursions of the Aksu basin would be recognisable throughout the Quaternary. The distinct terracing of both the tufa and the ?Holocene fluvial deposits also imply that glacioeustatic effects have been superimposed on a gradual regional uplift. This is analogous to the Quaternary coastal terrace and fanglomerate sequences on Cyprus which are almost certainly related to a superposition of glacioeustatic cycles on the uplift centred around Troodos (Poole and Robertson, 1991).

Further evidence for uplift is the profile A-A' in Fig. 5.2, reproduced in Fig. 5.14) The mature slope surface of the Kemer fan, which can be traced out to sea, is clearly disrupted by a palaeocliffline, 75m in height, caused by marine corrosion into the uplifting slope surface. Larger cliffs are cut in the other profiles but it is not clear how much of this is due to faulting and how much due to uplift (Plate 5.3F). Notches in the tufa along the Antalya coastline show that the cliffs have been uplifted relative to sea-level.

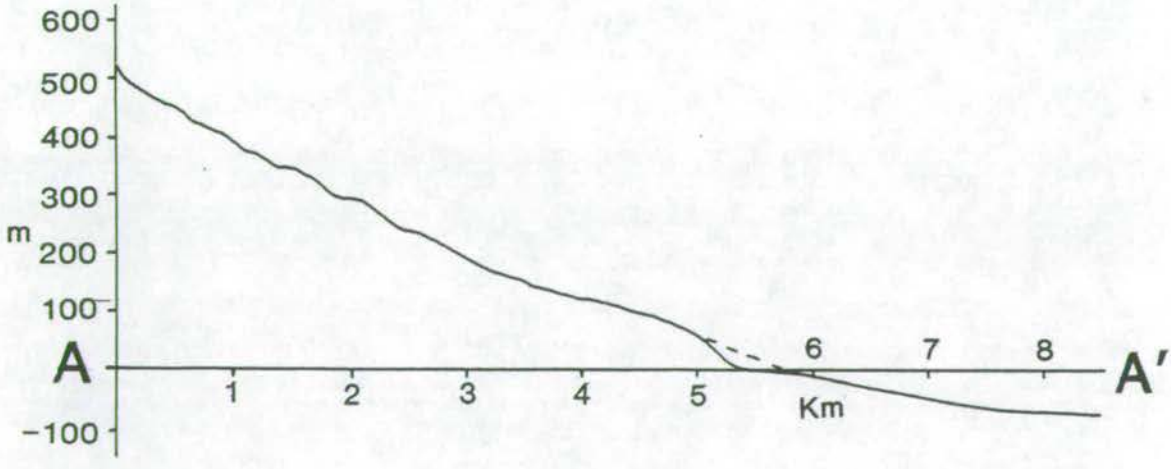

Fig 5.14: Profile A-A' from Fig. 5.2. The smooth slope surface of the Phaselis fan can be traced offshore, but is interrupted by a sea-cliff 75m in height, which demonstrates the regional uplift of the coastline.

The shorelines of the eastern Mediterranean document the regional nature of this uplift. The coastline of western Turkey is typical of a drowned coastline with complex coastal morphology, flooded estuaries and beaches. Rates of subsidence in western Turkey were calculated by Flemming (1971). Eastwards from Antalya the coastline of southern Turkey, Syria and Israel is relatively straight, often with sea-cliffs. This documents a regional uplift (Piarozzoli *et al*, 1991). Regional uplift is also documented in Cyprus (Poole and Robertson, 1991). The tectonic reasons for this are discussed further in chapter 6. This regional uplift is the background for more local tectonic events. Thus, the Quaternary faulting which will be discussed in chapter 6 causes a relative subsidence of the Aksu basin with relation to the Taurus mountains, but relative to sea-level, uplift has occurred.

5.9: Conclusions

1) Mature slope surfaces have been developing since the Early Pliocene with the devlopment of coarse fanglomerates (Kemer Fanglomerates) and the smoothing of the Taurus mountain limestones.

2) A period of faulting during the ?Early Quaternary, after development of the slope surfaces to a mature satge and prior to tufa deposition uplifted the Taurus mountains, cutting through the mature slope surfaces.

3) Subsequent fluvial incision, as a result of the uplift event, has destroyed and dissected much of the original fan surface.

4) The fault scarps show typical degraded Mediterranean scarp profiles (Stewart and Hancock, 1989) with step-faults and a rugged surface.

5) The tufa terraces infilled this faulted topography to from an essentially flat surface which has subsequently been eroded by base-level changes. Faulting may play some role in terrace formation along the eastern basin margin.

6) Conglomerate terraces of the Aksu Çay are the result of climatically controlled aggradation events superimposed on regional uplift.

7) Terra rossa formed on the tufa and the Mesozoic limestone during a climatic period of characterised by hot-dry summers. This was washed into the basin during flash floods forming extremely steep sided channels.

8) Gradual regional uplift has affected the area throughout the Quaternary and probably since the Pliocene. This uplift is the background against which other tectonic and sedimentological events occur.

Chapter 6: Neotectonic evolution

The Mediterranean has long been of interest to tectonic geologists due to its status as a zone of incipient collision. Indeed, the Mediterranean itself is on the brink of disappearing, as the last remnants of the Tethys finally close. Understanding the associated tectonics of the area is of particular importance, as this final phase of orogenesis frequently causes lateral and rotational displacement of large regions, which will later be preserved in the resulting mountain belt. Understanding such an early collisional setting has important consequences for the way in which we unravel collision margins of past eras.

The eastern Mediterranean basin to the south of the Mediterranean ridge is thought to be a remnant of the Mesozoic Tethyan ocean crust and margin. The Mediterranean ridge itself is a mud dominated accretionary complex that, locally, is in an early collisional setting (e.g. Sirte region). By contrast, in the central western Mediterranean only a small remnant of Mesozoic crust remains in the Ionian sea and the main basins are younger (e.g. Tyrrhenian sea).

Western Turkey, Greece, the Aegean and the Hellenic active margin have been the focus of much geophysical and geological research. The well exposed neotectonics, geology and good modern and historical earthquake data have meant

that rapid progress has been made in understanding both of large-scale tectonics of the region, particularly its development during the Pliocene and Quaternary, and small-scale tectonics. Despite this progress the complexity of the region is such that there remains much controversy concerning many aspects of its geological evolution.

Broadly, the eastern Mediterranean may be considered as an area where seismicity defines zones of deformation surrounding rigid microplates (McKenzie, 1970). Although the comparison with large-scale plate tectonics is not exact, due to internal deformation of the microplates, the broad comparison is a good starting point for considering the behaviour of the area. Dewey and Sengör (1979) emphasise the complexity of the boundary zones between these microplates. Collision between the northward moving African and Arabian plates and Eurasia is hypothesised to have caused westward translation of the central Anatolian plateau (tectonic escape) and extension in the Aegean and western Turkey (McKenzie, 1970, 1972). This occurred along the Bitlis suture in the middle to early-Late Miocene (Lhanghian-Serravalian). The details of this tectonic behaviour are discussed in the following sections. These two areas may be considered as part of a semi-rigid plate bounded by the North Anatolian fault zone (NAFZ), East Anatolian Fault (EAF) and the Cyprus and Hellenic active margins. The nature of the boundary between the two microplates is not yet defined. One of the purposes of this study is to look in more detail at this transition zone.

Much of the Mediterranean consists of continental or "transitional" crust with oceanic crust thought to remain only in the deeper parts of the basins (Lort, 1977). The presence of this oceanic crust allows northward subduction to occur along the western part of the Cyprus active margin and along the Hellenic active margin. The crust has been shown to change from a thickness of 22-32km thick in the Aegean (Makris, 1976; Makris and Vees, 1977; Makris and Stobbe, 1984) to 40-50km thick under the Anatolian Plateau (Mindavelli and Mitchell, 1989).

6.1: Eastern Mediterranean tectonics

In order to understand the tectonic evolution of the Antalya region we need first to review in more detail the behaviour and development of tectonic escape in the eastern Mediterranean. The tectonic, bathymetric and geographic features discussed in this section are summarised in Fig. 6.1. We have already seen that the tectonics of the eastern Mediterranean are dominated by the collision of the African and Arabian plates with the Eurasian plate. Karig and Kozlu (1990) show that in the Maras region of eastern Turkey only small changes in the relative motions of the plates can cause dramatic changes in the stress regime.

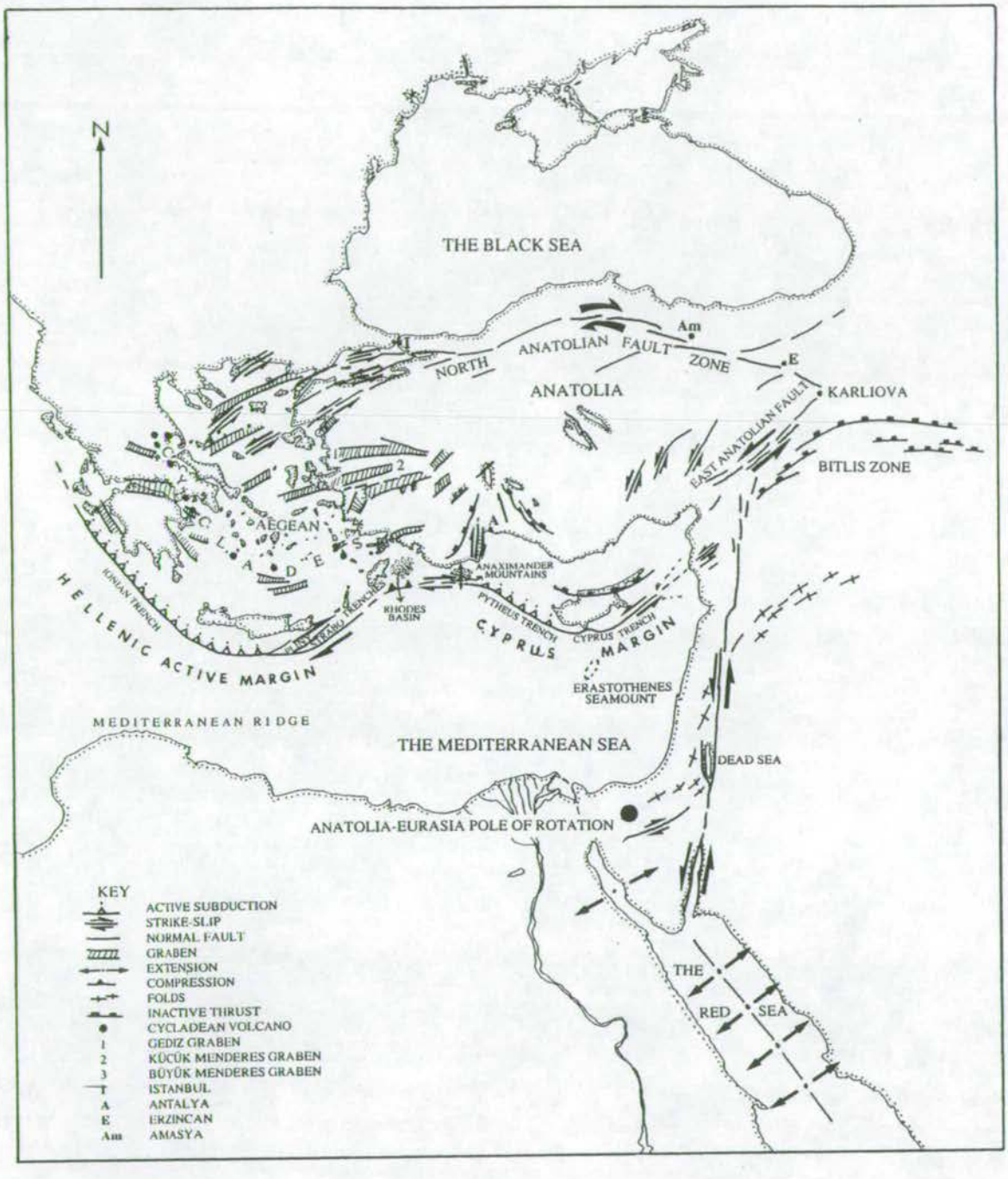

Fig. 6.1: Map of the eastern Mediterranean area showing the principal tectonic, bathymetric and geographic features of the region.

	Absolute motion poles
Africa 30-6 Ma	33°N 35°W
Africa 6-0 Ma	19°N 16°W (= SW shift in absolute motion)
	Corresponding counterclockwise rotation
Euler pole of rotation	48°S 84°E
Angular velocity (ω)	0.085° / Ma
	Increase of absolute velocity of Arabia to Africa
Arabia 5-0 Ma	16mm / yr

Table 6.1: Summary of motion of the African plate between 30 Ma and present from Pollitz (1991)

This observation presumably applies to the entire eastern Mediterranean area.

Livermore and Smith (1984) calculated the relative motion of Africa and Eurasia in the vicinity of Turkey from improved Atlantic ocean-floor data and geologic and geomagnetic time scales. Their determinations are, however, somewhat broad, with a northwards movement of Africa relative to Eurasia and a N 06° movement of Arabia relative to Eurasia, remaining unchanged since 37 Ma.

Pollitz (1991) was able to produce a much more detailed assessment of relative plate motions in the eastern Mediterranean region by integrating local geological data, primarily using hotspot tracks and analysis of propagating rifts together with the marine magnetic, anomaly and fracture zone data. It seems that a change in absolute plate motion occurred between 8 and 4 Ma. Northward convergence changed to become the present-day northwestward convergence. This transition is consistent with the observed large counterclockwise rotation of the western European stress field during the Late Miocene. This is attributed to hotspot activity in the Afar region causing increased mantle flow away from the Red Sea rift region at this time (Bergerat, 1987; Le Pichon and Gaulier, 1988). Hempton (1987) suggested that the Arabian plate travelled as part of the African plate until the mid Oligocene and then moved independently until the mid Miocene. It once again moved as part of the African plate until the Pliocene, between 5 and 4 Ma. At this time–strike-slip motion restarted along the Dead Sea transform and the Arabian region acquired faster northward motion in comparison to the African plate. Quantification of the kinematics discussed here is given in Table 6.1.

6.1.1: The Red Sea, Gulf of Aden and the Dead Sea transform

The relative motion of the African and Arabian plates is an important controlling factor of tectonic escape. As Arabia collides faster more material is driven out to the west. This differential motion of the African and Arabian plates is

controlled by rifting of the Red Sea/Gulf of Aden. Rifting began in the Red Sea and Gulf of Aden around the Eocene to Early Oligocene (35-30 Ma, Pollitz, 1991). Arabian plate motion, as determined by Hempton (1987), points to an episodic history of extension in the Red Sea and the Gulf of Aden. Hempton (1987) argued that extension began in the mid-late Eocene. This phase halted in the Mid Miocene with the collision of the Arabian plate with Eurasia, along the Bitlis zone. Movement along the Dead Sea transform began and extension in the Red Sea restarted in the Early Pliocene, when tectonic escape became established, allowing the Arabian plate to move faster than the African plate. Sea-floor spreading is thought by Hempton (1987) to have commenced at the start of this second episode of extension, perhaps because the Arabian plate separated faster than previously. In the Gulf of Aden sea floor spreading commenced at least 10 Ma ago (Cochran, 1981). Le Pichon and Gaulier (1988) calculated that the Red Sea has been opening for the same period of time. To model the opening they had to use a different pole of rotation for the pre-5 Ma calculations and the post-5 Ma calculations. They came to a very different conclusion from Hempton, arguing that rifting occurred from 13 Ma and again relating it to onset of extrusion tectonics, in the earlier "proto stage" of Sengör, Görür and Saroğlu (1985). Le Pichon and Gaulier (1988) did not envisage oceanic spreading in the northern part of the Red sea until 4-7 Ma ago. It is noteworthy that their heat flow models do not allow the cases of rifting occurring at 13 Ma and 4.5 Ma to be differentiated. It seems that their arguments are neither entirely against nor can discount a two-phase rifting process such as that described by Hempton (1987). Much earlier Le Pichon and Francheteau (1978) had suggested that the main opening in the Gulf of Aden/Red Sea system started in the Middle Miocene (25 Ma) and ended in the Late Miocene (6 Ma). Opening resumed 4-5 Ma ago and resulted in a 40-45km motion along the Levant shear, total movement on the shear has been 60-65km. They proposed that movement along the North Anatolian fault zone occurred during both these periods with a compressional event in between.

6.1.2: The North Anatolian fault zone and the East Anatolian fault

The North Anatolian and East Anatolian strike-slip lineaments are generally considered to be the bounding faults of westward tectonic escape of Turkey.

Sengör *et al* (1985) considered that westward escape of Turkey began at approximately 12 Ma. Barka and Hancock (1984) recognised a broad shear zone which can be considered as a proto-North Anatolian fault zone in the Mid to Late Miocene; a fully fledged North Anatolian fault zone existed in the Pliocene. The transition between the two almost certainly took place in the latest Miocene

(Messinian) when the fault zone narrowed, but its geomorphological expression first appeared during the Early Pliocene. Total offset on the zone is calculated to be 85km ± 5km (Barka and Hancock, 1984).

There is no clear evidence to date the inception of the East Anatolian fault zone but it seems that its development was later than that of the North Anatolian fault zone and it was certainly already active by the Pliocene. The total offset since its initiation is similar to that of the North Anatolian fault zone during the same period (25km and 22km) (Barka and Hancock, 1984). Sengör *et al* (1985) suggested that prior to this, lateral displacement was taken up by the Bitlis suture zone. Rotstein (1984) also considered the two faults in some detail and felt that the two were not equivalent. He argued that the East Anatolian Fault is an arcuate structure similar to those that curve into the Anatolian block from Amasya and Erzincan. However, the evidence from Sengör *et al* (1985) argued strongly against this. In addition, much of Rotstein's (1984) arguments based on earthquake solutions can be explained by different geometric conditions along the two zones (Barka and Kadinsky-Kade, 1988). It seems clear that the North Anatolian and East Anatolian faults do indeed bound the westward moving Anatolian plate.

Barka and Kadinsky-Kade (1988) postulated that the North Anatolian fault dates from the uppermost Miocene to Early Pliocene, with total displacement varying from 40km near Erzincan to 15km in the Marmaris region. These estimates are considerably lower than others, but the significant decrease in displacement towards the west might be expected.

Although the geometry of the North Anatolian fault zone is confined to a narrow band along much of its length in the Marmaris region, starting about 150km east of the Sea of Marmara, it divides into three main graben-bounding strands.

6.1.3: The Anatolian Block

England and McKenzie (1982, 1983) argued that buoyancy forces arising from crustal thickness differences drive tectonic escape. Snyder and Barazangi (1986) state that the Zagros mountains have uplifted at least 1mm/yr since the Late Pliocene. They compared this uplift to the two-stage crustal thickening models of the Himalayas (Lyon-Caen and Molnar, 1985). In their model, the lower crust deforms plastically between the brittle upper crust and a rigid uppermost mantle lid. Two decoupling zones exist, allowing the different levels to behave independently. Isostatic forces cause the plastic lower crust to raise the surface and depress the Moho. Additional flexural forces, affecting the whole Arabian lithosphere, and horizontal compression produce basement thickening.

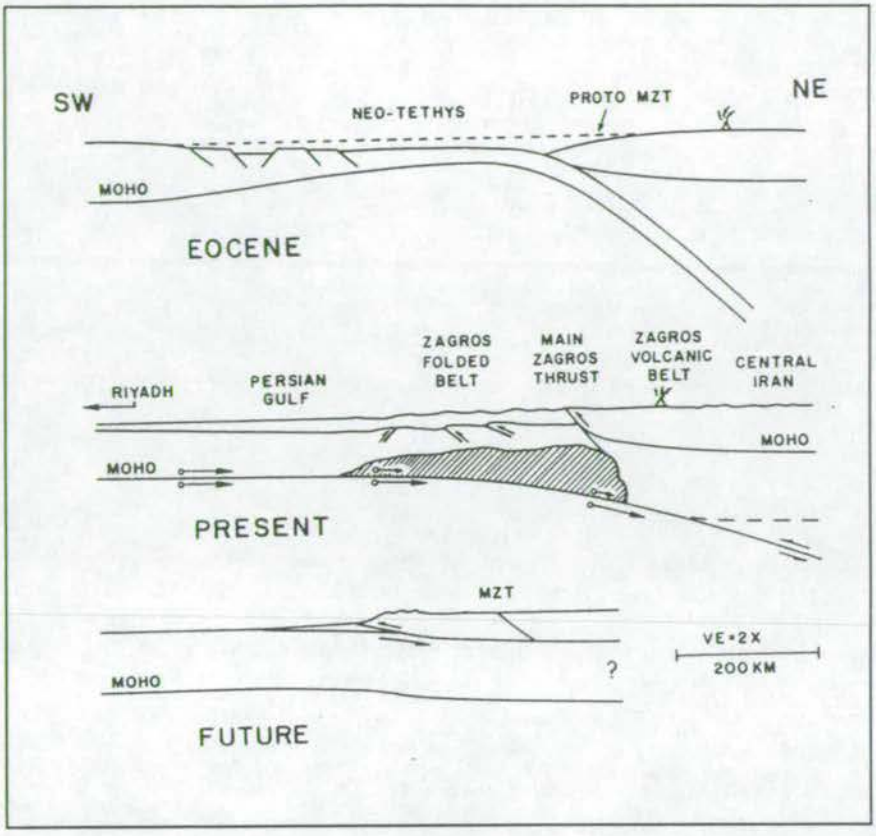

Fig. 6.2: Three stage evolutionary model of the Zagros from Snyder and Barazangi (1986)

It is suggested that the Zagros area represents an early stage in the development of the Himalayas. This model is illustrated in Fig. 6.2. The consequence of Himalayan-style uplift in this region is a gravitational potential which helps drive the western escape of Turkey and will continue to do so until collison ceases and the Mediterranean becomes another continental suture zone. Sengör *et al* (1985) favoured boundary forces as the driving force of tectonic escape, but did not expand on the mechanics of this process.

Rotstein (1984) first argued for counterclockwise rotation of the Anatolian block. His criticism of the models which use a single pole of rotation is that they assume the Anatolian transform fault to be an ideal transform which describes all of the motion between Arabia and the Black Sea. The Satellite Laser Ranging (SLR) results of Le Pichon, Chamot-Rooke, Huchon and Luxey (1993), also suggest a counterclockwise rotation of the whole Anatolian block, about a Euler pole located north of the Sinai peninsula. Oral, Reilinger, Toksöz, King, Barka, Kinik, and Lenk (1995) showed very similar GPS results. Their Euler pole is in an almost identical position to that of Le Pichon *et al* (1993). Both sets of GPS data show that transfer of

motion between Africa and Eurasia is complete and the Anatolian plate and the Aegean plate are moving as a single (Turkish) plate in the present day. Oral *et al* (1995) calculated that the extension observed in the Aegean region is approximately one third of values previously given.

The observation of Rotstein (1984) that the Anatolian block deforms internally is a valid one. Active margin-like faults splay from the eastern part of the North Anatolian fault zone, in particular from near Erzincan and Amasya, and transfer deformation well into the Anatolian block. Data on the behaviour of the bounding shear zones of the Anatolian block, in particular the southern boundary, are used to deduce the behaviour of the block itself (Rotstein, 1984). The result is a combined model of westward extrusion and rigid-plastic deformation, such as that described by Molnar and Tapponier (1975) for central Asia, which requires counterclockwise rotation of Anatolia. McKenzie (1972) and Le Pichon and Angelier (1979) define poles of rotation for the movement along the strike-slip block from the shape of the North Anatolian fault zone. Rotstein (1984) pointed out that to compute a pole of rotation the Aegean extension and the deformation taken up on the splay faults must also be accounted for. These views have subsequently been updated by the GPS data. The slightly faster northwards movement of Arabia in relation to Africa and the subduction in the Aegean may well be expected to cause a torque on the eastern Anatolian plate, possibly a cause of rotation. Taking into account all these factors gives a relative motion of the area trending NE-SW with a counterclockwise rotational component. The rotation of the Anatolian plateau is probably taken up by a number of continental slivers bounded by the splay faults discussed above, each rotating a small amount and translating SW.

6.1.4: The Cyprus and Hellenic active margins and their relationship

The present day Cyprus active margin was established in the Lower Miocene when the arc jumped from just south of the Kyrenia range in Cyprus to its current position south of the island due to collision of the Cyprus with the Kyrenia lineament (Robertson and Woodcock, 1986; Eaton and Robertson, 1993).

Subduction under the Cyprus active margin is an extremely slow process. No widespread arc volcanism is associated with the Cyprus arc, although Neogene volcanics in southern Turkey may be related to early subduction (Innocenti, Manetti, Mazzouli, Pasquare and Villari, 1982). The torque created by the faster moving Arabian plate and the consequent rotation of the Anatolian plateau may account for

the very slow behaviour of the Cyprus active margin and the lack of associated volcanism. Ben Avraham, Kempler and Ginzburg (1988) showed from geophysical properties of the region and multichannel seismic reflection profiles that subduction almost certainly occurs only in the western part of the active margin between the Eratosthenes Seamount and the Anaximander area. South of Cyprus, breakup of the Eratosthenes Seamount is taking place and fragments of the Seamount are thrust beneath Cyprus (Kempler and Ben Avraham, 1987). The breakup of the Eratosthenes seamount was shown extremely well on seismic profiles shot by the recent TTR3 cruise of the R.V. *Gelendzhik*, documented in Limonov, Woodside and Ivanov (1994) and Robertson *et al* (1994). The eastern continuation of the active margin is relatively poorly understood. McKenzie (1970, 1972) suggested, from regional considerations, that the active margin became a strike-slip zone connecting through the Çukarova area to the East Anatolian fault. Alternatively, it has been proposed that active convergence and thrusting continued in the region, extending into the Bitlis zone (Le Pichon and Angelier, 1979; Rotstein and Kafka, 1982). Ben Avraham *et al* (1988) suggest that the active margin could connect with the complex strike-slip zone of the Dead Sea transform which occurs to the north of the Sea of Galilee, i.e. considerably further south then previously suggested. This interpretation is supported by the work of Anastakis and Kelling (1991) who considered that the subducting part of the active margin terminates at the eastern edge of Cyprus and is connected to the Hatay/Baer Bassit overthrust zone in Syria by a lineament characterised by alternating transpression and transtension. Recent seismic data from the Tredmar 2 cruise of the *R.V. Gelendzhik* show evidence of strike-slip deformation along a number of strike-slip lineaments which join the Arabian margin between Çukarova and Hatay. Compressional features are also observed in the area (Woodside and the scientific party, 1992).

Field data presented by Kelling, Gökçen, Floyd and Gökçen (1987) from the Misis complex in the Çukarova basin indicate that a pre-Pliocene strike-slip zone existed in the region. Field study of the late Palaeogene and Neogene basins in the Aslāntas fault zone (which runs to the north of and parallel to the East Anantolian fault) and the Bitlis compressional zone (Karig and Kozlu, 1990) shows that thrust tectonics may not have been as important a process as was previously suggested and they also believe that strike-slip motion dominated the region throughout the Neogene. They also give evidence for a phase of extensional tectonism during the Miocene. Transpressive displacement occured along the Aslantas fault zone into the Pliocene and a recent switch to transtension followed. They showed that these changes in kinematics do not require large changes in relative motion of the major

plates. This pattern of basin development is comparable to present day obliquely convergent and divergent margins of the circum-Pacific region (Ogawa, Horiucki, Tamiguchi and Naka, 1985).

It is widely accepted that the Hellenic active margin differs little from typical subducting margins. Active underthrusting, intermediate seismicity, a large free air gravity anomaly, an active volcanic arc (the Cyclades chain) and a Plio-Pleistocene trench system are all evidence that oceanic crust subducts northwards (Le Pichon and Angelier, 1979; Fytikas, Innocenti, Manetti, Mazzuoli, Peccerillo and Villeri, 1984).

Papadopoulos, Kondopouloi, Levantakis and Pavlides (1986) studied active deformation of the Aegean lithosphere using fault plane solutions and neotectonic field studies to show that the forearc part of the Hellenic arc is dominated by thrust faulting while the back arc is primarily extensional. A transition belt of strike-slip faults with a predominantly thrust component separates the two. Thrusting in the downgoing slab was also recognised. Re-analysis of earthquake mechanisms in the Hellenic Trench (Taymaz, Jackson and Westaway, 1990) shows 4 groups of earthquake mechanisms to exist in the region: a) normal faults trending N-S in the overriding material; b) low-angle thrusts with an E-W strike at about 40km depth; c) high-angle reverse faults, also with an E-W strike but somewhat shallower; d) events within the subducting lithosphere with approximate E-W trending P axes. The thrust earthquakes in b) and c) probably relate to the subducting sediment cover, underplating and uplifting Crete.

Mercier, Sorel and Simeakis (1987) summarised the present-day situation. The 50-100km wide region of the Ionian islands is currently under compression, whilst the Aegean sea is extensional. They recognise strong, but short-lived, compressional events, which deformed the active margins in the past. The details of these Aegean stress states are discussed further below. Mercier *et al* (1987) tentatively assigned these regional stress patterns to variations in subduction style under the Hellenic active margin. Thus, in the Pliocene, they viewed seaward migration of a long sinking slab as the cause of a low horizontal compression, which in turn caused σ_3 to be radial to the active margin boundary. In the present day, the extensional tectonic regime is thought to be due to maximum compression in the vertical plane as a consequence of the thickness of the continental crust, thus σ_3 is orthogonal to the slab push.

The possible presence of an earlier slab beneath the Aegean, which may account for some anomalous earthquakes in the area, was first discussed by Pazapachos *et al* (1973). Mercier *et al* (1987) also recognised the presence of an older active margin which they call the "Ionian Arc". They suggested that it extended

into western Turkey to join the "Lycian Arc" and suggested that the arc jumped southwards to its present position at the beginning of the Pliocene, although no hard evidence is put forward for this. From the Mid Pleistocene to the Present they described the active margin boundary as being subjected to a ENE-WSW (in the Ionian islands) and a NE-SW (south of Crete) trending compression. The Aegean sea undergoes NNW-SSE extension in the north and NW-SE extension around the south Aegean active margin. Kissel, Laj, Poisson, Savaşçin, Simeakis and Mercier (1986) used palaeomagnetic data from the Aegean islands to suggest that from the mid-Miocene onwards the Hellenic arc was straight and that since then gradual curvature of the arc has taken place. Anastakis and Kelling (1991) supported this view.

Other workers have also suggested that subduction began around the beginning of the Pliocene at 5 Ma (McKenzie, 1978; Mercier, 1981). Le Pichon and Angelier (1979) considered the geometry and kinematics of the trench system and the sinking slab to propose that subduction has been occurring since approximately 13 Ma. The observed extension in the Aegean region and particularly in Crete seems to independently suggest that this was the case. They proposed from this evidence that subduction under the Hellenic active margin occurs due to gravitational spreading and associated migration of the trench system to the S and SW, hence independent of the westward extrusion of Turkey. Dewey and Sengör (1979) came to a similar conclusion. The Neogene volcanics strongly support a Mid Miocene onset of subduction along the present-day Hellenic active margin (Fytikas *et al*, 1984). The distribution and age of the volcanics shows that during the Oligocene to Mid Miocene an arc existed to the north of the present day active margin and migrated south with time. In the Mid-Miocene volcanism associated with this arc ceased and new volcanism did not begin until the Cycladean volcanics became active in the Pliocene. This data fits well with the jumping of the arc to the south at about 12 Ma. The cessation of volcanism in the mid Miocene probably ties well with the cessation of subduction of the "Ionian arc". It is to be expected that it will take some time after initiation of a new arc to begin to melt the subducting crust and produce volcanics. However, Le Pichon *et al* (1993) used recent Geodetic - Satellite Laser Ranging (SLR) and Global Positioning Satellite (GPS) results to test the velocity of westward extrusion of Anatolia. The measured velocities indicate that transfer of motion from Arabia to Anatolia is complete. This implies therefore that the McKenzie model (1970, 1972) is correct and negates the model of Le Pichon *et al* (1979). Meulenkamp, Wortel, van Wamel, Spakman and Hoogerduyn-Strating (1988) arrived at an age of 26 Ma for initiation of subduction. Seismic tomography of the upper mantle in the region of the subducting slab suggests the slab is 800km long as

opposed to the 280-500 km estimated by Le Pichon and Angelier (1979). In order to subduct 800 km of slab at least 26 Ma is required. They proposed that fragmentation of Crete which began about 12 Ma was due to initiation of roll-back of the subduction zone. They tentatively attributed this to the onset of the final stages of collision between Africa/Arabia and Turkey. An age of 26 Ma is probably too old to fit with the observed geology of the Aegean. Meulenkamp *et al* (1988) considered it doubtful that the short length of the slab deduced by Le Pichon and Angelier (1979) is sufficiently long to produce large enough gravitional forces for subduction to occur. However, if gravitational forces are not responsible for subduction perhaps a shorter slab is the preferable solution. It is suggested in this thesis that the remnant "Ionian" slab may cause the tomographic results to indicate a slab of 800km in length.

Earthquake solutions associated with the two active margins give maximum depths of about 80km in Cyprus to 120km between the active margins and 160km in the Hellenic active margin (Rotstein, 1984). This implies that subduction occurs at a faster rate and that the slab penetrates the mantle at a steeper angle in the Hellenic region.

The relationship between the Hellenic and Cyprus active margins is poorly understood and a number of different suggestions have appeared in the literature. These vary between a continuous system (Rotstein and Kafka, 1982; Rotstein, 1984; Anastakis and Kelling, 1991); a discontinuous system (Aubuoin, 1975; Le Pichon and Angelier, 1979; Mercier, 1981); and a sharp cusp (McKenzie 1970, 1972; Dewey, Pitman, Ryan and Bonin, 1973; Nur and Ben Avraham, 1978; Dewey and Sengör, 1979).

Anastakis and Kelling (1991) used detailed consideration of bathymetric and seismic reflection data from the whole eastern Mediterranean area to assess the nature of the Cyprus active margin and its connection with the Hellenic active margin. The western subducting portion of the Cyprus active margin is bathymetrically defined by the Pytheus trench and the authors recognised a curve in this trench which enables it to achieve tectonic connection with the Strabo trench of the eastern part of the Hellenic active margin. In this area, south of the Rhodes basin, northward thrusting has been observed (Jongsma and Mascle, 1981). This compression represents a sector where a particular stress regime can be defined. In other sectors, e.g the Anaximander area, extensional stresses dominate. Seismic shot by the Tredmar 2 cruise of the *R.V. Gelendzhik* showed that the Anaximander mountains appear to be asymmetric, fault-bounded blocks. One (A-2) appears to be a giant fold. High gravity anomalies indicate that the mountains are currently rising

and are probably allochthonous (Woodside *et al*, 1991). Thus, it seems that a complex convergence zone in the region consists of alternate sectors of thrusting and strike-slip deformation accompanied by transpressional/transtensional deformation on the adjacent sectors of the overriding plate. This section of the active margin may represent a boundary transform fault where similar mechanisms have been shown to occur (Gilliland and Meyer, 1976). The convex-northward geometry of the active convergence zone to the southwest of Rhodes is attributed to this transform motion. Rotstein and Kafka (1982) note that the seismicity in the region indicates the active margin runs to the south of the Anaximander Mountains and the Florence rise.

It is probable that the Rhodes/Anaximander areas are behaving in a similar, but more advanced mode to the Eratosthenes seamount, causing subduction to cease and collisional tectonics to occur over a small region (Rotstein and Kafka 1982). Present-day seismicity in Antalya Bay (see also section 6.3.1) probably relates to the earlier subducting slab. It is likely that the Rhodes and Finike basins contain remnants of oceanic crust (Anastakis and Kelling, 1991) and the Anaximander Mountains are an accreted, broken-up, continental fragment, possibly of North African origin although some parts may also be related to the Bey Dağ lari. As yet no data exists to clarify the exact nature of the Anaximander Mountains.

6.1.5: The Aegean and western Turkey extensional regime

The region discussed in this section will be referred to as the Aegean region, but in fact includes both the Aegean and the area of western Turkey characterised by the Gediz, Büyük Menderes and Kücük Menderes Grabens. This area was called the West Anatolian extensional province by Sengör *et al* (1985) and as the name suggests is under extension.

Dewey and Sengor (1979) noted that the timing of the onset of extension in western Turkey, recorded in the graben sediments, is very close to initiation of motion on the North Anatolian fault zone, which occurred in the Late Miocene. However, in general, thick sedimentary sequences did not develop until the Late Pliocene and in some cases the Pleistocene, when full collapse of the basins occurred.

Structural field studies in western Turkey (Dumont, Poisson and Sahinci, 1979; Angelier, Dumont, Karamanderesi, Poisson, Simsek, and Uysal, 1981; Zanchi, Kissel and Tapirdirmaz, 1993) have resulted in consistent results concerning the tectonic evolution of Aegean region. All authors observed from their data that the

area underwent a Mid-Late Miocene NNE-SSW extension followed by Pliocene N-S extension, which changed to NE-SW extension sometime during the Quaternary (Fig. 6.3). Structural data from the Aegean islands (Mercier, Sorel, Vergely and Simeakis, 1989) showed an initial Late Miocene WNW-ESE phase followed by a Pliocene to Mid Pleistocene NE-SW phase and a succeeding N-S phase. Although the direction of events is somewhat different in the Aegean the timing of significant directional changes is remarkably similar in the two areas, Mercier *et al* (1989) considered the fault kinematics to be the results of changes in the regional stress patterns. The importance of the North Anatolian fault zone is also briefly discussed by Mercier *et al* (1989). The present-day tectonic regime is extensional and right-lateral slip will occur on NE-SW trending faults. During the Pliocene right-lateral strike-slip components were present all along the North Aegean Trough fault zone. This may have caused clockwise rotation of the material.

Eydoğan (1988) quantified the deformation in western Turkey from symmetric moment tensors of earthquakes occurring in the region between 1943 and 1983. He concluded that N-S extension in the area increases from north to south while E-W compression in the Marmaris region changes to E-W extension in southwestern Anatolia. In addition the dominant mode of deformation in the Marmara province is right-lateral strike-slip associated with the North Anatolian fault zone. The field evidence of Angelier *et al*, (1981); Zanchi *et al*, (1993) and Mercier *et al*, (1989) suggests that this regime has been active since the mid-Quaternary. Zanchi and Angelier (1993) reviewed focal mechanisms of earthquakes in the region and came to the conclusion that NE-SW extension is the current tectonic regime. This trend enhances the E-W directed right-lateral simple shear which dominates much of the area (Zanchi *et al,* 1993). In their model right-lateral shear is only initiated during the Quaternary and if the block rotations observed are related to this shear, as suggested in many of the models, the authors believe that this would require an unrealistic rate of rotation. They therefore feel that none of the models proposed to explain block rotations in the area are satisfactory. We have already seen, however, that right-lateral movement along the North Anatolian fault zone has almost certainly been underway since the Mid Miocene. This does not fit with the conclusions of Zanchi *et al* (1993) and it is suggested that the observed block rotations in the Aegean area are indeed related to right-lateral shear.

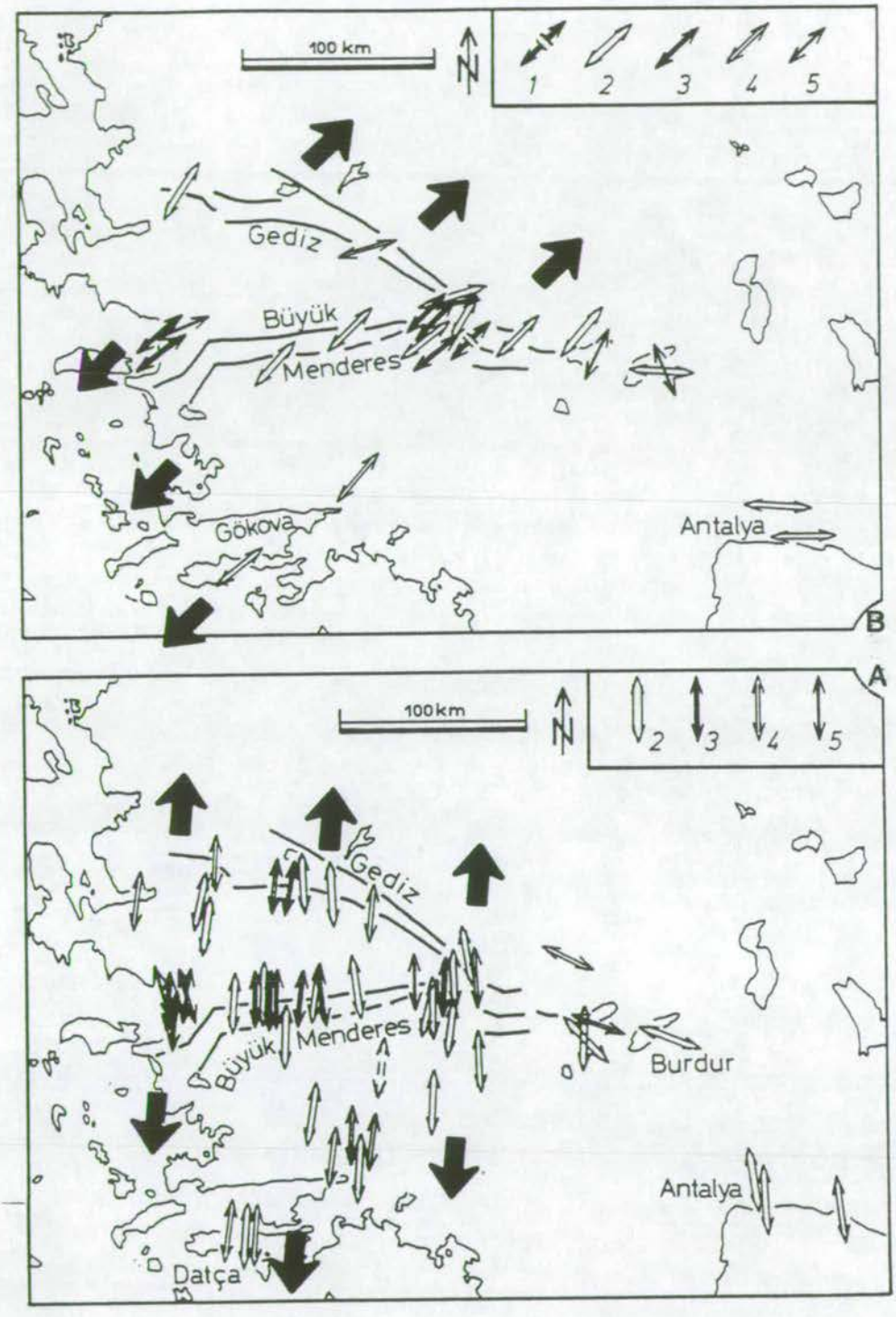

Fig. 6.3: Principal stress directions in western Turkey from Angelier *et al* (1981). Pliocene N-S extension (**A**), changed to NE-SW extension, sometime during the Quaternary (**B**). 1 = historic exension, 2 = direction of σ_3 computed for fault populations, 3 = as 2 with good chronology, 4 = direction of σ_3 using measurements of a main fault, 5 = as 4 with good chronology.

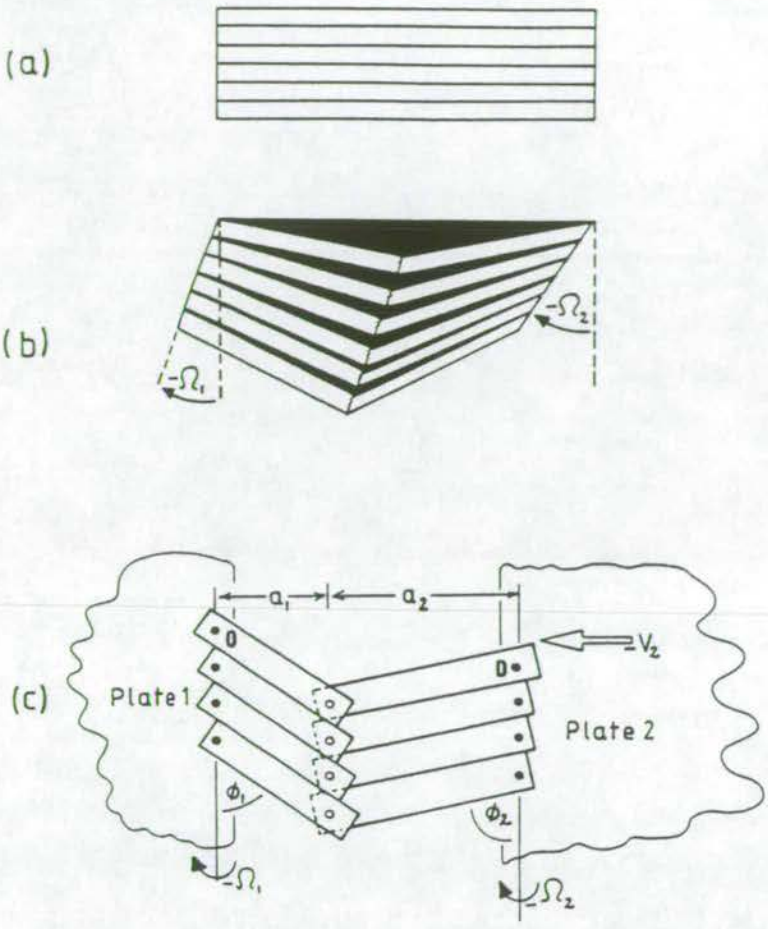

Fig 6.4: Sketches to illustrate the rotation of parallel slats from Taymaz *et al* (1991).
(a) starting configuration
(b) The effect of rotating the right-hand margin more than the left. Shortening parallel to the slats has been compensated by the rotation and breaking of the slats, which separate to produce gaps.
(c) model of rotating slats which can be constructed with wood. The central screws (open circles) join only the two arms of each broken slat. The filled circles are screws that join the slats to the margins of plates 1 and 2. The margins rotate at different rates.

Taymaz, Jackson and McKenzie (1991) used improved earthquake focal mechanisms to more accurately assess the active motions of the Aegean region and western Turkey. They arrived at the "broken slat model", shown in Fig. 6.4., which they quantitatively assessed (Fig. 6.5) and found to correspond remarkably well with earthquake observations from the Aegean area. The model works because continental collision between NW Greece-Albania and the Apulia-Adriatic platform prevents rotation being rapid enough to accommodate the distributed E-W right-lateral shear. Laj, Jamet, Sorel and Valante (1982) documented the rotations in the Ionian islands, along this margin. They found that rotation began about 5 Ma ago and proceeded at about 5°/Ma. No significant rotation has occurred in Crete. This fits well with the predicted rotations of Taymaz *et al* (1991) and puts some time constraint onto the model. Although the model explains well the Aegean and Greek neotectonic activity, the effect of the the extending Gediz, Büyük Menderes and Kücük Menderes Grabens on the eastern edge of the model are not accounted for. On its eastern margin the model is controlled by screws, assumed to have a fixed separation throughout the duration of the model.

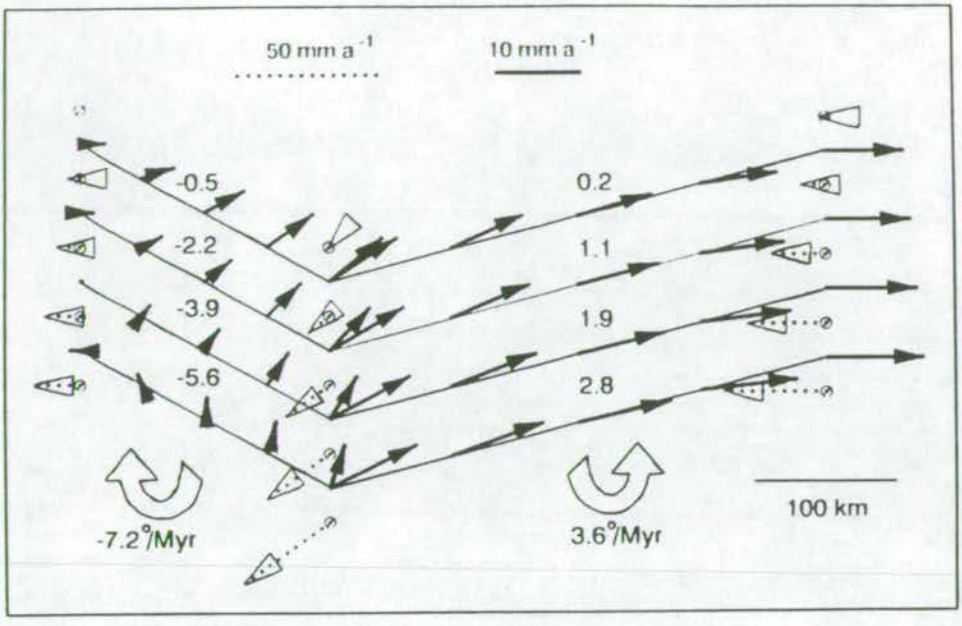

Fig. 6.5: Velocities and rotation rates for the broken slat model calculated by Taymaz *et al* (1991). Thick lines with arrows represent slip vectors. The length of each arrow is proportional to the magnitude of the velocity (see scale at top). Broken lines show the velocity vector of each screw relative to the origin (again length is proportional to velocity; scale at top). Curled open arrows show the sense of rotation of the slats. Numbers given are rotation rates for the bottom slats. Rotation rates for the other slats are also given (°/Ma). Rates increase downwards.

In addition, the edge effects of these elongate slats are not considered and no model is given for the interaction with the adjacent stable zone of the Anatolian plateau. The opening of the Gediz, Büyük Menderes and Kücük Menderes Grabens must clearly be taking up some of the strain but are there other effects that occur at this boundary? Price and Scott (1994) suggested that an anticlockwise rotation of the eastern margin of the Aegean region must occur. This is discussed further in section 6.2.1. However, we have already seen that the Anatolian plateau itself may be rotating anticlockwise which would be expected to cause approximately right-lateral shear along the eastern edge of the Aegean region. These large-scale right-lateral features are not, however, observed in this region. We should expect to see these effects in the Isparta angle area, discussed in section 6.2., and in the new data.

Jolivet, Brun, Gautier, Lallement and Patriat (1994) advocate that the ductile flow of the lower crust can be deduced from the metamorphic rocks on Naxos, Paros and elsewhere. They recognise a continuous ductile flow in the crust and a decoupling between the upper and lower crust. The metamorphics predominantly show top-to-the-north shear structures.

Gautier, Brun, Sokoutis, Jolivet, van den Driesseche, Martinod and Hatzfeld (1995) suggested that the patterns of graben formation in the Aegean sea are the result of "back arc" spreading driven by the gravitational spreading of thickened Alpine lithosphere. This was experimentally modelled, and produced a pattern of grabens similar to that seen in the Aegean. However, the "free" southern boundary was rather artificially fixed at its edges and it is felt that the details of this model do not fit the actual boundary conditions of the Aegean. Thus, the model of Taymaz *et al* (1991) is favoured as it models the boundary conditions that actually exist in the Mediterranean.

6.1.6: Synthesis of eastern Mediterranean tectonics during the Pliocene and Quaternary

A number of criteria were used to evaluate the validity of the above models, to fit them into a broad picture of the neotectonics of the eastern Mediterranean. Those models based on field observations and good earthquake solutions are favoured above more theoretical ones. The models are also required to fit together. It would be useless to favour inconsistent models in adjacent areas when trying to synthesise the movements of the whole area. Timing of events is also very important and in many cases this can be very difficult to ascertain. Again consistency over the whole area was sought.

One of the principal problems with understanding the evolution of the region is ascertaining whether major changes occurred at around 4-6 Ma ago or at around 10-13 Ma ago. Consideration of all the data suggests that the present-day system began to evolve around 12-13 Ma ago. A number of significant events took place at this time. At about 14 Ma terminal collision of the Arabian plate with Eurasia occurred along the Bitlis suture zone. According to Hempton (1987) this halted extension in the Red Sea and movement along the Dead Sea transform. Le Pichon *et al* (1988), in stark contrast, considered this event to mark the onset of rifting in the Gulf of Aden and Red Sea and transform motion of the Dead Sea fault zone. However, there seems to be nothing in their model that negates the idea of an earlier initiation, pause and restart as advocated by Hempton (1987). The Hempton model fits the data from other areas rather better and is thus favoured here. Field observations along the North Anatolian fault zone point to the existence of a broad shear zone at this stage. Whereas the Cyprus active margin was in its present day position from the Early Miocene onwards it is likely that subduction at the Hellenic active margin probably began at about 12 Ma, jumping southward from the position of the "Ionian arc". It is considered that the geological evidence from Crete, the onset

of volcanism along the Cyclades chain and the requirement for a driving force from the west are all good evidence for this. Rotations in the the Aegean sea also began around this time.

There is considerable evidence that despite the initiation of the current regime at approximately 12 Ma the system did not truly start to operate in its present form until about the beginning of the Pliocene (5 Ma) and it may be this that causes many of the conflicting observations. Certainly, at about the start of the Pliocene onset of rifting in the Red Sea, renewed onset of motion along the Dead Sea transform and associated increase in the relative motion of the Arabian plate can be related to the narrowing of the North Anatolian fault zone into a proper strike-slip zone. The East Anatolian fault zone seems to have first become active at this time, probably taking over from the Bitlis zone which may previously have been accommodating left-lateral shear. This phase therefore represents the initiation of true extrusion tectonics, expressed as the westward movement of the Turkish block. It was probably at this stage that gravitational driving forces of the Eastern Plateau (Iran) and boundary forces began to control the tectonics of the region, which may previously have been subduction controlled. This probably had the effect of accelerating the whole process, causing some of the events observed at this time such as the dramatic increase in depth of the western Turkish grabens. No major changes in the general plate tectonic setup have occurred since 5 Ma, but analysis of stress regimes in the Aegean region show a change from N-S extension to NE-SW extension in the mid Pleistocene. A minor change in the absolute motion of the northward moving African and Arabian plates may be responsible for this change of stress field. The change in stress field around the Hellenic active margin, from σ_3 radial to the active margin boundary in the Pliocene to σ_3 orthogonal to the active margin boundary at present, may also be related to this switch, but the timing of the change is unknown. Mercier *et al* (1989) related it to changes in crustal composition of the subducting slab.

There is no information avaliable about the past behaviour of the Anatolian plateau, but there is good present-day evidence that it currently undergoes counterclockwise rotation.

There is moderate evidence to suggest that the Rhodes basin and Anaximander mountains represent a zone of accreted continental material which is acting as a right-lateral transform between the two active margins. The outward bowing of the Hellenic active margin almost certainly accommodates the subduction, which might otherwise have occurred along this transform.

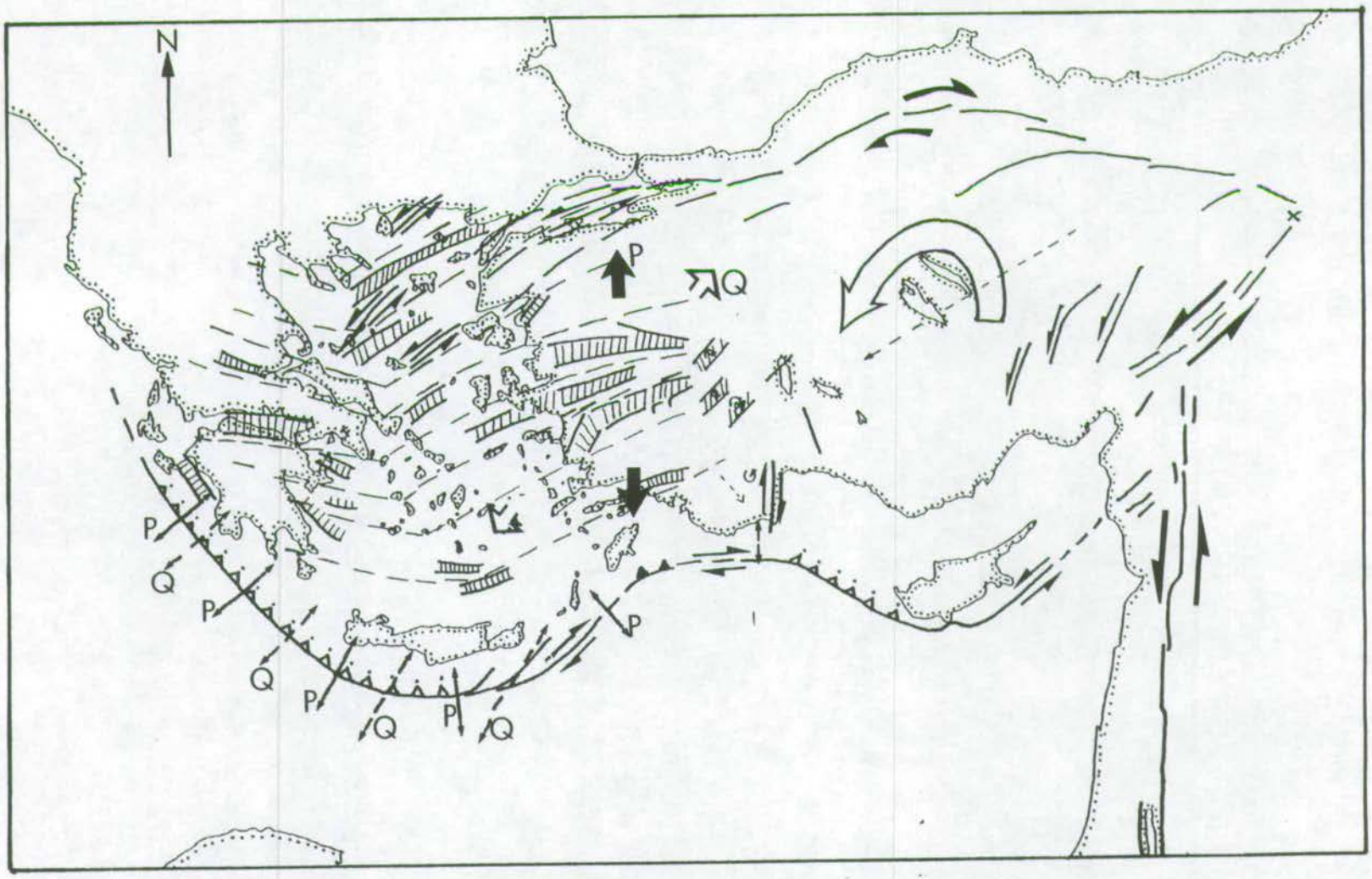

Fig. 6.6: Synthesised map of the tectonics of the eastern Mediterranean. P = Pliocene stress fields, Q = Quaternary stress fields. The dotted lines represent a possible fit of the "slats" of the Taymaz *et al* (1991) model to the Aegean graben structure. The large curved arrow represents the rotation of the Anatolian plateau and the dotted arrow through it the net translation. This is very schematic: the rotation is not as intense as the arrow suggests and is probably taken up by rotation and translation of slivers bounded by the strike-slip faults that break up the plateau.

There is no evidence in either of these cases that the situation has changed since the beginning of the Pliocene and it is assumed that the present situation broadly represents the situation during the last 5 Ma. The Taymaz *et al* (1991) model is adopted here to represent the development of the Aegean region through the Pliocene, as it quantitatively fits the present situation remarkably accurately. The synthesised model for the behaviour of the eastern Mediterranean during the Pliocene and Quaternary is summarised in Fig. 6.6.

6.2: Tectonics of the Isparta Angle

The Antalya (Aksu, Köprü and Manavgat) basins, and the Burdur, Acigöl and Baklan grabens occupy the zone which should represent the change between these two major tectonic realms. Whilst there have been studies of the Burdur and associated grabens, which are more obviously associated with the Gediz, Büyük Menderes and Kücük Menderes Grabens in western Turkey, the Antalya basins have been little studied. They should be responding to both extension in the west and extrusion and rotation of the Anatolian Plateau and thus tell us something about the interaction and development, through time, of these areas. To fully understand the tectonic evolution of the eastern Mediterranean the existence and fault activity of the Antalya basins must be explained.

6.2.1: The Pre-Pliocene tectonic history of the Isparta Angle

As already seen in chapter 1 the Isparta angle consists of a number of continental and oceanic fragments which were accreted to the Turkish margin in the late Cretaceous. Emplacement of the Beysehir-Hoyran-Hadim Nappes during the Eocene and the Lycian Nappes during the Miocene has created a series of thrusts which bound the area, defining a triangular region, hence the name Isparta angle. Thus, the predominant fabric in the area is NE-SW in the western Taurus mountains and NW-SE in the eastern Taurus mountains. These fabrics are shown in chapter 1 (Fig. 1.3). During the Late Miocene a SE-vergent compressional event related to final emplacement of the Lycian nappes and onset of westward movement of the Turkish continent affected the whole area. This has been called the "Aksu" phase (Poisson, 1977).

6.2.2: Burdur, Acigöl and Baklan grabens

The Burdur, Acigöl and Baklan grabens lie to the northwest of the study area. Taymaz and Price (1992) and Price and Scott (1994) observed that the grabens trend in a NE-SW direction, similar to a cross graben north of the Gediz graben. This leads

to the suggestion that they may be genetically related to the Gediz, Büyük Menderes and Kücük Menderes Grabens. Quaternary faulting superimposes an earlier Pliocene faulting associated with a more widely spaced system of grabens. Price and Scott (1994) suggested that in the Burdur graben this caused the Pliocene fault to rotate to its present shallow angle and subsequently to act as a detachment. Regional stress calculations (Taymaz and Price, 1992) show that the stress required to support the end Neogene topography was greater than that required today. The closer spacing of the Quaternary graben system is postulated to be a result of gravitational collapse which created smaller blocks, able to rotate more freely within the stress field. Pliocene σ_3 determinations east and west of the Burdur region (Angelier *et al*, 1981) indicate a regional N-S extension. Price and Scott (1994) observed a left-lateral strike-slip component on the basin bounding faults which led them to suggest that the area has undergone a clockwise block rotation, around vertical axes, in the regional N-S stress field. Unfortunately, as yet, there is no palaeomagnetic data to support this. To fit the Burdur region observations to the model of Taymaz *et al* (1991) Price and Scott (1994) proposed an anticlockwise rotation of the eastern margin of the Aegean region, accommodated by an approximately N-S trending deformation across which a right-lateral displacement occurs and within which NE-SW trending fault-blocks rotate in a clockwise sense. To incorporate all the faults in the area this zone needs to be at least 90km wide.

6.2.3: The Taurus and Bey Dağlari

Kissel and Poisson (1987) used palaeomagnetic evidence from 26 sites in Neogene sediments located in the Bey Dağlari to show that the Bey Dağlari massif has undergone anticlockwise rotation of 30° since 15 Ma. They attributed this to curvature of the Aegean active margins. In the eastern Taurides Kissel *et al* (1993) used palaeomagnetic evidence to demonstrate a post-Eocene clockwise rotation of approximately 40°. Together with the previous work of Kissel and Poisson (1987) they concluded that the Isparta angle was formed first by a clockwise rotation of the eastern Taurides and then by an anticlockwise rotation of the western Taurides (Bey Dağlari), deforming an originally straight (Late Cretaceous) collision front. They therefore considered the first event to have occured in the Late Oligocene to Eocene and the second in the Middle Miocene. One of the data sites sampled by Kissel and Poisson (1987) is within the Pliocene sediment, but the site was rejected due to weak magnetisation. Morris and Robertson (1993) also found a 30° counterclockwise rotation of the western Taurides. Their data from the Antalya complex identifies a remagnetisation event in the Early - Middle Miocene. This constrains the lower age

limit of the rotation. Robertson and Woodcock (1982) consider the event to have occurred in the Late Miocene, related to the final emplacement of allochthonous units on to the Bey Dağlari SW of the area, and convergence and bending of the Hellenic arc. There is no data on the upper age limit to fully constrain this interpretation. It may be that the rotation was slower than proposed by any of the previous studies and continued into the Pliocene.

Kocaefe and Ataman (1976) studied focal mechanisms of earthquakes in the region bounded by Antalya, Fethiye and Denizli, and associated these with lineaments observed on satellite images to conclude that the entire area is slipping southeastwards (Fig. 6.7). This southeastward movement could be responsible for the anticlockwise rotation observed by Kissel and Poisson (1987).

Dumont *et al* (1979) carried out a preliminary study of faulting in SW Turkey, a significant proportion of which was in the Taurides around Eğirdir, Beysehir and Burdur lakes, and around Camilar (between Fethiye and Finike). Their preliminary results in the region of the three lakes show a NW-SE extension. Traces of left-lateral movement are seen in this region. This corresponds well to the recent extension documented in Burdur and suggests that the Burdur results can also be applied across at least the northern portion of the Taurides, if not more extensively.

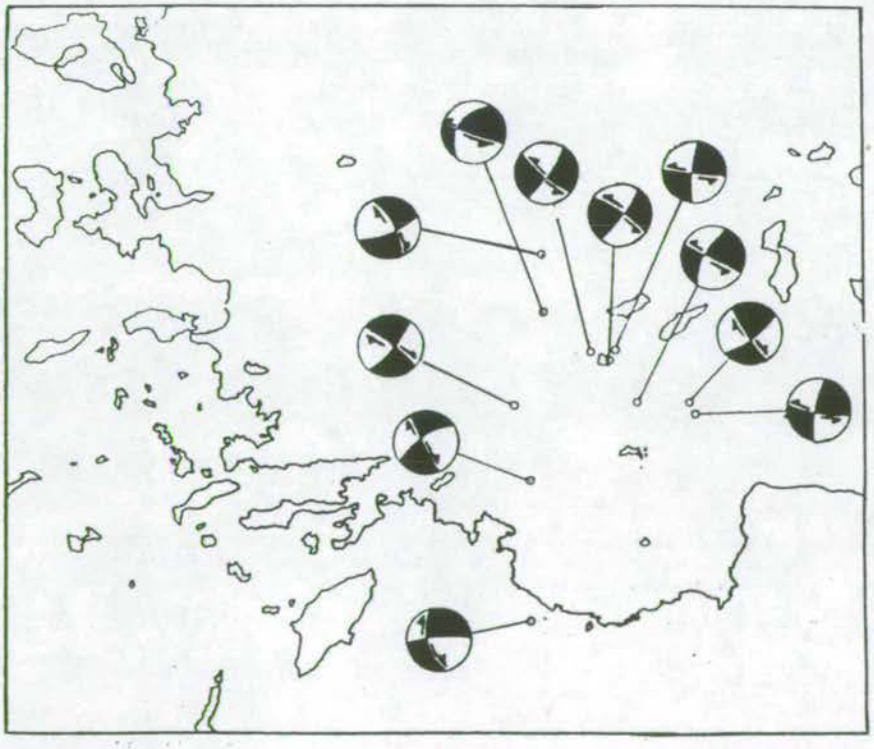

Fig. 6.7: Earthquake mechanisms of Kocaefe and Ataman (1976), which suggest that the region bounded at its corners by Antalya - Fethiye - Denizli is moving towards the SE.

Dumont *et al* (1979) also note that the large NW-SE trending faults are mostly found in the Beysehir region and cut through all previous tectonic structures including the Late Miocene Aksu phase compression, thus limiting this phase to the Pliocene and later.

6.2.4: The Aksu, Köprü and Manavgat basins

Palaeomagnetic study of the Neogene formations of the Aksu, Köprü and Manavgat basins (Kissel and Poisson, 1986) implies that there has been no rotation of the area since at least 15Ma. Thirty sites ranging from the Miocene and Pliocene of the southern part of the Aksu basin and three from the Isparta area, in the lavas and ignimbrites of the Gölçük region, were sampled for this study. Kissel, Averbuch, Frizon de Lamotte, Monod and Allerton (1993) believed that the insignificant rotation of the Antalya basin shown by their previous results implies the existence of a major decoupling zone between the eastern and western Taurides, probably along the base of the Antalya Complex. This observation is in agreement with Marcoux, Ricou, Burg and Brun (1989), but as discussed in chapter 1 their data probably confuses older structures with neotectonic structures. As shown by Morris and Robertson (1993) the allochthonous Antalya Complex also rotates, implying that no decoupling between the two exists, but rather that the strain is taken up over a broad band of shear.

Pliocene σ_3 determinations Angelier *et al* (1981) east and west of the Burdur region indicate N-S extension. Price and Scott (1994) note that to the east of their study area (i.e.in the Antalya basins) Quaternary σ_3 values are east-west trending.

Studies on the Neogene sediments of the Antalya basins are limited to two related French contributions which concentrate on the Miocene tectonics of the region. Du Poux (1984) studied the Plio-Quaternary tectonics of the region as part of an MSc thesis on the Neogene neotectonics of the Antalya and Cyprus basins. His data base was very limited. Sample sites were the Kovada graben, the border of the Aksu basin, and the Korkuteli region. His conclusion was that Plio-Quaternary tectonics occurring at the end of the Early Pliocene are purely extensional in the Aksu basin and activate or reactivate NS or NW-SE features. In the Bey Dağlari a distensive tensor is recognised with a principal ESE-WSW (σ_3) alignment and a secondary NNE-SSW (σ_2) alignment. He considered this activity to have brought the pre-Miocene erosion surface to 2000m altitude. Frizon de Lamottte, Poisson, Aubourg and Temiz (1994) used the data from Du Poux (1984) and others to reinterpret the Neogene tectonics of the area. The result is 350 kinematic indicators from 11 localities around the Isparta angle. The sites are concentrated along the

thrust zones of the area. They interpreted the area as having undergone two phases of tectonic transport, the first as a result of thrusting from the west and second as a result thrusting to the south. Both were attributed to the Aksu phase. However, much of this is based on the analysis of normal and strike-slip faults with no good tie on the timing of events. Flecker (1995) also recognised east vergent structures (faults and recumbant folds) from detailed sedimentological and structural analysis in the Miocene sediments of the Manavgat, Köprü and Aksu basins. She argued that the Aksu compressional phase was controlled by a final phase of south-eastward thrusting of the Lycian nappes and westward thrusting from the beginnings of westward movement of Anatolia. She recognised no southward vergent structures in the area. It is suggested here that many of the strike slip and normal faults incorporated into the model of Frizon de Lamotte *et al* (1994) may be later neotectonic features which can be explained by the model presented in section 5.6.

Two studies mapping tectonic lineaments from satellite images have been conducted. Değirminci and Günay (1992) mapped lineaments primarily over the Köprü basin and eastern Taurides to produce the strain ellipse reproduced in Fig. 6.8. This shows NNW-SSE normal faults, NW-SE right-lateral faults cutting NE-SW left-lateral faults (presumably of lesser importance). Aydar and Dumont (1979) looked specifically at lineaments cutting through the tufa and found NE-SW directions, cross-cut by NW-SE lineaments, cross-cut by N-S lineaments.

The major lineament running down the coast from Antalya to Olympos via Kemer is here called the Kemer zone or Kemer lineament. In none of the published maps of neotectonic faults in the eastern Mediterranean does the Kemer zone feature, although many have strike-slip motion inferred along the Kirkkavak fault.

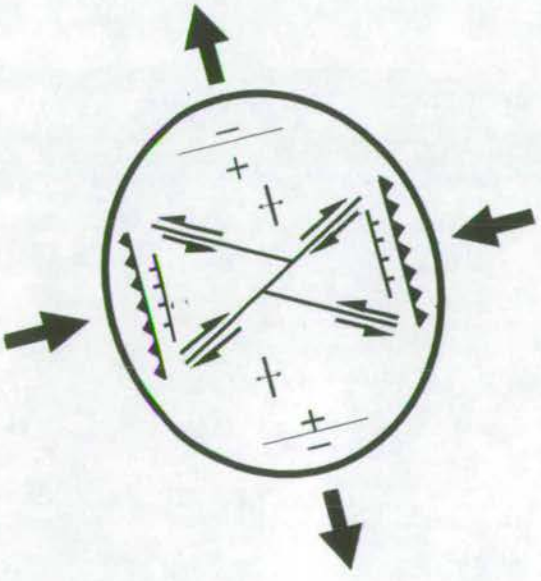

Fig. 6.8: Strain ellipse produced by Değirminci and Günay (1992) from lineaments identified on satellite images.

6.2.5: Summary of the observed tectonics of the Taurus Mountains and the Bey Dağlari and Antalya basins

The summary diagram (Fig. 6.9), of the Isparta angle, including the Burdur region, shows the observed Late Miocene and Pliocene tectonics described above. The hypothesised block rotations of Price and Scott (1994) are shown for the Burdur region. Briefly, the important observations to be considered are the lack of rotation in the Antalya basins themselves (Kissel and Poisson, 1986b) and the 30° counterclockwise rotation of the Bey Dağlari and Antalya complex (Kissel and Poisson, 1986a; Morris and Robertson, 1993) which has occurred since the Mid Miocene and may continue into the Pliocene. In addition, the southeastwards movement of the Antalya-Fethiye-Denizli block is thought to have some relevance and may be related to the rotation of the Bey Dağlari. The Burdur grabens undergo a period of gravitational collapse at the end of the Pliocene resulting in more closely spaced grabens during the Quaternary (Price and Scott, 1992).

The observed fault/lineament directions for the area, summarised in Table 6.2, are in agreement with each other and with the new data and thus support the model presented below.

Price and Scott (1994)	Burdur grabens	NW-SE	normal
Du Poux (1983)	Aksu basin	N-S, NW-SE	σ_3
	Bey Dağlari	ESE-WSW	σ_3
		NNE-SSW	σ_2
Değirminci and Günay (1992)	Köprü basin	NNW-SSE	normal
		NW-SE	right-lateral
		NE-SW	left-lateral
Aydar and Dumont (1979)	Aksu basin	NE-SW	1st generation
		NW-SE	2nd generation
		N-S	3rd generation

Table 6.2: Published fault lineament directions in the Isparta angle region.

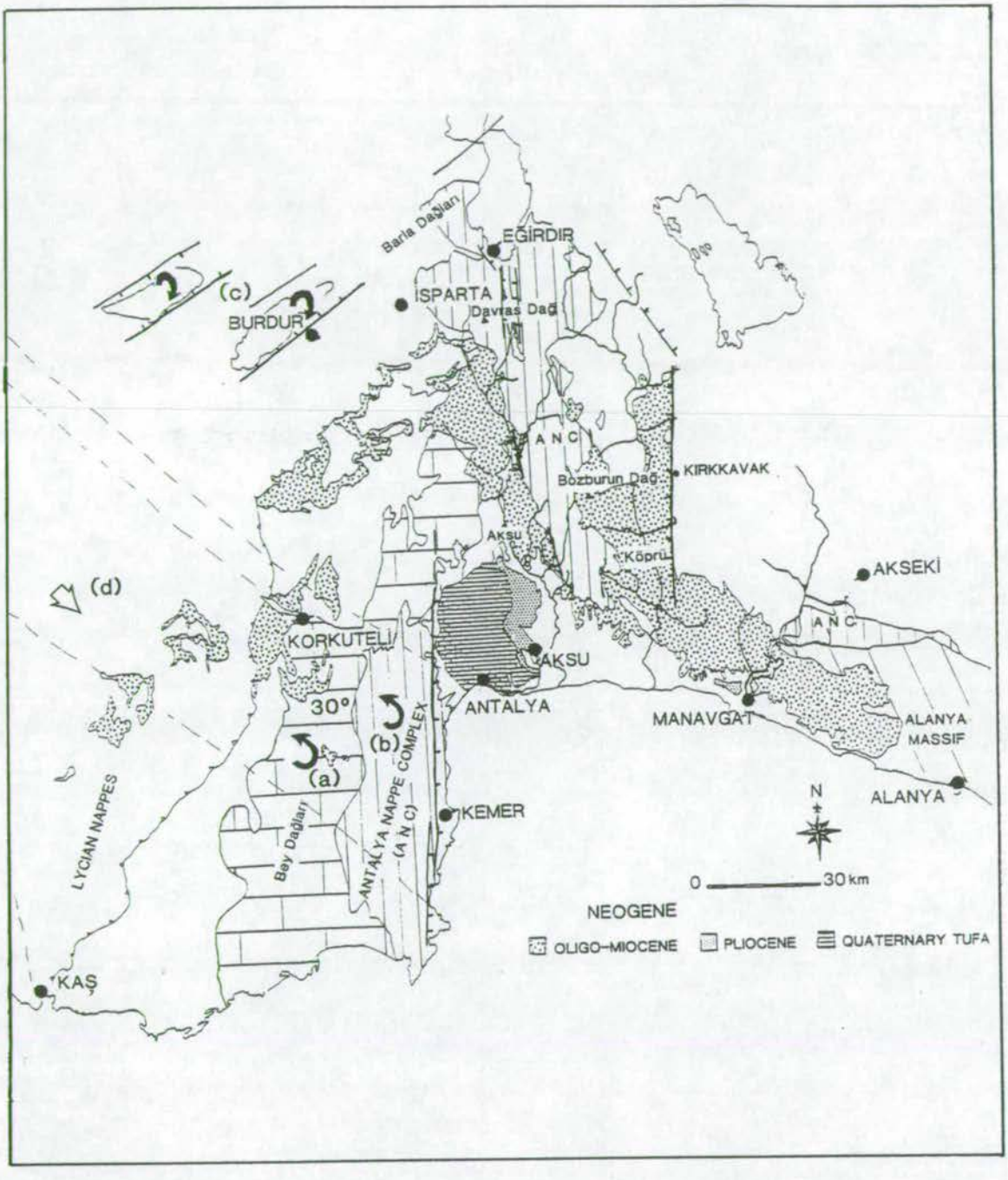

Fig. 6.9: Summary diagram of the observed tectonics of the Isparta angle and the Burdur region (a) Palaeomagnetic observation of Kissel and Poisson (1986); (b) Palaeomagnetic observation of Morris and Robertson (1993); (c) Burder and Acigöl graben model of Price and Scott (1994); (d) Transport direction of Kocaefe and Ataman (1976). The fine lineaments defining the region are from their observations.

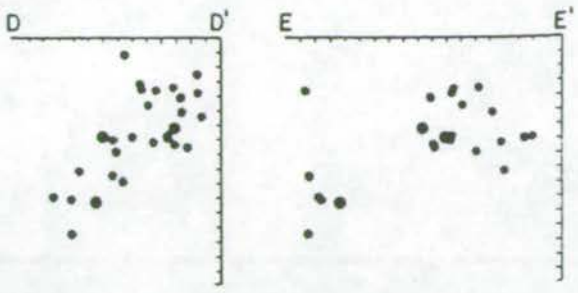

Fig. 6.10: Cross sections of seismicity in the Antalya Bay, associated with the Cyprus margin from Rotstein and Kafka (1982)

6.3: Seismic evidence for structure in the Antalya basin

6.3.1: Seismicity studies

Rotstein and Kafka (1982) describe the seismicity of Antalya Bay. Deep seismic activity is associated with a detached subducted slab north of the Anaximander Mountains, distinctly different from the present-day active subduction. (Fig. 6.10 part of their Fig. 6 note that 6b and 6c are nearly perpendicular to each other)

The 4 fault plane solutions for the Antalya area presented in Jackson and McKenzie (1984) are all associated with this remnant slab and are predominantly low-angle thrusts with one strike-slip solution. Earthquake epicentres reported during 1961-1980 for the region are plotted. They show earthquakes at depths of 50-100 km in Antalya Bay and >100km under Antalya itself. Some earthquakes between Antalya and Eğirdir are marked as shallower than 50km but no fault plane solutions are available (Fig. 6.11). Thus, at present, modern seismicity can add little to our knowledge of the neotectonics, except to suggest that current activity is limited to the western basin margin.

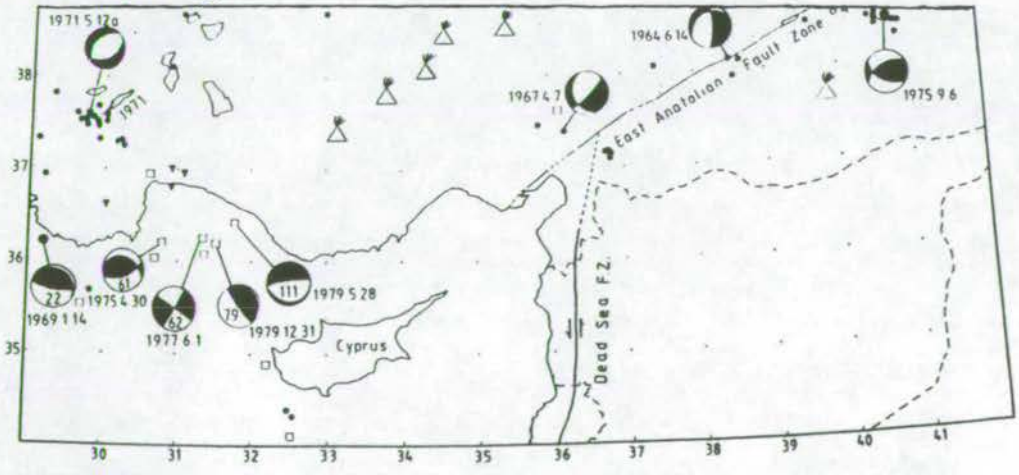

Fig. 6.11: Earthquake epicentres in the Antalya region (1961-1980): Jackson and McKenzie (1984)

6.3.2: Seismic reflection data

The seismic data from Antalya Bay have already been discussed in chapter 3. The 5 available lines are presented here as a fence diagram (Fig. 6.12) in order to show the structure of the basin, related to the coastline and to the bathymetry (inset). As discussed in chapter 3 the data are of poor quality and it is intended to provide an indication of the structural style of the basin rather than an exact interpretation. The most important result arising from the seismic data is that the Pliocene sediments are deposited on a block-faulted topography. This topography defines a graben which widens to the south. Sediment channels are identified within this graben, indicating a long-axis transport direction. The sediments which have been correlated with the marine Pliocene deltaic sediments are situated on the eastern block. They infill a block faulted topography, but only a few of these faults cut through the sediment packages. Only small syn-rift packages are present and it is thus inferred that normal faulting post-dated deposition of the marine Pliocene. The overall basin structure is that of a graben, although the faults on the western basin margin are smaller than those on the east, if the onshore Kemer faults are included.

6.4: Mesofracture analysis of the Taurus Mountains and Antalya basins

We have already seen in the previous chapter that the landscape is dominated by large-scale, normal fault scarps, grabens and terraces which result from significant normal faulting in the region, probably sometime during the Quaternary. This chapter is concerned with the analysis of brittle mesofractures in an attempt to quantitatively define the regional stress regime. Eyal and Reches (1983) considered that kinematically diagnostic mesostructures can yield more reliable stress directions than macrostructures. In terrains of weakly deformed sedimentary rocks mesofractures may be the only widespread structures present. However, "they are more reliable indicators of regionally significant stress strain trajectories in weakly deformed rocks than in thrust-fold belts, grabens and transcurrent fault zones where there may have been substantial vertical or horizontal rotations" (Hancock, 1985). In this study particular care must be taken to recognise areas where significant rotations may have occurred. As already shown in the earlier part of this chapter the complex tectonic regimes of western Turkey are often responsible for rotation about vertical axes. That these rotations have affected the study area is verified by the palaeomagnetic data of Kissel and Poisson (1986a, 1986b), Morris and Robertson (1993) and Kissel *et al* (1993).

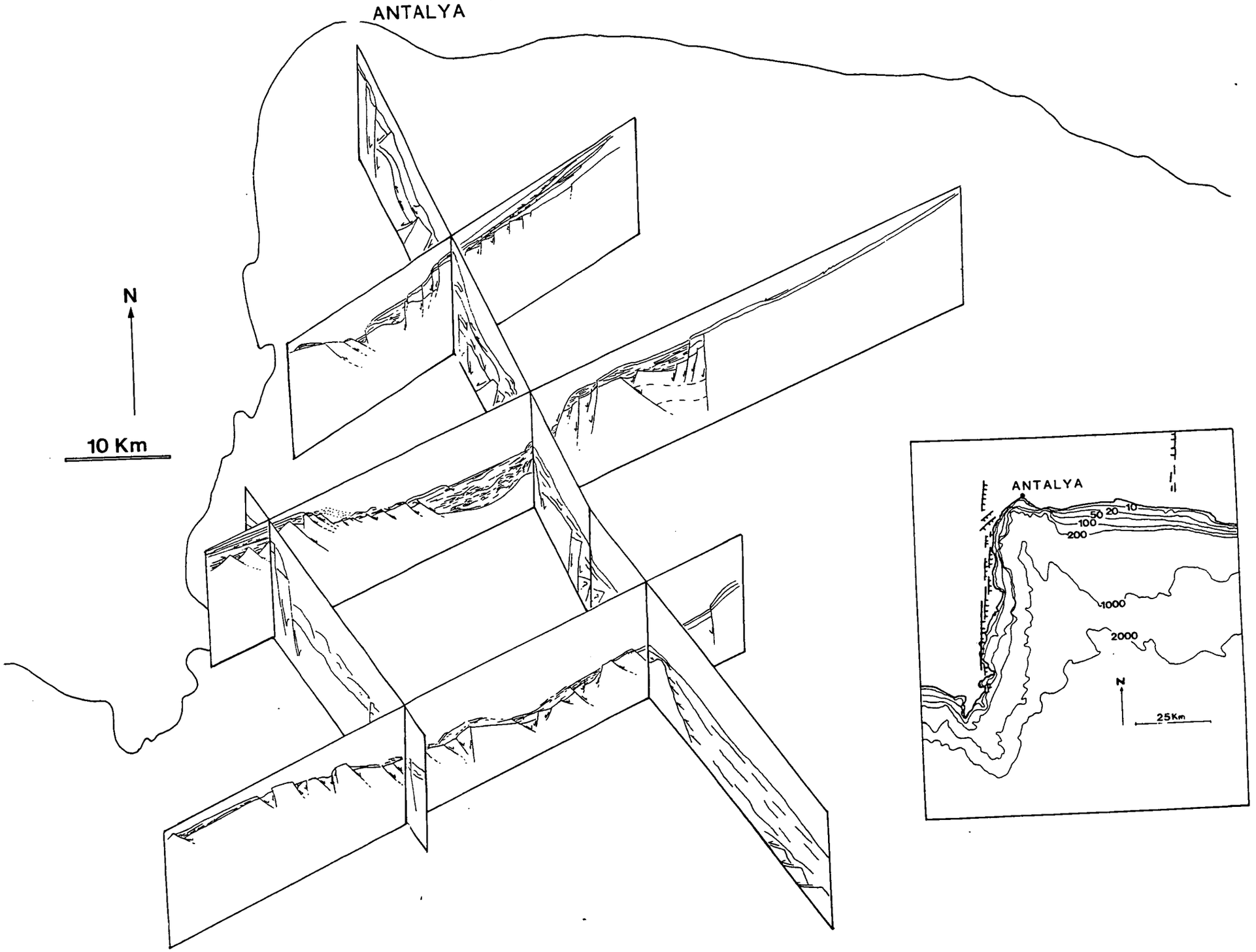

Fig. 6.12: Fence diagram of interpreted MTA seismic lines in Antalya Bay.

The strong tectonic fabric in the area discussed in section 6.2.1 is liable to reactivate in appropriate stress fields. It has been shown that the East African Rift zones, Lakes Tanganyika and Malawi (Versfelt and Rosendahl, 1989; Scott, Etheridge and Rosendahl 1992) are strongly controlled by the pre-existing fabric. It is shown that these rift zones consist of a number of half grabens, the polarity of which switch down the rift valley. The overall orientation of the valley is influenced by major pre-existing sub-vertical fault zones. Complex accommodation zones act as transfers between the main bounding faults. Scott *et al* (1992) analysed the dip directions of imaged blocks to find the direction of maximum fault block rotation and showed that the extension direction is oblique to the trend of the regional rift axis. They found a dominant compartmentalisation of structures into SE-ESE and NW-WNW directions in a NW-SE extensional field. This is interpreted as reflecting the predominance of pre-existing structural control on the overall geometry of the basin. However, the individual dips of blocks still give an indication of the regional stress field. In this way, the smaller scale structures provide a better impression of the overall kinematics of the area than the macro-stucture.

Structural data were collected throughout the region in areas where significant numbers of fault plane measurements could be made. Measurements were made on meso-scale (a few centimetres to a few metres) scarps of all quality. In practice, large polished fault planes are very rare and measurements were usually made on centimetre scale planes, often with only traces of slickenfibres remaining. These slickenfibres were used to ascertain the sense of motion. Occasionally other kinematic indicators, such as pits and frictional wear were used. Hancock (1985) recommended that data of this type be collected from small sampling sites, in structurally homogeneous domains away from major faults. This principle was largely adhered to, although often data were not sufficiently abundant and larger, rather scattered, areas were used to represent a region. Areas close to major neotectonic fault lineaments (e.g. Kemer, Kirkkavak) were studied on the grounds that the fault style is relatively simple in these areas, consisting of zones of high-angle normal faults. It is possible that detachment along the layer of Messinian evaporites occurs, but this is not indicated on seismic profiles. It is, therefore, assumed that the mesofaults belong to the same class as the associated macrofaults.

Most data were collected from Mesozoic limestones of the Taurus mountains. Nearly 1000 measurements were taken in total. The limestones behaved in a brittle manner and formation of slickenfibres was common. In contrast, fault planes in the Neogene sediments rarely have kinematic indicators, and can often only be seen when the section is freshly cut. In the unconsolidated Pliocene sediments, in

particular, fault planes were often taken by sighting. Kinematic indicators are extremely rare. The principal problem with this is that faulting cannot definitely be tied down to a period unless it is seen to cut through sediments prior to that period. Thus, measurements for Cretaceous limestones can only show that faulting occurred post-Cretaceous. However, if patterns of faulting in the Mesozoic can be shown to be similar or the same as patterns of faulting in the Neogene, then it is reasonable to assume that all the faulting measured relates to the same tectonic events. This means that kinematic indicators from Cretaceous and earlier limestones may be used to infer Neogene tectonics. In this case we also have good control on the Mesozoic history of the region. It is known that compression during the late Miocene tilted some Miocene sediments to almost vertical. Faults measured in these sediments, which cut the vertical sediments steeply, are inferred to be post "Aksu" phase compression. In addition an understanding of the underlying tectonic fabric enables us to assess the amount of reactivation.

Regions where concentrated data were collected are indicated on the map in Fig. 6.13. Localities are numbered according to their appearance in the text. The general appearence of the mesofractures, density of data, quality of data and results from each of these areas will be discussed below, working clockwise from the southwest. Data were plotted on rose diagrams and equal area, lower hemisphere stereographic projections using Stereoplot for Apple Macintosh©. Left-lateral, right-lateral and normal faults, where determined in the field, were plotted separately. No assumptions were made about the sense of a fault if it could not be determined from kinematic data. Patterns of faulting shown by all data can then be compared with the plots of kinematic data. Rose diagrams were plotted of strike direction (non-directional), dip of fault planes and pitch of the slickenside direction i.e. the plunge direction of the slickenside measurement. In general, all the measured faults were steep, plotting between 45° and 90°.

6.4.1: Western basin margin - Kemer and Olympos

In the previous chapter it was shown that the coastal section from Antalya to Kemer is dominated by large neotectonic, normal fault scarps. These major normal faults are inaccessible. Along the main road section new cuttings have been made through the limestones exposing numerous small fault scarps. One hundred and thirty-one meso-fault planes were measured, of which 77 had measurable kinematic indicators; a sense of movement was clear from 65 of these. No superposition of slickensides was observed.

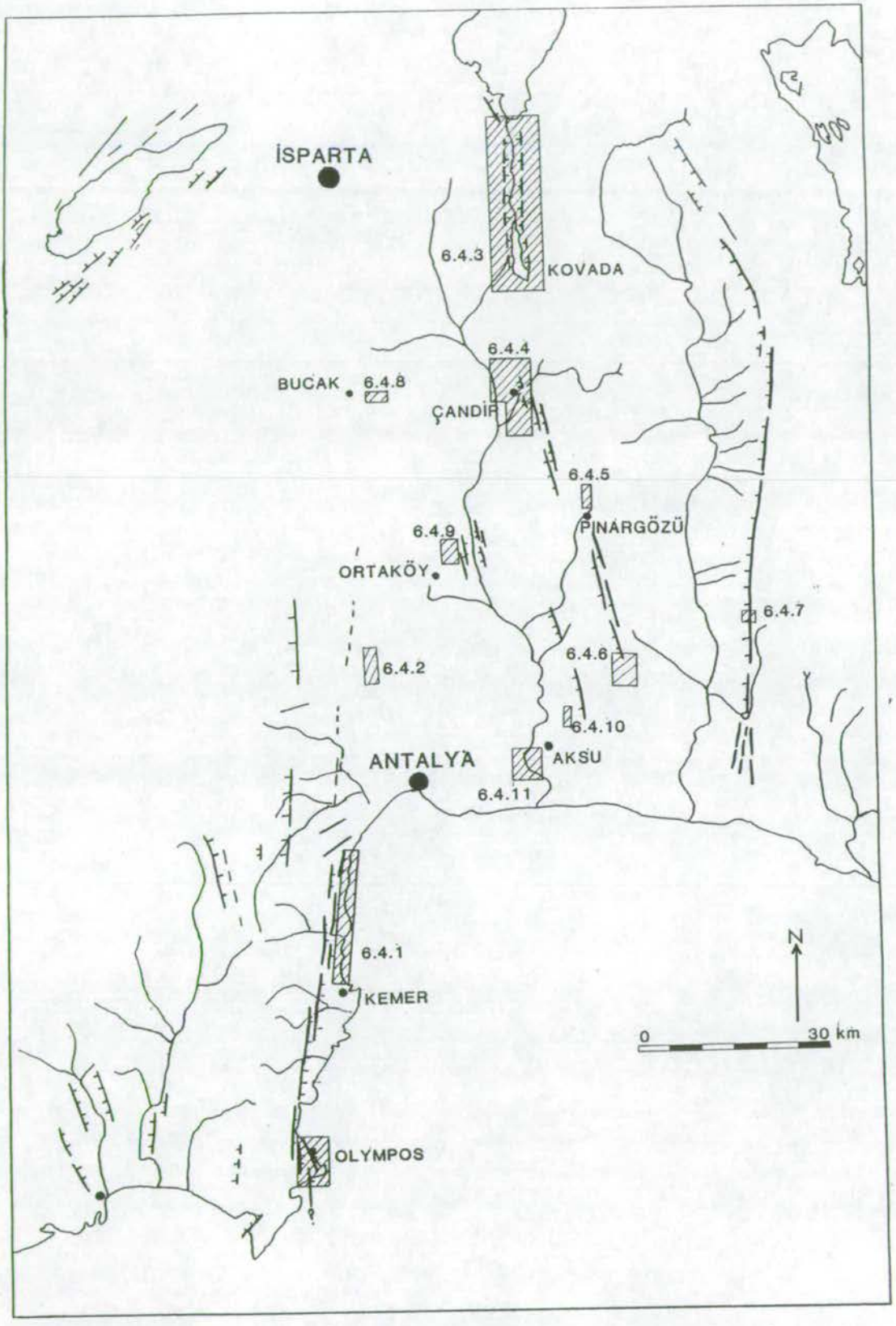

Fig. 6.13: Map of the Isparta angle showing major neotectonic lineaments and meso-fracture data collection localities. The localities are numbered according their section number in the text.

The stereographic projections (Fig. 6.14) and rose diagrams (Fig. 6.15) of directional data clearly show right-lateral faults running NE-SW and NW-SE. The stereographic projection plot of all data is more scattered, but generally accentuates the clusters shown in the plot of data of known kinematics. Normal faults are well clustered around the direction NNE-SSW. The Kezme gorge data, in contrast, show predominantly left-lateral slip with a dominant E-W orientation and some NW-SE faults. This is interpreted as a linking transform between two fault strands of the main Kemer lineament. The Olympos data were collected from the back of Olympos beach and from the mountain immediately to the south of Adrasan bay. This area represents the southernmost expression of the lineament before it runs offshore. It is clear that the data (Fig. 6.16) give almost identical results, except that the dip direction of the fault planes is more to the SW in the Olympos area and to the NE in the Kemer zone. This is almost certainly a function of the geometry of the particular areas. It can be confidently stated that the Antalya-Kemer lineament is a zone which has undergone extensive right-lateral shear. The current normal nature of the fault scarps masks this and is the product of NNE-SSW faulting which is also strongly picked up in the mesofracture analysis. Thus, a period of right-lateral shear preceded a period of normal faulting. A graph of dip of the plane versus pitch of the slickensides for normal and right-lateral faults (Fig. 6.15ii) shows that the measured normal faults are very close to pure dip-slip (black line) whilst the right-lateral faults are distinctly oblique slip.

6.4.2: Western basin margin - main Antalya road

Where the main road from Antalya to Isparta leaves the upper tufa plateau and ascends into the Taurus mountains the cuttings once again pass through Mesozoic carbonates which display numerous mesofault planes, including a few very striking polished surfaces, a few metres across. This region is not in the vicinity of a major set of fault scarps. Along this stretch of road, before the steep ascent begins, 74 fault planes were measured, yielding 25 kinematic indicators, and 20 sense directions. One plane had superposition of a more normal slickenside on a strike-slip direction. All data cluster around a NW-SE direction (Fig. 6.17) and no differentiation can be made between normal, left-lateral and right-lateral faults on the basis of strike directions. The full data set plotted as slickensides on great circles (Fig. 6.18) suggest that many of these NW-SE trending faults are normal.

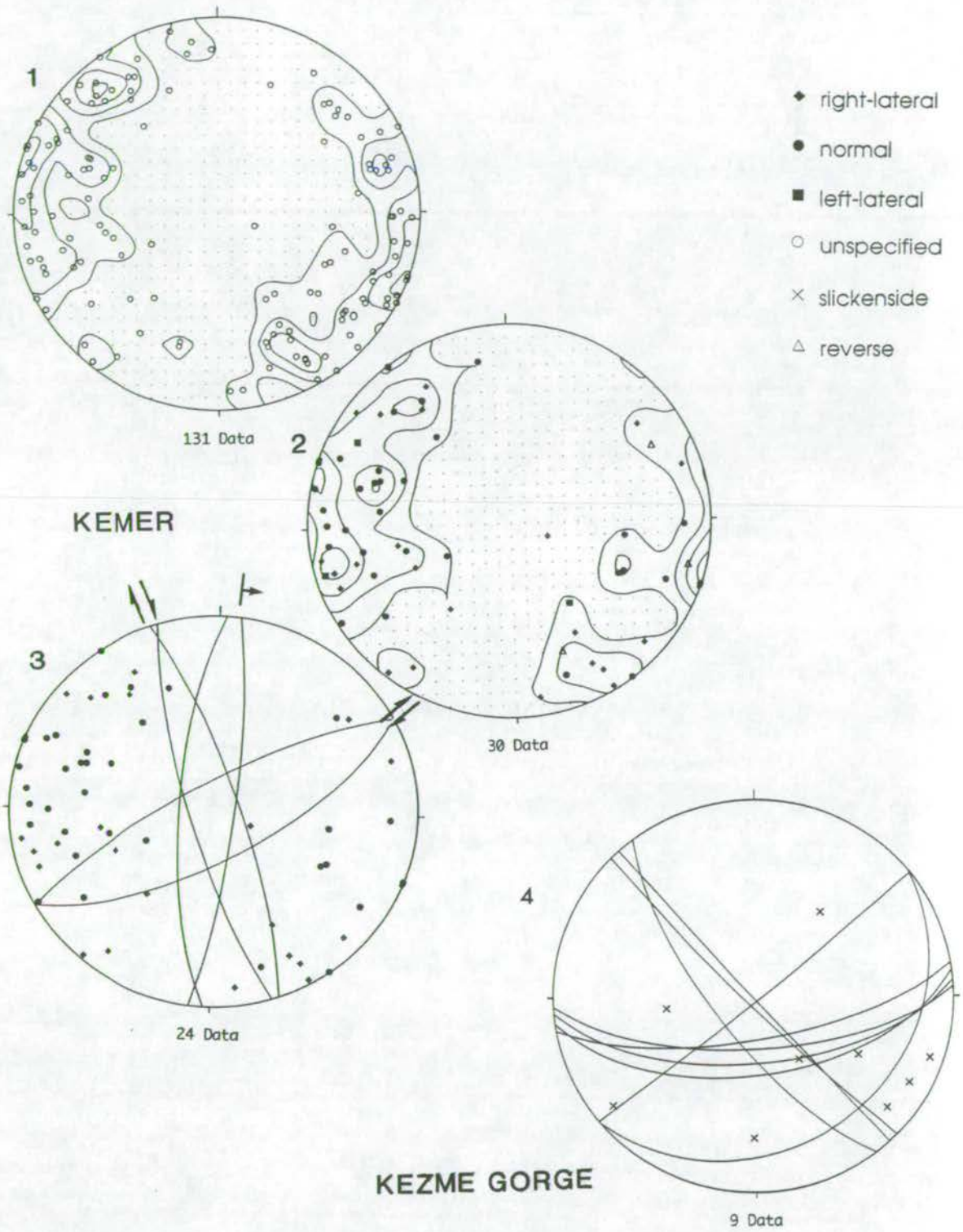

Fig. 6.14: Stereographic projections of poles to planes from the Kemer zone and from Kezme gorge. **1** = contoured plot of poles to planes of all data from the Kemer zone. **2** = contoured plot of poles to planes of data with known sense direction. Note that approximately the same regions are defined as in 1. **3** = plot of poles to planes for normal and right-lateral faults, with great circles of typical planes included. **4** = plot of poles to planes of data from Kezme gorge, interpreted as a transform between two normal faults.

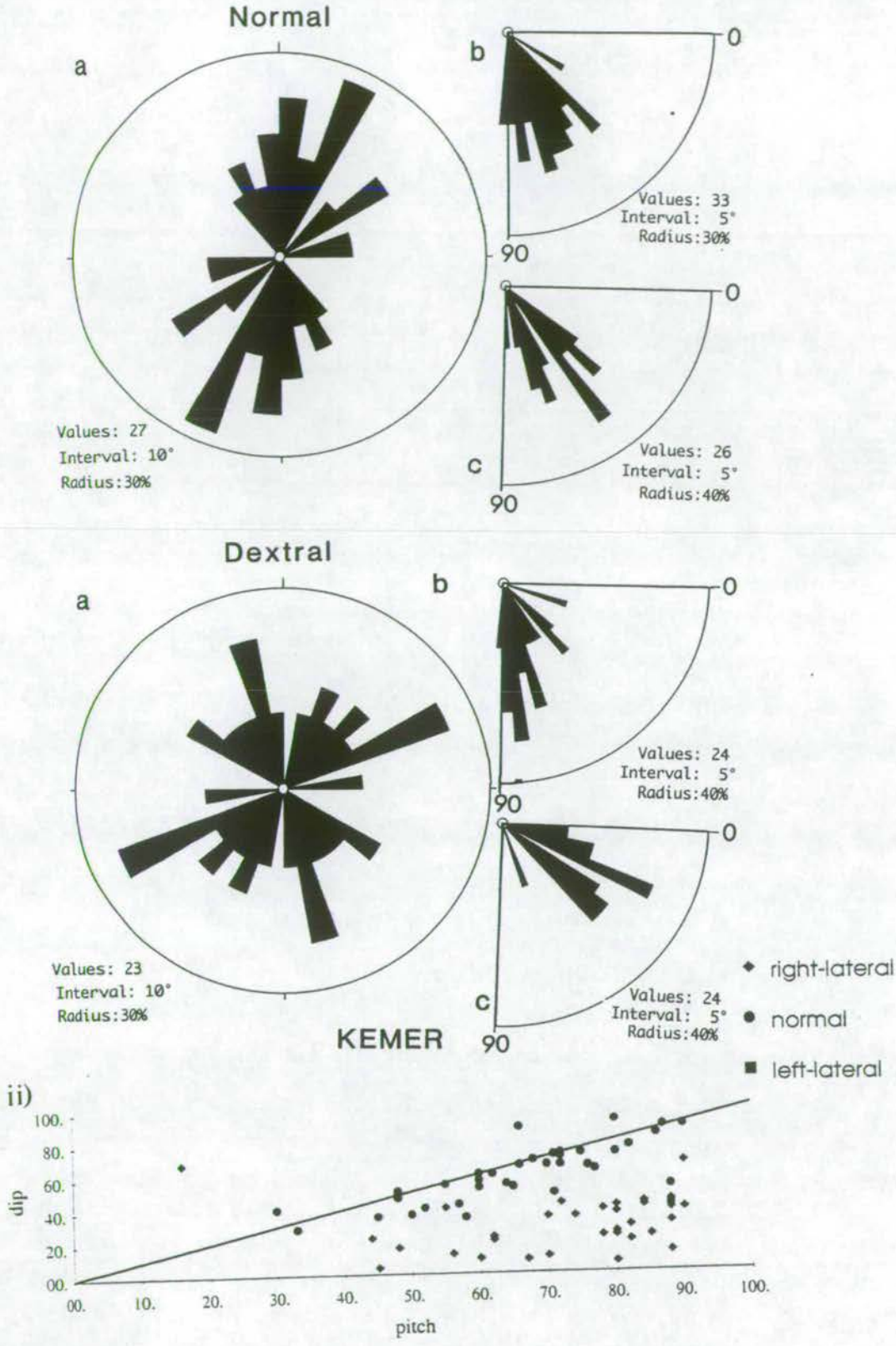

Fig. 6.15: i) Rose diagrams of normal and right-lateral faults measured in the Kemer zone. a) fault plane strike (non-directional) b) fault plane dip c) pitch of slickensides ii) plot of dip versus pitch of the faults. The solid line represents the plot of pure dip slip faults. The normal and right-lateral faults are clearly distinct.

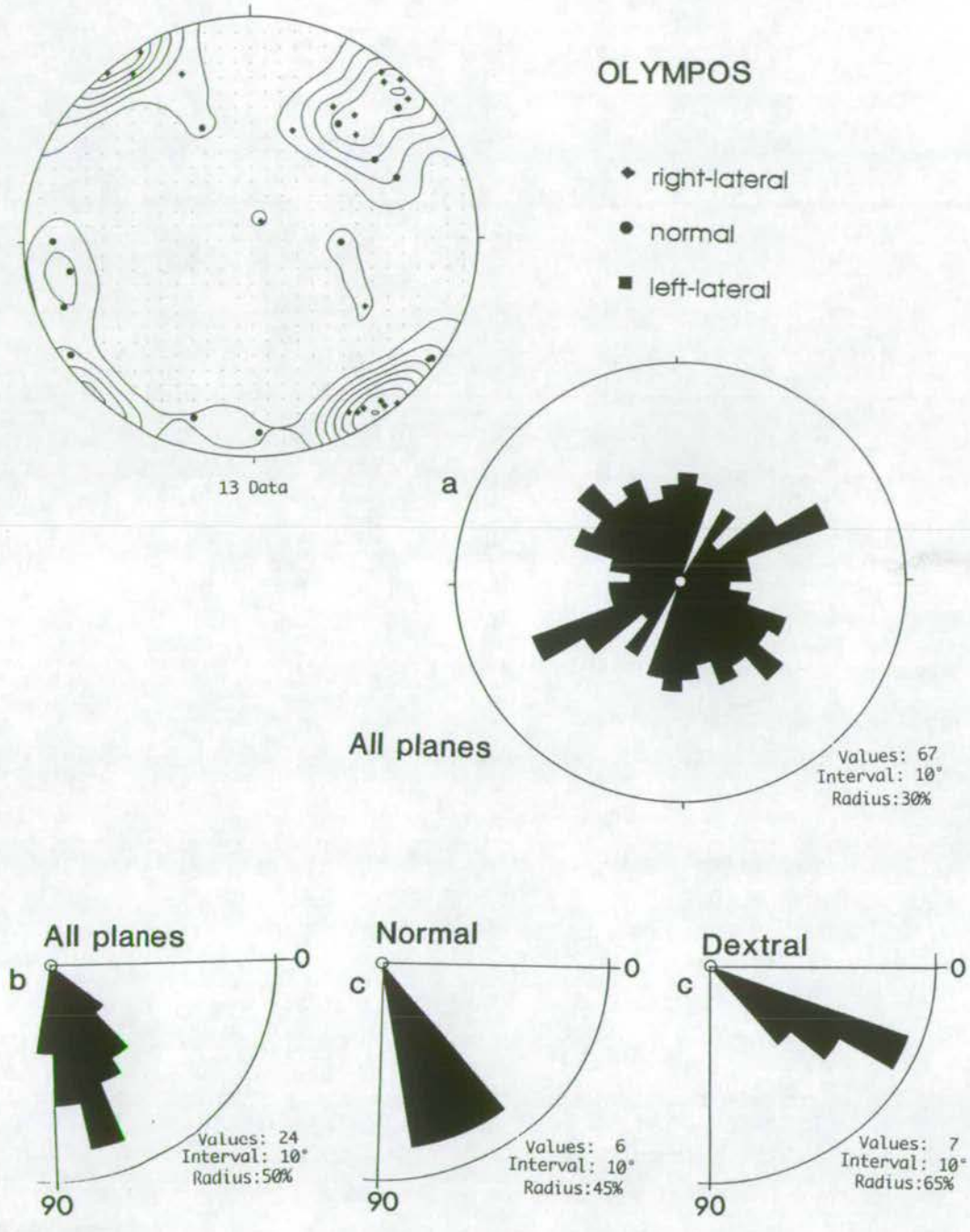

Fig. 6.16: Stereographic projection and rose diagram of fault plane measurements from the Olympos area. Note the similarity between these and the data from the Kemer zone. a) fault plane strike (non-directional) b) fault plane dip c) pitch of slickensides

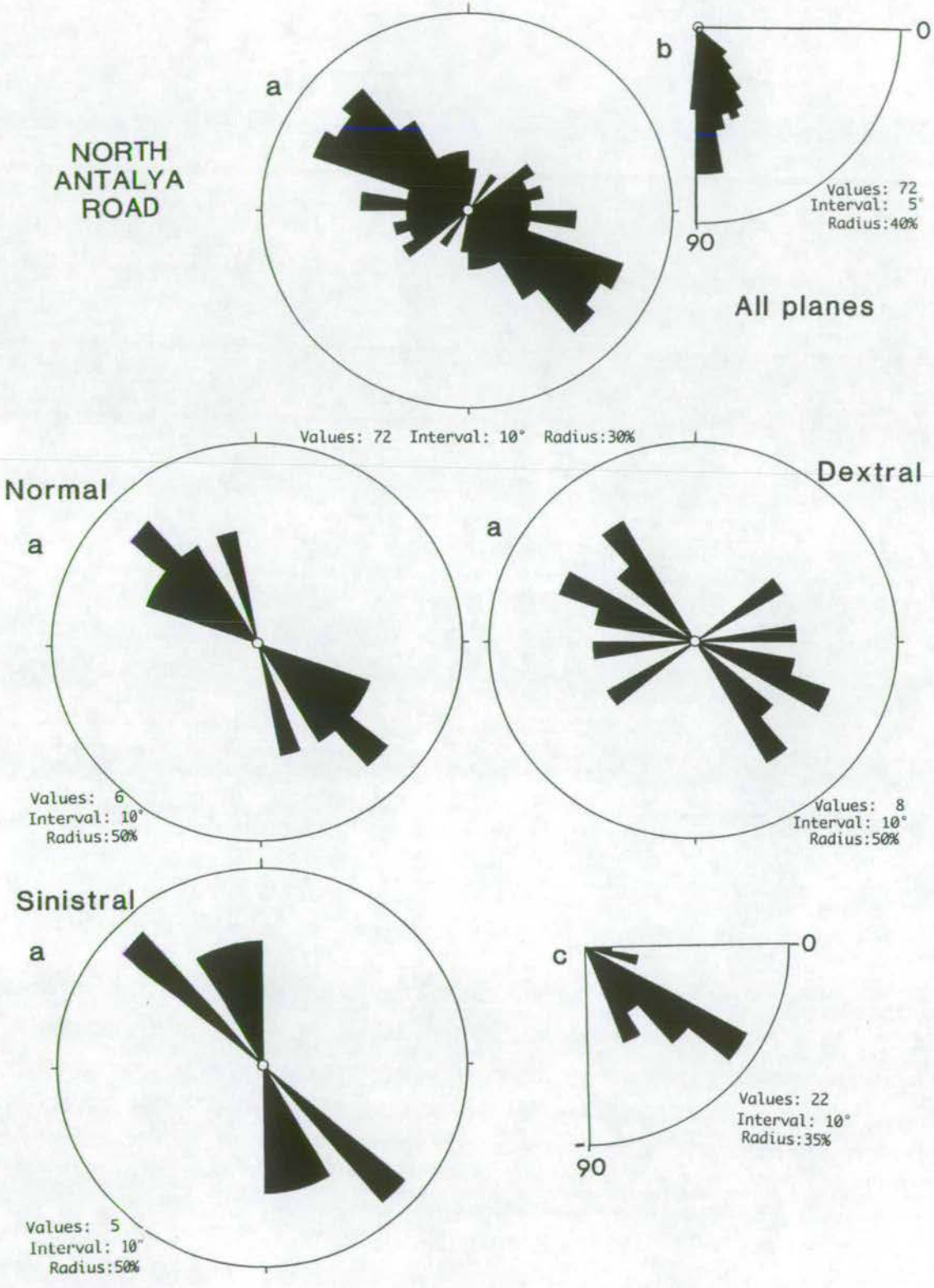

Fig. 6.17: Rose diagrams of faults on the North Antalya road. The plot of all data clearly shows that all faults follow the same trend. This is interpreted as the result of a strong pre-existing structural fabric in the area. a) fault plane strike (non-directional) b) fault plane dip

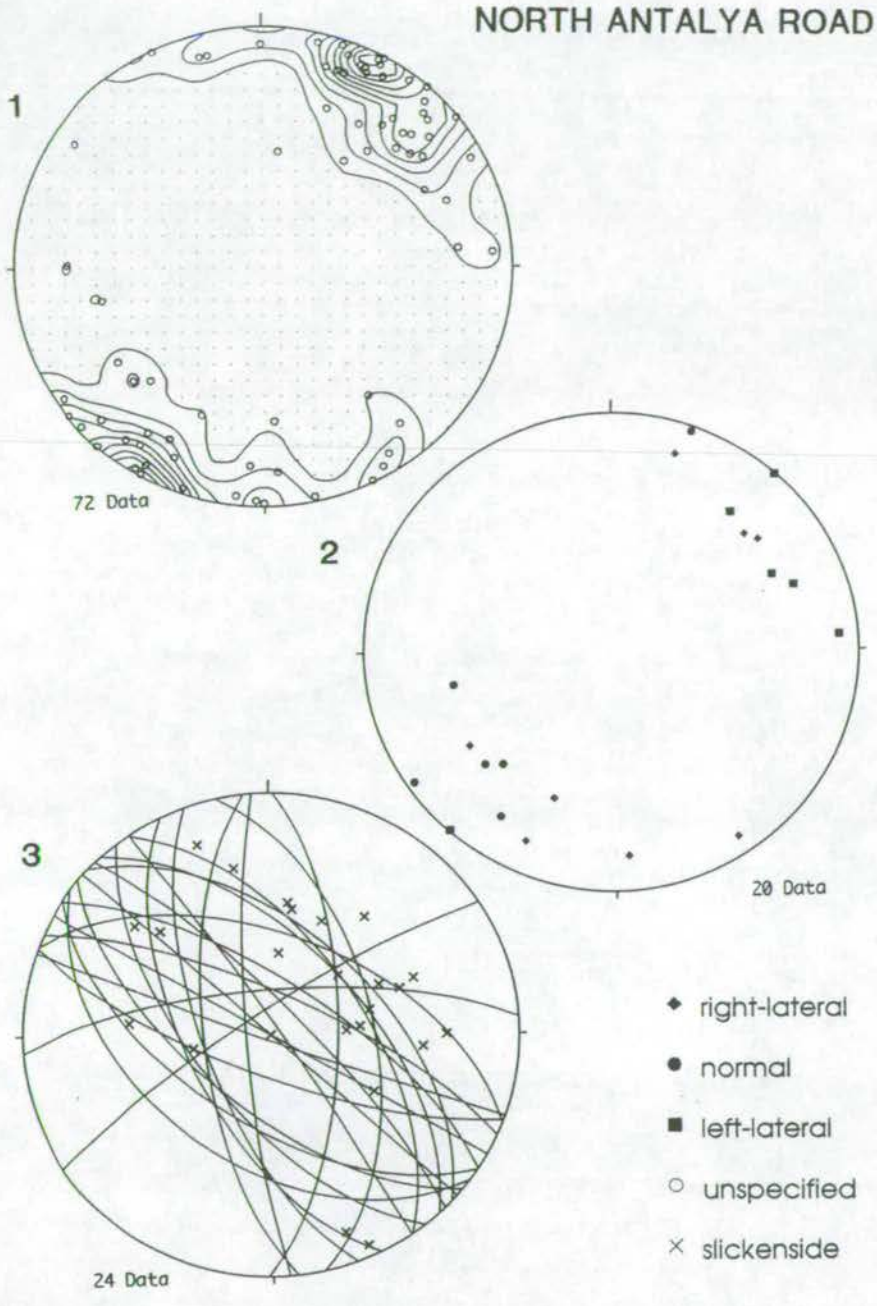

Fig. 6.18: Stereographic projections of faults on the North Antalya road. **1** = contoured plot of poles to planes of all data. **2** = plot of poles to planes of data giving a sense of movement. **3** = all data plotted as great circles with slickenside pitches plotted as crosses. Note the clustering of the data and the mix between normal and strike-slip movement.

6.4.3: Northern Taurides - Kovada graben

The Kovada graben is a linear graben, 25km long and 2-3km wide, running north-south from the southern end of Eğirdir lake. Kovada lake is situated at its southern end. The lake has retreated significantly in historical times and local reports of it filling much of the graben can still be heard. Despite the clear graben structure of this depression active fault scarps are not present and finding any trace of faulting is difficult. A total of 43 small, planes with slickensides were found on the eastern and western sides of the graben. The prominent fault direction is scattered around N-S, but is not N-S (Fig. 6.19), and it appears that the majority of the faults measured were not parallel to the graben edges. Slickenside data plotted on great circles show that many of the faults are normal. Splitting the data into that from the eastern and western margins of the graben (Fig. 6.20) shows that the western side is dominated by NNW-SSE and NE-SW strike directions and the eastern margin by NNE-SSW and NW-SE strike directions. The two sides are, in fact, not far off mirror images of one another. The mesofracture data does not directly reflect the overall graben orientation, but is more closely related to the other areas studied.

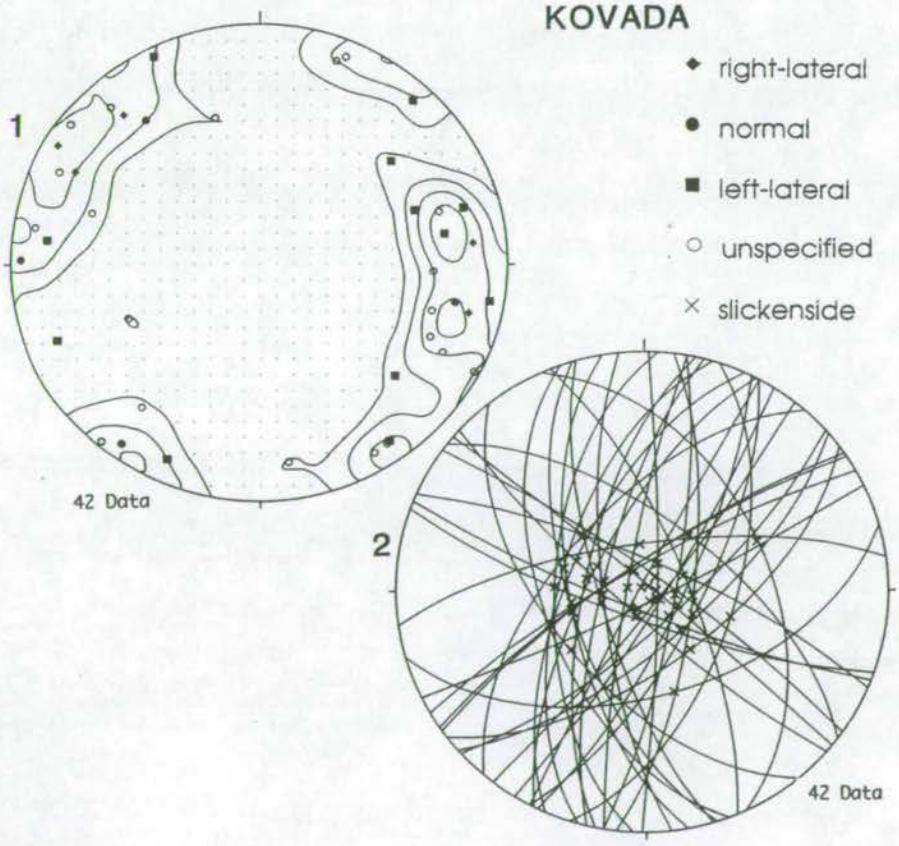

Fig. 6.19: Stereographic projections of faults measured in the Kovada graben. **1** = contoured plot of poles to planes of all data with sense data included. **2** = great circle plot of all data with slickenside pitch marked as crosses. Most faults are close to normal, but some strike-slip faults also exist.

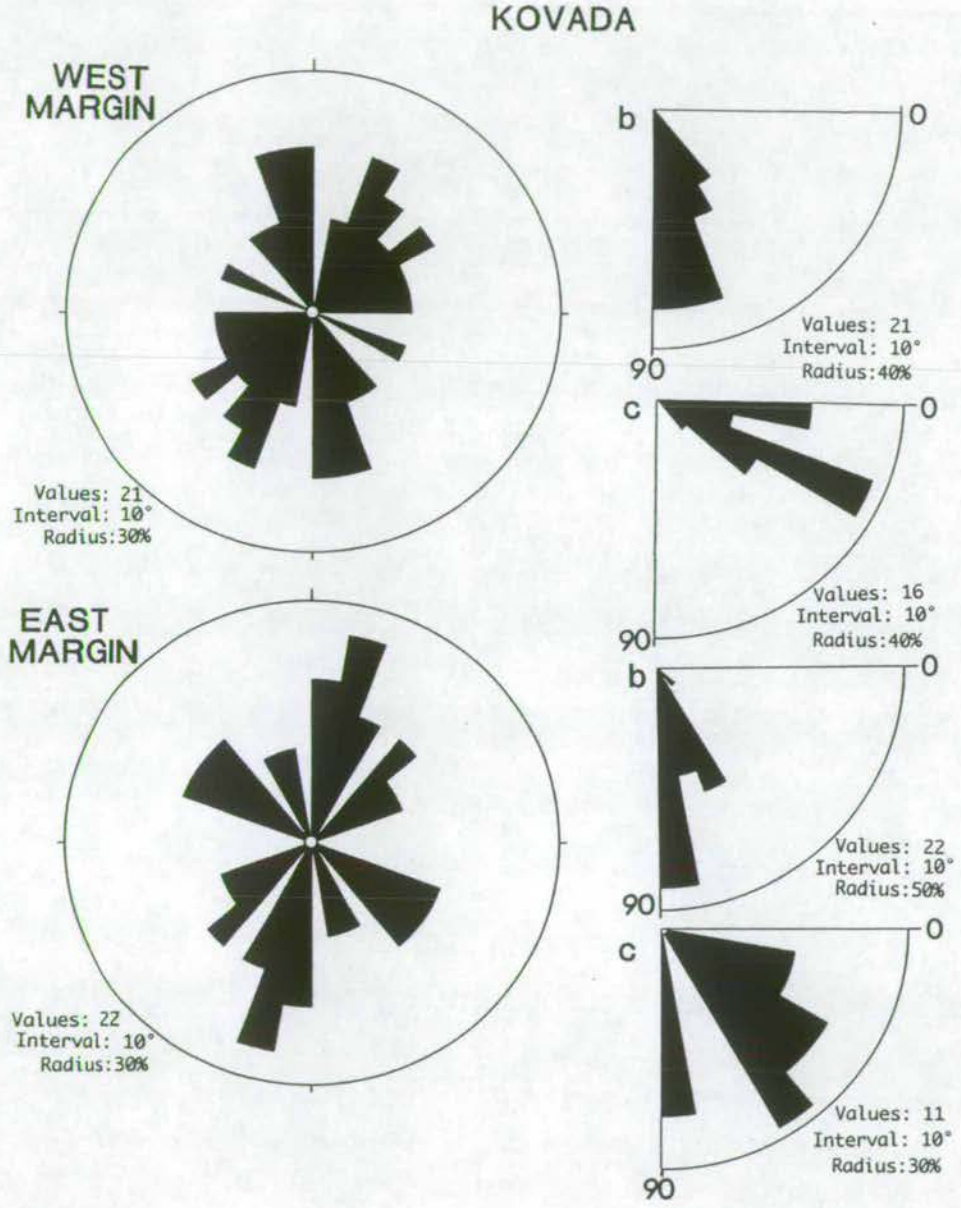

Fig. 6.20: Rose diagrams of fault data from the Kovada graben. Data from the west margin and east margin are presented separately. a) fault plane strike (non-directional) b) fault plane dip c) pitch of slickensides.

6.4.4: Central Isparta angle - Çandir

Çandir lies to the south of the Kovada graben, in the heart of the Taurus mountains. Travelling southwards on the road leading directly from the southern end of the Kovada graben to Çandir it is striking that directly to the east of Çandir village there are numerous steep, largely N-S trending, neotectonic normal faults which are not seen between the area and the Kovada graben. Once again it was not possible to come within the vicinity of the major scarps.

Fault data were rather sparsely distributed, often only a few measurements of small planes could be made in the area of one outcrop. In order to avoid random data collection in this rather distributed area care was taken to measure only those planes which showed slickensides or those that were very obviously fault planes. One hundred and forty three fault planes were measured along the roads marked on Fig. 6.24. A total of 53 sense directions were found on 128 striated planes. Superposition was observed on one plane and indicated that normal faulting occurred post left-lateral faulting.

In contrast to the Kemer lineament, where the vast majority of strike-slip faulting was right-lateral, both left-lateral and right-lateral faults are present. Left-lateral faulting is, however, more common. As shown on the rose diagrams (Fig. 6.21) and stereoplots (Fig. 6.22) the left-lateral faulting occurs dominantly in two directions NNE-SSW and NW-SE. Right-lateral faulting tends to be in a NE-SW direction, although is rather poorly defined, and normal faulting is in NNW-SSE (tending towards NW-SE) and NNE-SSW orientations. The normal and right-lateral fault trends lie approximately along the line of the major fault scarps seen in the area. Along the valley edge one ridge clearly shows right-lateral offset of the ridge with a flat dividing fault scarp between the two sections (Fig. 6.23). The gorge just to the north of Çandir shows predominantly strike-slip faulting (Fig 6.22) and is interpreted as a transform between fault strands, comparable to the Kezme gorge on the Kemer lineament.

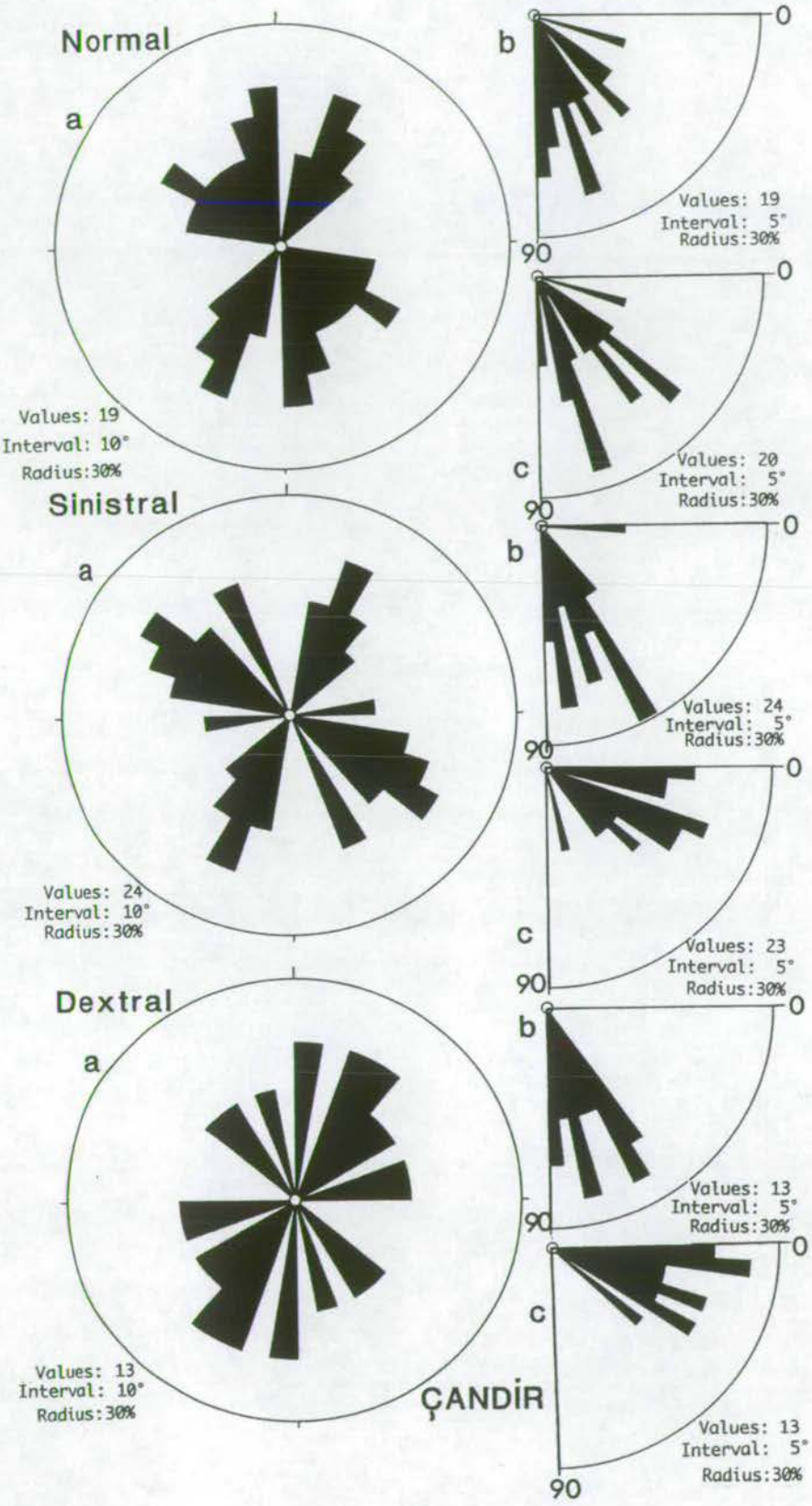

Fig. 6.21: Rose diagrams of faults measured in the Çandir region. a) fault plane strike (non-directional) b) fault plane dip c) pitch of slickensides.

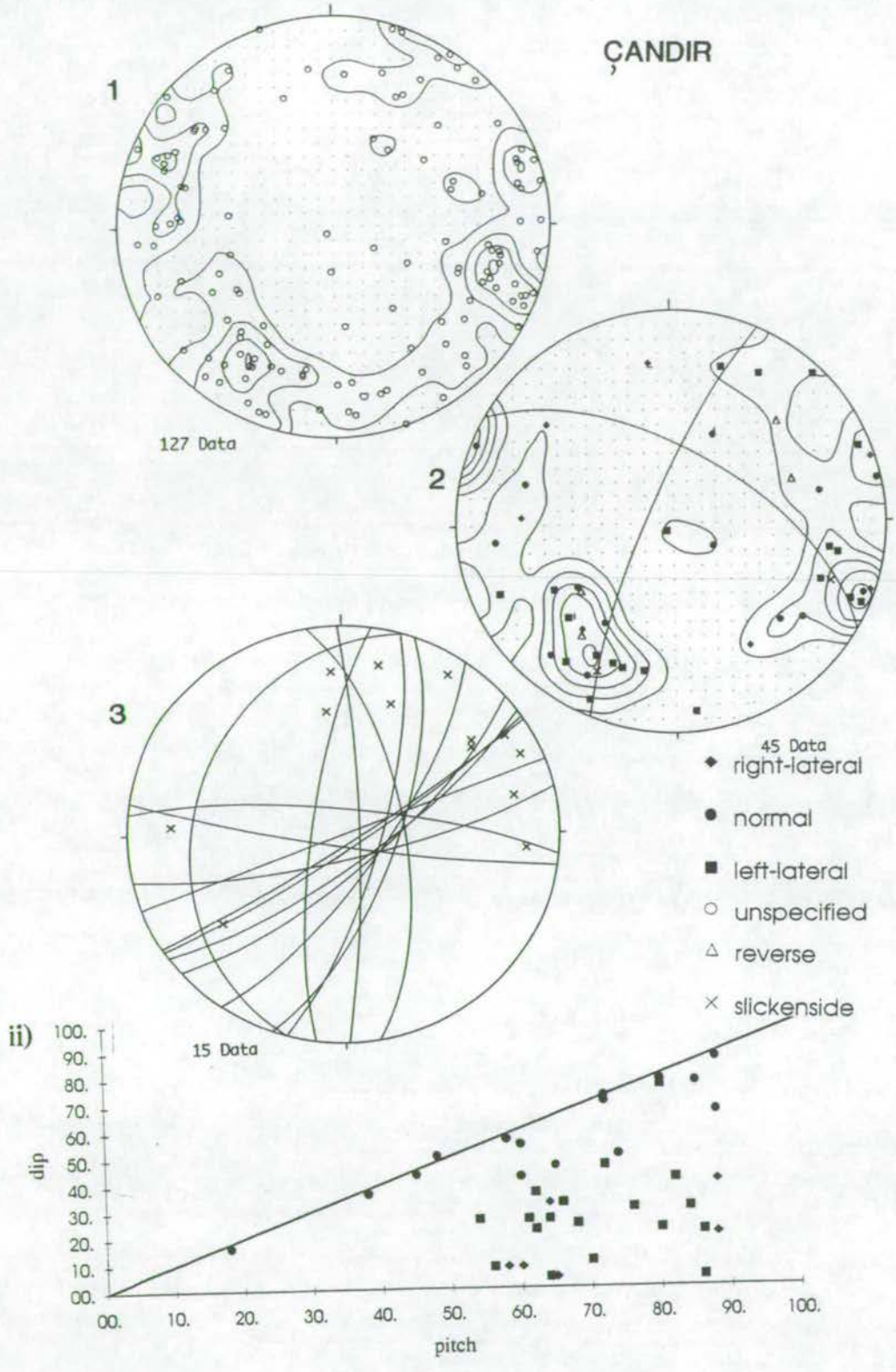

Fig. 6.22: Stereographic projections of faults measured in the Çandir area. **1** = contoured plot of poles to planes of all data. **2** = plot of poles to planes of data with known sense directions. Two typical planes are also plotted as great circles. **3** = plot of poles to planes of data from the Çandir gorge. The slickensides show predominantly strike-slip movement. This is interpreted as a transform similar to the Kezme gorge in the Kemer zone. ii) plot of dip versus pitch of the faults. A separation exists between the normal and strike-slip faults.

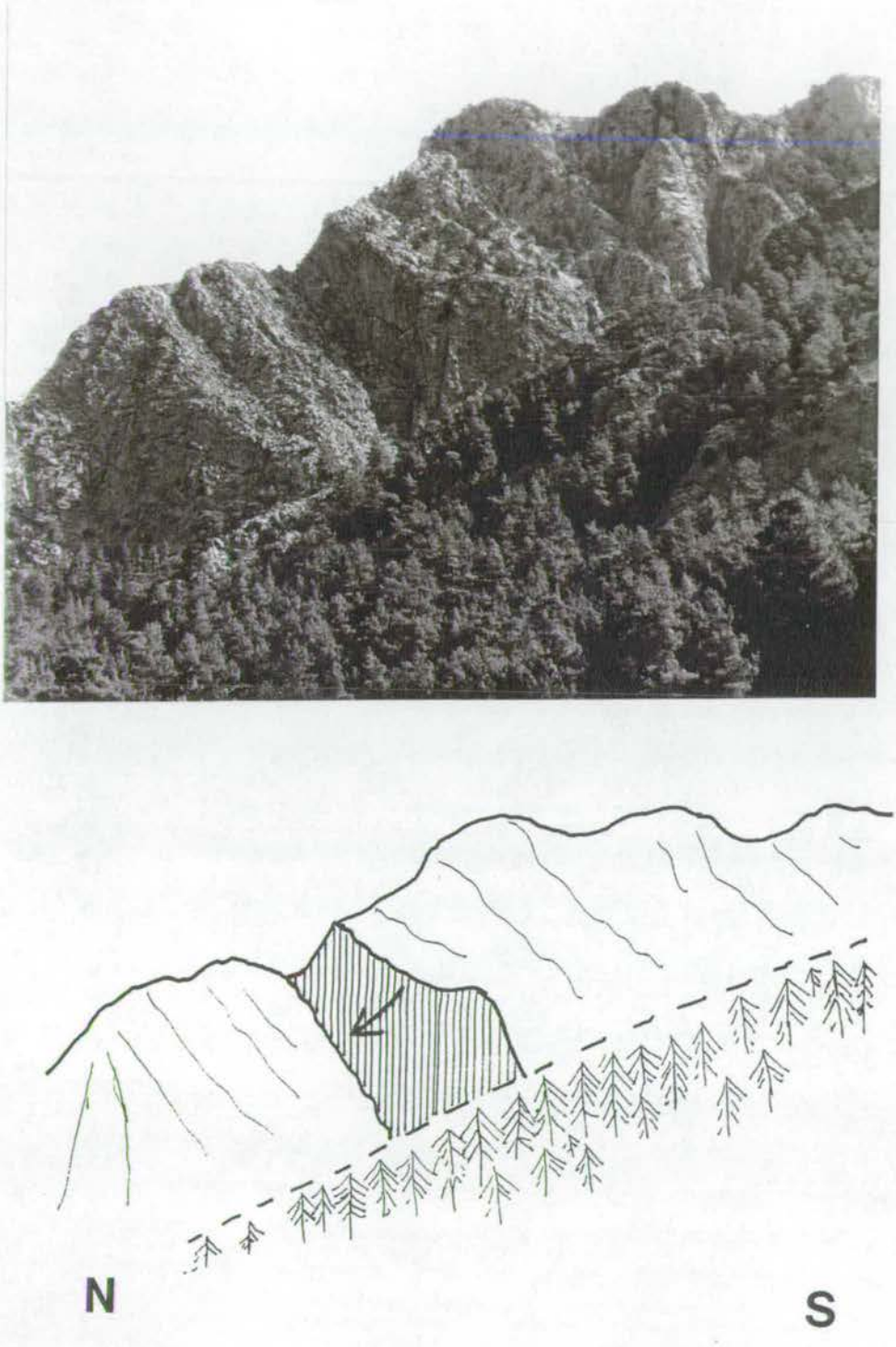

Fig. 6.23: Photograph and field sketch of one of the major fault scarps in the Çandir region. The ridge on the mountain has been offset in a right-lateral sense.

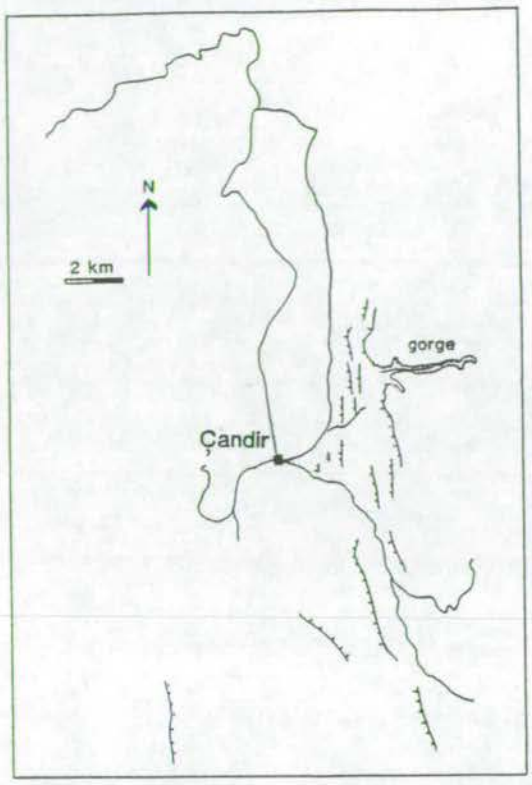

Fig. 6.24: Sketch map of the Çandir area. Data were collected along the marked roads. Note the set of fault scarps developed to the east of Çandir itself.

6.4.5: Eastern Aksu basin margin - Pinargözü

The lineament at Pinargözü is a strong NNW-SSE trending limestone block containing numerous mesofault scarps, the majority of which have good slickenside lineations. Normal, reverse, right-lateral and left-lateral senses were observed. On 78 measured planes 73 slickenside measurements were taken, of which 67 indicated clearly the sense of motion. A clear superposition of reverse followed by right-lateral followed by normal faulting could be seen. Left-lateral faults were less common and did not clearly fit into the sequence.

Unfortunately, the data collected are not considered useful in a regional analysis because of the apparent strong influence of the lineament itself, defined by the competent limestone, on the faulting directions. As can clearly be seen in the rose diagrams (Fig. 6.25) and the stereographic projections (Fig. 6.26) the reverse, strike-slip and normal faults all strike in the same NNW-SSE orientation, strongly implying that each successive phase of faulting was superimposed on the previous phase. A slight shift towards N-W of the normal and strike-slip faults from the original reverse direction can be seen. It can also be argued that the right-lateral faults are orientated slightly more N-S than the reverse or the normal faults. The advantage of this close directional relationship of fault phases is that good control is obtained on the sequence of events. The superposition data from this area are far better than from any other region.

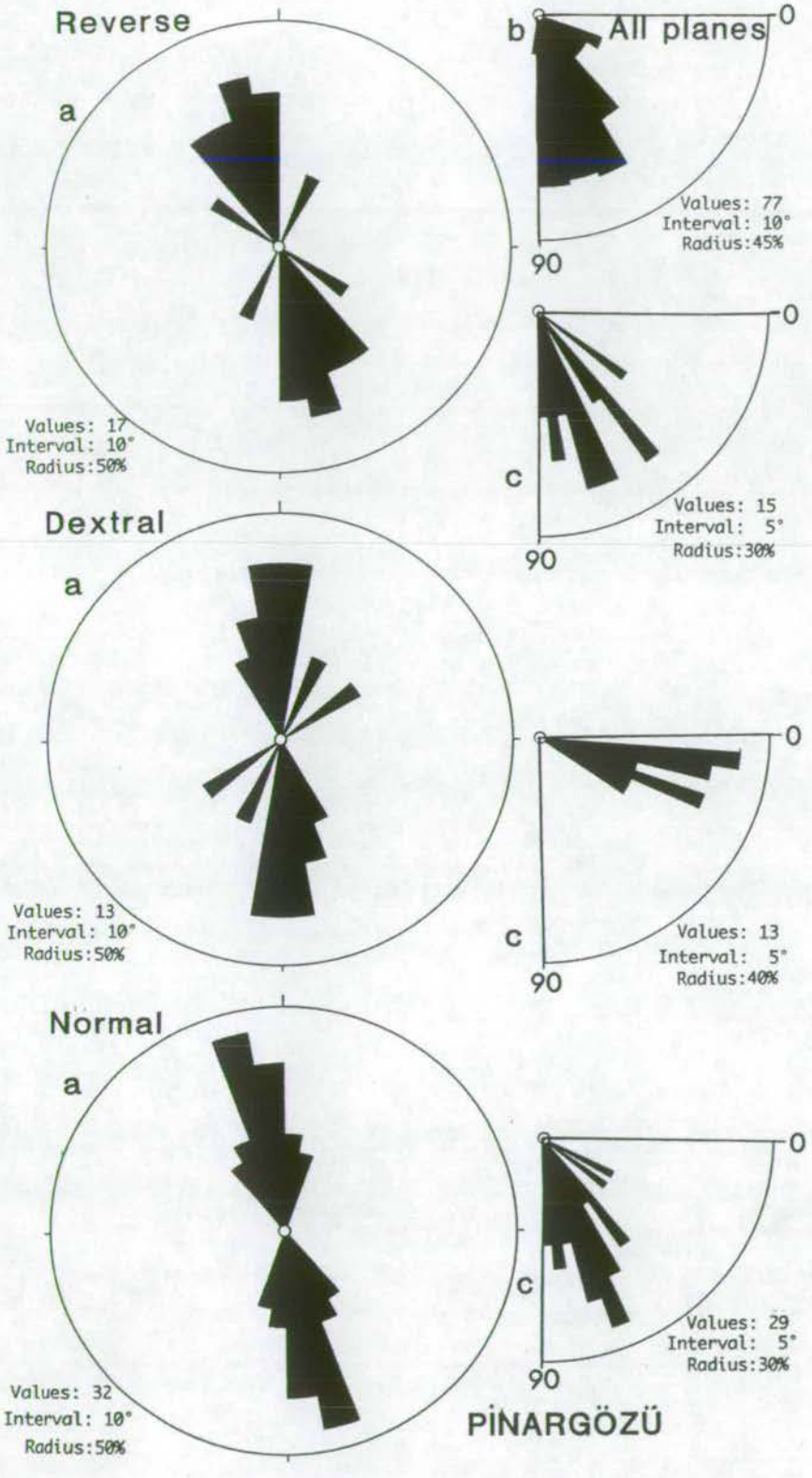

Fig. 6.25: Rose diagrams of the fault data collected at Pinargözü. Note the similarity in direction of all three fault types. a) fault plane strike (non-directional) b) fault plane dip c) pitch of slickensides.

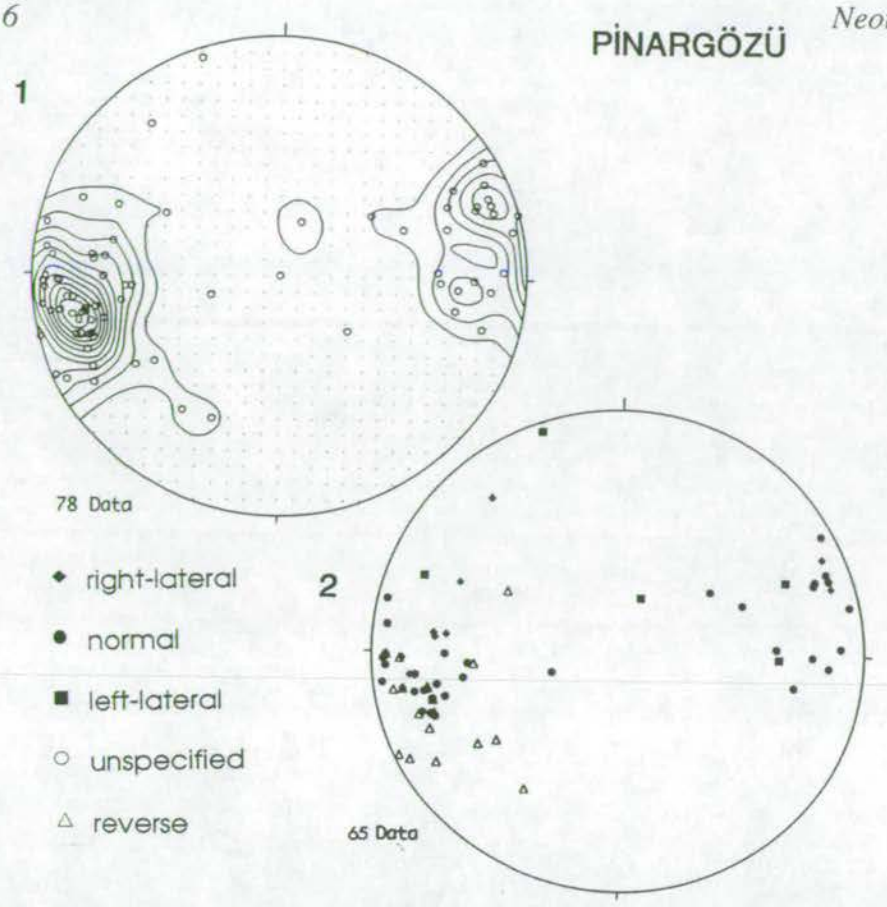

Fig. 6.26: Stereographic projections of faults measured in the Pinargözü region. **1** = contoured plot of poles to planes of all data. **2** = poles to planes of sense data. Note the slight difference in trend between the reverse faults and all others, otherwise the data are very tightly grouped and cannot be distiguished by distribution.

6.4.6: Eastern Aksu basin margin - Ovacik Dağlari

The Ovacik Dağlari also provided very poor data. It was particularly hoped to obtain information from this region as it forms the southern part of the eastern Asku basin margin and the southward continuation of the Pinargözü lineament. Most of the rocks in this range are soft Mesozoic serpentinites and radiolarites. In order to preserve good fault data hard limestones are needed. This was only found in one area. Sixty one measurements were made from this relatively small region. Fifty nine slickenside lineations were obtained, from which a sense of direction was given by 57 planes. A clear superposition pattern of normal faults superceding both right-lateral and left-lateral faults is seen in this area. The data presented in Figs. 6.27 and 6.28 show that this area is not reliable for a regional analysis. This was in many ways expected because of the difficulties in collecting the data and the poor condition of the rocks from which the data were collected. The faults of all types follow the same lineation directions. The great circle stereoplot (Fig.6.27) implies that many of the NW-SE trending faults are strike-slip.

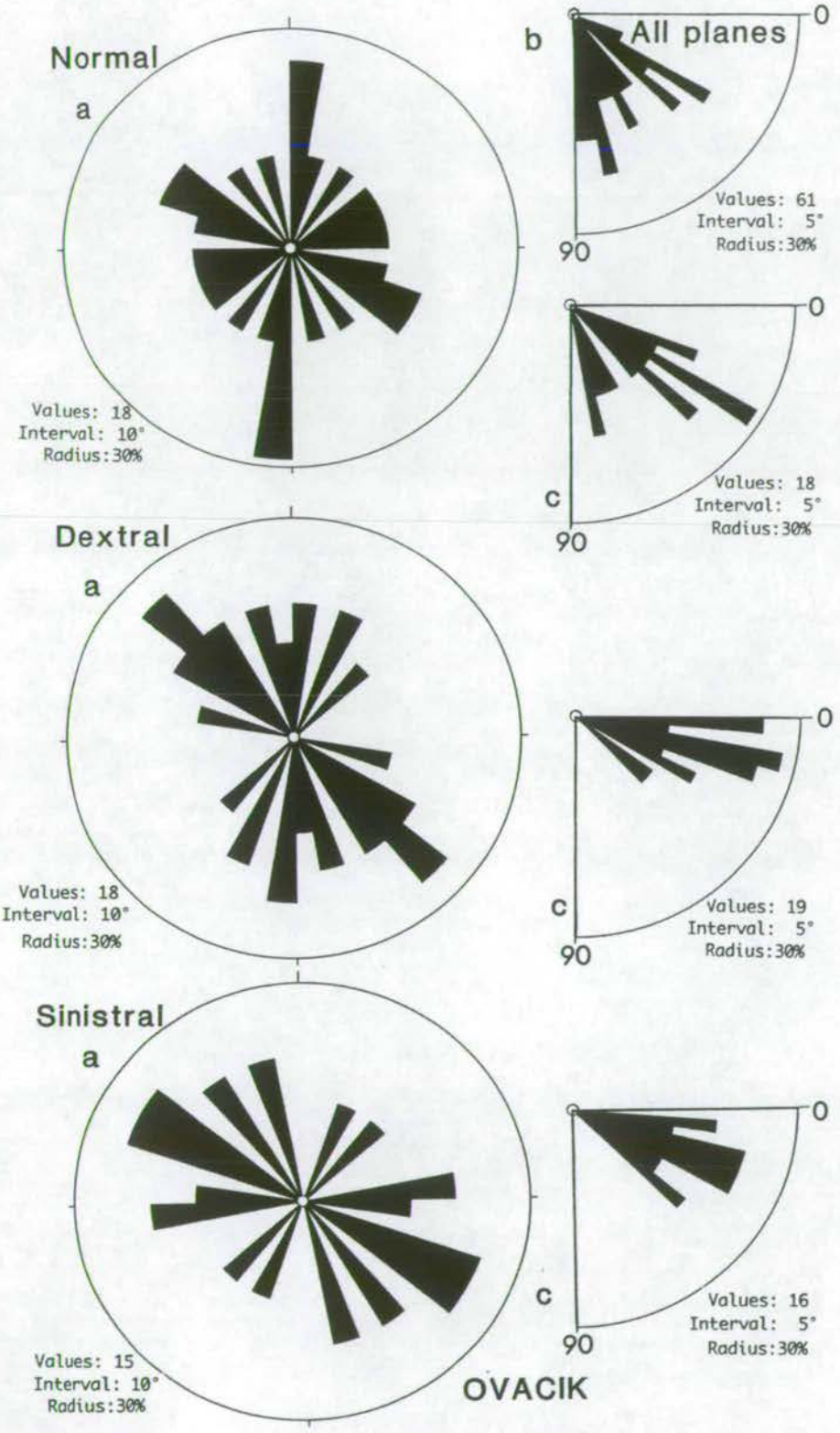

Fig. 6.27: Rose diagrams of the fault data collected near Ovacik. Note the similarity in fault directions between all fault types. Also, the normal faults show a particularly broad distribution. a) fault plane strike (non-directional) b) fault plane dip c) pitch of slickensides.

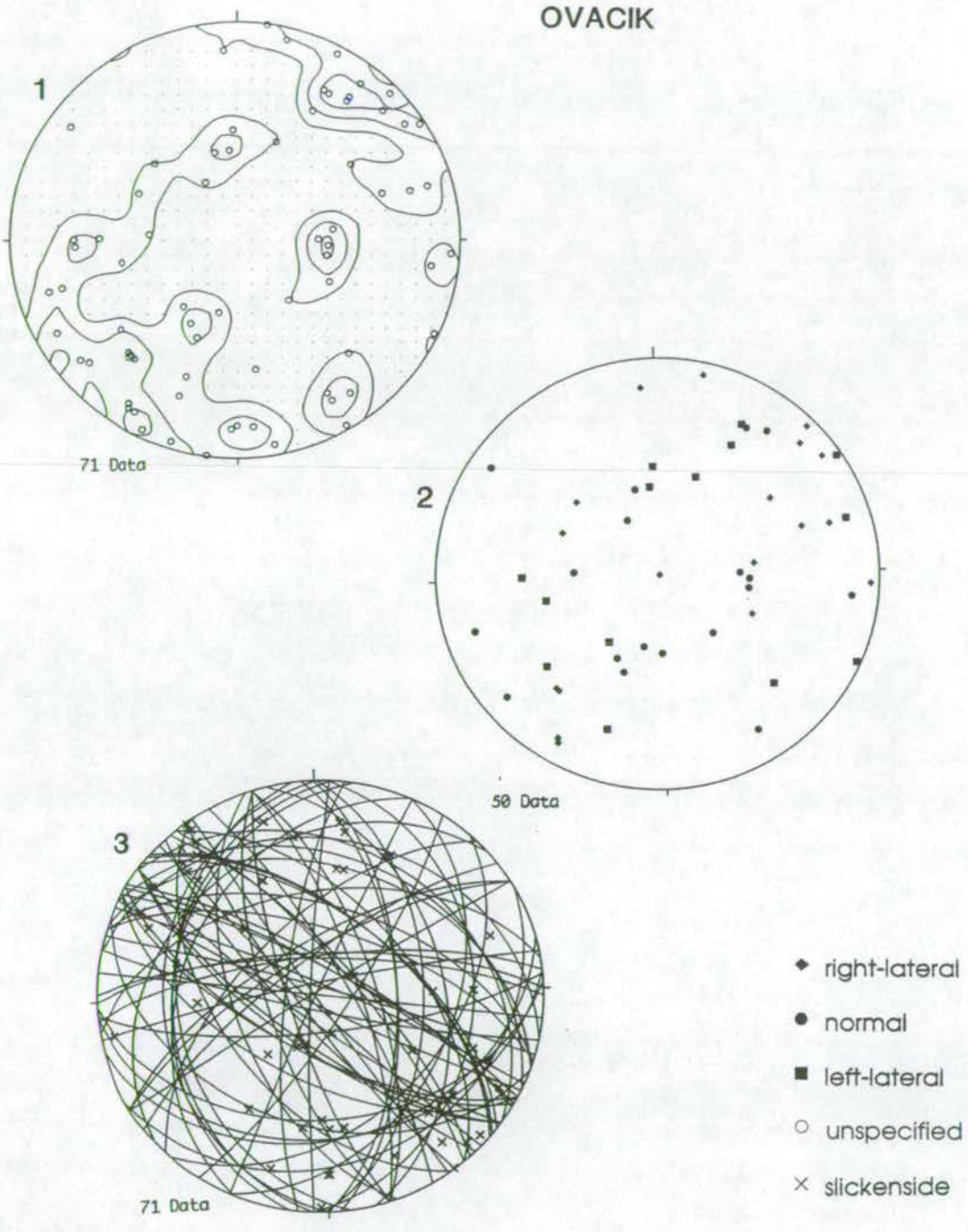

Fig. 6.28: Stereographic projections of the fault data collected near Ovacik. **1** = contoured plot of poles to planes of all data. **2** = plot of poles to planes of directional data. **3** = great circle plot with slickenside data. Note that a large proportion of the faults are strike-slip.

6.4.7: Eastern Köprü basin margin - Kirkkavak

Despite being a major neotectonic fault lineament the Kirkkavak fault yielded very little data for this study. Only along the road up to the radio station between Deliler and Mutlu could rocks with reasonable meso fault planes be found. However, even here the quality of the planes that were measured was poor. Only 22 planes were measured; all but one gave slickenside data with 12 providing a sense of direction. However, the directions are very mixed and normal, left-lateral and right-lateral motions were all observed. The great circle plot (Fig. 6.28) of all the measured planes and slickensides shows that strike-slip faulting has been important along the lineament and that the observed orientations are very similar to those from many other areas.

The quantity and quality of the data mean that no reliable conclusions can be drawn from this lineament.

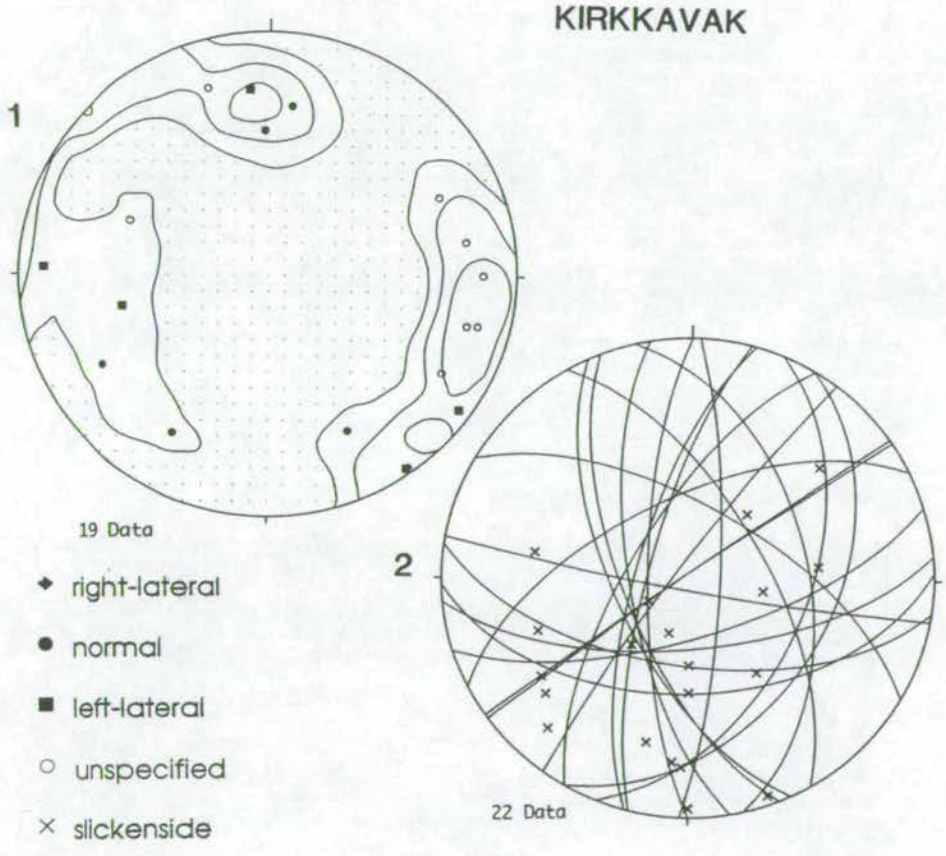

Fig. 6.29: Stereographic projections of fault data collected on the Kirkkavak fault. **1** = contoured plot of poles to planes of all data with sense data included. **2** = Great circle plot of all data with slickensides marked as crosses. An even spread between strike-slip and normal faults is shown in both plots.

6.4.8: Miocene sediments - Ortaköy

Just south of the tunnel works near Ortaköy a number of faults are clearly exposed, primarily in the Miocene sediments. A few measurements were taken in the Late Pliocene/Early Quaternary fanglomerates. In total 49 mesofault planes were measured. On these planes 39 slickenside lineations were found, yielding 35 sense of direction results. Left-lateral, right-lateral and normal faults were found. The steep dip of the fault planes (60° to 90°) indicate that faulting occurred after the sediments were tilted and are, therefore, post Miocene in age. It is clear from the stereoplot of directional data (Fig. 6.30) that the faults can be divided into distinct groups and that these trends are accentuated when all data are plotted and contoured. This is also clearly shown on the rose diagrams (Fig. 6.31). The right-lateral slip-planes have a strong NE-SW orientation, left-lateral planes, in contrast, are ESE-WSW with an E-W fraction. The normal planes are not so well defined, nor so common, but give orientations of NNW-SSE and N-S. A rose plot of all data is dominated by the ESE-WSW trending left lateral planes.

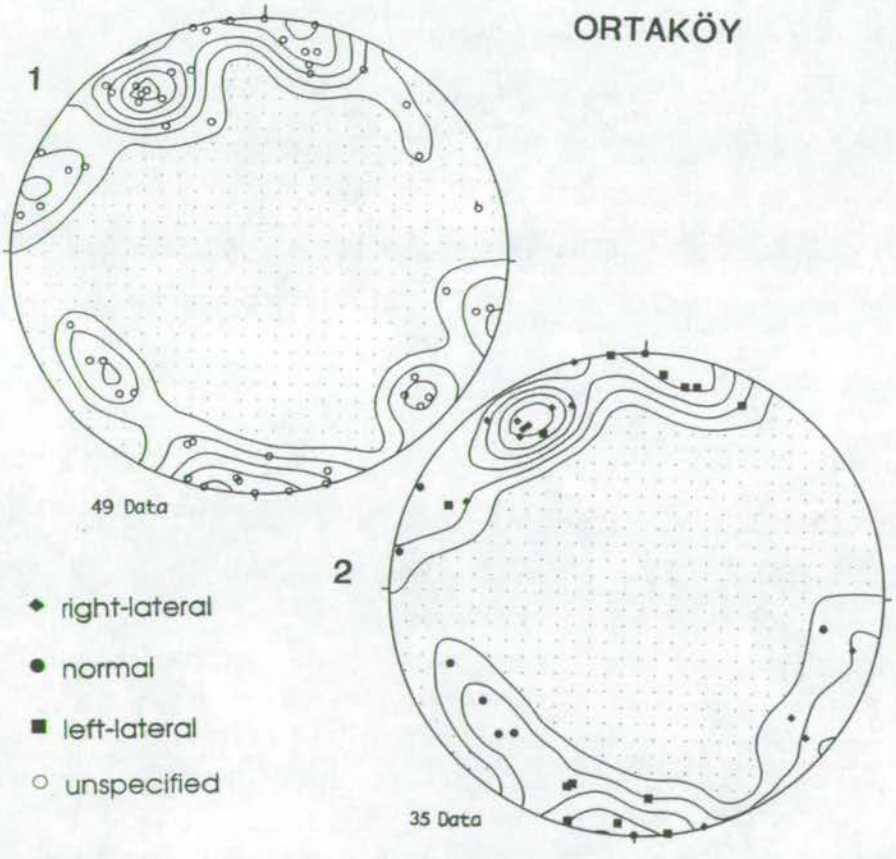

Fig. 6.30: Stereographic projections of fault data from Ortaköy, just south of the new tunnel. **1** = contoured plot of poles to planes of all data. **2** = contoured plot of poles to planes of directional data. The same patterns show in both data sets and allow left-lateral, right-lateral and normal faults to be distinguished.

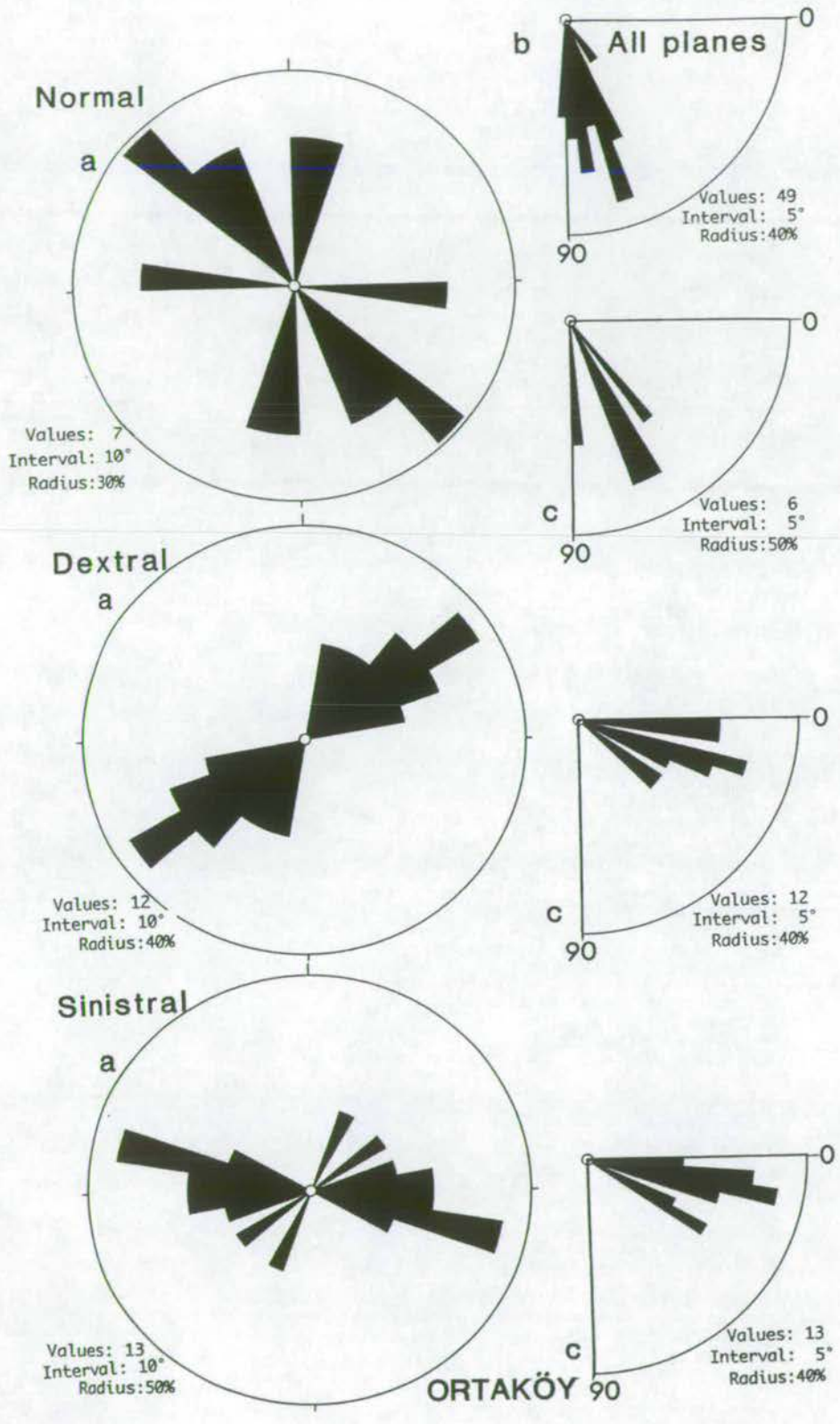

Fig. 6.31: Rose diagrams of fault data measured in the Ortaköy area. Normal fault data is sparse and unclear. Right-lateral and left lateral faults are more closely grouped.

6.4.9: Miocene sediments - Bucak

Fault planes were measured in the Miocene conglomerates outcropping on the road from Bucak to Kargi. In total 25 values were collected, with four slickenside readings but no sense determinations. The results are shown plotted stereographically (Fig. 6.32) The general orientations observed are NNE-SSW and NE-SW The limited slickenside data suggest that many of the faults are strike-slip. A small number of E-W faults are also observed.

6.4.10: Miocene sediments - Abdurrahmanlar and Gebiz

Freshly exposed Miocene sections along new irrigation works in the Abdurrahmanlar area exposed many faults. In places the bedding is near vertical, probably a result of Aksu phase compression. The fault planes cut through these sediments and are therefore interpreted to postdate the Aksu phase. Unfortunately no kinematic data were found. In total 67 planes were measured. A reasonable grouping is seen in the plot of the data (Fig. 6.32) with faults grouped around NE-SW, NW-SE and notably ESE-WNW. These directions are comparable enough to other areas to be attributed to the same faulting periods.

Data collected in the Gebiz limestone are inconclusive. One plane clearly shows strike-slip movement. The others have a NW-SE trend. This is approximately coincident with the trend of the limestone itself which is assumed to be fault controlled.

6.4.11: Pliocene sediments - Çalkaya

Faults are common in the Pliocene sediments around Çalkaya, but, due to the unconsolidated nature of the sediment in the area, are very difficult to measure. Of 68 measurements only 2 kinematic indicators were found. Both indicate normal faulting. The rose diagram and stereographic projection show a range of directions for the faults in the Pliocene sediments of this region (Fig. 6.33). This is undoubtedly partly due to the difficulties and imprecision of field measurement in an area where planes themselves are rarely exposed. The only kinematic data available, shown on the stereographic projection, indicate that the NNE-SSW directions are due to normal faults. Some of the E-W directions may be part of the synsedimentary faulting observed in the Aksu area and thus synsedimentary formation in the delta and nothing to do with the subsequent tectonics. Some degree of cluster can be identified in the NE-SW and NW-SE orientations.

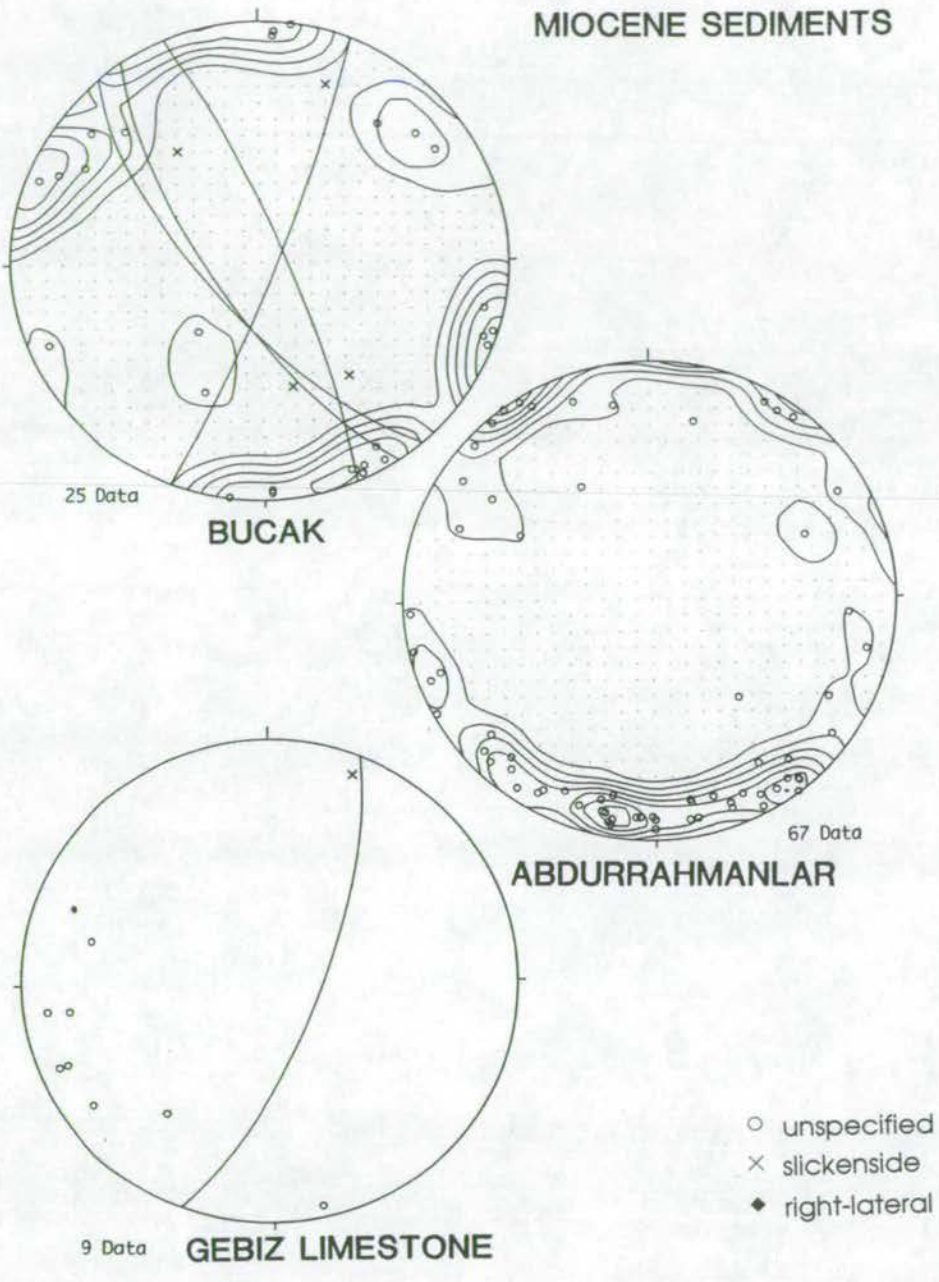

Fig. 6.32: Stereographic projections of fault data collected in Miocene sediments of the Aksu basin. **1** = contoured plot of poles to planes of data collected at Bucak. Great circles with slickenside data are also plotted. **2** = contoured plot of poles to planes of all data collected at Abdurrahmanlar. **3** = plot of poles to planes of data collected at Gebiz with great circle and pitch of slickenside of the one plane that gave a sense direction.

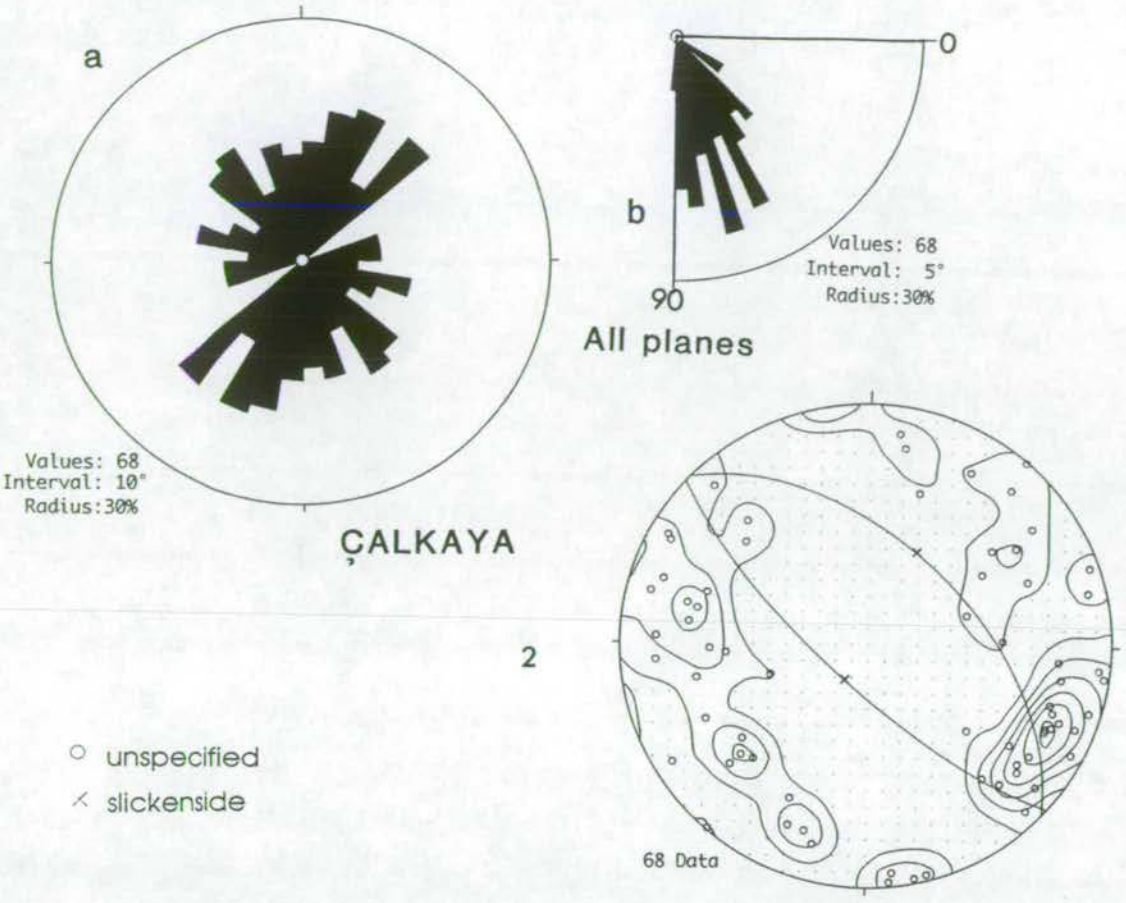

Fig. 6.33: Plot of fault data from the Pliocene sediments around Çalkaya. **1** = Rose diagram of all data. a) fault plane strike (non-directional) b) fault plane dip. **2** = contoured plot of poles to planes of all data with the two faults which gave a sense of direction plotted as gerat circles with slickensides. Both are normal faults.

6.4.12: Faulting in the Quaternary tufa

Minor faults in the Antalya tufa indicate that faulting has continued through the Quaternary. These faults are generally orientated SSW-NNE, but only a few measurements were made. The observed faults typically had a minor normal offset or were observed as fissures on the surface of the tufas. These fissures were sometimes filled with a few centimetres of breccia in a red matrix, which is assumed to be related to Terra rossa formation.

6.4.13: Summary of mesofracture results from the study area

Table 6.3. summarises the results obtained. It can very quickly be seen that all the data lie approximately in two principal directions NE-SW and NW-SE. In most areas right-lateral and normal faulting dominate. Left-lateral faulting is found around Çandir and Ortaköy and at Ovacik. The data from Ovacik and Kirkkavak are not considered good enough to draw any conclusions. Fig 6.34 shows plots of all data for 6 of the areas discussed above. Good comparison can be made between the data from Kovada, Kemer and Abdurrahmanlar and between Çandir and Ovacik, suggesting that it may be possible to draw some conclusions about the regional tectonic regime.

Although the Pinargözü and Antalya road data strongly suggest that very strong reactivation has occurred, it is in these two regions that the best superposition data can be found. This gives a very clear result that the reverse faulting, presumably of the Aksu phase, was followed by a phase of strike-slip faulting and then a phase of normal faulting. As the present-day topography is dominated by normal scarps it is easy to realise that normal faulting was a major event in the region. It is not so easy to determine how important the strike-slip faulting was.

NORMAL		
	Kemer and Olympos	NNE-SSW
	Çandir	NW-SE and NNW-SSE (most dominant)
	Ovacik	NW-SE and N-S (tentative)
	Ortaköy	NNW-SSE and N-S
	Çalkaya	NW-SE
RIGHT-LATERAL		
	Kemer	NE-SW and NW-SE
	Çandir	NE-SW
	Ortaköy	NE-SW
	Bucak	NE-SW and NNE-SSW (tentative)
LEFT-LATERAL		
	Çandir	NNE-SSW and NW-SE
	Ortaköy	WNW-ESE
	Ovacik	from E-W to SSE-NNW (large spread)
ALL PLANES	Pinargözü	NNW-SSE
	Antalya Road	NW-SE

Table 6.3: Summary of the principal strike directions obtained from the different study areas.

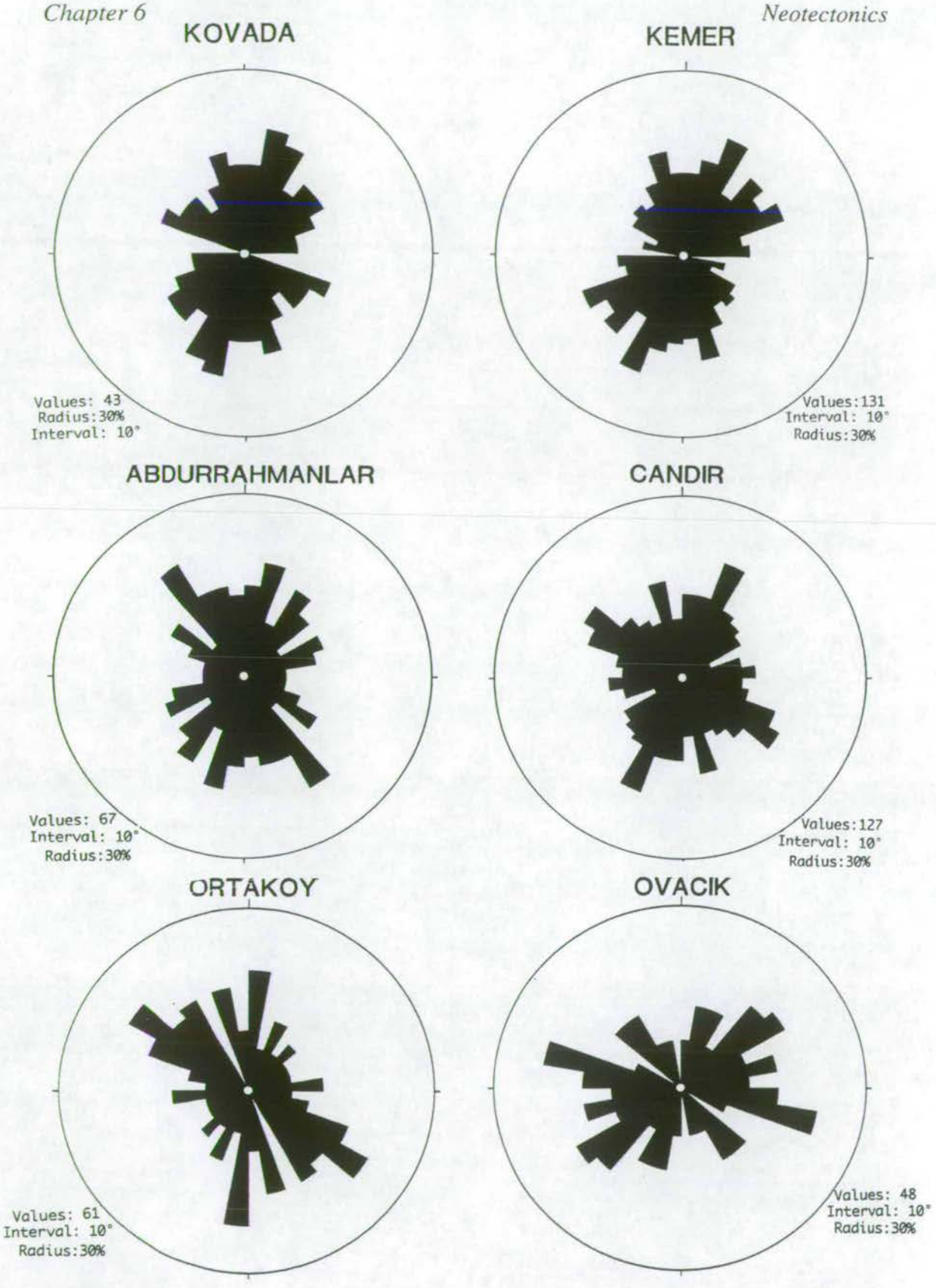

Fig. 6.34: Rose diagrams of all data from different regions in the Isparta angle. In particular comparison can be made between the general directions in the Kovada, Kemer and Abdurrahmanlar plots and between the Çandir and Ovacik plots.

6.5: Neotectonic development of the study area

The data from Pinargözü, the North Antalya road and the Ovacik Dağlari appear to be strongly controlled by a pre-existing structure, in the case of Pinargözü area this is a lithological control. The Antalya road and Ovacik data are probably also affected by lithology in that, particulary in the Ovacik Dağlari, the basement is very heterogeneous. These areas do give good superposition data, showing that, subsequent to the compressional deformation of the "Aksu phase", strike-slip and then normal faulting has affected the region. This is backed up by the geomorphological observation that the present-day scarps are clearly degraded normal faults.

A study on the Tanganika and Malawi Lakes (Scott *et al*, 1992) showed that in cases of oblique extension there is a dominant segregation of faults into orthogonal directions. It is a possibility that this is the cause of the two strong directions picked up in the current study. Although near dip-slip normal faults, steeply-dipping oblique faults and subvertical strike-slip faults have all been observed in the complex linked fault system that make up the East African rift valleys, the majority of the East African faults are oblique-slip in nature. The early phase of right-lateral faulting has a strong oblique-slip signature split into two orthogonal fault directions and may be the result of extension oblique to pre-existing basement structures. In the current study the plots of dip versus pitch of strike-slip faults show that those assigned to normal origin only have a small oblique component. The same normal faults also tend to have a more constrained orientation, often bisecting the strike-slip directions. This suggests that the stress field may have been relatively orthogonal during the period of normal faulting. The Pinargözü, North Antalya and geomorphological data suggest that normal faulting occurred after strike-slip faulting. It is, thus, possible that the change from dominantly strike-slip to dominantly normal faulting merely represents a change from extension oblique to pre-existing structural lineaments to extension orthogonal to structural lineaments.

A second possibility is suggested by the orthogonal pattern of the strike-slip fault directions. In cases of three-dimensional strain both experimentally (Reches and Dietrich,1983; Aydin and Reches, 1982), theoretically (Reches, 1978, 1983) and in field observations (Reches, 1978; Aydin and Reches, 1982) a complex orthogonal pattern of faulting, containing three or four fault directions, is observed. Plan views of the fault patterns and stereographic plots show a conjugate or orthorhombic symmetry which closely resembles the fault patterns seen in much of the current data, particularly the strike-slip data. Important features of faults developed in three-dimensional strain fields are that they dip steeply, and that both strike-slip and dip-

slip displacements occur on the fault surface. These features can all be seen in the study area. It may be that the early, dominantly strike-slip phase of deformation took place under three-dimensional strain whilst the later normal phase occurred as a result of two dimensional strain, after a brief period of gravitational collapse. It has already been noted that the Burdur area is thought to have been under gravitational stress during the Pliocene and it is likely the Isparta angle was under similar conditions. Whether this gravitational force was sufficient to cause a three dimensional strain style of faulting is open to debate.

The Kovada graben fault patterns in many ways resemble a mini Lake Tanganika or Malawi. The overall fault directions relate very well to the fault directions observed in other areas of the Taurus Mountains. However, the graben itself does not trend in the same direction as its bounding faults. The location of the Kovada graben is critical to understanding its formation. The map and section (Fig. 6.35) from Robertson (1993) show that a suture zone between the Davras Dağ limestones and the Sütçüler limestones runs approximately N-S down the graben. The numerous "islands" in the southern part of the Kovada graben are Mesozoic carbonates, probably representing blocks of carbonate platform margin sediments which, due to pre-existing weaknesses, flaked off the margins during extension. The presence of a graben structure at this location is almost certainly a direct result of the presence of the suture zone. It is probable that σ_3 was oblique to the opening direction. We have here a strong case for reactivation of a pre-existing lineament (Fig. 6.36). The situation here is slightly different to that of Lakes Tanganika and Malawi. Here the reactivated suture trends N-S, although is almost certainly not straight, and the actual faulting results from an oblique strain, which causes the faults to be at an angle to the main graben direction. In the East African rift it is the fault directions themselves that are controlled by the pre-existing weaknesses, although the extension direction is oblique to the main graben orientation. The overall graben structure is a combination of changing fault directions along the length of the rift. In both cases, by measuring the maximum dip created by individual faults, an indication of the maximum extensional direction can be ascertained.

In the Çandir and Ortaköy areas a dominant left-lateral fault set is observed. In addition, the rose diagram data of all planes from these two areas are not comparable with the general trends seen elsewhere. The fundamental difference between these areas and the previous areas is that the faults are not defined by strong lineaments but are distributed over a wide area.

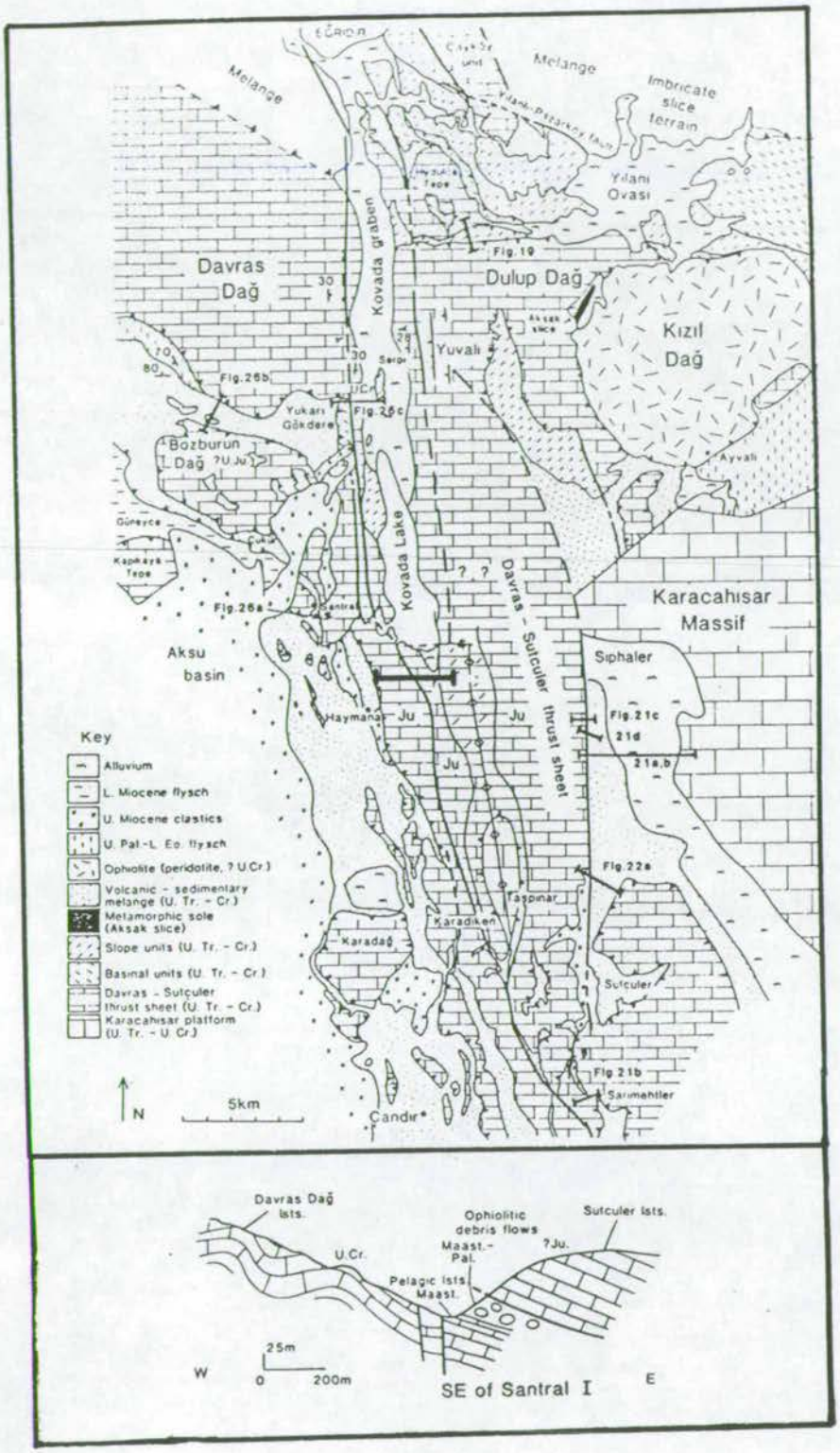

Fig. 6.35: Map of the Mesozoic geology of the Kovada graben area from Robertson (1993) The suture zone parallel to the graben almost certainly controls the opening direction of the graben itself.

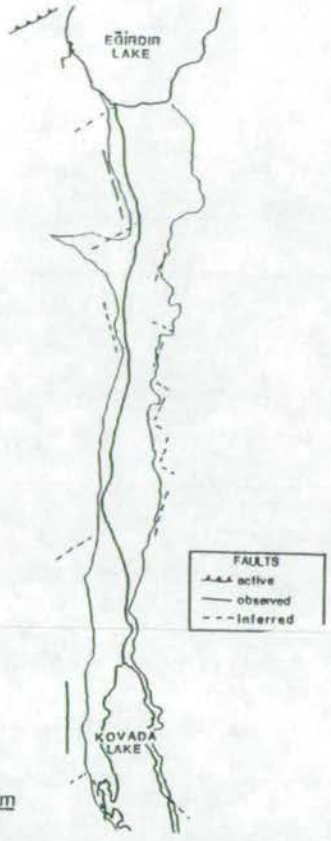

Fig. 6.36: Model of tectonic system of the Kovada graben. The marked faults are centred at the locations of data sites and approximately correspond to the data at those sites.

However, field observation of the main fault scarp at Çandir does suggest that the major lineaments in the region have been subject to right-lateral and then normal faulting. One of the left-lateral fault directions closely parallels the Burdur and Acigöl graben-bounding faults. The second is almost perpendicular. As shown schematically in Fig. 6.37 it is envisaged that the region is characterised by a diffuse deformation of small, clockwise rotating blocks bounded by left-lateral movement. This style of block rotation within a strike-slip zone has been well observed in California and Israel both palaeomagnetically and from earthquake and fault data (Christie Blick and Biddle, 1985; Nicholson, Seeber, Williams and Sykes, 1986; Ron, Nur and Eyal, 1990). Terres and Sylvester (1981) observed block rotations in a ploughed field on a scale less than 20cm. In the Çandir area blocks are almost certainly not large enough or coherent enough to leave anything but a left-lateral signature in the mesofracture analysis of broad, seemingly undeformed areas. It is recognised that no significant rotations of the Antalya basin were found palaeomagnetically. (Kissel and Poisson, 1986b).

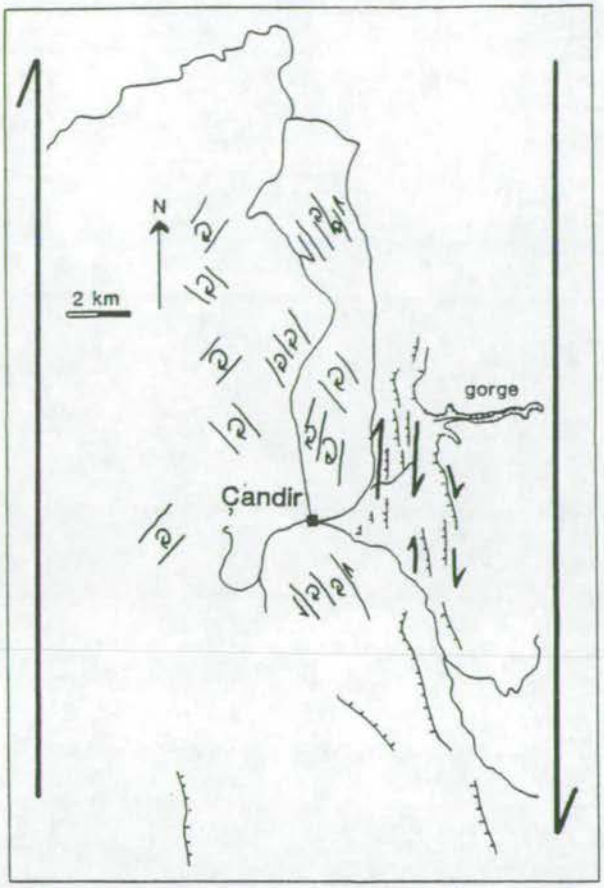

Fig. 6.37: Model of the distributed deformation accommodating right-lateral shear in the Çandir region. The locations of left-lateral faults are not intended to map real faults, but to give a general idea of the overall behaviour of the area.

It is doubtful, because of the apparent small size and probable incoherence of the blocks, whether any discernable rotation would be detected. In addition, this style of accommodation of right-lateral shear is almost certainly confined to zones where shear is particularly distributed. In the Çandir region this is most likely due to a strong pre-existing fracture pattern. In the Ortaköy area the reasons are not so clear.

Rose diagrams plotted for all faults measured at localities where pre-existing structures are not thought to strongly control the fault orientations were presented in Fig. 6.34. The data strongly suggest that σ_3 is ESE-WNW. This is in agreement with data from the late Miocene Aegean islands (Mercier *et al*, 1989), but not from the western Turkish grabens. It can be argued that, in an area where such strong reactivation of pre-existing structural lineaments occurs, a regional stress cannot be deduced. However, two lines of evidence suggest that it is possible to do so in this case. The first is that in the East African rift a stress direction can be determined by calculating the dip of fault blocks within the system. Measuring mesofractures has the same effect of using maximum dips and not macro-structures to deduce the regional σ_3 direction. Secondly, it seems likely from regional considerations that the

pre-existing structures are already aligned in a favourable orientation for reactivation within the stress field. This will be discussed further in section 6.7. The similarity between the fault orientations from the Kemer zone, Çalkaya and Kovada is very clear. The Kemer data support a right-lateral shear producing conjugate fault sets orientated NNW-SSE and NNE-SSW.

A later phase of normal faulting bisects these conjugate sets showing that the same weakened lineament was exploited. This observation does not distinguish whether the system changed from oblique extension to orthogonal extension or whether gravitational collapse changed the overall stress from a three-dimensional one to a two-dimensional one. The Neogene sediments allow us to constrain the timing of these events. At Abdurrahmanlar and Ortaköy the measured faults all cut through steeply dipping Miocene age sediments. This is strong evidence that faulting occurred post Aksu phase.

The Pliocene sediments are typically tilted in a westerly direction, towards the main Kemer fault scarps. There is no evidence that shear occurred as the sediments were deposited. The field occurrence of many of the faults in the Pliocene sediments is normal in character Offsets are often small, but always imply a normal component. They are also nearly always single planes. If significant shear had affected the sediments, broader zones containing multiple strands of fault planes would be expected. Unfortunately, the lack of slickenside information from within the sediments gives us no good empirical control on the style of faulting during the Pliocene. The two data which do exist are normal in character. In addition, the sediments are relatively undeformed in most areas and dip uniformly and more shallowly than might be expected in a shear zone. The general lack of evidence for shear faulting within the Pliocene sediments suggests that they have only been affected by the later stage of normal faulting. The similarity between the fault directions measured in the Pliocene around Çalkaya and those from the Kemer zone suggests that basement structures have been a strong influence on these unconsolidated sediments.

Finally, if the whole sequence of tectonic events observed in the Isparta angle did not begin until the mid Pliocene, an extremely rapid development of a large right-lateral shear zone and subsequent switch to normal faulting would need to be inferred. This does not seem possible as there are no obvious mechanisms to facilitate this.

In conclusion, the entire area can be seen as a zone which has undergone strong right-lateral shear accommodated by narrow right-lateral lineaments, which follow pre-existing structural weaknesses plus scattered regions of small clockwise

lateral shear zone and subsequent switch to normal faulting would need to be inferred. This does not seem possible as there are no obvious mechanisms to facilitate this.

In conclusion, the entire area can be seen as a zone which has undergone strong right-lateral shear accommodated by narrow right-lateral lineaments, which follow pre-existing structural weaknesses plus scattered regions of small clockwise rotating blocks bounded by left-lateral faults, which may be confined to areas where the basement is particularly weak. The conjugate and rhombohedral patterns of faulting may be due to oblique extension relative to the pre-existing fault weaknesses and/or a possible gravitational effect producing three-dimensional strain. It is not possible to distinguish between the two, although the former scenario seems more likely. The strike-slip phase dominated in the Late Miocene-Early Pliocene. It may have existed prior to the Aksu phase of compression (Flecker, 1995). For most of the Pliocene, a phase of tectonic quiescence existed during which the Pliocene sediments were deposited and mature erosion surfaces began to evolve (chapter 5). In the Late Pliocene-Early Quaternary the Pliocene deposits were tilted and the erosion surfaces dissected during what was probably a rapid phase of normal faulting. This can be attributed to a change of regional stress direction, also seen in the western Turkish grabens, which brought the stress field orthogonal to the major structural weaknesses of the area. The current degraded state of the major normal fault scarps indicates that normal faulting has not been intense throughout most of the Quaternary. The generally horizontal nature of the Quaternary tufa deposits and the lack of significant quantities of faulting within the tufa also suggest that recent activity has been limited. The gravitational collapse of the Burdur grabens which has been documented (Taymaz and Price, 1992) occurred in the earliest Quaternary, about the time that the Isparta angle appears to have undergone a brief but rapid period of normal faulting. It is highly possible that these two events are related and the collapse occurred over the whole region, possibly as the regional stress field changed. In the Isparta angle this change in regional stress was to a direction more orthogonal to the pre-existing weaknesses. Uplift of the Bey Dağlari relative to the rest of the Taurides due to underthrusting of the Anaximander mountains may have facilitated this.

6.6: Model of neotectonic evolution of the Isparta angle within the eastern Mediterranean framework

Since the Isparta angle lies in the probable boundary region between the extensional Aegean province and the more stable Anatolian plateau, it is important to review how the neotectonic field observations fit into the more regional tectonic

regime. It has been shown that the present-day tectonic regime started to develop during the Mid Miocene with the collision of Arabia and the onset of broad shear along the North Anatolian fault zone. It is suggested that during the Early Pliocene activity was particularly high as the previously slow system was suddenly able to operate more freely and an initial surge of activity, which has since slowed, occurred. It is assumed that models presented for the present day tectonic system are applicable back to the Late Miocene/Early Pliocene.

The rotating slats model of Taymaz *et al* (1993) is the starting point for this discussion. As the eastern margin rotates to drive the model it leaves a space where material has moved away. This space is naturally filled by the westward-moving, semi-rigid Anatolian block. However, this block is not just moving westward, it is broadly rotating in an anticlockwise manner. Clockwise rotation of the southeastern segment affected by the Taymaz *et al* (1993) system is expected. The combination of these two rotations would produce a broad right-lateral shear zone. This same conclusion was reached by Price and Scott (1994). They suggested the zone must be at least 90 km wide to accommodate the Burdur features. It may, in fact, be wider. In the Burdur region Price and Scott (1994) showed that right-lateral shear is probably accommodated by clockwise blocks rotating between NE-SW faults with a left-lateral shear component. It has already been suggested that this occurs in a much more diffuse manner in the northern region of the Isparta angle. In addition, the Isparta angle is characterised by a number of strong NNE-SSW trending lineaments which show strong right-lateral shear. The Kemer zone is the most important of these. North of the Burdur region no expression of right-lateral shear has been reported. The zone is thus represented as a broadly triangular region around the Isparta angle (Fig. 6.38). This zone may be "propagating" northwards as a "proto" plate boundary.

The distinct change in fault style from north to south within this broad right-lateral shear zone is represented in Fig. 6.39. Although the Taymaz model fits the tectonics seen in the Aegean and Greece well, the model is controlled from its eastern margin and the slats do not represent the reality of the western Turkish graben system. In the northern part of the zone the grabens almost certainly have an important role in accommodating the right-lateral displacement. The general N-S extension of the Aegean region due to subduction and forearc extension means that it is kinematically favourable for the crust to extend through a series of E-W graben to accommodate the strain imposed by the rigid Anatolian plate. In addition the North Anatolian Fault Zone takes up much of the strain in the region.

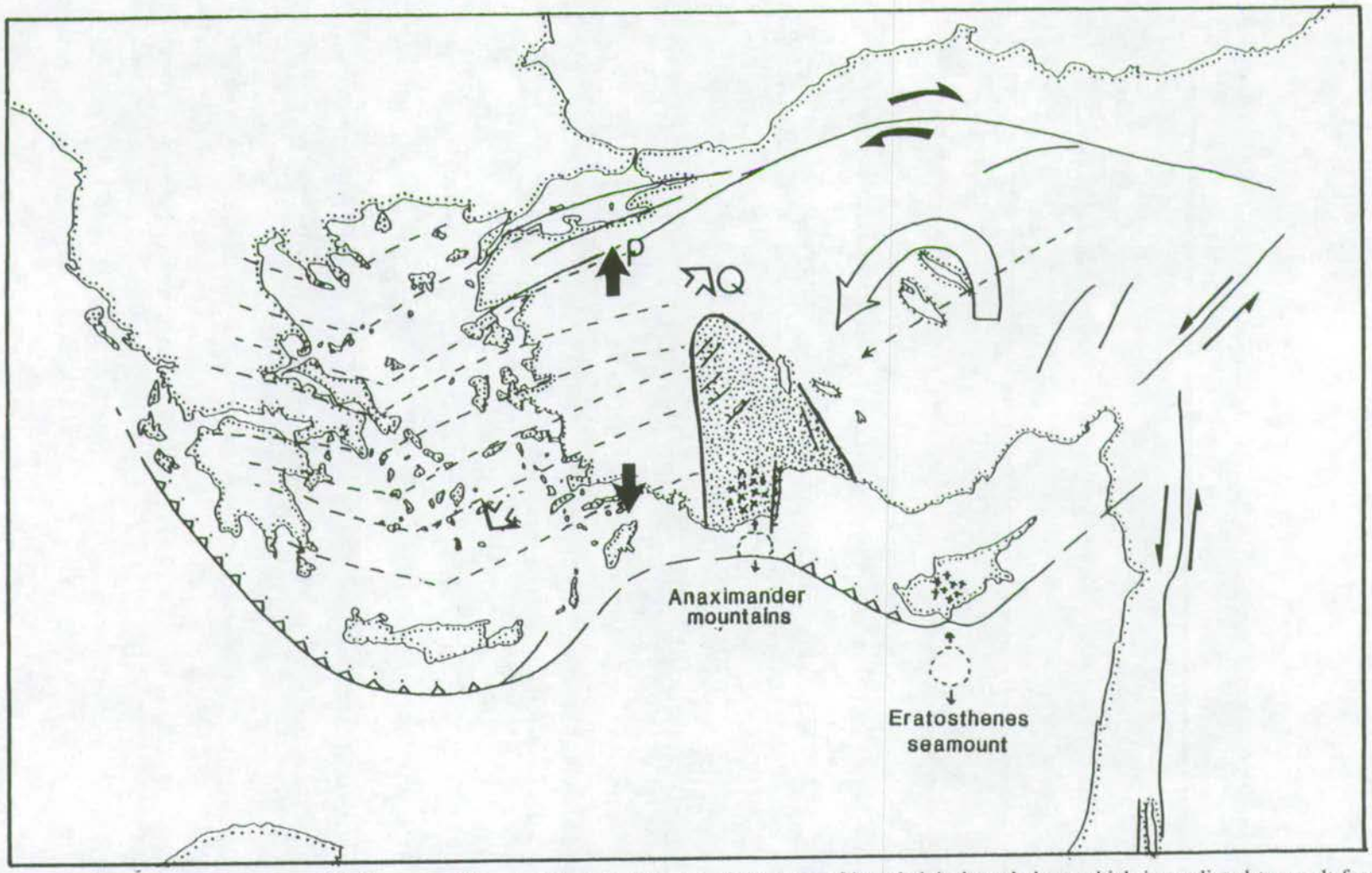

Fig. 6.38: Model of tectonics of the eastern Mediterranean. The shaded zone indicates of the zone of broad right-lateral shear which is predicted to result from the interaction of the Anatolian plateau with the extending Aegean region. The areas marked by small crosses (Bey Daǧlari and Troodos) are areas experiencing uplift due to the underthrusting of blocks of continental material (Anaximander mountains and Eratosthenes seamount). The following features are simplified from Fig. 6.6: P = Pliocene stress fields, Q = Quaternary stress fields. The dotted lines represent the model of Taymaz *et al* (1991). The large curved arrow represents the rotation of the Anatolian plateau and the dotted arrow through it the net translation.

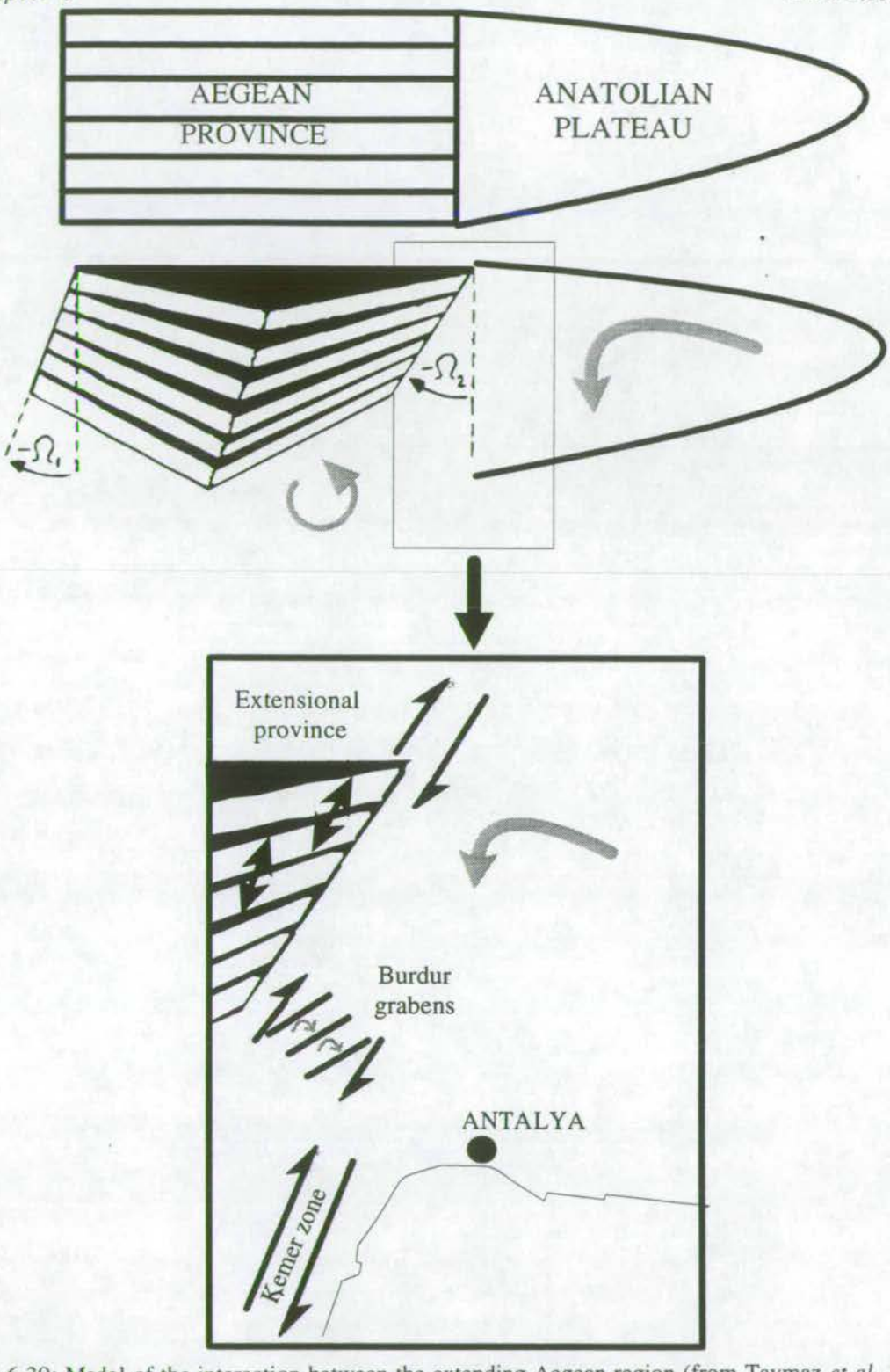

Fig. 6.39: Model of the interaction between the extending Aegean region (from Taymaz *et al*, 1991) and the rotating Anatolian block. The right-lateral shear increases from north to south. In the north most of the shear is accommodated by the extending grabens. In the Burdur and Acigöl grabens the shear is accommodated by clockwise block rotation between left-lateral faults (Price and Scott 1994). In the Isparta angle the shear is taken up as narrow shear zones reactivating pre-existing structures and, probably, as distributed shear in broader regions, similar to the Burdur/Acigöl grabens, but on a much smaller scale.

Further south, in the region dealt with in this thesis, the situation is different. Here the shear is almost certainly stronger as this is the region where clockwise rotation of the southeastern segment of the Aegean province is expected (Taymaz *et al*, 1990). This rotation is confirmed by the palaeomagnatic data (Kissel and Poisson, 1986a; Morris and Robertson, 1993) and the earthquake observations of Kocaefe and Ataman (1982). If the observed 30° counterclockwise rotation of the Bey Dağlari was not a brief Late Miocene event but has been a more gradual phenomenon then a very simple calculation can be made.

The Taymaz *et al* (1993) model predicts that the southeastern area of the Aegean province will rotate counterclockwise by 3.7°/Ma. If this rotation rate has been steady and applicable since the onset of rotation then 8.3 Ma are required to produce 30° of rotation. This suggests that rotation has been occurring since the mid-Miocene and fits well with the general observation that the current tectonic regime began to function at about that time. The Marcoux *et al* (1989) and Kissel and Poisson (1986) model requires a decoupling zone along the base of the Antalya complex. It has been already shown that the Antalya Complex rotates with the Bey Dağlari (Morris and Robertson, 1993) and it has been demonstrated here that this rotation can be produced entirely a result of right-lateral shear throughout the region. Hence, the decoupling model is invalidated.

Around the Isparta angle major linear weaknesses already existed and right-lateral shear was easily accommodated along a number of narrow N-S shear lineaments thoroughout the region. In addition, the crust in the Lycian Nappes area was not under the same N-S extensional stresses as further north and west and E-W graben formation was not a favourable solution to the problem. The right-lateral shear observed along the Kemer zone and along the Çandir-Pinargözü zone supports this hypothesis. Unfortunately, due to lack of good data we do not know if the Kirkkavak fault also sheared. It is probable that it did, as right-lateral displacement has been documented in the Miocene sediments bordering the fault scarp (Dumont and Kerey, 1975).

The Burdur region lies somewhere between these two zones. N-S extension is not strong enough to create E-W grabens (as to the north) to accommodate the shear and no well-orientated structural weaknesses (as in the Isparta Angle) exist to facilitate simple right-lateral shear. In this area right-lateral shear is accommodated by clockwise rotation of blocks along left-lateral oblique faults striking NE-SW. This fault direction is probably influenced by the NE-SW joint pattern in the pre-Pliocene basement (Price and Scott, 1994).

A number of lines of evidence suggest that regional uplift is the background tectonic signature over which local tectonic and sea-level effects are superimposed. The overall shallowing of sediments in the basin, from Pliocene marine marls to Quaternary tufa and fluvial sediments, implies that the basin has been lifted out of the range of glacioeustatic sea-level change (chapter 5). Areas such as Elmali, Isparta and Konya are all high plateau regions. High plateaux are indicative of uplift (cf. Tibetan plateau). There are a number of causal mechanisms which can be invoked, but it is not possible to more than tentatively speculate as no data are available to confirm or refute hypotheses at this stage. There is good evidence that the uplift of Cyprus since the Mid Miocene is related to the onset of subduction south of the island (Poole and Robertson, 1991; McCallum, 1989). Wortel, Spakman, de Jonge and Meijer (1995) showed that the presence of a detached slab below a region was a probable cause of uplift. More rapid uplift of Cyprus since the mid-Pliocene is probably related to underthrusting of the Eratosthenes seamount since its collision with the active margin (Robertson *et al*, 1993). Similar processes may be affecting the southern Turkish margin. It is known that a remnant subducted slab exists under Antalya Bay and this still causes deep seismic events (Rotstein and Kafaka ,1982; section 6.3.1). It is also suspected that the Anaximander Mountains are a collided continental fragment which has broken up and, if Eratosthenes is typical of collisional seamounts, has almost certainly underthrust the Turkish plate (south of Finike). This may be expected to produce local uplift. There is no direct evidence that the Anaximander mountains are underthrusting the Turkish plate. However, comparison with the Eratosthenes seamount and the observation that the Bey Dağ lari appears to uplift relative to the surrounding Taurides, marked by the dramatic faulting along the Kemer lineament, suggest that underthrusting has taken place throughout the Quaternary and probably earlier. Areas of uplift caused by the underthrusting of the Erastothenes and Anaximander blocks are shown on Fig. 6.38. There is no indication of what size the original Anaximander block may have been and thus no control on the scale of underthrusting that needs to be considered. A second possible cause of uplift is the general uplift, centered in the far east of Turkey and in Iran, and documented as a Himalayan-style uplift due to collision of Arabia and Eurasia along the Bitlis zone (Snyder and Barazangi, 1986). The effects of this uplift are likely to be broad, and to reduce towards the west. It is proposed that the broad uplift causing the development of the high plateau is a direct result of the Himalayan-style uplift in the east. Superimposed on this the underthrusting Anaximander Mountains cause a local uplift centered beneath the Bey Dağ lari which produces a half graben to the east. Lack of good data from the Kirkkavak fault, and

the general tilt and younging of the Pliocene sediments in a westerly direction suggest the present-day Aksu basin is a half graben structure and that the Kirkkavak margin is relatively passive. Earthquake data also suggests that current activity is concentrated on the western basin margin (section 6.3.1). This situation is comparable to the Mesaoria basin in northern Cyprus where active faulting was concentrated on the uplifting Troodos margin in the south and the northern Kyrenia margin was generally inactive (McCallum and Robertson, 1990).

As discussed above, the gravitational collapse observed in the Burdur region during the Early Pleistocene (Taymaz and Price, 1992) may be simultaneous with a gravitational collapse of the Isparta angle grabens, as a new favourable stress regime allowed fairly rapid strain release and basin collapse during a short period of normal faulting. Slight changes in relative plate motions probably caused a change of σ_3 in the Aegean province in the Early Quaternary from N-S extension in the Pliocene to NE-SW sometime during the Quaternary. The NW-SE trending faults were, thus, orthogonal to the new stress regime and the right-lateral faults were reactivated as normal faults, causing the major topography we see today. Since then a period of fault scarp degradation has resulted in the present-day appearance of relatively inactive neotectonic normal faults discussed in chapter 5. Lack of present-day earthquake data does not allow us to ascertain whether right-lateral shear or normal faulting dominate the present day zone. In whichever case, it is likely to be a relatively slow process.

The data collected in this study give σ_3 as ESE-WNW. This direction fits well with the regional influences caused by rotation (and net southwestward transport) of the Anatolian block, which would create a NNE-NE compressional force, and rotation of the eastern margin of the Aegean province around a N-S axis, which would create a WNW extensional force.

The pre-existing basement structures of the Isparta angle and the Burdur/ Acigöl region strongly influence the resulting tectonic style. From both areas it can be deduced that the zone between the extensional Aegean province and the more rigid Anatolian block has undergone a significant period of right-lateral shear. It is important to realise that, whilst structural weaknesses will always reactivate, it is frequently still possible to deduce the controlling regional tectonic regime. In this situation the pre-existing fabric was very closely aligned with the shear direction and hence very easily reactivated. If the shear direction had been more oblique then a much more complex pattern would have been observed.

6.7: Conclusions

1) Review of current knowledge concerning eastern Mediterranean tectonics suggests the following regional tectonic evolution: during the mid-late Miocene (12 Ma) a number of regional tectonic events mark the slow initiation of the current tectonic regime. Terminal collision of Arabia with Eurasia along the Bitlis suture zone is probably the dominant cause of this. As a result, a broad shear zone along the North Anatolian fault developed. At the same time subduction moved from the Aegean sea to the present day Hellenic active margin and from along the Kyrenia range in Cyprus to the position of the current Cyprus active margin. At the start of the Pliocene (5 Ma) this system seems to have received a boost, possibly due to the new gravitational driving force of the uplifting eastern Anatolian (Iran) region. Onset of motion along the East Anatolian fault and the narrowing of the North Anatolian fault zone to its present width mark the onset of relatively rapid westward tectonic expulsion of the Turkish plate. Change in absolute motion of the African plate may be a driving force for this speeding up of the system. It is probable that during the Latest Miocene - Early Pliocene, as this change occurred, an initial surge of activity took place as built-up stresses were released. In the late Pliocene - Early Quaternary changes in stress regime along the Hellenic arc and in the western Turkish grabens have been detected. The Burdur region is thought to have undergone gravitational collapse at this time (Taymaz and Price, 1992). The tectonic regime operating since 5 Ma can be described by SW translation and counterclockwise rotation of the Anatolian plateau and the rotating slats model (Taymaz *et al*, 1993) of the Aegean province. Between the Anatolian plateau and the Aegean province a broad zone of right-lateral shear is expected. This shear increases in intensity from south to north and was probably dominant in the Early Pliocene, when regional tectonic activity is thought to have been particularly rapid.

2) Meso-fracture fault analyses are summarised in Table 6.3. Fault directions are NE-SW, NW-SE, N-S and orientations which lie between (e.g NNW-SSE). Normal faults are superimposed on right-lateral faults, which in turn are superimposed on reverse faults related to the Aksu phase of deformation.

3) Right-lateral shear, probably during the Late-Miocene/Early Pliocene caused right-lateral strike-slip faulting along pre-existing structural lineaments. The conjugate pattern of strike-slip faults is probably a result of slight oblique

extension but may be due to gravitational forces causing three-dimensional strain. Areas of more diffuse deformation probably responded as small scale, clockwise block rotations bounded by left-lateral faults. The right-lateral shear is thought to be the result of interaction between the extending Aegean province and the westward translation and rotation of the Anatolian block. This shear zone may be a "proto" plate boundary.

4) A phase of normal faulting is recognised which created the present-day topography. This is thought to be early Quaternary in age and to be related to gravitational collapse brought about by regional uplift affecting the entire Tauride chain and a change in stress field direction, which rotated the stress field orthogonal to the pre-existing structural weaknesses. It is likely that this was coincident with collapse of the Burdur grabens (Taymaz and Price, 1992). The faulting was concentrated along the western margin, forming a half-graben topography. This may be due to a more local uplift of the Bey Dağ lari, thought to be caused by the underthrusting Anaximander mountains.

5) Despite the differences in tectonic style due to pre-existing structures observations can still be made concerning the regional stresses by considering the meso-scale data. σ_3 during the Early Pliocene is suggested to be ESE-WNW. A NNE-NE compressional force due to rotation (and net south-westward transport) of the Anatolian block, and a WNW extensional force due to rotation of the eastern margin of the Aegean province around a N-S axis may be the prime controls on σ_3.

6) Local tectonic effects are superimposed on a general tectonic uplift probably related to uplift of eastern Anatolia.

Chapter 7:
Conclusions & basin evolution

As considerable discussion can be found within individual chapters, the principal sedimentological and tectonic conclusions are simply restated, with reference to important diagrams and details in the preceding chapters. Finally, the data are synthesised and a model of basin evolution is presented.

7.1: Principal conclusions

1) The stratigraphic framework of the Pliocene sediments has been reorganised (chapter 2). This is based on: biostratigraphic dating which showed the onshore part of the marine Pliocene to be mid-Pliocene (*Globorotalia puncticulata-Globorotalia margaritae* zone) in age; U-Th dating which showed the tufa deposit to be >400,000 years; and sedimentological and climatological observations. Attention is drawn to Figure 2.4 (page 35).

2) The bioclastic Gebiz Limestone is thought to be Tortonian in age due to the large numbers of *Porites* corals. It is interpreted as a shallow-water limestone, probably developed very close to a palaeoshoreline (chapter 3, section 3.2.3). It

appears that Messinian evaporites are unconformable over the Gebiz limestone, but none were found *in situ* (chapter 3, section 3.3).

3) The marine Pliocene is divided into three Formations: the Yenimahalle Formation; the Çalkaya Formation; and the Kemer Fanglomerates (chapter 2).

The Yenimahalle Formation is characterised by a coarsening-up sequence from silts and marls to shallow-marine sands. Benthic foraminifera suggest that the deepest part of the sequence was of the order of 150m water depth, and that the upper part of the sequence was not deeper than 50m (chapter 3, section 3.7.1).

The Yenimahalle Formation passes gradationally into the Çalkaya Formation. In the north the Çalkaya Formation is a terrestrial braided stream deposit, which has at its head a small fanglomerate deposit. In the south the deposit is mostly marine, with some interbeds of terrestrial and marginal marine deposits. Interbedded tuffs are interpreted as the basal surge deposits of a small phreatomagmatic tuff ring. It is interpreted as a shoal water, type C delta with wave influence (Postma, 1990) (chapter 3, section 3.7.2).

Seismic data suggest that the marine Pliocene deposit is approximately 500m thick and contains three transgressive sequences (chapter 3, section 3.9). This allows the timing of deposition and the principal control on deposition to be related to the lower Pliocene highstand (Vail and Wornadt, 1991).

The Yenimahalle and Çalkaya Formations are very similar to the Nicosia and Kakkristra Formations of Cyprus (McCallum, 1989). The fundamental difference is the degree of tectonic control. The Cyprus deltas are steep Gilbert type deltas and reflect the tectonic uplift of the Troodos during deposition. In Cyprus, the change between the two depositional styles is sharp and is related to a pulse of tectonic uplift (McCallum and Robertson, 1987). The Aksu basin delta system is very shallow and thought to be deposited in a period of tectonic quiesence.

The Kemer Fanglomerates were deposited along the western margin of the Aksu basin as mature slope surfaces began to evolve. Coarse conglomerate fans with alluvial and debris flow conglomerate deposits were shed from the mountains as the scarp slope surfaces smoothed. Some of these fans probably extended into Antalya Bay to become marine fandeltas and a correlation is made with offshore sediment packages. The fans have not subsequently emerged and so this cannot be verified. These fans are comparable with the fandeltas of the Kasaba basin (Hayward, 1982) and the Gulf of Elat (Gvirtzman and Buchbinder, 1978) (chapter 3, section 3.8.1).

4) The development of the Kemer Fanglomerates and associated smoothing of the profile of the scarp slopes represents a period of tectonic quiesence, although some gradual uplift at this stage cannot be ruled out (chapter 5, section 5.2).

5) The Antalya tufa was deposited in a environment of swamps, lakes and rivers (chapter 5). All these environments were active tufa depositing environments. This produced a complex facies association, varying rapidly both laterally and vertically. All the facies types described by Pedley (1990) are present and two further facies have been recognised: tufa breccia and inorganic pisolith tufa. The integral nature of all the facies led to the proposal of a new classification of terrestrial carbonates (page 106).

Tufa is a relatively understudied rock type and the particularly large and well preserved Antalya tufa deposit provided an excellent opportunity to further understanding. The model of tufa formation that has been developed is presented in sections 4.13 and 4.14 (pages 138-156) and should be referred to for details.

6) In the western part of the basin the tufa is thought to be deposited onto a block-faulted topography. Deposition to the west is thought to be limited by the fault block topography which created a topographic ridge at the eastern edge of the tufa, protecting it from the erosion of the Aksu river and creating a barrier to contain the supersaturated spring water. Clastic input from the Aksu Çay prevented any deposition in the central part of the basin. (chapter 4, section 4.15). This initially created lacustrine environments, but as the hollow topography infilled, the surface water became generally shallower. Eventually a flat expanse of tufa formation filled the basin until the climate became too arid for significant tufa formation (see Figures 4.16 and 4.17). During the Holocene karstification of the tufa during the cold wet glacials and minimal tufa deposition during the interglacials has modified the original topography.

7) Right-lateral shear is though to have occurred from the Late Miocene through to the Early Pliocene (chapter 6, section 6.5). Flecker (1995) recognises this as part of the Aksu phase deformation. No evidence for dextral deformation was seen in the Pliocene sediments. Right-lateral shear is thought to relate to the initial development of the current neotectonic regime. Evidence from around the eastern Mediterranean suggests that this regime was incipient from the Mid Miocene onwards and that in the latest Miocene-Early Pliocene a burst of activity produced the narrow microplate boundaries and microplates that are present

today (chapter 6, section 6.1.6). The Antalya region occupies the boundary position between the extensional Aegean region and the translational/rotational Anatolian plateau. Analysis of the kinematics of this interaction predicts right-lateral shear (chapter 6, section 6.6). This observation was also made in the Burdur lakes region just to the northwest of the Isparta angle (Price and Scott, 1994). Refer to Figure 6.38 (page 259)

8) Evidence for regional uplift during the Quaternary period comes from the fluvial terraces of the Aksu basin; the lack of Quaternary marine sediments after the Pliocene; and the wave cut cliffs cutting into the remnant mature slope surfaces at Kemer. More regionally the change from drowned coastlines to the west of Turkey to uplifted coastlines around Antalya bay and along to Adana documents that this uplift is a regional phenomenon (chapter 5, section 5.8).

9) A second phase of tectonic activity is thought to have occurred during the Late Pliocene-Early Quaternary. It tilts the Early Pliocene sediments to the west, but does not affect the Mid Quaternary tufas. Faulting is greatest along the western margin. Evidence for this event is concentrated along the Kemer coastline. Thus, the basin structure is a half graben structure. The degraded nature of the fault scarps testifies that fault activity did not continue throughout the Quaternary (chapter 5, section 5.3). A combination of regional uplift and localised uplift of the Bey Dağlari, due to underthrusting of the Anaximander mountains, is thought to have led to gravitaional instability. In the ?late Pliocene/ early Quaternary a regional stress change rotated the stress field to a direction orthogonal to the pre-existing structural weaknesses, causing them to activate as normal faults. Evidence from the Burdur region lakes and grabens also suggests that a gravitational collapse occurred during the Early Quaternary (Taymaz and Price, 1992) (chapter 6, section 6.6).

10) The shaping of the tufa terraces is thought to be a result of base level changes due to glacio-eustatic effects during the Pliocene and Quaternary (chapter 5, section 5.5.2).

11) During favourable climatic conditions in the Quaternary, Terra rossa soils formed on the tufa and the Mesozoic carbonates. These were washed into the central basin during flash floods carving extremely steep-sided channels in the fluvial conglomerates (chapter 5, section 5.7).

7.2: Basin evolution

The conclusions drawn above can be synthesised to produce a model of basin evolution which is outlined in the following paragraphs.

The Plio-Quaternary sediments were deposited in a pre-existing Miocene basin, which was formed during the Early Miocene. The earliest datable sediments were Lower-Mid Miocene in age (Burdighalian-Lhangian); terrestrial conglomerates at the base of the sequence are probably Aquitanian. The Antalya basins were essentially the northern margins of the Cilicia basin, which stretches from Antalya to Adana and between the Turkish coast and the Cyprus margin (Flecker, 1995). The timing of basin formation ties in with the formation of the Kasaba basin; a foreland basin in front of the advancing Lycian nappes (Hayward, 1982). The mechanisms of basin formation are thought to be block-faulting related to loading by the Lycian nappes (Flecker 1995). The Gebiz limestone which has been included in this study, as it was originally though to be Messinian in age (Akay and Uysal, 1985), is thought most likely to have been deposited towards the end of this period.

The final stages of emplacement of the Lycian nappes caused compression and uplift of the basin. The Gebiz limestone was probably uplifted at this stage. Subsequent dessication of the basin led to deposition of evaporites, probably in small lagoons or silled basins, analagous to the sub basins of Cyprus (Robertson *et al*, 1995).

Right-lateral shear deformed the basin during the Late Miocene-Early Pliocene. In particular, this activated right-lateral strike-slip faulting along pre-existing structural weaknesses, which were slightly oblique to the principal stress direction. This probably relates to the development of the current neotectonic regime of the eastern Mediterranean.

Flooding of the Mediterranean, after the Messinian salinity crisis, returned the basin to normal marine conditions. This resulted in deposition of the Yenimahalle Formation, which onlaps the Gebiz limestone near Gebiz; the Mesozoic further north near Haciosmanlar; and the Miocene near Manavgat. The marine Pliocene is largely controlled by eustatic sea-level effects and three transgressive phases are recognised. This was a phase of tectonic quiesence and the mature slope surfaces started to evolve in the Taurus Mountains, particularly in the west. Deposition of coarse fandeltas (the Kemer Fanglomerates) resulted from this and they form part of the mature slope profile.

A phase of neotectonic faulting, probably Early Quaternary in age, subsequently cut through these erosion surfaces, tilting the Pliocene sediments to the west. No fault activity is recognised on the eastern margin at this time and the basin

appears to be a half graben. It is thought that localised uplift of the Bey Dağ lari, dure to underthrusting of the Anaximander mountains, is responsible for this asymmetry. The uplift that this produced has caused deep incision of fluvial systems through the mature slope surfaces on the western basin margin. This phase of faulting is thought to relate to gravitational collapse, possibly as the result of a swing in the regional stress field which brought the maximum extension direction orthogonal to the pre-existing fault lineaments.

Deposition of the Antalya tufa is thought to have occurred during the Mid Quaternary, when climatically favourable conditions for tufa deposition existed over a long (0.5 Ma) time. The tufa deposited into the fault-block topography, which resulted from the Early Quaternary normal faulting event and was limited to the west by tilted fault blocks, which created a topographic high at the eastern margin of the tufa depositing area. A complex lacustrine/paludal/fluvial environment developed which shallowed-up through time.

These local events are all superimposed on a regional uplift, which is identified throughout the Quaternary, but may have begun earlier. Thus, subsidence of the basin caused by the Early Quaternary faulting is a relative subsidence of the basin compared to the Taurides, but a relative uplift compared to sea-level.

During the Late Quaternary, strong climatic fluctuations related to the glacial cycles have superimposed their signature on this regional uplift. The result is the exposure of climatically controlled fluvial aggradation terraces in the central Aksu basin. Terra rossa soils are the most recent deposit in the basin, occurring in steep sided channels cut into the fluvial terrace conglomerates, as a result of flash flood events. They are also found in pockets in the tufa, where some of the Terra rossa originally formed.

At the present time tectonic and sedimentary activity in the basin is minimal and erosional processes dominate. The tufa gradually collapses as cave systems undermine the structure and sink holes develop (i.e. the spur north of Antalya). Fluvial incision cuts away at the terrace edges during glacial periods when runoff is high. The main depositional process is that of Aksu conglomerate terrace formation.

7.3: Coda

This project has shed light on the previously undescribed sediments and the tectonics of the Plio-Quaternary of the Aksu basin. It has also provided an excellent opportunity to study an unusually large deposit of tufa and to contribute to a growing field of sedimentological interest. It is hoped that this work will be a useful starting point for other, more focused projects. I believe that further seismic profiling and

coring of the Antalya bay sediments could provide an invaluable record of eustatic sea-level changes in the Mediterranean Pliocene and Quaternary. The relatively stable tectonic conditions recognised at this time and the excellent foraminiferal record uncovered by this study give high hope for success. The Antalya tufa may also be an ideal place for further research. In particular, more detailed observations on facies changes and relationships could be undertaken, and on the role of bacteria and algae in tufa deposition. Better dating might be achieved by a study of ostracods or from pollen within the soils. It would also be interesting to compare the model produced with lacustrine depositional environments, in order to identify similarities between facies variations and to further develop the links recognised between terrestrial carbonates.

Finally, I hope the information contained in this thesis will also be useful for researchers compiling more general studies of tectonics and sedimentation in the eastern Mediterranean and in regions of incipient collision.

References

Adamia Sh. A., Chkhotua T., Kekelia M., Lordkipanidze M., Shavishili I. and Zakariadze G. (1981) Tectonics of the Caucasus and adjoining regions: implications for the evolution of the Tethys ocean. *Journal of Structural Geology*, **3**, 437-447.

Adamia Sh.A. and Belov A.A. (1989). Problems on the Paleozoic and paleodynamic domains and their alpidic evolution in the Caucasus. **In:** Papanikolu D.J. and Sassi F.P. (eds) IGCP Project No. 276, Newsletter 1. *Geological Society of Greece Special Publication*, **1**, 11-18.

Akay, E and Uysal, S (1985) Orta toroslarin batisindaki (Antalya) Neojen çökellerinin stratigrafisis, sedimentolojisi ve yapisal jeolojisi, MTA

Akay E., Uysal S., Poisson A., Cravatte J. and Müller C. (1985) Antalya Neojen havzasinin straigrafisi. *Bulletin of the Geological Society of Turkey*, **28**, 105-119.

Alexander J., Nichols G.J. and Leigh S. (1990) The origins of marine conglomerates in the Pindus foreland basin, Greece. *Sedimentary Geology*, **66**, 243-254.

Altunel E. and Hancock P.L. (1993) Active fissuring and faulting in Quaternary Travertines at Pammukale, western Turkey. *Zeitschrift für Geomorphologie. Neue Forschung*, **94**, 285-302.

Altunel E. and Hancock P.L. (1993) Morphology and structural setting of Quaternary Travertines at Pammukale, Turkey. *Geological Journal*, **28**, 335-346.

Amundson R. and Kelly E. (1987) The chemistry and mineralogy of a CO_2-rich Travertine depositing spring in the California Coast Range. *Geochimica et Cosmochimica Acta*, **51**, 2883-2890.

Anastasakis G. and Kelling G. (1991) Tectonic connection of the Hellenic and Cyprus arcs and related geotectonic elements. *Marine Geology*, **97**, 261-277.

Angelier J., Dumont J.-F., Karamanderesi H., Poisson A., Simsek S. and Uysal S. (1981) Analysis of fault mechanisms and expansion of southwestern Anatolia since the Late Miocene. *Tectonophysics*, **75**, T1-T9.

Anketell, J.M., Cegla J. and Dzulynski S. (1970) On the deformational structures in systems with reverse density gradients. *Annales Societatis Geologorum Poloniae*, **40**, 3-30.

Auboin J. (1975) Alpine tectonics and plate tectonics: thoughts about the eastern Mediterranean. **In:** Ager D.V. and Brooks M. (eds) *Europe from crust to core*. Wiley, New York.

Aydar C. and Dumont J-V. (1979) Antalya travertinlerinde görülen dizilmelerde elde edilen Landsat görüntüleri üzerinde yapilan gözlemler: Neotektonik ve hidrojeoloji arasinda olabilecek bagintilarin tartismasi. *Maden Tetkik ve Arama Enstitusu dergisi*, Nisan 1979, **92**, 131-134.

Aydin A and Reches Z. (1982) Number and orientation of fault sets in the field and in experiments. *Geology*, **10**, 107-112.

Bally A.W. (1982) Musings over sedimentary basin evolution. *Philosophical Transactions of the Royal Society of London*, **A305**, 325-338.

Barger K.E. (1978) Geology and thermal history of Mammoth Hot Springs, Yellowstone National Park, Wyoming: *U.S. Geological Survey Bulletin*, **1444**, pp55.

Barka A.A. and Hancock P. (1984) Neotectonic deformation patterns in the convex northwards arc of the North Anatolian fault zone. **In:** Dixon J.E. and Robertson A.H.F. (eds) The geological evolution of the eastern Mediterranean. *Geological Society of London Special Publication*, **17**, 763-774.

Barka A.A. and Kadinsky-Cade K. (1988) Strike-slip fault geometry in Turkey and its influence on earthquake activity. *Tectonics*, **7**, 663-684.

Barnes I. (1965) Geochemistry of Birch Creek, Inyo County, California a Travertine depositing creek in an arid climate. *Geochimica et Cosmochimica Acta*, **29**, 85-112.

Ben-Avraham Z., Kempler D. and Ginzburg A. (1988) Plate convergence in the Cyprean arc. *Tectonophysics*, **146**, 231-240.

Bergerat F. (1987) Stress fields in the European platform at the time of the Africa-Eurasia collision. *Tectonics*, **6**, 99-132.

Bloom A.L., Broecker W.S., Chappell J.M.A., Matthews R.K. and Mesolella K.J. (1974) Quaternary sea-level fluctuations on a tectonic coast: new $^{230}Th/^{234}U$ dates from the Huon Peninsula, New Guinea. *Quaternary Research*, **4**, 185-205.

Bluck B.J. (1967) Sedimentation of beach gravels: examples from South Wales. *Journal of Sedimentary Petrology*, **37**, 128-156.

Boardman R.S., Cheetham A.H. and Rowell A.J. (eds) (1987) *Fossil invertebrates.* Blackwell Scientific Publications. pp713.

Bougeois J. and Leithold E.L. (1984) Wave-worked conglomerates - depositonal processes and criteria for recognition. **In:** Koster E.H. and Steel R.J. (eds) *Sedimentology of gravels and conglomerates.* Canadian Society of Petroleum Geologists, Memoir **10**, Calgary, Alberta, Canada, 331-343.

Bowen D.Q. (1978) *Quaternary Geology: A stratigraphic framework for multidisciplinary work.* Pergamon press, New York, Oxford. pp 221.

Brancaccio L., D'Argenio B., Ferrei V., Stanzione D., Bruno T. and Maria P.M. (1986) Caratteri tessiturali e geochimici dei Travertini di Rocchetta a Volturno (Molise). *Bolletino Societa Geologica Italiana*, **105**, 265-277.

Brancaccio L., D'Argenio B., Ferreri V., Stanzione D., Taddeuci A. and Voltaggio M. (1988) I Travertini di Rocchetta a Volturno (Molise). Datzioni con ^{230}Th e modello deposizionale. *Memorie Societa Geologica Italiana*, **41**, 673-683.

Brunn J.H., Dumont J.F., Graciansky P.C. de, Gutnic M., Juteau T, Marcoux J., Monod O. and Poisson A. (1971) Outline of the geology of the western Taurides. **In:** Campbell A.S. (ed) *Geology and History of Turkey.* Petroleum Exploration Society of Libya. Tripoli. 225-255.

Brunn J.H. (1974) Le problème de l'origine des nappes et leurs translations dans les Taurides occidentales. *Bulletin de la Société Géologique de France*, **16**, 101-106.

Buccino G., D'Argenio B., Ferreri V., Brancaccio L., Ferreri M., Panichi C. and Stanzione D. (1978) I Travertini della bassa valle del Tanagro (Campania) Studio Geomorphologico, Sedimentologico e Geochimico. *Bolletino Societa Geologica Italiana*, **97**, 617-646.

Buczynski C. and Chafetz H.S. (1991) Habit of bacterially induced precipitates of calcium carbonate and the influence of medium viscosity on mineralogy. *Journal of Sedimentary Petrology*, **61**, 226-233.

Bull W.B. (1990) Stream terrace genesis: implications for soil development. *Geomorphology*, **3**, 251-367.

Bull W.B. and Kneupfer P.L.K. (1987) Stream adjustment to uplift and climatic change, Charwell river, New Zealand. *Geomorphology*, **1**, 15-32.

Burger D. (1989) The travertine complex of Antalya/southwest Turkey. *International atlas of karst phenomena.* sheet **9**.

Burger D. (1990) The Travertine Complex of Antalya/Southwest Turkey. *Zeitschrift für Geomorphologie. Neue Forschung*. Suppl. Bd. **77**, 25-46.

Burger D. (1992) *Quantifizierung Quartärer subtropischer verwitterung auf kalk: das Beispiel Travertinkomplex von Antalya - Südwesttürkei.* Gebrüder Borntraeger, Berlin, Stuttgart. pp 131.

Carson M.A. and Kirkby M.J. (1972) *Hillslope form and process*. Cambridge university press, Cambridge.

Casanova J. (1986) East African Rift stromatolites. **In:** Frostick L.E. *et al.* (eds.) Sedimentation in the African Rifts. *Geological Society Special Publication*, **25**, 201-10.

Casanova J. and Nury D. (1989) Biosédimentologie des stromatolites fluvio-lacustres du fossè Oligocéne de Marseille. *Bulletin de la Société Géologique de France,* **V (6)**, 1173-1184.

Castanier S., Maurin A. and Perthuisot J-P. (1989) Production Bactérienne expérimentale de Corpuscles Carbonatés, Sphéroïdaux à Structure Fibro-radiare. Réflexions sur la Définition des Ooïdes. *Bulletin de la Société Géologique de France*, serie 8, **V (3)**, 589-595.

Chafetz H.S., Rush P.F. and Utech N.M. (1991) Microenvironmental controls on mineralogy and habit of $CaCO_3$ precipitates: an example from an active Travertine system. *Sedimentology*, **38**, 107-126.

Chafetz H.S. and Folk R.L. (1984) Travertines: depositional morphology and their bacterially constructed constituents. *Journal of Sedimentary Petrology*, **54**, 289-316.

Chappell J.M.A. (1983) A revised sea-level record for the last 300,000 years on Papua New Guinea. *Search*, **14**, 99-101.

Chaput G. and Darkot B. (1953) Sur le Pliocène des Environs D'Antalya (Turquie). *Compte Rendus Académie des Sciences*, **236**, 2259-2260.

Christie-Blick N. and Biddle K.T. (1985) Deformation and basin formation along strike-slip faults. **In:** Biddle K.T. and Christie Blick N. (*eds*) Strike-slip deformation, basin formation and sedimentation. *SEPM special publication*, **37**,1-34.

Cita M.B. (1975) Studi sul Pliocene e sugli strati di passagio dal Miocene al Pliocene. VIII. Planktonic foraminiferal biozonation of the Mediterranean Pliocene deep sea record. A revision. *Riv. Italia Paleontologica*, **81**, 527-44.

Clift P.D. (1990) Mesozoic/Cenozoic sedimentation and tectonics of the Southern Greek Neotethys (Argolis Peninsula) *Unpublished PhD thesis, University of Edinburgh.* pp336.

Clifton H.E. (1973) Pebble segregation and bed lenticularity in wave-worked versus alluvial gravel. *Sedimentology*, **20**, 173-187.

Cloetingh S. (1986) Intraplate stresses: a new tectonic mechanism for fluctuations of sea-level. *Geology*, **14**, 617-620.

Cochran J.R. (1981) The Gulf of Aden: structure and evolution of a young ocean basin and continental margin. *Geophysical Research*, **86**, 263-288.

Colella A. (1988) Pliocene-Holocene fan deltas and braid plain deltas in the Crati basin, southern Italy: a consequence of varying tectonic conditions. **In:** Nemec W. and Steel R.J. (eds) *Fan deltas: sedimentology and tectonic settings*. Blackie and Son, London, 50-74.

Cortesi C. and Leoni M. (1955) Studio sedimentologica a geochimica del travertino di un sondaggio a Bagni di Tivoli. *Periodica di Mineralogia*, **27**, 407-458.

Couteaux M. (1969) Formation et chronologie palynologique des Tufs calcaires du Luxembourg Belgo-Grand-Ducal. *Bulletin de l'Association Francaise pour l'Etude du Quaternaire*, **3**, 179-206.

Crimes T.P. (1975) The stratigraphical significance of trace fossils. **In:** Frey R.W. (ed) *The study of trace fossils*. Springer Verlag. New York. 109-130.

D'Argenio B., Ferreri V., Stanzione D., Brancaccio L. and Ferreri M. (1983) I Travertini di Pontecagnano (Campania) geomorfologia, sedimentologia, Geochimica. Bull. Geol. Soc It., **102**, 123-136.

Dalrymple G.B. and Lanphere M.A. (1969) *Potassium-Argon dating: principles, techniques and applications to geochronology*. W.H. Freeman and Co. San Francisco. pp258.

Darkot B.and Erinç S. (1947) Aksu batisinda Antalya traverten taraçalari. *Instanbul Üniversitesi Çoğ rafya Enstitüt Dergisi*, **1**, 56-65.

Davies A.M. (1935) *Tertiary Faunas. Vol.1: The composition of Tertiary faunas*. Thomas Murby & Co. pp 406.

Değ irmenci M. and Günay G. (1992) Analysis of Hydrologic Relations between Eğ irdir-Beysehir-Suğ la Lakes system and adjacent basins by means of remote sensing techniques (southern Turkey). *Environmental Geology and Water Sciences*, **19**, 41-45.

Défarge C., Trichet J. and Couté A. (1994) On the appearance of Cyanobacterial calcification in modern stromatolites. *Sedimentary Geology*, **94**, 11-19.

Degnan P.J. (1992) Tectono-sedimentary evolution of a passive margin: the Pindos zone of the NW Peleponnese, Greece. *Unpublished PhD thesis, University of Edinburgh*. pp400.

Demitrack A. (1986) The late Quaternary geologic history of the Larissa Plain, Thessaly, Greece: tectonic, climatic and human impact on the landscape. *Unpublished PhD thesis. Stanford University*, USA.

Depape J. and Arènes G. (1952) Contribution à l'étude des flores fossiles d'Asie Minuere. *Bulletin du Muséum, Paris*, Serie 2. **XXIV**, 328-332.

Dewey J.F., Pitman W.C. III, Ryan W.B.F and Bonin J. (1973) Plate tectonics and the evolution of the Alpine System. *Geological Society of America Bulletin*, **84**, 3137-3180.

Dewey J.F. and Sengör A.M.C. (1979) Aegean and surrounding regions: complex multiplate and continuum tectonics in a convergent zone. *Geological Society of America Bulletin*, **90**, 84-92.

Dilek Y. and Rowland J.C. (1993) Evolution of a conjugate passive margin pair in Mesozoic southern Turkey. *Tectonics*, **12**, 954-970.

Douglas R.G. (1979) Benthic foraminiferal ecology and paleoecology: a review of concepts and methods. **In:** Lipps J.H., Berger W.H., Buzas M.A., Douglas R.G. and Ross, C.A. *Foraminiferal ecology and paleoecology*. SEPM short course No. **6**. Society of Economic Paleontologists and Mineralogists, Houston. 21-53.

Du Poux B. (1983) Étude compareé de la tectonique néogène des bassins du sud de Chypre et du bassin d'Antalya (Turquie). *Unpublished MSc Thesis, Université de Paris-Sud, Orsay* pp 122.

Dumont J.F., Gutnic M., Marcoux J., Monod O. and Poisson A. (1972) Le Trias des Taurides occidentales (Turquie). Definition du bassin Pamphylien: Un nouveau domain à ophiolites à la marge extreme de la chaine taurique. *Zeitshcrift für Deutsche Geologische Geschichte*, **123**, 385-409.

Dumont J.F. and Uysal S., Simsek S., Kahramanderesi H. and Letouzey J. (1979) Formation of the grabens in southwestern Anatolia. *Bulletin of the Mineralogical and Research Exploration Institite of Turkey*, **92**, 7-18.

Dunne L.A. and Hempton M. R. (1984) Deltaic sedimentation in the Lake Hazar pull-apart basin, south-eastern Turkey. *Sedimentology*, **31**, 401-412.

Eaton S. (1987) The sedimentology of Mid to Late Miocene carbonates and evaporites in southern Cyprus. *Unpublished PhD thesis, University of Edinburgh.*

Eaton S. and Robertson A.H.F. (1993) The Miocene Pakhna Formation, southern Cyprus and its relationship to the Neogene tectonic evolution of the Eastern Mediterranean. *Sedimentary Geology*, **86**, 273-296.

Eggleston J.R. and Dean W.E. (1976) Freshwater stromatolitic bioherms in Green Lake, New York. **In:** Walter M.R. (ed.) *Stromatolites. Developments in Sedimentology*, **20**, 479-488.

Emeis K.-C., Richnow H.-H. and Kempe S. (1987) Travertine formation in Plitvice National Park, Yugoslavia: chemical versus biological control. *Sedimentology*, **34**, 595-609.

England P. and McKenzie D.P. (1983) Correction to: a thin viscous sheet model for continental deformation. *Geophysical Journal of the Royal Astronomical Society*, **73**, 523-532.

Eyal Y. and Reches Z. (1983) Tectonic analysis of the Dead Sea Rift regions since the late-Cretaceous based on mesostructures. *Tectonics*, **2**, 167-185.

Eyidoğan H. (1988) Rates of crustal deformation in western Turkey as deduced from major earthquakes. *Tectonophysics*, **148**, 83-92.

Faure G. (1991) *Principles and applications of inorganic geochemistry*. Maxwell Macmillan International Editions, New York. pp626.

Fisher R.V. and Schminke H.-U. (1984) *Pyroclastic rocks* . Springer Velag, Berlin. pp472.

Fisher R.V. and Waters A.C. (1970) Base surge bed forms in maar volcanoes. *American Journal of Science*, **268**, 157-180.

Flecker R.M., Robertson A.H.F., Poisson A. and Müller C. (1995) Facies and tectonic significance of two contrasting Miocene basins in south coastal Turkey. *Terra Nova*, **7**, 221-232.

Flecker R.M. (1995) Miocene basin evolution of the Isparta angle, S.Turkey. *Unpublished PhD thesis, University of Edinburgh.*

Flemming N.C. (1971) Eustatic and tectonic factors in the relative vertical displacement of the Aegean coast. **In:** Stanley D.J., Kelling G. and Weiler Y. (eds) The Mediterranean Sea: a natural sedimentation laboratory, 189-201.

Flügel E. (1972) Microfazielle Untersuchungen in der Alpinen Trias. Methoden und Probleme. *Mitteilungen für Gesellschaft der Geologisches Bergbaustudium*, **21**, 9-64.

Flugel E. (1978) *Mikrofazielle Untersuchungesmethoden von Kalken*. Springer-Verlag, Berlin, pp454.

Flügel E. (1982) *Microfacies Analysis of Limestones*. Springer-Verlag, Berlin, pp633.

Folk R.L. (1959) Practical petrographic classification of limestones. *Bulletin of the American Association of Petroleum Geologists*, **43**, 1-38.

Folk R.L. (1962) Spectral subdivision of limestone types. **In:** Ham W.E. (ed) Classification of carbonate rocks. *Memoir of the American Association of Petroleum Geologists*, **1**, 62-84.

Folk R.L. (1974) *Petrology of sedimentary rocks*. Hemphill Publishing Company, Austin, Texas. pp159.

Folk R.L. and Chafetz H.S. (1983) Pisoliths (pisoids) in Quaternary Travertines of Tivoli, Italy. **In:** Peryt T.M. (ed.) *Coated grains*. Springer-Verlag, Berlin, Heidelberg. pp474-487.

Follows E.J. (1990) Sedimentology and tectonic setting of Miocene reefs and related sediments in Cyprus. *Unpublished PhD thesis, University of Edinburgh*.

Ford T.D. (1989) Tufa: a freshwater limestone. *Geology Today*, Mar-Apr 1989, 60-63.

Frizon de Lamotte D., Poisson A., Aubourg C. and Temiz H. (1995) Chevauchements post Tortoniens vers L'ouest puis vers le sud au coeur de l'Angle d'Isparta (Taurus, Turquie). Conséquences Géodynaminques. *Bulletin de la Société Géologique de France*, **166**, 57-66.

Frostick L.E and Reid I. (1989) Climatic versus tectonic controls of fan sequences: lessons from the Dead Sea, Israel. *Journal of the Geological Society of London*, **146**, 527-538.

Fytikas M., Innocenti F., Manetti P., Mazzuoli R., Peccerillo A. and Villeri L. (1984) Tertiary to Quaternary evolution of volcanism in the Aegean region. **In:** Dixon J.E. and Robertson A.H.F. (eds) The geological evolution of the eastern Mediterranean. *Geological Society of London Special Publication*, **17**, 687-699.

Galloway W.E. (1975) Process framework for describing the morphology and stratigraphic evolution of the deltaic depositional systems. **In:** Broussard M.L. (ed) *Deltas: models for exploration.* Houston Geological Society, Houston. 87-98.

Gautier P., Brun J.P., Sokoutis D., Jolivet L., van den Driesseche J., Martinod J. and Hatzfeld D. (1995) The onset of Aegean extension: lateral extrusion vs gravity spreading of thickened lithosphere. *Terra abstracts:* supplement to *Terra Nova*, **7**, abstract XII-1(23), 171.

Gawthorpe R.L. and Colella A. (1990) Tectonic controls on coarse grained delta depositional systems in rift basins. **In:** Colella A. and Prior D.B. (eds) *Coarse-grained deltas.* Special publication of the International Association of Sedimentologists **10**, Blackwell Scientific Publications, 113-128.

Gerdes G., Dunajtschik-Piewak K., Riege H., Taher A.G., Krumbein W.E. and Reineck H.-E. (1994) Structural diversity of biogenic carbonate particles in microbial mats. *Sedimentology*, **41**, 1273-1294.

Gilliland and Mayer C.P. (1976) Two classes of transform faults. *Geological Society of America Bulletin*, **87**, 1127-1130.

Golubic S., Violante C., Ferreri V. and D'Argenio B. (1993) Algal control and diagenesis in Quaternary Travertine formation (Rochetta a Volturno, Central Appenines). **In:** Barattolo F. (*ed.*) Studies on Fossil Benthic Algae. *Bolletino della Societa Paleontologica Italiana*, Sp. Vol., **1**, 231-247.

Golubic S. (1969) Cyclic and non-cyclic mechanisms in the formation of Travertine. *Verhandlungen der Internationalen Vereinigung für Theoretische und Angewandte Limnologie*, **17**, 956-961.

Golubic S. (1991) Modern stromatolites: a review. **In:** Riding R. (ed.) *Calcareous algae and stromatolites*. Springer-Verlag, Berlin, Heidelberg. 541-561.

Gow C.E. (1981) Unusual occurance of biogenic (Cyanobacterial) carbonate sediments from a sink-hole lake in the western Transvaal, South Africa. *South African Journal of Science*, **77**, 564-565.

Gutnic, M., Monod O., Poisson A. and Dumont J.F. (1979) Géologie des Taurides occidentales (Turquie) *Mémoires de la Société Géologique de France*, **137**, 1-112.

Gvirtsman G. and Buchbinder B. (1978) Recent and Pleistocene coral reefs and coastal sediments of the Gulf of Elat. Post-congress guidebook. *Tenth International Congress of Sedimentology, Jerusalem*. 163-189.

Hack J.T. (1960) Interpretation of erosional topography in humid temperate regions. *American Journal of Science* (Bradley volume), **258-A**, 80-97.

Hancock P.L. (1985) Brittle microtectonics: principles and practice. *Journal of Structural Geology*, **7**, 437-457.

Hancock P.L. and Barka A.A. (1987) Kinematic Indicators on Active Normal Faults in Western Turkey. *Journal of Structural Geology*, **9**, 573-584.

Hardie L.A. and Eugster H.P. (1971) The depositional environment of marine evaporites: a case for shallow, clastic accumulation. *Sedimentology*, **16**, 187-220.

Harland W.B., Cox A., Llewellyn P.G., Pickton C.A.G., Smith A.G., Walter R. and Fancett K.E. (1982) *A geologic time-scale*. Cambridge University Press, pp131.

Hasegawa S., Sprovieri R. and Poluzzi A. (1990) Quantitative analysis of benthic foraminiferal assemblages from Plio-Pleistocene sequences in the Tyrrhenian sea, ODP leg 107. **In:** Kastens K.A., Mascle J. et al. *Proceedings of the Ocean Drilling Program, Scientific Results*, College Station, Texas, **107**, 461-478.

Haynes C.V. Jr. (1987) Curry Cochise County, Arizona. A late Quaternary stratigraphic record of Pleistocene extinction and paleo-Indian activities. *Geological Society of America, Centennial Field Guide*, Cordilleran Section, 23-28.

Haynes J.R. (1981) *Foraminifera*. Macmillan, London, pp 433.

Hayward A.B. (1982) Tertiary ophiolite-related sedimentation in S.W. Turkey. *Unpublished Ph.D thesis, University of Edinburgh.* pp420.

Hayward A.B. (1984) Miocene clastic sedimentation related to the emplacement of the Lycian Nappes and the Antalya Complex, SW Turkey. **In:** Dixon J.E. and Robertson A.H.F. (eds) The geological evolution of the eastern Mediterranean. *Geological Society of London Special Publication*, **17**, 287-300.

Heimann A. and Sass E. (1989) Travertines in the Northern Hula Valley, Israel. *Sedimentology*, **36**, 95-108.

Hempton M.R. (1987) Constraints on Arabian plate motion and extensional history of the Red Sea. *Tectonics*, **6**, 687-705.

Herman J.S. and Lorah M.M. (1987) CO_2 outgassing and calcite precipitation in Falling Spring Creek, Virginia, U.S.A. *Chemical Geology*, **62**, 251-262.

Horvatincic N. (1985) Radiocarbon age measurements of Tufa deposits from the Plitvice Lake Area. *Unpublished PhD thesis, University of Zagreb*.

Hsü K.J., Montadert L., Bernoulli D., Cita M.B., Erickson A., Garrison R.E., Kidd R.B., Mélières F., Müller C. and Wright R. (1978) History of the Mediterranean salinity crisis. **In:** Hsü K.J., Montadert L. *et al.*(1978) *Initial Reports of the Deep Sea Drilling Project*, **42**, (1). U.S. Government printing office, Washington. USA. 1053-1078.

Huntsman S.A. and Sunda W.G. (1980) **In:** (K. Morris, ed.) *The physiological ecology of phytoplankton*, Blackwell, 285-328.

Innocenti F., Manetti P., Mazzouli R., Pasquare G., and Villari L., (1982) Anatolia and north-west Iran. **In:** Thorpe R.S. (ed.) *Andesites*. Wiley, Chichester. 328-349.

Irion G. and Müller G. (1968) Mineralogy, petrology and chemical composition of some calcareous Tufa from the Schwabische Alb, Germany. **In:** Müller G. and Friedman I. (eds) *Recent developments in carbonate sedimentology in central Europe*. Springer-Verlag. 157-171.

Ivanovich M. and Harmon R.S. (eds.) (1982) *Uranium series disequilibrium: applications to environmental problems*. Clarendon Press. Oxford. pp571.

Jackson J.A. and McKenzie D. (1984) Active tectonics of the Alpine-Himalayan belt between western Turkey and Pakistan. *Geophysical Journal of the Royal astronomical Society*. **77**, 185-264.

Johnson H.D.and Baldwin C.T. (1978) Shallow siliciclastic seas. **In:** Reading H.G. (ed) *Sedimentary environments and facies*. Blackwell scientific publications, 229-282.

Jolivet, L., Brun J.-P., Gautier P., Lallemant S. and Patriat M. (1994) 3D Kinematics of extension in the Aegean region from the Early Miocene to the Present, insights from the ductile crust. *Bulletin de la Société Géologique de France*, **165**, 195-209.

Jones F.G. and Wilkinson B.H. (1978) Structure and growth of lacustrine pisoliths from Recent Michigan marl lakes. *Journal of Sedimentary Petrology*, **48**, 1103-1110.

Jones G. (1990) Tectono-stratigraphy and evolution of the Mesozoic Pindos ophiolite and associated units, northwestern Greece. *Unpublished PhD thesis, University of Edinburgh*. pp397.

Jongsma M. and Mascle J. (1981) Evidence for northward thrusting southwest of the Rhodes basin. *Nature*, **293**, 49-51.

Julia R. (1983) Travertines. **In:** Scholle P.A., Bebout D.G. and Moore C.H. (eds) Carbonate depositional environments. *Memoir of the American Association of Petroleum Geologists*, **33**, 64-72.

Jux U. and Kempf E.K. (1971) Stauseen durch Travertinabsatz im Zentralafghanischen Hochgebirge. *Zeitschrift für Geomorphologie, Neue Forschung*. Suppl. Bd. **12**, 107-137.

Karig D.E. and Kozlu H. (1990) Late Paleogene-Neogene evolution of the triple junction region near Maras, south-central Turkey. *Journal of the Geological Society, London*, **147**, 1023-1034.

Kaufmann A. (1993) An evaluation of several methods for determining $^{230}Th/U$ ages in impure carbonates. *Geochimica et Cosmochimica Acta*, **57**, 2303-2317.

Kelling G., Gökcen S.L., Floyd P A. and Gökcen N. (1987) Neogene tectonics and plate convergence in the eastern Mediterranean: new data from southern Turkey. *Geology*, **15**, 425-429.

Kempe S. and Emeis K. (1985) Carbonate chemistry and the formation of the Plitvice Lakes. **In:** Degens E., Kempe S. and Herrera (eds). *Transport of carbon and minerals in major world rivers*, Part 3. Mitteilungen der Geologie und Paläontologie Institüt, Universität Hamburg, **58**, 351-383.

Kempler D. and Ben Avraham Z. (1987) The tectonic evolution of the Cyprean Arc. *Annales Tectonicae*, **1**, 58-71.

Kennet J.P. and Srinivasan M.S. (1983) *Neogene planktonic foraminifera: a phylogenetic atlas*. Hutchison Ross, Pennsylvania, pp 263.

Kissel C., Laj C., Poisson A., Savaşçin Y., Simeakis K. and Mercier J.(1986) Paleomagnetic evidence for Neogene rotational deformations in the Aegean domain. *Tectonics*, **5**, 783-796.

Kissel C., Averbuch O., Frizon de Lamotte D., Monod O. and Allerton S. (1993) First paleomagnetic evidence for a post- Eocene clockwise rotation of the western Taurides thrust belt east of the Isparta re-entrant (southwestern Turkey). *Earth and Planetary Science Letters*, **117**, 1-14.

Kissel C. and Poisson A. (1986a) Étude paléomagnetique préliminare des formations Cénozoiques des Bey Daglari (Taurides occidentales - Turquie). *Comptes Rendus de l'Académie des Sciences*, Paris, **302, Série II (8)**, 343-348.

Kissel C. and Poisson A. (1986b) Étude paléomagnetique préliminare des formations Néogènes du bassin d'Antalya (Taurides occidentales - Turquie). *Comptes Rendus de l'Académie des Sciences*, Paris, **302, Série II (10)**, 711-716.

Kitano Y. (1963) Geochemistry of calcareous deposits found in hot springs. *Journal of Earth Sciences*, Nagoya University, **11**, 68-100.

Koban C.G. and Schweigert G. (1993) Microbial origin of Travertine fabrics - Two Examples from southern Germany (Pleistocene Stuttgart Travertines and Miocene Riedöschingen Travertine). *Facies*, (Stuttgart) **29**, 251-264.

Koceafe S. and Ataman G. (1976) Anadolu'da sismo-tectonik olayar - I Anatalya- Fethiye - Denizli Üçgeni içinde yerlalan bölgenin incelenmesi. (Seismo-tectonic events of Anatolia - I. Investigation of the region Antalya - Fethiye - Denizli Triangle. *Yerbilimleri* (Haceteppe University) **C.2 (1)**, 55-70.

Ku T.L. and Liang Z.C. (1984) The dating of impure carbonates with decay series isotopes. *Nuclear Instruments and Methods in Physics Research*, **223**, 563-571.

Kubiëna W.L. (1948) *Entwicklungslehre des Bodens*. Wien.

Kubiëna W.L. (1953) *The soils of Europe*. Thomas Murby and Co., London, pp317.

Kumar N. and Sanders J.E. (1976) Characteristics of modern shoreface deposits: modern and ancient examples. *Journal of Sedimentary Petrology*, **46**, 145-162.

Laj C., Jamet M., Sorel D. and Valente J.P. (1982) First palaeomagnetic results from Mio-Pliocene series of the Hellenic sedimentary arc. *Tectonophysics*, **86**, 45-67.

Lamarche V.C. (1968) Rates of slope degradation as determined from botanical evidence, White Mountains, California. *Professional Paper of the United States Geological Survey*, **352-I**, 341-377.

Laubscher H. P. and Bernouilli D. (1977) Mediterranean and Tethys,. **In:** Nairn A.E.M., Kanes W.H. and Stehl F.G. (eds) *The Ocean Basins and Margins, 4A, The Eastern Mediterranean*, Plenum, New York. 1-28.

Le Maitre R.W., Bateman P., Dudek A., Keller J., Lameyre Le Bas M.J., Sabine P.A., Scmid R., Sorenson H., Steckeisen A., Woolley A.R. and Zanettin B. (1989) *A classification of igneous rocks and glossary of terms*. Blackwell, Oxford.

Le Pichon X., Chamot-Rooke N., Huchon P. and Luxey P. (1993) Implications des nouvelles mesures de géodesie spatiale en Grèce et en Turquie sur l'extrusion latérale de l'Anatolie et de l'Égée. *Comptes Rendus de l'Académie des Sciences*, Paris, **316, Série II**, 983-990.

Le Pichon X. and Angelier J. (1979) The Hellenic arc and trench system: A key to the Neotectonic evolution of the Eastern Mediterranean area. *Tectonophysics*, **60**, 1-42.

Le Pichon X. and Francheteau J.-F.(1978) A plate tectonic analysis of the Red Sea - Gulf of Aden area. *Tectonophysics*, **46**, 369-406.

Le Pichon X. and Gaulier J.-M. (1988) The rotation of Arabia and the Levant fault system. *Tectonophysics*, **153**, 271-294.

Leeder M.R. and Alexander J.A. (1986) The Origin and Tectonic Significance of Asymmetrical Meander-belts. Sedimentology, **34**, 217-226.

Lefèvre C., Bellon H. and Poisson A. (1983) Présence de leucites dans le volcanisme pliocène de la région d'Isparta (Taurides occidentales, Turquie). *Comptes Rendus de l'Académie des Sciences,* Paris, **297, Série II**, 367-372.

Lefevre R. (1967) Un nouvel élément de la géologie du Taurus Lycien: les nappes d'Antalya (Turquie) *Comptes Rendus de l'Académie des Sciences,* Paris, **271**, 285-267.

Lewin J., Macklin M.G. and Woodward J.C. (1991) Late Quaternary Fluvial Sedimentation in the Voidomatis Basin, Epirus, Northwest Greece. Quaternary Research, **35**, 103-115.

Limanov, A.F., Woodside J.M. and Ivanov M.K. (eds) (1994) Mud volcanism in the Mediterranean and Black Seas and shallow structure of the Eratosthenes Seamount. Initial results of the geological and geophysical investigations during the third UNESCO-ESF "Training-through-Research" Cruise of RV *Gelendzhik* (June-July 1993). *UNESCO reports in Marine Geoscience,* **64**, pp173.

Link M.H., Osbourne R.H. and Awramik S.M. (1978) Lacustrine stromatolites and associated sediments of the Pliocene Ridge Route Formation, Ridge basin, California. *Journal of Sedimentary Petrology*, 48, 143-158.

Liritzis Y. and Galloway R.B. (1982) The $^{230}Th/^{234}U$ disequilibrium dating of cave travertines. *Nuclear instruments and methods*. **201**, 507-510.

Livermore R.A. and Smith A.G. (1984) Relative motions of Africa and Europe in the vicinity of Turkey. **In:** Tekeli O. and Göngüoğlu M.C. (eds) *Geology of the Taurus Belt*, MTA, Ankara, 1-10.

Loeblich A.R., Jr. and Tappan H. (1988) *Foraminiferal genera and their classification*. Von Nostran Reinhold, New York. pp869 + 847 plates (separate volume).

Logan B.W., Rezak R. and Ginsburg R.N. (1964) Classification and environmental significance of algal stromatolites. *Journal of Geology*, **72**, 68-83.

Lowe D.R. (1975) Water escape structures in coarse-grained sediments. *Sedimentology*, **22**, 157-204.

Lyon-Caen H. and Molnar P. (1985) Gravity anomalies, flexure of the Indian plate, and the structure, support and evolution of the Himalaya and Ganga basin. *Tectonics*, **4**, 513-538.

Magnin F., Guendon J-L., Quinf Y., Roiron P. and Thinon M. (1990) Datations isotopiques et étude des paléoenvironnements de la formation de la Papeterie Vasino (Meyrargues, Bouches-du-Rhône, France). Mise en Évidence de deux périodes de réchauffement durant le Riss. *Comptes Rendus de l'Académie des Sciences,* Paris, **310**, série II. 1285-1292.

Magnin F., Guendon J-L., Vaudour J. and Martin P. (1991) Les Travertins: accumulations carbonatées associées aux systèmes karstiques, séquences sédimentaires et paléoenvironnements Quaternaires. *Bulletin de la Société Géologique de France*, **162(3)**, 585-594.

Makris J. (1976) A dynamic model of the Hellenic arc deduced from geophysical data. *Tectonophysics*, **36**, 339-346.

Makris J. and Vees R. (1977) Crustal structure of the central Aegean Sea and the islands of Evvia and Crete, Greece, obtained from refraction seismic experiments. *Journal of Geophysics*, **42**, 329-341.

Marcoux J., Brun J.P., Burg J.P. and Ricou L.-E. (1989) Shear structures in the base of anhydrite at the base of thrust sheets (Antalya, southern Turkey). *Journal of Structural Geology*, **9**, 555-561.

Marcoux J., Ricou L.-E., Burg J.P. and Brun J.P. (1989) Shear-sense criteria in the Antalya and Alanya thrust system (southwestern Turkey): evidence for a southward emplacement. *Tectonophysics*, **161**, 81-91.

Marker M.E. (1971) Waterfall Tufas: A facet of karst geomorphology in South Africa. *Zeitschrift für Geomorphologie. Neue Forschung*. suppl. Bd. **12**, 138-152.

Marle L.J. van (1989) Benthic Foraminifera from the Banda Arc Region, Indonesia, and their Paleobathymetric Significance for Geological Interpretations of the Late Cenozoic Sedimentary Record. Free University Press, Amsterdam, pp271.

Marle L.J. van (1991) Eastern Indonesian, Late Cenozoic Smaller Benthic Foraminifera. North-Holland, Amsterdam, Oxford, New York, Tokyo. pp328.

Mather A.E., Silva P.G., Harvey A.M., Zazo C. and Goy J.L. (1992) The impact of neotectonic activity on Late Quaternary aggradational and dissectional sequences in the Mula basin, SE Spain. **In:** Lewin J., Macklin M.G. and Woodward J.C. (convenors) (1992) *Mediterranean Quaternary River Environments. An International Symposium*. Peterhouse, Cambridge. 28-29 Sept. 1992. {abstract}1-2.

McCallum J. E. and Robertson A.H.F. (1995a) Sedimentology of two fan delta systems in the Plio-Pleistocene of the Mesaoria basin. *Sedimentary Geology*, **98**, in press.

McCallum J. E. and Robertson A.H.F. (1995b) Late Pliocene-Early Pleistocene Athalassa Formation, N. central Cyprus: carbonate sand bodies in a shallow seaway between two emerging land masses. *Terra Nova*, **7**, 265-277.

McCallum J.E., Scrutton R.A., Robertson A.H.F. and Ferrari W. (1993) Seismostratigraphy and Neogene-Recent depositional history of the south central continental margin of Cyprus. *Marine and Petroleum Geology*, **10**, 426-438.

McCallum J.E. (1989) Sedimentation and tectonics of the Plio-Pleistocene of Cyprus. *Unpublished PhD. thesis, University of Edinburgh*. pp 263.

McCallum J.E. and Robertson A.H.F. (1990) Pulsed uplift of the Troodos Massif - evidence from the Plio-Pleistocene Mesaoria basin. **In:** Malpas J., Moores E.M., Panayiotou A. and Xenophontos C. (eds) Ophiolites, oceanic crustal analogues. *Proceedings of the Symposium "Troodos 1987". Geological Survey Department, Nicosia*, 217-230.

McKenzie D.P. (1970) Plate tectonics of the Mediterranean region, *Nature*, **220**, 239-243.

McKenzie D.P. (1972) Active tectonics of the Mediterranean region. *Geophysical Journal of the Royal astronomical Society*, **30**, 109-185.

McKenzie D.P. (1978) Active tectonics of the Alpine-Himalyan belt: the Aegean Sea and surrounding regions. *Geophysical Journal of the Royal astronomical Society*, **55**, 217-254.

McKenzie J.A., Palmer S.C. and Müller P.A. (1990) Strontium isotope stratigraphy of the deep-sea type section at ODP hole 653a. **In:** Kastens K.A., Mascle J. et al. *Proceedings of the Ocean Drilling Program, Scientific Results*, College Station, Texas, **107**, 401-404.

McKenzie J.A. and Sprovieri R. (1990) Paleoceanographic conditions following the earliest Pliocene flooding of the Tyrrhenian Sea. **In:** Kastens K.A., Mascle J. et al. *Proceedings of the Ocean Drilling Program, Scientific Results*, College Station, Texas, **107**, 405-414.

McPherson J.G., Shanmugam G. and Moiola R.J. (1987) Fan-deltas and braid-deltas: varieties of coarse grained deltas. *Bulletin of the Geological Society of America*, **99**, 331-340.

Mercier J.L (1981) Extensional compressional tectonics associated with the Aegean arc: comparison with the Andean Cordillera of south Peru - north Bolivia., *Philososophical transactions of the Royal society of London, series A*, **300**, 337-355.

Mercier J.L., Sorel D.,Vergeley P., Simeakis C. (1989) Extensional tectonic regimes in the Aegean basins during the Cenozoic. *Basin Research*, **2**, 49-71.

Mercier. J.L., Sorel D. and Simeakis K. (1987) Changes in the state of stress in the overriding plate of a subduction zone: the Aegean Arc from the Pliocene to the Present. *Annales Tectonicae*, **I**, 20-39

Merz M. and Zankl H. (1991) The influence of the sheath on carbonate cyanobacteria. **In:** Barattolo F. (ed) Studies on Fossil Benthic Algae. *Bolletino della Societa Paleontologica Italiana*, Sp. Vol., **1**.

Meulenkamp J.E. and Zacharisse W.J.(1973) Stratigraphic and structural framework of the Messinian deposits on Crete. **In:** Drooger C.W. (ed) *Messinian events in the Mediterranean.* North-Holland, Amsterdam. 202-205.

Meulenkamp J.E. Wortel M.J.R., Wamel van W.A., Spakman W. and Hoogerduyn Strating E. (1988) On the Hellenic subduction zone and the geodynamic evolution of Crete since the late Middle Miocene. *Tectonophysics*, **146**, 203-215.

Meusel H., Jäger E. and Weinert E. (1965) *Vergleichende chronologie der Zentral-europäischen Flora*, **I**, text-volume 583pp., map-volume 258pp.; Jena (G. Fischer).

Miall A.D. (1978) Summary of braided river deposits. **In:** Miall A.D. (ed) *Fluvial sedimentology.* Canadian Society of Petroleum Geologists, Memoir **5**, Calgary, Alberta, Canada, 597-604.

Mindavelli O., Oznur Y. and Mitchell B.J. (1989) Crustal structure and possible anisotropy in Turkey from seismic wave dispersions. *Geophysical Journal International*, **98**, 93-106.

Molnar P. and Tapponier P. (1975) Cenozoic tectonics of Asia: effects of continental collision. *Science*, **189**, 419-126.

Monod O. (1977) Réchérches géologiques dans le Taurus occidental au sud de Beysehir (Turquie). *Thése de Doctor de Sciences, Université de Paris Sud, Orsay*, pp 442.

Monty C.L. and Mas J.R. (1979) Lower Cretaceous (Wealdian) blue-green algal deposits of the province of Valencia, eastern Spain. **In:** Monty C.L.V. (ed) *Phanerozoic stromatolites*. Springer Verlag, Berlin. 85-120.

Monty C.L.V. (1976) The origin and development of cryptalgal fabrics. **In:** Walter M.R. (ed) Stromatolites. *Developments in Sedimentology*, **20**,193-249.

Monty C.L.V. and Hardie L.A. (1976) The geological significance of the freshwater blue-green algal calcareous marsh. In: Walter M.R. (ed) Stromatolites. *Developments in Sedimentology*, **20**, 447-477.

Morris A. (1990) Palaeomagnetic studies in Cyprus, Turkey and Greece. *Unpublished PhD thesis, University of Edinburgh.*

Morris A. and Robertson A.H.F (1993) Miocene remagnetisation of carbonate platform and Antalya Complex Units within the Isparta Angle, SW, Turkey. *Tectonophysics*, **220**, 243-266.

Murray J.W. (1985) *Atlas of invertebrate macrofossils.* Longman / The Palaeontological Association. pp241.

Murray J.W. (1991) *Ecology and paleoecology of benthic foraminifera.* Longman scientific and Technical, UK, pp 397.

Nanson G.C. and Croke J.C. (1992) A genetic classification of floodplains. Geomorphology, **4**, 459-487.

Nemec W. (1990a) Deltas - terminology and classification **In:** Colella A. and Prior D.B. (eds) *Coarse-grained deltas.* Special publication of the International Association of Sedimentologists **10**, Blackwell Scientific Publications, 3-12.

Nemec W. (1990b) Aspects of sediment movement on steep deltas. **In:** Colella A. and Prior D.B. (eds) *Coarse-grained deltas.* Special publication of the International Association of Sedimentologists **10**, Blackwell Scientific Publications, 29-73.

Nichols R.S., Sparks R.S.J. and Wilson C.J.N. (1994) Experimental studies of the fluidization of layered sediments and the formation of fluid escape structures. *Sedimentology*, **41**, 233-253.

Nicholson C., Seeber L., Williams P. and Sykes L.R. (1986) Seismic evidence for conjugate slip and block rotation within the San Andreas fault system, southern California. *Tectonics*, **5**, 629-648.

Nickel E. (1983) Environmental significance of freshwater oncoids, Eocene Guarga Formation, southern Pyrenees, Spain. In: Peryt T.M. (ed) *Coated grains*. Springer-Verlag, Berlin, Heidelberg. 308-329.

Nur A. and Ben-Avraham Z. (1978) The eastern Mediterranean and the Levant: tectonics of continental collision. *Tectonophysics*, **46**, 297-311.

Ogawa Y., Horiucki K., Tamiguchi H. and Naka J. (1985) Collision of the Izu arc with Honshu and the effects of oblique subduction in the Miura-Bosos Peninsula. *Tectonophysics*, **119**, 349-379.

Okay A.I., Siyako M. and Burkan K.A. (1991) Geology and tectonic evolution of the Biga Peninsula, northwest Turkey, *Bulletin of the Technical University of Istanbul*, **44**, 191-256.

Okay A.I. (1989) Alpine-Himalayan blueschists. *Annual Review of Earth and Planetary Sciences*, **17**, 55-87.

Oral M.B., Reilinger R.E., Toksöz M.N., King R.W., Barka A.A., Kinik I. and Lenk (1995) Global Positioning System offers evidence of plate motions in eastern Mediterranean. *EOS*, **76**, 9,11.

Ordóñez S. and García del Cura M.A. (1983) Recent and Tertiary fluvial carbonates in central Spain. **In:** Collinson J.D. and Lewin J. (eds) Modern and ancient fluvial systems. *Special Publication of the International Association of Sedimentologists*, **6**, 485-497.

Orton G.J. (1988) A spectrum of middle Ordovician fan deltas and braidplain deltas, North Wales: a consequence of varying fluvial clastic input. **In:** Nemec W. and Steel R.J. (eds) *Fan deltas: sedimentology and tectonic settings*. Blackie and Son, London, 23-49.

Osbourne R.H., Licari G.R. and Link M.H. (1982) Modern lacustrine stromatolites, Walker Lake, Nevada. *Sedimentary Geology*, **32**, 39-61.

Osmond J.K., May J.P.and Tanner W.F. (1970) Age of the Cape Kennedy Barrier-and-Lagoon complex. *Journal of Geophysical Research*. **75**, 469-479.

Özgür N., Pekdeger A., Schneider H.-J. and Bilgin A. (1990) Pliocene volcanism of the Gölçük area, Isparta/western Taurides. **In:** Savaşçin M.Y. and Eronat A.H. (eds) *Proceedings of the International Earth Sciences Congress on Aegean regions*. Volume II, IESCA publication No: **2**, 411-419.

Özüs S. (1992) Antalya Travertines, hydrology and geochemistry *Unpublished PhD Thesis, University of Çukarova*, Adana, Turkey. pp.177.

Papadopoulos G.A., Kondopouloi D.P., Levantakis G.-A. and Pavlides S.B. (1986) Seismotectonics of the Aegean region. *Tectonophysics*, **124**, 67-84.

Papazachos B.C. (1973) Distribution of seismic foci in the Mediterranean and surrounding area and its tectonic implications. *Geophysical Journal of the Royal astronomical Society*, **33**, 421-430.

Parihar N.S. and Pant G.B. (1975) Bryophytes as rockbuilders - Some calcicole mosses and liverworts associated with Travertine formation at Sahasradhara, Dehra Dun. *Current Science*. **44**, 61-62.

Payne A.S. (1995) Tectonic and sedimentary evolution of the Polis graben system, west Cyprus. *Unpublished PhD thesis, University of Edinburgh.*

Pedley H.M. (1980) The occurence and sedimentology of a Pleistocene Travertine in the Fiddien Valley, Malta. *Proceedings of the Geological Association*, **91**, 195-202.

Pedley H.M. (1990) Classification and environmental models of cool freshwater Tufas. *Sedimentary Geology*, **68**(100), 143-154.

Pedley H.M. (1992) Freshwater (Phytoherm) reefs: The role of biofilms and their bearing on marine reef cementation. *Sedimentary Geology*, **79**, 255-274.

Pedley H.M. (1993) Sedimentology of the Late Quaternary barrage Tufas in the Wye and Lathkill Valleys, N. Derbyshire. *Proceedings of the Yorkshire Geological Society*, **49**, 197-206.

Penck A. and Bruckner E. (1909). *Die Alpen im Eiszeitalter*, Leipzig.

Penck W. (1918) *Die tektonischen Grundzuge west Kleinasiens*, Stuttgart.

Pentecost A. (1978) Blue-green algae and freshwater carbonate deposits. *Proceedings of the Royal Society of London*, **200**, 43-61.

Pentecost A. (1990) The formation of Travertine shrubs: Mammoth Hot Springs, Wyoming. *Geological Magazine*, **127(2)**, 159-168.

Pentecost A. and Bauld J. (1988) Nucleation of calcite on the sheaths of cyanobacteria using a simple diffraction cell. *Geomicrobiology Journal*, **6**, 129-135.

Pentecost A. and Lord T. (1988) Postglacial Tufas and Travertines from the Craven District of Yorkshire. *Cave Science*, **15**, 15-19.

Pentecost A. and Terry C. (1988) Inability to demonstrate calcite precipitation by bacterial isolates from travertine. *Geomicrobiology Journal*, **6**, 185-194.

Peters J.M., Troelstra S.R. and van Harten D. (1985) Late Neogene and Quaternary vertical movements in eastern Crete and their regional significance. *Journal of the Geological society of London*, **142**, 501-513.

Peterson (1985) Equilibrium tendency and piedmont scarp denudation, Wasatch Front, Utah. **In:** Morisawa M. and Hack J.T. (eds) *Tectonic Geomorphology*, Allen and Unwin Boston, 209-233.

Pettijohn F.J. (1975) *Sedimentary rocks*, Harper and Row, New York. pp628

Phillipson A. (1918) *Kleinasien, Handbuch der Regionalen Geologie*, 2/2, pp183. Carl Winters Universitätsbuchhandlung, Heidelberg.

Piazzolli P.A., Laborel J., Saliege J.F., Erol O., Kayan I. and Person A. (1991) Holocene raised shorelines on the Hatay coasts (Turkey): palaeoecological and tectonic implications. *Marine Geology*, **96**, 295-311.

Picard M.D. (1971) Classification of fine-grained sedimentary rocks. *Journal of Sedimentary Petrology*, **41**, 230-242.

Pickett E.A. (1994) Tectonic evolution of the Palaeotethys ocean in NW Turkey. *Unpublished PhD thesis, University of Edinburgh*, 1994, pp525.

Planhol X. de (1952) Sur le réseau hydrographique et les dernières phases de soulèvement du Taurus Occidental. *Comptes Rendus de l'Académie des Sciences*, **234**, 1386-1388.

Planhol X. de (1956a) Contribution a l'étude geomorphologique de Taurus Occidental et ses plaines bordières. *Revue de Géographie Alpine*, **44**, 609-685.

Planhol X. de (1956b) Position stratigraphique et signification morphologie des Travertins Subtauriques de L'Anatolie Sud-occidental. *Report of the IV. International Congress on the Quaternary*, Rome-Pisa. 467-471 .

Poisson A., Akay E., Dumont J.-F. and Uysal S. (1984) The Isparta Angle: a Mesozoic palaeorift in the Western Taurides. In: Tekeli O. and Göngüoğlu C. (eds) *International Symposium on the Geology of the Taurus Belt.* Special Publication M.T.A., 1984, Ankara.

Poisson A., Akay E., Cravatte J., Muller C. and Uysal S. (1983) Données nouvelles sur la chronologie de la mise en place des nappes d'Antalya au centre de l'Angle d'Isparta (Taurides Occidentales, Turquie). *Comptes Rendus de l'Académie des Sciences*, Paris, **296**, 923-926.

Poisson A. (1977) Récherches géologiques dans les Taurides occidentales (Turquie) *Unpublished PhD Thesis, Université de Paris-Sud, Orsay.*

Poisson A. (1984) The extension of the Ionian trough into southwestern Turkey. **In:** Dixon J.E. and Robertson A.H.F. (eds) The geological evolution of the eastern Mediterranean. *Geological Society of London Special Publication*, **17**, 242-279.

Pollitz F.F. (1991) Two-stage model of African absolute motion during the last 30 million years. *Tectonophysics*, **194**, 91-106.

Pons A., Suc J.P., Reille M. and Combourrieu Nebout N. (1991) The past history of dryness in regions with a Mediterranean climate. **In:** Di Castri G., and Mooney H.A. (eds) *Time scales of water stress response of Mediterranean biota*, Berlin.

Poole A.J. (1992) Sedimentology, neotectonics and geomorphology related to tectonic uplift and sea-level change: Quaternary of Cyprus. *Unpublished PhD thesis, University of Edinburgh.*

Poole A.J., Shimmield G.B. and Robertson A.H.F. (1990) Late Quaternary uplift of the Troodos Ophiolite, Cyprus: Uranium series dating of Pleistocene coral. *Geology*, **18**, 894-897.

Poole A.J. and Robertson A.H.F. (1991) Quaternary uplift and sea-level change at an active plate boundary, Cyprus. *Journal of the Geological Society of London*, **148**, 909-921.

Pope K.O. and Van Andel T.H. (1984) Late Quaternary alluviation and soil formation in the Southern Argolid: its history, causes and archaeological implications. *Journal of Archaeological Science*, **11**, 281-306.

Postma G. (1990) Depositional architecture and facies of river anf fan deltas: a synthesis. **In:** Colella A. and Prior D.B. (eds) *Coarse-grained deltas.* Special publication of the International Association of Sedimentologists **10**, Blackwell Scientific Publications, 13-27.

Price S.P. and Scott B. (1994) Fault-block rotations at the edge of a zone of continental extension; southwest Turkey. *Journal of Structural Geology*, **16**, 381-392.

Reches Z. (1978) Analysis of faulting in three-dimensional strain fields. *Tectonophysics*, **47**, 109-129.

Reches Z. (1983) Faulting of rocks in three-dimensional strain fields II. Theoretical analysis. *Tectonophysics*, **95**, 133-156.

Reches Z. and Dietrich J.H. (1983) Faulting of rocks in three-dimensional strain fields I. Failure of rocks in polyaxial servo-control experiments. *Tectonophysics*, **95**, 111-132.

Ricci Lucci F. (1973) Resedimented evaporites: indicators of slope instability and deep basin conditions in Peri-Adriatic Messinian (Appenines foredeep, Italy). **In:** Drooger C.W. (ed) *Messinian events in the Mediterranean.* North-Holland, Amsterdam. 124-141.

Ricou, L.-E., Marcoux J. and Poisson A. (1979) L'Alloctonie des Bey Daǧ lari orienteux. Reconstruction palinspastique des Taurides Occidentales. *Bulletin de la Société Géologique de France*, **7, XXI**, 125-133.

Ricou L.-E., Argyriadis I, and Lefèvre R. (1974) Proposition d'une origin interne pour les nappes d'Antalya et le massif d'Antalya (Taurides occidentales, Turquie) *Bulletin de la Société Géologique de France*, **16**, 107-111.

Ricou L.E., Argyriadis I. and Marcoux J. (1975) L'axe calcaire du Taurus, un alignement de fenêtres Arabo-Africaines sous des nappes radiolaritique, ophiolitiques et métamorphiques. *Bulletin de la Société Géologique de France*, series **7**, **XVII**, 1024-1043.

Ricou L.E., Marcoux J. and Whitechurch H. (1984) The Mesozoic organisation of the Taurides. **In:** Dixon J.E. and Robertson A.H.F. (eds) The geological evolution of the eastern Mediterranean. *Geological Society of London Special Publication*, **17**, 349-359.

Riding R. (1983) Cyanoliths (cyanoids): Oncoids formed by calcified cyanophytes. **In:** Peryt T.M. (ed) *Coated grains*. Springer-Verlag, Berlin, Heidelberg. 276-283.

Riding R. (1991a) Classification of microbial carbonates. **In:** Riding R. (ed) *Calcareous algae and stromatolites*. Springer-Verlag, Berlin, Heidelberg. 21-51.

Riding R. (1991b) Calcified Cyanobacteria. **In:** Riding R. (ed.) *Calcareous algae and stromatolites*. Springer-Verlag, Berlin, Heidelberg. 55-87.

Rio D., Raffi I. and Villa G. (1990) Pliocene-Pleistocene calcareous nannofossil distribution patterns in the western Mediterranean. **In:** Kastens K.A., Mascle J. et al. *Proceedings of the Ocean Drilling Program, Scientific Results*, College Station, Texas, **107**, 513-533.

Robertson A.H.F., Eaton S., Follows E.J. and Payne A.S. (1995) Depositional processes and basin analysis of Messinian evaporites in Cyprus. *Terra Nova*, **7**, 233-253.

Robertson A.H.F., Kidd R.B., Ivanov M.K., Limonov A.F., Woodside J.M., Galindo-Zaldivar J. and Nieto L. and the scientific party of the 1993 TTR-3 Cruise. (1994) Probing continental collision in the Mediterranean Sea. *EOS*, **75**, 233, 239.

Robertson A.H.F., Clift P.D., Degnan P.J. and Jones G. (1991) Palaeogeographic and palaeotectonic evolution of the eastern Mediterranean Neotethys. *Palaeogeography, Palaeoclimatology, Palaeoecology*, **87**, 291-343.

Robertson A.H.F. (1993) Mesozoic-Tertiary sedimentary and tectonic evolution of Neotethyan carbonate platforms, margins and small ocean basins in the Antalya Complex, southwest Turkey. *Special Publication of the International Association of Sedimentologists*, **20**, 415-465.

Robertson A.H.F. and Dixon J.E. (1984) Introduction: Aspects of the geological evolution of the eastern Mediterranean **In:** Dixon J.E. and Robertson A.H.F. (eds) The geological evolution of the eastern Mediterranean. *Geological Society of London Special Publication*, **17**, 1-77

Robertson A.H.F. and Woodcock N.H. (1982) Sedimentary history of the south-western segment of the Mesozoic-Tertiary Antalya continental margin, south-western Turkey. *Ecologae Geologica Helvetica*, **75/3**, 517-562.

Robertson A.H.F. and Woodcock N.H. (1984) The SW segment of the Antalya Complex, Turkey as a Tethyan Mesozoic-Tertiary continental margin **In:** Dixon J.E. and Robertson A.H.F. (eds) The geological evolution of the eastern Mediterranean. *Geological Society of London Special Publication*, **17**, 251-271.

Robertson A.H.F. and Woodcock N.H. (1986) The role of the Kyrenia Range lineament, Cyprus, in the geological evolution of the Eastern Mediterranean Area. *Philosophical Transactions of the Royal Society of London.* **A 317**, 141-177.

Ron H., Nur A. and Eyal Y. (1990) Multiple strike-slip fault sets: a case study of the Dead Sea transform. *Tectonics*, **9**, 1421-1431.

Rosholt J.N. (1980) *Uranium-trend dating of Quaternary sediments.* Open File Report U.S. Department of the Interior Geological Survey. pp33.

Rotstein Y. (1984) Counterclockwise rotation of the Anatolian Block. *Tectonophysics*, **108**, 71-91.

Rotstein Y. and Kafka A. (1982) Seismotectonics of the northern boundary of Anatolia, eastern Mediterranean region: subduction collision and arc jumping. *Geophysical Journal of the Royal astronomical Soc*iety, **87**, 7694-7706.

Rowley D.B. and Lottes A. (1988) Plate-kinematic reconstructions of the North Atlantic and Arctic: Late Jurassic to Present. *Tectonophysics*, **155**, 73-120.

Ruddiman W.F., Sarnthein M., Backman J., Baldauf J.G., Curry W., Dupont L.M., Janacek T., Pokras E.M., Raymo M.E., Stabell B., Stein R. and Tiedemann R. (1989) Late Miocene to Pleistocene evolution of climate in Africa and the low-latitude Atlantic: overview of leg 108 results. **In:** Ruddiman W.F., Sarnthein M. et al. *Proceedings of the Ocean Drilling Program, Scientific Results*, **108**, 463-484.

Ruddiman W.F. and Raymo M.E. (1982) Northern Hemisphere climate regimes during the past 3 Ma; possible tectonic connections. **In:** The past three million years evolution of climatic variability in the North Atlantic region; a discussion. *Philosophical transactions of the Royal society of London.* Series B, **318**, 411-430.

Rust B.R. (1978) Depositional models for braided alluvium. **In:** Miall A.D. (ed) *Fluvial sedimentology.* Canadian Society of Petroleum Geologists, Memoir **5**, Calgary, Alberta, Canada, 605-625.

Schneider S., Schroder H.G. and Le Campion-Alsumard Th. (1983) Algal micro-reefs - coated grains from freshwater environments. **In:** Peryt T.M. (ed) *Coated grains*. Springer-Verlag, Berlin, Heidelberg. 284-298

Scholl D.W. and Taft W.H. (1964) Algae, contributors to the formation of calcareous tufa, Mono Lake, California. *Journal of Sedimentary Petrology*, **34**, 309-319.

Schumm S.A. (1962) Erosion on miniature pediments in Badlands National Monument, South Dakota, *Bulletin of the Geological Society of America*, **73**, 719-724.

Schwarcz H.P. (1979) Uranium series dating of contaminated travertines: a two-component model. *McMaster University technical memo.*, **79**, pp14.

Schwarcz H.P. (1980) Absolute age determination of archaeological sites by Uranium series dating of travertines. *Archaeometry*, **22(1)**, 3-24.

Schwarcz H.P. and Latham A.G. (1989) Dirty Calcites: 1. Uranium-series dating of contaminated calcite using leachates alone. *Chemical Geology*, **80**, 35-43.

Scotese C.R., Gahagan L.M. and Larson R.L. (1988) Plate tectonic reconstructions of the Cretaceous and Cenozoic ocean basins. *Tectonophysics*, **155**, 27-48.

Scott D., Etheridge M.A. and Rosendahl B.R. (1992) Oblique-slip deformation in extensional terranes: a case study of the lakes Tanganyika and Malawi rift zones. *Tectonics*, **11**, 998-1009.

Sengör, A.M.C. (1979) Mid-Mesozoic closure of the Permo-Triassic Tethys and its implications. *Nature*, **279**, 590-593.

Sengör A.M.C., Görür N. and Saroğ lu F. (1985) Strike-slip faulting and related basin formation in zones of tectonic escape: Turkey as a case study. **In:** Biddle K.T. and Christie Blick N. (eds) Strike-slip deformation, basin formation and sedimentation. *SEPM Special Publication* No. **37**, 227-264.

Sengör A.M.C., Yilmaz Y. and Sungurlu O. (1984) Tectonics of the Mediterranean Cimmerides: nature and evolution of the western termination of Palaeotethys. **In:** Dixon J.E. and Robertson A.H.F. (eds) The geological evolution of the eastern Mediterranean. *Geological Society of London Special Publication*, **17**, 77-112.

Sengör A.M.C., Yilmaz Y.and Ketin I. (1980) Remnants of pre-Late Jurassic ocean in northern Turkey: Fragments of Permian-Triassic Palaeo-Tethys? *Bulletin of the Geological Society of America*, **91**, 599-609.

Sharp I. R. (1995) The Triassic to Tertiary sedimentary, tectonic and magmatic evolution of the Pelagonian and Vardar (Axios) zones, Macedonia, Northern Greece. *Unpublished PhD thesis, University of Edinburgh*. pp785.

Smith A.G., Hurley A.M. and Briden A.C. (1981) *Phanerozoic paleocontinental world maps*. Cambridge Univeraity Press, Cambridge, pp102.

Snyder D.B. and Barazangi M. (1986) Deep crustal structure and flexure of the Arabian Plate beneath the Zagros collisional mountain belt as inferred from gravity observations. *Tectonics*, **5**, 361-373.

Sprovieri R. (1978) I foraminiferi bentonici della sezione Plio-Pleistocenica di Capo Rossello (Agrigento, Sicily). *Bolletino della Societa Paleontologica Italiana*, **30**, 68-97.

Sprovieri R. and Hasegawa S. (1990) Plio-pleistocene benthic foraminifera stratigraphic distribution in the deep-sea record of the Tyrrhenian sea (ODP leg 107). **In:** Kastens K.A., Mascle J. et al. *Proceedings of the Ocean Drilling Program, Scientific Results*, College Station, Texas, **107**, 429-460.

Stewart I.A. and Hancock P.L. (1989) Normal fault zone evolution and fault scarp degradation in the Aegean region. *Basin Research*, **1**, 139-153.

Suc J.P.(1984) Origin and evolution of the Mediterranean vegetation and climate in Europe. *Nature*, **307**, 429-432.

Szulc J. and Cwizewicz M. (1988) The Lower Permian freshwater carbonates of the Slawkow graben, southern Poland: sedimentary facies context and stable isotope study. *Palaeogegraphy, Palaeoclimatology, Palaeoecology*, **70**, 107-120.

Taymaz T., Jackson J. and Westaway R. (1990) Earthquake mechanisms in the Hellenic trench near Crete. *Geophysical Journal International*, **102**, 695-731.

Taymaz T., Jackson J. and McKenzie D. (1991) Active tectonics of the north and central Aegean Sea. *Geophysical Journal International*, **106**, 433-490.

Taymaz T. and Price S. (1992) The 1971 May 12 Burdur earthquake sequence, SW Turkey: a synthesis of seismological and geological observations. *Geophysical Journal International*, **108**, 589-603.

Terres R.R. and Slyvester A.G. (1981) Kinematic analysis of rotated fractures and blocks in simple-shear. *Bulletin of the Seismological Society of America*, **71**, 1593-1605.

Thienemann A. (1954) *Die Binnegewasser Band* **XX** *Chironomus*. E.Schweizerbart'sche Verlag, Stuttgart, 157-162.

Thunnell R., Williams D., Tappa E., Rio D. and Raffi I. (1990) Pliocene-Pleistocene stable isotope record for Ocean Drilling Program site 653, Tyrrehnian basin: implications for the paleoenvironmental history of the Mediterranean Sea. **In:** Kastens K.A., Mascle J. et al. *Proceedings of the Ocean Drilling Program, Scientific Results*, College Station, Texas, **107**, 387-399.

Tietze E. (1885) Beiträge sur Geologie von Lykien. *Jahrbuch der K.K. Geologischen Reichsanstalt, Vienne*, **XXV**, 283-386.

Tucker M.E. (1982) *The field description of sedimentary rocks*. Geological Society of London Handbook. Open University Press. pp112.

Tucker M.E. and Wright P.V. (1990) *Carbonate sedimentology*. Blackwell Scientific Publications. Oxford. pp482.

Tüysüz O. (1990) Tectonic evolution of a part of the Tethyside orogenic collage: the Kargi massif, northern Turkey. *Tectonics*, **9**, 141-160.

Ünlügenç U.C. and Gürbüz K. (1992) Tertiary stratigraphy of the Adana basin. *Field excursion guide. 1st international symposium on Eastern Mediterranean Geology*. University of Çukarova, Adana. pp11.

Ustaömer T. (1993) Pre-Late Jurassic tectonic-sedimentary evolution of north Tethys: Central Pontides, N Turkey. *Unpublished PhD thesis, University of Edinburgh*. pp389.

Ustaömer T. and Robertson A.H.F. (1993) A late-Palaeozoic - early Mesozoic marginal basin along the active southern continental margin of Eurasia: evidence from the central Pontides, (Turkey) and adjacent regions. *Geological Journal*, **28**, 219-238.

Ustaömer T. and Robertson A.H.F. (1994) Late Palaeozoic marginal basin and subduction accretion: the Palaeotethyan Küre complex, central Pontides, northern Turkey. *Journal of the Geological Society of London*, **151**, 291-305.

Vail P.R., Mitchum R.M. and Thompson S. III (1977a) Relative changes of sea-level from coastal onlap. **In:** Payton C.E. (ed) Seismic stratigraphy - applications to hydrocarbon Exploration. *American Association of Petroleum Geologists. Memoir*, **26**, 63-82.

Vail P.R., Mitchum R.M. and Thompson S. III (1977b) Seismic stratigraphy and global changes in sea-level Part 4: global cycles of relative changes of sea-level. **In:** Payton C.E. (ed) Seismic stratigraphy - applications to hydrocarbon Exploration. *American Association of Petroleum Geologists. Memoir*, **26**, 83-97.

Van der Swann, G.J. (1983) Quantative analyses and the reconstruction of benthic foraminiferal communities. *Utrecht Micropaleontological Bulletin*, **30**, 49-69.

Varol O. (1982) Calcareous nannofossils from the Antalya Basin, Turkey. *Neues Jahrbuch für Paläontologie Mh.* **H 4**, 244-256.

Vergnaud Grazzini C.R., Saliège J.F., Urrutiager M.J. and Iannece A. (1990) Oxygen and Carbon isotope stratigraphy of ODP hole 653A and site 654: the Pliocene-Pleistocene glacial history recorded in the Tyrrhenian basin (west Mediterranean). **In:** Kastens K.A., Mascle J. et al. *Proceedings of the Ocean Drilling Program, Scientific Results*, College Station, Texas, **107**, 361-386.

Versfelt J.W. and Rosendahl B.R. (1989) Relationships between pre-rift structure and rift architecture in Lakes Tanganyika and Malawi, East Africa. *Nature*, **337**, 354-357.

Violante C., Ferreri V., D'Argenio B. and Golubic S. (1994) Excursion A1: Quaternary Travertines at Rocchetta a Volturno (Isernia, Central Italy). Facies analysis and sedimentary model of an organogenic carbonate system. *15th IAS Regional Meeting Ischia, Italy. Excursion Guide*. 5-22.

Vita-Finzi C. (1969) *The Mediterranean Valleys: Geological changes in Historical times*. Cambridge University Press, Cambridge.

Waldron J.W.F. (1981) Mesozoic sedimentary and tectonic evolution of the northeastern Antalya Complex, Eğridir, SW Turkey. *Unpublished PhD thesis, University of Edinburgh*. pp239.

Waldron J.W.F. (1984) Structural history of the Antalya Complex in the "Isparta angle", southwest Turkey. **In:** Dixon J.E. and Robertson A.H.F. (eds) The geological evolution of the eastern Mediterranean. *Geological Society of London Special Publication*, **17**, 272-286.

Warren J.K. (1982) The hydrological setting, occurrence and significance of gypsum in late Quaternary salt lakes in South Australia. *Sedimentology*, **29**, 609-637.

Wegener A. (1924) *The origin of continents and oceans*. Meuthen, London, pp212. (English translation of 3rd German edition of 1922).

Weijermars R., Mulder-Blanken C.W. and Wiegers J. (1986) Growth rate observation from the moss-built Checa Travertine terrace, central Spain. *Geological Magazine*, **123(3)**, 279-286.

Whitton D.G.A. and Brooks J.R.V. (1988) *A Dictionary of Geology* (2nd edition). Penguin Reference Books. pp495.

Wilson J.L.(1975) *Carbonate facies in geologic history*. Springer-Verlag, Berlin, pp471.

Wilson J.T. (1965) A new class of faults and their bearing on continental drift. *Nature*, **207**, 343-347.

Wilson J.W. (1994) The origin and tectono-stratigraphic evolution of the Meso-Hellenic Trough, northern Greece and Albania. *Unpublished PhD thesis, University of Edinburgh.*

Woodside J.M. (1977) Tectonic elements and crust of the eastern Mediterranean. *Marine Geophysical Research*, **3**, 317-354.

Woodside J.M. and the scientific party (1991) West Cyprus - Anaximander Mountains and Florence Rise survey. **In:** Geological and geophysical investigations in the Mediterranean and Black Sea areas. Initial reports of the Training through Research Cruise of RV *Gelendzhik* in the Eastern Mediterraneean and the Black Sea (June-July 1991) *UNESCO reports in marine science*, **56**, 120-170.

Woodside J.M. and the scientific party (1992) East Cyprus - West Tartus Ridge survey **In:** Geological and geophysical investigations in the Mediterranean and Black Sea areas. Initial reports of the Training through Research Cruise of RV *Gelendzhik* in the Eastern Mediterranean and the Black Sea (June-July 1991) *UNESCO reports in marine science*, **56**, 61-119.

Wornardt W.W. and Vail P.R. (1991) Revision of the Plio-Pleistocene cycles and their application to sequence stratigraphy and shelf and slope sediments in the Gulf of Mexico. *Transactions of the Gulf Coast Association geological society*, **41**, 719-744.

Wortel M.J.R., Spakman W., de Jonge M.R., Meijer P.T. (1995) The evolution of the Mediterranean region: from structure and kinematics to dynamics. *Terra abstracts:* supplement to *Terra Nova*, **7**, abstract XII-1(3), 169.

Wright R. (1978) Neogene paleobathymetry of the Mediterranean based on benthic foraminifers from DSDP leg 42A. **In:** Hsü K.J., Montadert L. *et al.*(1978) *Initial Reports of the Deep Sea Drilling Project*, **42**, (1). U.S. Government printing office, Washington, USA, 1053-1078.

Yalçin M.N. and Görür N. (1984) Sedimentological evolution of the Adana basin. *International symposium on the Geology of the Taurus belt*. Ankara. 165-167.

Yetis C. (1988) Reorganisation of the Tertiary Stratigraphy in the Adana Basin, Southern Turkey. *Newsletter of Stratigraphy*, **20**, 43-58.

Zacharisse W.J. and Spaak P. (1983) Middle Miocene to Pliocene paleoenvironmental reconstructions of the Mediterranean and adjacent Atlantic ocean: planktonic foraminiferal records of Southern Italy. *Utrecht Micropaleontological Bulletin*, **30**, 91-110.

Zanchi A., Kissel C.and Tapirdamaz C. (1993) Late Cenozoic and Quaternary brittle continental deformation in western Turkey. *Bulletin de la Société Géologique de France*, **164**, 507-517.

Zanchi A. and Angelier J. (1993) Seismotectonics of western Anatolia: regional stress orientation from geological and geophysical data. *Tectonophysics*, **222**, 259-274.

Appendix 1:

Benthic and planktic foraminifera: Manavgat and Yurtpinar sections

sample planktic/benthic	BENTHICS	PLANKTICS
MANAVGAT		
Ma1/92b 0.63 n=114	*Bulimina gibba* *Cibicides kullenbergi* *Cibicides lobatulus* *Globocassidulina subglobosa* *Lenticulina rotulata* *Lenticulina sp.* *Planulina arimensis* *Trifarina sp.* *Uvigerina peregrina*	*Globigerina bulloides* *Globigerina falconenesis* *Globigerina nepenthes* *Globigerina rubescens* *Globigerina sacculifera* *Globigerinella siphonifera* *Globigerinoides obliquus* *Globigerinoides obliquus extremus* *Globigerinoides ruber* *Globigerinoides tenellus* *Globigerinoides triloba* *Neogloboquadrina acostoensis* *Orbulina universa*
Ma2/92b 0.82 n=71	*Cibicides kullenbergi* *Cibicides lobatulus* *Cibicides refulgens* *Planulina arimensis* *Trifarina bradyi* *Uvigerina peregrina.* *Uvigerina sp.*	*Globigerina bulloides* *Globigerina falconensis* *Globigerina nepenthes* *Globigerina sacculifera* *Globigerinoides obliquus* *Globigerinoides ruber* *Globigrinoides triloba* *Globorotalia puncticulata* *Orbulina universa*
Ma3/92b 1.57 n=113	*Bolivina robusta* *Cibicides kullenbergi* *Cibicides lobatulus* *Lenticulina sp.* *Planulina arimensis* *Pullenia osloensis* *Uvigerina peregrina* *Uvigerina sp.*	*Globigerina bulloides* *Globigerina falconensis* *Globigerina nepenthes* *Globigerina sacculifera* *Globigerinoides obliquus* *Neogloboquadrina acostoensis* *Orbulina universa*
Ma4/92b 1.36 n=130	*Bulimina spinensis* *Cibicides kullenbergi* *Globocassidulina subglobosa* *Karreriella bradyi* *Lenticulina* *Melonis affinis* *Reussella simplex* *Sigmoilinitae tenuis* *Trifarina sp.* *Uvigerina peregrina* *Uvigerina sp.*	*Globigerina bulloides* *Globigerina sacculifera* *Globigerinoides obliquus* *Globigerinoides obliquus extremus* *Globigerinoides ruber* *Globigerinoides tenellus* *Globigerinoides triloba* *Globorotalia punctilata* *Orbulina universa*

Ma5/92b 1.84 n=179	*Amphicoryna sp.* *Brizalina macella* *Bulimina alazensis* *Bulimina sp.* *Cibicides kullenbergi* *Cibicides lobatulus* *Dentalina filiformis* *Dentalina sp.* *Gyroidina laevigata* *Hanzawaia rhodoensis* *Lagena sp.* *Lenticulina rotulata.* *Lenticulina sp.* *Melonis affinis* *Nonion sp.* *Planulina arimensis* *Pleurostomella alternans* *Pullenia osloensis* *Sigmoilinitae tenuis* *Siphonia reticulata* *Stilostomella antillea*	*Globigerina bulloides* *Globigerinella siphonifera* *Globigerinoides obliquus* *Globigerinoides obliquus extremus* *Globigerinoides ruber* *Globigerinoides tenellus* *Globigrinoides triloba* *Globorotalia inflata ?* *Globorotalia margaritae* *Orbulina bilobata* *Orbulina universa* *Sphaeroidinellopsis kochi*
Ma6/92b 6.02 n=309 *Globigerinella siphonifera* 120 *Orbulina universa* 79 other planktics 66 benthics 44	*Bolivina robusta* *Bulimina A* *Cibicides lobatulus* *Cibicides kullenbergi* *Lenticulina rotulata* *Melonis affinis* *Panulina sp.* *Planulina arimensis* *Rectobolivina sp.* *Sigmoilinitae tenuis* *Siphonia reticulata* *Stilostomella antillea* *Valvulinera sp.*	*Globigerina bulloides* *Globigerina falconensis* *Globigerinella siphonifera* *Globigerinoides tenellus* *Globogerinoides obliquus* *Globogerinoides obliquus extremus* *Globorotalia margaritae* *Orbulina bilobata* *Orbulina universa*
Ma7/92b 0.68 n=101	*Bolivina robusta* *Bulimina gibba* *Bulimina sp.* *Cibicides kullenbergi* *Cibicides lobatulus* *Dyocibicides biserialis* *Egerella bradyi* *Globocassidulina subglobosa* *Lenticulina rotulata* *Lenticulina sp.* *Melonis affinis* *Nonion fabum* *Pleurostomella alternans* *Pullenia osloensis* *Stilostomella antillea* *Uvigerina perigrina* *Uvigerina pigmea* *Uvigerina sp.* *Valvulinera sp.*	*Globigerina bulloides* *Globigerina sacculifera* *Globigerinoides obliquus extremus* *Globigerinoides ruber* *Globigerinoides triloba* *Globorotalia margaritae* *Neogloboquadrina acostoensis* *Orbulina universa*

Ma8/92b 0.42 n=27	*Bolivina robusta* *Brizalina alata* *Bulimina gibba* *Neoconorbina terquem* *Neolenticulina sp.* *Praeglobobulimina pupoides* *Stilostomella antillea* *Valvulinera sp.*	*Globigerina bulloides* *Globigerina sacculifera* *Globigerinoides obliquus extremus*
Ma9/92b 3.68 n=117	*Brizalina sp.* *Melonis affinis* *Praeglobobulimina pupoides* *Uvigerina peregrina* *Valvulinera sp.*	*Globigerina bulloides* *Globigerina decoroperta* *Globigerina rubescens* *Globigerina sacculifera* *Globigerinella siphonifera* *Globigerinoides ruber* *Globigerinoides tenellus* *Globigrinoides triloba* *Orbulina universa* *Orbulina universa*
Ma10/92b	*Cibicides lobatulus* *Lenticulina sp. A,* *Stilostomella antillea*	*Globigerina bulloides*
Ma12/92b 8.67 n=87	*Bolivina robusta* *Bulimina gibba* *Cibicides kullenbergi* *Cibicides lobatulus*	*Globigerina bulloides* *Globigerina falconensis* *Globigerinoides tenellus* *Neogloboquadrina acostoensis*
Ma13/92b 7.75 n=70	*Bulimina spinensis* *Cibicides lobatulus* *Elphidium advenum* *Melonis affinis*	*Globigerina bulloides* *Neogloboquadrina acostoensis*
Ma14/92b 2.38 n=54	*Bulimina spinensis* *Cibicides kullenbergi* *Cibicides lobatulus* *Elphidium advenum* *Lenticulina sp.* *Melonis affinis* *Neoconorbina terquem* *Valvulinera sp.*	*Globigerina bulloides* *Globigerina nepenthus* *Globigerina sacculifera* *Globigerinoides obliquus* *Globigerinoides tenellus* *Globorotalia margaritae* *Globorotalia punctilata* *Orbulina universa*
Ma16/92b 11.50 n=50	*Bolivina robusta* *Cibicides lobatulus*	*Globigerina bulloides* *Globigerinoides obliquus* *Globigerinoides ruber*
Ma17/92b 7.29 n=58	*Bolivina robusta* *Brazilina macella* *Bulimina gibba* *Karreriella bradyi* *Uvigerina peregrina*	*Globigerina bulloides* *Globigerina sacculifera* *Globigerinoides obliquus extremus* *Globigerinoides rubescens*
Ma18/92b 5.38 n=51	*Bolivina plicatella* *Brizalina macella* *Bulimina gibba* *Lagena sp.* *Valvulinera sp.*	*Globigerina bulloides* *Globigerinoides obliquus* *Globigerinoides ruber* *Globigerinoides tenellus* *Neogloboquadrina acostoensis* *Orbulina suturalis*

YURTPINAR		
Yu1/92b 0.2 n=5	*Cibicides refulgens* *Haynesia depressula* *Neolenticulina sp.* *Pattellina sp.*	*Globigerina bulloides*
Yu2/92b 0.18 n=47	*Ammonia beccarii* *Brizalina subreticulata* *Cibicides refulgens* *Cibicides lobatulus* *Cibicides kullenbergi* *Elphidium advenum* *Hanzawaia rhodoensis* *Nonion fabum* *Patellina sp.* *Quinqueloculina sp* *Uvigerina sp. A,* *Valvulinera sp.*	*Globigerina bulloides* *Globigerina falconensis* *Globigerina sacculifera* *Orbulina bilobata*
Yu3/92b 0 n=5	*Ammonia beccarii* *Aubygnina perlucida*	
Yu4/92b 1.27 n=34	*Bolivina robusta* *Cibicides lobatulus* *Eggerella propinqua* *Haynensia depressula* *Karriella bradyi* *Neoconorbina terquem,* *Nonion fabum* *Planorbulina mediterranensis*	*Globigerina bulloides* *Globogerina falconensis* *Glogigerinoides tenellus* *Globigerinoides triloba*
Yu6/92b 0.37 n=52	*Ammonia beccarii* *Cibicides lobatulus* *Elphidium advenum* *Gyroidina laevigata* *Hanzawaia rhodoensis* *Haynesia depressula* *Neoconorbina terquem* *Nonion fabum* *Patellina sp.* *Quinqueloculina sp.* *Spheroidina bulloides* *Stilostomella antillea* *Trifarina sp.* *Valvulinera sp.*	*Globigerina bulloides* *Globogerina falconensis* *Glogigerinoides tenellus* *Globigerinoides ruber* *Sphaeroidinellopsis kochi*

Yu8/92b 0.25 n=35	*Ammonia beccarii* *Bolivina robusta* *Brizalina macella* *Cibicides lobatulus* *Haynensia depressula* *Neoconorbina terquem* *Nonion fabum* *Uvigerina peregrina*	*Globigerinoides triloba* *Globorotalia margaritae*
Yu10/92b 0.13 n=51	*Ammonia beccarii* *Bolivina robusta* *Brizalina alata* *Bulimina spinensis.* *Cancris oblongus* *Cibicides kullenbergi* *Cibicides lobatulus* *Elphidium advenum* *Haynensia depressula* *Neoconorbina terquem* *Nonion fabum* *Praeglobobulimina pupoides* *Sigmoilinitae tenuis* *Trifarina Bradyi*	*Globigerina bulloides* *Globigerina falconensis* *Globigerina sacculifera*
Yu13/92b 0.2 n=18	*Ammonia beccarii* *Bolivina plicatella,* *Cibicides lobatulus* *Elphidium spp.* *Fursenkonia sp.* *Haynensia depressula* *Neoconorbina terquem,* *Nonion fabum* *Ruessella simplex* *Uvigerina peregrina,* *Valvulinera sp.*	*Globigerina bulloides* *Globigerina falconensis* *Globigerinoides obliquus*
Yu14/92b 0.18 n=20	*Cibicides lobatulus* *Globocassidulina subglobosa* *Haynensia depressula* *Neoconorbina terquem* *Spheroidina bulloides* *Uvigerina peregrina*	*Globigerinoides triloba*
Yu15/92b 0.30 n=13	*Ammonia beccarii* *Cibicides kullenbergi* *Elphidium advenum* *Melonis affinis* *Nonion fabum*	*Globigerina bulloides* *Globigerinoides obliquus* *Globigerinoides triloba*

Yu17/92b 0.313 n=42	*Ammonia beccarii* *Bolivina robusta* *Cibicides kullenbergi* *Elphidium advenum* *Elphidium crispum* *Elphidium macellum* *Nonion fabum* *Nonion sp.* *Stilostomella antillea* *Uvigerina sp.* *Valvulinera sp.*	*Globigerina bulloides* *Globigerina nepenthes ?* *Globigerinoides ruber* *Globigerinoides tenellus* *Sphaeroidinellopsis kochi*
Yu18/92b 0.41 n=72	*Ammonia beccarii* *Bolivina robusta* *Cancris oblongus* *Cibicides kullenbergi* *Cibicides lobatulus* *Cibicides refulgens* *Elphidium advenum* *Elphidium cf macellum* *Florius bouneum* *Fursenkonia sp.* *Haynensia depressula* *Melonis affinis* *Neoconorbina terquem* *Nonion fabum* *Patellina sp.* *Planorbulina mediterranensis* *Pleurostomella alternans* *Reusella simplex* *Textularia agglutinans* *Valvulinera sp.*	*Globigerina bulloides* *Globigerina falconensis* *Globigerina sacculifera* *Globigerinoides obliquus* *Globigerinoides ruber* *Globigerinoides rubescens* *Sphaerroidenellopsis kochi*
Yu19/92b 0.2 n=36	*Ammonia beccarii* *Bolivina sp.* *Cancris oblongus* *Cibicides kullenbergi* *Cibicides lobatulus* *Cibicides sp.* *Elphidium cf macellum* *Elphidium crispum* *Hanzawaia rhodoensis* *Haynensia depressula* *Melonis affinis* *Neoconorbina terquem* *Nonion fabum* *Planorbulina mediterranensis* *Valvulinera sp.*	*Globigerina falconensis* *Globigerinoides ruber* *Globigerinoides tenellus*

Yu22/92b 0.36 n=34	*Bolivina robusta* *Brizalina macella* *Bulimina gibba* *Bulimina spinensis.* *Cibicides lobatulus* *Cibicides sp.* *Elphidium advenum* *Globocassidulina subglobosa* *Haynensia depressula* *Melonis affinis* *Nonion fabum* *Patellina sp.* *Stilostomella antillea* *Valvulinera sp.*	*Globigerina bulloides* *Globigerina falconensis* *Globigerina sacculifera* *Globigerinoides rubescens*
Yu23/92b 0.10 n=34	*Ammonia beccarii* *Bolivina robusta* *Cancris oblongus* *Cibicides kullenbergi* *Cibicides lobatulus* *Elphidium cf macellum* *Elphidium macellum* *Elphidium sp. A,* *Florilus bouneaum* *Neoconorbina terquem* *Quinqueloculina sp.*	*Globigerina bulloides* *Globorotalia margaritae*
Yu24/92b	*Nonion sp.* *Elphidium sp. A*	
Yu25/92b 0.17 n=84	*Ammonia beccarii* *Bolivina sp. E,* *Brizalina hastula* *Bulimina gibba* *Cancris oblongus* *Cibicides lobatulus* *Elphidium cf macellum* *Elphidium crispum* *Elphidium excavatum* *Elphidium macellum* *Elphidium sp. A* *Florilus bouneaum* *Fursenkonia sp.* *Haynensia depressula* *Neoconorbina terquem* *Nonion Fabum* *Quinqueloculina sp.* *Textularia agglutinans* *Valvulinera sp.*	*Globigerina bulloides* *Globigerina rubescens* *Globigerina sacculifera* *Globigerinoides triloba* *Neogloboquadrina acostoensis* *Orbulina bilobata* *Orbulina universa*

Yu26/92b 0.33 n=133	*Ammonia beccarii* *Aubygnina perlucida* *Bolivina robusta* *Bolivina sp. H* *Brizalina A* *Bulimina spinensis.* *Cancris oblongus* *Cibicides kullenbergi* *Cibicides lobatulus* *Cibicides refulgens* *Cibicides spp.* *Dyocibicides biserialis* *Elphidium advenum* *Elphidium cf macellum* *Elphidium crispum* *Elphidium excavatum* *Elphidium macellum* *Elphidium sp. A* *Florilus bouneaum* *Hanzawaia rhodoensis*	*Globigerina bulloides* *Globigerina falconensis* *Globigerina rubescens* *Globigerina sacculifera* *Globigerinoides obliquus* *Globigerinoides ruber* *Globigerinoides tenellus* *Globigerinoides triloba* *Globorotalia margaritae* *Neogloboquadrina acostoensis*
	Haynensia depressula *Haynesia depressula* *Neoconorbina terquem* *Nonion fabum* *Oolina sp.* *Patellina sp* *Planorbulina mediterranensis* *Pyrgo sp.* *Reusella simplex* *Textularia agglutinans*	
Yu27/92b 0.18 n=20	*Bolivina plicatella* *Bolivina robusta* *Bolivina sp. C* *Cibicides lobatulus* *Elphidium macellum* *Elphidium advenum* *Elphidium sp. A* *Florilus bouneaum* *Fursenkonia sp.* *Neoconorbina terquem* *Quinqueloculina spp.*	*Globigerina bulloides* *Globorotalia margaritae*
Yu28/92b 0.25 n=15	*Bolivina sp.* *Cibicides kullenbergi* *Cibicides refulgens* *Elphidium advenum* *Elphidium excavatum* *Elphidium sp. A* *Fursenkonia sp.* *Haynensia depressula* *Neoconorbina terquem*	*Globigerinoides ruber* *Orbulina universa*

Yu29/92b 0.28 n=50	*Ammonia beccarii* *Bolivina robusta* *Bulimina spinensis* *Cibicides lobatulus* *Cibicides refulgens* *Elphidium macellum* *Fursenkonia sp.* *Haynensia depressula* *Melonis affinis* *Neoconorbina terquem* *Nonion fabum* *Planorbulina mediterranensis* *Quinqueloculina sp.* *Stilostomella antillea*	*Globigerina bulloides* *Globigerina falconensis*
Yu30/92b 0.42 n=30	*Ammonia beccarii* *Aubygnina perlucida,* *Cancris oblongus* *Cibicides lobatulus* *Cibicides refulgens* *Elphidium excavatum* *Elphidium sp.* *Haynensia depressula* *Neoconorbina terquem* *Nonion fabum*	*Globigerina bulloides* *Globigerina falconensis* *Globigerina rubescens* *Globigerinella siphonifera* *Globigerinoides obliquus extremus* *Neogloboquadrina acostoensis* *Orbulina universa*
Yu32/92b 0.47 n=50	*Ammonia beccarii* *Bolivina robusta* *Brizalina subreticulata* *Cancris oblongus* *Cibicides kullenbergi* *Cibicides lobatulus* *Cibicides refulgens* *Elphidium advenum* *Elphidium cf macellum* *Elphidium excavatum* *Neoconorbina terquem* *Nonion fabum* *Uvigerina peregrina* *Valvulinera sp.*	*Globigerina bulloides* *Globigerinoides ruber* *Globigrinoides triloba* *Globogerina sacculifera* *Globorotalia margaritae*
Yu33/92b 0.52 n=58	*Ammonia beccarii* *Bolivina robusta* *Bulimina spinensis* *Cancris oblongus* *Cibicides kullenbergi* *Cibicides lobatulus* *Elphidium advenum* *Elphidium macellum* *Neoconorbina terquem* *Nonion fabum* *Reusella simplex* *Textularia agglutinans*	*Globigerina bulloides* *Globigerina falconensis* *Globigerinoides ruber*

Yu35/92b 0.33 n=48	*Ammonia beccarii* *Bolivina sp.* *Cancris oblongus* *Cibicides kullenbergi* *Cibicides lobatulus* *Elphidium advenum* *Elphidium excavatum* *Neoconorbina terquem*	*Globigerina falconensis*
Yu36/92b 0.67 n=50	*Ammonia beccarii* *Cancris oblongus* *Cibicides kullenbergi* *Cibicides lobatulus* *Elphidium macellum* *Fursenkonia sp* *Haynensia depressula* *Melonis affinis* *Neoconorbina terquem* *Nonion fabum* *Textularia agglutinans*	*Globigerina bulloides* *Globigerina falconensis* *Globigerina sacculifera* *Globigerinella siphonifera* *Globigerinoides obliquus* *Globigerinoides ruber* *Globigerinoides tenellus*
Yu37/92b 0.35 n=23	*Ammonia beccarii* *Bolivina sp.* *Cibicides lobatulus* *Elphidium advenum* *Haynensia depressula* *Melonis affinis* *Nonion fabum* *Patellina sp.* *Uvigerina peregrina*	*Globigerina bulloides* *Globigerina falconensis* *Globigerina sacculifera*
Yu38/92b 0.39 n=78	*Bolivina robusta* *Cibicides kullenbergi* *Cibicides lobatulus* *Cibicides refulgens* *Elphidium advenum* *Elphidium excavatum* *Elphidium macellum* *Melonis affinis*	*Globigerina bulloides* *Globigerina falconensis* *Globigerina sacculifera* *Globigerinoides ruber* *Globorotalia margaritae*

Appendix 2:

2.1 Laboratory Procedure for Uranium and Thorium separations

A) DIGESTION

1. Wet the sample with **distilled water (H_2O)** in a **Teflon** beaker marked with the sample identity.
2. Add **20ml** of **Hydrochloric (HCl)** acid and **5ml** of **HNO_3**.
3. Spike the mixture with **0.025ml** (total) of **^{232}U & ^{228}Th**. Swill the mixture around carefully.
4. Place onto a hot plate to evaporate.
5. After the mixture has evaporated to a pastey consistency, transfer from the Teflon beaker to a **glass** beaker by swilling the mixture around with **10-20ml** of **7.8M HCl**.
6. Place onto a hot plate to evaporate.
7. When the mixture has evaporated down (not entirely), wash with a little **7.8 M HCl** and, if any particles are seen, heat (with a lid) until they dissolve. *** Do not heat to much or the acid strength will be altered.**

Ether extraction to remove Fe

Tufas contain a high content of iron. This needs to be extracted as it can be taken up on the column, thereby reducing the uptake of uranium.

1. After evaporation of the U sample, add **7.8 M HCl** to **25ml** and pour this solution into a separation flask, washing the beaker clean with **7.8 M HCl**.
2. Pour in an **equal amont** of **General Purpose Di-isopropyl Ether** and mix, regularly releasing the stopper to allow gas to escape.
3. Shake for **2 minutes** to transfer the Fe into the ether.
4. Place in a holder and extract the U - HCl mixture into a sample beaker, leaving the ether in the flask with the Fe (pour the ether into a dish and leave to evaporate in fume cupboard).
5. Evaporate U sample to a very small quantity, add **25ml** of **7.8 M HCl**, the sample is now ready for the first column.

B) SAMPLE TREATMENT

COLUMN 1

1. Fill column(s) with **Anion Exchange Resin** (AG 1-XG, 100-200 mesh, chloride form) mixed with **1 Molar (M) Hydro-Chloric (HCl) acid** (**resin needs to come to the level of 1 cm from the top of the column**).
2. **Wash** the column through with **25 mls** of **1 M HCl**
3. **Equilibrate** the column with **50 mls** of **7.8 M HCl**.
4. **Add** the digested sample to the column, washing all traces of the sample out of the beaker with **7.8 M HCl**. Ensure collecting beaker is marked with the sample identity.
5. **Wash** the column **3 times** with **15mls 7.8 M HCl**, to remove all Th which then collects in the beakers.
6. Place the collected Th sample on the hot plate (temperature about 7) and evaporate down to about 5 - 10 mls.
7. **Elute** the U collected in the column by washing through with **50 mls** of **1 M HCl**, collecting this in a clean beaker marked with the sample name.
8. **Evaporate** the U sample to very small quantity (a few drops).
9. U sample to: C) Electroplating.

Th sample conversion to Nitric (from 7 above)

1. Add **Concentrated HNO_3** to about **25 mls** and evaporate, making sure not to bake onto beaker.
2. Evaporate **3 times**.
3. Add **25ml of 8M HNO_3** and evaporate. When evaporation is complete, add another **25ml of 8M HNO_3** and heat with a lid until clear. Sample is now ready for the second column.

COLUMN 2

1. Half fill columns with **Resin** mixed with **0.1 M HNO_3**
2. **Wash** with **50 mls** of **0.1 M HNO_3**.
3. **Equilibrate** columns with **50 mls** of **8 M HNO_3**.
4. **Add** Th sample, washing out the sample beaker with **8 M HNO_3** so as to fill half way up funnel.

5. **Wash 3 times** with **15 mls** of **8 M HNO_3, .**
6. **Elute** Th with **50 mls** of **9 M HCl.**
7. Evaporate to a very small amount, being sure not to bake it.
8. Th sample to: C) Electroplating.

C) ELECTRO - PLATING

Preparing samples

1. Add **5 drops** of **Sulphuric acid (H_2SO_4)**
2. **Evaporate** until white fumes are produced, indicating only sulphuric acid remains.
3. Add **3 mls** (with Pastuer pipette) of **Ammonium Sulphate** and swirl the mixture.
4. Add **3 drops** (with Pastuer pipette) of **Thymol Blue** (if solution appears bitty, dissolve gently over hot plate).
5. Add sample to plating tubes, washing the beaker out gradually with **8ml** of **Ammonium Sulphate.**
6. Add **Concentrated Ammonia Solution**, one drop at a time, until solution turns **salmon pink**.

Electro-plating

1. Mark plating discs with sample identity, peel off the green/blue film, and clean with acetone.
2. Put the disk into the brass plate, polished surface up, recording which numbered or lettered plate the sample is in.
3. Push the Teflon tube onto the plate, ensuring that the platinum wire **does not** touch the disc.
4. Place brass collar onto the tube and tighten the screws.
5. Put a stirring bean into the tube, and place onto stirrer.
6. Add the sample to the tube, using ammonia sulphate solution to wash out the beaker. Turn on stirrer.
7. **Wire Connections.** The red wire from the distribution box connects to the platinum wire so as **not** to touch the brass of the plate. The black wire attaches to one of the brass screws.
8. Ensure the distribution box is switched off and the control knob at minimum before turning on the power supply box.
9. Keep the levels down on the power supply, then switch on the distribution box and adjust the two instruments until the distribution box has a level of at least **0.8**

amps (power supply will be around **12 volts**). As plating continues the current may drop, therefore tweak up the level on the distribution box.

10. Plate for about **1.5 hours**.
11. At the end of plating, squirt in 1 pippette of **concentrated ammonia solution**, while the current is still on, then switch off.
12. Remove the discs from the plates using tweezers and wash with **distilled water**.
13. Gently waft the disc, at an angle, in a bunsen flame until dry.

α-counting

The samples are counted on an alpha spectrophotometer (brand) for a period of 4 days at a vacuum of $8x10^{-2}$ Mbs and at 4 MeV. Counts are made within defined regions of interest, corresponding to the emission spectrum of the isotope. Background counts are made, in the same region, for a minimum of 2 days prior to loading of the sample. Conuts are chacked and adjusted by hand before being loaded into the spreadsheet.

2.2 Spreadsheets

The following pages are the spreadsheets containing all the data and basic calculations for each of the following samples:

Ca6/92bi	Ca8/92bii
Ca6/92bii	Ca8b/92b
Ca6/92biii	A1.1/91
Ca6/92biv	Ha/92b
Ca4/92b	Ko/92b
Ca5a/92b	Ku1/92b
Ca8/92bi	Ku2/92b

Summary of Results:

230Th/234U(a) is calculated using the L/L correction scheme for detrital Thorium (Kaufman, 1993). r^2 is the correlation value of the regression curve.

	230Th/234U(a)	r^2		234U/238U	error
Calkaya 6	1.078	0.970	4 data	1.084	0.066
Calkaya 8	1.031	0.995	3 data	1.086	0.070
all data	0.973	0.989	14 data	1.015	0.069

CALCULATING URANIUM & THORIUM DATA SAMPLE Antalya

SUB-SAMPLE Ca6/92bi SAMPLE WEIGHT 2.11023 SPIKE VOLUME 0.01976 Error 0.00009

Isotope	Gross count	Live Time	CPM	Background	Live Time	CPM	Adjusted CPM
U238	617	257982.00	0.14350	5	167579.40	0.00179	0.14171
U234	703	257982.00	0.16350	12	167579.40	0.00430	0.15920
U232	10657	257982.00	2.47855	101	167579.40	0.03616	2.44238
TH232	22	258014.80	0.00512	2	168252.40	0.00071	0.00440
TH230	789	258014.80	0.18348	9	168252.40	0.00321	0.18027
TH228	14012	258014.80	3.25842	88	168252.40	0.02348	3.23494
RA224	3789	258014.80	0.88111	443	168252.40	0.15798	0.72314

Isotope	Adjusted CPM	Error(+/-)
U238	0.14171	0.00583
U234	0.15920	0.00629
U232	2.44238	0.02428
TH232	0.00440	0.00120
TH230	0.18027	0.00662
TH228	3.23494	0.02768
RA224	0.72314	0.01616

Adjusting TH228 for RA224 ingrowth

CPM	Error(+/-)
3.19438	0.02772

Isotope	Activity(DPM)	Error(+/-)
U238	0.34000	0.01524
U234	0.38198	0.01655
TH232	0.00892	0.00244
TH230	0.36516	0.01479

SPIKE ACTIVITIES

U232	Error(+/-)	TH228	Error(+/-)
62.58063	0.87613	69.10286	0.96744

U234/U238 Activity Ratio		TH230/U234 Activity Ratio	
Ratio	Error(+/-)	Ratio	Error(+/-)
1.12346	0.06409	0.95599	0.05636

COUNTER EFFICIENCIES(%) Uranium= 33.41 Thorium= 32.80

CHEMICAL YIELDS (%) Uranium= 59.11746 Thorium= 71.31689

CONCENTRATION (PPM) Uranium= 0.45515 Thorium= 0.03622

SUB-SAMPLE	Ca6/92bii	SAMPLE WEIGHT		2.12962	SPIKE VOLUME		0.01976	Error	0.00009

Isotope	Gross count	Live Time	CPM	Background	Live Time	CPM	Adjusted CPM
U238	601	258104.70	0.13971	8	169934.10	0.00282	0.13689
U234	650	258104.70	0.15110	9	169934.10	0.00318	0.14792
U232	11413	258104.70	2.65311	116	169934.10	0.04096	2.61215
TH232	14	258133.40	0.00325	1	170119.60	0.00035	0.00290
TH230	745	258133.40	0.17317	6	170119.60	0.00212	0.17105
TH228	12810	258133.40	2.97753	130	170119.60	0.03834	2.93919
RA224	3631	258133.40	0.84398	426	170119.60	0.15025	0.69373

Isotope	Adjusted CPM	Error(+/-)
U238	0.13689	0.00579
U234	0.14792	0.00602
U232	2.61215	0.02512
TH232	0.00290	0.00094
TH230	0.17105	0.00640
TH228	2.93919	0.02656
RA224	0.69373	0.01578

Adjusting TH228 for RA224 ingrowth

CPM	Error(+/-)
2.90160	0.02659

Isotope	Activity(DPM)	Error(+/-)
U238	0.30429	0.01393
U234	0.32882	0.01458
TH232	0.00641	0.00208
TH230	0.37798	0.01560

SPIKE ACTIVITIES

U232	Error(+/-)	TH228	Error(+/-)
62.58063	0.87613	69.10286	0.96744

U234/U238 Activity Ratio		TH230/U234 Activity Ratio	
Ratio	Error(+/-)	Ratio	Error(+/-)
1.08063	0.06341	1.14948	0.06922

COUNTER EFFICIENCIES(%)	Uranium=	33.17	Thorium=	33.46
CHEMICAL YIELDS (%)	Uranium=	63.68880	Thorium=	63.50629
CONCENTRATION (PPM)	Uranium=	0.40735	Thorium=	0.02604

CALCULATING URANIUM & THORIUM DATA

SAMPLE Antalya

SUB-SAMPLE Ca6/92biii SAMPLE WEIGHT 2.19297 SPIKE VOLUME 0.01976 Error 0.00009

Isotope	Gross count	Live Time	CPM	Background	Live Time	CPM	Adjusted CPM
U238	576	258166.90	0.13387	4	170354.70	0.00141	0.13246
U234	648	258166.90	0.15060	9	170354.70	0.00317	0.14743
U232	13940	258166.90	3.23976	62	170354.70	0.02184	3.21793
TH232	28	258193.70	0.00651	2	170483.00	0.00070	0.00580
TH230	629	258193.70	0.14617	7	170483.00	0.00246	0.14371
TH228	13649	258193.70	3.17180	88	170483.00	0.02801	3.14379
RA224	3582	258193.70	0.83240	168	170483.00	0.05913	0.77327

Isotope	Adjusted CPM	Error(+/-)
U238	0.13246	0.00562
U234	0.14743	0.00601
U232	3.21793	0.02758
TH232	0.00580	0.00133
TH230	0.14371	0.00590
TH228	3.14379	0.02733
RA224	0.77327	0.01464

Adjusting TH228 for RA224 ingrowth

CPM	Error(+/-)
3.09932	0.02737

Isotope	Activity(DPM)	Error(+/-)
U238	0.23211	0.01062
U234	0.25835	0.01142
TH232	0.01166	0.00267
TH230	0.28871	0.01285

SPIKE ACTIVITIES

U232	Error(+/-)	TH228	Error(+/-)
62.58063	0.87613	69.10286	0.96744

U234/U238 Activity Ratio

TH230/U234 Activity Ratio

Ratio	Error(+/-)	Ratio	Error(+/-)
1.11303	0.06550	1.11751	0.06972

COUNTER EFFICIENCIES(%) Uranium= 33.33 Thorium= 33.87

CHEMICAL YIELDS (%) Uranium= 78.08502 Thorium= 67.02167

CONCENTRATION (PPM) Uranium= 0.31072 Thorium= 0.04735

SUB-SAMPLE	Ca6/92biv	SAMPLE WEIGHT	2.01251	SPIKE VOLUME	0.01976	Error	0.00009

Isotope	Gross count	Live Time	CPM	Background	Live Time	CPM	Adjusted CPM
U238	475	258216.70	0.11037	9	170663.90	0.00316	0.10721
U234	486	258216.70	0.11293	10	170663.90	0.00352	0.10941
U232	14486	258216.70	3.36601	64	170663.90	0.02250	3.34351
TH232	41	258247.50	0.00953	5	170891.20	0.00176	0.00777
TH230	301	258247.50	0.06993	9	170891.20	0.00316	0.06677
TH228	9008	258247.50	2.09288	84	170891.20	0.02498	2.06790
RA224	2432	258247.50	0.56504	257	170891.20	0.09023	0.47481

Isotope	Adjusted CPM	Error(+/-)
U238	0.10721	0.00517
U234	0.10941	0.00524
U232	3.34351	0.02811
TH232	0.00777	0.00168
TH230	0.06677	0.00417
TH228	2.06790	0.02225
RA224	0.47481	0.01277

Adjusting TH228 for RA224 ingrowth

CPM	Error(+/-)
2.03638	0.02232

Isotope	Activity(DPM)	Error(+/-)
U238	0.19702	0.01008
U234	0.20107	0.01022
TH232	0.02589	0.00562
TH230	0.22248	0.01447

SPIKE ACTIVITIES

U232	Error(+/-)	TH228	Error(+/-)
62.58063	0.87613	69.10286	0.96744

U234/U238 Activity Ratio		TH230/U234 Activity Ratio	
Ratio	Error(+/-)	Ratio	Error(+/-)
1.02056	0.06939	1.10645	0.09105

COUNTER EFFICIENCIES(%)	Uranium=	34.81	Thorium=	31.70
CHEMICAL YIELDS (%)	Uranium=	77.66432	Thorium=	47.05018
CONCENTRATION (PPM)	Uranium=	0.26375	Thorium=	0.10516

CALCULATING URANIUM & THORIUM DATA

SAMPLE Antalya (T2)

SUB-SAMPLE Ca4/92b SAMPLE WEIGHT 2.02237 SPIKE VOLUME 0.01976 Error 0.00009

Isotope	Gross count	Live Time	CPM	Background	Live Time	CPM	Adjusted CPM
U238	692	257176.40	0.16145	4	169150.70	0.00142	0.16003
U234	769	257176.40	0.17941	11	169150.70	0.00390	0.17551
U232	10618	257176.40	2.47721	105	169150.70	0.03724	2.43997
TH232	52	257184.50	0.01213	6	169157.90	0.00213	0.01000
TH230	691	257184.50	0.16121	18	169157.90	0.00638	0.15482
TH228	10504	257184.50	2.45054	186	169157.90	0.05122	2.39932
RA224	3220	257184.50	0.75121	832	169157.90	0.29511	0.45610

Isotope	Adjusted CPM	Error(+/-)
U238	0.16003	0.00618
U234	0.17551	0.00658
U232	2.43997	0.02431
TH232	0.01000	0.00189
TH230	0.15482	0.00631
TH228	2.39932	0.02429
RA224	0.45610	0.01673

Adjusting TH228 for RA224 ingrowth

CPM	Error(+/-)
2.36651	0.02438

Isotope	Activity(DPM)	Error(+/-)
U238	0.40118	0.01706
U234	0.43999	0.01825
TH232	0.02853	0.00543
TH230	0.44163	0.01969

SPIKE ACTIVITIES

U232	Error(+/-)	TH228	Error(+/-)
62.60382	0.87645	69.08892	0.96724

U234/U238 Activity Ratio

TH230/U234 Activity Ratio

Ratio	Error(+/-)	Ratio	Error(+/-)
1.09674	0.05900	1.00374	0.06076

COUNTER EFFICIENCIES(%) Uranium= 33.41 Thorium= 32.80

CHEMICAL YIELDS (%) Uranium= 59.03706 Thorium= 52.84481

CONCENTRATION (PPM) Uranium= 0.53705 Thorium= 0.11590

SUB-SAMPLE Ca5a/92b SAMPLE WEIGHT 2.03267 SPIKE VOLUME 0.01976 Error 0.00009

Isotope	Gross count	Live Time	CPM	Background	Live Time	CPM	Adjusted CPM
U238	830	257144.00	0.19367	5	169167.30	0.00177	0.19189
U234	906	257144.00	0.21140	7	169167.30	0.00248	0.20892
U232	8956	257144.00	2.08972	124	169167.30	0.04398	2.04574
TH232	13	257135.40	0.00303	1	169177.50	0.00035	0.00268
TH230	1001	257135.40	0.23357	10	169177.50	0.00355	0.23003
TH228	11520	257135.40	2.68808	173	169177.50	0.04947	2.63860
RA224	3222	257135.40	0.75182	670	169177.50	0.23762	0.51420

Isotope	Adjusted CPM	Error(+/-)
U238	0.19189	0.00677
U234	0.20892	0.00709
U232	2.04574	0.02243
TH232	0.00268	0.00091
TH230	0.23003	0.00747
TH228	2.63860	0.02539
RA224	0.51420	0.01612

Adjusting TH228 for RA224 ingrowth

CPM	Error(+/-)
2.61021	0.02542

Isotope	Activity(DPM)	Error(+/-)
U238	0.57086	0.02271
U234	0.62150	0.02398
TH232	0.00689	0.00235
TH230	0.59188	0.02188

SPIKE ACTIVITIES

U232	Error(+/-)	TH228	Error(+/-)
62.60382	0.87645	69.08892	0.96724

U234/U238 Activity Ratio		TH230/U234 Activity Ratio	
Ratio	Error(+/-)	Ratio	Error(+/-)
1.08872	0.05328	0.95233	0.05049

COUNTER EFFICIENCIES(%) Uranium= 33.17 Thorium= 33.46

CHEMICAL YIELDS (%) Uranium= 49.86031 Thorium= 57.14028

CONCENTRATION (PPM) Uranium= 0.76420 Thorium= 0.02800

CALCULATING URANIUM & THORIUM DATA — SAMPLE

SUB-SAMPLE Ca8/92bi — SAMPLE WEIGHT 1.99292 — SPIKE VOLUME 0.01976 — Error 0.00009

Isotope	Gross count	Live Time	CPM	Background	Live Time	CPM	Adjusted CPM
U238	535	248261.90	0.12930	2	177859.80	0.00067	0.12862
U234	630	248261.90	0.15226	6	177859.80	0.00202	0.15023
U232	13035	248261.90	3.15030	63	177859.80	0.02125	3.12905
TH232	118	248260.40	0.02852	7	177860.10	0.00236	0.02616
TH230	568	248260.40	0.13728	14	177860.10	0.00472	0.13255
TH228	12462	248260.40	3.01184	223	177860.10	0.05991	2.95193
RA224	3813	248260.40	0.92153	908	177860.10	0.30631	0.61522

Isotope	Adjusted CPM	Error(+/-)
U238	0.12862	0.00561
U234	0.15023	0.00612
U232	3.12905	0.02772
TH232	0.02616	0.00277
TH230	0.13255	0.00590
TH228	2.95193	0.02735
RA224	0.61522	0.01806

Adjusting TH228 for RA224 ingrowth

CPM	Error(+/-)
2.89501	0.02751

Isotope	Activity(DPM)	Error(+/-)
U238	0.25457	0.01194
U234	0.29734	0.01315
TH232	0.06197	0.00666
TH230	0.31403	0.01502

SPIKE ACTIVITIES

U232	Error(+/-)	TH228	Error(+/-)
62.45983	0.87444	69.17252	0.96842

U234/U238 Activity Ratio		TH230/U234 Activity Ratio	
Ratio	Error(+/-)	Ratio	Error(+/-)
1.16801	0.06972	1.05612	0.06845

COUNTER EFFICIENCIES(%) Uranium= 33.33 Thorium= 33.87

CHEMICAL YIELDS (%) Uranium= 76.08 Thorium= 62.54

CONCENTRATION (PPM) Uranium= 0.34079 Thorium= 0.25170

SUB-SAMPLE	Ca8/92bii	SAMPLE WEIGHT		1.96206	SPIKE VOLUME		0.01976	Error	0.00009

Isotope	Gross count	Live Time	CPM	Background	Live Time	CPM	Adjusted CPM
U238	634	258852.10	0.14696	11	328343.90	0.00201	0.14495
U234	612	258852.10	0.14186	10	328343.90	0.00183	0.14003
U232	13507	258852.10	3.13082	149	328343.90	0.02723	3.10360
TH232	58	258211.30	0.01348	10	328342.60	0.00183	0.01165
TH230	704	258211.30	0.16359	30	328342.60	0.00548	0.15810
TH228	13698	258211.30	3.18297	364	328342.60	0.05160	3.13137
RA224	4006	258211.30	0.93087	1632	328342.60	0.29823	0.63264

Isotope	Adjusted CPM	Error(+/-)
U238	0.14495	0.00587
U234	0.14003	0.00576
U232	3.10360	0.02703
TH232	0.01165	0.00186
TH230	0.15810	0.00625
TH228	3.13137	0.02737
RA224	0.63264	0.01646

Adjusting TH228 for RA224 ingrowth

CPM	Error(+/-)
3.08809	0.02744

Isotope	Activity(DPM)	Error(+/-)
U238	0.29378	0.01291
U234	0.28381	0.01265
TH232	0.02628	0.00422
TH230	0.35667	0.01537

SPIKE ACTIVITIES

U232	Error(+/-)	TH228	Error(+/-)
62.45983	0.87444	69.17252	0.96842

U234/U238 Activity Ratio		TH230/U234 Activity Ratio	
Ratio	Error(+/-)	Ratio	Error(+/-)
0.96608	0.05577	1.25670	0.07748

COUNTER EFFICIENCIES(%)	Uranium=	34.81	Thorium=	31.70
CHEMICAL YIELDS (%)	Uranium=	72.23092	Thorium=	71.27768
CONCENTRATION (PPM)	Uranium=	0.39328	Thorium=	0.10675

SUB-SAMPLE	Ca8b/92b	SAMPLE WEIGHT	1.99066	SPIKE VOLUME	0.01976	Error	0.00009

Isotope	Gross count	Live Time	CPM	Background	Live Time	CPM	Adjusted CPM
U238	361	248263.60	0.08725	9	177853.80	0.00304	0.08421
U234	397	248263.60	0.09595	4	177853.80	0.00135	0.09460
U232	15030	248263.60	3.63243	67	177853.80	0.02260	3.60983
TH232	237	248268.20	0.05728	10	177855.10	0.00337	0.05390
TH230	335	248268.20	0.08096	16	177855.10	0.00540	0.07556
TH228	13510	248268.20	3.26502	171	177855.10	0.04408	3.22094
RA224	3759	248268.20	0.90845	807	177855.10	0.27224	0.63621

Isotope	Adjusted CPM	Error(+/-)
U238	0.08421	0.00470
U234	0.09460	0.00486
U232	3.60983	0.02976
TH232	0.05390	0.00387
TH230	0.07556	0.00462
TH228	3.22094	0.02835
RA224	0.63621	0.01765

Adjusting TH228 for RA224 ingrowth

CPM	Error(+/-)
3.13523	0.02863

Isotope	Activity(DPM)	Error(+/-)
U238	0.14463	0.00844
U234	0.16247	0.00879
TH232	0.11805	0.00872
TH230	0.16549	0.01053

SPIKE ACTIVITIES

U232	Error(+/-)	TH228	Error(+/-)
62.45983	0.87444	69.17252	0.96842

U234/U238 Activity Ratio		TH230/U234 Activity Ratio	
Ratio	Error(+/-)	Ratio	Error(+/-)
1.12335	0.08526	1.01855	0.08480

COUNTER EFFICIENCIES(%)	Uranium=	34.81	Thorium=	31.70
CHEMICAL YIELDS (%)	Uranium=	84.01260	Thorium=	72.36576
CONCENTRATION (PPM)	Uranium=	0.19362	Thorium=	0.47949

CALCULATING URANIUM & THORIUM DATA SAMPLE

SUB-SAMPLE A1.1/91 SAMPLE WEIGHT 1.95578 SPIKE VOLUME 0.01976 Error 0.00009

Isotope	Gross count	Live Time	CPM	Background	Live Time	CPM	Adjusted CPM
U238	554	248254.20	0.13390	4	177855.80	0.00135	0.13255
U234	617	248254.20	0.14912	9	177855.80	0.00304	0.14609
U232	13124	248254.20	3.17191	121	177855.80	0.04082	3.13109
TH232	217	248256.00	0.05245	10	177854.90	0.00337	0.04907
TH230	576	248256.00	0.13921	19	177854.90	0.00641	0.13280
TH228	13232	248256.00	3.19799	330	177854.90	0.08732	3.11067
RA224	4353	248256.00	1.05206	1423	177854.90	0.48005	0.57200

Isotope	Adjusted CPM	Error(+/-)
U238	0.13255	0.00573
U234	0.14609	0.00609
U232	3.13109	0.02794
TH232	0.04907	0.00372
TH230	0.13280	0.00598
TH228	3.11067	0.02833
RA224	0.57200	0.02040

Adjusting TH228 for RA224 ingrowth

CPM	Error(+/-)
3.03299	0.02859

Isotope	Activity(DPM)	Error(+/-)
U238	0.26716	0.01243
U234	0.29445	0.01328
TH232	0.11307	0.00879
TH230	0.30600	0.01479

SPIKE ACTIVITIES

U232	Error(+/-)	TH228	Error(+/-)
62.46479	0.87451	69.16975	0.96838

U234/U238 Activity Ratio

Ratio	Error(+/-)
1.10215	0.06617

TH230/U234 Activity Ratio

Ratio	Error(+/-)
1.03921	0.06836

COUNTER EFFICIENCIES(%) Uranium= 33.41 Thorium= 32.80

CHEMICAL YIELDS (%) Uranium= 75.93 Thorium= 67.65

CONCENTRATION (PPM) Uranium= 0.35764 Thorium= 0.45926

SUB-SAMPLE	Ha/92b	SAMPLE WEIGHT		2.10767	SPIKE VOLUME		0.01976	Error	0.00009

Isotope	Gross count	Live Time	CPM	Background	Live Time	CPM	Adjusted CPM
U238	507	248257.00	0.12253	7	177854.30	0.00236	0.12017
U234	542	248257.00	0.13099	13	177854.30	0.00439	0.12661
U232	9240	248257.00	2.23317	260	177854.30	0.08771	2.14546
TH232	206	248258.70	0.04979	5	177861.60	0.00169	0.04810
TH230	728	248258.70	0.17595	19	177861.60	0.00641	0.16954
TH228	12618	248258.70	3.04956	297	177861.60	0.08116	2.96840
RA224	4022	248258.70	0.97205	1128	177861.60	0.38052	0.59153

Isotope	Adjusted CPM	Error(+/-)
U238	0.12017	0.00551
U234	0.12661	0.00576
U232	2.14546	0.02386
TH232	0.04810	0.00355
TH230	0.16954	0.00668
TH228	2.96840	0.02765
RA224	0.59153	0.01906

Adjusting TH228 for RA224 ingrowth

CPM	Error(+/-)
2.89072	0.02789

Isotope	Activity(DPM)	Error(+/-)
U238	0.32802	0.01623
U234	0.34559	0.01696
TH232	0.10790	0.00819
TH230	0.38033	0.01643

SPIKE ACTIVITIES

U232	Error(+/-)	TH228	Error(+/-)
62.46479	0.87451	69.16975	0.96838

U234/U238 Activity Ratio		TH230/U234 Activity Ratio	
Ratio	Error(+/-)	Ratio	Error(+/-)
1.05355	0.06806	1.10052	0.07158

COUNTER EFFICIENCIES(%)	Uranium=	33.17	Thorium=	33.46
CHEMICAL YIELDS (%)	Uranium=	52.40698	Thorium=	63.20688
CONCENTRATION (PPM)	Uranium=	0.43912	Thorium=	0.43828

SUB-SAMPLE Ko/92b SAMPLE WEIGHT 2.14251 SPIKE VOLUME 0.01976 Error 0.00009

Isotope	Gross count	Live Time	CPM	Background	Live Time	CPM	Adjusted CPM
U238	289	258213.10	0.06715	8	328346.60	0.00146	0.06569
U234	350	258213.10	0.08133	11	328346.60	0.00201	0.07932
U232	13857	258213.10	3.21990	154	328346.60	0.02814	3.19176
TH232	66	258212.10	0.01534	26	328346.60	0.00475	0.01059
TH230	400	258212.10	0.09295	34	328346.60	0.00621	0.08673
TH228	12119	258212.10	2.81606	504	328346.60	0.07317	2.74289
RA224	3798	258212.10	0.88253	2072	328346.60	0.37862	0.50391

Isotope	Adjusted CPM	Error(+/-)
U238	0.06569	0.00398
U234	0.07932	0.00439
U232	3.19176	0.02745
TH232	0.01059	0.00211
TH230	0.08673	0.00477
TH228	2.74289	0.02584
RA224	0.50391	0.01656

Adjusting TH228 for RA224 ingrowth

CPM	Error(+/-)
2.70711	0.02594

Isotope	Activity(DPM)	Error(+/-)
U238	0.11857	0.00747
U234	0.14317	0.00829
TH232	0.02494	0.00498
TH230	0.20439	0.01180

SPIKE ACTIVITIES

U232	Error(+/-)	TH228	Error(+/-)
62.46479	0.87451	69.16975	0.96838

U234/U238 Activity Ratio		TH230/U234 Activity Ratio	
Ratio	Error(+/-)	Ratio	Error(+/-)
1.20742	0.09913	1.42765	0.11635

COUNTER EFFICIENCIES(%) Uranium= 33.33 Thorium= 33.87

CHEMICAL YIELDS (%) Uranium= 77.59361 Thorium= 58.48358

CONCENTRATION (PPM) Uranium= 0.15873 Thorium= 0.10132

CALCULATING URANIUM & THORIUM DATA — SAMPLE

SUB-SAMPLE Ku1/92b — SAMPLE WEIGHT 1.92876 — SPIKE VOLUME 0.01976 — Error 0.00009

Isotope	Gross count	Live Time	CPM	Background	Live Time	CPM	Adjusted CPM
U238	528	258209.60	0.12269	11	328353.00	0.00201	0.12068
U234	491	258209.60	0.11409	16	328353.00	0.00292	0.11117
U232	15027	258209.60	3.49181	240	328353.00	0.04386	3.44796
TH232	77	258208.10	0.01789	21	328350.20	0.00384	0.01406
TH230	609	258208.10	0.14151	47	328350.20	0.00859	0.13293
TH228	15765	258208.10	3.66332	436	328350.20	0.06150	3.60183
RA224	4799	258208.10	1.11515	1989	328350.20	0.36345	0.75169

Isotope	Adjusted CPM	Error(+/-)
U238	0.12068	0.00537
U234	0.11117	0.00520
U232	3.44796	0.02863
TH232	0.01406	0.00220
TH230	0.13293	0.00587
TH228	3.60183	0.02937
RA224	0.75169	0.01804

Adjusting TH228 for RA224 ingrowth

CPM	Error(+/-)
3.55019	0.02946

Isotope	Activity(DPM)	Error(+/-)
U238	0.22399	0.01067
U234	0.20633	0.01026
TH232	0.02805	0.00443
TH230	0.26533	0.01255

SPIKE ACTIVITIES

U232	Error(+/-)	TH228	Error(+/-)
62.46479	0.87451	69.16975	0.96838

U234/U238 Activity Ratio		TH230/U234 Activity Ratio	
Ratio	Error(+/-)	Ratio	Error(+/-)
0.92119	0.05949	1.28592	0.08786

COUNTER EFFICIENCIES(%) Uranium= 33.41 Thorium= 32.80

CHEMICAL YIELDS (%) Uranium= 83.61203 Thorium= 79.18398

CONCENTRATION (PPM) Uranium= 0.29985 Thorium= 0.11395

CALCULATING URANIUM & THORIUM DATA SAMPLE

SUB-SAMPLE Ku2/92b SAMPLE WEIGHT 1.96727 SPIKE VOLUME 0.01976 Error 0.00009

Isotope	Gross count	Live Time	CPM	Background	Live Time	CPM	Adjusted CPM
U238	379	258206.00	0.08807	13	328350.70	0.00238	0.08569
U234	482	258206.00	0.11200	21	328350.70	0.00384	0.10817
U232	8662	258206.00	2.01281	530	328350.70	0.09685	1.91596
TH232	99	258211.60	0.02300	19	328347.30	0.00347	0.01953
TH230	951	258211.60	0.22098	36	328347.30	0.00658	0.21440
TH228	14679	258211.60	3.41092	461	328347.30	0.06588	3.34505
RA224	4330	258211.60	1.00615	2010	328347.30	0.36729	0.63886

Isotope	Adjusted CPM	Error(+/-)
U238	0.08569	0.00457
U234	0.10817	0.00517
U232	1.91596	0.02203
TH232	0.01953	0.00245
TH230	0.21440	0.00725
TH228	3.34505	0.02837
RA224	0.63886	0.01735

Adjusting TH228 for RA224 ingrowth

CPM	Error(+/-)
3.29357	0.02848

Isotope	Activity(DPM)	Error(+/-)
U238	0.28060	0.01586
U234	0.35418	0.01818
TH232	0.04120	0.00521
TH230	0.45229	0.01714

SPIKE ACTIVITIES

U232	Error(+/-)	TH228	Error(+/-)
62.45983	0.87444	69.17252	0.96842

U234/U238 Activity Ratio

Ratio	Error(+/-)
1.26224	0.09041

TH230/U234 Activity Ratio

Ratio	Error(+/-)
1.27700	0.08103

COUNTER EFFICIENCIES(%) Uranium= 33.17 Thorium= 33.46

CHEMICAL YIELDS (%) Uranium= 46.80 Thorium= 72.01

CONCENTRATION (PPM) Uranium= 0.37563 Thorium= 0.16736

Appendix 3:

Standard geochemical techniques and XRF data

3.1: X-ray flourescence

Whole rock chemical analysis of samples was carried out by X-ray flouresence (XRF) at the department of Geology and Geophysics, Edinburgh University. After removing veins and weathered surfaces with a diamond saw, samples were crushed and ground to a grain size of <200μm.

For major element analysis measured quantities were added to previously ignited rock powder and the samples were fused at 1100°C to obtain glass discs. The samples were analysed for 10 major elements on a Phillips PW1480 wavelength dispersive sequential XRF spectrometer. Data obtained follows in table I.

For trace element analysis the rock powders were pressed into pellets and were analysed for 17 trace elements using the Phillips PW1480 spectrometer. Samples were calibrated using USGS and CRPG international standards. Data obtained follows in table II

3.2: X-ray diffraction

Powders for X-ray diffraction (XRD) analysis were crushed and ground as for XRF analysis. The samples were packed into a pellet-shaped container and analyzed on the Phillips PW 1800 diffractometer at the Department of Geology and Geophysics, University of Edinburgh. The samples were scanned from 5-60°θ using a Cu K alpha source. The resulting traces were compared with mineral analyses contained within a databank of standardized minerals and compounds.

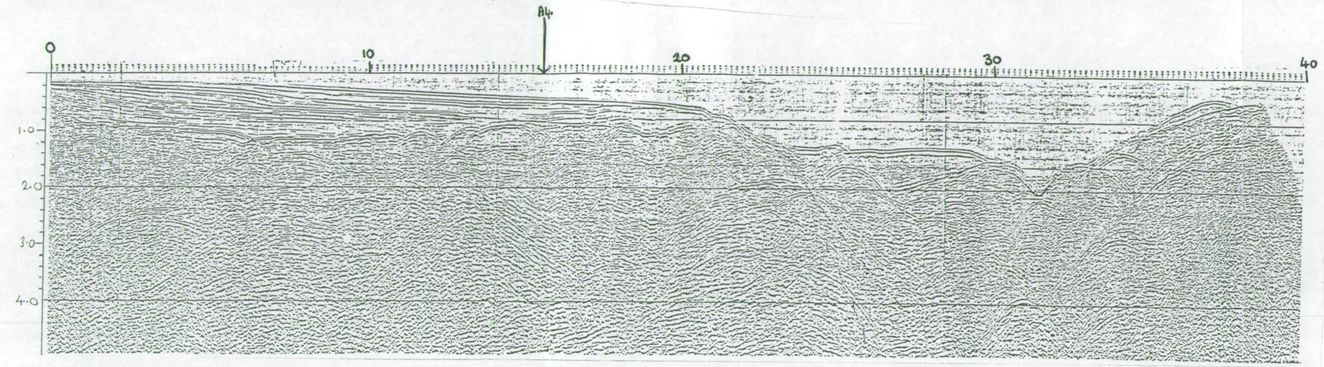

A1

A2

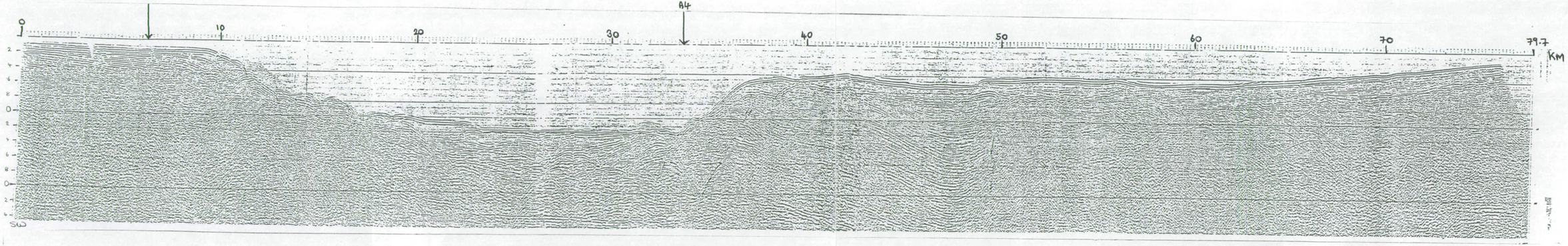

WT%	TUFF1	TUFF2	TUFF3	TUFF5	TU1	TU5A	TU5B	TU5C	TU5D	TU5E	TU5F	TU8-A
SiO2	63.56	63.33	63.79	63.62	64.16	64.61	63.81	64.27	64.53	65.53	64.53	65.19
Al2O3	16.75	16.5	16.26	15.52	16.63	15.95	15.88	15.84	15.84	16.04	15.83	16.23
Fe2O3	3.09	3.24	2.85	3.74	2.88	3.05	3.25	3.17	3.19	2.69	2.85	3.01
MgO	1.37	1.38	1.11	0.85	1.22	0.84	1.13	1.12	0.84	0.83	0.88	0.78
CaO	3.21	3.33	3.19	2.3	2.91	2.42	2.94	2.66	2.21	2.16	2.36	2.15
Na2O	5.15	5.13	4.42	3.94	4.93	4.36	4.25	4.71	3.93	4.14	4.2	4.34
K2O	4.535	4.479	4.907	5.502	4.758	5.327	5.458	5.369	5.837	5.835	5.462	5.665
TiO2	0.449	0.44	0.405	0.366	0.441	0.349	0.38	0.392	0.349	0.359	0.368	0.344
MnO	0.069	0.078	0.061	0.071	0.068	0.067	0.083	0.062	0.056	0.058	0.069	0.055
P2O5	0.222	0.203	0.233	0.144	0.236	0.165	0.188	0.197	0.161	0.153	0.162	0.13
LOI	1.06	1.08	2.52	2.9	1.31	2.42	2.25	1.7	2.65	2.65	2.62	2.2
Total	99.47	99.18	99.74	98.96	99.54	99.55	99.61	99.5	99.6	100.45	99.32	100.11

WT%	TU8-B	TU8-C	TU8-D	TU8-E	TU8-F	TU8-G	TU8-H	YE11	YE13Bi	YE13Bii	YE13C	P1/92
SiO2	64.7	65	65.17	63.6	64.84	64.95	64.96	47.75	63.41	59.81	35.69	64.5
Al2O3	16.2	16.1	16.56	16.64	16.08	16.3	15.93	19.99	17.65	20.31	16.24	15.98
Fe2O3	2.7	2.77	2.94	3.05	3	2.79	2.77	5.11	2.24	3.19	3.78	2.82
MgO	0.92	0.81	0.85	0.92	0.81	0.87	0.77	2.05	0.92	0.63	1.03	0.83
CaO	2.49	2.18	2.19	2.67	2.25	2.27	2.15	7.86	1.68	1.52	18.86	2.27
Na2O	4.35	4.22	4.3	3.83	4.33	4.1	4.32	1.76	4.06	4.95	1.45	3.96
K2O	5.728	5.863	5.657	4.736	5.378	5.751	5.558	2.728	6.228	5.66	2.021	5.847
TiO2	0.369	0.352	0.359	0.358	0.355	0.359	0.339	0.692	0.754	0.554	0.447	0.365
MnO	0.063	0.057	0.05	0.069	0.07	0.076	0.064	0.072	0.016	0.032	0.037	0.058
P2O5	0.148	0.139	0.134	0.133	0.131	0.144	0.123	0.631	0.516	0.315	0.346	0.157
LOI	1.97	2.3	2.17	3.74	2.31	2.21	2.27	10.79	1.89	2.45	19.51	2.52
Total	99.63	99.78	100.38	99.75	99.56	99.82	99.25	99.42	99.36	99.43	99.4	99.31

Table I

	Ba	Rb	Th	Nb	La	Ce	Sr	Nd	Zr	Y	LOI
Chondrite	6.9	0.35	0.042	0.35	0.329	0.865	11.8	0.63	0.684	2	
Calkaya Tuff											
Tuff2/93	2182.3	141.1	31.8	44.3	116.4	209.6	3122.8	66.2	328	23.8	1.076
Tuff3/93	1818.6	180.3	41.7	48.5	110.1	214.2	2403.4	64.8	326.2	22.6	2.52
Tuff1/93	2237.1	139.1	32.8	46.1	120.1	215	3162.5	70	364.4	25.1	1.06
Tu1/92b	2067.6	159.7	36.6	48.2	116.2	215.9	2896.6	69.2	378.8	25	1.309
Tuff5/93	1536.9	182.3	52.8	51.4	133.5	235.8	1940.9	65	319.8	22.1	2.972
Tu5/92bA	1516.9	178.8	51.4	50.6	113.4	200.1	2074.1	58.9	305.9	22.1	2.424
Tu5/92bB	1662.3	184.6	51.3	49.2	155.5	247.5	2186.1	71.1	319.1	24.8	2.253
Tu5/92bC	1577.9	213.4	54.4	51	146.3	245	2314.3	70.3	327.3	23.9	1.7
Tu5/92bD	1505.7	203.7	55.9	50.6	136.5	231.2	2062	59.7	318.1	22.5	2.652
Tu5/92bE	1493.3	193.4	54.6	52.4	121.3	215.5	2052	61	332.5	23.4	2.652
Tu5/92bF	1528.2	194.1	49	50.4	119	202.2	2062.2	63.3	315.4	21.8	2.62
P1/92	1543.5	194	53.6	50.8	134.2	235.9	2087.4	73.1	312.7	23	2.134
Yenimahalle channel											
Ye13b/93E	2036.9	192.4	62.8	63.4	141.7	252.5	1947	87.7	427.2	31.2	2.448
Ye13b/93A	2307.8	216.9	49.4	60	140.4	204.8	1640.4	83.9	524.9	30.1	1.892
Ye13c/93	2689.5	46.8	44.2	35.6	190.5	302.3	1743.4	104.2	298.5	18	19.21
Ye11/93	2487.4	89	55.7	51.3	178.9	361.3	1838.1	93.6	444.2	21.7	10.79
Isparta Ignimbrite											
I1/91	1532.3	200.2	95.6	70.7	93.4	235.8	1952.2	93.4	512	26.3	4.606
Gol1/93	2827.2	135.9	55.1	48.9	150.2	401.2	4834.1	150.2	476.2	32.1	1.329
Gol2/93	4046.9	203.7	59.9	49.4	191.1	595.2	5249.9	191.1	478.5	36.1	2.854
Gol3/93	2758.6	164.8	68.5	76.3	123.8	444.1	4786.4	123.8	582.5	33.6	1.157
Gol4/93	2983.8	145.1	53.5	49.7	167	488.8	4393.6	167	443.7	35.7	0.0181
Gol5/93	2391.4	117.4	68.9	51.7	158.1	451.1	4309.1	158.1	500.7	29.8	3.094

Table II

Appendix 4:

Seismic profiles

Seismic data were shot by MTA Sismiki in Antalya Bay and provided courtesy of Prof. Dr. M. Ergün. Lines A1-A5 produce a broad grid over the Antalya Bay area.

WT%	TUFF1	TUFF2	TUFF3	TUFF5	TU1	TU5A	TU5B	TU5C	TU5D	TU5E	TU5F	TU8-A
SiO2	63.56	63.33	63.79	63.62	64.16	64.61	63.81	64.27	64.53	65.53	64.53	65.19
Al2O3	16.75	16.5	16.26	15.52	16.63	15.95	15.88	15.84	15.84	16.04	15.83	16.23
Fe2O3	3.09	3.24	2.85	3.74	2.88	3.05	3.25	3.17	3.19	2.69	2.85	3.01
MgO	1.37	1.38	1.11	0.85	1.22	0.84	1.13	1.12	0.84	0.83	0.88	0.78
CaO	3.21	3.33	3.19	2.3	2.91	2.42	2.94	2.66	2.21	2.16	2.36	2.15
Na2O	5.15	5.13	4.42	3.94	4.93	4.36	4.25	4.71	3.93	4.14	4.2	4.34
K2O	4.535	4.479	4.907	5.502	4.758	5.327	5.458	5.369	5.837	5.835	5.462	5.665
TiO2	0.449	0.44	0.405	0.366	0.441	0.349	0.38	0.392	0.349	0.359	0.368	0.344
MnO	0.069	0.078	0.061	0.071	0.068	0.067	0.083	0.062	0.056	0.058	0.069	0.055
P2O5	0.222	0.203	0.233	0.144	0.236	0.165	0.188	0.197	0.161	0.153	0.162	0.13
LOI	1.06	1.08	2.52	2.9	1.31	2.42	2.25	1.7	2.65	2.65	2.62	2.2
Total	99.47	99.18	99.74	98.96	99.54	99.55	99.61	99.5	99.6	100.45	99.32	100.11

WT%	TU8-B	TU8-C	TU8-D	TU8-E	TU8-F	TU8-G	TU8-H	YE11	YE13Bi	YE13Bii	YE13C	P1/92
SiO2	64.7	65	65.17	63.6	64.84	64.95	64.96	47.75	63.41	59.81	35.69	64.5
Al2O3	16.2	16.1	16.56	16.64	16.08	16.3	15.93	19.99	17.65	20.31	16.24	15.98
Fe2O3	2.7	2.77	2.94	3.05	3	2.79	2.77	5.11	2.24	3.19	3.78	2.82
MgO	0.92	0.81	0.85	0.92	0.81	0.87	0.77	2.05	0.92	0.63	1.03	0.83
CaO	2.49	2.18	2.19	2.67	2.25	2.27	2.15	7.86	1.68	1.52	18.86	2.27
Na2O	4.35	4.22	4.3	3.83	4.33	4.1	4.32	1.76	4.06	4.95	1.45	3.96
K2O	5.728	5.863	5.657	4.736	5.378	5.751	5.558	2.728	6.228	5.66	2.021	5.847
TiO2	0.369	0.352	0.359	0.358	0.355	0.359	0.339	0.692	0.754	0.554	0.447	0.365
MnO	0.063	0.057	0.05	0.069	0.07	0.076	0.064	0.072	0.016	0.032	0.037	0.058
P2O5	0.148	0.139	0.134	0.133	0.131	0.144	0.123	0.631	0.516	0.315	0.346	0.157
LOI	1.97	2.3	2.17	3.74	2.31	2.21	2.27	10.79	1.89	2.45	19.51	2.52
Total	99.63	99.78	100.38	99.75	99.56	99.82	99.25	99.42	99.36	99.43	99.4	99.31

Table I

	Ba	Rb	Th	Nb	La	Ce	Sr	Nd	Zr	Y	LOI
Chondrite	6.9	0.35	0.042	0.35	0.329	0.865	11.8	0.63	0.684	2	
Calkaya Tuff											
Tuff2/93	2182.3	141.1	31.8	44.3	116.4	209.6	3122.8	66.2	328	23.8	1.076
Tuff3/93	1818.6	180.3	41.7	48.5	110.1	214.2	2403.4	64.8	326.2	22.6	2.52
Tuff1/93	2237.1	139.1	32.8	46.1	120.1	215	3162.5	70	364.4	25.1	1.06
Tu1/92b	2067.6	159.7	36.6	48.2	116.2	215.9	2896.6	69.2	378.8	25	1.309
Tuff5/93	1536.9	182.3	52.8	51.4	133.5	235.8	1940.9	65	319.8	22.1	2.972
Tu5/92bA	1516.9	178.8	51.4	50.6	113.4	200.1	2074.1	58.9	305.9	22.1	2.424
Tu5/92bB	1662.3	184.6	51.3	49.2	155.5	247.5	2186.1	71.1	319.1	24.8	2.253
Tu5/92bC	1577.9	213.4	54.4	51	146.3	245	2314.3	70.3	327.3	23.9	1.7
Tu5/92bD	1505.7	203.7	55.9	50.6	136.5	231.2	2062	59.7	318.1	22.5	2.652
Tu5/92bE	1493.3	193.4	54.6	52.4	121.3	215.5	2052	61	332.5	23.4	2.652
Tu5/92bF	1528.2	194.1	49	50.4	119	202.2	2062.2	63.3	315.4	21.8	2.62
P1/92	1543.5	194	53.6	50.8	134.2	235.9	2087.4	73.1	312.7	23	2.134
Yenimahalle channel											
Ye13b/93E	2036.9	192.4	62.8	63.4	141.7	252.5	1947	87.7	427.2	31.2	2.448
Ye13b/93A	2307.8	216.9	49.4	60	140.4	204.8	1640.4	83.9	524.9	30.1	1.892
Ye13c/93	2689.5	46.8	44.2	35.6	190.5	302.3	1743.4	104.2	298.5	18	19.21
Ye11/93	2487.4	89	55.7	51.3	178.9	361.3	1838.1	93.6	444.2	21.7	10.79
Isparta Ignimbrite											
I1/91	1532.3	200.2	95.6	70.7	93.4	235.8	1952.2	93.4	512	26.3	4.606
Gol1/93	2827.2	135.9	55.1	48.9	150.2	401.2	4834.1	150.2	476.2	32.1	1.329
Gol2/93	4046.9	203.7	59.9	49.4	191.1	595.2	5249.9	191.1	478.5	36.1	2.854
Gol3/93	2758.6	164.8	68.5	76.3	123.8	444.1	4786.4	123.8	582.5	33.6	1.157
Gol4/93	2983.8	145.1	53.5	49.7	167	488.8	4393.6	167	443.7	35.7	0.0181
Gol5/93	2391.4	117.4	68.9	51.7	158.1	451.1	4309.1	158.1	500.7	29.8	3.094

Table II

Appendix 4:

Seismic profiles

Seismic data were shot by MTA Sismiki in Antalya Bay and provided courtesy of Prof. Dr. M. Ergün. Lines A1-A5 produce a broad grid over the Antalya Bay area.

A4

40

50

NE

58

0

Sec

K3

A3

TWT

2

A3

4

A4

A3

50

60

70

80

88 Km

SES

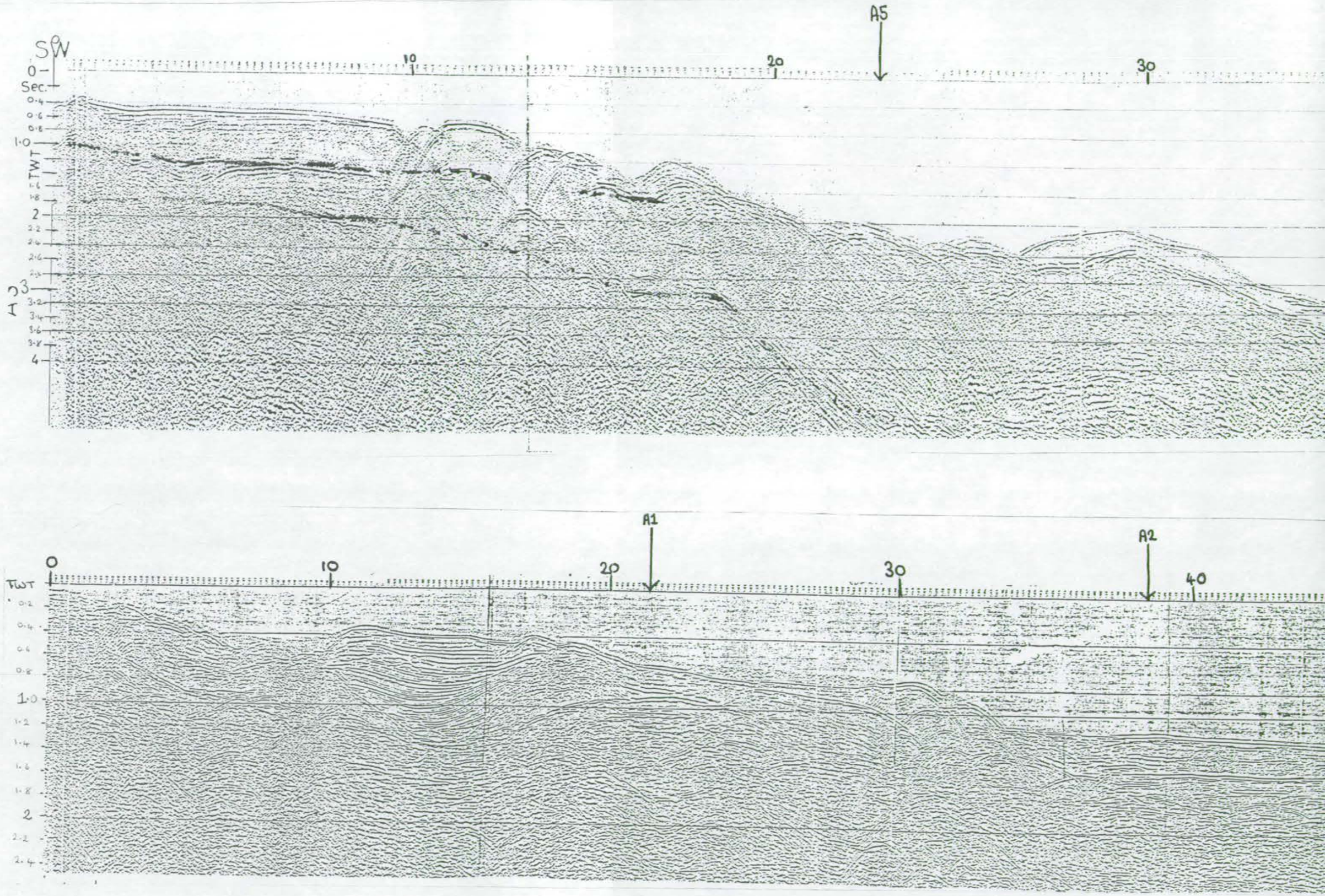
SW
0
Sec.
0·4
0·6
0·8
1·0
TWT
1·6
1·8
2
2·2
2·4
2·6
2·8
3
3·2
3·4
3·6
3·8
4
10
20
30
A5
A3
A1
0
10
20
30
40
A2
TWT
0·2
0·4
0·6
0·8
1·0
1·2
1·4
1·6
1·8
2
2·2
2·4

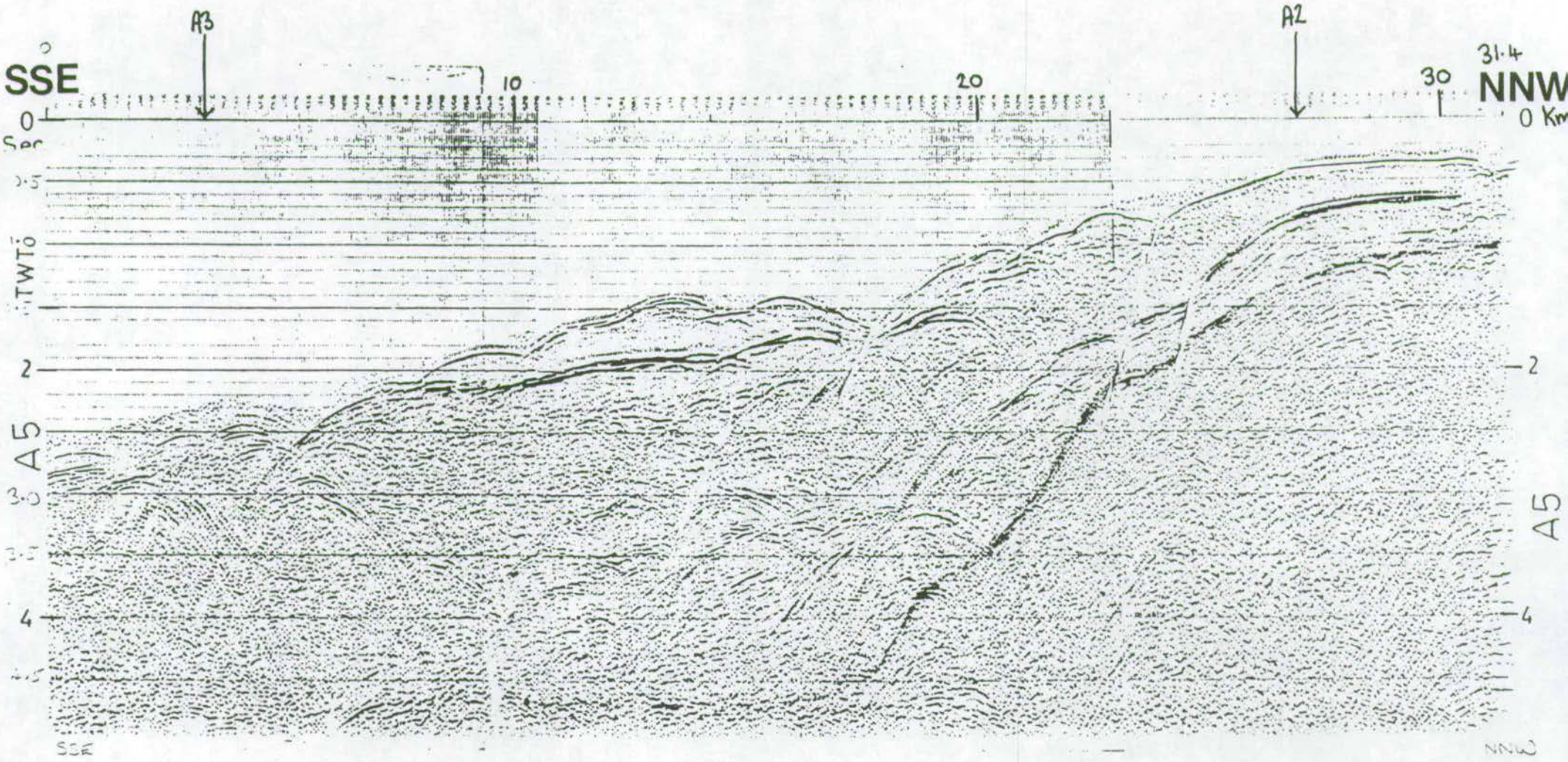

A5

SUMMARY FRAMEWORK

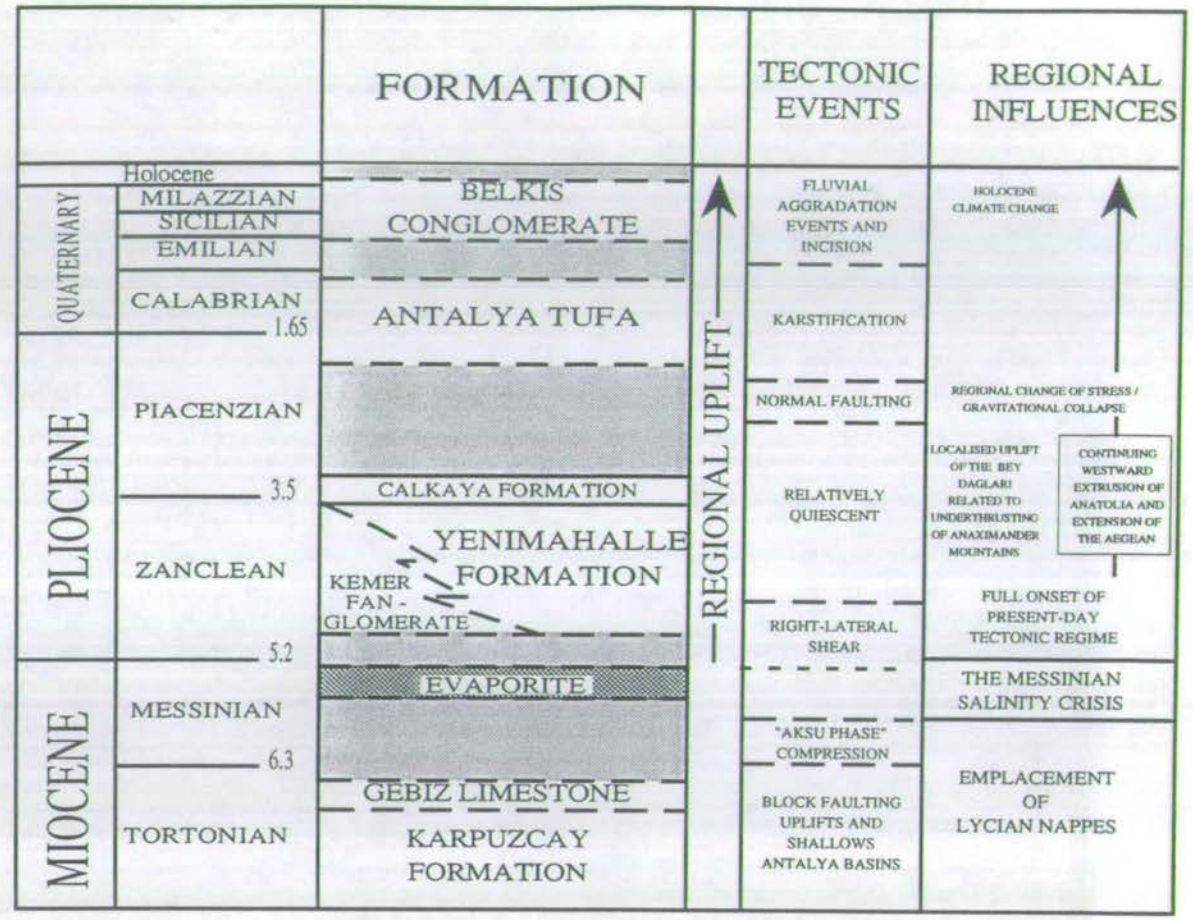

SUMMARY FRAMEWORK